SHEEP AND GOAT GENE EXPLORATION

EDITED BY: Shaobin Li, Rui Su and Xin Wang

PUBLISHED IN: Frontiers in Genetics and Frontiers in Veterinary Science

frontiers Research Topics

ISSN 1664-8714
ISBN 978-2-88974-986-7
DOI 10.3389/978-2-88974-986-7

About Frontiers

Frontiers is more than just an open-access publisher of scholarly articles: it is a pioneering approach to the world of academia, radically improving the way scholarly research is managed. The grand vision of Frontiers is a world where all people have an equal opportunity to seek, share and generate knowledge. Frontiers provides immediate and permanent online open access to all its publications, but this alone is not enough to realize our grand goals.

Frontiers Journal Series

The Frontiers Journal Series is a multi-tier and interdisciplinary set of open-access, online journals, promising a paradigm shift from the current review, selection and dissemination processes in academic publishing. All Frontiers journals are driven by researchers for researchers; therefore, they constitute a service to the scholarly community. At the same time, the Frontiers Journal Series operates on a revolutionary invention, the tiered publishing system, initially addressing specific communities of scholars, and gradually climbing up to broader public understanding, thus serving the interests of the lay society, too.

Dedication to Quality

Each Frontiers article is a landmark of the highest quality, thanks to genuinely collaborative interactions between authors and review editors, who include some of the world's best academicians. Research must be certified by peers before entering a stream of knowledge that may eventually reach the public - and shape society; therefore, Frontiers only applies the most rigorous and unbiased reviews.
Frontiers revolutionizes research publishing by freely delivering the most outstanding research, evaluated with no bias from both the academic and social point of view. By applying the most advanced information technologies, Frontiers is catapulting scholarly publishing into a new generation.

What are Frontiers Research Topics?

Frontiers Research Topics are very popular trademarks of the Frontiers Journals Series: they are collections of at least ten articles, all centered on a particular subject. With their unique mix of varied contributions from Original Research to Review Articles, Frontiers Research Topics unify the most influential researchers, the latest key findings and historical advances in a hot research area! Find out more on how to host your own Frontiers Research Topic or contribute to one as an author by contacting the Frontiers Editorial Office: frontiersin.org/about/contact

SHEEP AND GOAT GENE EXPLORATION

Topic Editors:
Shaobin Li, Gansu Agricultural University, China
Rui Su, Inner Mongolia Agricultural University, China
Xin Wang, Northwest A&F University, China

Citation: Li, S., Su, R., Wang, X., eds. (2022). Sheep and Goat Gene Exploration. Lausanne: Frontiers Media SA. doi: 10.3389/978-2-88974-986-7

Table of Contents

frontiers in Genetics

EDITORIAL
published: 31 March 2022
doi: 10.3389/fgene.2022.802709

Editorial: Sheep and Goat Gene Exploration

Shaobin Li[1]*, *Xin Wang*[2] *and Rui Su*[3]

[1]Gansu Key Laboratory of Herbivorous Animal Biotechnology, Faculty of Animal Science and Technology, Lanzhou, China, [2]College of Animal Science and Technology, Northwest A & F University, Xianyang, China, [3]College of Animal Science, Inner Mongolia Agricultural University, Hohhot, China

Keywords: functional gene, phenotype, economic traits, goat, sheep

Editorial on the Research Topic

Sheep and Goat Gene Exploration

Domestic sheep (*Ovis aries*) and goats (*Capra hircus*) are valuable farm animals that provide meat, milk, and textile-fiber for people's daily lives. Most of these traits are quantitative and controlled by multiple genes and environments. Elucidating the genetic and epigenetic mechanisms of these economic traits is critical to understanding how a trait comes into being. However, it is difficult and time-consuming work. The development of biotechnology and sequencing technology has accelerated the process of finding functional genes, which is beneficial to improving the economic traits of sheep and goat production.

Meat is the main product of sheep and goats, which is mainly affected by carcass traits (including fat), and some functional genes have been identified previously. *Myostatin* and *Callipyge* (*CLPG*) are two typical genes that can directly affect sheep carcass weight by changing hindquarters phenotype. The regulation of the expression of *MyHC* isoforms can change the myofiber types and thus change the meat quality in sheep (Bao et al.). The content of intramuscular fat (IMF) has a direct effect on the quality and flavor of the meat. A deficiency of Acetyl-CoA acyltransferase 1 (*ACAA1*) leads to an increases in the triglyceride content and lipid accumulation and promote differentiation of sheep preadipocytes, while with the overexpression of this gene a reverse phenomenon appears with a decrease of triglyceride content and lipid accumulation and inhibition of adipogenesis (Wang et al.). *APOA2*, *GALK1*, *ADIPOQ,* and *NDUFS4* may be involved in the deposition of fat in the tail of Chinese indigenous sheep (Zhu et al.). Some microRNAs (miRNAs) involved in adipocyte differentiation may be used to improve sheep meat quality and IMF content as new biomarkers (Xiao et al.), and miRNA-mRNA networking can co-regulate goat polyunsaturated fatty acid (PUFA) metabolism and synthesis (Xie et al.).

Wool and cashmere are some of the other important products of sheep and goat production. Some genes associated with the development of hair follicles or encoded fiber structural protein may have an effect on fiber traits. Besides, some miRNAs can also indirectly influence wool traits through regulating these genes. Fibroblast growth factors (FGF) and Wnt and some other signaling pathways have an important function in regulating the development of hair follicles (Harshuk-Shabso et al., 2020; Houschyar et al., 2020). *WNT2* could promote the growth and development of sheeps' skin and hair follicles (Tian et al.). Further, some *FGF5* variations are associated with wool length, greasy wool weight, and mean fiber diameter in Fine wool sheep (Zhao et al.). Sulfur is a special component in animal fibers which mainly exists as organic sulfur-containing amino acids (SAAs), and has an important function on wool fiber quality. Melatonin may regulate sulfur metabolism by regulating genes related to the skin cell cycle and energy metabolism (Chai et al.), and it regulates cashmere growth via up-regulating*β-catenin* and *Wnt10b* expression (Liu et al.). circRNA may regulate the growth and development of hair

OPEN ACCESS

Edited and reviewed by:
Martino Cassandro, University of Padua, Italy

***Correspondence:**
Shaobin Li
lisb@gsau.edu.cn

Specialty section:
This article was submitted to Livestock Genomics, a section of the journal Frontiers in Genetics

Received: *27 October 2021*
Accepted: *07 March 2022*
Published: *31 March 2022*

Citation:
Li S, Wang X and Su R (2022) Editorial: Sheep and Goat Gene Exploration. Front. Genet. 13:802709. doi: 10.3389/fgene.2022.802709

follicles by the NF-kappa B signaling pathway and Notch signaling pathway in cashmere goats (Shang et al.).

Litter size is an important trait for muti-lamb sheep and goat breeds. Fecundity booroola (*FecB*) is a major gene on sheep prolificacy (Hua and Yang, 2009). A *FecB* variant shows moderate ovulation and litter size, and a shorter estrous cycle which can be highly recommended in sheep crossbreeding systems for commercial mutton production (Wang et al.). A 13-bp indel mutation in the 3′ UTR of A-kinase anchoring protein 12 gene (*AKAP12*) is significantly associated with litter size in Shanbei white cashmere goats of China (Kang et al.). miRNAs are related to the regulation of around 1/3 of all genes in mammals and are wildly involved in all kinds of biological and physiological processes including reproduction (Reza et al., 2019). chi-miR-324-3p inhibits the proliferation of goat granulosa cells by targeting *DENND1A* (Liu et al.). Some lncRNAs play a role in regulating cell division during ovarian development in goat (Li et al.) and may participate in the regulation of seasonal reproduction in sheep (Xia et al.).

In brief, this Research Topic highlights the diversity of functional genes and miRNAs related to sheep and goat economic traits, and their biological functions would be unraveled gradually. Furthermore, the establishment of some databases, eg iSheep (Wang et al.), is undoubtedly the icing on the cake.

AUTHOR CONTRIBUTIONS

All authors listed have made a substantial, direct, and intellectual contribution to the work, and approved it for publication.

FUNDING

This work is supported by the National Natural Science Foundation of China (32060140), Distinguished Young Scholars fund of Gansu Province (21JR7RA857), and Fuxi Young Talents Fund of Gansu Agricultural University (Gaufx-03Y04).

REFERENCES

Harshuk-Shabso, S., Dressler, H., Niehrs, C., Aamar, E., and Enshell-Seijffers, D. (2020). Fgf and Wnt Signaling Interaction in the Mesenchymal Niche Regulates the Murine Hair Cycle Clock. *Nat. Commun.* 11, 5114. doi:10.1038/s41467-020-18643-x

Houschyar, K. S., Borrelli, M. R., Tapking, C., Popp, D., Puladi, B., Ooms, M., et al. (2020). Molecular Mechanisms of Hair Growth and Regeneration: Current Understanding and Novel Paradigms. *Dermatology* 236, 271–280. doi:10.1159/000506155

Hua, G.-H., and Yang, L.-G. (2009). A Review of Research Progress of FecB Gene in Chinese Breeds of Sheep. *Anim. Reprod. Sci.* 116, 1–9. doi:10.1016/j.anireprosci.2009.01.001

Reza, A. M. M. T., Choi, Y.-J., Han, S. G., Song, H., Park, C., Hong, K., et al. (2019). Roles of microRNAs in Mammalian Reproduction: from the Commitment of Germ Cells to Peri-Implantation Embryos. *Biol. Rev.* 94, 415–438. doi:10.1111/brv.12459

Conflict of Interest: The authors declare that the research was conducted in the absence of any commercial or financial relationships that could be construed as a potential conflict of interest.

Publisher's Note: All claims expressed in this article are solely those of the authors and do not necessarily represent those of their affiliated organizations, or those of the publisher, the editors and the reviewers. Any product that may be evaluated in this article, or claim that may be made by its manufacturer, is not guaranteed or endorsed by the publisher.

frontiers in Veterinary Science

ORIGINAL RESEARCH
published: 19 March 2021
doi: 10.3389/fvets.2021.647192

A Comparative Study of Sheep Breeds: Fattening Performance, Carcass Characteristics, Meat Chemical Composition and Quality Attributes

G. M. Suliman[1,2*], *A. N. Al-Owaimer*[1], *A. M. El-Waziry*[3], *E. O. S. Hussein*[1], *K. Abuelfatah*[2] *and A. A. Swelum*[1,4*]

[1] Department of Animal Production, College of Food and Agriculture Sciences, King Saud University, Riyadh, Saudi Arabia,
[2] Department of Meat Production, Faculty of Animal Production, University of Khartoum, Khartoum North, Sudan,
[3] Department of Animal Production and Fishery, Faculty of Agriculture, University of Alexandria, Alexandria, Egypt,
[4] Department of Theriogenology, Faculty of Veterinary Medicine, Zagazig University, Zagazig, Egypt

OPEN ACCESS

Edited by:
Rui Su,
Inner Mongolia Agricultural University, China

Reviewed by:
Begoña Panea,
Aragon Agrifood Research and Technology Center (CITA), Spain
Bülent Ekiz,
Istanbul University-Cerrahpasa, Turkey
Ana Kaić,
University of Zagreb, Croatia

***Correspondence:**
G. M. Suliman
gsuliman@ksu.edu.sa
A. A. Swelum
aswelum@ksu.edu.sa

Specialty section:
This article was submitted to Livestock Genomics, a section of the journal Frontiers in Veterinary Science

Received: *29 December 2020*
Accepted: *09 February 2021*
Published: *19 March 2021*

Citation:
Suliman GM, Al-Owaimer AN, El-Waziry AM, Hussein EOS, Abuelfatah K and Swelum AA (2021) A Comparative Study of Sheep Breeds: Fattening Performance, Carcass Characteristics, Meat Chemical Composition and Quality Attributes. Front. Vet. Sci. 8:647192. doi: 10.3389/fvets.2021.647192

Fattening performance, Carcass characteristics, chemical composition, and meat quality were evaluated in three sheep breeds: Awassi, Harri, and Najdi. Forty-five lambs of similar weight and age were raised for 90 days under similar conditions. The Harri and Najdi breeds had higher dressing-out percentages than Awassi sheep. The Awassi and Harri breeds had thicker backfat than the Najdi breed. No significant difference was found in moisture, protein, and intramuscular fat among the breeds. However, the Harri breed had a higher ash content than the Awassi and Najdi breeds. The Najdi breed had higher ultimate pH and lower cooking loss than the Awassi and Harri breeds. Awassi and Harri sheep had a higher myofibril fragmentation index, longer sarcomere length, and lower hardness and chewiness than Najdi sheep. Subjectively, no significant differences were detected between the breeds, except for flavor intensity while the Awassi sheep were rated in between and not significantly different. In conclusion, breed affected carcass characteristics, meat composition, and the quality of sheep. The dressing yield was higher in Harri and Najdi than Awassi sheep. Awassi sheep showed superior meat quality characteristics followed by Harri sheep. However, Najdi sheep had the best cooking loss percentage and flavor intensity score.

Keywords: sheep, breed, carcass, meat quality, muscle

INTRODUCTION

The primary livestock species producing red meat in Saudi Arabia are sheep, goats, cattle, and camels. Their total population is estimated to be 13,444,435 heads (1), distributed as follows: 9,055,438, 3,563,017, 354,276, and 471,704 heads, respectively. Therefore, sheep represent the majority (72%) of the livestock population, although the Kingdom of Saudi Arabia imports large numbers of sheep to satisfy its needs. Notably, sheep meat tops the preferred meat list of Saudi citizens followed by camel meat. Saudi Arabia don't produce sheep meat enough, a part is imported and Australia is the main source of this importation. The Business Monitor International (BMI) (2)

reported that there was an expanding market for Australian red meat exports to Saud Arabia in the first 5 months of 2013, with estimated shipments up 171% annually. In this context, mutton exports have grown to a total of 7,584 tones, projecting an increase of 65% for the same period. The only way to shorten the distance between production and consumption, aiming at lowering the importation rates of sheep meat is to prize our assets, following the economic principle. The first step to follow is evaluating sheep breeds for their performance, productivity, the differences between them, the points of strength and weakness, and the quality of their products. Then, based on the outcomes, strategic plans and short- and long-term visions can be developed. It is hypothesized that the carcass characteristics, meat chemical composition and quality attributes can be varied depend on sheep breed. Moreover, the information available about meat quality characteristics of Awassi, Harri, and Najdi sheep is scant, though these are the main sheep breeds in Saudi Arabia being adaptive to local environment, resistant to indigenous parasites and diseases, have good meat producing ability and much preferred by the natives compared to the other sheep breeds. Surprisingly enough, there is no study (up-to-date) comparing theses three sheep breeds under search regarding their fattening performance, carcass characteristics and meat quality; while, some of them gained higher standing among consumers and in markets than the others without any solid base and facts. Hence, the necessity arises to compare between these breeds to explore their exact capabilities and particularities. Therefore, this study was conducted to evaluate carcass characteristics, meat chemical composition and, quality attributes of Awassi, Harri, and Najdi sheep breeds.

MATERIALS AND METHODS

Animals, Housing, Feed, and Feeding

The experiment was conducted at the farm of the Department of Animal Production, College of Food and Agricultural Sciences, King Saud University, Riyadh, Saudi Arabia (24.8051° N, 46.5203° E). Three indigenous Saudi sheep breeds, Awassi (locally known as Ne'aimi), Harri, and Najdi, were used in this comparative study. A total of 45 intact lamb males (15 animals of each breed), with an age ranged from 84 to 95 days old and weight ranged from 23.40 to 25.87 kg, were included in this trial. The lambs were ear-tagged, treated against internal and external parasites, and housed in partially shaded pens supplied with individual feeding and watering facilities and subjected to a feeding period of 90 days after an adaptation period of 14 days. All the lambs were kept under the same conditions and fed the same diet, which was formulated to meet the nutrient requirements of lambs (3) and was offered *ad libitum*. The animals were fed iso-nitrogenous and iso-caloric commercial pelleted feed. The feed ingredients included alfalfa hay, maize, barely, soybean meal, minerals + trace elements supplements and vitamins. The feed chemical composition was 13.75, 8.16, 2.11, 8.6, and 67.38% for crude protein (CP), crude fiber (CF), ether extract (EE), ash and nitrogen free extract (NFE), respectively. Metabolizable energy (ME) of feed was 2.7 Mcal/kg. Drinking water and salt licks were made available around the clock. The experiment was conducted following the guidelines outlined by the Ethical Committee (Ethics Reference No. KSU-SE-20-17).

Fattening Performance

Live weight was recorded at the start and end of the experimental period (90 days). Feed intake was determined daily as the difference between the amounts of feed offered and refusals. Average daily intake (ADI), average daily gain (ADG), and feed conversion ratio (FCR) were calculated.

Animal Slaughtering, Carcass Evaluation, and Muscle Sampling

At the end of fattening period (90 days), eight animals were randomly selected from each breed and slaughtered following the approved Halal meat protocol directed by the legislation of Islam. Carcass and non-carcass components were weighed immediately after slaughter, and the weight of the digestive contents was computed as the difference between the full and empty digestive tract. The empty body weight (EBW) was computed as the difference between the slaughter weight and weight of digested content. All carcasses were chilled (at 4°C) for 24 h. Then, the cold weight was taken, and the carcasses were split into two halves from the pelvis to the neck along the vertebral column. The left side of the chilled carcass was cut between the 12th and 13th ribs to determine the extent of the rib-eye area and thickness of the back and body wall fats. The *Longissimus thoracis* (LT) muscles from the 9th to 12th thoracic vertebrae of both sides were removed for analyses. In brief, reading of pH and color components were performed on the steak. Drip loss and water-holding capacity tests needed meat samples of around 20 and 2 g, respectively. The cooking loss test needed a steak of approximately 2.5 cm (around 300 g). Texture profile analysis needed a sample similar to that of CL test (300 g). The shearing force was performed using the same sample of CL determination after being cooked. Sarcomere length and MFI tests required 10 and 4 g, respectively. Meat chemical composition and taste panel tests needed meat samples of around 100 and 200 g, respectively.

Meat Chemical Composition

The LT muscle was used to estimate the moisture, crude protein, crude fat, and ash based on the protocol outlined by GASTAT (1).

Meat Quality Analysis

pH and Color Measurements

The ultimate pH (pHu) of each carcass was measured at 24 h postmortem using a portable pH meter (Model pH 211, Hanna Instruments, Woonsocket, Rhode Island, USA) consistently on the left *Longissimus* muscle caudal to the 12th rib. LT samples were analyzed for color characteristics: lightness (L*), redness or red–green scale (a*), and yellowness or yellow–blue scale (b*). The color measurements were assessed using a colorimeter (Konica Minolta, CR-400-Japan; Measuring aperture: 8 mm; Illuminant: CIE D65; Observer angle: CIE 2° Standard Observer). Before measuring, a blooming time of 30 min was applied. Three readings were taken on the muscle surface, and a mean value was processed. Values of a* and b* were used to calculate color saturation (chroma), hue angle (H°) and b* to a* ratio based on

the following equations: chroma (C^*) = $(a^{*2} + b^{*2})^{1/2}$ and hue angle (H°) = $\tan^{-1}$ (b^*/a^*) described by Mancini and Hunt (4) and Olfaz et al. (5).

Cooking Loss

Cooking loss (CL) was calculated following the procedures described by Al-Owaimer et al. (6). The samples were placed in an electric commercial stainless-steel grilling oven and cooked at 200°C to an internal temperature of 70°C. After cooking, the steaks were cooled down to room temperature (20°C), surface dried with filter paper, reweighed, and the CL was expressed as the percentage weight change.

Water-Holding Capacity

The water-holding capacity (WHC) was determined following the methodology described by Wilhelm et al. (7). A meat sample of approximately 2 g was analyzed in duplicate. Initially, the sample was placed between two filter papers and then left under a 10 kg weight for 5 min. Finally, the WHC was determined as the difference between the initial and final weight of the sample and expressed as a ratio relative to the original weight.

Drip Loss

To evaluate drip loss (DL), a meat sample of around 20 g was taken and placed in sealed polyethylene plastic bag, thereafter stored in a chiller at (4°C) for 24 h. Then, the sample was removed from the bag, gently wiped, and reweighed. The DL was expressed as a percentage of the weight change.

Myofibril Fragmentation Index

The myofibril fragmentation index (MFI) of the LT samples from the three breeds was calculated following Culler et al. (8). In brief, 4 g of the muscle sample was minced using scissors. Then, it was homogenized in a mixer with 40 ml of cold (2°C) MFI buffer. Thereafter, several washes were performed, and then, the absorbance of the resultant 0.5 mg/ml solution was read at 540 nm using a spectrophotometer (HACH DR/3000 Spectrophotometer, USA). The MFI of each sample was calculated by multiplying the absorbance at 540 nm by 200.

Sarcomere Length (SL)

The sarcomere length (SL) was performed following the method described by Cross et al. (9). Briefly, three longitudinal muscle samples (3 cm × 3 cm × 2 cm) were removed and stored in 5% glutaradehyde solution for 4 h at 4°C. The SL was then determined by laser diffraction.

Shear Force and Texture Profile Analysis

A 2.5-cm-thick muscle sample (approximately 300 g) was taken to perform the test. The sample was placed in an electric commercial stainless-steel grilling oven and cooked at 200°C to an internal temperature of 70°C. The internal temperature was adjusted by inserting a thermocouple probe (Ecoscan Temp JKT, Eutech Instruments, Pte Ltd., Keppel Bay, HarbourFront, Singapore) into the center of each steak. The shear force (SF) of the LT was assessed following Wheeler et al. (10). Three round cores (1.27 cm in diameter) were removed from each cooked muscle sample parallel to the longitudinal orientation of the muscle fibers. The SF was obtained as the maximum force (N/cm^2) perpendicular to the fibers using a TA.HD texture analyzer (Stable Micro Systems, Surrey, UK) outfitted with a Warner–Bratzler attachment. The texture profile analysis (TPA) was conducted using the texture analyzer (TA.HD, Stable Micro Systems, Surrey, UK) fitted with a compression-plate attachment. Each sample underwent two cycles of 80% compression. The components determined were hardness, cohesiveness, springiness, and chewiness.

Sensory Evaluation

The test was performed using a 2.5-cm-thick meat steak (about 400 g). The meat samples were prepared and cooked under precise and uniform conditions, and then presented to panel members in specialized testing room. The taste panel room equipped with individual booths and prepared to meet all the specifications required to perform accurate and reliable sensory evaluation test as room temperature and ventilation, booth dimensions, red color light to mask color differences between meat samples, and other requirements. The room was connected to a small kitchen for sample preparation and handling. The kitchen was equipped with electrical grilling oven, warming food cabinets, refrigerator, and general kitchen supplies. The meat sample was placed in an electric commercial stainless-steel grilling oven and cooked at 200°C to an internal temperature of 70°C. The internal temperature of the sample was monitored by inserting a thermocouple probe (Ecoscan Temp JKT, Eutech Instruments, Pte Ltd., Keppel Bay, HarbourFront, Singapore) into the center of each steak. The category scaling method was used to categorize the meat samples on an 8-point category scale following Suliman et al. (11, 12). A panel of eight trained panelists assessed the cooked meat samples for flavor, tenderness and juiciness. The panel members were chosen for their ability to distinguish meat attributes under consideration and trained in how to score different characteristics. Each panelist was asked to score four samples per treatment at each session. Two sessions were held to complete the test. The samples were about 2 cm in size (∼50 g) that presented in a disposable plastic container. The panelists were requested to avoid food and smoking 2 h before meat tasting. Water and crackers were available to remove any residual flavor of the previous samples.

Statistical Analysis

Differences in the means of the different treatment groups were tested using analysis of variance in SPSS® software program version 21 (SPSS, Chicago, IL), while separation of the means was performed using Duncan's Multiple Range Test. Data were expressed as the mean ± standard error of the mean (SEM).

RESULTS AND DISCUSSION

Fattening Performance

All the experimental animals started the growth period that extended for 90 days with an initial live weight (ILW) of approximately 24.56 kg. The ILW did not differ significantly between the treatment animals. On the other hand, the final live weight (FLW) differed between the treatment groups where

Awassi breed attained the highest ($P < 0.05$) FLW followed by Najdi then Harri. Average daily intake (ADI), average daily gain (ADG) and feed conversion ratio (FCR) were significantly different between the sheep breeds. The Awassi sheep breed reported the highest ($P < 0.05$) ADI followed by Najdi > Harri, and the best ($P < 0.05$) ADG and FCR compared to the other two sheep breeds (**Table 1**). The superior FLW of Awassi sheep is attributed to the eminent ADG and FCR over Najdi and Harri breeds. The Harri breed showed a growth performance that located intermediate between the other two breeds.

Slaughter Weights and Carcass Characteristics

At the end of experimental period (90 days), the slaughter weight and carcass characteristics of three sheep breeds at there shown in **Table 2**. The slaughter body weight (SBW), EBW, and hot carcass weight (HCW) were significantly ($P < 0.05$) greater in Awassi and Najdi breeds than the Harri breed. The Najdi breed had a higher cold carcass weight (CCW) than the Harri sheep ($P < 0.05$). The dressing-out percentage (DP) based on SBW or EBW is one of the primary variables used to evaluate carcass characteristics, and it has considerable economic importance. In small ruminants, the DP based on SBW ranged from 36 to 60%, and it was affected by different factors (13). In this study, the SBW-based and EBW-based DP were in the range of 47.6–50.8 and 51.75–54.96, respectively. These results are similar to those previously reported (2, 3, 6, 14). The Harri and Najdi breeds had significantly ($P < 0.05$) higher DP (SBW) and DP (EBW) than Awassi sheep. No significant difference was detected in the gut fill of the different sheep breeds (**Table 3**). Therefore, the differences in DP can be attributed to the effect of the breed; besides effects of carcass weight, non-carcass components and internal body fat. Several studies have indicated that breed is one of the primary factors affecting DP (2, 3, 6–8, 14, 15). While Peña et al. (16) indicated that carcass weight had a significant influence on DP and other carcass quality traits.

There were no significant differences in chiller shrinkage (CS), rib-eye area, and body wall fat among the different sheep breeds. The Awassi and Harri breeds exhibited significantly ($P < 0.05$) thicker back fat than the Najdi breed. CS or evaporative weight losses have previously been reported to account for 2% of the HCW during the initial 24 h of chilling beef, pork, and lamb (17). Body fat cover is the primary variable linked with CS (18). In this study, the CS was higher than that reported by Greer and Jones (17). This could be due to low body wall fat in sheep breeds, which ranged from 3.53 to 4.35 mm. Generally, tropical sheep

TABLE 1 | Fattening performance of the three sheep breeds fed the experimental diet ($n = 15$/group).

Item	Breed			Limits		SEM
	Awassi	Harri	Najdi	Minimum	Maximum	
Initial live weight, kg	24.31	24.70	24.68	23.40	25.87	0.23
Final live weight, kg	50.52[a]	44.51[b]	48.54[a]	42.00	53.70	0.86
ADI kg/day	1.69[a]	1.41[b]	1.64[a]	1.35	1.87	16.12
ADG kg/day	0.31[a]	0.24[b]	0.28[a]	0.20	0.34	10.11
FCR	5.49[b]	6.91[a]	5.95[b]	5.16	6.81	0.20

ADI, Average daily intake; ADG, Average daily gain; FCR, Feed conversion ratio.
[a,b]Means within rows not sharing the same letter (s) differ significantly ($p < 0.05$).

TABLE 2 | Slaughter weight and Carcass characteristics of three sheep breeds ($n = 8$/group).

Component	Breed			Limits		SEM
	Awassi	Harri	Najdi	Minimum	Maximum	
SBW (kg)	50.53[a]	45.19[b]	49.54[a]	43.05	57.20	0.74
EBW (kg)	46.48[a]	41.70[b]	45.46[a]	39.50	51.50	0.64
HCW (kg)	24.04[a]	22.93[b]	24.69[a]	21.15	27.94	0.30
CCW (kg)	23.35[a,b]	22.39[b]	24.06[a]	20.67	27.10	0.29
DP (SBW)	47.60[b]	50.80[a]	49.50[a]	45.30	53.00	0.47
DP (EBW)	51.75[b]	54.96[a]	54.38[a]	49.40	57.40	0.51
CS%	2.90[a]	2.39[b]	2.53[a,b]	1.89	3.49	0.09
Rib-eye area (cm^2)	7.77	8.94	8.67	6.07	11.90	0.30
Back fat (mm)	2.58[a]	1.99[a]	1.29[b]	0.88	3.94	0.16
Body wall fat (mm)	3.99	3.53	4.35	2.01	6.40	0.22

[a,b]Means within rows with different superscripts are significantly different ($p < 0.05$).
SBW, slaughter body weight; EBW, empty body weight; DP (EBW), dressing percentage per empty body weight; DP (SBW), dressing percentage per full body weight; HCW, hot carcass weight; CCW, cold carcass weight; CS, chiller shrinkage.

TABLE 3 | Non-carcass components and fat content of the three sheep breeds ($n = 8$/group).

*Component%	Breed			Limits		SEM
	Awassi	Harri	Najdi	Minimum	Maximum	
Head	7.57	6.94	7.58	6.15	8.56	0.15
Heart	0.69	0.60	0.68	0.54	0.90	0.02
Lungs and trachea	2.30[a]	1.81[b]	2.18[a]	1.52	3.16	0.08
Liver	3.21	2.95	3.09	2.24	3.69	0.07
Spleen	0.29	0.27	0.29	0.20	0.38	0.01
Kidneys	0.51[a]	0.44[b]	0.48[a,b]	0.37	0.57	0.01
Tail	11.59	13.78	12.64	6.58	21.23	0.71
Stomach empty	7.97	7.05	7.18	5.59	8.90	0.22
Intestine empty	6.27[a]	4.43[c]	5.43[b]	3.53	7.84	0.21
Gut fill	16.85	15.16	16.48	10.90	21.80	0.66
Pericardial fat	0.45	0.49	0.48	0.32	0.56	0.02
Omental fat	3.06	3.42	2.90	1.41	5.13	0.20
Mesenteric fat	2.09	1.66	1.62	0.90	3.78	0.14
KKCF	2.37	3.06	1.86	0.19	6.61	0.14

*****Components were computed as a percentage of hot carcass weight.*

[a,b,c]Means within rows with different superscripts are significantly different ($p < 0.05$).

KKCF, kidney knob and channel fat.

breeds tend to deposit less subcutaneous fat than temperate sheep breeds (19).

Non-carcass Components and Fat Content

There were no significant differences between breeds for the head, heart, liver, spleen, tail, stomach (empty), and internal fat deposits (kidney knob and channel fat [KKCF], pericardial, omental, and mesenteric) (**Table 2**). The Awassi and Najdi breeds had heavier lungs and trachea than the Harri breed. The kidneys were heavier ($P < 0.05$) in the Awassi than Harri breed. The weight of the empty intestine varied significantly between sheep breeds: the Awassi breed had the heavier intestine, followed by the Najdi breed.

Meat Chemical Composition

The chemical compositions of the meat of the three sheep breeds are provided in **Table 4**. The moisture and protein contents of the meat ranged from 73.34 to 74.40% and 20.62 to 20.86%, respectively, with no significant differences between the three sheep breeds. The Awassi breed had the highest percentage of intramuscular fat (4.74%) followed by the Najdi breed (3.95%), and lastly, the Harri breed (3.84%). However, the difference was not significant. The ash content was significantly higher in the Harri breed (1.11%) than the Awassi and Najdi breeds, which had similar ash content (1.07%). In general, the chemical composition of meat is affected by numerous factors, including diet, carcass weight, and breed (10, 11, 13, 15, 17–27). The moisture content of the three sheep breeds was in the range reported by Abdullah and Qudsieh (28) for Awassi sheep. Our findings for protein content were in the range reported by Corazzin et al. (13) for sheep meat. In terms of the effect of sheep breed on protein content (29) did not find any effect of breed on meat protein. However, Rodrigues et al. (20) and Bjelanović et al. (30) found that breed has a significant effect on protein content. In the current study, the three sheep breeds had almost similar protein content, suggesting that breed has no effect on the protein content of sheep meat.

The intramuscular fat content of sheep meat commonly ranges between 1.5 and 9.5% (31), depending on many factors. However, meat with a moderate quantity of intramuscular fat is preferred by the consumer (32). In the current study, the three sheep breeds had intramuscular fat ranging between 3.84 and 4.74%, which is considered a moderate preferred quantity of intramuscular fat (33). This result is inconsistent with the findings of (21, 34), who reported a higher intramuscular fat of Najdi than Awassi.

Meat Quality Characteristics

Table 4 shows the meat quality characteristics of the three sheep breeds. The pHu values of the three sheep breeds ranged from 5.80 to 5.89. Generally, the pHu of the sheep meat declines from seven upon slaughter to reach approximately 5.3–5.8 at 24 h (35). In this study, there were significant differences between the breeds. The Najdi breed had a higher pHu than the Awassi (5.82) and Harri (5.80) breeds. Variation in pHu in different breeds was also reported by El Hassan et al. (22) and Hopkins and Fogarty (36), and this may be attributed to differences in glycogen levels in muscles and pre-slaughter stress (37).

The CL for the three sheep breeds ranged from 28.9 to 34.5%. Generally, the sheep meat had CL values ranging from 14 to 41% (13). The meat from Najdi sheep had a significantly lower CL (28.9%) than that of Harri (33.47%) and Awassi (34.54%) sheep. The effect of breed on the CL of sheep meat has also been reported by Mateo et al. (23) and Kuchtík et al. (29) and is probably because of the different pHu. In a living animal the muscle pH is approximately 7.2. After animal death, glycogen is broken down to lactic acid when muscle turns into meat. The ultimate pHu of meat, at 24 h post-mortem, can range from 5.2 to 5.8. Both the rate and extent of post-mortem pH fall will

TABLE 4 | Meat chemical composition of the three sheep breeds ($n = 8$/group).

Composition %	Breed			Limits		SEM
	Awassi	Harri	Najdi	Minimum	Maximum	
Moisture	73.34	74.40	74.37	70.73	75.85	0.28
Protein	20.86	20.64	20.62	19.48	21.97	0.12
Fat	4.74	3.84	3.95	1.28	8.29	0.35
Ash	1.07^{b}	1.11^{a}	1.07^{b}	1.00	1.16	0.01

^{a,b}*Means within rows with different superscripts are significantly different ($p < 0.05$).*

influence meat quality characteristics. A low ultimate pHu results in meat proteins having decreased water-holding capacity, while a higher ultimate pHu will give less cooking loss. In this study, the Najdi breed had the highest pHu and the lowest CL percentage. The WHC and drip loss of the three sheep breeds were in the range of 1.23–1.41 and 4.33–3.73, respectively, with no significant differences between breeds.

The color of meat is the most important quality attribute. The decision to purchase meat is affected more by the appearance of the meat than any other aspect of quality (4). There were no significant differences in the ultimate color characteristics of lightness (L*), redness (a*), and yellowness (b*) among the three sheep breeds. The values of a* were in the range of 16.22 to 16.62, and the values of b* were in the range of 4.91–5.76. These values were higher than those reported in the Omani sheep breed by Burke et al. (24) and Al-Khalasi and Mahgoub (38) and lower than the reported by Esenbuga et al. (39). The variation may be due to age and/or diet differences. The values of L* and a* color components reported in this study are looked acceptable as consumers consider fresh sheep meat with a* and L* values equal to or exceeding 9.5 and 34, respectively, as acceptable (40). Consumers consider fresh sheep meat with a* and L* values equal to or exceeding 9.5 and 34, respectively, as acceptable (40). The sheep breeds under investigation did not show any significant differences between them regarding chroma, b*/a* ratio or hue angle. Awassi breed revealed the highest values of these components comparing to the other two breeds followed by Harri then Najdi. Once again, Harri located in-between the two breeds with an average color components' value. This may be attributed to the common ancestry of the three breeds. In a study (41) reported that Harri and Najdi breeds were categorized within the same gene pool based on a structure analysis. Moreover, a second study that evaluated the genetic diversity of these three breeds using microsatellite markers, concluded there was low population differentiation among the three sheep populations (42).

Tenderness is the most important eating quality characteristic, and it determines consumer acceptability (43). Meat tenderness depends on many intrinsic and extrinsic factors. Many studies have reported a positive correlation between meat tenderness and MFI (15, 17, 18, 44) and sarcomere length (45). Therefore, MFI and SL were investigated. As shown in **Table 5**, the different sheep breeds exhibited different MFI values, which ranged from 110.87 to 77.56. Awassi and Harri sheep had significantly higher MFI than Najdi sheep. The SL ranged from 1.63 to 1.85 μm with significant differences between the sheep breeds. The Awassi breed had the longest SL, and the Najdi breed had the shortest, while the Harri breed fell in between them. Sarcomere is the smallest contractile unit of a muscle fiber and serves as the basic force-producing machinery of striated muscles. The sarcomere length (SL) have only indirect effects on meat quality while an animal is living, but soon postmortem there will be pertinent impacts (46). The postmortal sarcomere length has marked effects on textural properties of raw and cooked meat, and on water-holding especially in raw meat as well as indirect effects on color and taste. This could explain the intermediate position of Harri breed between Awassi and Najdi breeds with respect to most investigated carcass and meat quality parameters in this study. The SL values observed in this study are similar to those reported by Gaili (19) and Devine et al. (47).

The SF, which was defined as the maximum load needed to cut the meat perpendicular to fibers, is inversely associated with tenderness. Red meat is classified as tender until a SF of 34.72 N/cm^2, intermediate from 40.01 to 52.96 N/cm^2, and tough if the SF exceeds 57.86 N/cm^2 (48, 49). In this study, the three sheep breeds had SF mean values ranging from 28.34 to 32.17 N/cm^2. According to the above classification, the meat of three breeds is considered as tender meat. The Awassi breed had a particular quality with the highest MFI and SL values and lowest SF value. The three sheep breeds differed significantly ($P < 0.05$) in hardness and chewiness, but not in springiness and cohesiveness. Again, the Awassi breed showed the lowest value of hardness and chewiness followed by the Harri breed. The three sheep breeds differed significantly ($P < 0.05$) in hardness and chewiness, but not in springiness and cohesiveness. Again, the Awassi breed showed the lowest value of hardness and chewiness followed by the Harri breed. Nevertheless, it reported the highest ($P > 0.05$) shear force indicating less tender meat compared to the other two breeds. Hardness is the force needed to achieve a given deformation. It represents the hardness of the sample at first bite. While shear force is the force necessary to shear a piece of meat (50). Once again, Harri breed located intermediate between Awassi and Najdi breeds when texture profile parameters were considered.

Sensory Evaluation

Sensory evaluation scores of the three sheep breeds are provided in **Table 6**. The sheep breeds only differed significantly ($P < 0.05$) in flavor intensity, and the Najdi breed gained the highest score followed by the Awassi breed.

TABLE 5 | Meat quality characteristics, myofibril fragmentation index (MFI) and texture profile analysis (TPA) of the three sheep breeds ($n = 8$/group).

Characteristic	Breed			Limits		SEM
	Awassi	Harri	Najdi	Minimum	Maximum	
pH_u	5.82[b]	5.80[b]	5.89[a]	5.60	5.90	0.02
Cooking loss%	34.54[a]	33.47[a]	28.96[b]	22.12	41.81	0.86
WHC	1.23	1.38	1.41	0.23	1.53	0.05
Drip loss%	4.33	3.73	3.88	2.60	6.60	0.23
Ultimate color values						
L*	34.63	33.50	35.39	31.05	40.75	0.54
a*	16.62	16.49	16.22	14.24	18.98	1.40
b*	5.76	5.17	4.91	3.92	7.29	0.18
Chroma (C*)	17.60	17.29	16.97	14.87	20.08	0.30
b*/a* Ratio	0.35	0.31	0.30	0.22	0.40	0.01
Hue Angle (H°)	19.14	17.42	16.79	12.63	22.03	0.50
MFI	110.87[a]	104.0[a]	77.56[b]	45.70	153.55	6.27
SL (μm)	1.85[b]	1.79[a]	1.63[b]	1.26	2.10	0.04
***TPA**						
Shear force (N/cm^2)	32.17	29.03	28.34	18.54	38.93	0.13
Hardness (N/cm^2)	3.83[b]	6.47[a]	6.67[a]	3.04	13.04	0.06
Springiness	0.58	0.60	0.61	0.49	0.70	0.01
Cohesiveness	0.53	0.50	0.53	0.41	0.59	0.01
Chewiness	0.13[b]	0.21[a,b]	0.23[a]	0.13	0.43	0.02

[a,b]Means within rows with different superscripts are significantly different ($p < 0.05$).
**TPA, texture profile analysis.*

TABLE 6 | Sensory evaluation of the meat of three sheep breeds ($n = 8$/group).

Attribute*	Breed			Limits		SEM
	Awassi	Harri	Najdi	Minimum	Maximum	
Juiciness	5.23	4.88	5.36	4.00	6.40	0.13
Tenderness	5.58	5.46	5.85	4.50	6.80	0.13
Flavor intensity	5.53[a,b]	5.19[b]	5.89[a]	4.60	6.90	0.11

[a,b]Means within rows with different superscripts are significantly different ($p < 0.05$).
**Sensory evaluation was performed using an eight-point hedonic scale (1 = the least; 8 = the best).*

CONCLUSIONS

This study revealed that there were prominent differences between the sheep breeds under investigation. Awassi, Harri and Najdi sheep showed noticeable variations regarding carcass characteristics, meat composition and quality. Awassi breed reflected better meat quality attributes than the other two breeds, nevertheless, Harri appeared to have the best dressing yield. In addition, Harri has the less non-carcass components besides an intermediate body fat content that suits today's healthy eating behavior. It is a fact that Awassi breed has a good reputation among Saud citizens and being the favorable source of meat for a long time, but it is the time for Harri breed to gain his place. In conclusion, we recommend a future breeding program ending in a new cross-sheep breed that have the best of Awassi and Harri.

DATA AVAILABILITY STATEMENT

The raw data supporting the conclusions of this article will be made available by the authors, without undue reservation.

ETHICS STATEMENT

The animal study was reviewed and approved by the King Saud University Ethical Committee (Ethics Reference No: KSU-SE-20-17).

AUTHOR CONTRIBUTIONS

GS and AE-W: conceptualization. AA-O and GS: methodology. EH and KA: software. AS and EH: investigation. KA and AE-W: data curation. GS and AS: writing—original draft preparation,

review and editing. AA-O: visualization. All authors have read and agreed to the published version of the manuscript.

FUNDING

This research was funded by the Deputyship for Research & Innovation, Ministry of Education in Saudi Arabia through the project number IFKSUHI-43.

ACKNOWLEDGMENTS

The authors extend their appreciation to the Deputyship for Research & Innovation, Ministry of Education in Saudi Arabia for funding this research work through the project number IFKSUHI-43. Thanks are also extended to the Deanship of Scientific Research and RSSU at King Saud University for their technical support.

REFERENCES

1. GASTAT. Agriculture, water and environment. In: *General Authorityi for Statistics*. Statistical Yearbook of 2018. (2018). Available online at: https://www.stats.gov.sa/en/1011 (accessed March 3, 2021).
2. Business Monitor International – Industry Reports. *Saudi Arabia Food and Drink Report Aug 27, 2016*. New York, NY: Alacra Store (2016). Retrieved from: http://www.alacrastore.com/storecontent/Business-Monitor-International-Industry-Reports/Saudi-Arabia-Food-and-Drink-Report-2026-454 (accessed March 03, 2021).
3. NRC. *Nutrient Requirements of Small Ruminants: Sheep, Goats, Cervids, and New World Camelids;* Washington, DC: The National Academies Press (2007). p. 384. doi: 10.17226/11654
4. Mancini RA, Hunt MC. Current research in meat color. *Meat Sci*. (2005) 71:100–21. doi: 10.1016/j.meatsci.2005.03.003
5. Olfaz M, Ocak N, Erener G, Cam MA, Garipoglu AV. Growth, carcass and meat characteristics of Karayaka growing rams fed sugar beet pulp, partially substituting for grass hay as forage. *Meat Sci*. (2005) 70:7–14. doi: 10.1016/j.meatsci.2004.11.015
6. Al-Owaimer AN, Suliman GM, Sami AS, Picard B, Hocquette JF. Chemical composition and structural characteristics of Arabian camel (*Camelus dromedarius*) m. longissimus thoracis. *Meat Sci*. (2014) 96:1233–41. doi: 10.1016/j.meatsci.2013.10.025
7. Wilhelm AE, Maganhini MB, Hernández-Blazquez FJ, Ida EI, Shimokomaki M. Protease activity and the ultrastructure of broiler chicken PSE (pale, soft, exudative) meat. *Food Chem*. (2010) 119:1201–4. doi: 10.1016/j.foodchem.2009.08.034
8. Culler RD, Parrish FC Jr, Smith GC, Cross HR. Relationship of myofibril fragmentation index to certain chemical, physical and sensory characteristics of bovine longissimus muscle. *J Food Sci*. (1978) 43:1177–80. doi: 10.1111/j.1365-2621.1978.tb15263.x
9. Cross HR, West RL, Dutson TR. Comparison of Methods for measuring sarcomere length in beef semitendinosus Muscle. *Meat Sci*. (1981) 5:261–6. doi: 10.1016/0309-1740(81)90016-4
10. Wheeler TL, Shackelford SD, Koohmaraie M. Sampling, cooking, and coring effects on Warner–Bratzler shear force values in beef. *J Anim Sci*. (1996) 74:1553–62. doi: 10.2527/1996.7471553x
11. Suliman GM, Babiker SA, Eichinger HM. Effect of Hibiscus seed-based diet on chemical composition, carcass characteristics and meat quality traits of cattle. *Indian J Anim Res*. (2017) 51:694–9. doi: 10.18805/ijar.11458
12. Suliman GM, Alowaimer AN, Hussein EOS, Ali HS, Abdelnour SA, Abd El-Hack ME, et al. Chemical composition and quality characteristics of meat in three one-humped camel (camelus dromedarius) breeds as affected by muscle type and post-mortem storage period. *Animals*. (2019) 9:834. doi: 10.3390/ani9100834
13. Corazzin M, Del Bianco S, Bovolenta S, Piasentier E. Carcass characteristics and meat quality of sheep and goat. In: Lorenzo JM, Munekataa P, Barba FJ, Toldrá F, editors. *More than Beef, Pork and Chicken–The Production, Processing, and Quality Traits of Other Sources of Meat for Human Diet*. Cham: Springer (2019). p. 119–65. doi: 10.1007/978-3-030-05484-7_6
14. AOAC. Official methods of analysis. In: Herlick K, et al., editors. *Association of Official Analytical Chemists*. 15th ed. Arlington, VA (2007).
15. Ayele S, Urge M, Animut G, Yusuf MJ. Comparative slaughter performance and carcass quality of three Ethiopian fat-tailed hair sheep breeds supplemented with two levels of concentrate. *Trop Anim Health Prod*. (2019) 51:187–98. doi: 10.1007/s11250-018-1675-7
16. Peña F, Cano T, Domenech V, Alcalde Ma J, Martos J, García- Martinez A, et al. Influence of sex, slaughter weight and carcass weight on "non-carcass" and carcass quality in segureña lambs. *Small Ruminant Res*. (2005) 60:247–54 doi: 10.1016/j.smallrumres.2004.12.011
17. Greer GG, Jones SD. Quality and bacteriological consequences of beef carcass spray-chilling: effects of spray duration and boxed beef storage temperature. *Meat Sci*. (1997) 45:61–73. doi: 10.1016/S0309-1740(96)00073-3
18. Smith GC, Carpenter ZL. Postmortem shrinkage of lamb carcasses. *J Anim Sci*. (1973) 36:862–7. doi: 10.2527/jas1973.365862x
19. Gaili ESE. Effect of breed-type on carcass weight and composition in sheep. *Trop Anim Health Prod*. (1979) 11:191–8. doi: 10.1007/BF02237800
20. Rodrigues S, Cadavez V, Teixeira AJ. Breed and maturity effects on Churra Galega Bragancana and Suffolk lamb carcass characteristics: killing-out proportion and composition. *Meat Sci*. (2006) 72:288–93. doi: 10.1016/j.meatsci.2005.07.019
21. Gardner GE, Williams A, Ball, AJ, Jacob RH, Refshauge G, Hocking Edwards J, et al. Carcase weight and dressing percentage are increased using Australian Sheep Breeding Values for increased weight and muscling and reduced fat depth. *Meat Sci*. (2015) 99:89–98. doi: 10.1016/j.meatsci.2014.07.031
22. El Hassan G, Abuelfatah K, Babiker S, Alsiddig M. Feedlot performance and carcass characteristics of some Sudan desert sheep ecotypes and their crosses. *Int J Agric Sci Vet Med*. (2017) 5:25–32.
23. Mateo J, Caro I, Carballo DE, Gutiérrez-Méndez N, Arranz JJ, Gutiérrez-Gil BJ. Carcass and meat quality characteristics of Churra and Assaf suckling lambs. *Anim Int J Ani Biosci*. (2018) 12:1093–101. doi: 10.1017/S1751731117002270
24. Burke JM, Apple JK, Roberts WJ, Boger CB, Kegley EB. Effect of breed-type on performance and carcass traits of intensively managed hair sheep. *Meat Sci*. (2003) 63:309–15. doi: 10.1016/S0309-1740(02)00087-6
25. Pérez P, Maino M, Tomic G, Mardones E, Pokniak JJ. Carcass characteristics and meat quality of Suffolk Down suckling lambs. *Small Ruminant Res*. (2002) 44:233–40. doi: 10.1016/S0921-4488(02)00076-7
26. Ponnampalam E, Butler K, Hopkins D, Kerr M, Dunshea F, Warner R. J. Genotype and age effects on sheep meat production. 5. Lean meat and fat content in the carcasses of Australian sheep genotypes. *Aust J Exp Agric*. (2008) 48:893–7. doi: 10.1071/EA08054
27. Karaca S, Yilmaz A, Kor A, Bingöl M, Cavidoglu I, Ser GJ. The effect of feeding system on slaughter-carcass characteristics, meat quality, and fatty acid composition of lambs. *Arch Anim Breed*. (2016) 59:121–9. doi: 10.5194/aab-59-121-2016
28. Abdullah AY, Qudsieh RIJ. Effect of slaughter weight and aging time on the quality of meat from Awassi ram lambs. *Meat Sci*. (2009) 82:309–16. doi: 10.1016/j.meatsci.2009.01.027
29. Kuchtík J, Zapletal D, Šustová KJ. Chemical and physical characteristics of lamb meat related to crossbreeding of Romanov ewes with Suffolk and Charollais sires. *Meat Sci*. (2012) 90:426–30. doi: 10.1016/j.meatsci.2011.08.012
30. Bjelanović M, Grabež V, Vučić G, Martinović A, Lima LR, Marković B, et al. Effects of different production systems on carcass and meat quality of sheep and lamb from western Balkan and Norway. *Biotechnol Anim Husbandry*. (2015) 31:203–21. doi: 10.2298/BAH1502203B
31. Pannier L, Pethick DW, Geesink GH, Ball AJ, Jacob RH, Gardner GE. Intramuscular fat in the longissimus muscle is reduced in lambs from sires selected for leanness. *Meat Sci*. (2014) 96(2 Pt B):1068–75. doi: 10.1016/j.meatsci.2013.06.014

32. Joo ST, Kim GD, Hwang YH, Ryu YC. Control of fresh meat quality through manipulation of muscle fiber characteristics. *Meat Sci*. (2013) 95:828–36. doi: 10.1016/j.meatsci.2013.04.044
33. Miller RK. Factors affecting the quality of raw meat. In: Jerry K, edior. *Meat Processing, Improving Quality (Woodhead Publishing Series in Food Science, Technology and Nutrition)*. (2002). p. 27–63 doi: 10.1533/9781855736665.1.27
34. Al-Suwaiegh SB. Comparative study of carcasses characteristics and fatty acid composition of intramuscular and subcutaneous fat of Awassi and Najdi sheep. *Asian J Anim Vet Adv*. (2015) 10:119–31. doi: 10.3923/ajava.2015.119.131
35. Savell JW, Mueller SL, Baird BE. The chilling of carcasses. *Meat Sci*. (2005) 70:449–59. doi: 10.1016/j.meatsci.2004.06.027
36. Hopkins D, Fogarty NJ. Diverse lamb genotypes-−2. Meat pH, colour and tenderness. *Meat Sci*. (1998) 49:477–88. doi: 10.1016/S0309-1740(98)00051-5
37. Stewart SM, McGilchrist P, Gardner GE, Pethick DW. Association between loin ultimate pH and plasma indicators of pre-slaughter stressors in Australian lamb. *Meat Muscle Biol*. (2018) 2:254–64. doi: 10.22175/mmb2017.10.0050
38. Al-Khalasi S, Mahgoub O. Carcass and meat quality characteristics of omani sheep fed diets based on raw or processed mesquite (Prosopis Juliflora) pods. *J Vet Sci Ani Husb*. (2018) 6:206. doi: 10.15744/2348-9790.6.301
39. Esenbuga N, Macit M, Karaoglu M, Ksakal V, Aksu MI, Yoruk MA, et al. Effect of breed on fattening performance, slaughter and meat quality characteristics of Awassi and Morkaraman lambs. *Livestock Sci*. (2009) 123:255–60. doi: 10.1016/j.livsci.2008.11.014
40. Khliji S, Van de Ven R, Lamb TA, Lanza M, Hopkins DL. Relationship between consumer ranking of lamb colour and objective measures of colour. *Meat Sci*. (2010) 85:224–9. doi: 10.1016/j.meatsci.2010.01.002
41. Al-Atiyat RM, Aljumaah RS, Alshaikh MA, Abudabos AM. Microsatellite-based genetic structure and diversity of local Arabian sheep breeds. *Front Genet*. (2018) 9:408. doi: 10.3389/fgene.2018.00408
42. Mahmoud AH., Abou-Tarboush FM., Rady A, Al-Anazi KM, Abul Farah M, Mohammed OB. Genetic variability of sheep populations of Saudi Arabia using microsatellite markers. *Indian J Anim Res*. (2018) 54:409–12. doi: 10.18805/ijar.B-775
43. Miller MF, Carr MA, Ramsey CB, Crockett KL, Hoover LC. Consumer thresholds for establishing the value of beef tenderness. *J Anim Sci*. (2001) 79:3062–8. doi: 10.2527/2001.79123062x
44. Vestergaard M, Therkildsen M, Henckel P, Jensen LR, Andersen HR, Sejrsen K. Influence of feeding intensity, grazing and finishing feeding on meat and eating quality of young bulls and the relationship between muscle fibre characteristics, fibre fragmentation and meat tenderness. *Meat Sci*. (2000) 54:187–95. doi: 10.1016/S0309-1740(99)00098-4
45. Veiseth E, Shackelford SD, Wheeler TL, Koohmaraie M. Factors regulating lamb longissimus tenderness are affected by age at slaughter. *Meat Sci*. (2004) 68:635–40. doi: 10.1016/j.meatsci.2004.05.015
46. Ertbjerg P, Puolanne E. Muscle structure, sarcomere length and influences on meat quality: a review. *Meat Sci*. (2017) 132:139–52. doi: 10.1016/j.meatsci.2017.04.261
47. Devine CE, Payne SR, Peachey BM, Lowe TE, Ingram JR, Cook CJ. High and low rigor temperature effects on sheep meat tenderness and ageing. *Meat Sci*. (2002) 60:141–6. doi: 10.1016/S0309-1740(01)00115-2
48. Boleman SJ, Boleman SL, Miller RK, Taylor JF, Cross HR, Wheeler TL, et al. Consumer evaluation of beef of known categories of tenderness. *J Anim Sci*. (1997) 75:1521–4. doi: 10.2527/1997.7561521x
49. Hopkins DL, Hegarty RS, Walker PJ, Pethick DW. Relationship between animal age, intramuscular fat, cooking loss, pH, shear force and eating quality of aged meat from sheep. *Aust J Exp Agric*. (2006) 46:879–84. doi: 10.1071/EA05311
50. de Huidobro FR, Miguel E, Bla'zquez B, Onega E. A comparison between two methods (Warner–Bratzler andtexture profile analysis) for testing either raw meat or cooked meat. *Meat Sci*. (2005) 69:527–36. doi: 10.1016/j.meatsci.2004.09.008

Conflict of Interest: The authors declare that the research was conducted in the absence of any commercial or financial relationships that could be construed as a potential conflict of interest.

frontiers in Genetics

ORIGINAL RESEARCH
published: 21 May 2021
doi: 10.3389/fgene.2021.648256

Goat *AKAP12*: Indel Mutation Detection, Association Analysis With Litter Size and Alternative Splicing Variant Expression

Zihong Kang[1,2], Yangyang Bai[2], Xianyong Lan[2] and Haiyu Zhao[1]**

[1] School of Life Sciences, Lanzhou University, Lanzhou, China, [2] College of Animal Science and Technology, Key Laboratory of Animal Genetics, Breeding and Reproduction of Shaanxi Province, Northwest A&F University, Yangling, China

OPEN ACCESS

Edited by:
Shaobin Li,
Gansu Agricultural University, China

Reviewed by:
Wenlin Bai,
Shenyang Agricultural University, China
Ran Di,
Institute of Animal Sciences, Chinese Academy of Agricultural Sciences, China

***Correspondence:**
Xianyong Lan
lanxianyong79@nwsuaf.edu.cn
Haiyu Zhao
haiyuzhao1988@126.com

Specialty section:
This article was submitted to Livestock Genomics, a section of the journal Frontiers in Genetics

Received: *19 January 2021*
Accepted: *29 April 2021*
Published: *21 May 2021*

Citation:
Kang Z, Bai Y, Lan X and Zhao H (2021) Goat AKAP12: Indel Mutation Detection, Association Analysis With Litter Size and Alternative Splicing Variant Expression. Front. Genet. 12:648256. doi: 10.3389/fgene.2021.648256

A-kinase anchoring protein 12 (*AKAP12*) plays key roles in male germ cells and female ovarian granulosa cells, whereas its influence on livestock litter size remains unclear. Herein we detected the genetic variants of *AKAP12* gene and their effects on litter size as well as alternative splicing variants expression in Shaanbei white cashmere (SBWC) goats, aiming at exploring theoretical basis for goat molecular breeding. We identified two Insertion/deletions (Indels) (7- and 13-bp) within the *AKAP12* gene. Statistical analyses demonstrated that the 13-bp indel mutation in the 3′ UTR was significantly associated with litter size (n = 1,019), and the carriers with DD genotypes presented lower litter sizes compared with other carriers ($P < 0.01$). Bioinformatics analysis predicted that this 13-bp deletion sequence could bind to the seed region of miR-181, which has been documented to suppress porcine reproductive and respiratory syndrome virus (PRRSV) infection by targeting PRRSV receptor CD163 and affect the pig litter size. Therefore, luciferase assay for this 13-bp indel binding with miRNA-181 was performed, and the luciferase activity of pcDNA-miR-181-13bp-Deletion-allele vector was significantly lower than that of the pcDNA-miR-181-13bp-Insertion-allele vector ($P < 0.05$), suggesting the reduced binding capability with miR-181 in DD genotype. Given that alternative spliced variants and their expression considerably account for the Indel genetic effects on phenotypic traits, we therefore detected the expression of the alternative spliced variants in different tissues and identified that *AKAP12-AS2* exhibited the highest expression levels in testis tissues. Interestingly, the *AKAP12-AS2* expression levels of homozygote DD carriers were significantly lower than that of individuals with heterozygote ID, in both testis and ovarian tissues ($P < 0.05$), which is consistent with the effect of the 13-bp deletion on the reduced litter size. Taken together, our results here suggest that this 13-bp indel mutation within goat *AKAP12* might be utilized as a novel molecular marker for improving litter size in goat breeding.

Keywords: goat, *AKAP12* gene, insertion/deletion, litter size, mRNA expression, alternative splicing

INTRODUCTION

High prolificacy in goat breeding brings huge economic values. The lambing of goats as an important reproductive trait, is directly related with the economic benefits of the goat industry, therefore the breeding of goat variety with high fecundity is essential and necessary (Wang et al., 2020a, 2021; Zhang et al., 2020). Shaanbei white cashmere goat (SBWC) is an excellent domestic goat variety with fine cashmere and meat quality. However, its potential reproductive capacity has not been fully developed and the litter size traits urgently need to be improved. Compared with the traditional Cross-breeding, molecular marker-assisted selection (MAS) has higher efficiency and accuracy (Collard and Mackill, 2008; Mills et al., 2011). By using molecular markers like Insertion/Deletion (InDel), breeders can improve the reproductive ability of goats while retaining other excellent traits, which is of great significance to the rapid development of goat industry (Li et al., 2019; Ren et al., 2019).

A-Kinase Anchoring Protein 12 (*AKAP12*) is a structurally diverse protein that shares common features to bind the protein kinase A regulatory subunit (Qasim and McConnell, 2020; Seo et al., 2021). Previous studies have suggested that *AKAP12* plays a potential role in male germ cells and ovarian granulosa cells in mammals (Erlichman et al., 1999; Binder et al., 2013). In addition, it was reported that follicle-stimulating hormone (FSH) could downregulate the expression of AKAPs in granulosa cells (Escamilla-Hernandez et al., 2008). The increased expression of *AKAP12* in the downstream FSH signaling pathway of estrogen receptor β (ERβ)-null granulosa cells suggested that FSH could only downregulate *AKAP12* under the action of ERβ, and the increased expression of *AKAP12* might lead to the isolation of PKA regulatory units, as well as an observed decrease in cAMP accumulation (Deroo et al., 2009). Together, these studies strongly suggest that *AKAP12* plays a key role in the regulation of fecundity in mammals.

Alternative splicing (AS) events can lead to multiple splicing variants of a gene and production of proteins with diverse functions therefore are necessary and fundamental in analyzing organism complexity, evolutionary pathways, and metabolic activities (Ule and Blencowe, 2019; Aísa-Marín et al., 2021). Generally, alternative splicing affects gene transcription and translation through splicing proteins and their regulatory factors, thus affecting gene functions. At present, two splicing variants of *AKAP12* gene have been documented in goats, designated as *AKAP12-AS1* and *AKAP12-AS2*. However, to date, DNA polymorphisms as well as gene expression profiles of the splicing variants of goat *AKAP12* have rarely been studied. Therefore, in this study, we investigated the genetic variants, alternative splicing and expression profiles of goat *AKAP12*, as well as their potential effects on the first-born litter size, in order to promote the application of marker-assisted selection (MAS) in goat breeding.

Abbreviations: bp, base pairs; *AKAP12*, A-kinase anchoring protein 12; indel, insertion/deletion; II, insertion/insertion; ID, insertion/deletion; DD, deletion/deletion; MAS, marker-assisted selection; SNPs, single nucleotide polymorphisms; SVs, structural variants; PCR, polymerase chain reaction; PKA, protein kinase A; PKC, protein kinase C; FSH, follicle-stimulating hormone; Ho, homozygosity; He, heterozygosity; PIC, polymorphism information content; HWE, Hardy-Weinberg equilibrium; AS, alternative splicing; qPCR, quantitative polymerase chain reaction.

MATERIALS AND METHODS

Sample and Data Collection

All experiments in this study involving animals were approved by the Faculty Animal Policy and Welfare Committee of Northwest A&F University (Ethic approval file No. NWAFAC1008). Moreover, the care and use of experimental animals completely conformed with local animal welfare laws, guidelines, and policies. We randomly collected the ear tissues of 1,019 Shaanbei white cashmere (SBWC) female goats from a local farm in Yulin, Shaanxi Province. These goats were all 2–3 years old, raised and managed under the same conditions (Cui et al., 2018; Kang et al., 2019). After weaning, all ewes were housed with a constant temperature and good ventilation, and litter sizes were recorded by the breeder. They were raised a nutritionally adequate diet and the ewes were free of disease. Goats included in the present study were randomly selected to ensure that the individuals had no genetic relationship, as much as possible (Chen et al., 2019a). The mean of litter size of SBWC goats was 1.46. In this study, we also collected the muscle, testis, brain, liver, and heart samples from six male goats, which were all healthy and at the same age. All goats used in this study were raised and managed under the same conditions after birth (Wang et al., 2020b). All tissue samples collected were fast frozen in liquid nitrogen and stored at −80°C after being brought back to the laboratory (Hui et al., 2020).

Genomic DNA Extraction

Genomic DNA of goat ear tissue was extracted using the salting-out method. The concentration and quality of genomic DNA were detected using a Thermo NanoDrop 2000 (Thermo Fisher Scientific). The integrity of DNA and the presence of RNA and protein contamination were detected by 1% agarose gel electrophoresis (Lan et al., 2007; Hui et al., 2020; Wang et al., 2020b). Each DNA sample was diluted to 50 ng/μL and a total of 96 samples were randomly selected to construct DNA pools. Touchdown PCR was used for identification of genetic variations as well as individual genotyping (Chen et al., 2019b).

RNA Extraction and Quantitative RT-PCR

The total RNA from the tissue samples was extracted by using the Trizol (TaKaRa Biotech Co. Ltd., Dalian, China) method, which mainly includes steps like sample cracking, extraction, precipitation, and dissolution. The same amount of RNA of each sample was reverse transcribed according to the instructions of the reverse transcription kit (TaKaRa Biotech Co. Ltd.). Primers for quantitative RT-PCR analysis are shown in **Table 1**, and the mRNA expression was detected using the CFX96 Real-Time PCR Detection System (Bio-Rad, United States) as described previously (Jia et al., 2015). The fluorescence signal was detected at the end of each cycle, and three replicates were set for each sample.

TABLE 1 | Primers for PCR amplifications.

Primer names	Sequences (5′–3′)	Fragment (bp)	Function	Location
9-bp	F: GGGTCACTGCTTTACATCCGTT	122/122	Indel detection	3′ UTR/3′ UTR
	R: ATGGTGGCATTGTTTCAGTACCT			
7-bp	F: TGTTTAATGGCGGTAGA	149/156	Indel detection	Intron 3/Promoter
	R: GAGGGTTTCAGAGTTGC			
13-bp	F: CACTCATCCTACTGGCAT	179/192	Indel detection	3′ UTR/3′ UTR
	R: TGTTAATAGCGTTCCTCC			
qPCR-AS1	F: AGAAGCCTTGCCTCAGGAGTTTG	156	qPCR	Exon 1–2
	R: CGCCTTCTCCAAATCGCAGG			
qPCR-AS2	F: TCCTCACGATCACAGTTGGAC	110	qPCR	Exon 1–2
	R: TCCCTCCTTCGTGATGTCCT			
GAPDH	F: AAAGTGGACATCGTTGCCAT	116	Internal control	Exon 3–4
	R: CCGTTCTCTGCCTTGACTGT			
pcDNA3.1-miR-181	F: GG**GGTACC**CCTCCAGATCCTCGCAGAT	337	Overexpression	
	R: CC**CTCGAG**GATCACGCTCGCACAATGC			
psi-CHECK2	F: CCG**CTCGAG**CACTCATCCTACTGGCAT	179/192	Targeting detection	3′ UTR
	R: AAGGAAAAAA**GCGGCCGC**TGTTAATAGCGT TCCTCC			

The bold font refers to the sequence of the restriction enzyme cutting site, the underlined font refers to the protective bases.

Plasmid Construction

We used RNAhybrid[1] to predict the potential miRNA binding sites of the goat *AKAP12* 13-bp region. The 179/192-bp DNA sequence containing the 13-bp region was cloned into psiCHECK-2 using T4 DNA Ligase and the insert was released by *Xho*I and *Not*I digestion (TaKaRa Biotech Co., Ltd.). The miR-181 sequence was cloned into the pcDNA3.1 vector (Invitrogen) as described previously (Kang et al., 2020; Hao et al., 2021), and the insert was released by *Kpn*I and *Xho*I digestion.

Cell Culture and Luciferase Reporter Assays

Human embryonic kidney 293T (HEK293T) cells were seeded in a 60-mm cell culture dish, and 4 mL of the growth medium was added. The details of the cell culture condition have been described previously (Chen et al., 2018). Before transfection, trypsin was used to digest the cells from the culture dish, and after centrifugation, 3×10^4 cells were seeded into 96-well plates and cultured overnight. After transfection for 24 h, the medium was discarded, 50 μL of 1 × PLB was added to each well, and the cells were shaken at room temperature for 30 min until full lysed. Cell lysates (5 μL) were added to the 96-well ELISA plate, and luciferase activity was measured using 20 μL of LARII and Stop&Go (Promega, Heidelberg, Germany). The data were processed and calculated as: luciferase activity = Renilla luciferase/firefly luciferase.

Statistical Analyses

Allele, genotype frequencies, and linkage disequilibrium (LD) analyses were conducted using the SHEsis software[2]. Genetic parameters were calculated using the Nei's methods (**Table 2**; Nei and Roychoudhury, 1974). According to the correlation coefficients (D'/r^2), the pattern of pairwise LD between the indel loci was estimated and visualized. The case of $D' = 1$ or $r^2 = 1$ is known as complete LD. Values of $D' < 1$; $r^2 > 0.33$ indicate strong LD. A least-squares mean (LSM) test was used to determine the litter size of goats with different indel genotypes according to the formula $Y_{ij} = \mu + HYS_i + G_j + e_{ij}$, where Y_{ij} is the phenotypic value of litter size, μ is the overall population mean, HYS_i is the fixed effect of the herd-year-season, G_j is the fixed effect of genotype, and e_{ij} is the random error (Cui et al., 2018).

For gene expression analysis, on the premise of ensuring amplification efficiency, *GAPDH* was used as the internal reference gene to correct the mRNA expression level, and $2^{-\Delta\Delta Ct}$ method was used to calculate the relative mRNA expression levels (Livak and Schmittgen, 2001).

RESULTS

Identification of Novel *AKAP12* Indel Loci

This study referred to three indel loci that were documented in the NCBI database[3], and their RS numbers were rs665726346 (9-bp), rs636798034 (7-bp), and rs639087618 (13-bp), respectively. The two indel loci (rs636798034 and rs639087618) were confirmed to be exist in this population. A DNA mixing pool was used as a template for PCR amplification. According to the results of gel electrophoresis, a 7-bp indel in the promoter of *AKAP12-AS2* (NC_030816: g.83323del ACTGCTG) and a 13-bp indel in the 3′ UTR (NC_ 030816.1: g.110266del TGGTCTTTTTGTG) were identified by PCR amplifications (**Figure 1**) using primers as shown in **Table 1**.

[1]https://bibiserv.cebitec.uni-bielefeld.de/rnahybrid/

[2]http://analysis.bio-x.cn

[3]https://www.ncbi.nlm.nih.gov/

TABLE 2 | Genotype and allele frequency of two indel loci within *AKAP12* gene in Shaanbei white cashmere (SBWC) goats.

Loci	Rs number	Observed genotypes (Sample size)	Frequencies		*Ho*	*He*	PIC	HWE χ^2 (*p*-values)
			Genotypes	Alleles				
7-bp (n = 665)	rs636798034	II (14)	0.021	0.212 (I)	0.666	0.334	0.278	13.613 (*P* = 0.0002)
		ID (254)	0.382	0.788 (D)				
		DD (397)	0.597					
13-bp (*n* = 1019)	rs639087618	II (12)	0.012	0.122 (I)	0.786	0.214	0.191	0.819 (*P* = 0.365)
		ID (224)	0.220	0.878 (D)				
		DD (783)	0.768					

Ho, homozygosity; He, heterozygosity; PIC, polymorphism information content; HWE, Hardywenberg epuilibrium.

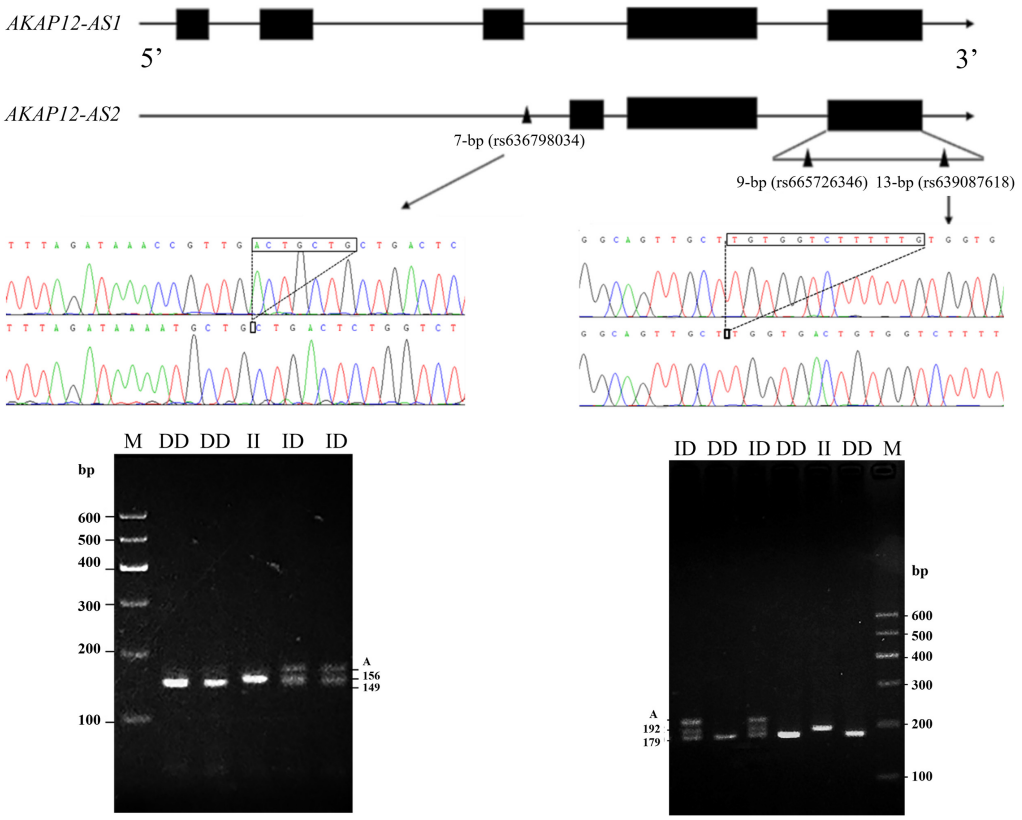

FIGURE 1 | The electrophoresis diagrams and sequencing diagrams of goat *AKAP12* gene indel loci. Black boxes: exon; Black triangle: mutation site; "A" means heteroduplex.

Genotype, Allele Frequency, and Linkage Disequilibrium Analysis

Both indel loci contain three genotypes: homozygotic deletion type (DD), homozygotic insertion type (II), and heterozygote type (ID). The allele and genotype frequencies are shown in **Table 2**. The PIC values indicated that the 7-bp indel locus had moderate polymorphism (PIC = 0.278), while the 13-bp indel locus had low polymorphism (PIC = 0.191) in SBWC. The genotypic frequency of the 13-bp indel locus was in accordance with the Hardy-Weinberg equilibrium (HWE) (χ^2-test, $P > 0.05$) while the 7-bp indel locus was not conform to HWE ($P < 0.05$) in this investigated goat population. Then, the LD of the indel loci was analyzed and the result showed that the r^2 value was low (0.03), while D′ value was high (0.99) (**Figure 2**), suggesting the minimal historical recombination between 7- and 13-bp indel loci.

Association Analysis Between First-Born Litter Size and Indel Genotypes

Next, the associations between *AKAP12* indel loci and their productive performance in female goats (single kid and multiple kids) were investigated. The results of the litter size relevance analysis are shown in **Table 3**. Since no significant association was identified between the genotypes of the 7-bp indel locus

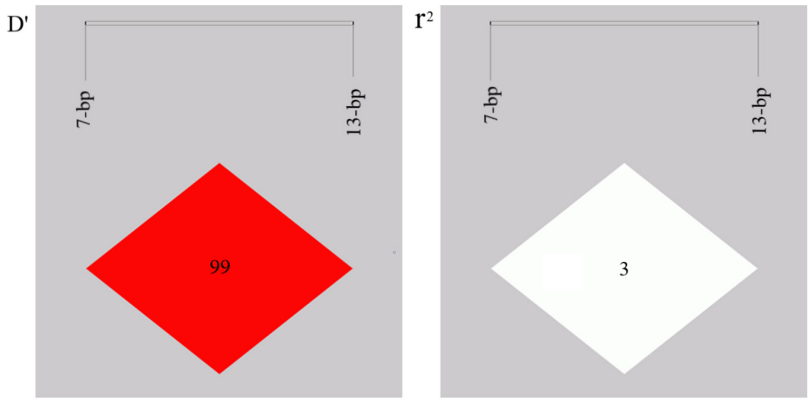

FIGURE 2 | Linkage disequilibrium plot of the *AKAP12* gene two indel loci.

TABLE 3 | Associations of two indel loci with first-born litter size in Shaanbei white cashmere (SBWC) goats.

Loci	Rs number	Genotypes			*p*-values
		II	ID	DD	
7-bp	rs636798034	1.36 ± 0.15 (*n* = 11)	1.51 ± 0.04 (*n* = 216)	1.53 ± 0.03 (*n* = 313)	0.635
13-bp	rs639087618	1.70^{AB} ± 0.15 (*n* = 10)	1.64^{A} ± 0.04 (*n* = 192)	1.45^{B} ± 0.02 (*n* = 631)	0.000078

Columns with different letters (A, B) mean P < 0.01.

and the litter size in 665 goats, we did not expand the sample size further in this locus. Interestingly, the 13-bp indel locus was significantly associated with the first-born litter size: the individuals with homozygote DD had a smaller first-born litter size, in comparison with the individuals with II and ID genotypes. We further analyzed the distribution of the genotype with the two indel variations in single and multi-lambing goat populations using the chi-square test. Consistent with the above correlation analysis, no significant difference was observed in the 7-bp indel genotype distribution, while the 13-bp indel demonstrated a significant differential genotype distribution ($P < 0.01$; **Table 4**).

The 13-bp Variation Influenced the Binding of miR-181 to Goat *AKAP12* 3′ UTR

Bioinformatic analysis using RNA hybrids predicted that the 13-bp deletion sequences within the *AKAP13* gene could bind to the seed region of miR-181 which was reported to suppress porcine reproductive and respiratory syndrome virus (PRRSV) infection by targeting PRRSV receptor CD163 and affect litter size. Therefore, luciferase activity evaluation for 13-bp indel in 3′ UTR biding with miRNA-181 was performed. Our results showed the binding of miR-181 and goat *AKAP12* 3′ UTR bases decreased when the 13-bp deletion was present (**Figure 3A**). In order to verify this predicted mechanism, the psiCHECK-2 plasmids (DD or II types) were transfected or co-transfected with pcDNA-miR-181 into the HEK293T cells, and the results indicated that the luciferase activity of II genotype vector was significantly higher than that of the DD genotype vector, and the luciferase activity of pcDNA-miR-181-Insertion allele vector was significantly higher than that of pcDNA-miR-181-Deletion allele vector (**Figure 3B**).

Identification of Genetic Variants Regulating *AKAP12* Expression

Given that mRNA expression and spliced variants may also account for Indel genotypic effects on phenotypic characteristics, we detected the mRNA expression of the spliced variants in different tissues of male goats and ovaries of female goats. Two alternative *AKAP12* splicing, named *AKAP12-AS1* and *AKAP12-AS2* and their sequence alignment analysis were shown in the file S1. Our results revealed that *AKAP12-AS2* was expressed in all tissues, whereas *AKAP12-AS1* was only expressed in the testis and brain. Notably, *AKAP12-AS2* exhibited the highest mRNA expression levels in the testis tissue (**Figures 4A–C**). Interestingly, the ovary *AKAP12-AS2* expression in goats with multiple lambs is relatively higher than those with single lamb (**Figure 4D**).

In addition, the genotypes of 7-bp indel locus didn't influence the *AKAP12* mRNA expression in both testis and ovary tissues ($P > 0.05$) (**Figures 4E,G**), whereas for the *AKAP12-AS2* 13-bp indel locus, the expression level of homozygote DD was significantly lower than that of individuals with heterozygote ID, in both testis and ovarian tissues ($P < 0.05$) (**Figures 4E,F**), which consistently explained the negative effects of the 13-bp deletion on the reduced goat litter size.

DISCUSSION

Reproductive capacity of goats are quantitative traits controlled by multiple genes with low heritability, therefore it is difficult

TABLE 4 | Genotype distribution between goats with single- and multi-lamb in Shaanbei white cashmere (SBWC) goats.

Loci	Rs number	Types	Sample size	Genotypes			Genotype frequencies			Independent χ^2-value, df, *P*-value
				II	ID	DD	II	ID	DD	
7-bp	rs636798034	Single compatriot	278	7	112	159	0.025	0.403	0.572	$\chi^2 = 0.721$ df = 2 $P = 0.697$
		multi- compatriots (≥2)	262	4	104	154	0.015	0.397	0.588	
13- bp	rs639087618	Single compatriot	432	3	73	356	0.007	0.169	0.824	$\chi^2 = 22.501$ df = 2 $P = 0.000013$
		Multi- compatriots (≥2)	398	7	119	272	0.018	0.299	0.683	

to achieve significant improvements with traditional breeding. Compared with the classical cross-breeding, molecular marker-assisted selection (MAS) has remarkably higher efficiency and accuracy (Collard and Mackill, 2008; Mills et al., 2011). Therefore, we can improve the reproductive ability of goats while retaining other excellent economical traits by using molecular markers. *AKAP12* has a common function of binding to the regulatory subunit of protein kinase A and protein kinase C signaling in regulation (Su et al., 2010). Previous studies have verified that the *AKAP12* gene plays potential roles in male germ cells and ovarian granulosa cells (Erlichman et al., 1999; Binder et al., 2013). However, to the best of our knowledge, there has been no relevant report on the effects of *AKAP12* polymorphisms on the reproductive performances of goats.

In this study, we identified two novel indel loci (7- and 13- bp) within *AKAP12* gene by PCR amplifications. The frequency of "D" allele was greater than that of "I" allele for both loci, and the minimum allele frequencies of 7 and 13-bp were 0.212 and 0.122, respectively. In addition, the genotypic frequency of the 13-bp indel locus was in accordance with the Hardweinberg equilibrium state ($P > 0.05$), while the 7-bp indel locus was not ($P < 0.05$), which might result from the effective artificial selection during breeding (Zhao et al., 2013).

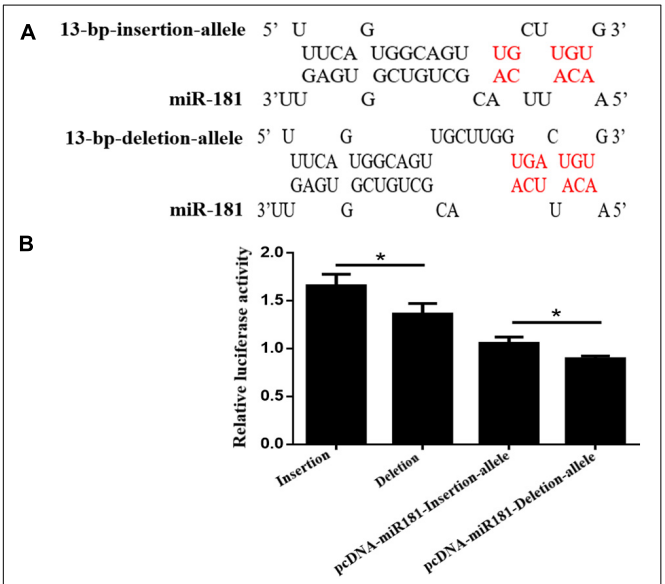

FIGURE 3 | (A) The 13-bp indel locus influences the binding of miR-181 and goat *AKAP12* 3′ UTR. **(B)** HEK293T cells transfected with the psiCHECK-2 plasmids (DD or II types) or co-transfected with pcDNA-miR-181. The relative luciferase activity was plotted on the Y axis and data were presented as means ± SE. *$P < 0.05$.

For the association analysis, in one way, practically we analyzed the effect of indel loci on first-born litter size of goats via two steps. Initially 665 individuals were used to analyze the correlation between first-born litter size and two indel mutations and the results showed that there was no significant association between the 7-bp indel locus and litter size, while the 13-bp locus was significantly correlated with goat litter size in the same population. Thus, we further extended the sample size from 665 to 1,019 and verified the association of the 13-bp indel locus with litter size. The individuals with DD genotype had fewer first-born litter sizes than those with the II and ID genotypes, thereby indicating that the allele "I" of *AKAP12* has a positive effect on the fertility of SBWC. Furthermore, linkage disequilibrium (LD) analyis was performed between 7 and 13-bp loci, and the low r^2 value indicated that there was no historical recombination between these two loci, which partially explained their different genetic effects on goat litter size.

In another way, we further analyzed the distribution of genotypes of the two indel loci in single and multi-lambing goat populations using the chi-square test. In different litter size types, there was not significant difference in the 7-bp indel genotype distribution, while in the 13-bp indel locus, significant difference in the genotype distribution was observed. In combination with the linkage analysis, our results demonstrate that the 7 and 13-bp indel loci do not affect litter size traits synergistically.

Based on the above statistical analyses, we revealed that the 13-bp locus significantly affected goat litter size in a good sample size. Herein, we gave the following explanations:

Firstly, as the 13-bp indel mutation was located on the 3′ UTR of goat *AKAP12*, we hypothesized that this indel region might be the binding site of specific miRNAs thereby influencing the *AKAP12* gene expression. It is well-known that miRNAs can bind to the 3′ UTR of target mRNA to inhibit gene expression (Abdollahzadeh et al., 2019). Thus, further bioinformatics analysis demonstrated that the 13-bp deletion sequences within the *AKAP13* gene could bind to the

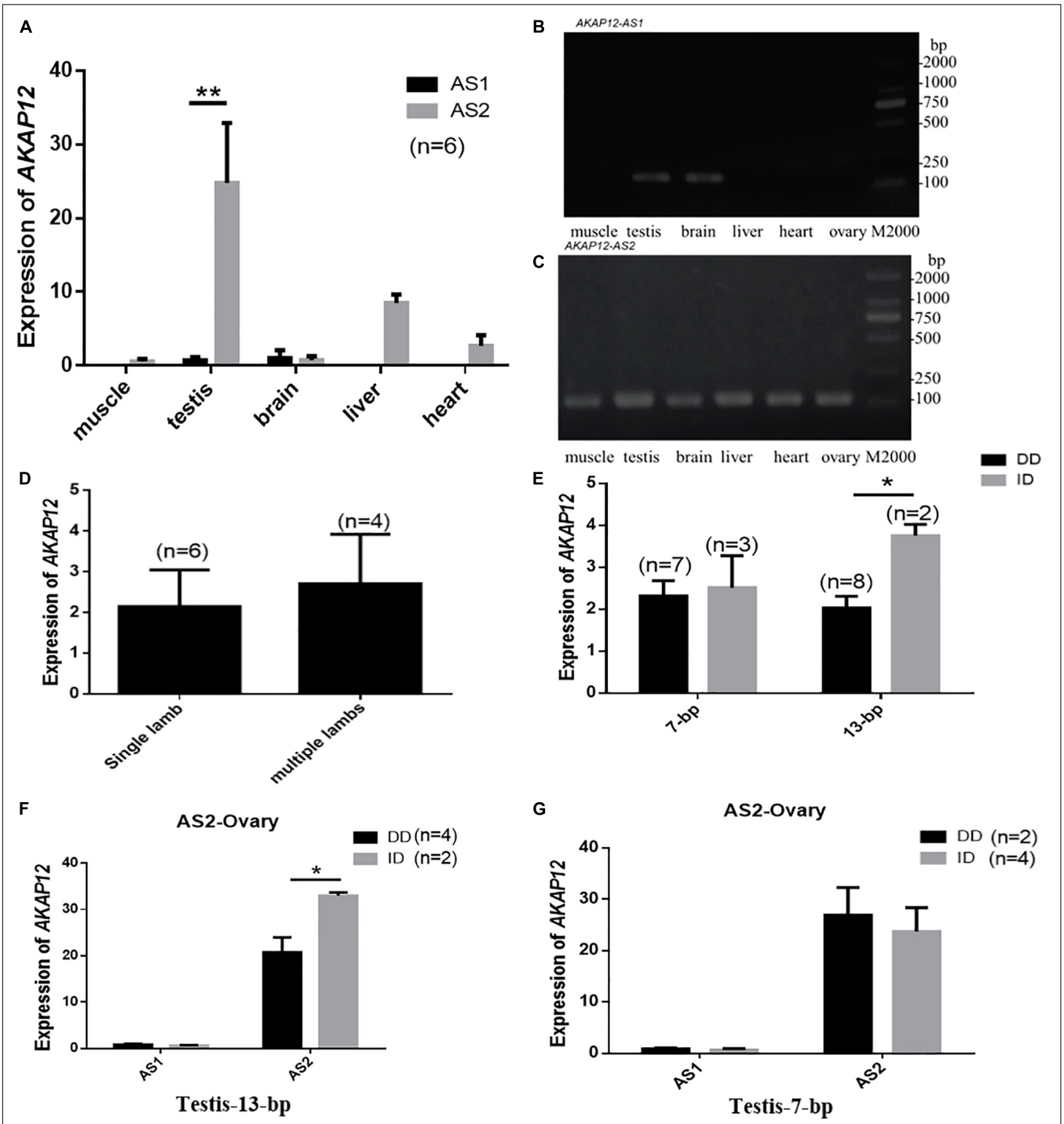

FIGURE 4 | *AKAP12* mRNA expression patterns in Shaanbei white cashmere goat. **(A)** Differential expression of *AKAP12-AS1* and *AKAP12-AS2* in different tissues of male goats. **(B)** RT-PCR analysis of *AKAP12-AS1* in different tissues. **(C)** RT-PCR analysis of *AKAP12-AS2* in different tissues. **(D)** Differential expression of *AKAP12* gene in ovary tissue of goats with single-lamb or multi-lambs. **(E–G)** The correlation between *AKAP12* mRNA expression in the ovary and testis and different genotypes of the 7-bp and 13-bp indel locus. Data represent means ± SE. $^{*}P < 0.05$, $^{**}P < 0.01$.

seed region within the miR-181 which has been reported to suppress porcine reproductive and respiratory syndrome virus (PRRSV) infection by targeting PRRSV receptor CD163 and affect reproductive capacity (Gao et al., 2013; Guo et al., 2013). In addition, it has been well established that genes related to embryo implantation and placental formation were regulated by miR-181a and miR-181c (Su et al., 2014). Therefore, luciferase activity evaluation for 13-bp indel in 3′ UTR biding with

miRNA-181 was performed. As expected, the luciferase activity of pcDNA-miR-181-13bp-Deletion-allele vector was significantly lower than that of the pcDNA-miR-181-13bp-Insertion-allele vector, suggesting that the locus with DD genotype exhibits significantly reduced binding capability with miR-181, partially accounting for the above associative analysis. Thus, the 13-bp indel might affect litter size traits of goats by interfering the binding of miR-181.

Moreover, genetic variations can affect gene expression thereby affecting phenotypic characters. Thus, we speculated that the results of the associative analysis might be caused by the influence of the genotypes of the indel locus on the expression levels of *AKAP12* mRNA. Therefore, we detected the mRNA expression of the spliced variants in different tissues of male goats and ovaries of female goats. The results showed that *AKAP12-AS2* was expressed in all tissues, but *AKAP12-AS1* was only expressed in the testis and brain. Notably, *AKAP12-AS2* exhibited the highest expression levels in testis tissues. Importantly, for the *AKAP12-AS2* 13-bp indel locus, the expression levels of homozygote DD were significantly lower than that of individuals with heterozygote ID, in both testis and ovarian tissues, which is consistent with the negative effects of the 13-bp deletion on the reduced litter size. It has been well established that alternative splicing might affect gene expression and translation through splicing proteins and other regulatory factors, thus affecting gene functions (Ule and Blencowe, 2019; Aísa-Marín et al., 2021). Thus, it's tempting to speculate that the 13-bp indel variation affects the binding of miRNAs, which in turn affected gene expression, resulting in a phenotypic difference.

Briefly, our study here revealed that the 13-bp indel within goat *AKAP12* gene significantly affected the first-born litter size by interfering with the binding of miR-181 and the expression of *AKAP12* spliced variants, therefore might promote the application of MAS in goat breeding.

DATA AVAILABILITY STATEMENT

The datasets presented in this study can be found in online repositories. The names of the repository/repositories and accession number(s) can be found below: https://www.ncbi.nlm.nih.gov/genbank/, rs636798034 and https://www.ncbi.nlm.nih.gov/genbank/, rs639087618.

ETHICS STATEMENT

The animal study was reviewed and approved by the Faculty Animal Policy and Welfare Committee of Northwest A&F University (Ethic approval file No. NWAFAC1008).

AUTHOR CONTRIBUTIONS

ZK and YB performed the experiments, analyzed the data, and prepared the manuscript. XL and HZ designed the experiments, discussed the results, and revised the manuscript. All authors contributed and approved the current submission.

FUNDING

This work was funded by the Fundamental Research Funds for the Central Universities (Grant No. lzujbky-2019-74), the "Double First-Class" Research Start-up Funds of Lanzhou University (Grant No. 561119201), and the National Natural Science Foundation of China (Grant No. 31172184).

ACKNOWLEDGMENTS

We greatly thank the staffs of Shaanbei white cashmere goat breeding farm, Shaanxi province, P.R. China for samples collecting. We thank Dr. Chuanying Pan, Xinyu Wang, and Enhui Jiang of Northwest A&F University for contributing to collect samples and recorded reproduction data. We greatly thank Prof. Dr. Lei Qu and his team as well as the staffs of Shaanbei white cashmere goat breeding farm, Shaanxi province, P.R. China for their kind help in sample collection.

SUPPLEMENTARY MATERIAL

The Supplementary Material for this article can be found online at: https://www.frontiersin.org/articles/10.3389/fgene.2021.648256/full#supplementary-material

Supplementary File 1 | Sequence alignment of *AKAP12-AS1* and *AKAP12-AS2*.

REFERENCES

Abdollahzadeh, R., Daraei, A., Mansoori, Y., Sepahvand, M., Amoli, M. M., and Tavakkoly-Bazzaz, J. (2019). Competing endogenous RNA (ceRNA) cross talk and language in ceRNA regulatory networks: a new look at hallmarks of breast cancer. *J. Cell. Physiol.* 234, 10080–10100. doi: 10.1002/jcp.27941

Aísa-Marín, I., García-Arroyo, R., Mirra, S., and Marfany, G. (2021). The alter retina: alternative splicing of retinal genes in health and disease. *Int. J. Mol. Sci.* 22:1855. doi: 10.3390/ijms22041855

Binder, A. K., Rodriguez, K. F., Hamilton, K. J., Stockton, P. S., Reed, C. E., and Korach, K. S. (2013). The absence of ER-β results in altered gene expression in ovarian granulosa cells isolated from in vivo preovulatory follicles. *Endocrinology* 154, 2174–2187. doi: 10.1210/en.2012-2256

Chen, M., Yan, H., Wang, K., Cui, Y., Chen, R., and Liu, J. (2019a). Goat SPEF2: expression profile, indel variants identification and association analysis with litter size. *Theriogenology* 139, 147–155. doi: 10.1016/j.theriogenology.2019.08.007

Chen, M., Yang, W., Liu, N., Zhang, X., Dong, W., and Lan, X. (2019b). Pig Hsd17b3: alternative splice variants expression, insertion/deletion (indel) in promoter region and their associations with male reproductive traits. *J. Steroid Biochem.* 195:105483. doi: 10.1016/j.jsbmb.2019.105483

Chen, R., Cui, Y., Zhang, X., Zhang, Y., Chen, M., and Zhou, T. (2018). Chlorpyrifos induction of testicular-cell apoptosis through generation of reactive oxygen species and phosphorylation of AMPK. *J. Agric. Food Chem.* 66, 12455–12470. doi: 10.1021/acs.jafc.8b03407

Collard, B. C., and Mackill, D. J. (2008). Marker-assisted selection: an approach for precision plant breeding in the twenty-first century. *Philos. Trans. R. Soc. Lond. B Biol. Sci.* 363, 557–572. doi: 10.1098/rstb.2007.2170

Cui, Y., Yan, H., Wang, K., Xu, H., Zhang, X., and Zhu, H. (2018). Insertion/deletion within the KDM6A gene is significantly associated with litter size in goat. *Front. Genet.* 9:91.

Deroo, B. J., Rodriguez, K. F., Couse, J. F., Hamilton, K. J., Collins, J. B., and Grissom, S. F. (2009). Estrogen receptor beta is required for optimal cAMP production in mouse granulosa cells. *Mol. Endocrinol.* 23, 955–965. doi: 10.1210/me.2008-0213

Erlichman, J., Gutierrez-Juarez, R., Zucker, S., Mei, X., and Orr, G. A. (1999). Developmental expression of the protein kinase C substrate/binding protein (clone 72/SSeCKS) in rat testis identification as a scaffolding protein containing an a-kinase-anchoring domain which is expressed during late-stage spermatogenesis. *Eur. J. Biochem.* 263, 797–805. doi: 10.1046/j.1432-1327.1999.00561.x

Escamilla-Hernandez, R., Little-Ihrig, L., Orwig, K. E., Yue, J., Chandran, U., and Zeleznik, A. J. (2008). Constitutively active protein kinase a qualitatively mimics the effects of follicle-stimulating hormone on granulosa cell differentiation. *Mol. Endocrinol.* 22, 1842–1852. doi: 10.1210/me.2008-0103

Gao, L., Guo, X. K., Wang, L., Zhang, Q., Li, N., and Chen, G. (2013). MicroRNA 181 suppresses porcine reproductive and respiratory syndrome virus (PRRSV) infection by targeting PRRSV receptor CD163. *J. Virol.* 87, 8808–8812. doi: 10.1128/jvi.00718-13

Guo, X. K., Zhang, Q., Gao, L., Li, N., Chen, X. X., and Feng, W. H. (2013). Increasing expression of microRNA 181 inhibits porcine reproductive and respiratory syndrome virus replication and has implications for controlling virus infection. *J. Virol.* 87, 1159–1171. doi: 10.1128/jvi.02386-12

Hao, D., Wang, X., Wang, X., Thomsen, B., Yang, Y., and Lan, X. (2021). MicroRNA bta-miR-365-3p inhibits proliferation but promotes differentiation of primary bovine myoblasts by targeting the activin a receptor type I. *J. Anim. Sci. Biotechnol.* 12:16.

Hui, Y., Zhang, Y., Wang, K., Pan, C., Chen, H., and Qu, L. (2020). Goat DNMT3B: an indel mutation detection, association analysis with litter size and mRNA expression in gonads. *Theriogenology* 147, 108–115. doi: 10.1016/j.theriogenology.2020.02.025

Jia, W., Wu, X., Li, X., Xia, T., Lei, C., and Chen, H. (2015). Novel genetic variants associated with mRNA expression of signal transducer and activator of transcription 3(STAT3) gene significantly affected goat growth traits. *Small Rumin. Res.* 129, 25–36. doi: 10.1016/j.smallrumres.2015.05.014

Kang, Z., Zhang, S., He, L., Zhu, H., Wang, Z., and Yan, H. (2019). A 14-bp functional deletion within the CMTM2 gene is significantly associated with litter size in goat. *Theriogenology* 139, 49–57. doi: 10.1016/j.theriogenology.2019.07.026

Kang, Z., Zhang, S., Jiang, E., Wang, X., Wang, Z., and Chen, H. (2020). CircFLT1 and lncCCPG1 sponges miR-93 to regulate the proliferation and differentiation of adipocytes by promoting lncSLC30A9 expression. *Mol. Ther. Nucleic Acids* 22, 484–499. doi: 10.1016/j.omtn.2020.09.011

Lan, X., Pan, C., Chen, H., Zhang, C., Li, J., and Zhao, M. (2007). An Alul PCR-RFLP detecting a silent allele at the goat POU1F1 locus and its association with production traits. *Small Rumin. Res.* 73, 8–12. doi: 10.1016/j.smallrumres.2006.10.009

Li, W., Liu, D., Tang, S., Li, D., Han, R., and Tian, Y. (2019). A multiallelic indel in the promoter region of the Cyclin-dependent kinase inhibitor 3 gene is significantly associated with body weight and carcass traits in chickens. *Poult. Sci.* 98, 556–565. doi: 10.3382/ps/pey404

Livak, K. J., and Schmittgen, T. D. (2001). Analysis of relative gene expression data using real-time quantitative PCR and the 2(-Delta Delta C (T)) method. *Methods* 25, 402–408. doi: 10.1006/meth.2001.1262

Mills, R. E., Pittard, W. S., Mullaney, J. M., Farooq, U., Creasy, T. H., and Mahurkar, A. A. (2011). Natural genetic variation caused by small insertions and deletions in the human genome. *Genome Res.* 21, 830–839. doi: 10.1101/gr.115907.110

Nei, M., and Roychoudhury, A. K. (1974). Sampling variances of heterozygosity and genetic distance. *Genetics.* 76, 379–390.

Qasim, H., and McConnell, B. K. (2020). AKAP12 signaling complex: impacts of compartmentalizing cAMP-dependent signaling pathways in the heart and various signaling systems. *J. Am. Heart Assoc.* 9:e016615.

Ren, T., Li, W., Liu, D., Liang, K., Wang, X., and Li, H. (2019). Two insertion-deletion variants in the promoter region of the QPCTL gene are significantly associated with body weight and carcass traits in chickens. *Anim. Genet.* 50, 279–282. doi: 10.1111/age.12741

Seo, J. H., Maki, T., Miyamoto, N., Choi, Y. K., Chung, K. K., and Hamanaka, G. (2021). AKAP12 supports blood-brain barrier integrity against ischemic stroke. *Int. J. Mol. Sci.* 21:9078. doi: 10.3390/ijms21239078

Su, B., Bu, Y., Engelberg, D., and Gelman, I. H. (2010). SSeCKS/Gravin/AKAP12 inhibits cancer cell invasiveness and chemotaxis by suppressing a protein kinase C-Raf/MEK/ERK pathway. *J. Biol. Chem.* 28, 4578–4586. doi: 10.1074/jbc.m109.073494

Su, L., Liu, R., Cheng, W., Zhu, M., Li, X., and Zhao, S. (2014). Expression patterns of microRNAs in porcine endometrium and their potential roles in embryo implantation and placentation. *PLoS One* 9:e87867. doi: 10.1371/journal.pone.0087867

Ule, J., and Blencowe, B. J. (2019). Alternative splicing regulatory networks: functions, mechanisms, and evolution. *Mol. Cell* 76, 329–345. doi: 10.1016/j.molcel.2019.09.017

Wang, K., Kang, Z., Jiang, E., Yan, H., Zhu, H., and Liu, J. (2020b). Genetic effects of DSCAML1 identified in genomewide association study revealing strong associations with litter size and semen quality in goat (*Capra hircus*). *Theriogenology* 146, 20–25. doi: 10.1016/j.theriogenology.2020.01.079

Wang, K., Liu, X., Qi, T., Hui, Y., Yan, H., and Qu, L. (2021). Whole-genome sequencing to identify candidate genes for litter size and to uncover the variant function in goats (*Capra hircus*). *Genomics* 113, 142–150. doi: 10.1016/j.ygeno.2020.11.024

Wang, Z., Pan, Y., He, L., Song, X., Chen, H., and Pan, C. (2020a). Multiple morphological abnormalities of the sperm flagella (MMAF)-associated genes: the relationships between genetic variation and litter size in goats. *Gene* 753:144778. doi: 10.1016/j.gene.2020.144778

Zhang, X., Zhang, S., Tang, Q., Jiang, E., Wang, K., and Lan, X. (2020). Goat sperm associated antigen 17 protein gene (SPAG17): small and large fragment genetic variation detection, association analysis, and mRNA expression in gonads. *Genomics* 112, 5115–5121. doi: 10.1016/j.ygeno.2020.09.029

Zhao, H., Wu, X., Cai, H., Pan, C., Lei, C., Chen, H., et al. (2013). Genetic variants and effects on milk traits of the caprine paired-like homeodomain transcription factor 2 (PITX2) gene in dairy goats. *Gene* 532, 203–210. doi: 10.1016/j.gene.2013.09.062

Conflict of Interest: The authors declare that the research was conducted in the absence of any commercial or financial relationships that could be construed as a potential conflict of interest.

frontiers in Genetics

ORIGINAL RESEARCH
published: 02 June 2021
doi: 10.3389/fgene.2021.649015

MicroRNA-mRNA Regulatory Networking Fine-Tunes Polyunsaturated Fatty Acid Synthesis and Metabolism in the Inner Mongolia Cashmere Goat

Yuchun Xie[1,2,3,4†], Zhihong Liu[1,2,3,4†], Juntao Guo[1,2,3,4†], Xin Su[1,2,3,4], Cun Zhao[1,2,3,4], Chongyan Zhang[1,2,3,4], Qing Qin[1,2,3,4], Dongliang Dai[1,2,3,4], Yanhong Zhao[1,2,3,4], Zhiying Wang[1,2,3,4], Ruijun Wang[1,2,3,4], Yanjun Zhang[1,2,3,4], Rui Su[1,2,3,4], Zhixin Wang[1,2,3,4] and Jinquan Li[1,2,3,4]**

[1] College of Animal Science, Inner Mongolia Agricultural University, Hohhot, China, [2] Key Laboratory of Animal Genetics, Breeding and Reproduction, Hohhot, China, [3] Key Laboratory of Mutton Sheep Genetics and Breeding, Ministry of Agriculture, Hohhot, China, [4] Engineering Research Center for Goat Genetics and Breeding, Hohhot, China

Fatty acid composition is an important aspect of meat quality in ruminants. Improving the beneficial fatty acid level in cashmere goat meat is important to its economic value. To investigate microRNAs (miRNAs) and mRNAs that regulate or coregulate polyunsaturated fatty acid (PUFA) synthesis and metabolism in the Inner Mongolia cashmere goat, we used longissimus dorsi muscle (WLM) and biceps femoris muscle (WBM) for transcript-level sequencing. RT-qPCR was used to evaluate the expression of mRNAs and miRNAs associated with PUFA synthesis and metabolism. The total PUFA content in the WBM was significantly higher than that in the WLM ($P < 0.05$). Our study is the first to systematically report miRNAs in cashmere goat meat. At the mRNA level, 20,375 genes were identified. *ACSL1*, *CD36* and *TECRL* were at the center of a gene regulatory network and contributed significantly to the accumulation and metabolic regulation of fatty acids. At the miRNA level, 426 known miRNAs and 30 novel miRNAs were identified. KEGG analysis revealed that the miRNA target genes were involved mainly in the PPAR signaling pathway. The mRNA-miRNA coregulation analysis showed that *ACSL1* was negatively targeted by nine miRNAs: chi-miR-10a-5p, chi-miR-10b-5p, chi-miR-130b-5p, chi-miR-15a-5p_R-1, chi-miR-15b-5p, chi-miR-16a-5p, chi-miR-16b-5p, chi-miR-181c-5p_R+1, and chi-miR-26b-5p. Finally, we speculated that the simultaneous silencing of *ACSL1* by one or more of these nine miRNAs through PPAR signaling led to low *ACSL1* expression in the WLM and, ultimately to high PUFA content in the WBM. Our study helps elucidate the metabolic regulation of fatty acids in Inner Mongolia cashmere goats.

Keywords: microRNA, mRNA, cashmere goat, ACSL1, fatty acid

OPEN ACCESS

Edited by:
Sonia Andrade,
University of São Paulo, Brazil

Reviewed by:
Siyuan Zhan,
Sichuan Agricultural University, China
Wenlin Bai,
Shenyang Agricultural University, China
Jun Luo,
Northwest A&F University, China

***Correspondence:**
Zhixin Wang
hhhtwzx@126.com
Jinquan Li
lijinquan_nd@126.com

† These authors have contributed equally to this work and share first authorship

Specialty section:
This article was submitted to Livestock Genomics, a section of the journal Frontiers in Genetics

Received: *15 February 2021*
Accepted: *29 April 2021*
Published: *02 June 2021*

Citation:
Xie Y, Liu Z, Guo J, Su X, Zhao C, Zhang C, Qin Q, Dai D, Zhao Y, Wang Z, Wang R, Zhang Y, Su R, Wang Z and Li J (2021) MicroRNA-mRNA Regulatory Networking Fine-Tunes Polyunsaturated Fatty Acid Synthesis and Metabolism in the Inner Mongolia Cashmere Goat. Front. Genet. 12:649015. doi: 10.3389/fgene.2021.649015

INTRODUCTION

The Inner Mongolian cashmere goat is a local breed that provides both cashmere and meat, but it is famous for its cashmere, which is known as "soft gold" (Su et al., 2015, 2020). The cashmere value of this goat has often caused its meat value to be ignored. Every year, nearly 700,000 cashmere goats are maintained, and the corresponding meat production is nearly 10,000 tons. Although the cashmere of this goat has been widely studied, its meat economic traits have not been reported. Fatty acid composition is a crucial aspect of meat quality in ruminants, as fatty acids often influence the flavor and juiciness of meat (Tvrzicka et al., 2011). In addition, fatty acids in meat are important for human health (Ladeira et al., 2018). Improving the quality of meat by increasing the concentrations of beneficial fatty acids to improve human health and reducing those of potentially detrimental fatty acids is an important undertaking (Scollan et al., 2014).

In the past few years, an increasing number of studies have demonstrated that microRNAs (miRNAs), once considered genomic "noise," can mediate the epigenetic, transcriptional, and posttranscriptional regulation of genes involved in fatty acid metabolism by participating in the fatty acid regulatory network (Xu et al., 2010; Long et al., 2019; Zhang et al., 2019). Such studies have linked fatty acid metabolism with miRNA-mRNA relationships, which may provide new ideas and directions for exploration of the regulatory mechanisms of fatty acid metabolism in animals. Lu et al. (2020) found that miR-212 regulates fatty acid synthase (*FASN*) and sterol regulatory element binding factor 1 (*SREBP1*) expression by targeting the silent information regulator 2 (*SIRT2*) gene and repressing its expression, ultimately promoting fat deposition in mammary epithelial cells. In intramuscular preadipocytes, overexpression of miR-17-5p suppresses the expression of nuclear receptor coactivator 3 (*NCOA3*), fatty acid binding protein 4 (*FABP4*), and peroxisome proliferator-activated receptor gamma (PPARγ) and inhibits the differentiation of preadipocytes (Han et al., 2017). Depending on the degree of complementarity between miRNAs and the 3′-untranslated region (UTR) or 5′-UTR sequences of target mRNAs, miRNAs regulate mRNAs in two ways (Bartel, 2009): If the sequences are fully complementary, the miRNAs degrade the target mRNAs, whereas if the sequences are incompletely complementary, the miRNAs repress mRNA translation and thereby protein synthesis. Both ways accomplish gene regulation. Ma et al. (2018) found that overexpression of bta-miR-130a/b inhibits the expression of adipocyte differentiation-related genes, including peroxisome proliferator activated receptor gamma (*PPARG)*, fatty acid binding protein 4 (*FABP4)*, lipin 1 (*LPIN1)*, and lipoprotein lipase (*LPL*). The aim of this study was to investigate polyunsaturated fatty acids (PUFAs) that are differentially present in different parts of the same goat, e.g., in the longissimus dorsi muscle (WLM) and biceps femoris muscle (WBM), and to use these two muscles as models to screen key miRNAs and mRNAs related to fatty acid synthesis and metabolism at the transcriptional level. Joint analysis of RNAs at both the mRNA and miRNA levels was further performed to construct a key miRNA-mRNA network associated with fatty acid metabolism and synthesis, which was further validated. The findings of this study help lay a foundation for the elucidation of the metabolic regulation of fatty acids in cashmere goats.

MATERIALS AND METHODS

Ethics Statement

Samples were collected in accordance with the Guidelines for Experimental Animals of the Ministry of Science and Technology (Beijing, China) and were approved by the experimental animal ethics committee of Inner Mongolia Agricultural University (Approval No. [2020]056).

Animals

The animals were slaughtered under controlled conditions after being electrically stunned. WLM and WBM tissues were excised immediately between the 12th and 13th ribs (right half carcass) and rapidly stored in liquid nitrogen and subsequently stored at −80°C until analysis. Three replicates were provided by Inner Mongolia cashmere goats (Yiwei White Cashmere Goat Breeding Farm, Erdos, Inner Mongolia). In semidesert pastures, all goats are grazed year-round and feed freely. Two muscles from three goats (25.2 ± 0.16 kg, wether, 2 years old) were used for fatty acid composition analysis, miRNA sequencing (miRNA-Seq) and mRNA sequencing (mRNA-Seq) and RT-qPCR.

Fatty Acid Composition Analysis

The extracted fatty acids were prepared with fatty acid methyl esters (Berton et al., 2016). The fatty acids were separated by an Agilent 5977B GC/MSD (Agilent, CA, United States) using a 100 m × 0.25 mm diameter SP-2560 capillary column of 0.02 mm thickness (Supelco, Bellefonte, PA) (Ebrahimi et al., 2014). Helium was used as a carrier gas with a spit ratio of 9:1. The experimental conditions for mass spectrometry were as follows: full scan mode, a solvent delay of 11 min, a gain factor of 10, an ion source temperature of 230℃, and a quadrupole temperature of 150℃. Qualitative Analysis B.07.00 software (Agilent) was used with the National Institute of Standards and Technology (NIST) database to identify the compound information for the reference standard (Sigma-Aldrich, United States) and samples. The results are expressed as a percentage of total fatty acids.

Total RNA Isolation, miRNA-Seq and mRNA-Seq

Total RNA was extracted using TRIzol reagent (Invitrogen, CA, United States) following the manufacturer's procedure. The 6000 Nano LabChip Kit (Agilent, CA, United States) with the Agilent Bioanalyzer 2100 system (Agilent Technologies, CA, United States) was used to assess RNA integrity. Approximately 1 μg of total RNA with an RNA integrity number (RIN) > 7.0 was used to prepare a small RNA library according to the protocol of a TruSeq Small RNA Sample Prep Kit (Illumina, San Diego, United States). Then, we performed single-end

sequencing (36 bp or 50 bp) on an Illumina HiSeq 2500. Approximately 10 μg of total RNA representing a specific adipose type was used to deplete ribosomal RNA with an Epicenter Ribo-Zero Gold Kit (Illumina). Following purification, the poly(A)- or poly(A)+ RNA fractions were fragmented into small pieces using divalent cations under elevated temperature. Then, the cleaved RNA fragments were reverse-transcribed to create the final cDNA library in accordance with the protocol for a mRNA-Seq sample preparation kit (Illumina), and the average insert size for the paired-end libraries was 300 bp (±50 bp). Then, we performed paired-end sequencing on an Illumina HiSeq 4000 (lc-bio, China) following the vendor's recommended protocol.

Raw Data Analysis for mRNAs and miRNAs

First, Cutadapt (Martin, 2011) was used to remove the reads that contained adaptor sequences, contamination, low-quality bases and undetermined bases. Then, sequence quality was verified with FastQC[1]. We used Bowtie2 (Langmead and Salzberg, 2012) and TopHat2 (Kim et al., 2013) to map reads to the genome of *Capra hircus*. The mapped reads of each sample were assembled with StringTie (Pertea et al., 2015). Subsequently, the whole transcriptome of *Capra hircus* was obtained. The samples were merged to reconstruct a comprehensive transcriptome using Perl scripts. After the final transcriptome was generated, StringTie and Ballgown (Frazee et al., 2015) were used to estimate the expression levels of all transcripts.

The raw reads were subjected to an in-house program, ACGT101-miR (LC Sciences, Houston, Texas, United States), to remove adapter dimers, contamination, low-complexity sequences, sequences of common RNA families (rRNA, tRNA, small nuclear RNA (snRNA), snoRNA) and repeats. Subsequently, unique sequences with lengths of 18–26 nucleotides were mapped to specific species precursors in miRBase 22.0 with the Basic Local Alignment Search Tool (BLAST) to identify known miRNAs and novel 3p- and 5p-derived miRNAs. Length variation at both the 3′ and 5′ ends and one mismatch within the sequence were allowed in the alignment. The unique sequences that mapped to the hairpin arms of mature species-specific miRNAs were identified as known miRNAs. The unique sequences that mapped to the arms of known species-specific precursors opposite the annotated mature miRNA-containing arm were considered to be novel 5p- or 3p-derived miRNA candidates. The remaining sequences were mapped to precursors from other selected species (excluding species-specific precursors) in miRBase 22.0 through BLAST search, and the mapped premiRNAs were further BLASTed against the specific species genomes to determine their genomic locations. We defined the miRNAs obtained through the above two methods as known miRNAs. The unmapped sequences were BLASTed against the specific genomes, and the hairpin RNA structures containing sequences were predicted from the flanking 80 nt sequences using RNAfold software[2].

Differential Expression Analysis of mRNAs and miRNAs Related to Fatty Acid Synthesis and Metabolism

StringTie was used to determine mRNA expression levels by calculating the fragments per kilobase of transcript per million mapped reads (FPKM) values. The differentially expressed mRNAs meeting the criteria of a log2 (fold change, FC) > 1 or a log2 (FC) < -1 and statistical significance ($P < 0.05$) were selected with the R package Ballgown.

The differential expression of miRNAs based on normalized deep-sequencing counts was analyzed through Student's *t*-test based on the experimental design. The significance thresholds were 0.01 and 0.05 in each test. For the prediction of the target genes of the most abundant miRNAs, two computational target prediction algorithms (TargetScan 5.0 and miRanda 3.3a) were used to identify miRNA binding sites. When using the miRanda database, the species of Capra hircus was used. Finally, the genes predicted by both algorithms were combined, and the overlapping genes were identified. The Gene Ontology (GO) terms and Kyoto Encyclopedia of Genes and Genomes (KEGG) pathways of the most abundant miRNAs and their targets were also annotated.

Validation of the RNA-Seq of mRNAs and miRNAs Related to Fatty Acid Synthesis and Metabolism

Total RNA from six samples (three goats) was extracted with TRIzol (Invitrogen, CA) according to the manufacturer's instructions. Total RNA was reverse-transcribed to cDNA using the PrimeScript RT reagent Kit (TaKaRa, Tokyo, Japan) and RT-qPCR was performed using SYBR Premix Ex Taq (TaKaRa, Tokyo, Japan). The mRNA primers were synthesized by Shanghai Shenggong, China (**Supplementary Table 9**). The relative mRNA levels were normalized to β-actin (Hou et al., 2016) expression for each sample; For miRNA detection, reverse transcription followed by stem-loop RT-qPCR was performed according to the manufacturer's protocols using the Bulge-LoopTM miRNA RT-qPCR Primer (RiboBio, Guangzhou, China). Quantification of miRNA was performed with a stem-loop real-time PCR miRNA kit (RiboBio). The relative miRNA levels were normalized to U6 small nuclear RNA (Carvalho et al., 2019) expression for each sample.

Statistical Analysis for RT-qPCR of mRNA and miRNA

The ct data from three goats and three technical replicates of all the candidate mRNA and miRNA obtained from the RT-qPCR experiments were evaluated with the $2^{-\Delta\Delta CT}$ method (Livak and Schmittgen, 2001). Student's *t*-test was performed for WBM and WLM using SPSS (IBM SPSS Statistics). The results are

[1]http://www.bioinformatics.babraham.ac.uk/projects/fastqc/

[2]http://rna.tbi.univie.ac.at/cgi-bin/RNAfold.cgi

presented as the mean ± standard deviation. A significance level of 0.05 was used.

RESULTS

Fatty Acid Content of WLM and WBM

To assess the fatty acid content, WLM and WBM tissues were collected from 2-year-old goats. A total of 34 fatty acids were found in the muscles of Inner Mongolian cashmere goats, including the omega-3 fatty acids C22:6 and C18:3n3 and the omega-6 fatty acids C18:2c9, C18:3n6, and C20:4 (**Supplementary Table 1**). Independent-sample *t*-tests were performed for fatty acids in different muscles (WBM and WLM). The results showed that the total PUFA content in WBM was significantly higher than that in WLM ($P < 0.05$) (**Figure 1** and **Supplementary Table 2**), and the levels of the PUFAs methyl linoleate (C18:2c9), cis-13-16-docosadienoic acid methyl ester (C22:2), gamma-linolenic acid methyl ester (C18:3n6), cis-11,14,17-eicosatrienoic acid methyl ester (C20:3n3), methyl cis-5,8,11,11, and 14-eicosatetraenoic acid (C20:4) in WBM were significantly higher than those in WLM ($P < 0.05$). The levels of the monounsaturated fatty acids (MUFAs) cis-10-pentadecenoic acid methyl ester (C15:1) and methyl erucate (C22:1) in WBM were significantly higher than those in WLM ($P < 0.05$). In other words, WBM and WLM were representative and could be used as models for the study of PUFAs.

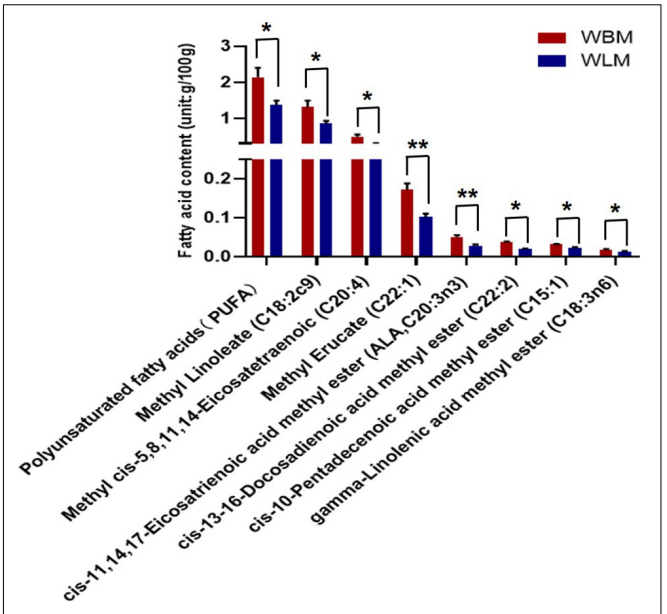

FIGURE 1 | Fatty acid content of longissimus dorsi muscle (WLM) and biceps femoris muscle (WBM). Red represents the high-fatty acid group (the WBM tissue group), while blue represents the low-fatty acid group (the WLM tissue group). The asterisks represent the levels of significance (*t*-test: $^{*}P < 0.05$, $^{**}P < 0.01$).

The Expression of mRNAs and miRNAs in Different Muscles of Inner Mongolia Cashmere Goats

To assess the mRNAs and miRNAs of the Inner Mongolia cashmere goat, we collected WLM tissues and WBM tissues for transcriptomic profiling of all mRNAs and miRNAs via high-throughput sequencing. For RNA-Seq library preparation, an average of 88,125,888 clean reads were obtained from the six samples tested, and 82.23–85.22% of these reads were uniquely aligned to the reference genome ARS1 in Ensembl. All 6 samples had at least 95.41% reads with quality equal to or exceeding Q30. An average of 20,375 genes were found in each sample of Inner Mongolia cashmere goat meat (**Supplementary Table 3**).

In addition, for the small RNA-Seq libraries, an average of 11,226,053 clean reads and 190,214 unique reads were obtained. An average of 426 known miRNAs and 30 novel miRNAs were obtained after a series of analyses (**Supplementary Table 4**).

Differentially Expressed Genes (DEGs) Related to Unsaturated Fatty Acid Synthesis and Metabolism

There were 245 DEGs in WBM compared with WLM (**Figure 2A** and **Supplementary Table 5**), of which 85 were upregulated and 160 were downregulated in WBM. These DEGs included 18 DEGs related to the regulation of fatty acid synthesis and metabolism, including acyl-CoA synthetase long chain family member 1 (*ACSL1*) (FC = 2.23), lactate dehydrogenase B (*LDHB*, FC = 3.44), acyl-CoA dehydrogenase (*ACADS*, FC = 2.02), long-chain fatty acid acyl-CoA dehydrogenase (*ACADVL*, FC = 2.56), and trans-2,3-enoyl-CoA reductase like (*TECRL*) (FC = 2.67). These genes are important for the accumulation and metabolism of PUFAs.

KEGG analysis revealed pathways associated with these DEGs (**Figure 2B** and **Supplementary Table 6**). Specifically, the DEGs were involved in 8 fatty acid-related signaling pathways, including the fat digestion and absorption (ko04975), fatty acid biosynthesis (ko00061), fatty acid metabolism (ko01212), fatty acid elongation (ko00062), PPAR signaling (ko03320), adipocytokine (ko04920) pathways, fatty acid degradation (ko00071), and glycerolipid metabolism(ko00561) pathways (**Table 1**). These eight signaling pathways are also important for the accumulation and metabolism of PUFAs. The mRNA-based KEGG network analysis of the above 18 DEGs and 8 signaling pathways revealed an indirect relationship among the 15 DEGs (**Figure 2C**). *ACSL1* was associated with 5 fatty acid metabolic process terms: the adipocytokine signaling pathway, fatty acid biosynthesis, fatty acid metabolism, fatty acid degradation, and PPAR signaling pathway were thus indirectly linked to 11 genes. *CD36* was found to participate in fat digestion and absorption, the PPAR signaling pathway and the adipocytokine signaling pathway and was indirectly linked to 11 genes. *TECRL* was revealed to be involved in fatty acid metabolism, fatty acid elongation and the biosynthesis of PUFAs and was indirectly linked to three genes. *ACSL1*, *CD36* and *TECRL* were at the center of the gene regulatory network, indicating that they contribute significantly to the accumulation and metabolic regulation of fatty acids.

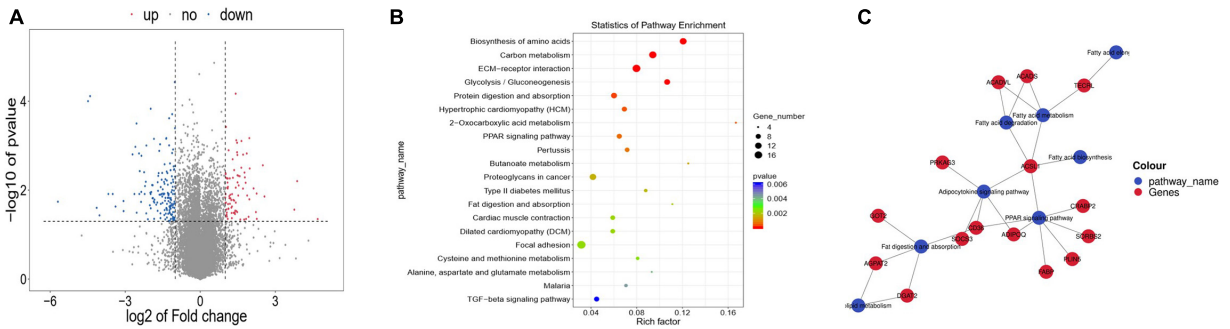

FIGURE 2 | Differentially expressed genes (DEGs) in skeletal muscle in the high-fatty acid group and the low-fatty acid group. **(A)** DEGs. The red and blue dots represent upregulated and downregulated mRNAs, respectively. **(B)** KEGG pathway analysis for the DEGs. Only the top 20 enriched pathways are presented here. **(C)** KEGG-DEGs pairs and regulatory network.

Differentially Expressed miRNAs (DEMs) Related to Unsaturated Fatty Acid Synthesis and Metabolism

Venn analysis of the 409 miRNAs found in cashmere goat muscle showed that a total of 343 miRNAs were co-expressed in both WBM and WLM, 39 were expressed only in WLM, and 27 were expressed only in WBM (**Supplementary Table 7**). A total of 32 ($P < 0.05$) DEMs were found in different parts of the muscle (**Figure 3A** and **Supplementary Table 8**), of which 14 were upregulated and 18 were downregulated in WBM. PC-3p-32774_108 and hsa-miR-615-3p_R-1 were upregulated ($P < 0.01$), whereas chi-miR-10b-3p, pol-let-7a-5p_R+3_1ss17AG, chi-miR-362-5p, and bta-let-7a-5p_R+2 were downregulated ($P < 0.01$).

KEGG analysis of the miRNA target genes (**Figure 3B** and **Supplementary Table 8**) revealed that they were associated mainly with biological processes such as fatty acid biosynthesis, the PPAR signaling pathway, and fatty acid degradation and absorption. The miRNA functional analysis results were consistent with the KEGG analysis results for the DEGs.

The miRNA target genes were predicted, and the transcriptome data were then used as a bridge to integrate the two sets of association data to obtain a miRNA-mRNA coregulatory network (**Figure 4A**). The constructed network contained 4 DEGs and 57 miRNAs. The network revealed that acetyl-CoA acyltransferase 2 (*ACAA2*) could be targeted by 8 miRNAs, while hydroxyacyl-CoA dehydrogenase trifunctional multienzyme complex subunit beta (*HADHB*) could be targeted by 11 miRNAs. *ACSL1* could be targeted by 15 miRNAs, and enoyl-CoA hydratase short chain 1 (*ECHS1*) could be targeted by 23 miRNAs. These results suggest that *ACAA2*, *HADHB*, *ACSL1,* and *ECHS1* may be the crucial genes mediated by miRNAs for the regulation of fatty acid metabolism.

To determine which specific miRNAs regulate the DEGs related to fatty acid metabolism, we performed clustering analysis of the expression patterns of the target genes (**Figure 4B**). The analysis revealed the existence of 9 miRNAs that negatively regulate the *ACSL1* gene in cashmere goats, including chi-miR-10a-5p, chi-miR-10b-5p, chi-miR-130b-5p, chi-miR-15a-5p_R-1, chi-miR-15b-5p, chi-miR-16a-5p, chi-miR-16b-5p, chi-miR-181c-5p_R + 1, and chi-miR-26b-5p. chi-miR-361-3p negatively regulates the *ACADS* gene in cashmere goats.

TABLE 1 | Eight significantly enriched pathways related to fatty acid metabolism.

Pathway_id	Pathway_name	Genes	DEG number	*P*-value
ko00062	Fatty acid elongation	*TECRL*	1	0.364156
ko00561	Glycerolipid metabolism	*AGPAT2*; *DGAT2*	2	0.292918
ko00061	Fatty acid biosynthesis	*ACSL1*	1	0.249221
ko00071	Fatty acid degradation	*ACADS*; *ACADVL*; *ACSL1*	3	0.073432
ko01212	Fatty acid metabolism	*ACADS*; *ACADVL*; *ACSL1*; *TECRL*	4	0.022678
ko04920	Adipocytokine signaling pathway	*ACSL1*; *ADIPOQ*; *CD36*; *PRKAG3*; *SOCS3*	5	0.019141
ko03320	PPAR signaling pathway	*ACSL1*; *ADIPOQ*; *CD36*; *CRABP2*; *FABP*; *PLIN5*; *SORBS2*	7	0.00259
ko04975	Fat digestion and absorption	*AGPAT2*; *CD36*; *DGAT2*; *GOT2*	4	0.002178

mRNA and miRNA Expression Related to Unsaturated Fatty Acid Synthesis and Metabolism

The expression of 6 DEGs related to unsaturated fatty acid synthesis and metabolism [*TECRL*, *CD36*, *ACSL1*, *ACADS*, *ACADVL* and diacylglycerol o-acyltransferase 2 (*DGAT2*)] was validated through RT-qPCR (**Figure 5**). The expression of

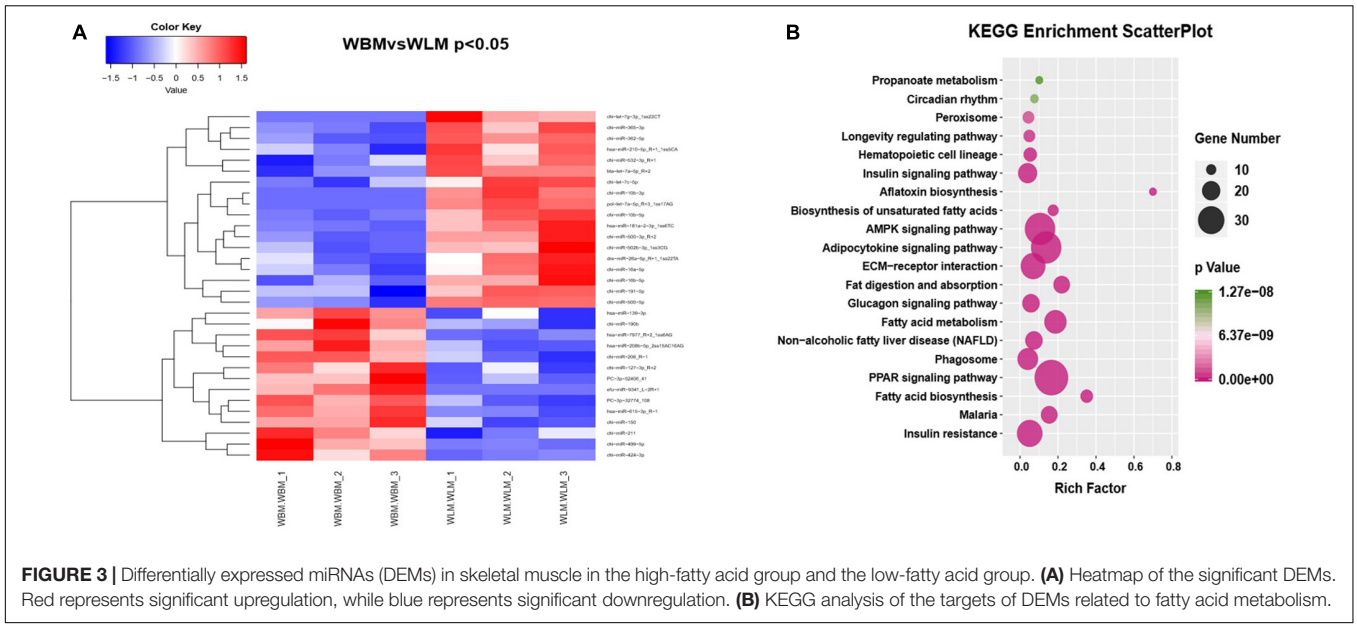

FIGURE 3 | Differentially expressed miRNAs (DEMs) in skeletal muscle in the high-fatty acid group and the low-fatty acid group. **(A)** Heatmap of the significant DEMs. Red represents significant upregulation, while blue represents significant downregulation. **(B)** KEGG analysis of the targets of DEMs related to fatty acid metabolism.

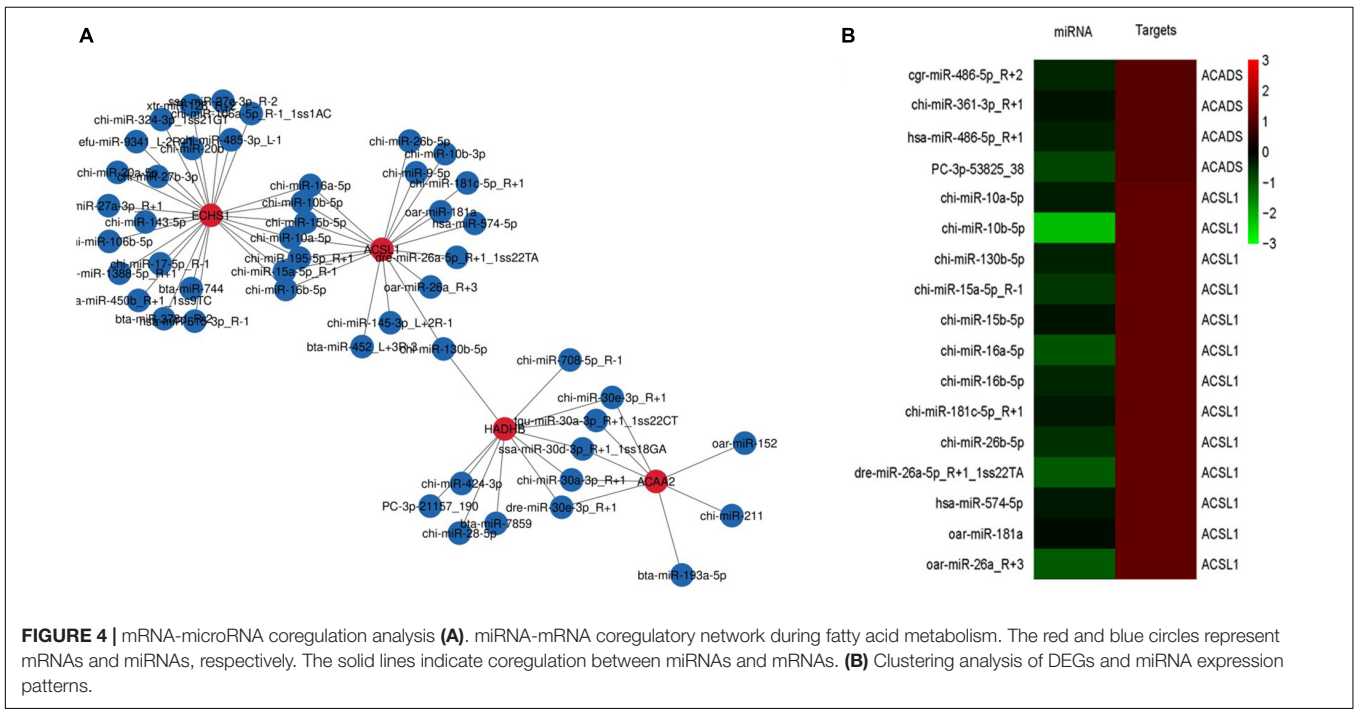

FIGURE 4 | mRNA-microRNA coregulation analysis **(A)**. miRNA-mRNA coregulatory network during fatty acid metabolism. The red and blue circles represent mRNAs and miRNAs, respectively. The solid lines indicate coregulation between miRNAs and mRNAs. **(B)** Clustering analysis of DEGs and miRNA expression patterns.

these selected transcripts was significantly higher in the WBM than in the WLM tissues ($P < 0.05$), and the expression patterns were highly consistent with those obtained by the RNA-Seq method.

The RNA-Seq results for chi-miR-16b-5p, chi-miR-10b-5p, chi-miR-365-3p, chi-miR-16a-5p, chi-miR-7c-5p, and chi-miR-191-5p were also validated through RT-qPCR (**Figure 6**). The expression of these selected miRNAs was significantly higher in the WLM than in the WBM tissues ($P < 0.01$), and the expression patterns were highly consistent with those obtained by the RNA-Seq method.

DISCUSSION

Our results show that Inner Mongolian cashmere goat meat contains a variety of omega-3 and omega-6 fatty acids that are beneficial to humans, such as C18:3n3 and C18:2c9, which have protective effects against cardiovascular and inflammatory diseases via the downregulation of proinflammatory genes (De Caterina et al., 2006; Yalcintan et al., 2018). There are two essential types of fatty acids in human nutrition: omega-3 fatty acids (alpha-linolenic acid) and omega-6 fatty acids (linoleic acid). The human body cannot synthesize essential fatty acids

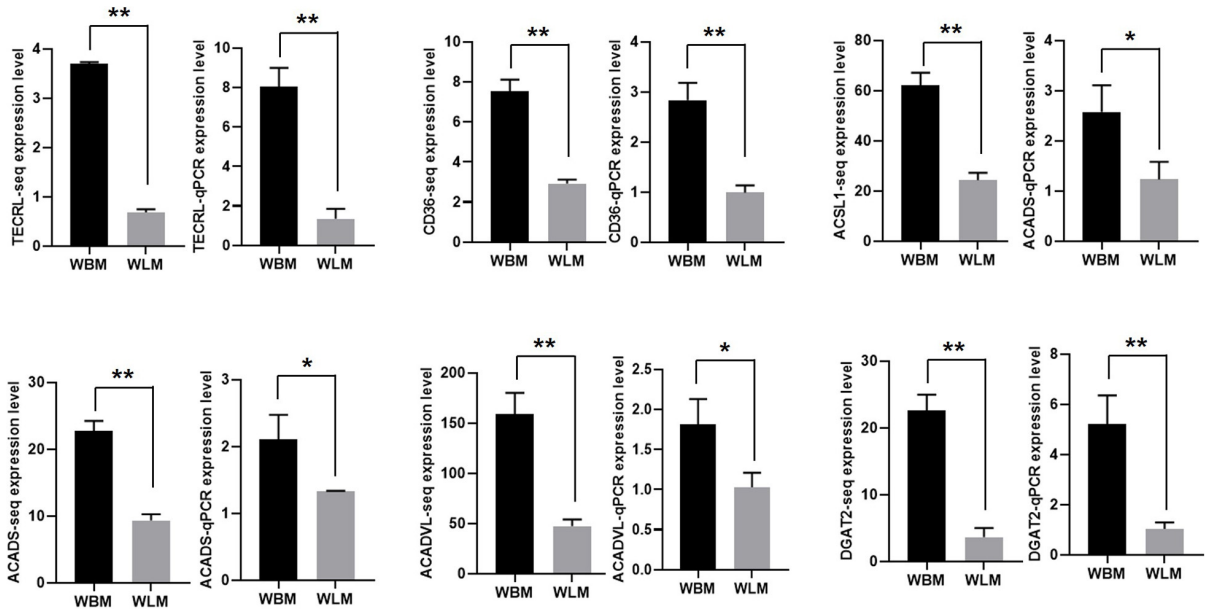

FIGURE 5 | The expression of mRNA related to unsaturated fatty acid synthesis and metabolism. Biceps femoris muscle (WBM): high-fatty acid content group. Longissimus dorsi muscle (WLM): low-fatty acid content group. Expression of genes were normalized by β-actin. The asterisks represent the levels of significance (*t*-test: $^{*}P < 0.05$, $^{**}P < 0.01$).

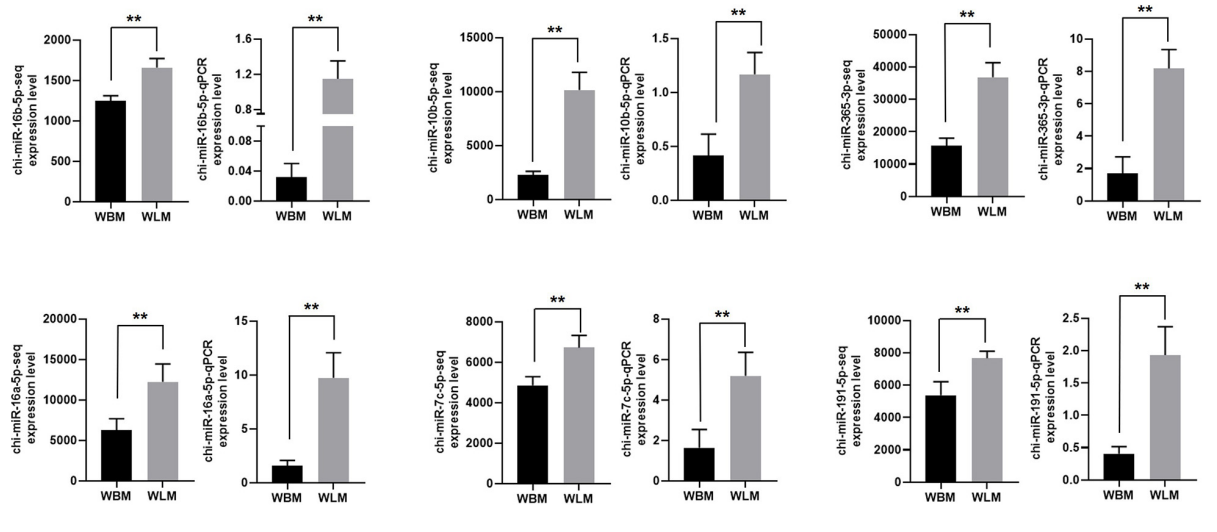

FIGURE 6 | Validation of the miRNA-Seq results. Biceps femoris muscle (WBM): high-fatty acid group. Longissimus dorsi muscle (WLM): low-fatty acid group. Expression of miRNAs were normalized by U6 snRNA. The asterisks represent the levels of significance (*t*-test: $^{**}P < 0.01$).

and thus must obtain them from food. Although seafood is the major dietary source of omega-3 fatty acids, a recent fatty acid intake survey indicated that red meat also serves as a significant source of omega-3 fatty acids for some populations (Sinclair et al., 1994). Therefore, understanding the molecular mechanisms related to fatty acids in the meat of the Inner Mongolian cashmere goat is vital. Improving our understanding of the sensory characteristics and nutritional value of goat meat is also key. Fatty acid composition is species- and tissue-specific. In our study, the PUFA content was significantly higher in WBM than in WLM. The findings indicate that the WBM and WLM of Inner Mongolia cashmere goats are effective models for research on the accumulation and metabolism of PUFAs.

Improving the beneficial fatty acid content of cashmere goat meat is important to improving the economic traits of cashmere goats. Thus, it is necessary to understand the molecules and molecular mechanisms that affect the accumulation and metabolism of fatty acids. To investigate which genes and miRNAs coregulate PUFA expression in Inner Mongolia cashmere goats, we selected WBM and WLM tissues with

significantly different PUFA contents for miRNA and mRNA sequencing. We identified 20,375 genes and 426 known miRNAs and 30 novel miRNAs in the meat of Inner Mongolia cashmere goats. At the mRNA level, 18 DEGs and 8 signaling pathways were related to fatty acid metabolism. The KEGG network analysis of the above 18 DEGs and 8 signaling pathways revealed that *ACSL1*, *CD36,* and *TECRL* are at the center of the gene regulatory network. *ACSL1* exists in fat cells and is considered to play an important role in activating the synthesis of triglycerides from fatty acids (Li et al., 2009). High expression of *ACSL1* reduces fatty acid β-oxidation through the PPARγ pathway, thereby increasing triglyceride levels (Li T. et al., 2020). In addition, *CD36* can activate fatty acid β-oxidation (Shi and Burn, 2004; Kennedy and Kashyap, 2011). $CD36^{+}CD44^{bright}$ cells express relatively high levels of three key enzymes involved in fatty acid β-oxidation (*ACADVL*, *ACADM,* and *HADHA*) (Pascual et al., 2017). *CD36* recognizes a number of lipid ligands, binds native and oxidized lipoproteins and then coordinates fat metabolism (Pepino et al., 2014). Furthermore, through GeneCards, we found that *TECRL* is a protein-coding gene. Among its related pathways are metabolism and fatty acyl-CoA biosynthesis. However, there have been no reports about *TECRL* in muscle tissue. In conclusion, the *ACSL1*, *CD36,* and *TECRL* genes are important participants in molecular mechanisms related to fatty acids in the Inner Mongolia cashmere goat.

At the miRNA level, our study is the first to systematically report that miRNAs regulate PUFA metabolism in the meat of Inner Mongolia cashmere goats. There were 214, 222, and 207 mature miRNAs in skeletal muscles of Landrace, Tongcheng, and Wuzhishan pigs, respectively (Hou et al., 2016). There were 767 known miRNAs in the WLM of Xinjiang brown cattle and Kazakh cattle (Li N. et al., 2020). In our study, we identified 426 known miRNAs and 30 novel miRNAs in the meat of cashmere goats. The number of miRNAs identified in the meat of cashmere goats was less than that in beef, but more than that in pork. Our results provide data to elucidate the molecular mechanisms affecting PUFA metabolism in Inner Mongolia cashmere goats. KEGG analysis showed that the miRNA target genes were mainly involved in fatty acid biosynthesis, fatty acid elongation, fatty acid degradation and absorption, and the PPAR signaling pathway. These results are consistent with those of the DEG KEGG analysis. Fatty acid uptake and decreased lipolysis are associated with increased intramuscular fat (IMF) deposition. Specifically, changes in the balance between synthesis and degradation can increase or decrease fatty acids (Teixeira et al., 2017). PPARs are a family of nuclear receptors that bind to fatty acids and perform significant functions in the regulation of nutrient metabolism and energy homeostasis (Lemay and Hwang, 2006). PUFAs can bind to PPARα at physiological concentrations and induce the expression of several genes involved in fatty acid metabolism, including fatty acid transport, synthesis and β oxidation (Rodríguez-Cruz and Serna, 2017). In conclusion, the PPAR pathway is important for fatty acid metabolism in the Inner Mongolia cashmere goat.

The mRNA-miRNA coregulation analysis showed that only *ACSL1* was negatively regulated by miRNAs in cashmere goats. *ACSL1* was negatively targeted by 9 miRNAs: chi-miR-10a-5p, chi-miR-10b-5p, chi-miR-130b-5p, chi-miR-15a-5p_R-1, chi-miR-15b-5p, chi-miR-16a-5p, chi-miR-16b-5p, chi-miR-181c-5p_R + 1, and chi-miR-26b-5p. *ACSL1* is involved in 5 fatty acid metabolic pathways: the adipocytokine signaling pathway, fatty acid biosynthesis, fatty acid metabolism, fatty acid degradation, and the PPAR signaling pathway; all pathways are related to PPAR signaling. Thus, we speculated that the simultaneous silencing of *ACSL1* by one or more of these nine negatively regulated miRNAs through PPAR signaling led to the low expression of the *ACSL1* gene in the WLM and finally to the high PUFA content in the WBM. A study by Lian showed that bta-miR-181a may contribute to the negative regulation of lipid synthesis in mammary cells by targeting *ACSL1* (Lian et al., 2016). In addition, miR-34a-5p can increase intracellular lipid content by reducing the *ACSL1* protein level (Tian et al., 2019). miR-126-3 might be involved in lipid metabolism in the mammary gland (Chu et al., 2017). However, there were no prior reports on the 9 miRNAs identified in our study and their association with fatty acids in cashmere goat meat. Furthermore, which miRNAs interact with *ACSL1* through PPAR signaling pathways to ultimately affect fatty acid synthesis or breakdown in the Inner Mongolia cashmere goat requires further cellular functional validation.

CONCLUSION

Our study is the first to systematically report miRNAs in cashmere goat meat and 426 known miRNAs and 30 novel miRNAs were identified. KEGG analysis revealed that the miRNA target genes were involved mainly in the PPAR signaling pathway. At the mRNA level, 20375 genes were identified. The mRNA-miRNA coregulation analysis showed that *ACSL1* was negatively targeted by nine miRNAs. We speculated that the simultaneous silencing of *ACSL1* by one or more of these nine miRNAs through PPAR signaling led to low *ACSL1* expression in the WLM and, ultimately, to high PUFA content in the WBM.

DATA AVAILABILITY STATEMENT

The data presented in the study are deposited in the SRA database (https://www.ncbi.nlm.nih.gov/sra) repository, accession number (SRA, PRJNA689238).

ETHICS STATEMENT

The animal study was reviewed and approved by the experimental animal ethics committee of Inner Mongolia Agricultural University [Approval No. (2020)056].

AUTHOR CONTRIBUTIONS

YX, ZL, and JG made substantial contributions to the conception and design of the experiments. YX, ZL, JG, XS, CYZ, and CZ

conceived and designed the experiments YX, RS, QQ, and DD performed the experiments. YX, ZL, ZYW, YJZ, and RW analyzed the data. YX, ZL, YHZ, and ZYW wrote the manuscript. JL and ZXW critically revised the manuscript. All authors read and approved the final manuscript.

FUNDING

This work received funding from the National Natural Science Foundation of China (31660640 and 32060742), the Major Science and Technology Projects of the Inner Mongolia Autonomous Region of China (2020ZD0004), the Key Technology Project of the Inner Mongolia Autonomous Region (2020GG0030), and National Key Research and Development Program of China (2018YFD0502000). The funding bodies played no role in the design of the study, collection, analysis, and interpretation of data or in the writing of the manuscript.

ACKNOWLEDGMENTS

We are thankful for the samples provided by the Aerbasi White Cashmere Goat Breeding Farm. JL provided the test platform, and the authors of this article, ZL helped in designing and conducting the experiments and in analyzing, evaluating and interpreting the results.

SUPPLEMENTARY MATERIAL

The Supplementary Material for this article can be found online at: https://www.frontiersin.org/articles/10.3389/fgene.2021.649015/full#supplementary-material

Supplementary Table 1 | Fatty acid content of cashmere goat muscle.

Supplementary Table 2 | Fatty acid classification.

Supplementary Table 3 | Overview of the data for RNA sequencing.

Supplementary Table 4 | Overview of the data for small RNA sequencing.

Supplementary Table 5 | Differentially regulated mRNAs.

Supplementary Table 6 | KEGG enrichment of DEGs.

Supplementary Table 7 | Detected miRNA.

Supplementary Table 8 | Differently expressed miRNAs.

Supplementary Table 9 | The primer information of mRNA.

REFERENCES

Bartel, D. P. (2009). MicroRNAs: target recognition and regulatory functions. *Cell* 136, 215–233. doi: 10.1016/j.cell.2009.01.002

Berton, M. P., Fonseca, L. F. S., Gimenez, D. F. J., Utembergue, B. L., Cesar, A. S., Coutinho, L. L., et al. (2016). Gene expression profile of intramuscular muscle in Nellore cattle with extreme values of fatty acid. *Bmc Genomics* 17:972. doi: 10.1186/s12864-016-3232-y

Carvalho, E. B., Gionbelli, M. P., Rodrigues, R. T. S., Bonilha, S. F. M., Newbold, C. J., Guimarães, S. E. F., et al. (2019). Differentially expressed mRNAs, proteins and miRNAs associated to energy metabolism in skeletal muscle of beef cattle identified for low and high residual feed intake. *BMC Genomics* 20:501. doi: 10.1186/s12864-019-5890-z

Chu, M., Zhao, Y., Feng, Y., Zhang, H., Liu, J., Cheng, M., et al. (2017). MicroRNA-126 participates in lipid metabolism in mammary epithelial cells. *Mol. Cell. Endocrinol.* 15, 77–86. doi: 10.1016/j.mce.2017.05.039

De Caterina, R., Zampolli, A., Del Turco, S., Madonna, R., and Massaro, M. (2006). Nutritional mechanisms that influence cardiovascular disease. *Am. J. Clin. Nutr.* 83, 421S–426S.

Ebrahimi, M., Rajion, M., and Goh, Y. (2014). Effects of oils rich in linoleic and α-linolenic acids on fatty acid profile and gene expression in goat meat. *Nutrients* 6, 3913–3928. doi: 10.3390/nu6093913

Frazee, A. C., Pertea, G., Jaffe, A. E., Langmead, B., Salzberg, S. L., and Leek, J. T. (2015). Ballgown bridges the gap between transcriptome assembly and expression analysis. *Nat. Biotechnol.* 33:243. doi: 10.1038/nbt.3172

Han, H. Y., Gu, S. H., Chu, W., Sun, W., Wei, W., Dang, X., et al. (2017). miR-17–5p Regulates differential expression of NCOA3 in pig intramuscular and subcutaneous adipose tissue. *Lipids* 52, 939–949.

Hou, X., Yang, Y., Zhu, S., Hua, C., Zhou, R., Mu, Y., et al. (2016). Comparison of skeletal muscle miRNA and mRNA profiles among three pig breeds. *Mol. Genet. Genomics* 291, 559–573. doi: 10.1007/s00438-015-1126-3

Kennedy, D. J., and Kashyap, S. R. (2011). Pathogenic role of scavenger receptor CD36 in the metabolic syndrome and diabetes. *Metab. Syndr. Relat. Disord.* 9, 239–245. doi: 10.1089/met.2011.0003

Kim, D., Pertea, G., Trapnell, C., Pimentel, H., Kelley, R., and Salzberg, S. L. (2013). TopHat2: accurate alignment of transcriptomes in the presence of insertions, deletions and gene fusions. *Genome Biol.* 14:R36. doi: 10.1186/gb-2013-14-4-r36

Ladeira, M. M., Schoonmaker, J. P., Swanson, K. C., Duckett, S. K., Gionbelli, M. P., Rodrigues, L. M., et al. (2018). Review: nutrigenomics of marbling and fatty acid profile in ruminant meat. *Animal* 12, s282–s294. doi: 10.1017/S1751731118001933

Langmead, B., and Salzberg, S. L. (2012). Fast gapped-read alignment with Bowtie 2. *Nat. Methods* 9, 357–359. doi: 10.1038/nmeth.1923

Lemay, D. G., and Hwang, D. H. (2006). Genome-wide identification of peroxisome proliferator response elements using integrated computational genomics. *J. Lipid Res.* 47, 1583–1587. doi: 10.1194/jlr.M500504-JLR200

Li, L. O., Ellis, J. M., Paich, H. A., Wang, S., Gong, N., Altshuller, G., et al. (2009). Liver-specific loss of long chain acyl-CoA synthetase-1 decreases triacylglycerol synthesis and beta-oxidation and alters phospholipid fatty acid composition. *J. Biol. Chem.* 284, 27816–27826. doi: 10.1074/jbc.M109.022467

Li, N., Yu, Q. L., Yan, X. M., Li, H. B., and Zhang, Y. (2020). Sequencing and characterization of miRNAs and mRNAs from the longissimus dorsi of Xinjiang brown cattle and Kazakh cattle. *Gene* 741:144537. doi: 10.1016/j.gene.2020.144537

Li, T., Li, X., Meng, H., Chen, L., and Meng, F. (2020). ACSL1 affects triglyceride levels through the PPARγ Pathway. *Int. J. Med. Sci.* 17, 720–727. doi: 10.7150/ijms.42248

Lian, S., Guo, J. R., Nan, X. M., Ma, L., Loor, J. J., and Bu, D. P. (2016). MicroRNA Bta-miR-181a regulates the biosynthesis of bovine milk fat by targeting ACSL1. *J. Dairy Sci.* 99, 3916–3924. doi: 10.3168/jds.2015-10484

Livak, K. J., and Schmittgen, T. D. (2001). Analysis of relative gene expression data using real-time quantitative PCR and the 2(-Delta Delta C(T)) method. *Methods* 25, 402–408. doi: 10.1006/meth.2001.1262

Long, J. K., Dai, W., Zheng, Y. W., and Zhao, S. P. (2019). miR-122 promotes hepatic lipogenesis via inhibiting the LKB1/AMPK pathway by targeting Sirt1 in non-alcoholic fatty liver disease. *Mol. Med.* 25:26. doi: 10.1186/s10020-019-0085-2

Lu, X., Xia, H., Jiang, J., Xu, X., Li, M., Chen, Z., et al. (2020). MicroRNA-212 targets SIRT2 to influence lipogenesis in bovine mammary epithelial cell line. *J. Dairy Res.* 87, 232–238. doi: 10.1017/S0022029920000229

Ma, X., Wei, D., Cheng, G., Li, S., Wang, L., Wang, Y., et al. (2018). Bta-miR-130a/b regulates preadipocyte differentiation by targeting PPARG and CYP2U1 in beef cattle. *Mol. Cell. Probes* 42, 10–17. doi: 10.1016/j.mcp

Martin, M. (2011). Cutadapt removes adapter sequences from high-throughput sequencing reads. *EMBnet J.* 24, 1138–1143. doi: 10.1089/cmb.2017.0096

Pascual, G., Avgustinova, A., Mejetta, S., Martín, M., Castellanos, A., Attolini, C. S., et al. (2017). Targeting metastasis-initiating cells through the fatty acid receptor CD36. *Nature* 541, 41–45. doi: 10.1038/nature20791

Pepino, M. Y., Kuda, O., Samovski, D., and Abumrad, N. A. (2014). Structure-function of CD36 and importance of fatty acid signal transduction in fat metabolism. *Annu. Rev. Nutr.* 34, 281–303. doi: 10.1146/annurev-nutr-071812-161220

Pertea, M., Pertea, G. M., Antonescu, C. M., Chang, T. C., Mendell, J. T., and Salzberg, S. L. (2015). StringTie enables improved reconstruction of a transcriptome from RNA-seq reads. *Nat. Biotechnol.* 33, 290–295. doi: 10.1038/nbt.3122

Rodríguez-Cruz, M., and Serna, D. S. (2017). Nutrigenomics of n-3 fatty acids: regulators of the master transcription factors. *Nutrition* 41, 90–96. doi: 10.1016/j.nut.2017.04.012

Scollan, N. D., Dannenberger, D., Nuernberg, K., Richardson, I., MacKintosh, S., Hocquette, J. F., et al. (2014). Enhancing the nutritional and health value of beef lipids and their relationship with meat quality. *Meat Sci.* 97, 384–394. doi: 10.1016/j.meatsci.2014.02.015

Shi, Y., and Burn, P. (2004). Lipid metabolic enzymes: emerging drug targets for the treatment of obesity. *Nat. Rev. Drug Discov.* 3, 695–710.

Sinclair, A. J., Johnson, L., O'Dea, K., and Holman, R. T. (1994). Diets rich in lean beef increase arachidonic acid and long-chain omega 3 polyunsaturated fatty acid levels in plasma phospholipids. *Lipids* 29, 337–343. doi: 10.1007/BF02537187

Su, R., Fu, S., Zhang, Y., Wang, R., Zhou, Y., Li, J., et al. (2015). Comparative genomic approach reveals novel conserved microRNAs in Inner Mongolia cashmere goat skin and longissimus dorsi. *Mol. Biol. Rep.* 42, 989–995. doi: 10.1007/s11033-014-3835-9

Su, R., Gong, G., Zhang, L., Yan, X., Wang, F., Zhang, L., et al. (2020). Screening the key genes of hair follicle growth cycle in Inner Mongolian Cashmere goat based on RNA sequencing. *Arch. Anim. Breed.* 63, 155–164. doi: 10.5194/aab-63-155-2020

Teixeira, P. D., Oliveira, D. M., Chizzotti, M. L., Chalfun-Junior, A., Coelho, T. C., Gionbelli, M., et al. (2017). Subspecies and diet affect the expression of genes involved in lipid metabolism and chemical composition of muscle in beef cattle. *Meat Sci.* 133, 110–118. doi: 10.1016/j.meatsci.2017.06.009

Tian, W. H., Wang, Z., Yue, Y. X., Li, H., Li, Z. J., Han, R. L., et al. (2019). miR-34a-5p increases hepatic triglycerides and total cholesterol levels by regulating ACSL1 protein expression in laying hens. *Int. J. Mol. Sci.* 20:4420. doi: 10.3390/ijms20184420

Tvrzicka, E., Kremmyda, L. S., Stankova, B., and Zak, A. (2011). Fatty acids as biocompounds: their role in human metabolism, health and disease–a review. Part 1: classification, dietary sources and biological functions. *Biomed. Pap. Med. Fac. Univ. Palacky Olomouc Czech. Repub.* 155, 117–130.

Xu, B., Gerin, I., Miao, H. Z., Vu-Phan, D., Johnson, C. N., Xu, R., et al. (2010). Multiple roles for the non-coding RNA SRA in regulation of adipogenesis and insulin sensitivity. *PLoS ONE* 5:e14199. doi: 10.1371/journal.pone.0014199

Yalcintan, H., Ekiz, B., and Ozcan, M. (2018). Comparison of meat quality characteristics and fatty acid composition of finished goat kids from indigenous and dairy breeds. *Trop. Anim. Health Prod.* 50, 1261–1269.

Zhang, B., Li, H. J., Li, D., Sun, H., Li, M., and Hu, H. (2019). Long noncoding RNA Mirt2 upregulates USP10 expression to suppress hepatic steatosis by sponging miR-34a-5p. *Gene* 700, 139–148. doi: 10.1016/j.gene.2019.02.096

Conflict of Interest: The authors declare that the research was conducted in the absence of any commercial or financial relationships that could be construed as a potential conflict of interest.

frontiers in Genetics

ORIGINAL RESEARCH
published: 11 June 2021
doi: 10.3389/fgene.2021.678825

Expression Profiling and Functional Analysis of Circular RNAs in Inner Mongolian Cashmere Goat Hair Follicles

Fangzheng Shang[1†], Yu Wang[2†], Rong Ma[3†], Zhengyang Di[1], Zhihong Wu[1], Erhan Hai[1], Youjun Rong[1], Jianfeng Pan[1], Lili Liang[1], Zhiying Wang[1], Ruijun Wang[1], Zhihong Liu[1], Yanhong Zhao[1], Zhixin Wang[1], Jinquan Li[2,3,4] and Yanjun Zhang[1]**

[1] College of Animal Science, Inner Mongolia Agricultural University, Hohhot, China, [2] Key Laboratory of Mutton Sheep Genetics and Breeding, Ministry of Agriculture, Hohhot, China, [3] Key Laboratory of Animal Genetics, Breeding and Reproduction, Hohhot, China, [4] Engineering Research Center for Goat Genetics and Breeding, Hohhot, China

OPEN ACCESS

Edited by:
Xin Wang,
Northwest A&F University, China

Reviewed by:
Wenlin Bai,
Shenyang Agricultural University, China
Zhibin Ji,
Shandong Agricultural University, China

***Correspondence:**
Jinquan Li
lijinquan_nd@126.com
Yanjun Zhang
imauzyj@163.com

[†]These authors share co-first authorship

Specialty section:
This article was submitted to Livestock Genomics, a section of the journal Frontiers in Genetics

Received: 10 March 2021
Accepted: 29 April 2021
Published: 11 June 2021

Citation:
Shang F, Wang Y, Ma R, Di Z, Wu Z, Hai E, Rong Y, Pan J, Liang L, Wang Z, Wang R, Liu Z, Zhao Y, Wang Z, Li J and Zhang Y (2021) Expression Profiling and Functional Analysis of Circular RNAs in Inner Mongolian Cashmere Goat Hair Follicles. Front. Genet. 12:678825. doi: 10.3389/fgene.2021.678825

Background: Inner Mongolian cashmere goats have hair of excellent quality and high economic value, and the skin hair follicle traits of cashmere goats have a direct and important effect on cashmere yield and quality. Circular RNA has been studied in a variety of tissues and cells.

Result: In this study, high-throughput sequencing was used to obtain the expression profiles of circular RNA (circRNA) in the hair follicles of Inner Mongolian cashmere goats at different embryonic stages (45, 55, 65, and 75 days). A total of 21,784 circRNAs were identified. At the same time, the differentially expressed circRNA in the six comparison groups formed in the four stages were: d75vsd45, 59 upregulated and 33 downregulated DE circRNAs; d75vsd55, 61 upregulated and 102 downregulated DE circRNAs; d75vsd65, 32 upregulated and 33 downregulated DE circRNAs; d65vsd55, 67 upregulated and 169 downregulated DE circRNAs; d65vsd45, 96 upregulated and 63 downregulated DE circRNAs; and d55vsd45, 76 upregulated and 42 downregulated DE circRNAs. Six DE circRNA were randomly selected to verify the reliability of the sequencing results by quantitative RT-PCR. Subsequently, the circRNA corresponding host genes were analyzed by the Gene Ontology (GO) and the Kyoto Encyclopedia of Genes and Genomes (KEGG) pathway. The results showed that the biological processes related to hair follicle growth and development enriched by GO mainly included hair follicle morphogenesis and cell development, and the signaling pathways related to hair follicle development included the Notch signaling pathway and NF-κB signaling pathway. We combined the DE circRNA of d75vsd45 with miRNA and mRNA databases (unpublished) to construct the regulatory network of circRNA–miRNA–mRNA, and formed a total of 102 pairs of circRNA–miRNA and 126 pairs of miRNA–mRNA interactions. The binding relationship of circRNA3236–chi-miR-27b-3p and circRNA3236–chi-miR-16b-3p was further verified by dual-luciferase reporter assays, and the results showed that circRNA3236 and chi-miR-27b-3p, and circRNA3236 and chi-miR-16b-3p have a targeted binding relationship.

Conclusion: To summarize, we established the expression profiling of circRNA in the fetal skin hair follicles of cashmere goats, and found that the host gene of circRNA may be involved in the development of hair follicles of cashmere goats. The regulatory network of circRNA–miRNA–mRNA was constructed and preliminarily verified using DE circRNAs.

Keywords: circRNA, cashmere goat, hair follicles, expression profile, functional analysis

BACKGROUND

There are two kinds of hair follicles in the skin of cashmere goats, namely, primary hair follicles and secondary hair follicles. Primary hair follicles produce coarse hairs, and secondary hair follicles produce cashmere. The structural characteristics of the skin and hair follicles of cashmere goats are not only important correlates of their biological characteristics but also have a direct and important effect on the yield and quality of cashmere. The hair follicle is a skin accessory organ with complex morphology and structure; it controls the growth of hair, and its most prominent feature is regeneration. The initiation of morphogenesis of primary and secondary hair follicles in cashmere goats occurs at different stages of embryonic development, and the initiation of primary hair follicles is earlier than that of secondary hair follicles. At the embryonic stage of 45–55 days, the skin forms a complete epidermal structure, and the hair follicles have not yet appeared; at 55–65 days, the primary hair follicles begin to develop in various parts of the fetus, and the keratinocytes in the basal layer of the epithelium are arranged in a fence to form hair buds, but the formation of primary hair follicles in the lateral part of the body is later than that in other parts (such as the top of the head, shoulder, and neck). At 65 days, obvious primary follicle hair buds are observed on the sides of the body. At 65–75 days, the primordial bodies of secondary hair follicles are observed in various parts of the fetus, and secondary hair follicles begin to occur and grow from the epidermis near the primary hair follicles. Similar to the primary hair follicles, the formation of secondary hair follicles in the lateral part of the body is later than that in other parts. At 75 days, obvious secondary hair follicle hair buds are observed on the side of the body (**Supplementary Figure 1**; Zhang et al., 2006, 2007).

The hair follicle traits of cashmere goats have a direct and important effect on the quantity and quality of cashmere. The ultimate goal of the research in the field of hair follicle growth and development in cashmere goats is to reveal the mechanism of cashmere growth and find the important genes related to cashmere growth. The morphogenesis and development of hair follicles may be related to some protein-coding genes. At present, it is considered that most of the signaling molecules regulating hair follicle morphogenesis belong to the Wnt pathway (Li et al., 2004), tumor necrosis factor (TNF) family, fibroblast growth factor (FGF) family (Milla, 2002), bone morphogenetic protein (BMP) family (Thomadakis et al., 1999), Sonic hedgehog (SHH) conduction pathway (McMahon et al., 2003), transforming growth factor (TGF) family (Ullrich and Paus, 2005), and NOTCH conduction pathway (Crowe et al., 1998). Some of these coding genes are stimulants of hair follicle development and some are inhibitors, which are repeatedly used to regulate each other.

miRNA is an early non-coding RNA in hair follicles. Researchers identified 22 new miRNAs and 316 conserved miRNAs in adult Inner Mongolia cashmere goats and speculated that miRNA-203 may play an important role in the growth of skin and hair follicles (Liu et al., 2012), and verified that miRNA-203 may regulate the development of cashmere goat hair follicles by targeting *DDOST* and *NAE1* (Ma et al., 2021). In recent years, the role of lncRNA in skin and hair follicles has been gradually a concern of researchers. Studies have found that lncRNA-000133 has a complex regulatory relationship with related miRNAs and their target genes. Overexpression of lncRNA-000133 leads to a significant increase in the relative expression of *ET-1*, *SCF*, *ALP*, and *LEF1* in dermal papilla cells (Zheng et al., 2019); lncRNA-599547 regulates the expression of *Wnt10b* gene by targeting miR-15b-5p, thus, inducing the differentiation of dermal papilla cells (Yin et al., 2020).

Circular RNA (circRNA) is a special kind of RNA, which has no free 5′ cap structure and 3′ poly (A) structure, and is insensitive to nuclease (William and Norman, 2014). CircRNAs can be divided into four types according to its origin: intron circRNA, exon circRNA, exon–intron circRNA, and intergenic circRNA (Chen and Li, 2015). The main mechanisms of action of circRNAs include regulating the expression of the host genes (Zhang et al., 2013; You et al., 2015), interacting with RNA-binding proteins (Xu et al., 2018); translating proteins (Conn et al., 2015); and acting as competitive endogenous RNA to regulate the expression of genes (Hansen et al., 2013; Memczak et al., 2013; Westholm et al., 2014). A current research focus is the action of circRNA, through competitive binding to miRNA, in regulating gene expression to complete the regulation of life activities that has become a research hotspot. Studies have shown that circLMO7 can enhance the *HDAC4* expression of the miR-378a-3p target gene through competitive binding of miR-378a-3p, promote muscle cell proliferation, and inhibit the differentiation of bovine myoblasts (Wei, 2017); CircARF3 adsorbs miR-103, to alleviate the targeted inhibition of miR-103 on *TRAF3* and alleviate adipose inflammation by promoting mitochondrial autophagy (Zhang, 2018). CircRNA3669 as competing endogenous RNA (ceRNA) adsorbs miR-26a and removes the downregulation of *RCN2* by miR-26a in dairy goat endometrial epithelial cells (Liu, 2019). However, circRNA studies on the regulation of hair follicle development in the embryonic stage of cashmere goats are still scarce.

Abbreviations: CircRNA, circular RNA; ceRNA, competing endogenous RNA; qRT-PCR, quantitative RT-PCR.

In the previous research of our group, we analyzed the regulatory role of miRNA–mRNA in the development of hair follicles at embryo stage in cashmere goats (Han et al., 2020). In this study, in order to explore the pattern of expression and functional role of circRNAs in the development of fetal hair follicles of cashmere goats, we first used a high-throughput sequencing technique to construct the circRNA expression profiling of cashmere goats during the fetal period (45, 55, 65, and 75 days), and identified the DE circRNAs in different comparison groups. At the same time, the host genes of DE circRNAs were analyzed by Gene Ontology (GO) and the Kyoto Encyclopedia of Genes and Genomes (KEGG) pathway. Following this, the regulatory network of circRNA–miRNA–mRNA was constructed by combining miRNA and mRNA databases, and the binding of circRNA–miRNA was verified by dual-luciferase reporter assays. This study has laid a foundation for further exploration of the regulatory role of circRNAs as ceRNAs in the hair follicles of cashmere goats and has also provided a new direction for the study of hair follicles development.

MATERIALS AND METHODS

Animals and Samples

In this experiment, 12 3-year-old ewes with good production performance, the same growth environment, and the same feed were selected for breeding in Inner Mongolia Jinlai Animal Husbandry Technology Co., Ltd. (Hohhot, Inner Mongolia), and the breeding time was recorded. The environment of the cashmere goat farm meets the relevant requirements of the experimental facilities in the Chinese national standard "Experimental Animal Environment and Facilities" (GB14925-2010). Health status, pathogenic microorganism infections, and zoonotic infections were monitored to ensure animal safety and all animal experiments were performed in accordance with the "Guidelines for Experimental Animals" of the Ministry of Science and Technology (Beijing, China). A total of 12 fetal skin samples were collected during the four periods of 45, 55, 65, and 75 days of gestation of goats, immediately treated with DPEC water, and placed in liquid nitrogen. The samples were then stored in a refrigerator at −80°C for RNA-seq and quantitative RT-PCR (qRT-PCR) tests. All fetal skin samples were collected in accordance with the International Guiding Principles for Biomedical Research Involving Animals and approved by the Special Committee on Scientific Research and Academic Ethics of Inner Mongolia Agricultural University, responsible for the approval of biomedical research ethics of Inner Mongolia Agricultural University [Approval No. (2020) 056]. No specific permissions were required for these activities, and no endangered or protected species were involved.

RNA Library Construction and Sequencing

This study sequenced 12 samples of lateral skin of cashmere goats at 45, 55, 65, and 75 days of fetal period. Total RNA was isolated and purified using Trizol reagent (Invitrogen, Carlsbad, CA, United States), following the manufacturer's procedure. The amount of RNA and purity of each sample were quantified using NanoDrop ND-1000 (NanoDrop, Wilmington, DE, United States). The RNA integrity was assessed using Agilent 2100. Approximately 5 μg of total RNA was used to deplete ribosomal RNA according to the instructions of the Ribo-Zero^{TM} rRNA Removal Kit (Illumina, San Diego, CA, United States), and the remaining RNA fragments were reverse transcribed using an RNA-seq Library Preparation Kit (Illumina) to form the final cDNA. Finally, we performed the paired-end sequencing on an Illumina Hiseq 4000 (LC Bio, Hangzhou, Zhejiang, China), following the vendor's recommended protocol.

Identification of Transcripts

According to the characteristics of circRNA structure and splicing sequence, and combined with literature reports, we used CIRCExploter2 (Zhang et al., 2014; Wang et al., 2020) and CIRI (Gao et al., 2015, 2018) to predict circRNAs, and integrate the results of the two software programs according to the starting and ending positions of circRNA. The following is the circRNA identification standard: (1) Mismatch $\leq$2; (2) back-spliced junctions reads $\geq$1; (3) two splice sites comprise less than 100 kb of the genome. According to the above identification and screening criteria, circRNA was identified more accurately.

Differential Expression Analysis

We used SRPBM as a normalization method to quantify the expression of circRNA.

SRPBM $= \frac{SR \times 10^9}{N}$, where SR is the number of spliced reads, and N is the total number of mapped reads in the sample. Analysis of differentially expressed circRNA was done using R package-edge, differential multiples (fold change) and P-values were used by default to screen differential circRNAs; that is, genes that simultaneously satisfy the absolute value of log2 (fold change) greater than or equal to 1 and P-value less than or equal to 0.05 are marked as yes; otherwise, they are marked as no.

Gene Ontology and Kyoto Encyclopedia of Genes and Genomes Pathway Enrichment Analysis

Gene Ontology and KEGG enrichment analysis is the use of all GO and KEGG annotated circRNA host genes. The gene ontology database[1] was used to perform functional annotations on DE transcripts of three components, namely, biological processes (BPs), molecular function (MF), and cellular component (CC). Pathway significant enrichment analysis can identify that the host genes are involved in the major biochemical metabolic pathways and signal transduction pathways using the KEGG database[2]. The hypergeometric test was used to analyze GO enrichment of host genes and the statistical enrichment of host genes in KEGG pathways. GO terms and KEGG pathways (corrected P-value < 0.05) were considered significantly enriched.

[1]http://www.geneontology.org/
[2]http://www.genome.jp/kegg/

Construction of CircRNA Regulatory Networks

In this study, two software programs, Targetscan[3] and miRanda[4], were used to predict the miRNA targeted by circRNA. The target genes targeting miRNA were predicted, and the circRNA–miRNA–mRNA regulatory network was constructed preliminarily. Finally, Cytoscape (Shannon et al., 2003) was used to visualize it.

qRT-PCR

In accordance with the manufacturer's instructions, we used Trizol reagent (Takara, Dalian, Liaoning, China) to extract the total RNA from 12 skin samples representing the fetal periods of cashmere goats. Subsequently, we used a PrimeScript RT Reagent Kit with gDNA Eraser (Takara, Dalian, Liaoning, China) to reverse transcribe RNA to cDNA. Following this, each sample with three duplicates, was tested on a LightCycler® 96 Real-Time PCR system (Roche, Basel, Switzerland) using TB GreenPremix Ex Taq II (Takara, Dalian, Liaoning, China). The qRT-PCR conditions were: 95°C for 30 s and then 40 cycles at 95°C for 10 s, 60°C for 30 s, followed by 72°C for 10 s. β-actin was used as the reference gene (Shen et al., 2020; Zhang et al., 2020). The validated primers used for RT-qPCR are listed in the **Supplementary Table 1**. The expression levels were calculated using the $2^{-\Delta\Delta CT}$ method (Schmittgen and Livak, 2008).

Dual-Luciferase Reporter Assays

Chi-miR-27b-3p mimics and chi-miR-16a-3p mimics were synthesized by Hanbio Biotechnology Company (Shanghai, China). The miRNA mimics were transfected into HEK 293T cells using the LipoFiter transfection reagent according to the manufacturer's instructions. The psiCHECK2-circRNA3236-WT construct was generated by inserting the circRNA3236 fragments containing the miRNA binding sequence into the psiCHECK-2 vector (Promega) at the 3′ end of the Renilla luciferase gene. The mutant psiCHECK2-circRNA3236-MUT construct was generated by mutating the miRNA-binding sequence to the complementary sequence using overlapping extension PCR. For circRNA3236 luciferase assays, the HEK 293T cells were transfected with miRNA mimics and either the psiCHECK2-circRNA3236-WT or mutated psiCHECK2-circRNA3236-Mut reporter plasmid. At 48 h post-transfection, luciferase activity was measured using a dual-luciferase reporter assay system (Promega) according to the manufacturer's instructions. The relative luciferase activities were calculated by comparing the Firefly/Renilla luciferase activity ratio.

Statistical Analysis

SPSS18.0 (Beijing, China) was used to calculate the Spearman correlation coefficient and dual-luciferase assay. Results are expressed as the mean ± SEM, and statistically significant differences between two means were analyzed using *t*-test. A value of $P < 0.05$ was considered statistically significant.

[3]http://www.targetscan.org/mamm_31/

[4]http://www.microrna.org/microrna/home.do

RESULTS

Identification and Characterization of CircRNAs in Hair Follicles of Cashmere Goats

In order to explore the expression pattern of circRNA in fetal skin hair follicles of cashmere goats, in this study, high-throughput sequencing was performed at four stages of the fetal phase of Inner Mongolian cashmere goats (Albas type). First, we constructed 12 libraries that removed ribosomal RNA of cashmere goats during the fetal period, which were named d45_1, d45_2, d45_3, d55_1, d55_2, d55_3, d65_1, d65_2, d65_3, d75_1, d75_2, and d75_3, respectively. These libraries were applied to the IlluminaHiseq4000 platform for RNA sequencing, and 1,063,299,566 raw reads were obtained from the 12 libraries (**Table 1**).

In these original reads, 1,023,889,360 effective reads were obtained by removing the reads with a connector (adaptor); the reads with N (N indicating that the base information cannot be determined) are greater than 5%, and those are of low quality (the bases with a quality value Q ≤ 10 accounting for more than 20% of the total reads) (**Table 2**). The Q20 (the proportion of bases with quality value ≥20, error rate <0.001) of each library was 99.90% and the Q30 (the proportion of bases with quality value ≥30, error rate <0.001) was above 98.1% (**Table 1**), indicating that the sequencing accuracy was high. Comparing the 1,023,889,360 effective reads with the reference genome, the percentage of the number of reads on the reference genome as a percentage of valid reads was more than 94%, the percentage of the number of reads compared with the unique location of the reference genome as a percentage of valid reads was more than 77%, and the number of reads compared with the multiple locations of the reference genome as a percentage of valid reads was more than 17%. Therefore, the utilization rate of the data was normal, and the original data obtained met the requirements of the subsequent circRNA analysis (**Table 2**) in terms of quantity and quality.

According to the characteristics of the circRNA structure and splicing sequence, we used CIRCExploter2 and CIRI to predict circRNAs. The results showed that the total number of specific circRNA identified in each sample was more than 2,800, and the corresponding parental genes numbered more than 1,700 (**Figure 1**). Studies have found that most circRNAs contain two to four exons (**Figure 2A**). At the same time, the exon length of circRNAs indicates that the length of a single exon is longer than that of circRNAs composed of multiple exons (**Figure 2B**). Chromosome distribution analysis showed that circRNAs were distributed on almost all chromosomes, and the number of circRNAs on chromosomes 1, 10, and 11 was higher than those on other chromosomes (**Figure 2C**). Finally, exon circRNAs accounted for 92.01% (**Figure 2D**) of all circRNAs in the cashmere goat skin hair follicles.

Analysis of Differences in CircRNAs

In order to explore further the regulatory role of circRNAs in the early development of cashmere goat hair follicles, we

TABLE 1 | Data quality control statistics.

Sample	Raw data		Valid data		Valid ratio (reads)	Q20 %	Q30 %	GC content %
	Read	Base	Read	Base				
d45_1	83,377,840	12.51G	80,991,260	12.15G	97.14	99.97	98.33	46
d45_2	80,073,650	12.01G	77,655,516	11.65G	96.98	99.97	98.33	45.50
d45_3	91,499,974	13.72G	87,070,648	13.06G	95.16	99.98	98.41	46
d55_1	100,354,248	15.05G	96,199,486	14.43G	95.86	99.98	98.45	46.50
d55_2	91,779,488	13.77G	88,089,256	13.21G	95.98	99.98	98.53	47
d55_3	94,888,486	14.23G	91,438,886	13.72G	96.36	99.98	98.48	47
d65_1	90,684,330	13.60G	87,483,330	13.12G	96.47	99.97	98.17	47
d65_2	102,708,880	15.41G	99,047,498	14.86G	96.44	99.98	98.47	46.50
d65_3	80,732,910	12.11G	77,823,688	11.67G	96.40	99.97	98.34	47
d75_1	81,140,600	12.17G	77,983,860	11.70G	96.11	99.98	98.45	45
d75_2	83,141,742	12.47G	80,115,068	12.02G	96.36	99.98	98.46	45
d75_3	82,917,418	12.44G	79,990,864	12.00G	96.47	99.97	98.33	46

TABLE 2 | Reference genome alignment read statistics.

Sample	Valid reads	Mapped reads (%)	Unique mapped reads (%)	Multi mapped reads (%)
d45_1	80,991,260	76,343,633 (94.26)	61,948,389 (76.49)	14,395,244 (17.77)
d45_2	77,655,516	74,877,365 (96.42)	61,031,456 (78.59)	13,845,909 (17.83)
d45_3	87,070,648	84,828,546 (97.42)	68,283,000 (78.42)	16,545,546 (19.00)
d55_1	96,199,486	93,762,003 (97.47)	76,182,223 (79.19)	17,579,780 (18.27)
d55_2	88,089,256	85,888,657 (97.50)	69,725,622 (79.15)	16,163,035 (18.35)
d55_3	91,438,886	89,149,678 (97.50)	71,925,770 (78.66)	17,223,908 (18.84)
d65_1	87,483,330	85,122,572 (97.30)	68,170,805 (77.92)	16,951,767 (19.38)
d65_2	99,047,498	96,402,904 (97.33)	79,282,917 (80.05)	17,119,987 (17.28)
d65_3	77,823,688	75,757,511 (97.35)	60,872,547 (78.22)	14,884,964 (19.13)
d75_1	77,983,860	75,996,848 (97.45)	62,127,737 (79.67)	13,869,111 (17.78)
d75_2	80,115,068	78,137,926 (97.53)	64,459,926 (80.46)	13,678,000 (17.07)
d75_3	79,990,864	77,918,087 (97.41)	63,626,735 (79.54)	14,291,352 (17.87)

divided the four stages into six comparison groups and analyzed the differential expression by calculating the SRPBM value of circRNAs (**Figures 3A,B**). The results are as follows: d75vsd45, circRNA upregulated by 59 and downregulated by 33; d75vsd55, circRNA upregulated by 61 and downregulated by 102; d75vsd65, circRNA upregulated by 32 and downregulated by 33; d65vsd55, circRNA upregulated by 67 and downregulated by 169; d65vsd45, circRNA upregulated by 96 and downregulated by 63; and d55vsd45, circRNA upregulated by 76 and downregulated by 42 (**Figure 4**). By further exploring the law of differential expression of circRNA, it was found that the differential expression of circRNA of d65vsd55 was the greatest, while the differential expression of circRNA of d75vsd65 was the lowest (**Figure 4** and **Supplementary Figure 2**).

Validation of CircRNAs by qRT-PCR

To validate the accuracy of the circRNA sequencing results, the relative expression of six DE circRNAs (circRNA2049, circRNA3411, circRNA2225, circRNA5681, circRNA1604, and circRNA4351) (**Supplementary Table 2**), were measured by qRT-PCR (**Figure 5**). The qRT-PCR results were consistent with the transcriptome sequencing data.

Gene Ontology and Kyoto Encyclopedia of Genes and Genomes Pathway Analysis of Host Genes

Gene Ontology analysis includes three domains describing the cellular and molecular roles of genes and gene products (BP, CC, and MF) (Harris et al., 2004). KEGG is a pathway database for the systematic analysis of gene function, linking genomic and functional information (Ogata et al., 1999). In order to explore the regulatory role of host genes of DE circRNAs in hair follicle genesis and development in cashmere goats, we analyzed the host genes of circRNA that were differentially expressed in different control groups by GO and KEGG pathway analyses. The results of GO enrichment showed that there was gene enrichment in the BPs related to the growth and development of hair follicles, such as hair follicle morphogenesis (GO:0031069), cell development (GO:0048468) MF including TGF beta receptor binding (GO:0005160), repressing transcription factor binding (GO:0070491), and CC including cell junction (GO:0030054), and transcription elongation factor complex (GO:0008023). A total of 54 pathways were significantly enriched in the six comparison groups. KEGG pathway analysis showed that there was gene enrichment in the

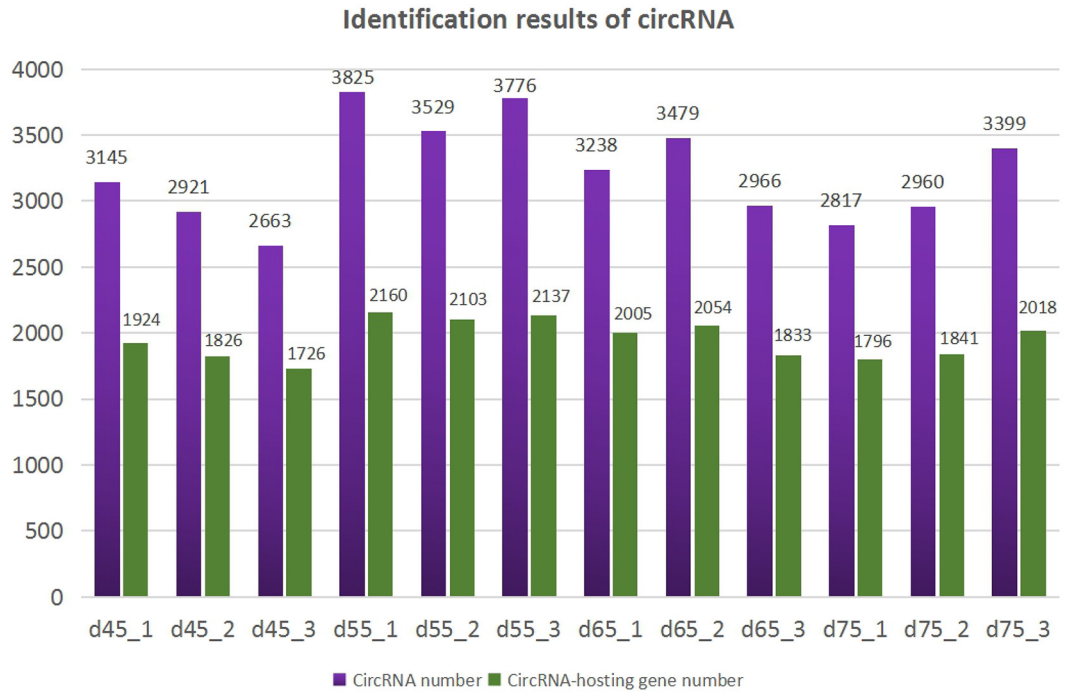

FIGURE 1 | Identification results of circRNAs. The purple columns represent the number of circRNAs, and the green columns represent the number of circRNA-hosting genes.

Notch signaling pathway (ko04330), NF-κB signaling pathway (ko04064), PI3K-AKt signaling pathway (ko04151), and other signal pathways (**Supplementary Figure 3**). Therefore, the host genes corresponding to differentially expressed circRNAs may be involved in the process of hair follicle growth and development, and then play a regulatory role.

Functional Analysis of CircRNA as an miRNA Sponge

The ceRNA hypothesis is a new model for post transcriptional gene regulation. According to the hypothesis, the expression of designated miRNAs is reduced by ceRNA (Wang et al., 2019). To construct the ceRNA network of circRNA–miRNA–mRNA, we integrated our miRNA library data (unpublished data) and mRNA library data to analyze the miRNA binding sites in the circRNAs and mRNA using miRanda and Targetscan. We selected DE exon circRNA in d75vsd45 for construction of the ceRNA regulatory network. In the up–down–up regulation pattern, we predicted 46 circRNA–miRNA and 49 miRNA–mRNA interactions (**Supplementary Table 3** and **Figure 6A**). As shown in **Figure 6A**, upregulated circRNA9106 may serve as a sponge for multiple miRNAs (chi-miR-1, chi-miR-18a-3p, and chi-miR-93-3p). Notably, three circRNAs, circRNA8058, circRNA6363, and circRNA8624 contained seed targets of chi-miR-133a-5p, which were identified by searching for miRNA target sites. Moreover, these miRNAs can downregulate the expression of their target genes (chi-miR-133a-5p was predicted to bind with *FLRT1*, *SOX5*, and RBPJL genes). We further constructed a down–up–down co-expression network using miRanda and Targetscan with a strict model, for which 56 circRNA–miRNA and 77 miRNA–mRNA interactions were predicted (**Supplementary Table 4** and **Figure 6B**). In the down–up–down co-expression network, three downregulated circRNAs, circRNA3382, circRNA1448, and circRNA1896, contained seed targets of chi-miR-26b-3p. chi-miR-26b-3p was predicted to bind with multiple target genes, including *MCTP1*, *MEF2C*, *GPC6*, and *FZD5*. At the same time, circRNA3236 was predicted to have two target miRNAs (chi-miR-27b-3p and chi-miR-16b-3p).

CircRNA3236 Binds to chi-miR-27b-3p and chi-miR-16b-3p

CircRNA3236 was downregulated in d75vsd45; Targetscan and miRanda software predicted that circRNA3236 was targeted to chi-miR-27b-3p and chi-miR-16b-3p, and there were two binding sites, respectively. Therefore, two mutant vectors were constructed to verify the specific binding sites (**Figures 7A,B**). The results showed that compared with the NC group, chi-miR-27b-3p and chi-miR-16b-3p significantly decreased the expression of luciferase in circRNA3236 WT ($P < 0.001$). It shows that there is a binding effect between the two in this experiment. After mu1 mutation, chi-miR-27b-3p failed to downregulate the expression of luciferase in circRNA3236-mut1 ($P > 0.05$), indicating that the mutation was successful. Mu1 is the binding site of chi-miR-27b-3p and circRNA3236-wt. After mu4 mutation, chi-miR-16b-3p failed to downregulate

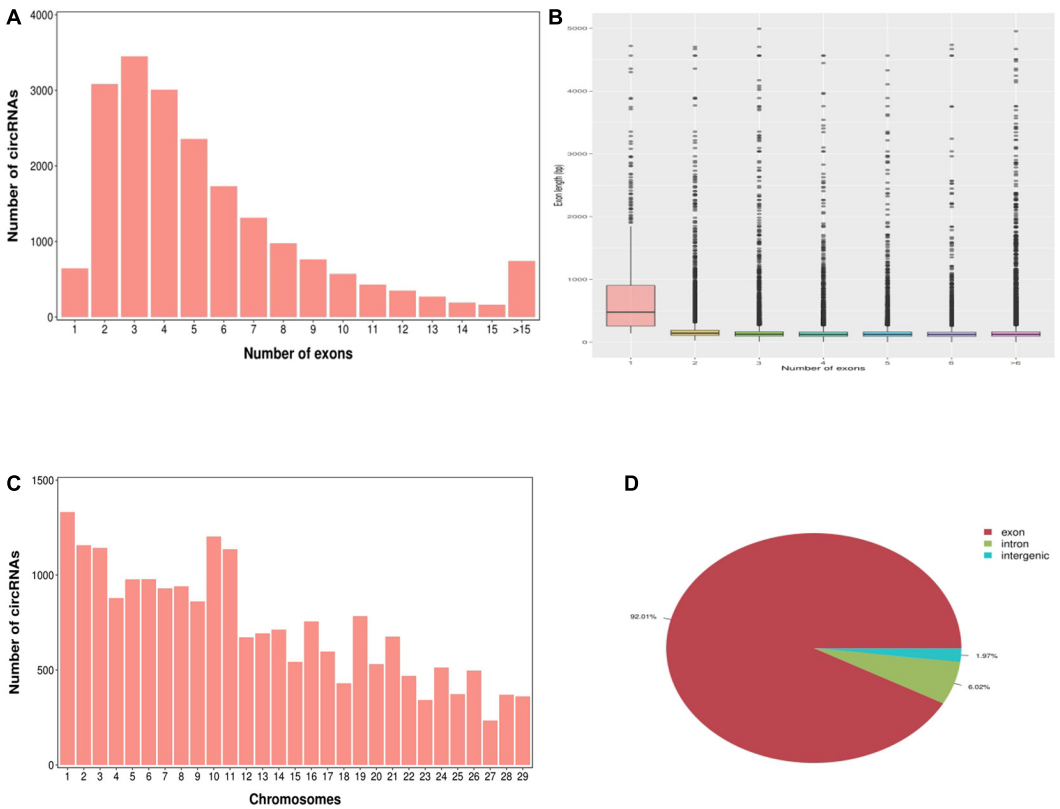

FIGURE 2 | Characteristics of circRNAs in hair follicles of cashmere goats. **(A)** Distribution of the number of circRNAs per gene. The *x*-axis represents the number of circRNAs/host gene and the *y*-axis represents the number of circRNA. **(B)** Box plot showing the exon length of exon-derived circRNAs. The *x*-axis represents the number of exons that the circRNA contains and the y-axis represents the exon length. **(C)** Distribution of the identified circRNAs in each chromosome. The *x*-axis represents the number of chromosomes and the *y*-axis represents the number of circRNAs classified by different chromosomes. **(D)** Classification of circRNAs in hair follicles of cashmere goats.

the expression of luciferase in circRNA236-mut4 ($P > 0.05$), indicating that the mutation was successful. Mu4 is the binding site of chi-miR-16b-3p and circRNA3236 (**Figures 7C,D**).

DISCUSSION

Studies have shown that circRNAs may affect biological function by regulating the level of linear mRNA expression (Kelly et al., 2015). In this experiment, the host genes of differential circRNAs were analyzed by GO and the KEGG pathway. The BP of GO enrichment includes hair follicle morphogenesis, hair follicle maturation, and cell growth; the pathway of KEGG enrichment includes the Notch signaling pathway and NF-kappa B signaling pathway. Previous studies have shown that there is a direct relationship between the Notch signal pathway and hair follicle morphogenesis (Lin et al., 2000), high expression of *Notch1* and *Notch2* can accelerate the formation of mouse hair substrate, and at the same time, it can inhibit the cells around the hair substrate to form substrate (Crowe et al., 1998). Ocu-miR-205 can promote the transition of Rex rabbit hair follicles from the growing stage to a degenerative quiescent stage by regulating the expression of related genes and proteins in Notch, BMP, and other signaling pathways, to change the hair density (Liu et al., 2020). Krieger used a mouse model to study the regulation of the NF-kappa B signaling pathway in the hair follicle cycle and found that the NF-kappa B signaling pathway is essential for the growth and activation of hair follicle stem cells (Krieger et al., 2018). The research of the NF-kappa B signaling pathway in mice showed that the NF-kappa B signaling pathway was activated downstream of EdaA1 and EDAR, thus, playing an important role in the development of hair follicles (Schmidt-Ullrich et al., 2006). Zhang et al. (2009) found that Wnt/β-catenin signaling transduction is a necessary signaling for NF-kappa B activation, and EDAR is the direct target gene of Wnt/β-catenin signaling pathway. The initial activation of the Wnt/β-catenin signaling pathway depends on the activity of EDA/EDAR/NF-kappa B in the prohair substrate of primary hair follicles. The complex interaction and interdependence of Wnt/ β-catenin and EDA/EDAR/NF-kappa B signaling pathways in the initiation and maintenance of primary hair follicle substrate were revealed (Zhang et al., 2009). Therefore, we speculate that circRNA may play a regulatory role in the primary stage of hair follicle development via the Notch signaling pathway and the NF-kappa B signaling pathway.

In the past few decades, there have been many studies on the regulatory role of miRNA and lncRNA in hair follicles (Sun et al., 2010; Liu et al., 2012; Yuan et al., 2013; Zhou, 2016, Wang et al., 2017; Zhou et al., 2018; Zhou, 2018). However, there

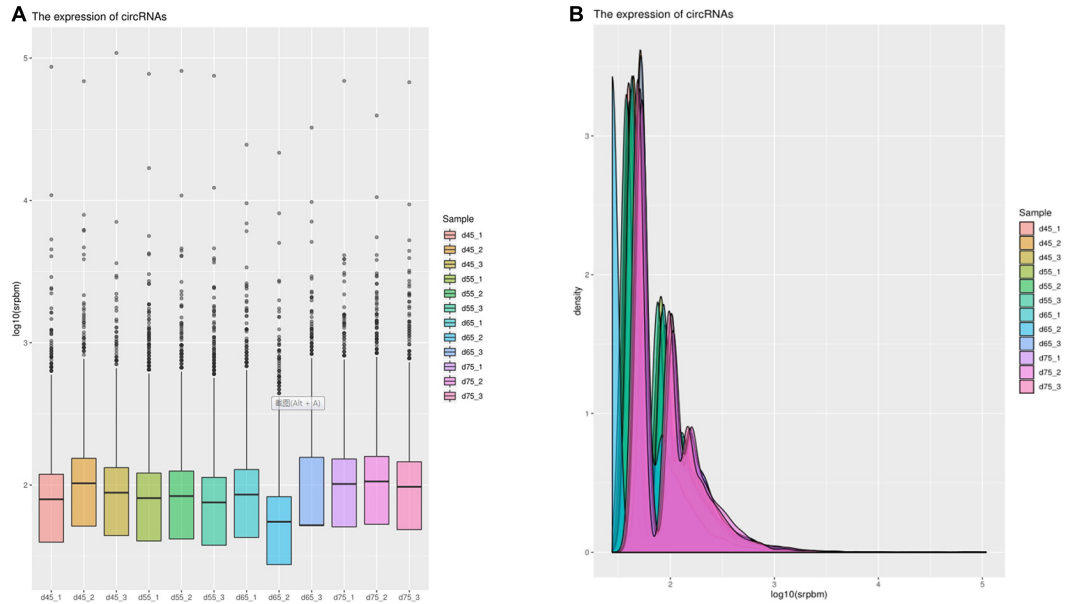

FIGURE 3 | The expression of circRNAs. **(A)** Box plot showing the expression abundance of circRNAs in each sample. **(B)** Density plot of the expression density distribution of circRNAs in each sample.

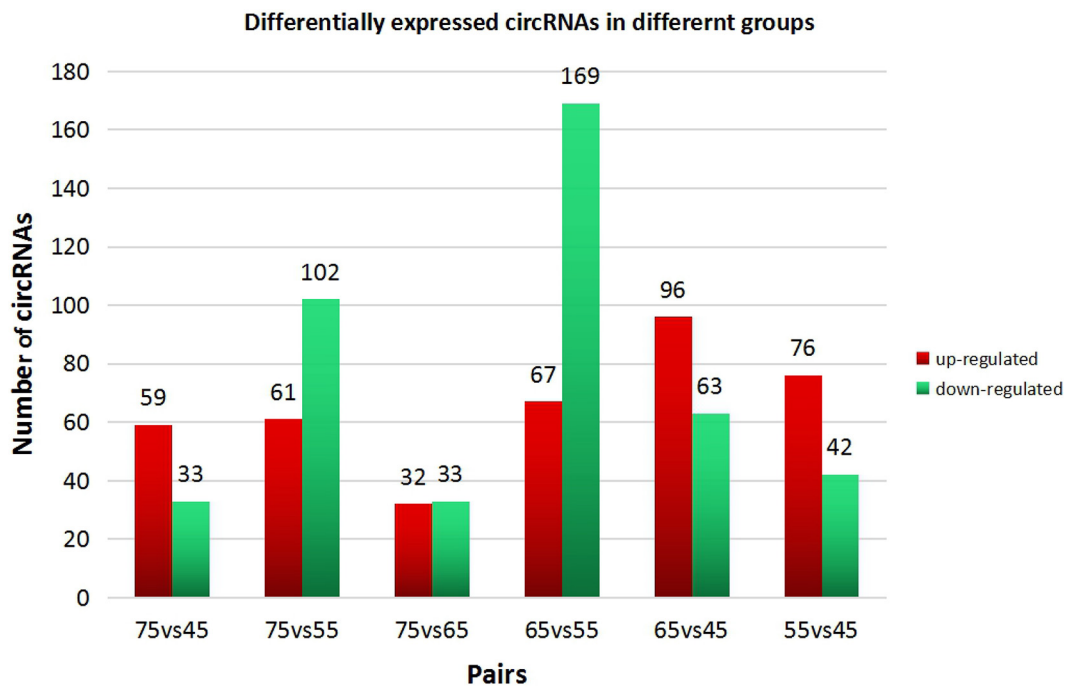

FIGURE 4 | Differential expression of circRNAs in different groups. The red columns represent upregulated circRNAs, and the green columns represent downregulated circRNAs.

is no report about circRNA related to hair follicle development. CircRNA is mostly located in the cytoplasm, and some circRNAs have MRE (a sequence recognized by miRNA), which can interact with miRNA and participate in molecular regulation as ceRNA. CeRNA was first proposed by the Pandolfi team at Harvard Medical School in *Cell* in 2011. It is pointed out that there are competitive endogenous RNA (ceRNA) molecules in cells. These ceRNA molecules (including lncRNA, circRNA, mRNA, pseudogenes, etc.) can compete through miRNA response elements (MRE) for a combination with the same miRNA in

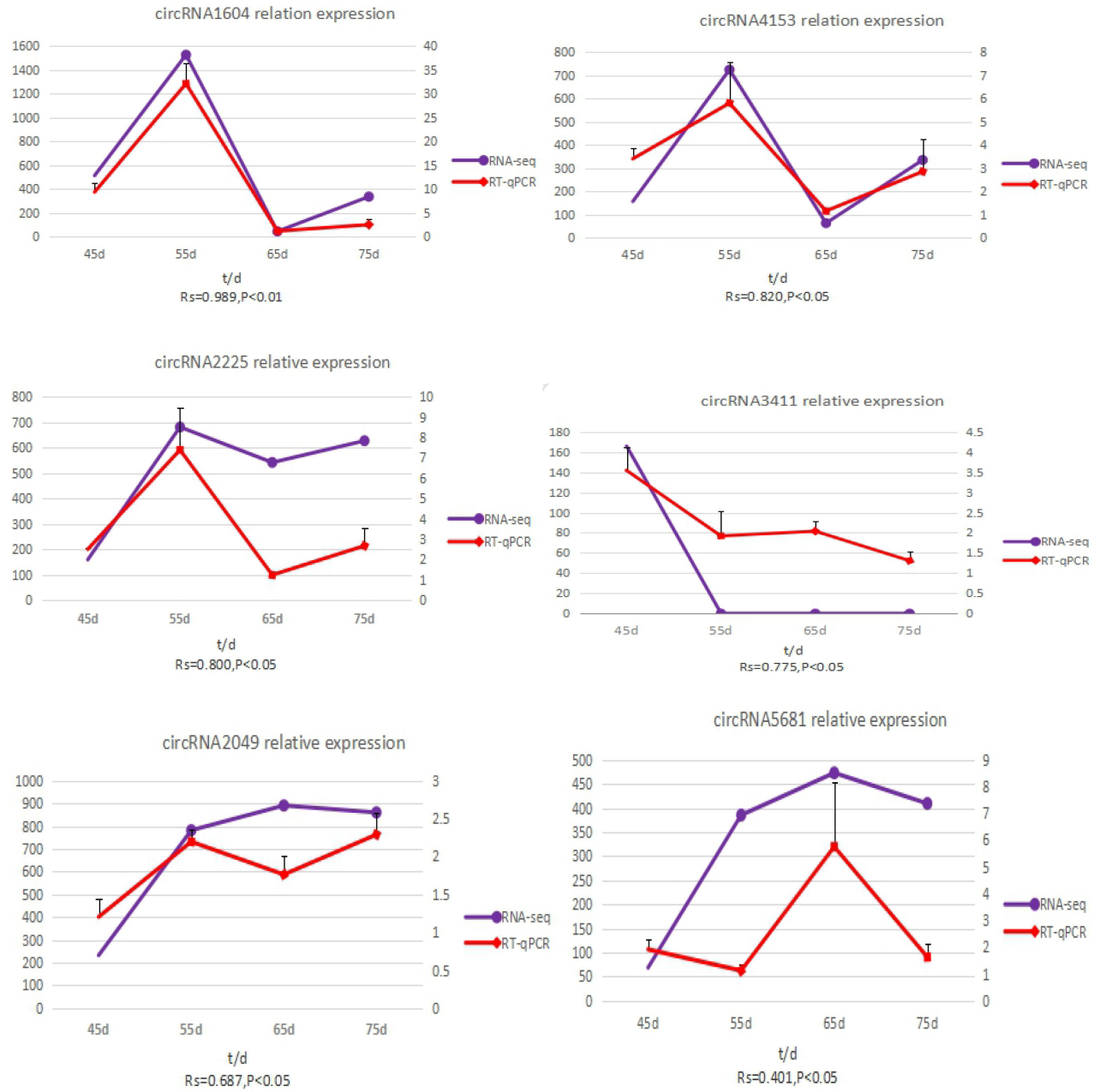

FIGURE 5 | The expression quantity and expression trend of circRNA in different periods. A total of $0.8 < |Rs| < 1$ indicates a strong correlation; $0.6 < |Rs| < 0.8$ indicates a strong correlation; $0.4 < |Rs| < 0.6$ indicates a moderate correlation; $0.2 < |Rs| < 0.4$ indicates a weak correlation; $0 < |Rs| < 0.2$ indicates no correlation; and the degree of proximity between |Rs| and 1 represents the degree of closeness and correlation between two variables.

order to regulate each other's expression levels (Salmena et al., 2011). In recent years, the involvement of circRNA as ceRNA in the regulation of biological life activities has become the focus of circRNA research. The research mainly focuses on human tumors and the regulation of life activities of some animals. In the field of human tumor research, researchers have constructed the circRNA–miRNA–mRNA regulatory network of liver cancer on the basis of high-throughput sequencing, which provided new insights that circRNA mediates the occurrence and development of liver cancer through a ceRNA mechanism (Zhao J. et al., 2019). It was found that circ_PUM1 could compete with miRNA-136, resulting in upregulation of *NOTCH3* expression, thus, promoting the occurrence and development of endometrial carcinoma (Zong et al., 2020). It was identified that hsa_circ_0000467 plays a regulatory role in gastric cancer by regulating the level of miRNA-326-3p, and that circRNA may be a potential diagnostic marker and therapeutic target in gastric cancer (He et al., 2020). It is verified that circFUT8

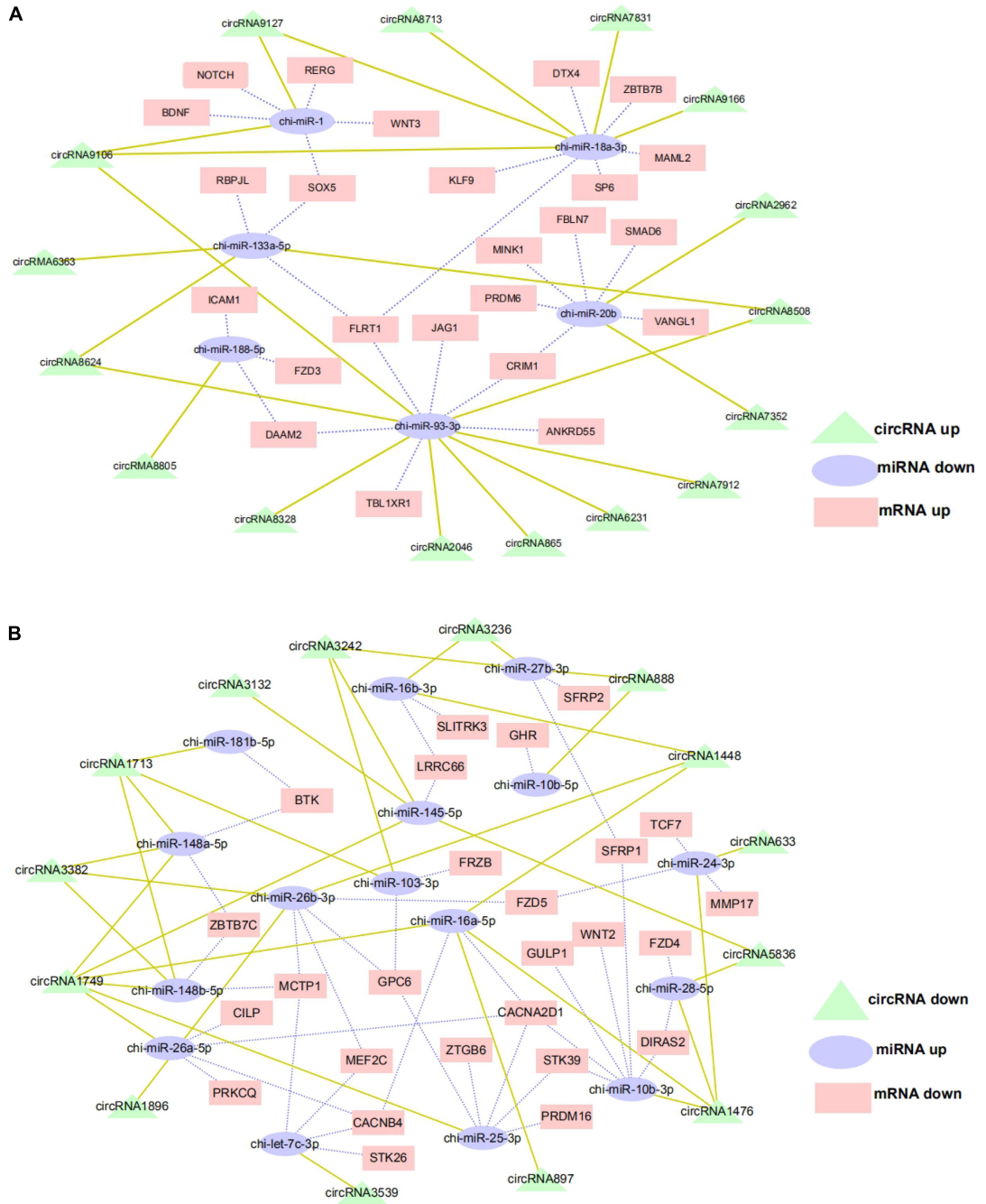

FIGURE 6 | CircRNA–miRNA–mRNA regulatory network analysis in cashmere goat hair follicle. **(A)** Upregulated circRNA networks and **(B)** downregulated circRNAs networks for d75vsd45.

plays an inhibitory role in bladder cancer cells by targeting miRNA-570-3p/KLF10 (Mo et al., 2020). In non-human animal research, Zhang et al. (2020) found that circRNA-006258 regulates the growth and lactation of goat mammary epithelial cells through a circRNA-006258-miR-574-5p-EVI5L regulatory network. Wang et al. (2020) constructed a circRNA expression profile related to milk fat metabolism under heat stress and established the related ceRNA regulatory network. Li et al. (2020) analyzed the differentially expressed circRNA, between fast contractile muscle and slow contractile muscle of porcine skeletal muscle and established a ceRNA network by combining the differentially expressed circRNA with miRNA and mRNA databases, which was preliminarily verified by double luciferase. However, there are no reports on circRNA related to fetal hair follicle development in cashmere goats. In this study, a total of 21,784 circRNA were identified in four stages of fetal skin

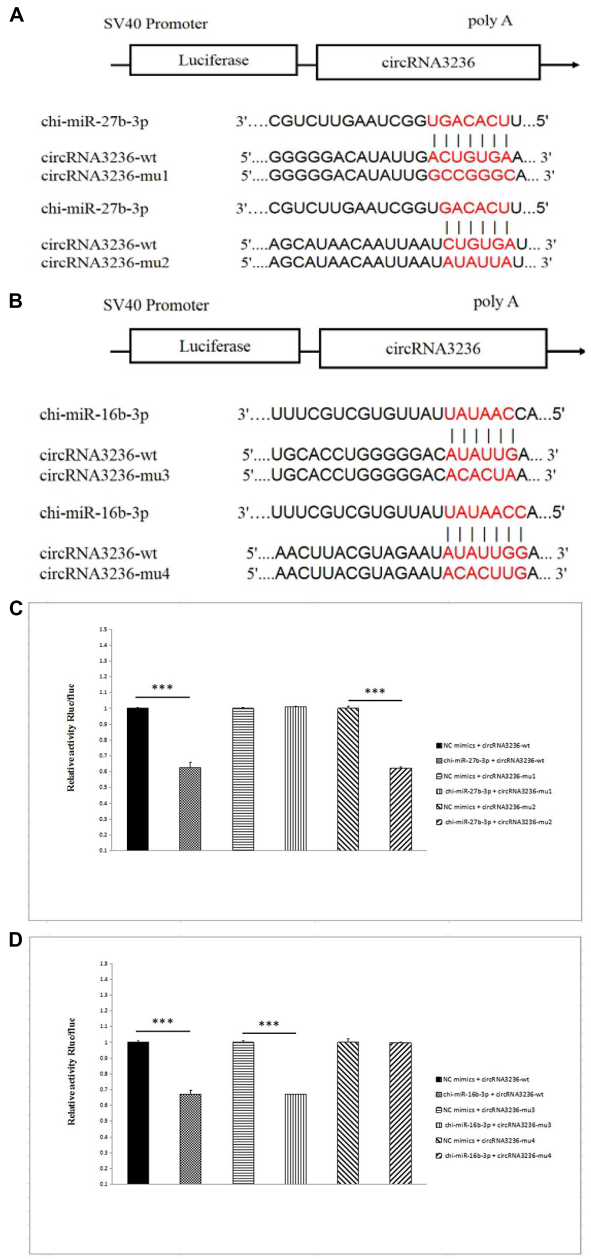

FIGURE 7 | CircRNA3236 sponged with chi-miR-27b-3p andchi-miR-26a-3p. **(A)** The predicted binding site and mutated site of chi-miR-27b-3p in circRNA3236. **(B)** The predicted binding site and mutated site of chi-miR-16a-3p in circRNA3236. **(C)** Detection of interaction between circRNA3236 and chi-miR-27b-3p by dual luciferase reporter gene assay. **(D)** Detection of interaction between circRNA3236 and chi-miR-16b-3p by dual luciferase reporter gene assay. ***$P < 0.001$ shows that the difference is extremely significant.

hair follicles of cashmere goats. The differentially expressed circRNA of each comparison group was screened, and the differential circRNAs were combined with miRNA and mRNA using the mode of upregulation–downregulation–upregulation or downregulation–upregulation–downregulation to construct the ceRNA network. Some circRNAs and differentially expressed circRNAs at different stages have been identified previously in the hair follicle development of Angora rabbits, but the total number of circRNAs, and differentially expressed circRNAs were greater, and a ceRNA network was established in this study. It is suggested that circRNAs may play an irreplaceable role in the development of hair follicles in cashmere goats (Zhao B.H. et al., 2019).

In order to explore further the functional mechanism of circRNA in the hair follicle development of cashmere goats, we predicted the miRNA targeted by circRNA and the target genes targeted by miRNA, which were differentially expressed by d75vsd45, and, thus, constructed the ceRNA network. Among them, 16 circRNAs targeted six miRNAs, and six miRNAs targeted 23 target genes in the upregulation–downregulation–upregulation model; 14 circRNAs targeted 16 miRNAs, and 16 miRNAs targeted 26 target genes in the downregulation–upregulation–downregulation model. We constructed circRNA2046-chi-miR-93-3p-FLRT1, circRNA2962-chi-miR-20b-SMAD6, circRNA3236-chi-miR-27b-3p-SFRP, circRNA3236-chi-miR-16b-3p-SLITRK3, circRNA1476-chi-miR-10b-3p-WNT2, and other signaling pathways. Among them, *SFRP1* (Hawkshaw et al., 2018), *WNT3* (Millar et al., 1999), *SMAD6* (Lv et al., 2019), and other genes are all involved in important pathways that have been related to hair follicle development in previous studies, including WNT, TGF-β, TNF, and other signal pathways. Therefore, we further speculate that circRNA, as ceRNA, may play a regulatory role in fetal skin hair follicles of cashmere goats through related genes such as WNT, TGF- β, and TNF. The results of the double luciferase experiment show that circRNA3236 and chi-miR-27b-3p, and circRNA3236 and chi-miR-16b-3p have a targeted binding relationship. It is suggested that the exon circRNA regulates gene expression by binding miRNA, and then regulates the growth and development of cashmere goat hair follicle. This is consistent with previous studies on the functional mechanism of circRNA.

CONCLUSION

We constructed the expression profiling of circRNAs in the hair follicles of Inner Mongolia cashmere goats at different embryonic stages (45, 55, 65, and 75 days), and a total of 21,784 circRNA were identified. The results of GO and KEGG analysis of host genes showed that there may be some relationship between circRNA and its host genes, and circRNA may play a role in the BP of hair follicle growth and development in cashmere goats through the Notch signaling pathway and NF-kappa B signaling pathway. At the same time, the regulatory network of circRNA–miRNA–mRNA was constructed, and the interaction between 102 pairs of circRNA–miRNA and 126 pairs of miRNA–mRNA was studied. The results of the dual luciferase assay showed that circRNA3236 and chi-miR-27b-3p, and circRNA3236 and chi-miR-16b-3p have a targeted binding relationship. The specific binding sites were verified, which provides an important basis for exploring the molecular mechanism of circRNA as ceRNA in the morphogenesis and development of hair follicles, and also

provides important information for studying the mechanism of action of circRNA in human hair follicles.

DATA AVAILABILITY STATEMENT

The RNA-Seq data were submitted to the SRA database under accession number (SRR13306949, SRR13306948, SRR13306947, SRR13306946, SRR13306945, SRR13306944, SRR13306943, SRR13306942, SRR13306941, SRR13306940, SRR13306939, SRR13306938). Additional data can be found in **Supplementary Material**.

ETHICS STATEMENT

All fetal skin samples were collected in accordance with the International Guiding Principles for Biomedical Research Involving Animals and approved by the Special Committee on Scientific Research and Academic Ethics of Inner Mongolia Agricultural University, responsible for the approval of biomedical research ethics of Inner Mongolia Agricultural University (Approval No. [2020] 056). No specific permissions were required for these activities, and no endangered or protected species were involved.

AUTHOR CONTRIBUTIONS

FS, RM, YJZ, and JL conceived the idea and designed the study. FS, YW, ZXW, LL, and JP participated in the sample collection. FS, RM, EH, ZW, YR, and ZL performed the experiments. ZYW, YHZ, RW, and YJZ analyzed the data. FS and ZD wrote the draft. FS, ZD, YW, and YJZ finalized the manuscript. All authors read and approved the final manuscript.

FUNDING

This study was supported by the Plan Project of Science and Technology in Inner Mongolia (2019GG243), the reported work was supported by the National Natural Science Foundation of China (31860627). The funding played a role in the design of the study and the collection, analysis, and interpretation of data.

ACKNOWLEDGMENTS

We thank the Inner Mongolia Jinlai Animal Husbandry for providing experimental samples and LC Biological (Huangzhou, China) for the RNA-seq sequencing in this study. We also thank the International Science Editing (http://www.internationalscienceediting.com) for editing this manuscript.

SUPPLEMENTARY MATERIAL

The Supplementary Material for this article can be found online at: https://www.frontiersin.org/articles/10.3389/fgene.2021.678825/full#supplementary-material

Supplementary Figure 1 | Changeable process in hair follicle morphogenesis of the Inner Mongolian cashmere goat in the fetal period.

Supplementary Figure 2 | Volcano plot of all DE circRNAs in six comparison groups.

Supplementary Figure 3 | GO and KEGG enrichment analysis of host genes of DE circRNAs.

Supplementary Table 1 | Primer information for qRT-PCR.

Supplementary Table 2 | CircRNAs verified by qRT-PCR and related information.

Supplementary Table 3 | CircRNA, miRNA, and mRNA in d45 vs d75 were differentially expressed in the up-down-up ceRNA regulatory network.

Supplementary Table 4 | CircRNA, miRNA, and mRNA in d45 vs d75 were differentially expressed in the down-up-down ceRNA regulatory network.

REFERENCES

Chen, L. L., and Li, Y. (2015). Regulation of circRNA biogenesis. *RNA Biol.* 12, 381–388. doi: 10.1080/15476286.2015.1020271

Conn, S. J., Pillman, K. A., Toubia, J., Conn, V. M., Salmanidis, M., Phillips, C. A., et al. (2015). The RNA binding protein quaking regulates formation of circRNAs. *Cell* 160, 1125–1134. doi: 10.1016/j.cell.2015.02.014

Crowe, R., Henrique, D., Horowicz, D., and Niswander, L. (1998). A new role for Notch and Delta in cell fate decisions patterning the feather array. *Development* 125, 767–775. doi: 10.1242/dev.125.4.767

Gao, Y., Wang, J. F., and Zhao, F. Q. (2015). CIRI: an efficient and unbiased algorithm for de novo circular RNA identification. *Genome Biol.* 16:4.

Gao, Y., Zhang, J. Y., and Zhao, F. Q. (2018). Circular RNA identification based on multiple seed matching. *Brief Bioinform.* 19, 803–810. doi: 10.1093/bib/bbx014

Han, W. J., Yang, F., Wu, Z. H., Guo, F. Q., Zhang, J. J., Hai, E. H., et al. (2020). Inner mongolian cashmere goat secondary follicle development regulation research based on mRNA-miRNA Co-analysis. *Sci. Rep.* 10:4519.

Hansen, T. B., Jensen, T. I., Clausen, B. H., Bramsen, J. B., Finsen, B., Damgaard, C. K., et al. (2013). Natural RNA circles function as efficient microRNA sponges. *Nature* 495, 384–388. doi: 10.1038/nature11993

Harris, M. A., Clark, J., Ireland, A., Lomax, J., Ashburner, M., Foulger, R., et al. (2004). The gene ontology (GO) database and informatics resource. *Nucleic Acids Res.* 32, D258–D261.

Hawkshaw, N. J., Hardman, J. A., Haslam, I. S., Shahmalak, A., Gilhar, A., Lim, X., et al. (2018). Identifying novel strategies for treating human hair loss disorders: cyclosporine a suppresses the Wnt inhibitor, SFRP1, in the dermal papilla of human scalp hair follicles[J]. *PLoS Biol.* 16:e2003705.

He, Q. Q., Yan, D., Dong, W., Bi, J. M., Huang, L. F., Yang, M. H., et al. (2020). circRNA circFUT8 upregulates Krüpple-like factor10 to inhibit the metastasis of bladder cancer via sponging miR-570-3p. *Mol. Ther. Oncolytics* 16, 172–187.

Kelly, S., Greenman, C., Cook, P. R., and Papantonis, A. (2015). Exon skipping is correlated with exon circularization. *J. Mol. Biol.* 427, 2414–2417. doi: 10.1016/j.jmb.2015.02.018

Krieger, K., Millar, S. E., Mikuda, N., Krahn, I., Kloepper, J. E., Bertolini, M., et al. (2018). NF-kappa B participates in mouse hair cycle control and plays distinct roles in the various pelage hair follicle. *J. Invest. Dermatol.* 138, 256–264. doi: 10.1016/j.jid.2017.08.042

Li, B. J., Yin, D., Li, P. H., Zhang, Z. K., Zhang, X. Y., Li, H. Q., et al. (2020). Profiling and functional analysis of circular RNAs in porcine fast and slow muscles. *Front. Cell Dev. Biol.* 8:322. doi: 10.3389/fcell.2020.00322

Li, G. Q., Ji, Y. C., and Li, Y. (2004). Molecular mechanism of hair follicle morphogenesis. *Foreign Med. Dermatol. Venereol.* 30, 38–40.

Lin, M. H., Leimeister, C., Gessler, M., and Kopan, R. (2000). Activation of the Notch pathway in the hair cortex leads to aberrant differentiation of the adjacent hair-shaft layers. *Development* 127, 2421–2432. doi: 10.1242/dev.127.11.2421

Liu, G. Y., Li, S., Liu, H. L., Zhu, Y. L., Bai, L. Y., Sun, H. T., et al. (2020). The functions of ocu-miR-205 in regulating hair follicle development in Rex rabbits. *BMC Dev. Biol.* 20:8. doi: 10.1186/s12861-020-00213-5

Liu, Y. X. (2019). *Molecular Mechanism of circna3669 as Cerna in Regulating Apoptosis of Endometrial Epithelial Cells in Dairy Goats*. Xianyang: Northwest agricultural and Forestry University.

Liu, Z. H., Xiao, H. M., Li, H. P., Zhao, Y. H., Lai, S. Y., Yu, X. L., et al. (2012). Identification of conserved and novel microRNAs in cashmere goat skin by deep sequencing[J]. *PLoS One* 7:e50001. doi: 10.1371/journal.pone.0050001

Lv, X. Y., Gao, W., Jin, C. Y., Wang, L. H., Wang, Y., Chen, W. H., et al. (2019). Preliminary study on microR-148a and microR-10a in dermal papilla cells of Hu sheep[J]. *BMC Genet.* 20:70. doi: 10.1186/s12863-019-0770-8

Ma, T., Li, J. Y., Li, J. P., Wu, S. F., Xiang, B., Jiang, H. Z., et al. (2021). Expression of miRNA-203 and its target gene in hair follicle cycle development of Cashmere goat[J]. *Cell Cycle* 20, 204–210. doi: 10.1080/15384101.2020.1867789

McMahon, A. P., Ingham, P. W., and Tabin, C. J. (2003). Developmental roses and clinical significance of hedgehog signaling. *Curr. Top. Dev. Biol.* 53, 1–114. doi: 10.1016/s0070-2153(03)53002-2

Memczak, S., Jens, M., Elefsinioti, A., Torti, F., Krueger, J., and Rybak, A. (2013). Circular RNAs are a large class of animal RNAs with regulatory potency. *Nature* 495, 333–338. doi: 10.1038/nature11928

Milla, S. E. (2002). Molecular mechanisms regulating hair follicle development Investiga-tive. *Dernatology* 118, 216–225. doi: 10.1046/j.0022-202x.2001.01670.x

Millar, S. E., Willert, K., Salinas, P. C., Roelink, H., Nusse, R., Sussman, D. J., et al. (1999). signaling in the control of hair growth and structure. *Dev. Biol.* 207, 133–149. doi: 10.1006/dbio.1998.9140

Mo, W. L., Jiang, J. T., Zhang, L., Lu, Q. C., Li, J., Gu, W. D., et al. (2020). Circular RNA hsa_circ_0000467 promotes the development of gastric cancer by competitively binding to MicroRNA miR-326-3p. *BioMed. Res. Int.* 2020:4030826.

Ogata, H., Goto, S., Sato, K., Fujibuchi, W., Bono, H., and Kanehisa, M. (1999). KEGG: kyoto encyclopedia of genes and genomes. *Nucleic Acids Res.* 27, 29–34.

Salmena, L., Poliseno, L., Tay, Y., Kats, L., and Pandolfi, P. P. (2011). A ceRNA hypothesis:the rosetta stone of a hidden RNA language? *Cell* 146, 353–358. doi: 10.1016/j.cell.2011.07.014

Schmidt-Ullrich, R., Tobin, D. J., Lenhard, D., Paus, R., and Scheidereit, C. (2006). NF-kappaB transmits Eda A1/EdaR signalling to activate Shh and cyclin D1 expression, and controls post-initiation hair placode down growth. *Development* 133, 1045–1057. doi: 10.1242/dev.02278

Schmittgen, T. D., and Livak, K. J. (2008). Analyzing real-time PCR data by the comparative CT method. *Nat. Protoc.* 3, 1101–1108. doi: 10.1038/nprot.2008.73

Shannon, P., Markiel, A., and Ozier, O. (2003). Cytoscape: a software environment for integrated models of biomolecular interaction networks. *Genome Res.* 13, 2498–2504. doi: 10.1101/gr.1239303

Shen, M. M., Li, T. T., Chen, F. X., Wu, P. F., Wang, Y., Chen, L., et al. (2020). Transcriptomic analysis of circRNAs and mRNAs reveals a complex regulatory network that participate in follicular development in chickens[J]. *Front. Genet.* 11:503. doi: 10.3389/fgene.2020.00503

Sun, W., Julie, L. Y., Huang, H. D., Shyy, J. Y. J., and Chien, S. (2010). microRNA:a master regulator of cellular processes for bioengineering systems. *Ann. Rev. Biomed. Eng.* 12, 1–27. doi: 10.1146/annurev-bioeng-070909-105314

Thomadakis, G., Ramoshebi, L. N., Crooks, J., Rueger, D. C., and Ripamonti, U. (1999). Immunolocalization of bone morphogenetic protein-2 and -3 and osteogenic protein-1 during murine tooth root morphogenesis and in other craniofacial structures. *Eur. J. Oral. Sci.* 107, 368–377. doi: 10.1046/j.0909-8836.1999.eos107508.x

Ullrich, R., and Paus, R. (2005). Molecular principles of hair follicle induction and morphogenesis. *BioEssays* 27, 247–261. doi: 10.1002/bies.20184

Wang, D. Y., Chen, Z. J., Zhuang, X. N., Luo, J. Y., Chen, T., Xi, Q. Y., et al. (2020). Identifification of circRNA-associated-ceRNA networks involved in milk fat metabolism under heat stress. *Int. J. Mol. Sci.* 21:4162. doi: 10.3390/ijms21114162

Wang, G. P., Guo, X. Q., Cheng, L. Y., Chu, P. P., Chen, M., Chen, Y. H., et al. (2019). An integrated analysis of the circRNA-miRNA-mRNA network reveals novel insights into potential mechanisms of cell proliferation during liver regeneration. *Artif. Cells Nanomed. Biotechnol.* 47, 3873–3884. doi: 10.1080/21691401.2019.1669623

Wang, S. H., Ge, W., Luo, Z. X., Guo, Y., Qu, L., Zhang, Z. Y., et al. (2017). Integrated analysis of coding genes and non-coding RNAs during hair follicle cycle of cashmere goat (*Capra hircus*). *BMC Genomics* 18:767. doi: 10.1186/s12864-017-4145-0

Wei, X. F. (2017). *Mechanism of miR-378a-3p, miR-107 and Related Circrna Regulating Bovine Myocyte Development*. Xianyang: Northwest A & F University.

Westholm, J. O., Miura, P., Olson, S., Shenker, S., Joseph, B., Sanfilippo, P., et al. (2014). Genome-wide analysis of drosophila circular RNAs reveals their structural and sequence properties and age-dependent neural accumulation. *Cell Rep.* 9, 1966–1980. doi: 10.1016/j.celrep.2014.10.062

William, R. J., and Norman, E. S. (2014). Detecting and characterizing circular RNAs. *Nat. Biotechnol.* 32, 453–461. doi: 10.1038/nbt.2890

Xu, Z. H., Li, P. Y., Fan, L., and Wu, M. H. (2018). The potential role of circRNA in tumor immunity regulation and immunotherapy. *Front. Immunol.* 22:9. doi: 10.3389/fimmu.2018.00009

Yin, R. H., Zhao, S. J., Wang, Z. Y., Zhu, Y. B., Yin, R. L., Bai, M., et al. (2020). LncRNA-599547 contributes the inductive property of dermal papilla cells in cashmere goat through miR-15b-5p/Wnt10b axis[J]. *Anim. Biotechnol.* 18, 1–15. doi: 10.1080/10495398.2020.1806860

You, X. T., Vlatkovic, I., Babic, I., Will, T., Epstein, I., Tushev, G., et al. (2015). Neural circular RNAs are derived from synaptic genes and regulated by development and plasticity. *Nat. Neurosci.* 18, 603–610. doi: 10.1038/nn.3975

Yuan, C., Wang, X. L., Geng, R. Q., He, X. L., Qu, L., and Chen, Y. L. (2013). Discovery of cashmere goat (*Capra hircus*) microRNAs in skin and hair follicles by Solexa sequence -ing. *BMC Genomics* 14:511.

Zhang, M., Ma, L., Liu, Y. H., He, Y. L., Li, G., An, X. P., et al. (2020). CircRNA-006258 sponge-adsorbs miR-574-5p to regulate cell growth and milk synthesis via EVI5L in goat mammary epithelial cells.[J]. *Genes (Basel)* 11:718. doi: 10.3390/genes11070718

Zhang, X. O., Wang, H. B., Zhang, Y., Lu, X. H., Chen, L. L., and Li, Y. (2014). Complementary sequence mediated exon circularization. *Cell* 159, 134–147. doi: 10.1016/j.cell.2014.09.001

Zhang, Y., Zhang, X. O., Tian, C., Xiang, J. F., Yin, Q. F., Xing, Y. H., et al. (2013). Circular intronic long noncoding RNAs. *Mol cell* 51, 792–806. doi: 10.1016/j.molcel.2013.08.017

Zhang, Y. H., Tomann, P., Andl, T., Gallant, N. M., Huelsken, J., Jerchow, B., et al. (2009). Reciprocal requirements for EDA/EDAR/NF-kappa B and Wnt/b-catenin signaling pathways in hair follicle induction. *Dev Cell.* 17, 49–61. doi: 10.1016/j.devcel.2009.05.011

Zhang, Y. J., Yin, J., Li, C. Q., and Li, J. Q. (2006). Study on the occurrence and development of hair follicles in fetal period of inner mongolia albas cashmere goat. *J. Anim. Husbandry Vet. Med.* 37, 761–768.

Zhang, Y. J., Yin, J., Li, J. Q., and Li, C. Q. (2007). Study on the structure and morphogenesis of cashmere follicles in Albas cashmere goats, Inner Mongolia. *Chin. J. Agric. Sci.* 40, 1017–1023.

Zhang, Z. Z. (2018). *Molecular Mechanism of miR-103 Regulating Adipose Development by Binding circRNAs*. Xianyang: Northwest A & F University.

Zhao, B. H., Chen, Y., Hu, S. S., Yang, N. S., Wang, M. M., Liu, M., et al. (2019). Systematic analysis of non-coding RNAs involved in the angora rabbit (*Oryctolagus cuniculus*) hair follicle cycle by RNA sequencing. *Front. Genet.* 10:407. doi: 10.3389/fgene.2019.00407

Zhao, J., Yang, X. W., Li, J. T., Wang, Q., Wang, L., and Wang, G. T. (2019). Construction and functional enrichment analysis of circrna miRNA mRNA regulatory network in hepatocellular carcinoma based on high-throughput sequencing. *Jo. Clin. Hepatobiliary Dis.* 35, 1740–1744.

Zheng, Y. Y., Wang, Z. Y., Zhu, Y. B., Wang, W., Bai, M., Jiao, Q., et al. (2019). LncRNA-000133 from secondary hair follicle of Cashmere goat: identification, regulatory network and its effects on inductive property of dermal papilla cells. *Anim. Biotechnol.* 31, 122–134. doi: 10.1080/10495398.2018.1553788

Zhou, G. X. (2018). *Screening of Key Genes of Secondary Hair Follicle cycle Cycle in Northern Shaanxi White Cashmere Goat and Functional Verification of Lhx2 and miR-144*. Xianyang: Northwest A & F University.

Zhou, G. X., Kang, D. J., Ma, S., Wang, X. T., Gao, Y., Yang, Y. X., et al. (2018). Integrative analysis reveal sncRNA-mediated molecular

regulatory network driving secondary hair follicle regression in cashmere goats. *BMC Genomics* 19:222. doi: 10.1186/s12864-018-4603-3

Zhou, X. B. (2016). *Optimization of Culture Medium Composition of Secondary Dermal Papilla Cells of Shanbei White Cashmere Goat and the effect of miR-206 on it Regulation research*. Xianyang: Northwest A & F University.

Zong, Z. H., Liu, Y., Chen, S., and Zhao, Y. (2020). Circ_PUM1 promotes the development of endometrial cancer by targeting the miR-136/NOTCH3 pathway. *J. Cell. Mol. Med.* 24, 4127–4135. doi: 10.1111/jcmm.15069

Conflict of Interest: The authors declare that the research was conducted in the absence of any commercial or financial relationships that could be construed as a potential conflict of interest.

frontiers in Genetics

ORIGINAL RESEARCH
published: 15 June 2021
doi: 10.3389/fgene.2021.675305

Ovine *FABP4* Variation and Its Association With Flystrike Susceptibility

*L. E. R. Burrows[1], H. Zhou[1], C. M. A. Frampton[2], R. H. J. Forrest[3] and J. G. H. Hickford[1]**

[1] Gene-Marker Laboratory, Faculty of Agriculture and Life Sciences, Lincoln University, Christchurch, New Zealand, [2] Department of Medicine, University of Otago, Christchurch, New Zealand, [3] Faculty of Education Humanities and Health Science, Eastern Institute of Technology, Napier, New Zealand

Flystrike is a major cost and a welfare issue for the New Zealand sheep industry. There are several factors that can predispose sheep to flystrike, such as having fleecerot, a urine-stained breech, and "dags" (an accumulation of fecal matter in the wool of the breech). The FABP4 gene (*FABP4*) has been associated with variation in ovine fleecerot resistance, with a strong genetic correlation existing between fleecerot and flystrike occurrence. In this study, blood samples were collected from sheep with and without flystrike for DNA typing. PCR-SSCP analyses were used to genotype two regions of ovine *FABP4*. Sheep with the A_1 variant of *FABP4* were found to be less likely (odds ratio 0.689, $P = 0.014$) to have flystrike than those without A_1. The likelihood of flystrike occurrence decreased as copy number of A_1 increased (odds ratio 0.695, $P = 0.006$). This suggests that *FABP4* might be a candidate gene for flystrike resilience in sheep, although further research is required to verify this association.

Keywords: *FABP4*, flystrike, PCR-SSCP, variation, sheep

OPEN ACCESS

Edited by:
Rui Su,
Inner Mongolia Agricultural University, China

Reviewed by:
Xianyong Lan,
Northwest A&F University, China
João Gouveia,
Universidade Federal do Vale do São Francisco, Brazil
Hegang Li,
Qingdao Agricultural University, China

****Correspondence:***
J. G. H. Hickford
Jonathan.Hickford@lincoln.ac.nz

Specialty section:
This article was submitted to Livestock Genomics, a section of the journal Frontiers in Genetics

Received: *02 March 2021*
Accepted: *24 May 2021*
Published: *15 June 2021*

Citation:
Burrows LER, Zhou H, Frampton CMA, Forrest RHJ and Hickford JGH (2021) Ovine FABP4 Variation and Its Association With Flystrike Susceptibility. Front. Genet. 12:675305. doi: 10.3389/fgene.2021.675305

INTRODUCTION

The breeding of sheep that are less susceptible to flystrike is an attractive proposition for reducing its impact on sheep production. If genetic variation associated with decreased susceptibility to flystrike could be identified, then this might provide greater accuracy for making breeding selections to reduce the prevalence of the disease.

In 2010, a single-nucleotide polymorphism (SNP) association study was undertaken by Smith et al. (2010) on sheep from the fleecerot and flystrike resistant and susceptible flocks in Australia. Among the genes identified as potentially being associated with fleecerot susceptibility was the fatty-acid binding protein 4 (FABP4) gene (*FABP4*). Given that fleecerot has been identified as an important predisposing factor to flystrike (Norris et al., 2008) and that a study by Raadsma (1991) reported a strong genetic correlation ($r > 0.9$) between the two conditions, there is justification for testing whether *FABP4* is also associated with the occurrence of flystrike.

The fatty-acid binding proteins are hydrophobic ligand-binding cytoplasmic proteins, and are thought to be involved in lipid metabolism through the binding and intracellular transport of long-chain fatty-acids (Furuhashi and Hotamisligil, 2008; Tsuda et al., 2009). Expression of *FABP4* has been reported in adipocytes and macrophages (Furuhashi and Hotamisligil, 2008). In skin, FABP4 has been shown to be localized in the sebaceous glands (Watanabe et al., 1997), and it has

been suggested to regulate their activity by modulating lipid-signaling and/or lipid metabolism in sebocytes (Lin and Khnykin, 2014).

Tsuda et al. (2009) revealed that *FABP4* was strongly expressed in phosphatase-and-tensin (*Pten*)-null keratinocytes. In this context, FABP4 has been suggested to selectively enhance the activities of peroxisome proliferator-activated receptor gamma (PPARγ), a member of the nuclear hormone receptor family, and one that regulates genes involved in sebaceous tissue differentiation (Michalik and Wahli, 2007). Keratinocyte-specific *Pten*-null mice display distinct phenotypes, which includes having wrinkled skin and ruffled and shaggy hair. Histological examination revealed that these mice had acanthosis, sebaceous gland hyperplasia, and accelerated hair follicle morphogenesis (Suzuki et al., 2003). The gene, *FABP4*, is therefore implicated in the development of these phenotypes. Given the loss of waxes and hydrophobicity is thought to be a major contributing factor in the development of fleecerot (Norris et al., 2008), then *FABP4* variation may also affect flystrike susceptibility in sheep. Furthermore, the FABP4 protein is also released from adipocytes and macrophages, and it is a proinflammatory signaling protein, with the level of FABP4 protein increasing in the blood of people with the skin inflammatory condition psoriasis (Baran et al., 2017). Inflammation is observed in skin tissues affected by fleece rot.

Yan et al. (2012) studied sequence variation in two regions of *FABP4*. In the first, which spanned parts of exon 2 and intron 2, five unique sequences were observed. These variants were a consequence of three nucleotide substitutions and one nucleotide deletion in intron 2. In the second region of the gene, which spanned parts of exon 3 and intron 3, four different sequences were detected, which come about as a consequence of four nucleotide substitutions.

To ascertain whether variation in *FABP4* is associated with variation in susceptibility to flystrike in New Zealand (NZ) sheep, animals with and without flystrike were identified at shearing time. Genetic variation within *FABP4* was analyzed using PCR-SSCP analyses, and associations with the occurrence of fleecerot and flystrike explored. Any association identified might provide a better understanding of biological role of *FABP4* in variation in susceptibility to flystrike.

MATERIALS AND METHODS

Sheep Studied and Identification of Flystrike

Eight-hundred and fourty-four sheep were studied in total. Of these, 441 either had flystrike or were recovering from flystrike. Sheep were diagnosed as having active flystrike when larvae could be seen on the skin, and the wool was discolored and bad smelling. Sheep that had had flystrike were identified through having areas of pink skin with no wool or shorter wool, evidence of scar tissue from maggot damage, or flaky dry skin. Where possible, for each sheep found with flystrike, another sheep from the same flock, but that had no evidence of flystrike was also chosen (n = 403). The sheep were identified over a period of 5 years (2013–2017) from both commercial and stud farms from six geographical regions and were of 20 different breeds or composites there-of.

Blood Collection

Blood samples from the sheep were collected onto FTA cards (Whatman, Middlesex, United Kingdom) and these were labeled with year, farm, breed, gender, age, and the presence (n = 441) or absence (n = 403) of flystrike as specified above. The blood was left to dry and then stored in darkness at room temperature. DNA stored in this way is suitable for subsequent analysis (Dash et al., 2020), and for genotyping the DNA was purified according to the method of Zhou et al. (2006).

FABP4 Genotyping

The genotypes for Region-1 and -2 of *FABP4* were determined according to the methods described in Yan et al. (2012). Primers were synthesized by Integrated DNA Technologies (Coralville, IA, United States). All 844 sheep were genotyped for Region-1, while 582 were genotyped for Region 2 (n = 291 with flystrike).

Statistical Analyses

All statistical analyses were performed using IBM SPSS Statistics version 24 (Chicago, IL, United States).

For both *FABP4* regions, the presence or absence of a sequence variant in each genotype was coded with a 1 or 0, respectively. For inclusion in statistical models, some variables and/or categories within variables were combined due to there being small numbers in some groups. Age and gender were merged into a single variable (age_gender) which had the following categories: animals under 2 years of age (gender was not known), 2 year-old ewes, 3 + year-old ewes, 2 year-old rams, and 3 + year-old rams. Sheep breed was compressed into four categories: black-face/terminal sheep (n = 173; Dorset Down + Finn x Texel Cross + Poll Dorset + Shropshire + South Down + South Suffolk + Texel + other Suffolk-crosses), Merino and Merino-cross sheep (n = 303; Merino + Corriedale + other Merino crosses), maternal cross-bred sheep (n = 236; Coopworth + Corriedale x Romney-cross + Perendale-cross + unspecified cross + Romney-cross + other composite maternal sheep) and pure-bred maternal sheep (n = 132; Romney + Perendale + Lincoln). The six geographical regions (Banks Peninsula, Mid-Canterbury, Northland, North Canterbury, Otago and South Canterbury) were combined into three general locations: mid-Canterbury, districts north of mid-Canterbury and districts south of mid-Canterbury.

Univariate Pearson Chi-square tests were then performed to explore the association between these variables: year (recognizing there is likely to be annual variation in flystrike occurrence), age_gender (recognizing there are likely to sheep age and gender effects on flystrike occurrence), breed (recognizing there may be breed effects in flystrike occurrence), and location (recognizing potential regional differences in flystrike occurrence), and the presence or absence of flystrike.

For each *FABP4* variant from the two regions of the gene, a Pearson Chi-squared test along with a binary logistic regression was performed to explore whether the presence or absence of the variant was associated with the presence or absence of flystrike, and to determine an odds-ratio (OR). If an association was detected, a subsequent binary logistic regression analysis was performed to determine the independent effects of the gene variants on the incidence of flystrike when year, breed, location, and age-gender were taken into account. A copy-number analysis was also performed in which the presence or absence of the variant was replaced with number of copies of the variant (0, 1, or 2) in the binary logistic regression models.

RESULTS

Sequence Variation in FABP4

The previously described A_1, B_1, C_1 and D_1 variants (exon 2—intron 2; Region-1) and A_2, B_2, and C_2 variants (exon 3-intron 3; Region-2) of *FABP4* (Yan et al., 2012) were identified. The E_1 (Region-1) and D_2 (Region-2) variants (Yan et al., 2012) were not detected in the sheep studied here. The sequence variation in the regions typed could, in part, be matched to the findings of Smith et al. (2010) with the SNPs c.348 + 166T > C, c.348 + 298T > C, and c.348 + 356T > C in Region-2 of *FABP4*, corresponding to FABIn30227, FABIn30360, and FABIn30420 respectively, defined in that study.

FABP4 Associations

The frequency of flystrike occurrence for sheep with different *FABP4* variants from each region of the gene, is shown in **Table 1**.

The results of the univariate analyses exploring the effect of the different independent effects on associations between the presence or absence of each *FABP4* Region-1 variant and flystrike presence and absence are shown in **Table 2**. Associations existed for each variable with at least one of the variants, and thus all the variables were retained in the subsequent multivariate analyses. The univariate Pearson chi-squared analyses to explore the association between the variables and the occurrence of flystrike detected no association for location ($P = 0.545$), year ($P = 0.132$), or breed ($P = 0.050$), but an association was detected with age_gender ($P < 0.001$). Only the association with age-gender persisted in the multivariate binary logistic models for each *FABP4* Region-1.

The presence of *FABP4* A_1 was found to be associated with a lower likelihood of flystrike (OR = 0.651, $P = 0.003$), which persisted when correcting for the effect of age_gender, breed, location and year (OR = 0.689, $P = 0.014$), while the presence of C_1 appeared to possibly be linked to an increased likelihood of flystrike (OR = 1.267, $P = 0.095$) in the chi-square, but this was lost when corrected for the other effects (**Table 3**).

The copy number analysis (correcting for year, breed classification, location, and age-gender) for *FABP4* A_1 revealed there was a 30.5% reduction in flystrike for each additional copy of *FABP4* A_1 (OR = 0.695, $P = 0.006$).

No associations between the occurrence of flystrike and the variants of *FABP4* Region-2 were detected (**Table 4**).

DISCUSSION

Smith et al. (2010) identified five SNPs in ovine *FABP4* from Merino sheep that are associated with fleecerot. Three of these SNPs were also identified by Yan et al. (2012, 2018) and in this study too. In Region-1, Yan et al. (2012) detected five variant sequences of *FABP4* (named A_1 -E_1) and four variant sequences (A_2-D_2) for Region-2 in 483 NZ sheep of various breeds. Variants A_1, B_1 and C_1 were the most common and observed in all breeds. Variant D_1 was observed in all the breeds except Poll Dorset sheep and E_1 was only observed in two breeds (Poll Dorset and Corriedale). In this study four of the *FABP4* Region-1 variants were detected (A_1-D_1), with E_1 not being found. More recently, Yan et al. (2018) reported the five previously identified Region-1 variants (A_1, B_1, C_1, D_1 and E_1) and three previously identified Region-2 variants (A_2, B_2 and C_2) were detected in NZ Romney sheep, describing fourteen different haplotypes spanning the two regions: A_1-A_2, A_1-B_2, A_1-C_2, B_1-A_2, C_1-A_2, C_1-C_2, D_1-A_2, B_1-B_2, C_1-B_2, D_1-C_2, E_1-B_2, E_1-A_2, D_1-B_2 and B_1-C_2.

In the context of the observed associations with Region-1 variant A_1 in this study, it must, therefore, be noted that A_1 could potentially be present in the sheep studied in one of three haplotypes across these two regions (A_1-A_2, A_1-B_2, and A_1-C_2), although the haplotypes were not established here as that require nucleotide sequencing of all 844 sheep. Variant C_1 was also found in three haplotypes (C_1-A_2, C_1-C_2, and C_1-B_2) by Yan et al. (2018), albeit in different breeds. Variants A_2 and B_2 occurred in haplotypes with all five Region-1 variants, and C_2 with all except E_1 (Yan et al., 2018). It is therefore not surprising that associations were not detected with Region-2 of the gene and future research focused on association studies using haplotypes is merited.

The SNPs described in *FABP4* in this study were all found in introns. Although introns do not code for amino acids, some SNPs in introns, silent substitutions in coding sequences and variation in regions flanking coding sequences can have a functional role, and/or affect gene expression. For example, SNPs in introns have been reported to affect primary transcript splicing efficiency, the stability of mRNA, and the translation of mRNA (Le Hir et al., 2003); and silent substitutions in coding regions (typically in position three of the codon) have also been shown to affect mRNA stability and pre-mRNA splicing (Duan et al., 2003; Supek et al., 2014). The *FABP4* SNPs identified do not fall into any known RNA splicing sites, however, they may be linked to sequence variation in other regions of *FABP4* that is of structural or functional importance. This has also been suggested by Smith et al. (2010) and Yan et al. (2012, 2018).

Given that the aim of this study was to determine if there was an association between the presence of flystrike and variation in ovine *FABP4*, then it is notable that sheep with the A_1 variant were less likely to have flystrike than those without A_1. It is, however, impossible to say if any given sheep carrying the A_1 variant will, or will not get flystrike, as some sheep in this study carrying A_1 also had flystrike and some sheep carrying two copies of A_1 were also struck, with them accounting for 2.5% of the struck genotypes. It must be remembered in this context that the analyses are only finding associations rather than causative mutations.

TABLE 1 | Frequencies of flystrike in sheep with *FABP4* Region-1 and Region-2 variants.

Variant	Number of sheep with variant*	Number of sheep with variant and flystrike	Frequency of flystrike in animals with variant (%)
Region-1	(844 sheep in total)		
A_1	314	143	46
B_1	483	257	53
C_1	521	284	55
D_1	94	48	51
Region-2	(582 sheep in total)		
A_2	489	246	50
B_2	278	147	53
C_2	19	9	47

**Includes heterozygous and homozygous sheep.*

TABLE 2 | *P*-values[a] from Pearson Chi-square analyses exploring associations between the variables, each *FABP4* Region-1 variant and flystrike occurrence.

Variable	*FABP4* Region-1 variants				Flystrike
	A_1	B_1	C_1	D_1	
Age_gender	**0.001**	0.782	0.232	0.215	**<0.001**
Breed	**<0.001**	0.535	**0.004**	0.332	**0.050**
Location	0.584	0.406	**0.002**	0.635	0.545
Year	**0.001**	**<0.001**	**<0.001**	0.868	0.132

[a] *$P \leq 0.05$ in bold.*

TABLE 3 | The association of the presence of each *FABP4* Region-1 variant with the occurrence of flystrike given the presence of a particular *FABP4* Region-1 variant.

Statistical model	Variant	Odds ratio	95% confidence interval		*P*-value[a]
			Upper	Lower	
Pearson Chi-square, Binary logistic regression analysis: Dependent variable = the presence or absence of flystrike; independent variable = the presence or absence of the gene variant.	A_1	0.651	0.492	0.862	**0.003**
	B_1	1.094	0.833	1.437	0.519
	C_1	1.267	0.959	1.673	0.095
	D_1	0.948	0.617	1.456	0.807
Binary logistic regression: dependent variable = the presence or absence of flystrike; independent variables = the presence or absence of the gene variant, year, breed, location, and the combined age_gender variable.	A_1	0.689	0.512	0.927	**0.014**
	B_1	1.110	0.832	1.480	0.478
	C_1	1.209	0.899	1.625	0.210
	D_1	1.001	0.638	1.570	0.996

[a] *$P \leq 0.05$ in bold.*

TABLE 4 | The association of the presence of each *FABP4* Region-2 variant with the occurrence of flystrike given the presence of a particular *FABP4* Region-2 variant.

Statistical model	Variant	Odds ratio	95% confidence interval		*P*-value
			Upper	Lower	
Pearson Chi-square, Binary logistic regression analysis: Dependent variable = the presence or absence of flystrike; independent variable = presence or absence of the gene variant.	A_2	1.080	0.693	1.683	0.734
	B_2	1.247	0.900	1.727	0.184
	C_2	0.897	0.359	2.240	0.816
Binary logistic regression: dependent variable = the presence or absence of flystrike; independent variables = the presence or absence of the gene variant, year, breed, location, and the combined age_gender variable.	A_2	1.100	0.687	1.762	0.691
	B_2	1.161	0.814	1.655	0.409
	C_2	1.075	0.402	2.872	0.886

The first associations between SNPs in or near *FABP4*, and fleecerot, were described by Smith et al. (2010). However, given there is a high genetic correlation ($r > 0.9$) between fleecerot and flystrike, it is perhaps not that surprising that an association has been found with flystrike susceptibility. The susceptibility of sheep to fleecerot and flystrike can also be assessed through

the measurement of indicator traits, including assessment of physical characteristics and chemical characteristics. In the context of the latter, wax and suint levels affect the wettability of the wool (Belschner, 1937; Norris et al., 2008), and thus susceptibility to disease. In fine wool sheep, bright (high luster), high yielding (but greasy) wool, which is white in color, is the most consistent wool type associated with fleecerot resistance, and wool of this type is highly heritable (Hayman, 1953; James et al., 1984; Raadsma, 1987). Fiber diameter is another highly heritable trait that has been associated with resistance to fleecerot (Raadsma, 1993), with a lower fiber diameter resulting in a greater resistance in Merino sheep (James and Ponzoni, 1992). Given these observations, the wax levels in the wool are possibly influenced by FABP4, and this could explain why variation in *FABP4* appears to be associated with fleecerot and flystrike resilience. In this context, exploring the relationship between *FABP4* expression and wool wax levels, along with other wool traits, could shed light on FABP4's role in flystrike resilience, although it has been reported that the phenotypic correlations between fleecerot, flystrike and other fleece characteristics, are typically low (Raadsma, 1987).

Bakhtiarizadeh et al. (2013) used Lori-Bakhtiari and Zel sheep to investigate the differences in *FABP4* expression in fat-tail tissue and visceral adipose tissue. Their results suggested that the expression of *FABP4* was higher in the fat-tail of Lori-Bakhtiari sheep, than expression in either the fat-tail or visceral tissue of the Zel sheep. The higher level of expression of *FABP4* in the fat-tail tissue of Lori-Bakhtiari sheep was related to there being more fatty-acid transportation into the fat-tail compared with the Zel sheep. If fat is a factor that affects flystrike resilience in sheep, then increased expression of *FABP4*, leading to more fatty-acid transport into different areas of the body could be an underlying mechanism for the variation in resilience. It would be interesting to look at the frequency of *FABP4* variants A_1-E_1 in Lori-Bakhtiari and Zel sheep to see if they have a higher frequency of the A_1 variant, especially as this variant has also been found to occur at a high frequency in a line of sheep that were deliberately bred for increased fatness (Yan et al., 2012). The Lori-Bakhtiari and Zel sheep could also be investigated to ascertain their resilience to flystrike in the context of *FABP4* variation.

Yan et al. (2012) found a vast difference between fat and lean lines of sheep and variation in *FABP4*. Sheep carrying the *FABP4* A_1 variant were predominantly in the fat line, while sheep carrying the C_1 variant was associated with the lean line. In the present study, sheep with the A_1 variant were the least likely to get flystrike. While the level of expression (if any) of this variant was not ascertained in either study, it might nevertheless speculated that sheep with a higher carcass fat content, may also have an increased or different lipid content in their wool. Wool wax contains fatty acids, and these coat the wool fibers and skin, where they inhibit bacterial growth by lowering the pH of the skin surface (Lambers et al., 2006). It might, therefore, be worthwhile, to investigate whether *FABP4* affects wool wax production (qualitatively and quantitatively) and whether this affects the likelihood of fleecerot and/or flystrike occurring. However, if the *FABP4* A_1 variant decreases flystrike susceptibility and increases the fat content in meat, then farmers would have to decide if they want to selectively breed sheep for both these traits. This could cause conflict with consumer demand for healthier sheep that produce leaner meat. In some markets, the current consumer demand is for leaner meat due to the common perception that fat is linked to obesity and cardiovascular disease (Volk, 2007; Pethick et al., 2011), and this demand is met by producing leaner slaughter animals on-farm (Pethick et al., 2011).

Fatty acid-binding protein 4 has also been shown to modulate inflammatory responses in macrophages (Furuhashi and Hotamisligil, 2008). In macrophages lacking FABP4 (*FABP4 -/-)* there are several signaling pathways that are suppressed, including the production of cytokines such as tumor-necrosis factor –α (TNF-α), interleukin 1 β (IL β) and IL6 (Makowski et al., 2005; Furuhashi and Hotamisligil, 2008). It is of interest that inflammatory cytokines and T cell-dependent cytokine IL-2 and IFN–γ are produced in the skin during flystrike (Bowles et al., 1994). FABP4 also acts to coordinate functional interactions between macrophages and adipocytes in the adipose tissue (Furuhashi and Hotamisligil, 2008). The adipocytes sit near the skin surface, thus these cells could play a role in the inflammatory response to flystrike in the skin. The "fatter" type sheep, as shown by Yan et al. (2012) to have a high frequency of A_1 variant, may therefore have greater resilience to flystrike by having an improved inflammatory response.

While the results of this study suggest that variation in *FABP4* might be used as a gene-marker for flystrike resilience in sheep and that breeding for sheep that carry the A_1 variant may decrease disease prevalence, the pleiotropic nature of the gene, including its potential effect on other important production traits, suggests considerably more research needs to be undertaken.

DATA AVAILABILITY STATEMENT

The raw data supporting the conclusions of this article will be made available by the authors, without undue reservation.

ETHICS STATEMENT

Ethical review and approval was not required for the animal study because the research we undertook was retrospective/observational (not experimental), with the animals analyzed being located on private farms where they are part of commercial sheep farming operations. They were not part of experimental flocks, and the flocks were not structured, or created for experimental purposes. The blood collection approach we employed falls within the allowable practices specified in Section 7.5 Animal Identification of the Animal Welfare (Sheep and Beef Cattle) Code of Welfare 2010, which is a code of welfare issued under the Animal Welfare Act 1999 (New Zealand Government).

AUTHOR CONTRIBUTIONS

HZ and JH contributed to conception and design of the study. LB collected the data, organized the database, performed the experiments, and wrote the first draft of the manuscript. LB, CF, and RF performed the statistical analysis. HZ, RF, and JH contributed to the manuscript revision. All authors read and approved the submitted version.

REFERENCES

Bakhtiarizadeh, M. R., Moradi-Shahrbabak, M., and Ebranhimie, E. (2013). Underlying functional genomics of fat deposition in adipose tissue. *Gene* 521, 122–128. doi: 10.1016/j.gene.2013.03.045

Baran, A., Świderska, M., Bacharewicz-Szczerbicka, J., Myśliwiec, H., and Flisia, I. (2017). Serum fatty acid-binding protein 4 is increased in patients with psoriasis. *Lipids* 52, 51–60. doi: 10.1007/s11745-016-4211-4

Belschner, H. G. (1937). Studies of the sheep blowfly problem. II. Observations on fleece rot and body strike in sheep, particularly in regards to their incidence, type of sheep susceptible, and economic importance. *Sci. Bull.* 54, 61–95.

Bowles, V. M., Meeusen, E. N. T., Chandler, K., Verhagen, A., Nash, A. D., and Brandon, M. R. (1994). The immune response of sheep infected with larvae of the sheep blowfly Lucilia cuprina monitored via efferent lymph. *Vet. Immunol. Immunopathol.* 40, 341–352. doi: 10.1016/0165-2427(94)90044-2

Dash, H. R., Shrivastava, P., and Das, S. (2020). *Reliable Use of Whatman^{TM} FTA^{TM} Cards for One-Step Collection and Isolation of DNA. In: Principles and Practices of DNA Analysis: A Laboratory Manual for Forensic DNA Typing*. New York: Springer.

Duan, J., Wainwright, M. S., Comeron, J. M., Saitou, N., Sanders, A. R., Gelernter, J., et al. (2003). Synonymous mutations in the human dopamine receptor D2 (DRD2) affect mRNA stability and synthesis of the receptor. *Hum. Mol. Genet.* 12, 205–216. doi: 10.1093/hmg/ddg055

Furuhashi, M., and Hotamisligil, G. S. (2008). Fatty-acid-binding proteins: role in metabolic disease and potential as drug targets. *Nat. Rev. Drug Discov.* 7, 489–503. doi: 10.1038/nrd2589

Hayman, R. (1953). Studies in fleecerot of sheep. *Crop Pasture Sci.* 4, 430–463. doi: 10.1071/AR9530430

James, P. I., Warren, G. H., and Neville, A. (1984). The effect of some fleece characters on the skin wax layer and fleecerot development in Merino sheep following wetting. *Aust. J. Agric. Res.* 35, 413–422. doi: 10.1071/ar9840413

James, P. J., and Ponzoni, R. W. (1992). Fibre diameter variability in South Australian Merinos- phenotypic and genetic relationships with wool quality parameters and fleece rot resistance. *Wool Technol. Sheep Breed.* 40, 25–26.

Lambers, H., Piessen, S., Bloem, A., Pronk, H., and Finkel, P. (2006). Natural skin surface pH is on average below 5, which is beneficial for its resident flora. *Int. J. Cosmet. Sci.* 28, 359–370. doi: 10.1111/j.1467-2494.2006.00344.x

Le Hir, H., Nott, A., and Moore, M. J. (2003). How introns influence and enhance eukaryotic gene expression. *Trends Biochem. Sci.* 28, 215–220. doi: 10.1016/s0968-0004(03)00052-5

Lin, M. H., and Khnykin, D. (2014). Fatty-acid transporters in skin development, function and disease. *Biochim. Biophys. Acta* 1841, 362–368. doi: 10.1016/j.bbalip.2013.09.016

Makowski, L., Brittingham, K. C., Reynolds, J. M., Suttles, J., and Hotamisligil, G. S. (2005). The fatty acid-binding protein, aP2, coordinates macrophages cholesterol trafficking and inflammatory activity. *J. Biol. Chem.* 280, 12888–12895. doi: 10.1074/jbc.m413788200

Michalik, L., and Wahli, W. (2007). Peroxisome proliferator-activated receptors (PPARs) in skin health, repair and disease. *Biochim. Biophys. Acta* 1771, 991–998.

Norris, B. J., Colditz, I. G., and Dixon, T. J. (2008). Fleecerot and dermatophilosis in sheep. *Vet. Microbiol.* 128, 217–230. doi: 10.1016/j.vetmic.2007.10.024

Pethick, D. W., Ball, A. J., Banks, R. G., and Hocquette, J. F. (2011). Current and future issues facing red meat quality in a competitive market and how to manage continuous improvement. *Anim. Prod. Sci.* 51, 13–18. doi: 10.1071/an10041

Raadsma, H. W. (1987). Flystrike control: an overview of management and breeding options. *Wool Technol. Sheep Breed.* 35, 174–185.

Raadsma, H. W. (1991). Fleece rot and body strike in Merino sheep. V. Heritability of liability to body strike in weaner sheep under flywave conditions. *Crop Pasture Sci.* 42, 279–293. doi: 10.1071/ar9910279

Raadsma, H. W. (1993). Fleece rot and body strike in Merino sheep. VI. Experimental evaluation of some physical fleece and body characteristics as indirect selection criteria for fleece rot. *Crop Pasture Sci.* 44, 915–931. doi: 10.1071/ar9930915

Smith, W. J. M., Li, Y., Ingham, A., Collis, E., McWilliam, S. M., Dixon, T. J., et al. (2010). A genomics-informed, SNP associated study reveals FBLN1 and FABP4 as contributing to resistance to fleecerot in Australian Merino sheep. *BMC Vet. Res.* 6:27. doi: 10.1186/1746-6148-6-27

Supek, F., Miñana, B., Valcárcel, J., Galbaldón, T., and Lehner, B. (2014). Synonymous mutations frequently act as driver mutations in human cancers. *Cell* 156, 1324–1335. doi: 10.1016/j.cell.2014.01.051

Suzuki, A., Itamia, S., Ohishi, M., Hamada, K., Inoue, T., Komazawa, N., et al. (2003). Keratinocyte-specific Pten deficiency results in epidermal hyperplasia, accelerated hair follicle morphogenesis and tumor formation. *Cancer Res.* 63, 674–681.

Tsuda, M., Inoue-Nartia, T., Suzuki, A., Itami, S., Blumenberg, M., and Manabe, M. (2009). Induction of gene encoding FABP4 in Pten-null keratinocytes. *FEBS Lett.* 583, 1319–1322. doi: 10.1016/j.febslet.2009.03.030

Volk, M. G. (2007). An examination of the evidence supporting the association of dietary cholesterol and saturated fats with serum cholesterol and development of coronary heart disease. *Altern. Med. Rev.* 12, 228–245.

Watanabe, R., Fujiib, H., Yamamotoa, A., Hashimotoa, T., Kamedac, K., Itoa, M., et al. (1997). Immunohistochemical distribution of cutaneous fatty-acid-binding protein in human skin. *J. Dermatol. Sci.* 16, 17–22. doi: 10.1016/s0923-1811(97)00615-4

Yan, W., Zhou, H., Hu, J., Luo, Y., and Hickford, J. G. H. (2018). Variation in the FABP4 gene affects carcass and growth traits in sheep. *Meat Sci.* 145, 334–339. doi: 10.1016/j.meatsci.2018.07.007

Yan, W., Zhou, H., Luo, Y., Hu, J., and Hickford, J. G. H. (2012). Allelic variation in ovine fatty-acid binding protein (FABP4) gene. *Mol. Biol. Rep.* 39, 10621–10625. doi: 10.1007/s11033-012-1951-y

Zhou, H., Hickford, J. G., and Fang, Q. (2006). A two-step procedure for extracting genomic DNA from dried blood spots on filter paper for polymerase chain reaction amplification. *Anal. Biochem.* 354, 159–161. doi: 10.1016/j.ab.2006.03.042

Conflict of Interest: The authors declare that the research was conducted in the absence of any commercial or financial relationships that could be construed as a potential conflict of interest.

frontiers in Genetics

ORIGINAL RESEARCH
published: 21 June 2021
doi: 10.3389/fgene.2021.649140

Effect of the *ACAA1* Gene on Preadipocyte Differentiation in Sheep

Yanli Wang[1†], Xin Li[1†], Yang Cao[2], Cheng Xiao[1], Yu Liu[1], Haiguo Jin[1] and Yang Cao[1]*

[1] *Institute of Animal Biotechnology, Jilin Academy of Agricultural Science, Changchun, China,* [2] *Institute of Animal Husbandry and Veterinary, Zhejiang Academy of Agricultural Sciences, Hangzhou, China*

Acetyl-CoA acyltransferase 1 (*ACAA1*) functions as a key regulator of fatty acid β-oxidation in peroxisomes by catalyzing the cleavage of 3-ketoacyl-CoA to acetyl-CoA and acyl-CoA, which participate in the extension and degradation of fatty acids. Thus, *ACAA1* is an important regulator of lipid metabolism and plays an essential role in fatty acid oxidation and lipid metabolism. Our previous study findings revealed that *ACAA1* is closely associated with the peroxisome proliferator-activated receptor (*PPAR*) signaling and fatty acid metabolism pathways, which are involved in fat deposition in sheep, leading to our hypothesis that *ACAA1* may be involved in fat deposition by regulating lipid metabolism. However, the associated molecular mechanism remains unclear. In the present study, to assess the potential function of *ACAA1* in sheep preadipocyte differentiation, we knocked down and overexpressed *ACAA1* in sheep preadipocytes and evaluated the pattern of *ACAA1* gene expression during preadipocyte differentiation by qRT-PCR. *ACAA1* was significantly expressed in the early stage of adipocyte differentiation, and then its expression decreased. *ACAA1* deficiency increased lipid accumulation and the triglyceride content and promoted sheep preadipocyte differentiation, whereas *ACAA1* overexpression inhibited adipogenesis and decreased lipid accumulation and the triglyceride content. Simultaneously, we demonstrated that *ACAA1* deficiency upregulated the expressions of the adipogenic marker genes *PPARγ* and *C/EBPα* in sheep preadipocytes, but *ACAA1* overexpression inhibited the expressions of these markers, indicating that *ACAA1* affects lipid metabolism by regulating adipogenic marker genes. Our results may promote a better understanding of the regulation of adipogenesis by *ACAA1*.

Keywords: *ACAA1* gene, preadipocyte differentiation, sheep, lipid metabolism, adipogenesis

OPEN ACCESS

Edited by:
Rui Su,
Inner Mongolia Agricultural University, China

Reviewed by:
Paolo Zambonelli, University of Bologna, Italy
Angela Cánovas, University of Guelph, Canada
Runjun Yang, Jilin University, China

***Correspondence:**
Yang Cao
caoyang003@163.com

[†] These authors have contributed equally to this work

Specialty section:
This article was submitted to Livestock Genomics, a section of the journal Frontiers in Genetics

Received: *04 January 2021*
Accepted: *18 May 2021*
Published: *21 June 2021*

Citation:
Wang Y, Li X, Cao Y, Xiao C, Liu Y, Jin H and Cao Y (2021) Effect of the ACAA1 Gene on Preadipocyte Differentiation in Sheep. Front. Genet. 12:649140. doi: 10.3389/fgene.2021.649140

INTRODUCTION

Adipose tissue, which comprises brown and white adipocytes, is essential for maintaining energy and metabolic homeostasis in animals and plays an essential role in animal endocrine function (Gesta et al., 2007; Galic et al., 2010). Furthermore, adipose tissue secretes several cytokines and hormones that affect the function of cells and tissues (Galic et al., 2010). In mammals, the normal that cleaves peroxisom development of adipose tissue is crucial to maintaining good health. The intramuscular fat content directly affects the meat quality and flavor in animal production, and the abnormal metabolism of adipose tissue can affect meat quality in livestock (Wood et al., 2008). Therefore, elucidating the molecular mechanisms involved in adipocyte differentiation is vital for disease treatment and improving the economic benefits of animal husbandry production.

Acetyl-coenzyme A acyltransferase (ACAA) is a thiolytic enzyme of the acyl-CoA superfamily of metabolic enzymes (Stim-Herndon et al., 1995; Vishwakarma et al., 2013; Ya, 2013). ACAA family members include *ACAA1* and *ACAA2*. *ACAA1*, also known as peroxisome 3-ketoacyl-CoA thiolase, is a crucial enzyme that regulates the β-oxidation of fatty acids in peroxisomes and plays an essential role in fatty acid metabolism (Wanders et al., 2001). The β-oxidation of fatty acids alters the fatty acid content of animals, affecting the meat quality of livestock and poultry.

Because of the changing dietary habits of individuals and the gradual strengthening of healthcare awareness, mutton has become favored by the general public as a green food because of its high protein content, low cholesterol levels, and excellent nutritional qualities (Cao, 2017). The meat quality of animals is closely associated with their fat content because an appropriate intramuscular fat content can increase marbling, reduce shear force, and increase meat flavor and palatability. Additionally, the intramuscular fat content has special significance for production efficiency and meat quality. Intramuscular fat is regulated by lipid metabolism and is synthesized from glycerol and fatty acids. The whole metabolic process is a complex and highly coordinated process (Fang, 2017). Genetic factors affect the accumulation of intramuscular fat by regulating *de novo* lipogenesis and adipocyte differentiation. In a previous screen for functional genes associated with lipid metabolism that affect meat quality, *ACAA2*, a member of the acetyl-CoA acyltransferase family, was identified as a key functional gene affecting lipid metabolism (Li, 2008). *ACAA1* is an important regulator of fatty acid metabolism (Wanders et al., 2001); presently, studies on *ACAA1* have primarily focused on human metabolic diseases, tumors, and cancer. As a regulator of lipid metabolism, few reports have investigated the involvement of *ACAA1* in animal meat quality breeding. In the present study, the pattern of *ACAA1* gene expression during the adipogenic differentiation of sheep preadipocytes was analyzed to assess its role in the adipogenic differentiation process. Investigating the effect of *ACAA1* gene expression on adipogenic differentiation at the cellular and molecular levels is crucial to further improve mutton quality.

MATERIALS AND METHODS

Experimental Animals

Three-month-old lambs were provided by the Institute of Animal Biotechnology (Jilin Academy of Agricultural Science, Changchun, China). All the experimental procedures were examined and approved by the Animal Welfare and Ethics Committee of Jilin Academy of Agricultural Sciences (AWEC 2019A05, May 16, 2019) and complied with the rules and regulations established by the Chinese Experimental Animal Ethics Committee.

Cell Isolation, Cultivation, and Adipocyte Differentiation

The precursor adipocytes were separated by the collagenase digestion method (Church et al., 2014). Sheep preadipocytes were isolated from the inguinal subcutaneous adipose tissue of 3-month-old male lambs. Next, the animals were anesthetized by air embolization and slaughtered in a specific slaughtering chamber; immediately after slaughter, their adipose tissue was collected under sterile conditions. Freshly isolated subcutaneous adipose tissues were cut into small pieces and weighed. Next, two volumes of 0.2% collagenase II (Sangon Biotech, Shanghai, China) were added per gram of tissue, and the sample was thoroughly mixed. The sample was digested in a water bath at 37°C for 40–90 min. After the digestion was terminated, the cells were obtained by filtration using 200- and 400-mesh filters, and the filtrate was centrifuged three times for 5 min at 1,500 rpm. Subsequently, the cells were cultured in Dulbecco's modified Eagle's medium (DMEM/F12; 1:1; Gibco, Shanghai, China) containing 10% fetal bovine serum (Gemini, Woodland, CL, United States) and 1% penicillin/streptomycin (Sangon Biotech) for 24 h at 37°C under an atmosphere with 5% CO_2. The non-adherent cells were washed away with phosphate-buffered saline (PBS; Gibco, Shanghai, China), and the buffered medium was changed every 48 h. Once the cell confluence reached 100% (0 days), the sheep preadipocytes were induced to differentiate by adding 10 μg/ml of insulin, 0.5 mM 3-isobutyl-1-methylxanthine (IBMX; Sigma, St. Louis, MO, United States) and 1.0 μM dexamethasone (DEX; Sigma) to the culture medium. The cells were then incubated for 2 days, after which 10 μg/ml of insulin (Sigma) was added and the cells were incubated for an additional 2 days (total of 4 days of incubation). Subsequently, the medium was changed every 48 h until the differentiation process was complete (after 8 days).

Oil Red O Staining and Detection of the Triglyceride Content

Differentiated adipocytes were washed three times with PBS and then fixed with 4% paraformaldehyde (Sangon Biotech, Shanghai, China) for 30 min at 37°C. Next, the cells were washed three times with PBS, stained with 2% oil red O (Sangon Biotech, Shanghai, China) solution at 37°C for 30 min, and washed three times with PBS before being visualized with a microscope for analysis. Subsequently, the oil red O solution was extracted with 100% isopropanol for 10 min, after which the absorbance of lipid droplets at 490 nm was measured on a microboard reader (Ramírezzacarías et al., 1992) (Thermo Fisher Scientific, Carlsbad, CA, United States). The triglyceride content in adipocytes was determined at room temperature using a triglyceride enzyme-linked assay kit E1030 (Applygen, Beijing, China).

Transfection of Sheep Preadipocytes

Cell transfection was performed as previously reported by Zhang et al. (2018) and Yun et al. '(2018). Both the recombinant overexpression plasmid ACAA1-PEX-4 (50 μg) and the empty vector PEX-4 (50 μg) used in the present study were obtained from GenePharma Company (Suzhou, China). ACAA1–PEX-4 was synthesized from PEX-4 and complementary DNA (cDNA) harboring the *ACAA1* gene, both of which were digested with the *Xho*I and *Eco*RI restriction endonucleases. PEX-4 was used as a

negative control (NC), and a vector containing enhanced green fluorescent protein (EGFP) was used to confirm the transfection efficiency. Sheep preadipocytes were transfected with 4 μg of the *ACAA1* overexpression plasmid (or NC plasmid) using 10 μl of FuGene HD Transfection Reagent (Promega, Madison, WI, United States) after reaching approximately 70–80% confluence in six-well plates, according to the manufacturer's instructions. Next, the cells were incubated for 24 h, after which the liquid was exchanged for fresh medium and the cells were induced for 48 h after transfection.

siRNA-ACAA1 (20 μM) and siRNA-NC (NC) were generated by GenePharma. siRNA-NC, as an NC, showed no homology with the target gene. Preadipocytes were cultured to 80% confluency in six-well plates and transfected with 10 μl of siRNA-ACAA1 (or NC) using 5 μl of Lipofectamine 2000 (Invitrogen, Carlsbad, CA, United States) according to the manufacturer's instructions. The cells were incubated for 8 h, transferred to fresh medium, and then induced 48 h after transfection. The small interfering RNA (siRNA) sequence information is shown in **Table 1**.

Quantitative Real-Time PCR Analysis

Fifteen samples from the normal differentiation period (0, 2, 4, 6, and 8 days, three repeats in each group), 18 samples from the overexpression group and the control group (0, 4, and 8 days, three repeats in the over-ACAA1 and over-NC groups), and 18 samples from the knockdown group and the control group (0, 4, and 8 days, three repeats in the siRNA-ACAA1 and siRNA-NC groups) were collected. Total RNA was isolated using TRIzol reagent (Invitrogen) and reverse transcribed to cDNA using a reverse transcription kit (TaKaRa, Shiga, Japan). Using the synthesized cDNA as a template, quantitative real-time polymerase chain reaction (qRT-PCR) was performed with a LightCycler® 480 II system (Roche) using SYBR Green I Master (Roche), with β-*actin* used as the internal control gene. The relative expression levels of the assayed genes were detected using the $2^{-\Delta\Delta Ct}$ method (Yang et al., 2018; Yun et al., 2018). The primer information is provided in **Table 2**.

Western Blot Analysis

Fifteen samples were collected from the normal differentiation period (0, 2, 4, 6, and 8 days, three repeats in each group), 12 samples were collected from the overexpression and control groups (4 and 8 days, three repeats in the over-ACAA1 and over-NC groups), and 12 samples were collected from the knockdown and control groups (4 and 8 days, three repeats in the siRNA-ACAA1 and siRNA-NC groups). The cells were washed three times with cold PBS, lysed with a protein lysis buffer (RIPA; Thermo Fisher Scientific) containing protease inhibitors (protease and phosphatase inhibitor cocktail), and then placed on ice for 2 min. Subsequently, the lysate was collected in a 1.5-ml centrifuge tube and placed on ice. The tube was lightly mixed every 5 min; after 30 min, the soluble proteins were obtained by centrifugation at 4°C at 12,000 rpm for 15 min. The protein concentration was determined using an enhanced bicinchoninic acid (BCA) protein detection kit (Beyotime, Shanghai, China). The protein samples were denatured at 95°C for 10 min, and then 20 μg protein sample was separated by sodium dodecyl sulfate–polyacrylamide gel electrophoresis (SDS-PAGE) on a 10% gel before being transferred to polyvinylidene difluoride (PVDF) membranes (Millipore, Burlington, MA, United States). The membranes were washed for 5 min with Tris-buffered saline containing Tween (TBST) and then blocked using 5% skimmed milk at room temperature for 2 h. Subsequently, the membranes were washed three times (5 min each) with TBST and then incubated with a primary antibody overnight at 4°C on a shaker. Next, the membranes were incubated with a corresponding secondary antibody [anti-rabbit or anti-mouse IgG horseradish peroxidase (HRP)-linked, 1:2,000 dilution; Cell Signaling Technology, Danvers, MA, United States] for 90 min at room temperature. The membranes were then washed three times with TBST, after which the immunoreactive bands were visualized using a ChemiScope 6000 Touch (Clinx, Shanghai, China) with an ECL-Plus kit (Applygen) (Yun et al., 2018). The band intensities were estimated by density measurements and normalized to β-actin using Clinx Chemi analysis software. Details regarding the primary antibodies used in the present study are provided in **Table 3**.

Statistical Analysis

The qRT-PCR results were statistically analyzed using the $2^{-\Delta\Delta Ct}$ method, and the gray values of the protein were

TABLE 1 | siRNA sequences.

Symbols	siRNA primer sequences (5′–3′)
siRNA-ACAA1	F: GCUGAGCGGUUUGGCAUUUTT R: AAAUGCCAAACCGCUCAGCTT
siRNA-NC	F: UUCUCCGAACGUGUCACGUTT R: ACGUGACACGUUCGGAGAATT

TABLE 2 | Primers used for quantitative real-time polymerase chain reaction.

Genes	Sequence (5′–3′)	Product size (bp)	GenBank accession number
ACAA1	F: TCAGGCTGTGTACTGTGTGGA R: AGCGTGATGACCTGTCGAG	120	XM_004018227.3
PPARγ	F: CCGTGGACCTTTCTATGATGG R: TACAGGCTCCACTTTGATTGC	194	NM_001100921.1
C/EBPα	F: AAGCCAAGAAGTCCGTGGAC R: AGCACCTTCTGTTGCGTCTCC	127	NM_001308574.1
β-*actin*	F: CCCTGGAGAAGAGCTACGAG R: GGTAGTTTCGTGAATGCCGC	131	U39357.2

TABLE 3 | Antibodies used for Western blot analysis.

Antibodies	Source, cat. no.	Species raised in mono-/polyclonal
ACAA1	Bioss, cat. no. bs-12566R	Rabbit polyclonal antibody
PPARγ	Bioss, cat. no. bs-4590R	Rabbit polyclonal antibody
C/EBPα	Bioss, cat. no. bs-1630R	Rabbit polyclonal antibody
β-*actin*	Abcam, cat. no. ab8224	Mouse monoclonal antibody

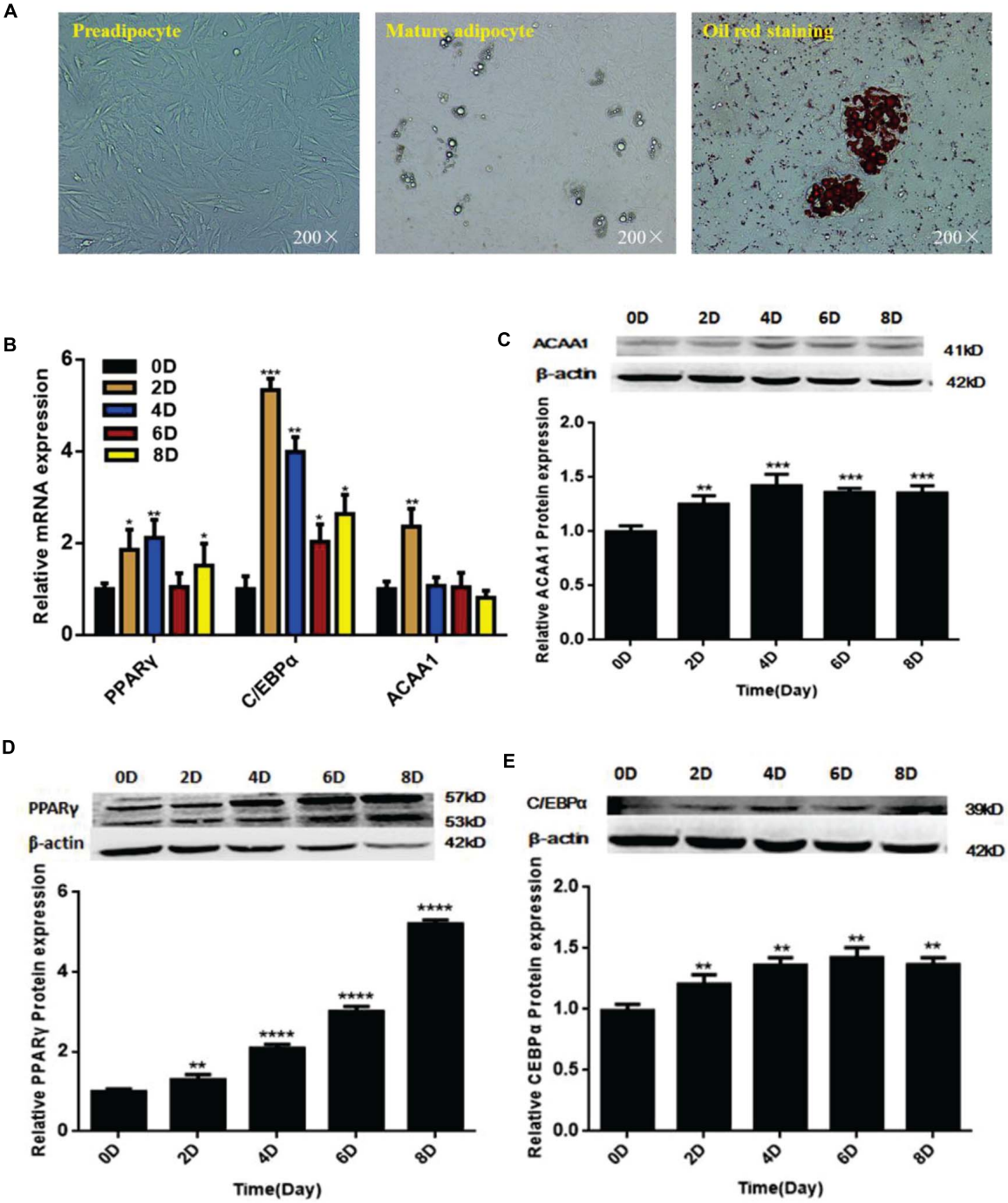

FIGURE 1 | *ACAA1* and adipogenic marker gene expression during sheep preadipocyte differentiation. **(A)** Sheep preadipocytes, mature adipocytes, and oil red O staining (200×). **(B)** Expression patterns of adipogenic marker genes (*PPARγ* and *C/EBPα*) in differentiating sheep adipocytes. **(C)** *ACAA1* protein expression in differentiating sheep adipocytes was determined by Western blot analysis. **(D,E)** The protein expression levels of *PPARγ* and *C/EBPα* during adipocyte differentiation were evaluated on days 0, 2, 4, 6, and 8. Densitometric analyses of the Western blots. With the differentiation of cells, the expression levels of adipogenic genes gradually increased (*$p < 0.05$, **$p < 0.01$, ***$p < 0.001$, and ****$p < 0.0001$). *ACAA1*, acetyl-CoA acyltransferase 1; *PPARγ*, peroxisome proliferator-activated receptor γ; *C/EBPα*, CCAAT/enhancer binding protein α.

analyzed using Clinx image analysis software. All the data are presented as the mean ± standard error of three independent experiments performed in triplicate. Calculations and figures were produced by one-way ANOVA using GraphPad Prism version 6.00 for Windows. The statistical significance levels were set at $p < 0.05$ (Yang et al., 2018).

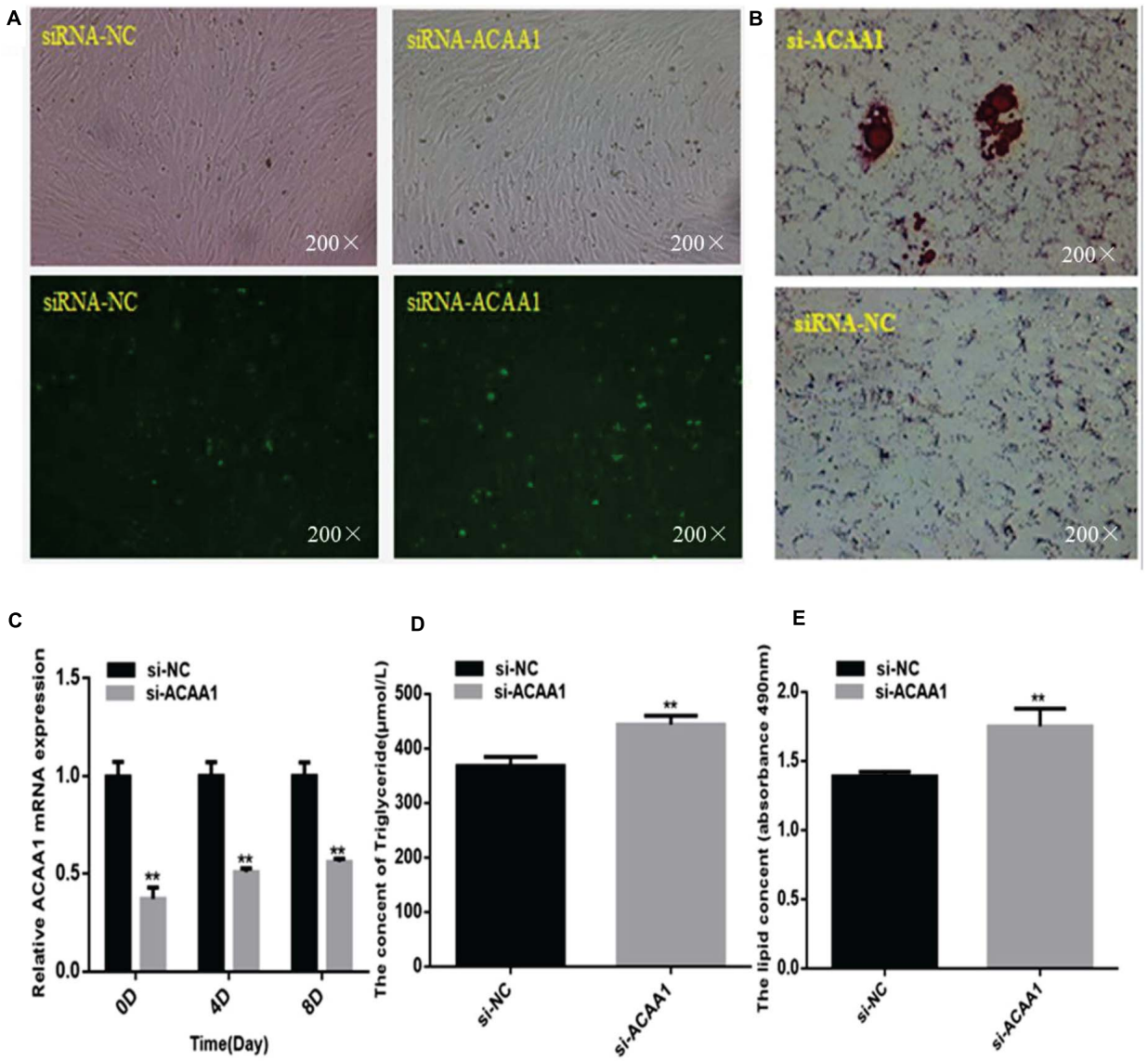

FIGURE 2 | *ACAA1* knockdown increases lipid accumulation and the triglyceride content during sheep preadipocyte differentiation. **(A)** Determination of the transfection efficiency of siRNA-ACAA1 (200×). **(B)** After 8 days of differentiation, the cellular lipid droplets were stained with oil red O (200×). **(C)** *ACAA1* mRNA expression was detected after siRNA-ACAA1 or NC transfection on days 0, 4, and 8 of adipogenic differentiation. The siRNA-ACAA1 groups all showed significantly lower expressions than the control group (**$p < 0.01$). **(D)** The triglyceride content after 8 days of induction in the siRNA-ACAA1 group was significantly higher than that in the control group (**$p < 0.01$). **(E)** The lipid droplet content measured at 490 nm after 8 days of induction was significantly higher in the siRNA-ACAA1 group than that in the control group (**$p < 0.01$). *siRNA*, small interfering RNA; *NC*, negative control.

RESULTS

ACAA1 Expression Pattern During Sheep Preadipocyte Differentiation

We isolated and used sheep preadipocytes as a model of adipogenesis to assess the associated changes in *ACAA1* expression. Sheep preadipocytes were stimulated to differentiate for 8 days using the "cocktail" method. The sheep preadipocytes exhibited obvious morphological changes after 8 days of differentiation and contained many cytoplasmic lipid droplets showing positive staining for oil red O, where typical round lipid droplets and smaller lipid droplets gathered into large lipid droplets were observed, all of which are typical characteristics of mature adipocytes (**Figure 1A**). The messenger RNA (mRNA) and protein levels of adipogenic markers (*PPARγ* and *C/EBPα*) were analyzed during sheep preadipocyte differentiation by qRT-PCR and Western blotting, respectively. During adipogenesis, the expression of adipogenic markers increased with the lipid accumulation in sheep adipocytes (**Figures 1B,D,E**), indicating that the isolated sheep preadipocytes could be used in subsequent experiments.

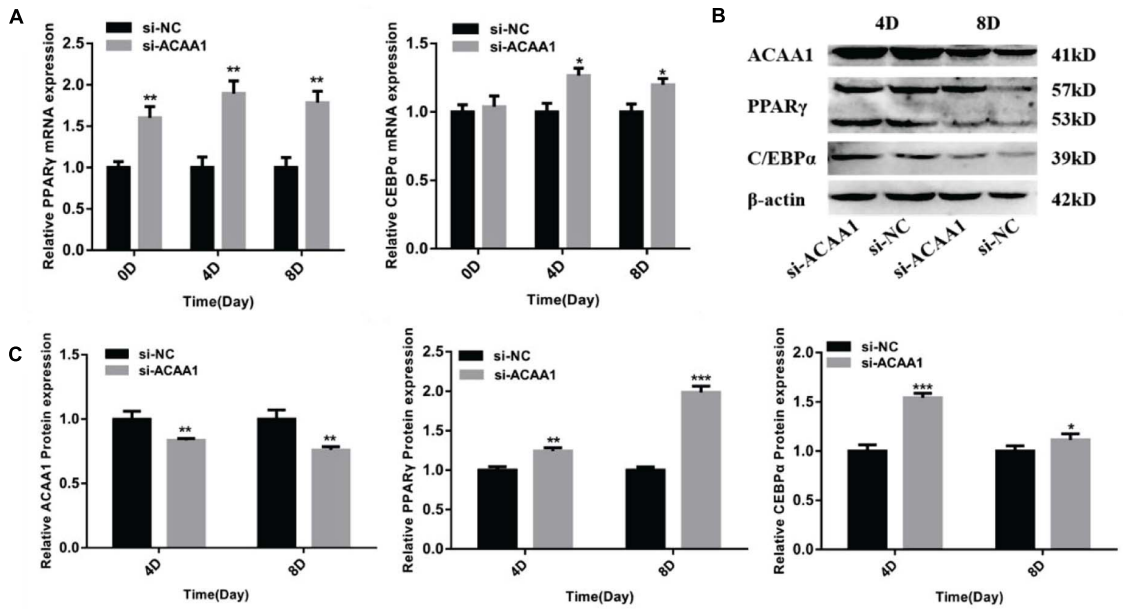

FIGURE 3 | *ACAA1* knockdown regulates adipogenic marker gene expression. **(A)** Sheep preadipocytes were transfected with siRNA-ACAA1 or siRNA-NC and differentiated into mature adipocytes. The mRNA expression levels of adipogenic marker genes *(PPARγ* and *C/EBPα)* were evaluated on days 0 (after cell amalgamation), 4, and 8 of adipogenic differentiation. On day 0 of adipogenic differentiation, the mRNA expression levels of the marker genes were higher than those of the control group, but only *PPARγ* reached a significant level (**$p < 0.01$). On days 4 and 8 of adipogenic differentiation, the mRNA expression levels of *PPARγ* and *C/EBPα* were significantly higher than those of the control group (*$p < 0.05$ and **$p < 0.01$). **(B)** Protein expression levels of *ACAA1* and adipogenic marker genes on days 4 and 8 of adipogenic differentiation. *Columns 1* and *2* are the siRNA-ACAA1 processing group and the siRNA-NC processing group, respectively (day 4). *Columns 3* and *4* are the siRNA-ACAA1 processing group and the siRNA-NC processing group, respectively (day 8). *β-actin* is the internal reference gene. **(C)** The protein expression levels of *ACAA1* and adipogenic marker genes were assessed on days 4 and 8 of adipogenic differentiation. The protein expression levels of *ACAA1* were significantly lower than those of the control group (**$p < 0.01$), and the protein expression levels of *PPARγ* and *C/EBPα* were significantly higher than those of the control group (*$p < 0.05$, **$p < 0.01$, and ***$p < 0.001$). *NC*, negative control.

Interestingly, the *ACAA1* mRNA expression levels were significantly increased in the first 2 days of sheep adipocyte differentiation and then gradually decreased (**Figure 1B**), while the *ACAA1* protein levels increased in the early stage of differentiation (0–4 days) before decreasing (**Figure 1C**). The *ACAA1* mRNA and protein expression trends were similar to those observed for the adipogenic marker *C/EBPα*. Adipogenesis involves the dynamic regulation of gene expression, and these results suggest that *ACAA1* may be involved in regulating sheep preadipocyte differentiation.

ACAA1 Knockdown Promotes Preadipocyte Differentiation

ACAA1 Knockdown Increases Lipid Accumulation and the Triglyceride Content

To assess whether *ACAA1* affects sheep preadipocyte differentiation, we knocked down *ACAA1* expression in sheep preadipocytes by transfecting siRNA-ACAA1 or siRNA-NC into sheep preadipocytes cultured to 80% confluency. The *ACAA1* mRNA and protein expression levels in the knockdown group were markedly downregulated compared with those in the NC group ($p < 0.01$; **Figures 2A,C**, **3B**). Oil red O staining and lipid droplet extraction analyses demonstrated that more lipids accumulated in adipocytes from the *ACAA1* knockdown group than from the NC group ($p < 0.01$; **Figures 2B,E**), and the triglyceride content of the knockdown group was also significantly greater ($p < 0.01$; **Figure 2D**).

ACAA1 Knockdown Enhances Adipogenic Marker Gene Expression

The mRNA expression levels of adipogenic marker genes (including *PPARγ* and *C/EBPα*) involved in differentiation were measured on days 0, 4, and 8 after induction (**Figure 3A**), while the protein expression levels were measured 4 and 8 days later (**Figure 3B**). The mRNA expressions of the adipogenic marker genes were upregulated following *ACAA1* knockdown ($p < 0.05$ and $p < 0.01$; **Figure 3A**), while the PPARγ and C/EBPα protein expressions were significantly increased by *ACAA1* deficiency ($p < 0.05$, $p < 0.01$, and $p < 0.001$; **Figure 3C**). Thus, the *ACAA1* gene may be a negative regulator of adipogenic differentiation.

ACAA1 Overexpression Inhibits Preadipocyte Differentiation

ACAA1 Overexpression Decreases Preadipocyte Lipid Accumulation and the Triglyceride Content

The effects of *ACAA1* overexpression on sheep preadipocyte differentiation were evaluated. The *ACAA1* mRNA and protein expression levels in the overexpression group were significantly

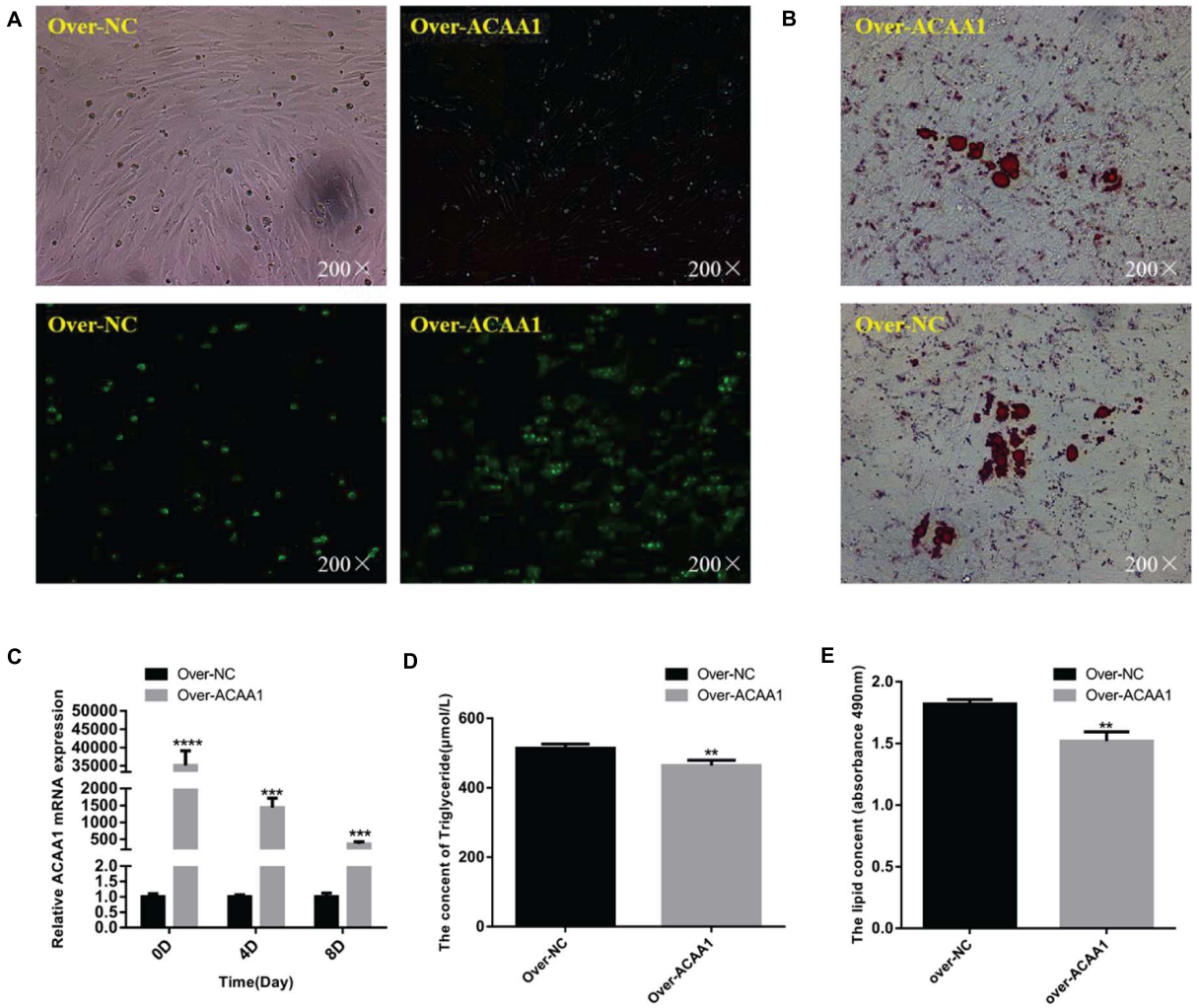

FIGURE 4 | *ACAA1* overexpression decreases lipid accumulation and the triglyceride content in preadipocytes. **(A)** Determination of the transfection efficiency of the *ACAA1* overexpression plasmid (200×). **(B)** After 8 days of differentiation, the cellular lipid droplets were stained with oil red O (200×). **(C)** *ACAA1* mRNA expression was assessed after cells were transfected with the *ACAA1* overexpression or the NC plasmids on days 0, 4, and 8 of adipogenic differentiation. The expression in the over-ACAA1 group was significantly higher than that in the control group (****$p < 0.01$ and ***$p < 0.001$). The difference was largest in the early stage of cell differentiation. **(D)** After 8 days of induction, the triglyceride content in the over-ACAA1 group was significantly lower than that in the control group (**$p < 0.01$). **(E)** The lipid droplet content measured at 490 nm after 8 days of induction in the over-ACAA1 group was significantly lower than that in the control group (**$p < 0.01$).

higher than those in the NC group ($p < 0.01$; **Figures 4A,C**, **5B**). Oil red O staining and lipid droplet extraction revealed that *ACAA1* overexpression significantly inhibited preadipocyte differentiation and lipid accumulation in sheep adipocytes ($p < 0.01$; **Figures 4B,E**). Additionally, the triglyceride content in the overexpression group was significantly lower than that in the NC group ($p < 0.01$; **Figure 4D**).

ACAA1 Overexpression Decreases Adipogenic Marker Gene Expression

ACAA1 overexpression remarkably downregulated the mRNA levels of the adipogenic marker genes *PPARγ* and *C/EBPα* on days 4 and 8 ($p < 0.05$, $p < 0.01$, $p < 0.001$, and $p < 0.0001$; **Figure 5A**). Consistent with these findings, Western blotting showed that *ACAA1* overexpression significantly decreased the protein levels of these adipogenic marker genes ($p < 0.01$ and $p < 0.001$; **Figures 5B,C**).

DISCUSSION

A strong correlation exists between the fat content and meat quality in animals, which can affect the sensory indexes of meat, such as tenderness, color, flavor, and nutritional value (Huan-Hsien, 2011). As one determinant of meat quality, fat content has become a research hotspot for livestock and poultry meat quality in recent years. However, presently, studies on the regulation of fat development and deposition have primarily focused on pigs (Zou et al., 2018), cattle (Park et al., 2018), and chickens (Fu et al., 2018), whereas such studies in sheep have been lacking.

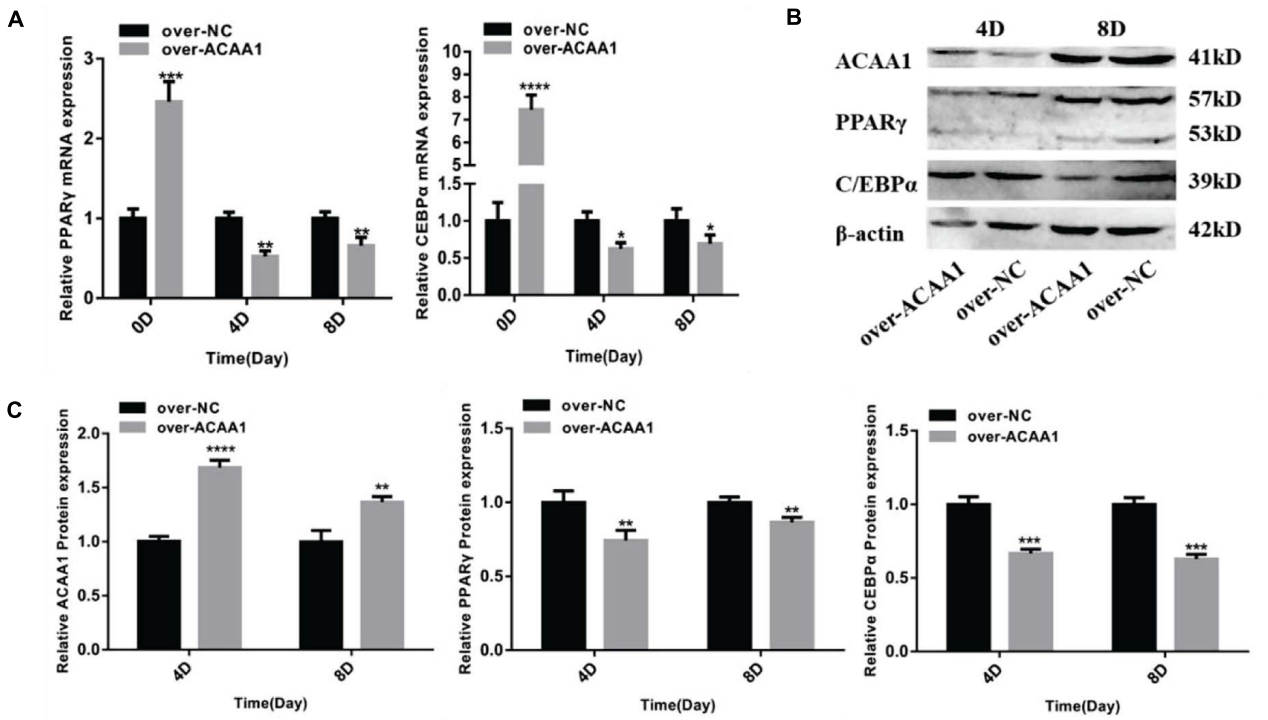

FIGURE 5 | *ACAA1* overexpression regulates adipogenic marker gene expression. **(A)** Sheep preadipocytes were transfected with *ACAA1* overexpression or negative control (NC) plasmids and differentiated into mature adipocytes. The mRNA expression levels of adipogenic marker genes (*PPARγ* and *C/EBPα*) were measured on days 0, 4, and 8 of adipogenic differentiation. Except day 0, the mRNA expression levels of *PPARγ* and *C/EBPα* were significantly lower than those of the control group (*$p < 0.05$, **$p < 0.01$, ***$p < 0.001$, and ****$p < 0.0001$). **(B)** Protein expression levels of *ACAA1* and adipogenic marker genes on days 4 and 8 of adipogenic differentiation. *Columns 1* and *2* are the over-ACAA1 processing and over-NC processing groups, respectively (day 4). *Columns 3* and *4* are the over-ACAA1 processing and over-NC processing groups, respectively (day 8). β-*actin* is the internal reference gene. **(C)** The protein expression levels of *ACAA1* and adipogenic marker genes were assessed on days 4 and 8 of adipogenic differentiation. The protein expression levels of *ACAA1* were significantly higher than those of the control group (****$p < 0.0001$ and **$p < 0.01$), and the protein expression levels of *PPARγ* and *C/EBPα* were significantly lower than those of the control group (**$p < 0.01$ and ***$p < 0.001$).

Mammalian adipogenesis is a complicated physiological process involving the expressions of multiple genes, signal transduction pathways, and network regulation to balance the proliferation and differentiation of preadipocytes (Gesta et al., 2007). The *ACAA1* gene encodes a thiolytic enzyme that cleaves peroxisomal 3-ketoacyl-CoA into acetyl-CoA and acyl-CoA, which participate in the extension and degradation of fatty acids. *ACAA1* is an important regulatory gene involved in cell lipid metabolism (Wanders et al., 2001) and is a target of biotherapy for human metabolic diseases (Colas et al., 2011; Park et al., 2012; Klimosch et al., 2013; Liu et al., 2015; Nwosu et al., 2018; Zhang et al., 2019). In a previous study, we investigated the transcriptome characteristics associated with the intramuscular fat content of the sheep longissimus dorsi muscle and observed significant differences in the transcriptional levels of *ACAA1*, which is associated with members of the PPAR signaling and fatty acid metabolism signaling pathways involved in fat deposition in sheep. Therefore, we speculated that *ACAA1* may be involved in fat deposition by regulating lipid metabolism.

In the present study, we analyzed the pattern of *ACAA1* gene expression during the differentiation of cultured sheep preadipocytes, and the results suggest that *ACAA1* may be a functional regulator of sheep fat deposition. Several studies have demonstrated that *ACAA1* plays an important role in animal lipid metabolism (Lisowski et al., 2014; Zhang and Wang, 2015; Zhu et al., 2016). For example, *ACAA1* gene upregulation is involved in fatty acid biosynthesis and lipid metabolism in beef cattle (Lisowski et al., 2014), as well as increased liver triglyceride metabolism, lipid decomposition, and fatty acid oxidation in mice fed a high-fat diet, which can reduce intestinal lipid absorption (Zhu et al., 2016). In the present study, to investigate the potential function of *ACAA1* in sheep preadipocyte differentiation, we assessed the effects of *ACAA1* knockdown and overexpression in sheep preadipocytes. After induction, we observed that *ACAA1* deficiency increased lipid accumulation and the triglyceride content and promoted adipogenesis. These results are consistent with those reported for chicken intramuscular preadipocytes, in which the inhibition of *ACAA1* gene expression in fatty acid peroxisomes was shown to promote the deposition of intramuscular fat in chickens (Li et al., 2019). However, *ACAA1* overexpression inhibits adipogenesis and decreases lipid accumulation and the triglyceride content. The upregulation of *ACAA1* expression has been shown to reduce the intramuscular fat content in the longissimus dorsi

of large white pigs (Yao, 2020). These results were consistent with previous findings (Xie et al., 2014; Zhang and Wang, 2015; Zhu et al., 2016). *ACAA1* gene upregulation enhanced fatty acid β-oxidation and triglyceride metabolism in the liver and decreased lipid accumulation in animals (Zhang and Wang, 2015). As a key enzyme of lipid metabolism, *ACAA1* may promote fatty acid metabolism and fatty acid degradation by participating in the β-oxidation of very long-chain fatty acids, affecting the function of fat metabolism in obese rats to achieve fat reduction and weight reduction (Meng, 2020). Fenofibrate (FB) significantly reduced abdominal fat and liver lipid accumulation in mice fed a high-fat diet by increasing *ACAA1* mRNA expression (Xie et al., 2014). Taken together, these results suggest that *ACAA1* may be a negative regulator of sheep preadipocyte differentiation and plays a crucial role in sheep fat deposition.

We found that *ACAA1* deficiency upregulates the expression of the adipogenic marker genes *PPARγ* and *C/EBPα* in sheep preadipocytes, but *ACAA1* overexpression inhibits *PPARγ* and *C/EBPα* expressions. Interestingly, the mRNA levels of these adipogenic marker genes on day 0 were significantly higher in the *ACAA1* overexpression group than those in the NC group, possibly because of a transcriptional delay effect for the different genes. PPARG is a key transcription factor in adipogenesis involved in maintaining the function of mature adipocytes (Imai et al., 2004; Schupp et al., 2009). The *ACAA1* gene is a downstream target gene of PPAR and is controlled by this regulator (Lake, 1995). In the PPAR signaling pathway, fatty acids serve as ligands that promote PPAR expression. PPAR activation can upregulate the expressions of downstream genes such as *ACAA1*, *ACOX1*, and *CPT-1* and stimulate fatty acid oxidation. Additionally, adipogenic gene upregulation resulting from PPAR activation can promote adipocyte differentiation (Li et al., 2019). *ACAA1* is closely related to the intramuscular fat content in pigs (Wu et al., 2013). The expression of *ACAA1* gene is regulated by the activation of the PPAR signaling pathway, which affects fat deposition and the intramuscular fat content in pigs (Yao, 2020). Based on previous study findings and those described herein, we hypothesize that the possible molecular mechanisms involved in preadipocyte differentiation are as follows. *ACAA1* knockdown reduces the oxidation of fatty acids in the PPAR signaling pathway, increasing the contents of saturated and unsaturated fatty acids in sheep adipocytes. The accumulated fatty acids further stimulate the transcriptional activity of PPAR, after which the expressions of downstream adipogenic genes become upregulated, promoting the differentiation of sheep preadipocytes.

In summary, our results suggest that *ACAA1* may be a transcriptional regulator of *PPARγ* and *C/EBPα* because of its ability to affect sheep preadipocyte differentiation. *ACAA1* deficiency promoted adipogenesis and lipid accumulation, while *ACAA1* overexpression inhibited sheep preadipocyte differentiation. These findings provide new molecular insights for further studies on the role of *ACAA1* in regulating fat metabolism and improving meat quality in sheep. However, further research is needed to elucidate the specific mechanism of *ACAA1* in regulating adipogenesis. There is still a long way to go for molecular breeding as a functional gene.

DATA AVAILABILITY STATEMENT

The raw data supporting the conclusions of this article will be made available by the authors, without undue reservation.

ETHICS STATEMENT

The animal study was reviewed and approved by the Animal Welfare and Ethics Committee of Jilin Academy of Agricultural Sciences.

AUTHOR CONTRIBUTIONS

YC (seventh author) designed the study. YW, XL, and YC (third author) performed the experiments. CX, YL, and YW analyzed the data. YW wrote the manuscript. HJ and YC (seventh author) corrected and approved the final version of the manuscript. All authors participated in the revision of the manuscript.

FUNDING

This study was supported by the National Natural Science Foundation of Jilin Province (20190201161JC) and China Agriculture Research System of MOF and MARA (CARS38).

SUPPLEMENTARY MATERIAL

The Supplementary Material for this article can be found online at: https://www.frontiersin.org/articles/10.3389/fgene.2021.649140/full#supplementary-material

REFERENCES

Cao, Y. (2017). *Comparative Analysis of Whole Genome Methylation and Transcriptome of the Longissimus Dorsi Muscle of Du Han and Small-Tail Han Sheep*. Changchun: Jilin University.

Church, C. D., Berry, R., and Rodeheffer, M. S. (2014). Isolation and study of adipocyte precursors. *Methods Enzymol.* 537, 31–46.

Colas, E., Perez, C., and Cabrera, S. (2011). Molecular markers of endometrial carcinoma detected in uterine aspirates. *Int. J. Cancer*. 129, 2435–2444. doi: 10.1002/ijc.25901

Fang, X. B. (2017). *Identification and Functional Verification of Candidate Genes for Beef Quality Traits Based on Transcriptome and Genome-Wide Methylation Analysis*. Changchun: Jilin University.

Fu, S., Zhao, Y., Li, Y., Li, G., Chen, Y., Li, Z., et al. (2018). Characterization of miRNA transcriptome profiles related to breast muscle development and intramuscular fat deposition in chickens. *J. Cell. Biochem.* 119, 7063–7079.

Galic, S., Oakhill, J. S., and Steinberg, G. R. (2010). Adipose tissue as an endocrine organ. *Mol. Cell. Endocrinol.* 316, 129–139.

Gesta, S., Tseng, Y. H., and Kahn, C. R. (2007). Developmental origin of fat: tracking obesity to its source. *Cell* 131, 242–256. doi: 10.1016/j.cell.2007.10.004

Huan-Hsien, C. (2011). *Study on Molecular Regulatory Network and Related Genes of Intramuscular Fat Formation in Broilers*. Beijing: Chinese Academy of Agricultural Sciences.

Imai, T., Takakuwa, R., Marchand, S., Dentz, E., Bornert, J. M., Messaddeq, N., et al. (2004). Peroxisome proliferator-activated receptor gamma is required in mature white and brown adipocytes for their survival in the mouse. *Proc. Natl. Acad. Sci. U.S.A.* 101, 4543–4547. doi: 10.1073/pnas.0400356101

Klimosch, S. N., Forstin, A., and Eckert, J. (2013). Functional TLR5 genetic variants affect human colorectal cancer survival. *Cancer Res.* 73, 7232–7242. doi: 10.1158/0008-5472.can-13-1746

Lake, B. G. (1995). Mechanisms of hepatocarcinogenicity of peroxisome-proliferating drugs and chemicals. *Annu. Rev. Pharmacol. Toxicol.* 35, 483–507. doi: 10.1146/annurev.pa.35.040195.002411

Li, G., Fu, S., Chen, Y., Jin, W., Zhai, B., Li, Y., et al. (2019). MicroRNA-15a regulates the differentiation of intramuscular preadipocytes by targeting *ACAA1*. *ACOX1* and *SCP2* in Chickens. *Int. J. Mol. Sci.* 20:4063. doi: 10.3390/ijms20164063

Li, W. J. (2008). *Screening and High-spirited Regulation of functional genes of Chicken related Fat Metabolism*. Beijing: Chinese Academy of Agricultural Sciences.

Lisowski, P., Kościuczuk, E. M., Gościk, J., Pierzchała, M., Rowińska, B., and Zwierzchowski, L. (2014). Hepatic transcriptome profiling identifies differences in expression of genes associated with changes in metabolism and postnatal growth between Hereford and Holstein-Friesian bulls. *Anim. Genet.* 45, 288–292. doi: 10.1111/age.12116

Liu, F., Li, H., Chang, H., Wang, J., and Lu, J. (2015). Identification of hepatocellular carcinoma-associated hub genes and pathways by integrated microarray analysis. *Tumori* 101, 206–214. doi: 10.5301/tj.5000241

Meng, Y. (2020). *Effects of Hypoxic Training on Liver Lipid Metabolism Related Genes and Serum Exocrine in Obese Rats*. Shandong: Qufu Normal University.

Nwosu, Z. C., Battello, N., and Rothley, M. (2018). Liver cancer cell lines distinctly mimic the metabolic gene expression pattern of the corresponding human tumours. *J. Exp. Clin. Cancer Res.* 37:211.

Park, S. J., Beak, S. H., Jung, D. J. S., Kim, S. Y., Jeong, I. H., Piao, M. Y., et al. (2018). Genetic, management, and nutritional factors affecting intramuscular fat deposition in beef cattle - A review. *Asian-Australas J. Anim. Sci.* 31, 1043–1061. doi: 10.5713/ajas.18.0310

Park, S. K., Yang, J. J., Oh, S., Cho, L. Y., Ma, S. H., Shin, A., et al. (2012). Innate immunity and non-Hodgkin's lymphoma (NHL) related genes in a nested case-control study for gastric cancer risk. *PLoS One* 7:e45274. doi: 10.1371/journal.pone.0045274

Ramírezzacarías, J. L., Castromuñozledo, F., and Kuriharcuch, W. (1992). Quantitation of adipose conversion and triglycerides by staining intracytoplasmic lipids with oil red O. *Histochemistry* 97, 493–497. doi: 10.1007/bf00316069

Schupp, M., Cristancho, A. G., and Lefterova, M. I. (2009). Re-expression of GATA2 cooperates with peroxisome proliferator-activated receptor-gamma depletion to revert the adipocyte phenotype. *J. Biol. Chem.* 284, 9458–9464. doi: 10.1074/jbc.m809498200

Stim-Herndon, K. P., Petersen, D. J., and Bennett, G. N. (1995). Characterization of an acetyl-CoA C-acetyltransferase (thiolase) gene from Clostridium acetobutylicum ATCC 824. *Gene* 154, 81–85. doi: 10.1016/0378-1119(94)00838-j

Vishwakarma, R. K., Ruby, Singh, S., Sonawane, P. D., Srivastava, S., and Kumari, U. (2013). Molecular cloning, biochemical characterization, and differential expression of an Acetyl-CoA C-Acetyltransferase Gene (AACT) of Brahmi (Bacopa monniera). *Plant Mol. Biol. Rep.* 31, 547–557. doi: 10.1007/s11105-012-0523-6

Wanders, R. J., Vreken, P., Ferdinandusse, S., Jansen, G. A., Waterham, H. R., van Roermund, C. W., et al. (2001). Peroxisomal fatty acid alpha- and beta-oxidation in humans: enzymology, peroxisomal metabolite transporters and peroxisomal diseases. *Biochem. Soc. Trans.* 29(Pt 2), 250–267. doi: 10.1042/bst0290250

Wood, J. D., Enser, M., Fisher, A. V., Nute, G. R., Sheard, P. R., Richardson, R. I., et al. (2008). Fat deposition, fatty acid composition and meat quality: a review. *Meat Sci.* 78, 343–358. doi: 10.1016/j.meatsci.2007.07.019

Wu, T., Zhang, Z. H., Yuan, Z. Q., Lo, L. J., Chen, J., Wang, Y., et al. (2013). Distinctive genes determine different intramuscular fat and muscle fiber ratios of the longissimus dorsi muscles in jinhua and landrace pigs. *PLoS One* 8:e53181. doi: 10.1371/journal.pone.0053181

Xie, W., Zhang, S., Lei, F., Ouyang, X., and Du, L. (2014). Ananas comosus L. Leaf Phenols and p-Coumaric acid regulate liver fat metabolism by upregulating CPT-1 expression. *Evid. Based Complement Alternat Med.* 2014:903258.

Ya, Y. Y. (2013). *Cloning and Quantitative Expression of 3-Ketoacyl-CoA Thiolase Gene in ISOCHRYSIS Globosa and Analysis of Fatty Acid Content Under Environmental Stress*. Shihezi: Shihezi University.

Yang, Y., Fang, X., Yang, R., Yu, H., Jiang, P., Sun, B., et al. (2018). MiR-152 regulates apoptosis and triglyceride production in MECs via targeting ACAA2 and HSD17B12 genes. *Sci. Rep.* 8:417.

Yao, C. G. (2020). *Identification of Gene Expression Patterns Affecting Porcine Fat Depositionusing GEO Public Database*. Changchun: Jilin University.

Yun, J., Jin, H., Cao, Y., Zhang, L., Zhao, Y., Jin, X., et al. (2018). RNA-Seq analysis reveals a positive role of HTR2A in adipogenesis in yan yellow cattle. *Int. J. Mol. Sci.* 19:1760. doi: 10.3390/ijms19061760

Zhang, B., Wu, Q., Wang, Z., Xu, R., Hu, X., Sun, Y., et al. (2019). The promising novel biomarkers and candidate small molecule drugs in kidney renal clear cell carcinoma: evidence from bioinformatics analysis of high-throughput data. *Mol. Genet. Genomic Med.* 7:e607. doi: 10.1002/mgg3.607

Zhang, L. Y., and Wang, Y. M. (2015). *Persistent Effects of Intake of Sea Cucumber Phospholipids on the Expression of Genes Related to Lipid Metabolism in Mice. Abstract of the Annual Meeting of Chinese Fisheries Society*. Hangzhou: China Fisheries Society.

Zhang, Y., Wang, Y., Wang, X., Ji, Y., Cheng, S., Wang, M., et al. (2018). Acetyl-coenzyme A acyltransferase 2 promote the differentiation of sheep precursor adipocytes into adipocytes. *J. Cell. Biochem. [Online ahead of print]* doi: 10.1002/jcb.28080

Zhu, S., Park, S., Lim, Y., Shin, S., and Han, S. N. (2016). Korean pine nut oil replacement decreases intestinal lipid uptake while improves hepatic lipid metabolism in mice. *Nutr. Res. Pract.* 10, 477–486. doi: 10.4162/nrp.2016.10.5.477

Zou, C., Li, L., Cheng, X., Li, C., Fu, Y., Fang, C., et al. (2018). Identification and functional analysis of long intergenic non-coding RNAs underlying intramuscular fat content in pigs. *Front Genet.* 27:102. doi: 10.3389/fgene.2018.00102

Conflict of Interest: The authors declare that the research was conducted in the absence of any commercial or financial relationships that could be construed as a potential conflict of interest.

frontiers in Veterinary Science

ORIGINAL RESEARCH
published: 22 June 2021
doi: 10.3389/fvets.2021.665872

Assessing Genetic Diversity and Estimating the Inbreeding Effect on Economic Traits of Inner Mongolia White Cashmere Goats Through Pedigree Analysis

Zhiying Wang[1†], Bohan Zhou[1†], Tao Zhang[1,2†], Xiaochun Yan[1], Yongsheng Yu[1], Jinquan Li[3,4,5], Bujun Mei[6], Zhixin Wang[1], Yanjun Zhang[1], Ruijun Wang[1], Qi Lv[1], Zhihong Liu[2], Yanhong Zhao[2], Chen Du[7] and Rui Su[1]**

[1] College of Animal Science, Inner Mongolia Agricultural University, Hohhot, China, [2] Inner Mongolia Bigvet Co., Ltd., Hohhot, China, [3] Key Laboratory of Mutton Sheep Genetics and Breeding, Ministry of Agriculture, Hohhot, China, [4] Key Laboratory of Animal Genetics, Breeding and Reproduction in Inner Mongolia Autonomous Region, Hohhot, China, [5] Engineering Research Center for Goat Genetics and Breeding, Inner Mongolia Agriculture University, Hohhot, China, [6] Department of Agriculture, Hetao College, Hetao University, Bayannaoer, China, [7] Reproductive Medicine Center, Affiliated Hospital of Inner Mongolia Medical University, Hohhot, China

Objective: The purpose of this study was to discover the population structure and genetic diversity of Inner Mongolia White Cashmere goats (IMCGs) and demonstrate the effect of inbreeding on the live body weight (LBW), cashmere yield (CY), fiber length (FL), and fiber diameter (FD) of IMCGs.

Materials and Methods: All data were collected from pedigree information and production performance records of IMCGs from 1983 to 2019. The population structure and genetic diversity were analyzed by Endog 4.8 software. Inbreeding coefficients were obtained by the pedigree package in R. Then, a linear regression model was used to analyze how inbreeding influences economic traits in IMCGs. Four levels of inbreeding coefficients (F_i) were classified in this study, including $F_i = 0$, $0 < F_i \leq 6.25$, $6.25 < F_i \leq 12.5$ and $F_i \geq 12.5$. Variance analysis was performed to determine whether inbreeding levels had a significant effect on economic traits in IMCGs.

Results: The proportions of rams and dams in IMCGs for breeding were relatively small, with values of 0.8 and 20.5%, respectively. The proportion of inbred animals in the entire population was high, with values up to 68.6%; however, the average inbreeding coefficient and relatedness coefficient were 4.50 and 8.48%, respectively. To date, the population has experienced 12 generations. The average generation interval obtained in the present study was 4.11 ± 0.01 years. The ram-to-son pathway was lowest (3.97 years), and the ewe-to-daughter pathway was highest (4.24 years). It was discovered that the LBW, CY, and FL increased by 3.88 kg, 208.7 g, and 1.151 cm, respectively, with every 1% increase in the inbreeding coefficient, and the FD decreased by 0.819 μm with every 1% increase in the inbreeding coefficient. Additionally, multiple comparison analysis indicated that when the inbreeding coefficient was higher than 6.25%, the LBW

Edited by:
Fabyano Fonseca Silva,
Universidade Federal de Viçosa, Brazil

Reviewed by:
Radovan Kasarda,
Slovak University of Agriculture, Slovakia
Mohammadreza Mohammadabadi,
Shahid Bahonar University of Kerman, Iran

***Correspondence:**
Chen Du
duchen1986072300@126.com
Rui Su
suruiyu@126.com

[†]These authors have contributed equally to this work and share first authorship

Specialty section:
This article was submitted to Livestock Genomics, a section of the journal Frontiers in Veterinary Science

Received: 09 February 2021
Accepted: 10 May 2021
Published: 22 June 2021

Citation:
Wang Z, Zhou B, Zhang T, Yan X, Yu Y, Li J, Mei B, Wang Z, Zhang Y, Wang R, Lv Q, Liu Z, Zhao Y, Du C and Su R (2021) Assessing Genetic Diversity and Estimating the Inbreeding Effect on Economic Traits of Inner Mongolia White Cashmere Goats Through Pedigree Analysis. Front. Vet. Sci. 8:665872. doi: 10.3389/fvets.2021.665872

showed an obvious decreasing trend. The threshold value of inbreeding depression in the CY is 12.5%. However, inbreeding depression has not been observed in the FL and FD.

Conclusion: Pedigree completeness needs to be further strengthened. The degree of inbreeding in this flock should be properly controlled when designing breeding programs.

Keywords: inner Mongolia white cashmere goats, genetic diversity, regression analysis, population structure, inbreeding

INTRODUCTION

As a typical small ruminant, cashmere goats are mainly distributed in dry and harsh climatic conditions in the tropics (1). Goat farming is practiced worldwide, with goat products having a favorable image (2, 3). The number of goats has increased globally, even in countries with high and intermediate incomes, despite major changes in agriculture due to industrial mergers, globalization, and technological advances in developed countries (4, 5). Most cashmere goats are dual-purpose breeds that produce cashmere, meat, and milk (6). China is the largest cashmere goat-producing country in the world. According to statistics, the total cashmere produced in China was ∼15,437.76 tons in 2018, accounting for more than 2/3 of the world's total output. The export volume of cashmere reached 3,212 tons (http://www.fao.org/home/en/). The genetic resources of cashmere goats are very rich throughout the world and are mainly distributed in Asia, including Mongolia, Iran, Afghanistan, Kazakhstan, Kyrgyzstan, and Tajikistan. Inner Mongolia White Cashmere goats (IMCGs) and Liaoning Cashmere goats (LNCGs) are key breeds in China (7). The male parents of most goat breeds in China come from both varieties (8). IMCGs and LNCGs are not allowed to be exported and are listed in the directory of genetic resource protection. The number of goat breeds in China is ∼69, including 18 cashmere goat breeds. There are 15 local varieties and 3 cultivated varieties (9).

Genetic diversity and population structure in animals are usually analyzed by using microsatellite and mitochondrial DNA variations (10, 11). In recent years, pedigree analysis has been an appropriate tool for evaluating genetic diversity and population structure in populations (12–16). Baena et al. (12) analyzed the genetic structure of the Mangalarga Marchador horse population in Brazil based on pedigree analysis and identified factors that may affect its genetic variability. Illa et al. (14) assessed the genetic diversity and population structure and appraised the efficiency of ongoing selective breeding programs in a closed nuclear herd of Nellore sheep through pedigree analysis. Vigeland (16) calculated relatedness coefficients by using pedigree information with inbred founders. Vatankhah et al. (15) described the population genetic structure and evaluated the state of conservation of genetic variability of Lori-Bakhtiari sheep in Iran. Goleman et al. (13) analyzed the degree of relatedness between individuals in the Polish hunting dog population and assessed the genetic variability of the population based on pedigree analysis. The analysis of genetic diversity and population structure will contribute to the conservation of animal genetic resources (14). IMCGs are an indigenous breed that is famous around the world due to its superior cashmere. In a previous study, the genetic diversity and population structure of IMCGs were analyzed by mitochondrial DNA and microsatellite polymorphism (17). This is the first study to analyze the population structure and genetic diversity of IMCGs based on pedigree information.

Many studies have reported that inbreeding in one flock may result in a decrease in production performance (14, 18). Yousefi et al. (19) quantified the effect of inbreeding on the average daily gain and the Kleiber ratio in native Mazandaran chickens. It was demonstrated that inbreeding had a significant effect on the average daily gain from hatching to 8 and 12 weeks of age (19). Paiva R demonstrated that MY305 was significantly affected by inbreeding (20). Todd et al. (18) analyzed the effects of inbreeding on covering success, gestation length, and foal sex ratio in Australian thoroughbred horses. Kiya et al. (21) reported that the inbreeding effect was significant for the longissimus muscle area and backfat thickness. In this study, the effect of the inbreeding coefficient on important economic traits in IMCGs was analyzed, which is helpful for properly designing mating schemes.

MATERIALS AND METHODS

Data Sources

In this study, genealogical information of IMCGs for a period of 37 years from 1983 to 2019 was collected for genetic diversity and population structure analysis. A total of 53,381 individuals were recorded, including 25,032 male lambs and 28,349 female lambs. The pedigree was edited to check the inconsistencies in dam and sire registration, birth date and sex registration. All of the individuals were sorted by date of birth for the next analysis.

The data were provided by Inner Mongolia Yiwei White Cashmere Goat Co., Ltd, China. The goats are reared at Etuoke Banner, Ordos City, Inner Mongolia Autonomous Region, China with arid and semiarid areas. IMCGs graze year round with supplementary feeding in the winter. Artificial insemination was used in this flock. The mating ratio of male to female sheep was ∼1:200–300. Mating usually occurred in early October of each year and lasted nearly 50 days. Lambs were born during the month of March. The feeding management and trait measurement methods have been described in detail in our previous studies (22). All birthing events were recorded, including the identification number, date of birth, birth status, sex, and birth weight. Pedigree information was comprehensive and clear with kids, sires, and dams. The traits evaluated in this study included the live body weight (LBW), cashmere yield (CY),

TABLE 1 | The basic statistics of economic traits of IMCGs.

Traits	*N*	MEAN	SD	C.V(%)
Live body weight	63,217	34.67	10.03	28.92
Cashmere yield	65,831	661.7	221.9	33.54
Fiber length	66,148	5.83	1.13	19.44
Fiber diameter	13,260	14.57	0.99	6.78

TABLE 2 | Pedigree structure of Inner Mongolia White Cashmere goats.

Item	*N*
Individuals in total	53,381
Males	25,032
Females	28,349
Sires in total	433
Dams in total	10,923
Base population	5,455
Individuals with known sire	49,274
Individuals with known dam	51,095
Individuals with both unknown parents	114
Individuals with both known parents	47,957
Individuals with no progeny	42,027

fiber length (FL), and fiber diameter (FD). The basic statistics for each trait are shown in **Table 1**.

Statistical Analysis

Analysis of Genetic Diversity and Population Structure

Endog 4.8 software was utilized to perform pedigree analysis and obtain corresponding parameters to illustrate the historical diversity and population structure (23). The depth and wholeness of the pedigree was determined by estimating the equivalent number of generations, and it was estimated by tracing back each ancestor in the pedigree history through numerous generations.

The founders are defined as individuals with one or both unknown parents. A 4-year time path was used to define the reference population because this time duration represents an approximate generation interval in goats (14). In the reference population, the effective number of founders and ancestors is useful to assess genetic diversity. The effective number of founders is characterized as the number of equally contributing founders that would be expected to produce the same genetic diversity as in the population under study (24). The formula is as follows:

$$f_e = \frac{1}{\sum_{k=1}^{f} q_k^2}$$

where q_k is the probability of gene origin for ancestor k. The effective number of ancestors (f_a) reflects the minimum number of animals required to estimate the genetic diversity of the population under study, and it is a useful measure to determine

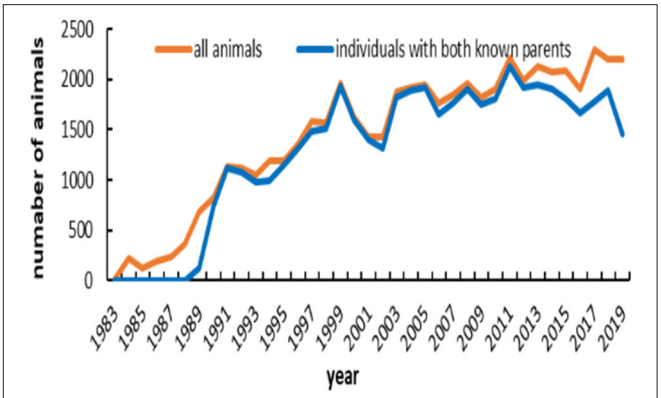

FIGURE 1 | Number of animals and number of individuals with both known parents across years.

the bottlenecks in the population that are the primary reason for genetic erosion in captive and domestic populations. It is estimated as:

$$f_a = \frac{1}{\sum_{j=1}^{a} q_j^2}$$

where q_j is the marginal contribution of ancestor j, which demonstrates the genetic contribution of an ancestor that is not explained by an earlier ancestor. In general, the effective number of ancestors should be smaller than the effective number of founders due to bottlenecks that reduce genetic variability.

The inbreeding coefficient (F) and the average relatedness (AR) coefficient were estimated by Meuwissen and Luo (24) and MaléCot (25), respectively. The AR coefficient of any animal is explained as the probability that an allele selected at random from the total population in the pedigree belongs to a particular animal; hence, it is equated as an account of the animal in the entire pedigree regardless of the pedigree information. F is defined as the probability that an individual has two identical alleles by descent. The change in breeding (ΔF) is estimated for each generation using the formulae suggested by Lacy (26).

$$\Delta F_i = 1 - \sqrt[t-1]{1 - F_i}$$

where F_i is the individual inbreeding coefficient and t is the equivalent complete generation for this individual. The estimate of effective population size (N_e) was computed from ΔF_i by averaging ΔF_i of n individuals included in a given reference subpopulation (27) as $N_e = 1/2\Delta\overline{F}$.

The genetic conservation index (GCI) for each of the individuals of the analyzed population was provided by Alderson (28). The index is computed from the genetic contributions of all of the identified founders as $GCI = \frac{1}{\sum p_i^2}$, where p_i is the proportion of genes of founder i in the pedigree of an animal. The index is based on the assumption that the objective of a conservation program is to retain the full range of alleles possessed by the base population. In this respect, the

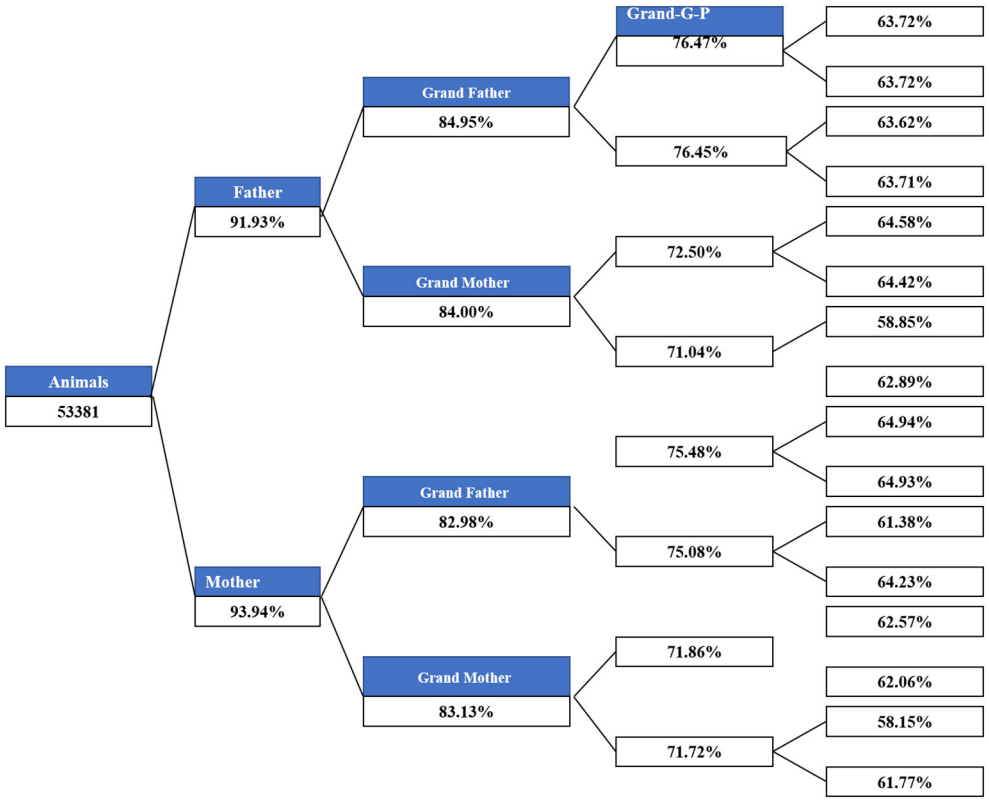

FIGURE 2 | Pedigree completeness across generations.

ideal individual would receive equal contributions from all of the founder ancestors in the population, and consequently, the higher the GCI value is, the higher the values of an animal for conservation (28). The following parameters were estimated for each individual: (1) the number of fully outlined generations, detailed as the number of generations delineating the offspring of the furthest generation where the ancestors of second-generation individuals are known, and ancestors with unknown parents are considered founders (generation 0); (2) the maximum number of generations observed, determined as the number of generations separating the individual from its ultimate ancestor; and (3) equivalent complete generations are detailed as the sum over all known ancestors of the terms calculated as the aggregate of $(1/2)^n$, where n is the number of generations separating the individual from each known ancestor. The average generation interval (GI) was pointed out as the average age of the birth of selected offspring. The estimate of GI for all of the pathways was estimated for the reference population, as this subpopulation is the most recent one that could accrue at least one generation on the farm.

Wright's (29) *F*-statistics are obtained as $F_{IS} = \frac{\tilde{F}-\bar{f}}{1-\bar{f}}$, $F_{ST} = \frac{\bar{f}-\tilde{f}}{1-\tilde{f}} = \frac{D}{1-\tilde{f}}$ and $F_{IT} = \frac{\tilde{F}-\tilde{f}}{1-\tilde{f}}$, where $\tilde{f}$ and $\tilde{F}$ are the mean coancestry and inbreeding coefficient for the entire metapopulation, respectively, and $\bar{f}$ is the average coancestry for the subpopulation. D is the kinship distance for molecular coancestry (30, 31).

The parameter of founder genome equivalents (f_g) can be defined as the number of founders that would be expected to produce the same genetic diversity as in the population under study if the founders were equally represented and no loss of alleles occurred. Parameter f_g was obtained by the inverse of twice the average coancestry of the individuals included in a predefined reference population (30).

Effect of Inbreeding on Important Economic Traits of IMCGs

The basic statistics of each trait in this study are shown in **Table 3**. Except for the fiber diameter, the other three traits were collected from 1990 to 2019. The individual inbreeding coefficient was obtained by pedigree packages in R (32). A multiple linear regression model was used to analyze how the inbreeding coefficient influenced the four traits. In this study, the impact factors of each trait included the production year (1990–2019), flocks (1–12), age of individuals (1–7), age of dams (2–7) birth status (1, 2), and gender (1, 2). The inbreeding coefficient (F_i) is continuously viable; however, other factors are discrete variables. Therefore, these discrete variables need to be centered first. Then, regression analysis was carried out by using the lm

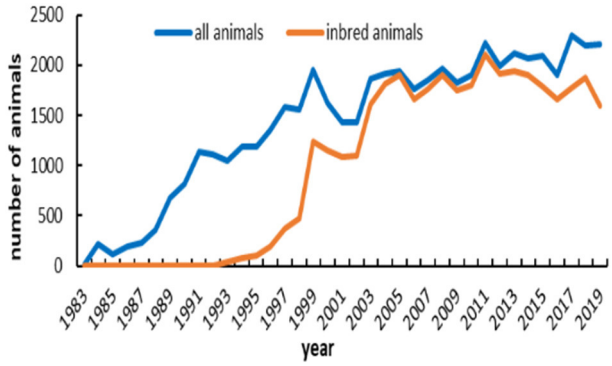

FIGURE 3 | Registered and inbred individuals of IMCGs from 1983 to 2019.

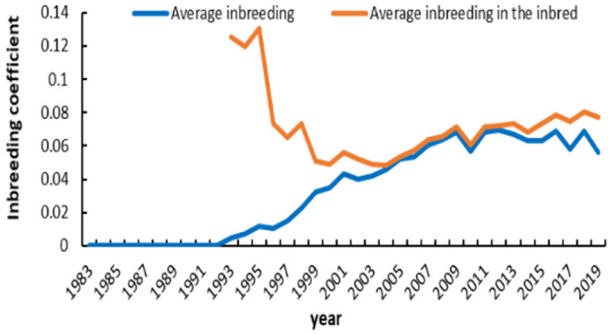

FIGURE 4 | Average inbreeding coefficient in registered and inbred individuals in IMCGs across years.

function of R language (33). The regression model is as follows:

$$y_i = \gamma_{00} + \gamma_{01} Year_i + \gamma_{02} Flock_i + \gamma_{03} Age_i + \gamma_{04} Dage_i + \gamma_{05} Sex_i + \gamma_{06} Bs_i + \gamma_{07} F_i + e_i$$

where y_i is the vector of the observed value of the i^{th}individual. $Year_i$, $Flock_i$, Age_i, $Dage_i$, Sex_i, Bs_i , and F_i are independent variables, while e_i is the residual. γ_{00} is an intercept, which was also used as the overmean. γ_{01}, γ_{02}, γ_{03}, γ_{04}, γ_{05}, γ_{06}, and γ_{07} are the slope coefficients of $Year_i$, $Flock_i$, Age_i, $Dage_i$, Sex_i, Bs_i , and F_i, which explained the incremental change in the dependent variable for each unit of change in the independent variables.

To assess how inbreeding influences the important economic traits of IMCGs, it is helpful to design a proper breeding scheme. Referring to corresponding studies (14), inbreeding coefficients (F_i) obtained by pedigree information were classified into four levels ($F_i = 0$; $0 < F_i \leq 6.25$; $6.25 < F_i \leq 12.5$; $F_i \geq 12.5$). Variance analysis of inbreeding levels on each trait was performed by the aov function of R language.

TABLE 3 | Parameters of the probability of gene origin for the reference population of IMCGs.

Item	Value
Number of animals in the reference population	8,592
Number of ancestors contributing to the reference population	1,977
Total number of founder animals in the reference population	1,980
Effective number of ancestors	23.42
Effective number of founders	27.87
Effective number of ancestors for the reference population	19
Effective number of founders for the reference population	24
Number of ancestors explaining 50%	6
Mean maximum generations	11
Increase in inbreeding by maximum generation	0.76%
Mean complete generations	7
Increase in inbreeding by complete generation	1.66%
Mean equivalent generations	8.55
Increase in inbreeding by equivalent generation	1.30%
Genetic conservation index	18.58
Wright *F*-statistics	5.7×10^{-5}
Founder genome equivalent	11.78

RESULTS

Analysis of Genetic Diversity and the Population Structure

The main demographic characteristics derived from genealogical data of IMCG flocks are summarized in **Table 2**. In this population, 0.8 and 20.5% are presented as sires and dams, respectively. Out of 53,381 animals, the number of founders (with one or more unknown parents) was 5,455, accounting for ∼10.22%. Of the total animals, the ratio of individuals with no progeny was ∼78.7%. The timeline trend of all animals and individuals with both known parents across years is presented in **Figure 1**. From 1983 to 1989, all animals in the pedigree were founders. The number of individuals with both unknown parents was relatively low from 1990 to 2012. After 1998, the number of individuals remained stable on this farm. Additionally, the pedigree completeness is shown in **Figure 2**. In total, of 53,381 animals, more than 90% had records with both parents. However, pedigree completion was poor when tracing back generations.

The number of registered and inbred animals across birth years is shown in **Figure 3**. No inbred animal was found until 1993. The proportion of inbred animals in all registered individuals was more than 63.4%. An overall increasing trend did exist in the inbred animals for IMCGs from 1999 to 2005 and then remained stable. The number of inbred animals even reached 97.7% of the registered animals in 2005. The timeline trend of the average inbreeding coefficients is presented in **Figure 4**. Increasing trends of average inbreeding coefficients were observed in all registered animals. However, there was no regular trend for average inbreeding coefficients in the inbred animals. A decreasing trend for average inbreeding coefficients was observed from 1993 to 1998 in the inbred animals.

The probabilities of gene origin parameters in the studied breed are presented in **Table 3**. Of the 8,592 animals in the reference population, there were 4,298 males and 4,303 females. The number of founder animals in the reference

TABLE 4 | Inbreeding, average relatedness, and effective population size in IMCGs.

Item	Value
Coefficient of inbreeding (Fi) in the whole population (%)	4.50%
Proportion of animals with Fi = 0%	16,779 (31.43%)
Proportion of animals with Fi = 0 to ≤6.25%	20,402 (38.22%)
Proportion of animals with Fi = >6.25 to ≤12.50%	13,270 (24.86%)
Proportion of animals with Fi = >12.5%	2,930 (5.49%)
Average relatedness (AR%)	8.48%
Realized effective population size (Ner)	15.16 ± 3.33

TABLE 5 | Mean value of inbreeding (*F*) and percentage of endogamic animals of IMCGs using the maximum number of generations traced.

Generation	Animals (*N*)	*F* (%)	% Inbred	Average *F* for inbred	Mean AR
0	2,086	0.00%			0.05%
1	3,604	0.00%			1.79%
2	3,845	0.82%	6.50%	12.55%	4.62%
3	4,431	2.12%	30.17%	7.04%	6.56%
4	4,635	3.39%	67.92%	4.99%	8.24%
5	3,737	4.57%	90.71%	5.04%	9.49%
6	5,385	5.09%	94.97%	5.36%	9.85%
7	6,303	6.27%	96.02%	6.53%	10.83%
8	6,594	6.50%	93.13%	6.98%	10.74%
9	6,498	6.50%	87.12%	7.46%	10.42%
10	4,713	6.89%	88.71%	7.77%	10.54%
11	1,494	6.82%	85.88%	7.95%	10.40%
12	56	6.21%	80.36%	7.73%	9.73%

TABLE 6 | Generation intervals (in years) for the four pathways of the IMCGs.

Pathway	*N*	GI ± SE (years)
Ram–Son	387	3.97 ± 0.07
Ram–Daughter	8,731	3.98 ± 0.01
Ewe–Son	387	4.03 ± 0.08
Ewe–Daughter	8,809	4.24 ± 0.02
Total	18,314	4.11 ± 0.01

population was 1980. The number of ancestors contributing to the reference population of IMCGs was 1977, which accounted for 99.8% of founders. The effective numbers of founders and ancestors in the studied population were 27.87 and 23.42, respectively. The effective numbers of founders and ancestors in the reference population were 24 and 19, respectively. The parameters of mean maximum generations, complete generations and equivalent generations were 11, 7, and 8.55, and the increases in inbreeding in the corresponding generations were 0.76, 1.66, and 1.30%, respectively. Fifty percent of genetic diversity was explained by six influential ancestors in the reference cohort. The founder genome equivalent of the reference population was 11.78. *F*-statistics were used to assess genetic differentiation in subdivided populations, and the value was 5.7×10^{-5}.

The distribution of the inbreeding coefficient among IMCGs is presented in **Table 4**. A total of 36,602 animals were inbred. Approximately 55.7% of inbred animals had inbreeding lower than 6.25%. The inbreeding coefficient ranged from 0.98 to 35.93%. A total of 3.96% of inbred animals had an inbreeding coefficient > 25%. The average inbreeding value and mean average relatedness in the entire studied population were 4.50 and 8.48%, respectively. The average inbreeding in the inbred individuals was 6.57%. It is presumed that effective population size is considered the number of animals that breed in an ideal population and engender an equal amount of inbreeding in the population under study. The realized effective population size (Ner) was 15.16 ± 3.33.

This population has gone through 12 generations by pedigree tracing (**Table 5**). With the increase in generations, the inbreeding coefficient and average relatedness coefficient show an overall increasing trend. More than 90% of the individuals in the population are inbred in the fifth generation. The mean relatedness coefficient ranged from 9.49 to 10.74% after the fifth generation, which was relatively high. In the first two generations, there were no inbred animals, and the average relatedness was also very low, with values of 0.05 and 1.79%. The estimation of generation intervals (in years) for the four pathways of the IMCGs is presented in **Table 6**. The average generation length obtained in the present study was 4.11 ± 0.01 years. The ram-to-son pathway was lowest (3.97 years), and the ewe-to-daughter pathway was highest (4.24 years). However, no significant differences in generation intervals were observed among the four pathways in IMCGs.

Effect of Inbreeding on Important Economic Traits of IMCGs

A linear regression model was established to assess the relationship between important economic traits and the inbreeding coefficients of IMCGs, and the results are shown in **Table 7**. The production year, herd, individual ages, age of dam, and sex had highly significant effects on all four traits ($P < 0.01$). The birth status had no significant effect on the FL and FD ($P > 0.05$), but the other three traits were significantly affected by the birth status ($P < 0.01$). Excluding the FL, the inbreeding coefficient had a significant effect on the other three traits. The results demonstrated that the LBW, CY, and FL increased by 3.88 kg, 208.7 g, and 1.151 cm, respectively, with every 1% increase in the inbreeding coefficient, and the FD decreased by 0.819 μm with every 1% increase in the inbreeding coefficient.

Variance analysis was performed to determine the threshold value of the inbreeding value for each trait. The results are shown in **Table 8**. Inbreeding levels had a significant effect on all of the traits ($P < 0.01$). Additionally, the multiple comparison analysis indicated that when the inbreeding coefficient was more than 6.25%, the LBW had an obvious decreasing trend. The threshold value of inbreeding depression in the CY is 12.5%. However, inbreeding depression has been observed in the FL and FD.

TABLE 7 | Regression analysis of inbreeding on the economic traits of IMCGs.

Effects	LBW		CY		FL		FD	
	Estimates	*P*-value	Estimates	*P*-value	Estimates	*P*-value	Estimates	*P*-value
Intercept	34.92	< 0.01**	660.93	< 0.01**	5.899	< 0.01**	14.070	< 0.01**
Year	0.49	< 0.01**	13.22	< 0.01**	0.050	< 0.01**	0.067	< 0.01**
Herd	−0.12	< 0.01**	0.89	0.027*	−0.017	< 0.01**	−0.046	< 0.01**
Age	3.04	< 0.01**	4.96	< 0.01**	0.019	< 0.01**	0.136	< 0.01**
Dage	0.11	< 0.01**	−4.13	< 0.01**	−0.018	< 0.01**	0.012	0.013*
bt	−0.54	< 0.01**	10.64	< 0.01**	0.018	0.069^{ns}	−0.009	0.591^{ns}
Sex	−14.65	< 0.01**	−58.20	< 0.01**	−0.378	< 0.01**	−0.203	< 0.01**
F	3.88	< 0.01**	208.73	< 0.01**	0.151	0.178^{ns}	−0.819	< 0.01**

*age, individual ages; dage, age of dams; bt, birth type; LBW, live body weight; CY, cashmere yield; FL, fiber length; FD, fiber diameter. **highy signifficant; *signifficant; ns, not signifficant.*

TABLE 8 | Variance analysis of inbreeding levels on important economic traits of IMCGs.

Traits	Class	*N*	Mean ± SD	*P*
LBW	Fi = 0%	34,213	30.56 ±8.56^{c}	<0.01**
	Fi = 0 to ≤6.25%	19,020	37.65 ±10.20^{a}	
	Fi = >6.25 to ≤12.50%	7,965	37.35 ±10.07^{b}	
	Fi > 12.5%	2,019	37.06 ±10.22^{b}	
CY	Fi = 0%	34,856	550.0 ±177.9^{c}	<0.01**
	Fi = 0 to ≤6.25%	20,258	759.1 ±211.6^{a}	
	Fi = >6.25 to ≤12.50%	8,573	764.9 ±208.3^{a}	
	Fi > 12.5%	2,144	745.7 ±204.8^{b}	
FL	Fi = 0%	34,908	5.49 ±1.00^{b}	<0.01**
	Fi = 0 to ≤6.25%	20,434	6.18 ±1.04^{a}	
	Fi = >6.25 to ≤12.50%	8,649	6.21 ±1.07^{a}	
	Fi > 12.5%	2,157	6.19 ±1.07^{a}	
FD	Fi = 0%	2,051	14.76 ±0.89^{a}	<0.01**
	Fi = 0 to ≤6.25%	7,278	14.56 ±1.00^{b}	
	Fi = >6.25 to ≤12.50%	3,154	14.57 ±0.99^{b}	
	Fi > 12.5%	777	14.49 ±0.97^{b}	

***highy signifficant.*

DISCUSSION

Analysis of Genetic Diversity and Population Structure

In this population, 0.8 and 20.5% are presented as sires and dams, respectively. The fraction of males and females selected in IMCGs was relatively low. Individuals with no progeny accounted for 78.7% of all animals. All of these animals were sold as stud stocks to other flocks to improve performance or eliminated at the market for goat meat. Artificial insemination is used in this flock, so very few sires were selected. Out of 53,381 animals, the number of founders (with one or more unknown parents) was 5,455, accounting for ∼10.22%. The results suggested a good depth in the pedigree in terms of completeness. Therefore, the accuracy of the estimated founders is reliable. The timeline trend of all animals with both known parents across the years indicated that the number of individuals with both unknown parents was low from 1990 to 2012; however, this value increased from 2013 to 2019. This may be related to incorrect pedigree information. After 1998, the population size remained stable. Our research team began to design a breeding plan for this flock in 1998, and thus, it had a reasonable population structure from then on.

This farm is representative of IMCGs. It has always undergone closed breeding and never introduced other breeds to cross. Therefore, the proportion of inbred animals among all registered individuals was more than 68.6%. A certain degree of inbreeding can improve production performance. Increasing trends of average inbreeding coefficients were observed in all registered animals. However, there was no regular trend for average inbreeding coefficients in the inbred animals. To maximize production performance, a reasonable mating plan is created every year. Most inbred animals showed inbreeding coefficients lower than 6.25%, and inbred animals with inbreeding coefficients > 25% accounted for ∼4%. This may be related to our strict implementation of the proper mating scheme. A small fraction of high inbreeding individuals may be caused by natural mating or poor management. The average inbreeding value in the entire studied population was 4.50%, which is lower than that in the cashmere goat breed of the South Khorasan and Iranian Adani goat breeds reported by Joezy-Shekalgorabi et al. (34, 35). However, Illa et al. (14) reported that the average inbreeding coefficient in Nellore sheep was 3.32%, which was lower than that in the IMCG population. This difference may be explained by population structure, sample size, and management mode. The average relatedness in this population is 8.48%, which is higher than that in other ruminant breeds (36, 37). It is presumed that the effective population size is considered the number of animals that breed in an ideal population and engender an equal amount of inbreeding in the population under study. According to the FAO guidelines on preserving animal genetic resources, an effective population size of < 50 affects the fitness of the breed (38). The realized effective population size (Ner) noted in this population is 15.16 ± 3.33, which is far lower than that reported in Nellore sheep and Latxa dairy sheep (14, 39). This is caused by the differences among breeds, mating schemes, and breed plans. The *F*-statistic in this population is very low, which is far lower than that reported in other studies (37, 40). This indirectly reflects the genetic differentiation among the population. Thus, this result indicated that the genetic differentiation in the IMCG population was low.

Shortening the generation interval is one of the methods to increase genetic progress. It also may result in better economic returns. This outcome is the best choice for production enterprises. However, decreasing the ability of individuals to stay on the farm will intensify genetic variability losses, especially rams. The genetic contribution of those animals will be lower because of their short lifespan. The population in this study has gone through 12 generations by pedigree tracing. The average generation length obtained in the present study was 4.11 ± 0.01 years, which is longer than that estimated in Beetal goats. Tomar et al. (41) reported that the generation interval was 2.04 years for Beetal goats. Similar results were observed in other breeds of goats (34, 35, 42). The generation length is ∼4 years for most goats. Compared to the sire–progeny pathways, a higher mean generation interval of the dam–progeny pathways was observed. This is probably attributable to the fact that breeding dams are usually kept for more years to produce offspring than sires. Similar results were obtained in Creole goats and Nellore sheep (14, 42). Animal conservation programs should balance the lowered generation intervals with decent annual genetic gains and breeding animals with sustained genetic variability on the farm.

Effect of Inbreeding on Important Economic Traits of IMCGs

The linear regression analysis demonstrated that the LBW, CY, and FL increased by 3.88 kg, 208.7 g, and 1.151 cm with every 1% increase in the inbreeding coefficient, and the FD decreased by 0.819 μm with every 1% increase in the inbreeding coefficient. It was illustrated that inbreeding had no negative impact on the economic traits under the current mating scheme. However, the variance of analysis of inbreeding levels indicated that when the inbreeding coefficient of most individuals was higher than 6.25 and 12.5%, the LBW and CY will produce inbreeding depression, respectively. Hence, the breeding plan should be updated appropriately. However, it is surprising to find that the increase in inbreeding resulted in a decrease in the FD, which is beneficial to the improvement of fiber quality. The results of this population are similar to those reported by Dai et al. (43). This study illustrated that inbreeding depression for fleece traits did not exist when the inbreeding coefficient reached 12.5%. Most studies have shown that inbreeding has no significant effect on fleece traits (36). Sousa et al. (44) reported that inbreeding had a significant effect on the body weight of Anglo Nubiana breed goats. Vostra-Vydrova et al. (37) indicated that inbreeding coefficients showed a significant negative influence on milk performance in the White Shorthair goat breed. This may be due to the differences in the studied traits, population structure, and data size.

CONCLUSION

Population structure across years in the Inner Mongolia Cashmere goat breed was documented in this study. A small number of unknown parents was found to be the reason for complete and detailed pedigree information. Although the proportion of inbred individuals in the entire population is high, the low average inbreeding coefficient and average relatedness obtained in the studied population indicated that the current mating scheme is relatively reasonable. Generally, animals with unknown parents are assumed to have no inbreeding. However, in reality, this will lead to underestimation of the inbreeding coefficient. An effective way to solve this problem is to ensure pedigree completeness. Alternatively, utilizing paternity testing methods helps to overcome the problem of pedigree incompleteness. Although inbreeding has not resulted in an obvious decrease in economic traits, it should be controlled properly when designing mating schemes.

DATA AVAILABILITY STATEMENT

The original contributions presented in the study are included in the article/supplementary material, further inquiries can be directed to the corresponding author/s.

AUTHOR CONTRIBUTIONS

TZ, XY, YY, and QL analyzed the data. RS, CD, and ZhiyW conceived of and coordinated the study. BM, RW, and JL helped in conceive of the study. ZhixW, YZhan, ZL, and YZhao help to collect data. ZhiyW and BZ wrote the manuscript. All authors read and approved the final manuscript.

ACKNOWLEDGMENTS

The authors of the article would like to send their sincere gratitude to the Natural Science Foundation of the Inner Mongolia Autonomous Region (2019 MS03070), the Science-Technology Project of Inner Mongolia Region (2020SGG2693), the Inner Mongolia Agricultural University for second levels of outstanding doctorate (NDYB2016-05), the Natural Science for Youth Foundation (31702086), the Natural Science Foundation of China (No. 31760660), and the Youth Science and Technology Talent Support Program of Inner Mongolia Autonomous Region (No. NJYT- 17-A21). Additionally, the authors would like to thank the Inner Mongolia Yiwei White Cashmere Goat Co., Ltd. for providing the necessary data to complete this study.

REFERENCES

1. Vazir NEA, Koshkooieh AE, Mehrjerdi AA, Mohammadabadi M, Babenko O, Bushtruk M, et al. Comparison of genetic diversity of leptin gene between wild goat and domestic goat breeds in iran. *Malaysian Appl Biol.* (2019) 48:85–93.
2. Gooki FG, Mohammadabadi M, Fozi MA, Soflaei M. Association of biometric traits with growth hormone gene diversity in raini cashmere goats. *Walailak J Sci Technol.* (2019) 16:499–508. doi: 10.48048/wjst.2019.3791
3. Khorshidi M, Mohammadabadi MR, Esmailizadeh AK, Barazandeh A, Babenko OI. Comparison of artificial neural network and regression models

for prediction of body weight in Raini Cashmere goat. *Iran J Appl Anim Sci.* (2019) 9:453–61.
4. Gholamhoseini Gooki F, Mohammadabadi MR, Asadi Fozi M. Polymorphism of the growth hormone gene and its effect on production and reproduction traits in goat. *Iran J Appl Anim Sci.* (2018) 8:653–9.
5. Shamsalddini S, Mohammadabadi MR, Esmailizadeh AK. Polymorphism of the Prolactin gene and its effect on fiber traits in goat. *Russ J Genet.* (2016) 52:405–8. doi: 10.1134/S1022795416040098
6. Moghadaszadeh M, Mohammadabadi MR, Esmailizadeh AK. Association of Exon 2 of BMP15 gene with the litter size in the Raini Cashmere goat. *Genet Millennium.* (2015) 13:4062–7.
7. Jin M, Lu J, Fei X, Lu Z, Quan K, Liu Y, et al. Genetic signatures of selection for cashmere traits in chinese goats. *Animals.* (2020) 10:1905. doi: 10.3390/ani10101905
8. Qi Y, Luo J, Han X, Zhu Y, Chen C, Liu J, et al. Genetic diversity and relationships of 10 Chinese goat breeds in the Middle and Western China. *Small Rumin Res.* (2009) 82:88–93. doi: 10.1016/j.smallrumres.2009.01.015
9. National livestock and Poultry Genetic Resources Committee. *Chinese Livestock and Poultry Genetic Resources. Special Livestock and Poultry, Sheep and Goats*. China Agricultural Publishing House (2011).
10. Diwedi J, Singh AW, Ahlawat S, Sharma R, Arora R, Sharma H, et al. Comprehensive analysis of mitochondrial DNA based genetic diversity in Indian goats. *Gene.* (2020) 756:144–9. doi: 10.1016/j.gene.2020.144910
11. Phyu PP, Pichler R, Soe O, Aung PP, Than M, Shamsuddin M, et al. Genetic diversity, population structure and phylogeography of Myanmar goats. *Small Rumin Res.* (2017) 148:33–42. doi: 10.1016/j.smallrumres.2016.12.028
12. Baena MM, Gervásio IC, Rocha RDFB, Procópio AM, de Moura RS, et al. Population structure and genetic diversity of Mangalarga Marchador horses. *Livestock Sci.* (2020) 239:104–9. doi: 10.1016/j.livsci.2020.104109
13. Goleman M, Balicki I, Radko A, Jakubczak A, Fornal A. Genetic diversity of the Polish Hunting Dog population based on pedigree analyses and molecular studies. *Livestock Sci.* (2019) 229:114–7. doi: 10.1016/j.livsci.2019.09.017
14. Illa SK, Gollamoori G, Nath S. Evaluation of selection program by assessing the genetic diversity and inbreeding effects on Nellore sheep growth through pedigree analysis. *Asian Aust J Anim Sci.* (2019) 33:1369–77. doi: 10.5713/ajas.18.0553
15. Vatankhah M, Sigdel A, Abdollahi-Arpanahi R. Population structure of Lori-Bakhtiari sheep in Iran by pedigree analysis. *Small Rumin Res.* (2019) 174:148–55. doi: 10.1016/j.smallrumres.2019.02.019
16. Vigeland MD. Relatedness coefficients in pedigrees with inbred founders. *J Math Biol.* (2020) 81:185–207. doi: 10.1007/s00285-020-01505-x
17. Ma Y, Su R, Fan Y, Qiao X, Li X, Zhang L, et al. The complete mitochondrial DNA analyses of Inner Mongolia Cashmere goat type of Erlangshan species. *Mitochondr DNA B.* (2018) 3:44–5. doi: 10.1080/23802359.2017.1419084
18. Todd ET, Hamilton NA, Velie BD, Thomson PC. The effects of inbreeding on covering success, gestation length and foal sex ratio in Australian thoroughbred horses. *BMC Genet.* (2020) 21:41. doi: 10.1186/s12863-020-00847-1
19. Yousefi B, Gholizadeh M, Hafezian H. Quantifying the effect of inbreeding on average daily gain and Kleiber ratio in Mazandaran native chickens. *Trop Anim Health.* (2020) 52:1–7. doi: 10.1007/s11250-020-02347-x
20. Paiva R, Sousa J, Ferreira J, Cunha EE, Facó O. Population structure and effect of inbreeding on milk yield of Saanen goats in Brazilian production systems. *Small Rumin Res.* (2020) 192:106–14. doi: 10.1016/j.smallrumres.2020.106194
21. Kiya CK, Pedrosa VB, Muniz K, Gusmo AL, Pinto L. Population structure of a nucleus herd of Dorper sheep and inbreeding effects on growth, carcass, and reproductive traits. *Small Rumin Res.* (2019) 177:141–5. doi: 10.1016/j.smallrumres.2019.06.015
22. Wang Z, Wang R, Zhang W, Wang Z, Wang P, Liu H, et al. Estimation of genetic parameters for fleece traits in yearling Inner Mongolia Cashmere goats. *Small Rumin Res.* (2013) 109:15–21. doi: 10.1016/j.smallrumres.2012.07.016
23. Gutiérrez JP, Goyache F. A note on ENDOG: a computer program for analysing pedigree information. *J Anim Breed.* (2005) 122:357–60. doi: 10.1111/j.1439-0388.2005.00512.x
24. Meuwissen T, Luo Z. Computing inbreeding coefficients in large populations. *Genet Select Evol.* (1992) 24:1–9. doi: 10.1186/1297-9686-24-4-305
25. MaléCot G. *Mathématiques de L'hérédité*. Paris: MassonetCie (1948).
26. Lacy RC. Analysis of founder representation in pedigrees: founder equivalents and founder genome equivalents. *Zool Biol.* (1989) 8:111–23. doi: 10.1002/zoo.1430080203
27. Gonzalez-Recio O, Maturana ELD, Gutierrez JP. Inbreeding depression on female fertility and calving ease in Spanish dairy cattle. *J Dairy Sci.* (2007) 90:5744–52. doi: 10.3168/jds.2007-0203
28. Alderson GHL. A system to maximize the maintenance of genetic variability in small populations. *Conserv Domest Livest.* (1991) 2:18–9.
29. Wright S. Coefficients of Inbreeding and relationship. *Am. Nat*. (1922) 56:330–8. doi: 10.1086/279872
30. Caballero A, Toro MA. Interrelations between effective population size and other pedigree tools for the management of conserved populations. *Genet Res.* (2000) 75:331–43. doi: 10.1017/S0016672399004449
31. Caballero A, Toro MA. Analysis of genetic diversity for the management of conserved subdivided populations. *Conserv Genet.* (2002) 3:289–99. doi: 10.1023/A:1019956205473
32. Therneau TM, Sinnwell J. Pedigree functions. *Acta Math Acad Sci Hungaricae*. (2015) 37:481–96. doi: 10.1007/BF01895150
33. Marschner I. Fitting generalized linear models [R package glm2 version 1.2]. *R J.* (2017) 3:12–5. doi: 10.32614/RJ-2011-012
34. Joezy-Shekalgorabi S, Maghsoudi A, Taheri-Yeganeh A, Rajabi-Marand B. Pedigree analysis of Cashmere goat breed of South Khorasan. *Ital J Anim Sci.* (2016) 15:590–4. doi: 10.1080/1828051X.2016.1221748
35. Joezy-Shekalgorabi S, Maghsoudi A, Taheri-Yeganeh A, Rajabi-Marand B. Genetic variability of Iranian adani goat breed using pedigree analysis. *J Anim Plant Sci.* (2017) 27:1774–80.
36. Mokhtari MS, Damaneh M, Gutierrez JP. Genetic variability and population structure of Raeini Cashmere goats determined by pedigree analysis. *J Livestock Sci Technol.* (2017) 5:43–50.
37. Vostra-Vydrova H, Hofmanova B, Moravcikova N, Rychtarova J, Vostry L. Genetic diversity, admixture and the effect of inbreeding on milk performance in two autochthonous goat breeds. *Livestock Sci.* (2020) 240:104–63. doi: 10.1016/j.livsci.2020.104163
38. FAO, IDAD, UNEP. Secondary Guidelines for Development of National Farm Animal Genetic Resources Management Plans. *Anim Record Medium Input Prod Environ.* (1998) 35:1369–75.
39. Granado-Tajada I, Rodríguez-Ramilo ST, Legarra A, Ugarte E. Inbreeding, effective population size, and coancestry in the Latxa dairy sheep breed. *J Dairy Sci.* (2020) 103:5215–26. doi: 10.3168/jds.2019-17743
40. Berihulay H, Li Y, Liu X, Gebreselassie G, Islam R, Liu W, et al. Genetic diversity and population structure in multiple Chinese goat populations using a SNP panel. *Anim Genet.* (2019) 50:242–9. doi: 10.1111/age.12776
41. Tomar SS, Arun K, Singh RB. Population analysis of a flock of Beetal goats for demographic parameters. *Indian J Anim Res.* (2000) 34:133–5.
42. Ginja C, Gama LT, Martin-Burriel I, Lanari MR, Revidatti MA, Aranguren-M endez JA, et al. Genetic diversity and patterns of population structure in Creole goats from the Americas. *Anim Genet.* (2017) 48:315–29. doi: 10.1111/age.12529
43. Dai S, Wang C, Wang Z, Wang Z, Zhang Y, Na Q, et al. Inbreeding and its effects on fleece traits of Inner Mongolia cashmere goats. *Small Rumin Res.* (2015) 128:50–3. doi: 10.1016/j.smallrumres.2015.04.007
44. Sousa JER, Paiva RDM, Sousa WH, Façanha DAE, Nunes SF, Morais JHG, et al. Endogamia em um rebanho de caprinos da raça Anglo Nubiana. *Arch Zoot.* (2018) 67:428–34. doi: 10.21071/az.v67i259.3801

Conflict of Interest: TZ is only employed by the company Inner Mongolia Bigvet Co., Ltd.

The remaining authors declare that the research was conducted in the absence of any commercial or financial relationships that could be construed as a potential conflict of interest.

frontiers in Genetics

ORIGINAL RESEARCH
published: 25 June 2021
doi: 10.3389/fgene.2021.648158

Identification and Comparative Analysis of Long Non-coding RNAs in High- and Low-Fecundity Goat Ovaries During Estrus

Yaokun Li[1], Xiangping Xu[1], Ming Deng[1], Xian Zou[2], Zhifeng Zhao[1], Sixiu Huang[1], Dewu Liu[1] and Guangbin Liu[1]**

[1] Guangdong Laboratory for Lingnan Modern Agriculture, College of Animal Science, South China Agricultural University, Guangzhou, China, [2] State Key Laboratory of Livestock and Poultry Breeding, Institute of Animal Science, Guangdong Academy of Agricultural Sciences, Guangzhou, China

OPEN ACCESS

Edited by:
Rui Su,
Inner Mongolia Agricultural University, China

Reviewed by:
Ran Di,
Institute of Animal Sciences, Chinese Academy of Agricultural Sciences, China
Zhibin Ji,
Shandong Agricultural University, China
Jiangjiang Zhu,
Southwest Minzu University, China
Adeyemi Adenaike,
Federal University of Agriculture, Abeokuta, Nigeria

***Correspondence:**
Dewu Liu
dwliu@scau.edu.cn
Guangbin Liu
gbliu@scau.edu.cn

Specialty section:
This article was submitted to Livestock Genomics, a section of the journal Frontiers in Genetics

Received: *31 December 2020*
Accepted: *06 May 2021*
Published: *25 June 2021*

Citation:
Li Y, Xu X, Deng M, Zou X, Zhao Z, Huang S, Liu D and Liu G (2021) Identification and Comparative Analysis of Long Non-coding RNAs in High- and Low-Fecundity Goat Ovaries During Estrus. Front. Genet. 12:648158. doi: 10.3389/fgene.2021.648158

The ovary is the most important reproductive organ in goats and directly affects the fecundity. Long non-coding RNAs (lncRNAs) are involved in the biological process of oocyte maturation. However, in the context of reproduction in goats, few studies have explored the regulation of lncRNAs. Therefore, we herein used the ovaries of high and low fecundity Leizhou black goats to identify differentially expressed lncRNAs (DElncRNAs) by high-throughput RNA sequencing; moreover, we analyzed the target genes of lncRNAs by functional annotation to explore the role of DElncRNAs in ovarian development. Twenty DElncRNAs were identified, of which six were significantly upregulated and 14 were significantly downregulated in high fecundity goats. Gene Ontology analyses suggested that MSTRG.3782 positively influences the expression of the corresponding gene *API5*, exerting regulative effects on the development of follicles, through which litter size might show variations. The target gene KRR1 of ENSCHIT00000001883 is significantly enriched in cell components, and ENSCHIT00000001883 may regulate cell growth and thus affect follicular development. Further, as per Kyoto Encyclopedia of Genes and Genomes pathway analyses, MSTRG.2938 was found to be significantly enriched, and we speculate that MSTRG.2938 could regulate ribosomal biogenesis in the pre-snoRNP complex as well as cell transformation in eukaryotes. Quantitative real-time PCR results were consistent with sequencing data. To conclude, our research results indicate that some lncRNAs play a key role in regulating follicle development and cell growth during goat' s ovarian development.

Keywords: long non-coding RNA, litter size, goats, reproduction, fertility, high-throughput nucleotide sequencing

INTRODUCTION

Litter size is influenced not only by nutrition levels and environment but also by inheritance (Cui et al., 2009). The ovary is the most important organ for the normal reproductive function of goats. It secretes estrogen to maintain sexual characteristics and cyclical reproductive activity; further, oocytes and ovulation have a major impact on the fertility of goats (Barnett et al., 2006;

Zhao et al., 2015). Studies have shown that the ovulation rate of goats is linked to high productivity (Pramod et al., 2013). lncRNAs play a chief role in reproduction-related processes in animals, but very limited information is available on the functions of lncRNAs in goats. In particular, in the context of reproduction in goats, few studies have explored the regulation of lncRNAs (Xing et al., 2014). Long non-coding RNAs are non-coding RNA transcripts of >200 nucleotides in length; they have a complex structure and lack the ability to code proteins (Jarroux et al., 2017). They can regulate gene expression and protein function to perform biological functions. Studies have reported that lncRNAs can regulate reproductive processes, such as ovarian development and maturation in female animals (Li et al., 2015; Ling et al., 2017; Liu et al., 2020). Therefore, it is crucial to study their role by exploring the function of key target genes.

High-throughput RNA sequencing and functional analyses have been used to elucidate the reproductive function of lncRNAs that were identified to be differentially expressed between the ovaries of multiparous and uniparous Anhui white goats; TCONS_00136407, TCONS_00146968, and TCONS_00320849, for example, were suggested to participate in oocyte meiosis (Ling et al., 2017). Using the same method to study the function of differentially expressed lncRNAs (DElncRNAs) in Chuanzhong black goats, ENSCHIT00000005909 and ENSCHIT00000005910 were suggested to regulate the viability and proliferation of keratinocyte-derived cells by influencing *IL1R2* (interleukin 1 receptor type II) thereby affecting ovarian function (Bouckenheimer et al., 2018). Leizhou black goat is a special local goat breed in southern China, which shows excellent adaptability to the living circumstance with high humidity and high temperature, and using high-throughput sequencing and bioinformatics analysis can help us to explore the novel functional DElncRNAs in the ovaries of goats.

Litter size is one of the most important economic traits in goat production, determining the benefit of farming enterprises. To provide a theoretical basis for goat breeding and improve the production efficiency of goat industry, it is vital to conduct in-depth research on the mechanisms regulating litter size. We herein screened DElncRNAs between the ovaries of high and low fecundity Leizhou black goats and predicted the target genes of DElncRNAs. In addition, Gene Ontology (GO) and Kyoto Encyclopedia of Genes and Genomes (KEGG) pathway analyses were used to analyze the function of target genes. Our results not only enrich the transcriptomic data of the goat ovary but also provide a theoretical basis for combining molecular breeding and conventional breeding technologies.

MATERIALS AND METHODS

Ethics Statement

All study protocols were approved by the Ethics Committee for the Care and Use of Laboratory Animals at the South China Agricultural University (permit no.: SYXK-2014-0136). Further, all experiments were performed in accordance with the guidelines of the South China Agricultural University.

Animals and Sample Collection

Seven healthy female Leizhou black goats (age, 3.5–4.5 years) were divided into high and low fecundity groups. The litter size of high-fecundity group (n = 3) and low-fecundity group (n = 4) were more than one and only one, respectively. Meanwhile, all of the samples in this study were from goats with three parity records of litter size. The female goats were injected with 0.1 mg cloprostenol to induce estrus (Perera et al., 1978; Martemucci and D'Alessandro, 2011; Fierro et al., 2013). The goats were kept under observation to determine whether they were in heat (bleating, searching for the male goat, frequent urination, hyperemia, edema, contraction of the vulva, and vaginal mucus discharge). The basis of estrus was the female goat shaking their tail, standing, and accepting to mate with the male goat (Taylor, 1978; Mekuriaw et al., 2016). The ovaries were collected within 24 h of estrus. The selected goats were killed and dissected, and both whole ovaries from each goat were collected immediately. The intact ovaries were collected and washed with 75% alcohol thrice. Then they were soaked into phosphate buffered saline. After the collection of the ovary, the ligaments and attached tissues were trimmed off under surgical anatomy microscope, ovarian follicles were isolated from the ovary, and the isolated ovarian tissue was frozen in liquid nitrogen and stored at –80°C.

Total RNA Isolation, cDNA Library Construction, and Transcriptome Sequencing

After thoroughly grinding the ovarian tissue, total RNA was extracted using TRIzol (Invitrogen, Carlsbad, CA, United States). NanoDrop ND-2000 was used to measure RNA concentration (Thermo Science, Wilmington, DE, United States). RNA integrity was assessed by denaturing agarose gel electrophoresis. Further, the cDNA library was constructed using 3 μl of total RNA from each sample, and double-terminal sequencing was performed on the HiSeq X-TEN sequencing platform by Shanghai Parsons Biotech Co., Ltd.

Quality Control of Raw Sequences

We used Cutadapt to remove reads with an average quality score below Q20. The Q20 value referred to the error probability of 1% for the identified bases in the process of base recognition. The reference genome index (GCF_001704415.1_ARS1_genomic[1]) was established by Bowtie 2, and the filtered reads were compared with the reference genome using TopHat 2. If the mismatch between the reads and the reference genome sequence was within 2, we considered the alignment to be successful (Kim et al., 2013).

Assembly and Novel lncRNA Prediction

According to the TopHat 2 results, StringTie was used for transcript assembly, and candidate lncRNAs were then selected

[1] http://www.ensembl.org/

based on the splicing results and structural features of lncRNAs. The screening conditions to identify lncRNAs were as follows: (1) transcripts with low expression levels, low credible single exon transcripts, and exon numbers < 2 were filtered out and (2) transcripts < 200 bp in length were excluded (Trapnell et al., 2010; Cabili et al., 2011). Moreover, Coding-Non-Coding-Index v2 (Barnett et al., 2006), Coding Potential Calculator (0.9-r2; Sun et al., 2013), Pfam Scan v1.3 (Punta et al., 2012), and phylogenetic codon substitution frequency (v20121028; Lin et al., 2011) were used for coding potential analyses. Transcripts without coding potential comprised the candidate set of lncRNAs. lncRNA expression at the transcription level was analyzed with StringTie. DESeq was used to analyze the expression of lncRNAs; the screening conditions were $|\text{Log2FoldChange}| > 1$ and $P < 0.05$ (Love et al., 2014). The ggplot 2 software package was used to construct a volcano map of DElncRNAs, and the pheatmap software package was used to perform clustering according to the expression level of same lncRNAs in different samples and that of different lncRNAs in the same sample. Distance was calculated with the Euclidean method and clustering was performed using hierarchical agglomerative clustering (Wang et al., 2010).

Target Gene Prediction

To explore the functions of lncRNAs, we predicted the target genes of DElncRNAs. Because the reliability of the analysis results is not high when the sample number is small, the function of trans-regulation can not be predicted. We searched the genes 100 kb downstream and upstream of lncRNAs and analyzed their functions.

GO and KEGG Pathway Analyses for Target Genes of DElncRNAs

GO analysis was performed with the predicted target genes using DAVID[2]. Furthermore, we used the KEGG database to analyze the potential functions of these genes in pathways[3] (Dennis et al., 2003; Han et al., 2012). A hypergeometric test was applied to discover the significant enrichment of GO terms and KEGG pathways so as to determine the main biological functions of differentially expressed genes (Wang et al., 2020; Huang et al., 2007). $P < 0.05$ indicated statistical significance.

Quantitative Real-Time PCR (qRT-PCR) for DElncRNAs

Total RNA (1 μg) was first reverse-transcribed using an RT Reagent Kit with gDNA Eraser (Takara, Dalian, China), according to manufacturer instructions. qRT-PCR was performed on a StepOnePlus Real-Time PCR System (Life Technologies, United StatesA), as per the standard protocol, using TB Green Fast qPCR Mix (Takara, Dalian, China). Primer Premier 5 used in primer design. Capra hircus β-actin served as the endogenous control for mRNA and lncRNA expression analyses.

[2]https://david.ncifcrf.gov

[3]http://www.genome.jp/kegg/

RESULTS

Sequencing Data Quality Control

The raw reads from the high and low fecundity groups were analyzed for quality control before further analyses. The Q30 value for each sample exceeded 93% (**Table 1**). Within the mapped reads, >85% of total reads were mapped to the reference genome without any mismatch (**Table 2**), indicating that the sequencing data was of high quality and suitable for subsequent analyses.

Screening and Validation of DElncRNAs

Of 4,462 lncRNAs, 20 were differentially expressed between the high and low fecundity groups. Compared with the low fecundity group, six lncRNAs were upregulated and 14 were downregulated in the high fecundity group ($P < 0.05$; **Figure 1A**). From the heatmap analysis, the expression level of the same lncRNA in the same group was essentially the same, indicating that there was little difference between the samples in the same group. Four and three samples belonging to the low and high fecundity groups, respectively, were clustered together, indicating that lncRNA expression patterns in the groups were different (**Figure 1B**). Six DElncRNAs were randomly selected for qRT-PCR to verify the reliability of RNA sequencing data. qRT-PCR results were fundamentally consistent with sequencing results, confirming that the sequencing data had high reliability (**Figure 1C**).

GO Analyses for Target Genes of lncRNAs

GO Analyses for Target Genes of All lncRNAs

The 4,462 lncRNAs corresponded to 2,870 genes, of which DElncRNAs corresponded to 19 target genes. To explore the biological function of lncRNAs involved in regulating litter size, we performed GO and KEGG pathway analysis to identify the functions of target genes. GO analyses revealed diverse biological functions, such as positive regulation of transcription from RNA polymerase II promoter, patterning of blood vessels, and palate development, and multiple target genes were involved, such as *CTNNB1* (encoding catenin beta-1), *WNT5A*, and *EDN1* (endothelin-1). Transcription factor complex, nucleus,

TABLE 1 | Quality control of RNA-seq data.

Sample	Clean reads (bp)	Clean reads (%)	Q30 (bp)	Q30 (%)
LL_ovarian1	102,568,128	99.71	14,469,811,737	93.78
LL_ovarian2	105,050,222	99.76	14,876,252,498	94.18
LL_ovarian3	101,304,042	99.66	14,193,808,086	93.09
LL_ovarian4	106,886,182	99.74	15,093,669,895	93.89
LH_ovarian1	101,039,510	99.51	14,381,870,205	94.43
LH_ovarian2	104,636,964	99.36	14,844,532,299	93.97
LH_ovarian3	101,631,476	99.59	14,245,966,824	93.07

Q30 value represents the error probability of 0.1% for the identified bases in the process of base recognition; LL_ovarian1–LL_ovarian4, low fecundity goats; LH_ovarian1–LH_ovarian3, high fecundity goats.

TABLE 2 | Statistics of the mapping result.

Sample	Total-mapped(bp)	Multiol-mapped(bp)	Uniquely-mapped(bp)
LL_ovarian1	87,722,258(85.53%)	3,401,453(3.88%)	84,320,805(96.12%)
LL_ovarian2	94,045,775(89.52%)	2,863,389(3.04%)	91,182,386(96.96%)
LL_ovarian3	88,004,353(86.87%)	2,413,301(2.74%)	85,591,052(97.26%)
LL_ovarian4	95,760,551(89.59%)	2,719,333(2.84%)	93,041,218(97.16%)
LH_ovarian1	90,985,423(90.05%)	2,200,033(2.42%)	88,785,390(97.58%)
LH_ovarian2	93,646,857(89.50%)	2,601,986(2.78%)	91,044,871(97.22%)
LH_ovarian3	89,517,832(88.08%)	2,404,052(2.69%)	87,113,780(97.31%)

Multiol-Mapped, the total number of sequences aligned to multiple positions; Uniquely mapped number of sequences with unique alignment positions on the reference sequence.

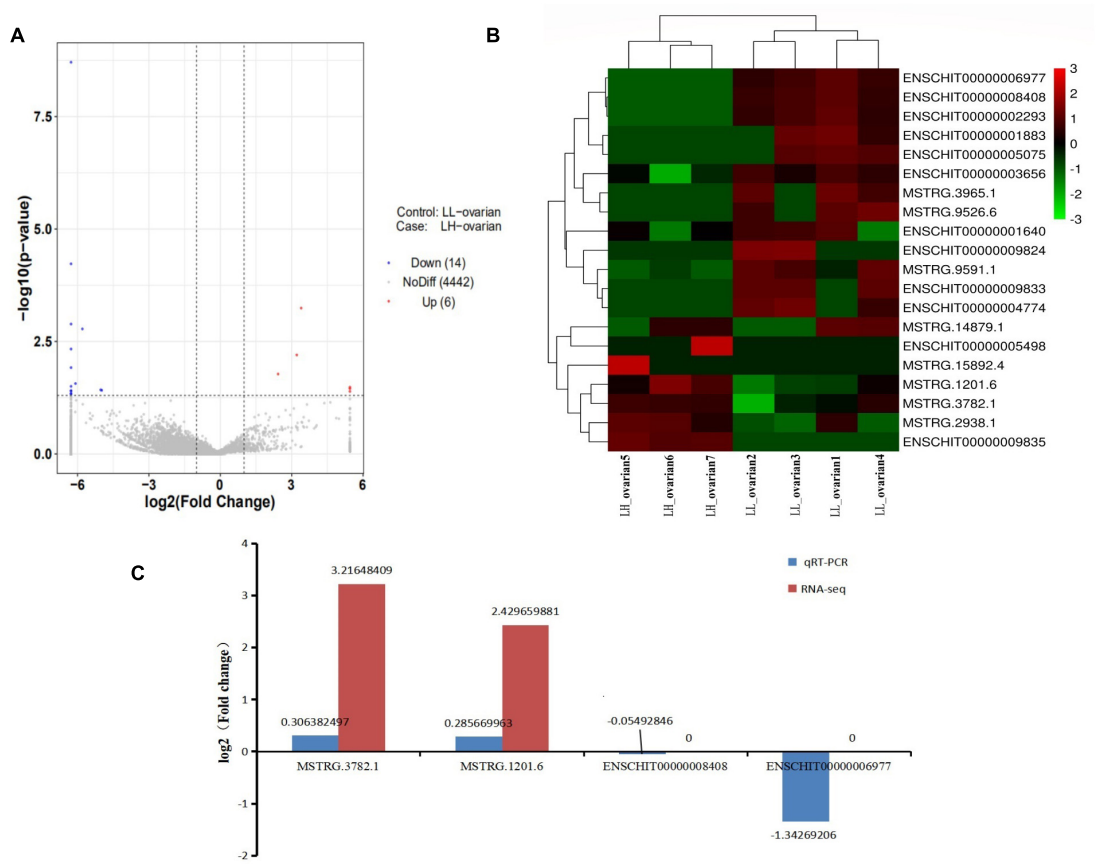

FIGURE 1 | Analysis and validation of DElncRNAs in RNA-seq libraries. **(A)** Volcano map in analyzing DElncRNAs between high fecundity group and low fecundity group. The red plot represented up-regulated expression in high fecundity group; the blue plot represented down-regulated expression in high fecundity group. **(B)** Hierarchical clustering analysis of lncRNA expression profiles from libraries with 20 DElncRNAs. Data were expressed as FPKM. Red: relatively high expression; Green: relatively low expression. **(C)** qRT-PCR results pertaining to DElncRNAs were compared with RNA-seq data. Red: RNA-seq; blue: qRT-PCR.

and integral component of plasma membrane were the top three terms significantly enriched in the cellular component, whereas transcriptional repressor activity, RNA polymerase II core promoter proximal region sequence-specific binding, sequence-specific DNA binding and RNA polymerase II core promoter proximal region sequence-specific DNA binding were the top three terms significantly enriched in the molecular function ($P < 0.05$; **Table 3** and **Figure 2A**). *ZNF536* and *SALL1* (sal-like 1) are noted to be involved in these functions.

GO Analyses for Target Genes of DElncRNAs

GO analysis revealed that 47 terms were significantly enriched between the high and low fecundity groups; the target genes involved were *IER2* (immediate early response protein 2), *TBXT*, *API5* (encoding apoptosis inhibitor 5), *KRR1*, *ARRDC4* (arrestin domain containing 4), *NOP56* (encoding nucleolar protein 56), and *OIP5* (encoding OPA-interacting protein 5) ($P < 0.05$). The target gene *API5* of MSTRG.3782 participated in 14 GO terms, including nuclear lumen, negative regulation

TABLE 3 | Top 10 significantly enriched Gene Ontology (GO) terms of target genes of all long non-coding RNAs (lncRNAs).

GO ID	GO name	Observed gene count	*P*
Molecular function			
GO:0001078	Transcriptional repressor activity, RNA polymerase II core promoter proximal region sequence-specific binding	25	8.11923E-09
GO:0043565	Sequence-specific DNA binding	50	2.81848E-07
GO:0000978	RNA polymerase II core promoter proximal region sequence-specific DNA binding	44	6.27029E-07
GO:0003682	Chromatin binding	44	7.63455E-06
GO:0001077	Transcriptional activator activity, RNA polymerase II core promoter proximal region sequence-specific binding	32	1.22538E-05
GO:0003700	Transcription factor activity, sequence-specific DNA binding	55	5.63408E-05
GO:0044212	Transcription regulatory region DNA binding	21	0.000261987
GO:0000977	RNA polymerase II regulatory region sequence-specific DNA binding	10	0.001142393
GO:0005249	Voltage-gated potassium channel activity	10	0.001653743
GO:0003705	Transcription factor activity, RNA polymerase II distal enhancer sequence-specific binding	7	0.001653743
Biological process			
GO:0045944	Positive regulation of transcription from RNA polymerase II promoter	79	4.46E-09
GO:0001569	Patterning of blood vessels	13	1.33E-07
GO:0060021	Palate development	20	6.08E-07
GO:0051965	Positive regulation of synapse assembly	16	1.60E-06
GO:0090090	Negative regulation of canonical Wnt signaling pathway	20	6.79359E-06
GO:0045665	Negative regulation of neuron differentiation	14	1.19474E-05
GO:0007411	Axon guidance	20	1.20265E-05
GO:0042493	Response to drug	18	1.83209E-05
GO:0042733	Embryonic digit morphogenesis	14	3.44706E-05
GO:0042475	Odontogenesis of dentin-containing tooth	13	3.71271E-05
Cellular component			
GO:0005667	Transcription factor complex	32	2.15852E-07
GO:0005634	Nucleus	232	6.64207E-07
GO:0005887	Integral component of plasma membrane	74	0.003866795
GO:0005615	Extracellular space	81	0.005325092
GO:0030424	Axon	16	0.006989932
GO:0005794	Golgi apparatus	50	0.007490282
GO:0005783	Endoplasmic reticulum	45	0.022593322
GO:0016592	Mediator complex	7	0.022693577
GO:0009897	External side of plasma membrane	20	0.022811136
GO:0071944	Cell periphery	5	0.031220242

of fibroblast apoptotic process, and regulation of fibroblast apoptotic process. The target gene *NOP56* of MSTRG.2938 participated in 13 GO terms, including nuclear lumen, histone methyltransferase binding, and pre-snoRNP complex. Further, we classified the function of the target genes into the three major GO categories of biological process, cellular component, and molecular function. Positive regulation of transcription from RNA polymerase II promoter involved in myocardial precursor cell differentiation, positive regulation of transcription from RNA polymerase II promoter involved in heart development, regulation of transcription from RNA polymerase II promoter involved in myocardial precursor cell differentiation were the top three abundant terms in the biological process category ($P < 0.05$). In the cellular component category, nuclear lumen, pre-snoRNP complex, and membrane-enclosed lumen were the top three abundant terms, whereas in the molecular function category, histone methyltransferase binding, protein binding, bridging involved in substrate recognition for ubiquitination, and snoRNA binding were the top three abundant terms ($P < 0.05$; **Table 4** and **Figure 2B**).

KEGG Pathway Analyses for Target Genes of lncRNAs

KEGG Pathway Analyses for Target Genes of All lncRNAs

As per KEGG pathway analysis, 20 pathways were significantly enriched ($P < 0.05$). The top 10 pathways were primarily associated with transforming growth factor-beta (TGF-β), signaling pathways regulating pluripotency of stem cells, pathways in cancer, basal cell carcinoma, Wnt signaling pathway, HTLV-I infection, neuroactive ligand-receptor interaction, proteoglycans in cancer, Hippo signaling pathway, and transcriptional misregulation in cancer (**Table 5** and **Figure 3A**). The target genes included *CTNNB1*, *WNT5A*, and *TGF-β2*, among others. The target gene *WNT5A* of ENSCHIG00000000774 was involved in seven signaling pathways, such as the Wnt signaling pathway, basal cell carcinoma, and HTLV-I infection.

KEGG Pathway Analyses for Target Genes of DElncRNAs

According to KEGG pathway enrichment analyses, the target genes involved ribosomal biogenesis in eukaryotes and olfactory transduction pathways, of which only the former showed significant enrichment ($P < 0.05$). The target gene *NOP56* of MSTRG.2938 was involved in this pathway (**Table 6** and **Figure 3B**).

DISCUSSION

The elucidation of mechanisms regulating litter size can provide a theoretical basis for breeding technologies in goats. Therefore, in this study, we used the ovaries of high and low fecundity Leizhou black goats to identify DElncRNAs by high-throughput RNA sequencing; moreover, we analyzed the target genes of lncRNAs to explore the role of DElncRNAs in ovarian development.

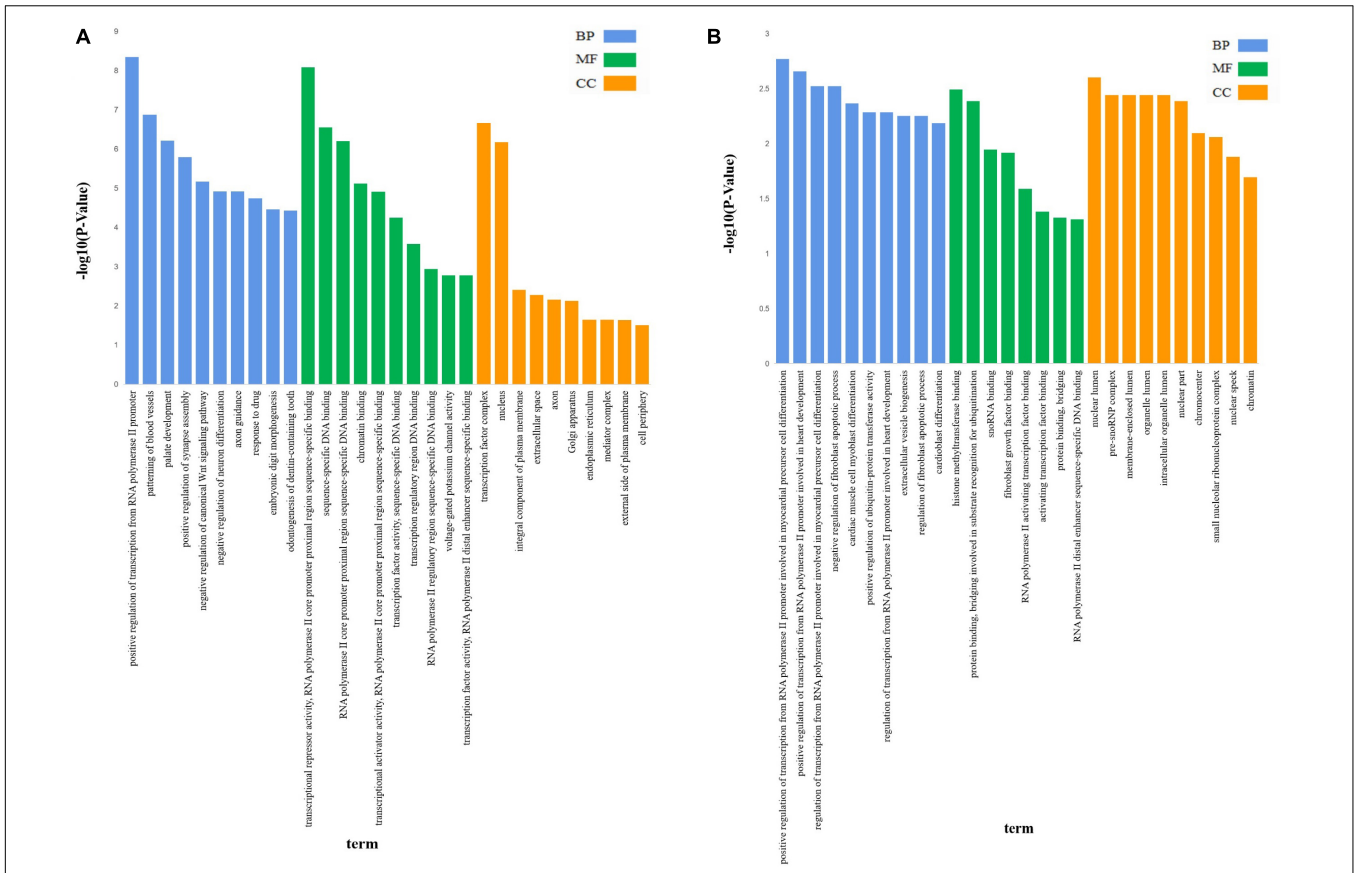

FIGURE 2 | The GO analysis of target genes of lncRNAs. GO analysis of lncRNA-target genes according to biological process (BP), cell component (CC), and molecular function (MF); **(A)** The GO analysis of target genes of all lncRNAs, *X*-axis was *P*-value(-log10), *Y*-axis was the GO term. **(B)** The GO analysis of target genes of DElncRNAs, X-axis was *P*-value(-log10), *Y*-axis was the GO term.

We herein identified enriched terms and signaling pathways; subsequently, we analyzed them as well as pertinent target genes involved in the regulation of reproduction. Fibroblasts are the main cellular component of loose connective tissue (Cai et al., 2012; Yeung et al., 2013). Carcinoma-associated fibroblasts evidently regulate the development of epithelial ovarian cancer by affecting the proliferation, apoptosis, migration, and invasive activity of ovarian cancer cells (Zhang et al., 2011). Fibroblast growth factor (FGFs) is involved in follicular development and follicular atresia (Costa et al., 2009; Miyoshi et al., 2010; Asgari et al., 2015; Coticchio et al., 2015). The expression of FGFs related to follicular development changes with the development of follicles. FGFs need to bind to distinct receptors to physiologically function (Basu et al., 2014). Apoptosis inhibitor 5, which is encoded by *API5*, is involved in regulating the cell cycle. Further, it promotes DNA synthesis and cell cycle G1/S transition, and regulates cell growth, proliferation, and apoptosis (Garcia-Jove Navarro et al., 2013). *API5* plays an important role in the termination of diapause and early embryonic development of Artemia sinica (Zhang et al., 2017). Through GO analysis, we found that the target gene *API5* of MSTRG.3782 was involved in the regulation of fibroblast apoptotic process and FGF binding. MSTRG.3782 was significantly upregulated in the high fecundity group. Accordingly, we hypothesized that lncRNA participates in cell growth, thereby affecting follicular development.

The nucleus is the main repository of genetic information in eukaryotic cells, and the site of DNA replication and transcription; it consequently controls genetic and metabolic activities (Lynch and Marinov, 2017). Chromosomes are the most important structures in the nucleus and carry hereditary information (Zetterström, 2008). A study found that OPA-interacting protein 5 (*OIP5*) was enriched in centrosomes during the G1 phase of the cell cycle and mediated the regulation of cell division (Naetar et al., 2007). In addition, *OIP5* reportedly has a fundamental role in maintaining the structure and function of centrosomes/centromeres (Fujita et al., 2007). *KRR1* encodes proteins present in early 90 S precursor particles of the small ribosomal subunit, and its locus has been implied to contribute to the development of polycystic ovary syndrome (Gromadka and Rytka, 2000; Zheng et al., 2014; Pau et al., 2017). In this study, we found that the target gene *OIP5* of MSTRG.1201 and the target gene *KRR1* of ENSCHIT00000001883 were significantly enriched in the cellular component of nuclear lumen, chromatin, organelle lumen, intracellular organelle lumen, among others. In the high fecundity group, MSTRG.1201 was significantly upregulated and ENSCHIT00000001883 was significantly

TABLE 4 | Top 10 significantly enriched Gene Ontology (GO) terms of target genes of differentially expressed long non-coding RNAs (DElncRNAs).

GO ID	GO name	Genes	*P*
Molecular function			
GO:1990226	Histone methyltransferase binding	NOP56	0.0032
GO:1990756	Protein binding, bridging involved in substrate recognition for ubiquitination	ARRDC4	0.0041
GO:0030515	snoRNA binding	NOP56	0.0113
GO:0017134	Fibroblast growth factor binding	API5	0.0121
GO:0001102	RNA polymerase II activating transcription factor binding	TBXT	0.0257
GO:0033613	Activating transcription factor binding	TBXT	0.0415
GO:0030674	Protein binding, bridging	ARRDC4	0.047
GO:0000980	RNA polymerase II distal enhancer sequence-specific DNA binding	TBXT	0.0486
GO:0060090	Molecular adaptor activity	ARRDC4	0.0563
GO:0001158	Enhancer sequence-specific DNA binding	TBXT	0.0602
Biological process			
GO:0003257	Positive regulation of transcription from RNA polymerase II promoter involved in myocardial precursor cell differentiation	TBXT	0.0017
GO:1901228	Positive regulation of transcription from RNA polymerase II promoter involved in heart development	TBXT	0.0022
GO:0003256	Regulation of transcription from RNA polymerase II promoter involved in myocardial precursor cell differentiation	TBXT	0.003
GO:2000270	Negative regulation of fibroblast apoptotic process	API5	0.003
GO:0060379	Cardiac muscle cell myoblast differentiation	TBXT	0.0043
GO:0051443	Positive regulation of ubiquitin-protein transferase activity	ARRDC4	0.0052
GO:1901213	Regulation of transcription from RNA polymerase II promoter involved in heart development	TBXT	0.0052
GO:0140112	Extracellular vesicle biogenesis	ARRDC4	0.0056
GO:2000269	Regulation of fibroblast apoptotic process	API5	0.0056
GO:0010002	Cardioblast differentiation	TBXT	0.0065
Cellular component			
GO:0031981	Nuclear lumen	IER2, TBXT, API5, KRR1, NOP56, OIP5	0.0025
GO:0070761	Pre-snoRNP complex	NOP56	0.0036
GO:0031974	Membrane-enclosed lumen	IER2, TBXT, API5, KRR1, NOP56, OIP5	0.0036
GO:0043233	Organelle lumen	IER2, TBXT, API5, KRR1, NOP56, OIP5	0.0036
GO:0070013	Intracellular organelle lumen	IER2, TBXT, API5, KRR1, NOP56, OIP5	0.0036
GO:0044428	Nuclear part	IER2, TBXT, API5, KRR1, NOP56, OIP5	0.0041
GO:0010369	Chromocenter	OIP5	0.008
GO:0005732	Small nucleolar ribonucleoprotein complex	NOP56	0.0087
GO:0016607	Nuclear speck	API5, OIP5	0.0131
GO:0000785	Chromatin	TBXT, OIP5	0.0202

TABLE 5 | Top 10 significantly enriched Kyoto Encyclopedia of Genes and Genomes (KEGG) pathways of target genes of all long non-coding RNAs.

KEGG pathway	Number of genes	*P*
TGF-beta signaling pathway	19	3.48E-06
Signaling pathways regulating pluripotency of stem cells	25	7.62E-06
Pathways in cancer	49	1.28E-05
Basal cell carcinoma	14	3.25E-05
Wnt signaling pathway	23	3.61E-05
HTLV-I infection	34	4.89E-05
Neuroactive ligand-receptor interaction	35	9.47E-05
Proteoglycans in cancer	25	0.00199537
Hippo signaling pathway	20	0.004450684
Transcriptional misregulation in cancer	20	0.004786637

downregulated. Therefore, we believe that MSTRG.1201 and ENSCHIT00000001883 affect follicular development by regulating cell division.

Mature snoRNP particles are composed of a series of small nucleolar RNA and core proteins. snoRNPs regulate the processing and modification of pre-rRNA and play an important role in ribosomal biogenesis (Richard and Kiss, 2006). Nucleolar protein 56 (encoded by *Nop56*) is involved in the synthesis of snoRNP as a core protein (Lykke-Andersen et al., 2018). Furthermore, an increase in the ribosome biosynthesis rate can promote the expression of the proto-oncogene *C-myc* and enhance the proliferative ability of cancer cells (Tomczak et al., 2015). *C-myc* encodes a transcription factor with a direct role in controlling translation (Ruggero, 2009). *Nol5a/Nop56* may be a critical gene involved in Myc-mediated oncogenic transformation (Cowling et al., 2014). According to our GO and KEGG pathway analyses, MSTRG.2938 was significantly upregulated in the high fecundity group, and its target gene *NOP56* was involved in ribosomal biogenesis in eukaryotes and the pre-snoRNP complex. We thus speculate that MSTRG.2938 regulates ribosomal biogenesis in the pre-snoRNP complex as well as cell transformation in eukaryotes. However, the specific mechanism of regulation of each lncRNA remains to be further investigated.

According to GO analyses, the target genes [Guanine Nucleotide Binding Protein, alpha 13(*GNA13*), Mothers against decapentaplegic homolog 2 (*SMAD*2), and Fibronectin Leucine Rich Transmembrane Protein 2 (*FLRT2*)] of all lncRNAs were mainly enriched in positive regulation of transcription from RNA polymerase II promoters, patterning of blood vessels, palate development, and positive regulation of synapse assembly. RNA polymerase II plays a pivotal role in the transcription of protein-encoding genes in all eukaryotic cells (Bernecky et al., 2016). *GNA13* participates in regulating cell movement and developmental angiogenesis (Offermanns et al., 1997). Moreover, *SMAD2* overexpression has been reported to repair secondary cleft palate by increasing apoptosis of medial edge epithelial cells in the TGF-β3 pathway (Miyazono et al., 2018). We thus report that these genes play a major role in maintaining the healthy growth of goats.

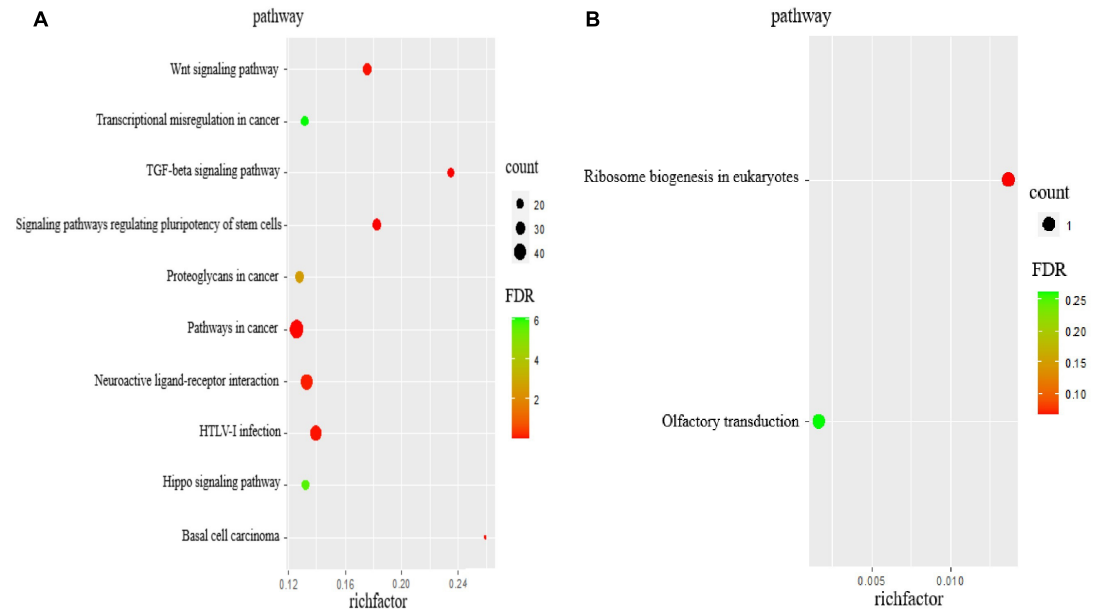

FIGURE 3 | The KEGG analysis of target genes of lncRNAs. **(A)** KEGG pathway analyses of target genes of all lncRNAs. KEGG enrichment was measured by rich factor, FDR and the number of genes enriched on this pathway. **(B)** KEGG pathway analyses of target genes of DElncRNAs. KEGG enrichment was measured by rich factor, FDR and the number of genes enriched on this pathway.

The Wnt signaling pathway and its downstream effectors not only regulate physiological processes such as cell growth and differentiation, cell migration, and genetic material stability but are also important for cancer progression, including for regulating tumor growth, cell senescence, and cell death. The Wnt/β-catenin signaling pathway is involved in various important processes, such as the regulation of embryo development, cell proliferation, and cell migration (Nusse and Clevers, 2017; Peng et al., 2017; Steinhart and Angers, 2018). β-Catenin is an essential structural component of cadherin-based adherens junctions and is a key component of Wnt/β-catenin signal transduction. Aberrant expression of *CTNNB1* and *WNT5A* has been observed to affect cell proliferation and lead to cancer occurrence. A mutation in *CTNNB1* is one of the many causes of β-catenin degradation (Kim et al., 2018). The Wnt/CTNNB1 pathway is a pivotal signaling pathway that regulates steroid production (Abedini et al., 2016). *WNT5A* is a highly evolved conservative non-classical Wnt ligand, which is required for normal ovarian follicle development (Abedini et al., 2016). *WNT5A* is differentially expressed during the development of mouse follicles, and it can significantly inhibit steroid production in atretic follicles (Lapointe and Boerboom, 2011; Abedini et al., 2016; Kumawat and Gosens, 2016). By blocking the function of FSH (follicle-stimulating hormone) and luteinizing protein, *WNT5A* can induce the down-regulation of *CTNNB1* and cAMP-response element binding protein (CREB), thus affecting follicle development and gonadotropin reactivity (Abedini et al., 2015). We found that the target gene *CTNNB1* of ENSCHIG00000000641 is one of the two signaling pathway members of Wnt and proteoglycans in cancer. ENSCHIG00000000641 was downregulated in the high fecundity group. Further, the target gene *WNT5A* of ENSCHIG00000000774 participated in the negative regulation of canonical Wnt signaling pathway terms and the Wnt signaling pathway. ENSCHIG00000000774 was also downregulated in the high fecundity group. Thus, we believe that ENSCHIG00000000641 and ENSCHIG00000000774 affect follicular development by regulating cell proliferation and steroid production, respectively.

The TGF-β superfamily participates in many physiological activities in mammals via autocrine and paracrine pathways, and TGF-β is mainly produced locally in the ovary. It has been reported that *TGF-β1* can promote the growth of mice follicles. Both TGF-β and activin A have proliferative action and cytodifferentiative action on granulosa cells (Liu et al., 1999). As a member of the transforming growth factor β family, TGF-β2 also plays an important role in the growth and development of follicles. TGF-β2 is located in follicular membrane cells and luteal cells and regulates the production of inhibitors and activins in granulosa cells and luteal cells (Knight and Glister, 2003). *Smad2/Smad3* are key molecules in the TGF-β/Smad signaling pathway that regulate ovarian

TABLE 6 | Top significantly enriched Kyoto Encyclopedia of Genes and Genomes (KEGG) pathways of target genes of differentially expressed long non-coding RNAs.

KEGG pathway	Number of genes	*P*
Ribosome biogenesis in eukaryotes	1	0.033754056
Olfactory transduction	1	0.261408061

growth and development and maintain ovarian function (Coutts et al., 2008; AlMegbel and Shuler, 2020). *Smad2* and *Smad3* can maintain normal fertility in women, and further support the Smad2/3 pathway in the ovary to participate in the regulation of signals produced by oocytes, which plays an important role in the coordination of ovulation (Li et al., 2008). In this study, we found that *TGF-β2*, *TGF-βR2*, and *Smad2* participated in the TGF-β signaling pathway, and they were regulated by ENSCHIG00000000886, ENSCHIG00000000609, and ENSCHIG00000002761, respectively. We accordingly speculate that these lncRNAs regulate follicle development, but the specific mechanism needs to be further studied.

To conclude, we found that target genes of all lncRNAs were mainly involved in protein transcription and played a role in maintaining the healthy growth of animals. In addition, the TGF-β and Wnt signaling pathways were found to be related to reproduction in animals. Based on functional analyses of target genes of DElncRNAs, fibroblast apoptotic process, FGF binding, pre-snoRNP complex, and ribosomal biogenesis in eukaryotes were associated with reproduction in goats. Our data improves the current understanding of the transcriptome of goats and provides valuable information for functional genomics resources and biological studies; moreover, we believe that our results are of great significance for in-depth studies of candidate lncRNAs in breeding techniques.

DATA AVAILABILITY STATEMENT

The datasets presented in this study can be found in online repositories. The names of the repository/repositories and accession number(s) can be found below: NCBI (accession: PRJNA728366).

ETHICS STATEMENT

The animal study was reviewed and approved by all study protocols were approved by the Ethics Committee for the Care and Use of Laboratory Animals at the South China Agricultural University (permit no. SYXK-2014-0136). Further, all experiments were performed in accordance with the guidelines of the South China Agricultural University.

AUTHOR CONTRIBUTIONS

YL: conceptualization, methodology, writing-reviewing, and editing. XX: data curation, writing-original draft preparation, software, and validation. MD: conceptualization. DL: visualization and investigation. GL: supervision. XZ: investigation. ZZ: investigation. All authors contributed to the article and approved the submitted version.

FUNDING

The Modern Agricultural Industrial Technology System of Guangdong Province (2019KJ127), the Guangdong Provincial Promotion Project of Modern Seed Industry, Guangdong Provincial Promotion Project on Preservation and Utilization of Local Breed of Livestock and Poultry, and Natural Science Foundation of Guangdong Province (2019B1515210017), and Natural Science Foundation of Guangdong Province, Regulation of miR-128 and miR-450 on proliferation and apoptosis of goat follicular granulosa cells (2021A1515010636).

ACKNOWLEDGMENTS

We would like to thank WENS Company for helping us with performing experiments.

SUPPLEMENTARY MATERIAL

The Supplementary Material for this article can be found online at: https://www.frontiersin.org/articles/10.3389/fgene.2021.648158/full#supplementary-material

Supplementary File 1 | The DElncRNAs in the ovary of high fecundity goats and low fecundity goats. (XLSX)

Supplementary File 2 | lncRNA primers sequences used for the qRT-PCR. (XLSX)

Supplementary File 3 | Protein-coding genes detected 100-kb upstream and downstream of the DElncRNAs. (XLSX)

Supplementary File 4 | GO enrichment analysis of target genes co-located with the all lncRNAs. (XLSX)

Supplementary File 5 | GO enrichment analysis of target genes co-located with the DElncRNAs. (XLSX)

Supplementary File 6 | KEGG enrichment analysis of target genes co-located with the all lncRNAs. (XLSX)

Supplementary File 7 | KEGG enrichment analysis of target genes co-located with the DElncRNAs. (XLSX)

Supplementary File 8 | Sequences of the DElncRNAs. (DOC)

REFERENCES

Abedini, A., Zamberlam, G., Boerboom, D., and Price, C. A. (2015). Non-canonical WNT5A is a potential regulator of granulosa cell function in cattle. *Mol. Cell Endocrinol.* 403, 39–45. doi: 10.1016/j.mce.2015.01.017

Abedini, A., Zamberlam, G., Lapointe, E., Tourigny, C., Boyer, A., Paquet, M., et al. (2016). WNT5a is required for normal ovarian follicle development and antagonizes gonadotropin responsiveness in granulosa cells by suppressing canonical WNT signaling. *FASEB J.* 30, 1534–1547. doi: 10.1096/fj.15-280313

AlMegbel, A. M., and Shuler, C. F. (2020). SMAD2 overexpression rescues the TGF-β3 null mutant mice cleft palate by increased apoptosis. *Differ. Res. Biol. Diversity* 111, 60–69. doi: 10.1016/j.diff.2019.10.001

Asgari, F., Valojerdi, M. R., Ebrahimi, B., and Fatehi, R. (2015). Three dimensional in vitro culture of preantral follicles following slow-freezing and vitrification of mouse ovarian tissue. *Cryobiology* 71, 529–536. doi: 10.1016/j.cryobiol.2015.11.001

Barnett, K. R., Schilling, C., Greenfeld, C. R., Tomic, D., and Flaws, J. A. (2006). Ovarian follicle development and transgenic mouse models. *Hum. Reprod. Update* 12, 537–555. doi: 10.1093/humupd/dml022

Basu, M., Mukhopadhyay, S., Chatterjee, U., and Roy, S. S. (2014). FGF16 promotes invasive behavior of SKOV-3 ovarian cancer cells through activation of mitogen-activated protein kinase (MAPK) signaling pathway. *J. Biol. Chem.* 289, 1415–1428.

Bernecky, C., Herzog, F., Baumeister, W., Plitzko, J. M., and Cramer, P. (2016). Structure of transcribing mammalian RNA polymerase II. *Nature* 529, 551–554. doi: 10.1038/nature16482

Bouckenheimer, J., Fauque, P., Lecellier, C. H., Bruno, C., Commes, T., Lemaître, J. M., et al. (2018). Differential long non-coding RNA expression profiles in human oocytes and cumulus cells. *Sci. Rep.* 8:2202. doi: 10.1038/s41598-018-20727-0

Cabili, M. N., Trapnell, C., Goff, L., Koziol, M., Tazon-Vega, B., Regev, A., et al. (2011). Integrative annotation of human large intergenic noncoding RNAs reveals global properties and specific subclasses. *Genes Dev.* 25, 1915–1927. doi: 10.1101/gad.17446611

Cai, J., Tang, H., Xu, L., Wang, X., Yang, C., Ruan, S., et al. (2012). Fibroblasts in omentum activated by tumor cells promote ovarian cancer growth, adhesion and invasiveness. *Carcinogenesis* 33, 20–29. doi: 10.1093/carcin/bgr230

Costa, I., Teixeira, N., Ripamonte, P., Guerra, D., Price, C., Buratini, J., et al. (2009). Fgf1 mRNA in. (bovine)antral follicles and corpora lutea. *Anim. Reprod.* 6, 409–415.

Coticchio, G., Dal Canto, M., Mignini Renzini, M., Guglielmo, M. C., Brambillasca, F., Turchi, D., et al. (2015). Oocyte maturation: gamete-somatic cells interactions, meiotic resumption, cytoskeletal dynamics and cytoplasmic reorganization. *Hum. Reprod. Update* 21, 427–454. doi: 10.1093/humupd/dmv011

Coutts, S. M., Childs, A. J., Fulton, N., Collins, C., Bayne, R. A., McNeilly, A. S., et al. (2008). Activin signals via SMAD2/3 between germ and somatic cells in the human fetal ovary and regulates kit ligand expression. *Dev. Biol.* 314, 189–199. doi: 10.1016/j.ydbio.2007.11.026

Cowling, V. H., Turner, S. A., and Cole, M. D. (2014). Burkitt's lymphoma-associated c-Myc mutations converge on a dramatically altered target gene response and implicate Nol5a/Nop56 in oncogenesis. *Oncogene* 33, 3519–3527. doi: 10.1038/onc.2013.338

Cui, H. X., Zhao, S. M., Cheng, M. L., Guo, L., Ye, R. Q., Liu, W. Q., et al. (2009). Cloning and expression levels of genes relating to the ovulation rate of the Yunling black goat. *Biol. Reprod.* 80, 219–226. doi: 10.1095/biolreprod.108.069021

Dennis, G. Jr., Sherman, B. T., Hosack, D. A., Yang, J., Gao, W., Lane, H. C., et al. (2003). DAVID: database for annotation, visualization, and integrated discovery. *Genome Biol.* 4:3.

Fierro, S., Gil, J., Viñoles, C., and Olivera-Muzante, J. (2013). The use of prostaglandins in controlling estrous cycle of the ewe: a review. *Theriogenology* 79, 399–408. doi: 10.1016/j.theriogenology.2012.10.022

Fujita, Y., Hayashi, T., Kiyomitsu, T., Toyoda, Y., Kokubu, A., Obuse, C., et al. (2007). Priming of centromere for CENP-A recruitment by human hMis18alpha, hMis18beta, and M18BP1. *Dev. Cell* 12, 17–30. doi: 10.1016/j.devcel.2006.11.002

Garcia-Jove Navarro, M., Basset, C., Arcondéguy, T., Touriol, C., Perez, G., Prats, H., et al. (2013). Api5 contributes to E2F1 control of the G1/S cell cycle phase transition. *PLoS One* 8:e71443. doi: 10.1371/journal.pone.0071443

Gromadka, R., and Rytka, J. (2000). The KRR1 gene encodes a protein required for 18S rRNA synthesis and 40S ribosomal subunit assembly in Saccharomyces cerevisiae. *Acta Biochim. Pol.* 47, 993–1005.

Han, L., Zhang, K., Shi, Z., Zhang, J., Zhu, J., Zhu, S., et al. (2012). LncRNA profile of glioblastoma reveals the potential role of lncRNAs in contributing to glioblastoma pathogenesis. *Int. J. Oncol.* 40, 2004–2012. doi: 10.3892/ijo.2012.1413

Huang, D. W., Sherman, B. T., Tan, Q., Kir, J., Liu, D., Bryant, D., et al. (2007). DAVID Bioinformatics Resources: expanded annotation database and novel algorithms to better extract biology from large gene lists. *Nucleic Acids Res.* 35, W169–W175. doi: 10.1093/nar/gkm415

Jarroux, J., Morillon, A., and Pinskaya, M. (2017). History, discovery, and classification of lncRNAs. *Adv. Exp. Med. Biol.* 1008, 1–46. doi: 10.1007/978-981-10-5203-3_1

Kim, D., Pertea, G., Trapnell, C., Pimentel, H., Kelley, R., and Salzberg, S. L. (2013). TopHat2: accurate alignment of transcriptomes in the presence of insertions, deletions and gene fusions. *Genome Biol.* 14:R36. doi: 10.1186/gb-2013-14-4-r36

Kim, G., Kurnit, K. C., Djordjevic, B., Singh, C., Munsell, M. F., Wang, W. L., et al. (2018). Nuclear β-catenin localization and mutation of the CTNNB1 gene: a context-dependent association. *Modern Pathol.* 31, 1553–1559. doi: 10.1038/s41379-018-0080-0

Knight, P. G., and Glister, C. (2003). Local roles of TGF-beta superfamily members in the control of ovarian follicle development. *Anim. Reprod. Sci.* 78, 165–183. doi: 10.1016/s0378-4320(03)00089-7

Kumawat, K., and Gosens, R. (2016). WNT-5A: signaling and functions in health and disease. *Cell. Mol. Life Sci. CMLS* 73, 567–587. doi: 10.1007/s00018-015-2076-y

Lapointe, E., and Boerboom, D. (2011). WNT signaling and the regulation of ovarian steroidogenesis. *Front. Biosci.* 3:276–285.

Li, J., Cao, Y., Xu, X., Xiang, H., Zhang, Z., Chen, B., et al. (2015). Increased new lncRNA-mRNA gene pair levels in human cumulus cells correlate with oocyte maturation and embryo development. *Reproductive Sci.* 22, 1008–1014. doi: 10.1177/1933719115570911

Li, Q., Pangas, S. A., Jorgez, C. J., Graff, J. M., Weinstein, M., and Matzuk, M. M. (2008). Redundant roles of SMAD2 and SMAD3 in ovarian granulosa cells in vivo. *Mol. Cell. Biol.* 28, 7001–7011. doi: 10.1128/MCB.00732-08

Lin, M. F., Jungreis, I., and Kellis, M. (2011). PhyloCSF: a comparative genomics method to distinguish protein coding and non-coding regions. *Bioinformatics* 27, i275–i282. doi: 10.1093/bioinformatics/btr209

Ling, Y., Xu, L., Zhu, L., Sui, M., Zheng, Q., Li, W., et al. (2017). Identification and analysis of differentially expressed long non-coding RNAs between multiparous and uniparous goat (Capra hircus) ovaries. *PLoS One* 12:e0183163. doi: 10.1371/journal.pone.0183163

Liu, G., Liu, S., Xing, G., and Wang, F. (2020). lncRNA PVT1/MicroRNA-17-5p/PTEN axis regulates secretion of E2 and P4, proliferation, and apoptosis of ovarian granulosa cells in PCOS. *Mol. Therapy. Nucleic Acids* 20, 205–216. doi: 10.1016/j.omtn.2020.02.007

Liu, X., Andoh, K., Abe, Y., Kobayashi, J., Yamada, K., Mizunuma, H., et al. (1999). A comparative study on transforming growth factor-beta and activin A for preantral follicles from adult, immature, and diethylstilbestrol-primed immature mice. *Endocrinology* 140, 2480–2485. doi: 10.1210/endo.140.6.6827

Love, M. I., Huber, W., and Anders, S. (2014). Moderated estimation of fold change and dispersion for RNA-seq data with DESeq2. *Genome Biol.* 15:550. doi: 10.1186/s13059-014-0550-8

Lykke-Andersen, S., Ardal, B. K., Hollensen, A. K., Damgaard, C. K., and Jensen, T. H. (2018). Box C/D snoRNP autoregulation by a cis-Acting snoRNA in the NOP56 Pre-mRNA. *Mol. Cell.* 72, 99–111.e5. doi: 10.1016/j.molcel.2018.08.017

Lynch, M., and Marinov, G. K. (2017). Membranes, energetics, and evolution across the prokaryote-eukaryote divide. *eLife* 6:e20437. doi: 10.7554/eLife.20437

Martemucci, G., and D'Alessandro, A. G. (2011). Induction/synchronization of oestrus and ovulation in dairy goats with different short term treatments and fixed time intrauterine or exocervical insemination system. *Anim. Reprod. Sci.* 126, 187–194. doi: 10.1016/j.anireprosci.2011.05.011

Mekuriaw, Z., Assefa, H., Tegegne, A., and Muluneh, D. (2016). Estrus response and fertility of Menz and crossbred ewes to single prostaglandin injection protocol. *Trop. Animal Health Prod.* 48, 53–57. doi: 10.1007/s11250-015-0919-z

Miyazono, K. I., Moriwaki, S., Ito, T., Kurisaki, A., Asashima, M., and Tanokura, M. (2018). Hydrophobic patches on SMAD2 and SMAD3 determine selective binding to cofactors. *Sci. Signal.* 11:eaao7227. doi: 10.1126/scisignal.aao7227

Miyoshi, T., Otsuka, F., Yamashita, M., Inagaki, K., Nakamura, E., Tsukamoto, N., et al. (2010). Functional relationship between fibroblast growth factor-8 and bone morphogenetic proteins in regulating steroidogenesis by rat granulosa cells. *Mol. Cell. Endocrinol.* 325, 84–92. doi: 10.1016/j.mce.2010.04.012

Naetar, N., Hutter, S., Dorner, D., Dechat, T., Korbei, B., Gotzmann, J., et al. (2007). LAP2alpha-binding protein LINT-25 is a novel chromatin-associated protein involved in cell cycle exit. *J. Cell Sci.* 120(Pt 5), 737–747. doi: 10.1242/jcs.03390

Nusse, R., and Clevers, H. (2017). Wnt/β-Catenin signaling, disease, and emerging therapeutic modalities. *Cell* 169, 985–999. doi: 10.1016/j.cell.2017.05.016

Offermanns, S., Mancino, V., Revel, J. P., and Simon, M. I. (1997). Vascular system defects and impaired cell chemokinesis as a result of Galpha13 deficiency. *Science* 275, 533–536. doi: 10.1126/science.275.5299.533

Pau, C. T., Mosbruger, T., Saxena, R., and Welt, C. K. (2017). Phenotype and tissue expression as a function of genetic risk in polycystic ovary syndrome. *PLoS One* 12:e0168870. doi: 10.1371/journal.pone.0168870

Peng, Y., Zhang, X., Feng, X., Fan, X., and Jin, Z. (2017). The crosstalk between microRNAs and the Wnt/β-catenin signaling pathway in cancer. *Oncotarget* 8, 14089–14106. doi: 10.18632/oncotarget.12923

Perera, B. M., Bongso, T. A., and Abeynaike, P. (1978). Oestrus synchronisation in goats using cloprostenol. *Vet. Record* 102:314. doi: 10.1136/vr.102.14.314-a

Pramod, R. K., Sharma, S. K., Singhi, A., Pan, S., and Mitra, A. (2013). Differential ovarian morphometry and follicular expression of BMP15, GDF9 and BMPR1B influence the prolificacy in goat. *Reprod. Domest. Anim.* 48, 803–809. doi: 10.1111/rda.12165

Punta, M., Coggill, P. C., Eberhardt, R. Y., Mistry, J., Tate, J., Boursnell, C., et al. (2012). The Pfam protein families database. *Nucleic Acids Res.* 40, D290–D301. doi: 10.1093/nar/gkr1065

Richard, P., and Kiss, T. (2006). Integrating snoRNP assembly with mRNA biogenesis. *EMBO Rep.* 7, 590–592. doi: 10.1038/sj.embor.7400715

Ruggero, D. (2009). The role of Myc-induced protein synthesis in cancer. *Cancer Res.* 69, 8839–8843. doi: 10.1158/0008-5472.CAN-09-1970

Steinhart, Z., and Angers, S. (2018). Wnt signaling in development and tissue homeostasis. *Development* 145:dev146589. doi: 10.1242/dev.146589

Sun, L., Luo, H., Bu, D., Zhao, G., Yu, K., Zhang, C., et al. (2013). Utilizing sequence intrinsic composition to classify protein-coding and long non-coding transcripts. *Nucleic Acids Res.* 41:e166. doi: 10.1093/nar/gkt646

Taylor D. J. (1978). Oestrus synchronisation in goats. *Vet. Rec.* 102:390.

Tomczak, K., Czerwińska, P., and Wiznerowicz, M. (2015). The Cancer Genome Atlas (TCGA): an immeasurable source of knowledge. *Contemporary Oncol.* 19, A68–A77. doi: 10.5114/wo.2014.47136

Trapnell, C., Williams, B. A., Pertea, G., Mortazavi, A., Kwan, G., van Baren, M. J., et al. (2010). Transcript assembly and quantification by RNA-Seq reveals unannotated transcripts and isoform switching during cell differentiation. *Nat. Biotechnol.* 28, 511–515. doi: 10.1038/nbt.1621

Wang, H., Nie, X., Li, X., Fang, Y., Wang, D., Wang, W., et al. (2020). Bioinformatics analysis and high-throughput sequencing to identify differentially expressed genes in nebulin gene (NEB) mutations mice. *Med. Sci. Monitor* 26:e922953. doi: 10.12659/MSM.922953

Wang, L., Feng, Z., Wang, X., Wang, X., and Zhang, X. (2010). DEGseq: an R package for identifying differentially expressed genes from RNA-seq data. *Bioinformatics* 26, 136–138. doi: 10.1093/bioinformatics/btp612

Xing, Z., Lin, A., Li, C., Liang, K., Wang, S., Liu, Y., et al. (2014). lncRNA directs cooperative epigenetic regulation downstream of chemokine signals. *Cell* 159, 1110–1125. doi: 10.1016/j.cell.2014.10.013

Yeung, T. L., Leung, C. S., Wong, K. K., Samimi, G., Thompson, M. S., Liu, J., et al. (2013). TGF-β modulates ovarian cancer invasion by upregulating CAF-derived versican in the tumor microenvironment. *Cancer Res.* 73, 5016–5028. doi: 10.1158/0008-5472.CAN-13-0023

Zetterström, R. (2008). The discovery of the structure and function of chromosomes: the basis of cytogenetics. *Acta Paediatrica* 97, 673–676. doi: 10.1111/j.1651-2227.2008.00755.x

Zhang, S., Yao, F., Jing, T., Zhang, M., Zhao, W., Zou, X., et al. (2017). Cloning, expression pattern, and potential role of apoptosis inhibitor 5 in the termination of embryonic diapause and early embryo development of Artemia sinica. *Gene* 628, 170–179. doi: 10.1016/j.gene.2017.07.021

Zhang, Y., Tang, H., Cai, J., Zhang, T., Guo, J., Feng, D., et al. (2011). Ovarian cancer-associated fibroblasts contribute to epithelial ovarian carcinoma metastasis by promoting angiogenesis, lymphangiogenesis and tumor cell invasion. *Cancer Lett.* 303, 47–55. doi: 10.1016/j.canlet.2011.01.011

Zhao, Z. Q., Wang, L. J., Sun, X. W., Zhang, J. J., Zhao, Y. J., Na, R. S., et al. (2015). Transcriptome analysis of the Capra hircus ovary. *PLoS One* 10:e0121586. doi: 10.1371/journal.pone.0121586

Zheng, S., Lan, P., Liu, X., and Ye, K. (2014). Interaction between ribosome assembly factors Krr1 and Faf1 is essential for formation of small ribosomal subunit in yeast. *J. Biol. Chem.* 289, 22692–22703. doi: 10.1074/jbc.M114.584490

Conflict of Interest: The authors declare that the research was conducted in the absence of any commercial or financial relationships that could be construed as a potential conflict of interest.

frontiers in Genetics

ORIGINAL RESEARCH
published: 09 July 2021
doi: 10.3389/fgene.2021.665834

Melatonin Regulates the Periodic Growth of Cashmere by Upregulating the Expression of *Wnt10b* and β-*catenin* in Inner Mongolia Cashmere Goats

Junyang Liu[1,2†], Qing Mu[1,2†], Zhihong Liu[1,2†], Yan Wang[1], Jiasen Liu[3], Zixian Wu[3], Wendian Gong[1,2], Zeyu Lu[1,2], Feifei Zhao[1,2], Yanjun Zhang[1,2], Ruijun Wang[1,2], Rui Su[1,2], Jinquan Li[1,2], Hongmei Xiao[1,4] and Yanhong Zhao[1,2]**

[1] College of Animal Science, Inner Mongolia Agricultural University, Hohhot, China, [2] Laboratory of Animal Genetic, Breeding and Reproduction, Hohhot, China, [3] Department of Inner Mongolia Academy of Agricultural Animal & Husbandry Sciences, Hohhot, China, [4] College of Life Science, Inner Mongolia Agricultural University, Hohhot, China

OPEN ACCESS

Edited by:
Shaobin Li,
Gansu Agricultural University, China

Reviewed by:
Wei Zhang,
China Agricultural University, China
Yuchun Pan,
Shanghai Jiao Tong University, China

***Correspondence:**
Hongmei Xiao
lhtdyx@126.com
Yanhong Zhao
13947196432@163.com

† These authors have contributed equally to this work

Specialty section:
This article was submitted to Livestock Genomics, a section of the journal Frontiers in Genetics

Received: 09 February 2021
Accepted: 24 May 2021
Published: 09 July 2021

Citation:
Liu J, Mu Q, Liu Z, Wang Y, Liu J, Wu Z, Gong W, Lu Z, Zhao F, Zhang Y, Wang R, Su R, Li J, Xiao H and Zhao Y (2021) Melatonin Regulates the Periodic Growth of Cashmere by Upregulating the Expression of Wnt10b and β-catenin in Inner Mongolia Cashmere Goats. Front. Genet. 12:665834. doi: 10.3389/fgene.2021.665834

Secondary hair follicle growth in cashmere goats has seasonal cycle changes, and melatonin (MT) has a regulatory effect on the cashmere growth cycle. In this study, the growth length of cashmere was measured by implanting MT in live cashmere goats. The results indicated that the continuous implantation of MT promoted cashmere to enter the anagen 2 months earlier and induce secondary hair follicle development. HE staining of skin tissues showed that the number of secondary hair follicles in the MT-implanted goats was significantly higher than that in the control goats ($P < 0.05$). Transcriptome sequencing of the skin tissue of cashmere goats was used to identify differentially expressed genes: 532 in February, 641 in October, and 305 in December. Fluorescence quantitative PCR and Western blotting results showed that MT had a significant effect on the expression of *Wnt10b*, β-*catenin*, and proteins in the skin tissue of Inner Mongolia cashmere goats. This finding suggested that MT alters the cycle of secondary hair follicle development by changing the expression of related genes. This research lays the foundation for further study on the mechanism by which MT regulates cashmere growth.

Keywords: melatonin, transcriptome sequencing, differently expressed genes, cashmere goats skin, *Wnt*/β-*catenin*

INTRODUCTION

In China, goat breeds can be divided into dairy type, cashmere type, and meat type according to their economic uses (Watkins and Buxton, 1992). Cashmere goats are precious livestock resources for the production of natural fiber with high quality (Liu et al., 2016; Su et al., 2018). Cashmere and wool are important components of goat hairs. A study on the characteristics of cashmere goat coats reported that the complex shape and structure of hair follicles control hair growth. In mammals, hair follicles attached to the skin structure are skin micro-organs (Cetera et al., 2017)

and develop through the interaction between epithelial and dermal cells. Regeneration is the most prominent characteristic of hair follicles (Zawilska et al., 1995; Tan et al., 1999). Follicles are divided into primary hair follicles and secondary hair follicles according to different developmental stages. Wool is developed by primary hair follicles, while cashmere is derived from secondary hair follicles of the skin (Zhu et al., 2013). Adult animals typically have one cashmere growth cycle in a year, with growth peaking in summer and slowing down in winter, and natural shedding occurring in spring (Mcdonald et al., 1987; Norton and Klören, 1995). In contrast, the growth of secondary hair follicles in adult cashmere goats is divided into the following three stages: anagen (from April to November), catagen (from December to January), and telogen (from February to March; Millar, 2002; Watabe et al., 2014; Messenger and Botchkareva, 2017). Studies by Zhang (2020) have shown that primary follicles and secondary follicles have different degrees of periodic changes throughout the year, with primary follicles being the last to grow during telogen. However, the cycle division was not completely consistent, and the activity of secondary follicles was the highest in October. November may be the transition stage of secondary follicles from anagen to catagen; January is the transition period of secondary follicles from catagen to telogen, and the follicles are still active, which can promote the growth of cashmere and finally the transition from telogen to anagen.

The growth of cashmere is affected by many factors, such as sunlight time, melatonin (MT), nutrition, genetics, and endocrine factors. The duration of direct sunlight directly affects the periodic growth of cashmere. As sunlight decreases, cashmere begins to emerge from the skin surface. As the light cycle becomes longer, the hairs fall off, and apoptosis occurs (Basheer and Abdulbari, 2018). In addition, the duration of direct sunlight affects the growth rate and yield of cashmere. The growth cycle of cashmere is also affected by the changes in light intensity. Some earlier assays have shown that with the increase in light intensity in summer, there is excessive secondary hair follicle growth from telogen to anagen, and the activity peaks in anagen. Another study showed that the length of Henderson illumination directly affected the growth of new trichomes but had no effect on the shedding of old trichomes (Salehian et al., 2015).

As an indole hormone, MT is mainly secreted by the pineal gland of the brain in humans and other mammals. Its secretion is affected by light and shows obvious diurnal changes. MT is found in the pineal gland and various other tissues and organs of vertebrates, including multifunctional molecules synthesized by the retina (Zawilska et al., 1995), bone marrow (Tan et al., 1999), gastrointestinal tract (Lepage et al., 2005), placenta (Lanoix et al., 2008), testis (Ji et al., 2012), and ovary (Tamura et al., 2017). Among its various physiological functions, MT exerts its powerful antioxidant capacity by directly scavenging free radicals and stimulating the activity of antioxidant enzymes (Reiter et al., 2017; Yang et al., 2020). In a study on the effects of light and MT implantation on cashmere production performance and regulation in Inner Mongolia white cashmere goats, periodic changes in light made the norepinephrine content periodic through the sympathetic nervous system, thus making the amount of 5-hydroxytryptamine (5-ht) and MT periodic (Tan et al., 1999). MT is secreted at higher levels at night and less in the daytime. After the summer solstice, the secretion quantities of MT increase gradually at night as the sunshine becomes increasingly shorter. After the winter solstice, as the days grow longer, and the nights grow shorter, the secretion time of MT is correspondingly shortened, and the secretion quantities are also gradually decreased (Lanoix et al., 2008; Ji et al., 2012; Tamura et al., 2017).

It was reported that MT can accelerate the hair follicle reconstruction process and induce secondary hair follicle development, which results in early entry into the next cashmere growth cycle and increases cashmere yields (Duan et al., 2017; Ge and Wang, 2018; Yang X. Z., 2020; Yang C. H., 2020). According to previous studies, two MT implants during the non-fleece period can improve the cashmere yields of Inner Mongolia cashmere goats to different degrees (Yang et al., 2020). Genes play a decisive role in the process of cashmere growth. Therefore, studying the related genes regulating cashmere growth based on MT is of great significance. *Wnt10b* is a key member of the *Wnt* family and is very important for the formation and maintenance of the hair matrix. *Wnt10b* not only promotes the development of hair follicles but also participates in the entire process of hair follicle development and cashmere periodic growth (Wu P. et al., 2020). Many studies on the classic *Wnt* signaling pathway have found that the *Wnt*/β-*catenin* signaling pathway plays an important role in hair follicle development (Lin et al., 2015; Wu Z.Y. et al., 2020). However, there is no clear mechanism by which MT regulates the cashmere growth cycle, and there is no conclusion about the role of *Wnt10b* and β-*catenin* in promoting cashmere growth through MT. In order to make up for the blank of this research, we performed many experiments in this study, including implanting MT in live cashmere goats, measuring the growth length of cashmere, observing the haematoxylin and eosin (HE) staining of skin tissues, performing Gene Ontology (GO) and Kyoto Encyclopedia of Genes and Genomes (KEGG) pathway analyses of transcript sequences of Inner Mongolia cashmere goat skins collected in February, October, and December, and using RT-PCR and western blot technology to examine the expression of the two key genes at the mRNA and protein levels. The research results provide a basis to investigate the mechanism of endogenous MT in the signaling pathway of cashmere growth in Inner Mongolia cashmere goats.

MATERIALS AND METHODS

Sample Collection and Ethics Statement

All the animals in this study came from the Jinlai animal husbandry farm in Inner Mongolia, and the use of the cashmere goats in the study was also approved by the owner. 12 adult (2-year-old) female goats with similar body weights (∼35 kg) were selected from Inner Mongolia cashmere goats and randomly assigned to two groups of six. MT was implanted

in the experimental group, while MT was not implanted in the control group.

MT Administration

The experimental study period was 12 months, that is, during the growth cycle of cashmere. MT (provided by the special economic animal laboratory of Northeast Forestry University) was implanted subcutaneously behind the ears of cashmere goats every 2 months. Based on previous studies (Duan et al., 2015), the MT dose was 2 mg/kg live weight. The control group was not implanted, and the experiment lasted 1 year. Skin samples (1 cm × 1 cm) of the shoulder blade side were collected in February, October, and December.

Experimental Procedures

The cashmere fiber samples were collected within 10 cm × 10 cm of the posterior part of the shoulder blade of goats. Samples were collected once a month 1 month after the start of the experiment. Each time, the sample was collected near the previous collection site on the side of the body but different from the previous collection site. Cashmere samples were collected for the determination of wool length and fineness. Skin samples of 1 cm × 1 cm on the side of the scapula of ewes were collected on the 22nd day of each month for 12 months, and the skin samples were stored in an ultralow temperature refrigerator at −80°C. Blood samples were collected immediately at 23:00 the day before each skin biopsy.

Determination of MT Concentration in Plasma of Cashmere Goats

Blood samples were collected from the jugular vein with a 10-ml EDTA-containing vacuum tube under low red light at 12 p.m.–2 p.m. The plasma was centrifuged at 3,000 rpm/min for 10 min at 4°C and stored at −20°C until analysis. The content of MT in plasma was determined by radioimmunoassay (RIA). MT content was determined by RIA according to the method provided by the Belgian company.

Hormone Test

Plasma MT concentrations were measured by RIA using commercial analysis equipment (Bar 3300, registered dietitian, Germany) with sensitivity and internal coefficient of variation (CV) of 2.3 pg/ml and 9.7–13.4% and 8.0–13.3%, respectively. Plasma cortisol concentrations were measured using RIA experimental tools (253 Hospital, Hohhot, Inner Mongolia), with sensitivity and internal variation coefficients (CV) of 2 ng/ml and <10% and <15%, respectively.

Cashmere Fiber Measurement

As described by Duan et al. (2015), the wool sample contains a mixture of coarse wool and cashmere fibers that must be washed with carbon tetrachloride and warm water and then air-dried in a fume hood. The length of the cashmere fiber is measured by fixing one end of the fiber at the zero point of the ruler and gently stretching the other end until there is no bending or kinking. The fiber length of each sample was determined by the average of 100 fibers.

Preparation of Frozen Skin Sections

The tissues were removed from −80°C, thawed at 4°C, placed in 4% paraformaldehyde solution, and fixed at 4°C overnight. The next day, the fixed tissues were washed with PBS three times for 3 min each time. After the filter paper was sucked dry, the tissues were put in 30% sucrose solution and dehydrated overnight at 4°C to the bottom of the tissues. The excess water was soaked up with filter paper, the appropriate angle was adjusted according to the section direction, the tissue was placed on the prefrozen section base, and then the tissue was embedded into the frozen section using an OTC embedding agent. The slicer was precooled 2 h in advance by setting the temperature of the apparatus at approximately −28°C, and then the tissue was sliced onto the base after it was completely frozen. Before sectioning, the sample was modified with a thickness of 20 mm. After the section was cut into the tissue, the section thickness was adjusted to 6 mm. For each section, the hair follicle shape was observed under a microscope to ensure completeness.

HE Staining of Skin Samples Over 3 Months

Frozen sections were fixed for 1 min, washed with water for 10 s, stained with haematoxylin for 1∼2 min, and washed under running water for 15∼20 s to wash away the stain. The sections were then incubated with 1% hydrochloric acid ethanol for 1 s, washed with water for 5 s, and rinsed with water again for 15∼20 s to restore the blue coloration. Next, the sections were stained with a 0.5% eosin solution for 5∼10 s, washed for 5 s with distilled water, dehydrated with 80 and 95% anhydrous ethanol for 30 s each, and cleared with dimethylbenzene xylene for 30 s. The sections were then sealed with neutral gum, and images were acquired under a microscope.

Determination of Relevant Parameters of Hair Follicle Groups

Images of hair follicles were taken by a microscope camera (Lycra ICC50W, Germany). Samples of sebaceous glands collected at different depths were observed with 10 fields of view each. The number of hair follicles in each counting area was calculated, plus the number of all trapped follicles at the top and left edge of the counting area. Follicles intercepted by the bottom and right margins were not included in the count.

RNA Extraction, Library Construction, and Sequencing

In the implanted MT group and the control group, six adult female Inner Mongolia white cashmere goats with similar physical characteristics were selected. After that, skin samples of 1 cm × 1 cm from the side of the scapula were collected in February, October, and December, stored in liquid nitrogen, and transported to the laboratory for extraction of total RNA. Total RNA was extracted from skin samples using TRIzol (Life Technologies, CA, United States) according to the manufacturer's instructions. RNA purity was checked using a NanoDrop 2000 spectrophotometer (NanoDrop Technologies, Wilmington, DE, United States), and the concentration and integrity of RNA were

assessed using an Agilent 2100 Bioanalyzer and Agilent RNA 6000 Nano Kit (Agilent Technologies, CA, United States).

Analysis of RNA-Seq Data

Approximately 4 μg of total RNA was used to prepare the RNA sequencing library using TruSeq RNA Sample Prep Kits (Illumina, San Diego, CA, United States) according to the kit's protocol. Finally, the libraries were sequenced on an Illumina HiSeq 2500 platform using 200-bp paired-end reads.

High-quality clean reads were obtained from the raw reads by removing low-quality and adapter-contaminated reads. After that, the filtered reads were aligned to the goat (*Capra hircus*) genome27 by TopHat57. The FPKM of each gene was calculated to estimate the gene expression level (Trapnell et al., 2010). The differentially expressed genes were obtained with the standards of |fold change| >1.5 and *P*-value < 0.05.

Pathway and Gene Enrichment Analysis

To explore the biological functions of differentially expressed genes, GO ad KEGG pathway enrichment analyses of these genes were performed. GO enrichment analyses of the differentially expressed genes were implemented by the GOseq R package. GO terms with corrected *P*-values < 0.05 were considered significantly enriched. KEGG[1] is a database that helps users assign related molecular processes, diseases, and pathways to genes by high-throughput technology.

Fluorescence Quantitative PCR

First, total RNA extracted was reverse transcribed into cDNA. Second, specific primers were designed by Primer 5.0 on the basis of the cDNA sequences of the goat *Wnt10b* and β-*catenin* actin genes published in NCBI and were synthesized by Shanghai Biological Engineering Co., Ltd. Next, cDNA obtained from total RNA by reverse transcription was used as a template in fluorescence quantitative PCR performed with SYBR® (TaKaRa, Tokyo, Japan). Amplification of each sample by PCR was performed with 3 technical replicates.

Western Blotting

In western blot experiments (Han et al., 2020), proteins were extracted from tissue samples in each group and quantified using the BCA Protein Assay Kit (Cat No. P0010S, Biyuntian, China). Equal amounts of proteins were subjected to SDS-PAGE and transferred to polyvinylidene fluoride membranes. Rabbit polyclonal *Wnt10b* (ab66721, 1:200, Abcam, United States) and rabbit monoclonal anti-β-*catenin* (ab17325, 1:100, Abcam, United States) antibodies were used as primary antibodies.

Statistical Analysis

In SAS 9.0, comparisons of experimental data from two groups were performed by *t*-test, and multiple comparisons of mean values were carried out by using the Duncan method. Correlation analysis of plasma MT, cashmere growth characteristics, etc., was performed.

[1]https://www.kegg.jp/

RESULTS AND ANALYSIS

MT Concentration in Plasma of Cashmere Goats Was Significantly Increased After MT Implantation

After implantation of MT, plasma MT levels increased from August to January of the following year, then began to decline after November, rose abruptly in February, and then declined gradually until June. The plasma MT content in the implanted group was approximately 10.42 times higher than that in the control group, and the MT concentration in the implanted group was significantly higher than that in the control group ($P < 0.01$; **Figure 1**).

MT Can Induce the Growth of Secondary Cashmere 2 Months Earlier

Goats in both the implanted group and the control were growing cashmere since August, and the growth basically stopped in January. From January to the cashmere period, the length of cashmere basically remains unchanged at 11 cm. Notably, in June, the MT implantation group started a new round of growth 2 months earlier than the control group, inducing secondary cashmere growth. Cashmere in the implantation group grew 3–4 cm, while no cashmere grew in the control group (**Figure 2**). From this experiment we found that, MT can induce the growth of secondary cashmere 2 months earlier.

Population of Primary and Secondary Hair Follicles in Cashmere Goats During the Early Growth Period

Hair follicle density (numbers of follicles per mm^2 of skin) and S:P (ratio of secondary to primary hair follicles) were used as indicators of the population of hair follicles in the skin of cashmere goats. In the present study, goat skin tissue histological examination showed that (**Figure 3**) the S:P ratio in the implanted group was significantly higher than that in the control group in May and June of the pregrowth period ($P < 0.05$, **Table 1**). There was no significant difference in the S:P ratio between the implanted group and the control group ($P > 0.05$, **Table 1**) from July to the growth period (September) or the declining period (December). Therefore, we focused on cashmere goat skin tissues in the pregrowth period (May and June) and growth period (September) with significant changes in the S:P ratio. In September of the growth period, the hair follicles in the skin of the implanted group and the control group began to shrink and increase, and the S:P ratio gradually decreased (**Figure 3**).

Screening of Differentially Expressed Genes Related to Hair Follicle Growth and Development in Cashmere Goats

Differentially expressed genes were identified by comparing the transcriptome data of the experimental group and the control group in February, October, and December. As shown in **Figure 4**, the co-expressed genes are outside the circle, while the differentially expressed genes are inside the circle. According

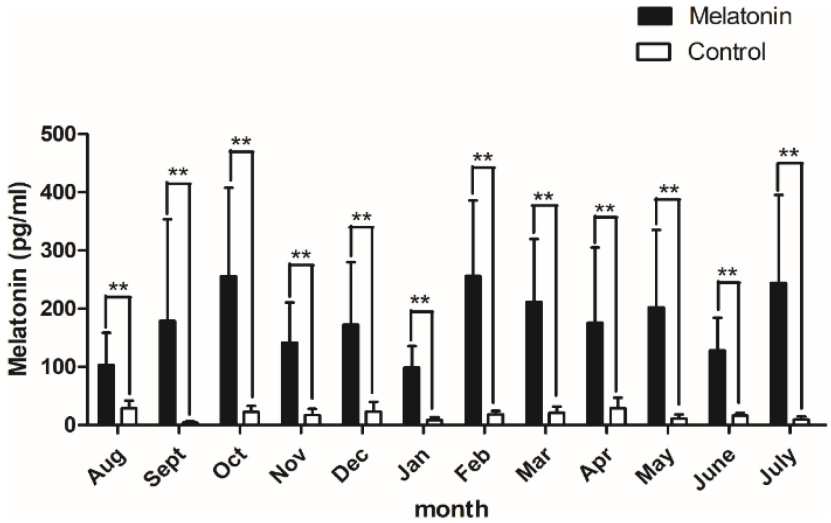

FIGURE 1 | Content of melatonin in plasma. Black histogram represents experimental group and white histogram represents control group. Control: no treatment; Melatonin: melatonin implantation. Values represent means ± SD, the punctuation ** represents $P < 0.01$.

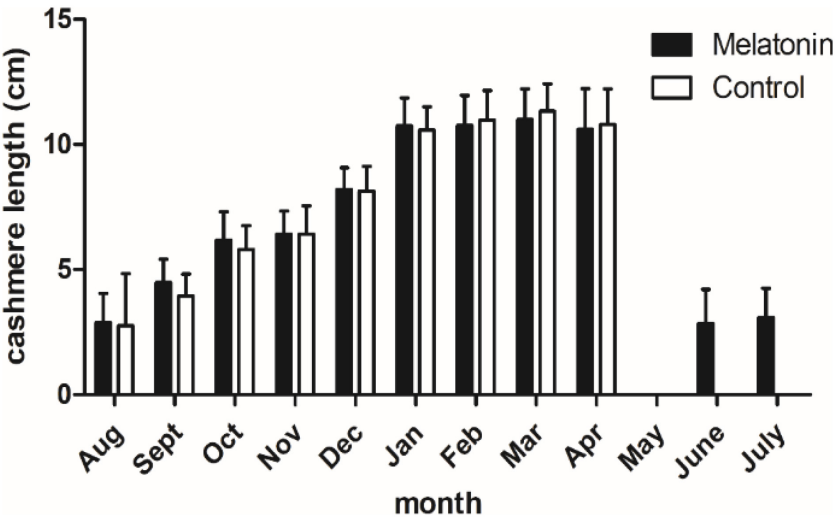

FIGURE 2 | Cashmere length of the cashmere goats in a year. Black histogram represents experimental group and white histogram represents control group.

to the differential expression analysis, 532 differentially expressed genes were identified between the experimental group and the control group in February, among which 148 were down-regulated and 384 were up-regulated. In October, 641 differentially expressed genes were identified, among which 178 were down-regulated and 463 were up-regulated. In December, 305 differentially expressed genes were identified, among which 138 genes were down-regulated and 167 genes were up-regulated.

Gene Functional Classification Analysis Related to Hair Follicle Growth and Development in Cashmere Goats

To better understand the biological behavior of HF and skin morphogenesis, according to GO classification statistics, 44 terms were categorized into three GO categories: cell components, molecular functions, and biological processes. Among them, in the cellular component category, the top GO term was cell part. In the molecular function category, most of the terms were related to binding. In the biological process category, most of the terms were related to cellular processes (**Figure 5**).

Kyoto Encyclopedia of Genes and Genomes is a very useful tool in searching for genes related to metabolic or signal transduction pathways. In this study, the screened genes were annotated with the KEGG database, and the metabolic pathways of some genes were analyzed. Some of the differentially expressed genes were enriched in *Wnt*, *MAPK*, *Notch*, and other signaling pathways, which are related to hair follicle development (Zhang et al., 2020). Two different genes, *Wnt10b* and β-*catenin*, that may

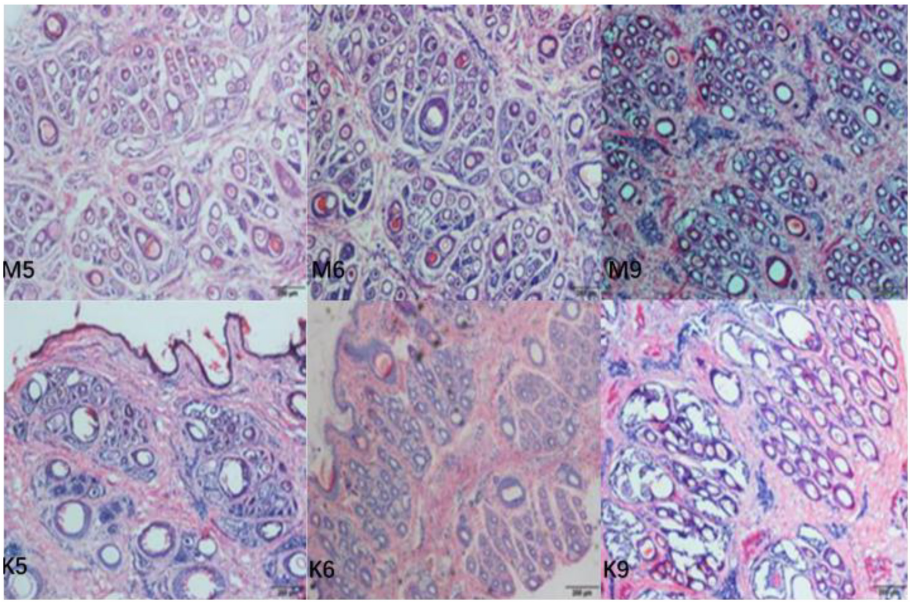

FIGURE 3 | Transverse incision of skin follicles of Inner Mongolia cashmere goats in May, June, and September. M represents trial group and K represents control group. The numbers 5, 6, and 9 represent May, June, and September, respectively.

TABLE 1 | Effect of administration of melatonin to cashmere goats in one cashmere growth cycle on primary and secondary hair follicle numbers.

Month	Control group		S:P	Implanted group		S:P
	PFD (n/mm^2)	SFD (n/mm^2)		PFD (n/mm^2)	SFD (n/mm^2)	
January	3.37 ± 0.34	37.51 ± 1.24	11.27 ± 1.55	4.30 ± 0.16	40.42 ± 2.23	9.43 ± 0.87
February	3.83 ± 0.49	40.49 ± 2.33	10.84 ± 2.20	4.36 ± 0.10	37.96 ± 2.00	8.71 ± 0.65
March	3.88 ± 0.40	43.92 ± 1.89	11.49 ± 1.80	4.20 ± 0.53	43.02 ± 2.28	10.49 ± 1.96
April	4.06 ± 0.40	30.64 ± 2.32	7.67 ± 1.40	4.35 ± 0.51	31.96 ± 2.23	7.52 ± 1.52
May	4.46 ± 0.43	36.71 ± 2.64	8.37^a ± 1.51	4.58 ± 0.43	56.83 ± 1.07	12.54^b ± 1.46
June	4.46 ± 0.23	37.71 ± 1.55	8.49^a ± 0.75	4.10 ± 0.50	54.71 ± 3.77	13.56^b ± 2.03
July	4.75 ± 0.43	50.04 ± 3.15	10.69 ± 1.74	4.81 ± 0.53	50.00 ± 2.20	10.59 ± 1.76
August	5.06 ± 0.42	55.07 ± 2.00	10.98 ± 1.37	5.18 ± 0.42	54.70 ± 1.17	10.64 ± 1.13
September	2.84 ± 0.42	41.68 ± 1.00	15.07 ± 2.90	3.28 ± 0.36	49.35 ± 0.14	15.26 ± 1.81
October	3.40 ± 0.42	49.32 ± 2.87	14.83 ± 2.91	3.57 ± 0.44	48.45 ± 0.54	13.77 ± 1.70
November	3.13 ± 0.44	43.60 ± 0.27	14.22 ± 2.18	3.25 ± 0.32	44.00 ± 0.56	13.71 ± 1.57
December	4.04 ± 0.34	50.58 ± 2.68	12.67 ± 1.83	4.37 ± 0.46	51.62 ± 1.87	11.99 ± 1.81

PFD, primary follicle density; SFD, secondary follicle density; S:P, ratio of secondary to primary follicles. The same letter represents no significant difference, while different letters represent significant difference in the table.

be related to hair follicles in these three pathways were selected for subsequent verification and analysis (**Tables 2**, **3**).

MT Promotes *Wnt10b* and β-*catenin* Gene Expression in the Skin of Inner Mongolia Cashmere Goats in Catagen and Telogen

Fluorescence quantitative PCR results showed that *Wnt10b* and β-*catenin* in the control group and the experimental group were expressed to varying degrees every month of the year. The expression of *Wnt10b* was significantly increased in the catagen and telogen periods after MT implantation ($P < 0.05$), and the expression of β-*catenin* was also increased in the late anagen period and telogen period. The above two genes play important roles in the process by which MT promotes the growth of cashmere (**Figures 6A,B**).

Extraction and Detection of Total RNA From Skin Tissues of Inner Mongolia Cashmere Goats

Total RNA was extracted from skin samples and detected by a NanoDrop 2000 UV spectrophotometer, and the products of 28S and 18S were detected by 1% agarose gel electrophoresis

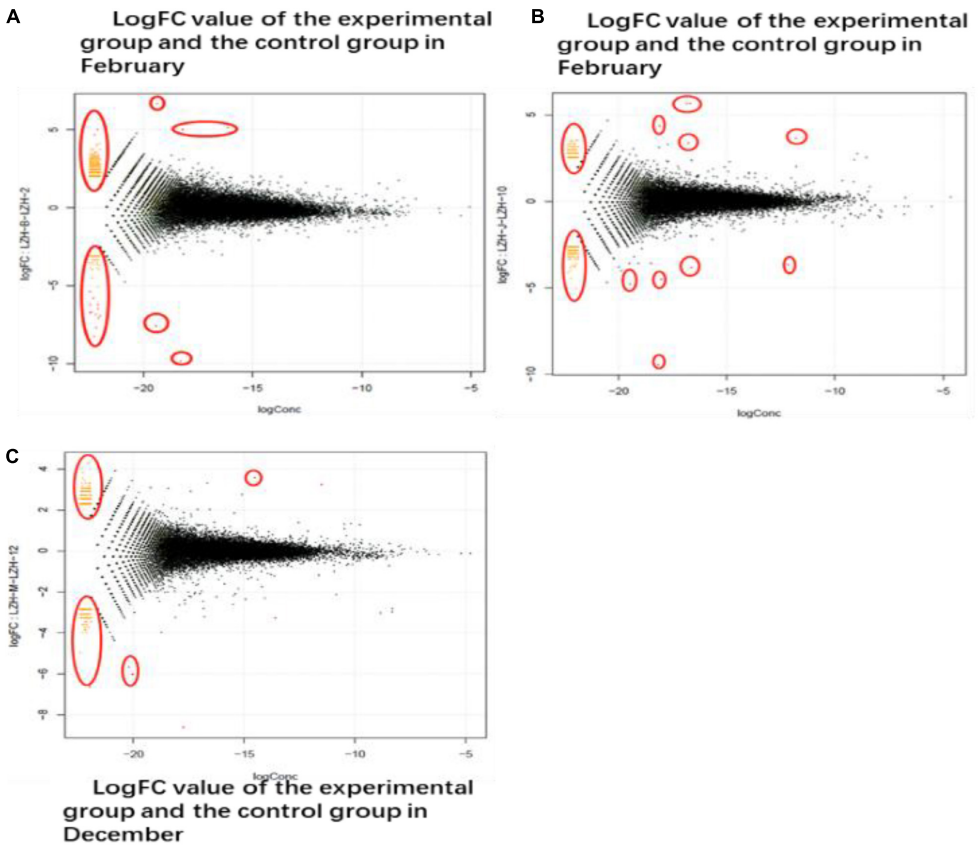

FIGURE 4 | DEG different period of cashmere. **(A)** LogFC value of the experimental group and the control group in February. The transcriptome data of the experimental group and the control group in February, October, and December were screened for differentially expressed genes. The co-expressed genes were on the outside and the different genes were on the inside. **(B)** October LogFC value of the experimental group and the control group. In October, 641 genes were screened out, of which 178 were down-regulated and 463 were up-regulated. **(C)** The LogFC value of the experimental group and the control group in December. In December, 305 differentially expressed genes were screened, among which 138 up-regulated genes had 167 differences.

without protein and organic reagent contamination (**Figure 7**) for subsequent experiments.

MT Had a Significant Effect on the Protein Expression of *Wnt10b* and β-*catenin* in Inner Mongolia Cashmere Goat Skin

To investigate the underlying mechanism of MT, western blot analysis was used to detect the effects of MT implantation on the expression of the *Wnt10b* protein and β-*catenin* protein in hair follicles of cashmere goats. The results showed that the expression level of *Wnt10b* protein in the experimental group was significantly higher than that in the control group in December and February. Moreover, the expression level of the β-*catenin* protein was also significantly higher in the experimental group than in the control group in October. Taking all the data into consideration, we concluded that the *Wnt10b* protein and β-*catenin* protein play a key role in the start-up and growth of hair follicles (**Figure 8**). MT regulates the periodic growth of cashmere by upregulating the expression of *Wnt10b* and β-*catenin* in Inner Mongolia cashmere goats.

DISCUSSION

The results to date clearly support our hypothesis that continuous injection of MT can stimulate the development of secondary hair follicles in cashmere goats and speed up the hair follicle reconstruction process in cashmere goats. Importantly, MT has beneficial effects on the growth of secondary hair follicles throughout the life cycle, and by upregulating the expression of genes related to hair follicle development in cashmere goats, MT regulates the periodic growth of cashmere and induces cashmere to enter the growing period in advance, leading to secondary cashmere growth and increasing cashmere yields.

MT Concentration in Plasma of Cashmere Goats in the Implanted Group and Control Group

The growth of cashmere has strong seasonal variation. The sunshine exposure time affects the cashmere growth rate and yield of cashmere goats. Under the influence of light intensity, MT concentration also undergoes obvious periodic changes. The secretion of MT has an important influence on the cashmere

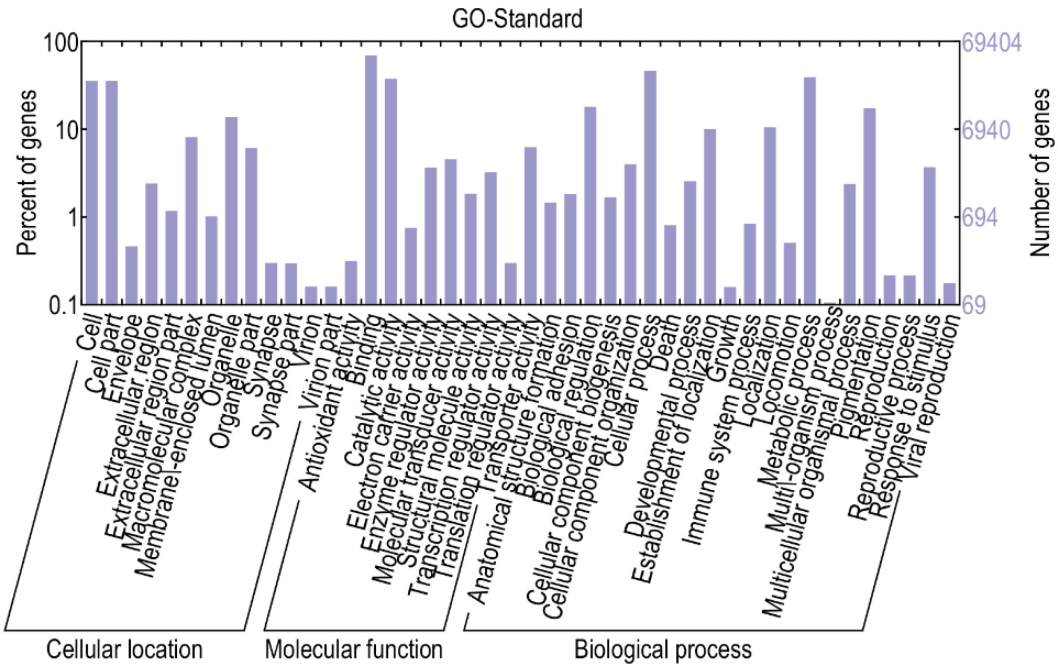

FIGURE 5 | GO analysis of differential genes. This figure, clustering analysis was performed on the differentially expressed genes of the implant group and the control group in different periods. The results are summarized in three main categories: biological process, cellular component, and molecular function. The *X*-axis indicates the second level term of gene ontology; The *Y*-axis shows the number of genes.

TABLE 2 | The primer sequences for RT-qPCR of cashmere goat gene.

gene Gene	Primer sequence (5′–3′) annealing temperature the sequence of primer Tm (°C)	Fragment length product size
Beta actin	F: GGCAGGTCATCACCATCGG 60	187 bp
	R: CGTGTTGGCGTAGAGGTCTTT	
Wnt10b	F: TGCTCACAACCGCAACTC 64	107 bp
	R: GGTCTCGCTCGCAGAAG	
Beta-catenin	F: GACCACAAGCAGAGTGCT 55	100 bp
	R: TGTCAGGTGAAGTCCTAAA	
SFRP1	F: GCACGACCGTGTGTCCTCCATGT 63	192 bp
	R: GCTTCTTCAGCTCCTTCTTCTTGAT	
FGF21	F: TCCCGAAAGTCTCTTGGAGC 57	110 bp
	R: ATCCGTACAGCTTCCCATCTG	
TCHHL1	F: GCCAGAAAGTGGCCCAAGATGTAT 58	192 bp
	R: CTCCAAACCATTCTCCTGTCTCAGT	

This table shows, the specific primers were designed by Primer 5.0 according to the cDNA sequences of goat Wnt10b, β-catenin, and the actin gene with a constant expression level published in NCBI and were synthesized by Shanghai Biological Engineering Co., Ltd.

TABLE 3 | Genes enriched in the signal pathways related to hair follicle growth.

Signaling pathways	Differential gene (ID)	Note
WNT	SFRP1 (ENSBTAP00000039575)	The DOWN
	WNT10b (NM003394)	The UP
	CHP2 (ENSBTAP00000016647)	The DOWN
	Beta – catenin (NM001076141)	The UP
MAPK	FGF21 (ENSP00000222157)	The UP
	NTRK2 (ENSBTAP00000053704 – d2)	The UP
	FGF14 (ENSP00000365301)	The DOWN
	NFKB1 (ENSBTAP00000027016.1)	The UP
Notch	DLL3 (ESNP000000205143)	The DOWN
	TCHHL1 (ENSBTAP00000021074)	The DOWN

This table, partial differential genes were enriched in Wnt, MAPK, Notch, and other signaling pathways. KEGG is a complete database, which serves as a bridge in major databases such as NCBI and SwissProt. The selected differential screened genes were annotated in the KEGG gene database, and some differential screened genes were analyzed in the metabolic pathway.

growth cycle. In this experiment, the content of MT in the plasma of the implanted and control groups was measured, and it was found that under natural light conditions, the content of MT in plasma of the control group at night was generally between 7 and 30 pg/ml, with an average of 17.34 pg/ml. After the implantation of MT, the content of MT in plasma was significantly increased. The data also indicated that the levels of MT in plasma vary greatly among different individuals at night. By implanting MT in Inner Mongolia cashmere goats, Yang found that the serum MT concentration in the treatment group was significantly higher than that in the control group, which was consistent with the experimental result of our study (Yang et al., 2020).

MT Affects Cashmere Growth in Cashmere Goats

The results of this study showed that MT implantation could stimulate the growth of cashmere (Duan et al., 2016), which

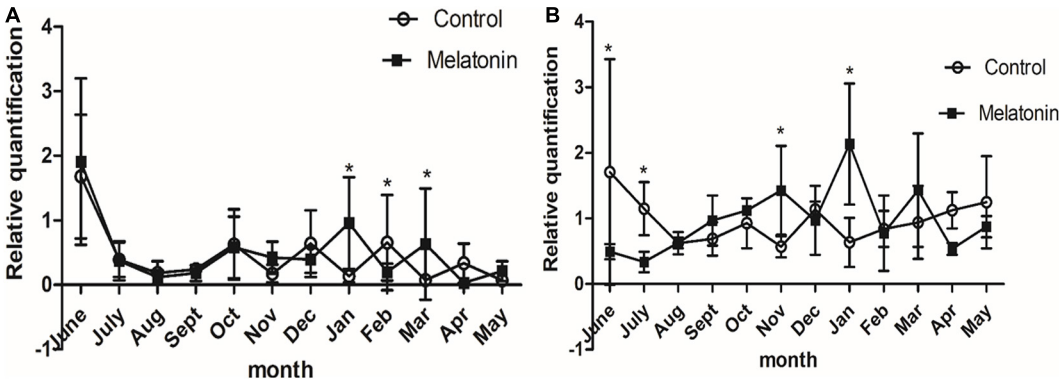

FIGURE 6 | Effects of melatonin on the expression of villi growth-related genes in Inner Mongolia cashmere goats. **(A)** The relative expression quantity of the *Wnt10b* gene. The square represents the experimental group; the circle represents the control group. The *Wnt10b* gene is expressed in different degrees in each month of the year in the control group and the experimental group. Control: no treatment; Melatonin: melatonin implantation. Values represent means ± SD, $^{*}P < 0.05$ vs. untreated group. **(B)** The relative expression quantity of β-*catenin* gene, the square represents experimental group; the circle represents control group. The expression level of human-catenin gene was different in each month of the year in the control group and the experimental group.

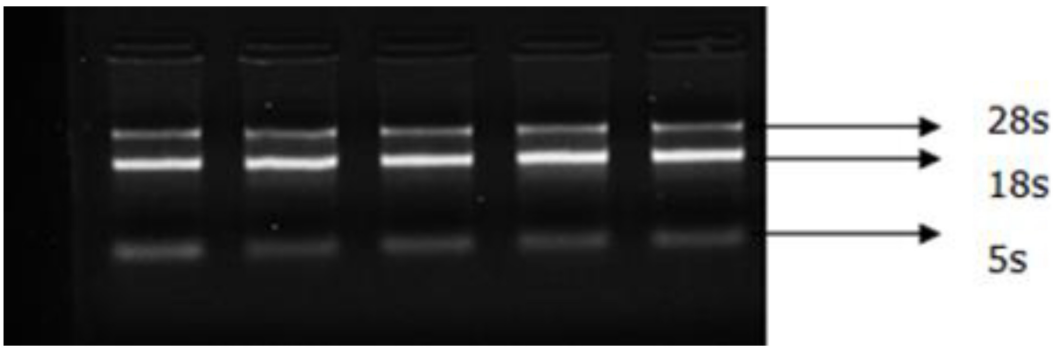

FIGURE 7 | Electrophoretogram of skin total RNA. Total RNA was extracted from skin samples and detected using the NanoDrop 2000 UV spectrophotometer (Thermo Fisher). Od260/280 values were all between 1.8 and 2.0. The bands with clear integrity of 28s and 18s were detected by 1% agarose gel electrophoresis.

was consistent with previous results. In this experiment, there was no significant difference in cashmere length between the treatment group and the control group. In June and July of the next year, kids in the MT implant group and the first-year goats had grown 3–4 cm growth of cashmere, while in the control group, no hair had grown on the surface. This indicates that continuous implantation of MT can promote the early growth of cashmere, stimulating the growth of secondary hair follicles and accelerating the hair follicle reconstruction process, which is consistent with the results of Wuliji et al. (2006). In this study, it was also found that MT implantation could reactivate secondary hair follicles in the resting period and restore fleece activity, which was manifested as an increase in cashmere density, but the specific mechanism remains to be further studied.

For the growth of cashmere, whether in the implanting group or the control group, the growth of cashmere started in August and stopped in January. In this experiment, the growth time of wool was longer than that of cashmere, indicating that the activity duration of primary hair follicles was longer than that of secondary hair follicles. The effect of MT on the development of hair follicles of cashmere goats is larger.

Observing the phenotypic characteristics of hair follicles in tissue sections, the differences in hair follicle characteristics between the MT implantation group and the control group in May, June, and September were preliminarily investigated. In this study, the effect of MT on the number of primary hair follicles in Inner Mongolia cashmere goats was consistent with the experimental results of unimplanted MT, indicating that MT has no effect on the number of primary hair follicles (Duan et al., 2015). In this study, HE staining results showed that in the same growth cycle of the experimental group and the control group, the overall development of the primary and secondary hair follicles was roughly the same, but there were significant differences in specific months. First, the number of secondary hair follicles in the experimental group was significantly higher than that in the control group only in May and June throughout the growth cycle. Second, in the early growth stage, the position of hair follicles in the experimental group from the epidermal layer was significantly shallower than that in the control group based on observation of the longitudinal cut of the skin, indicating that the hair follicles in the experimental group were very strong at this time, while the hair follicles in the control group had

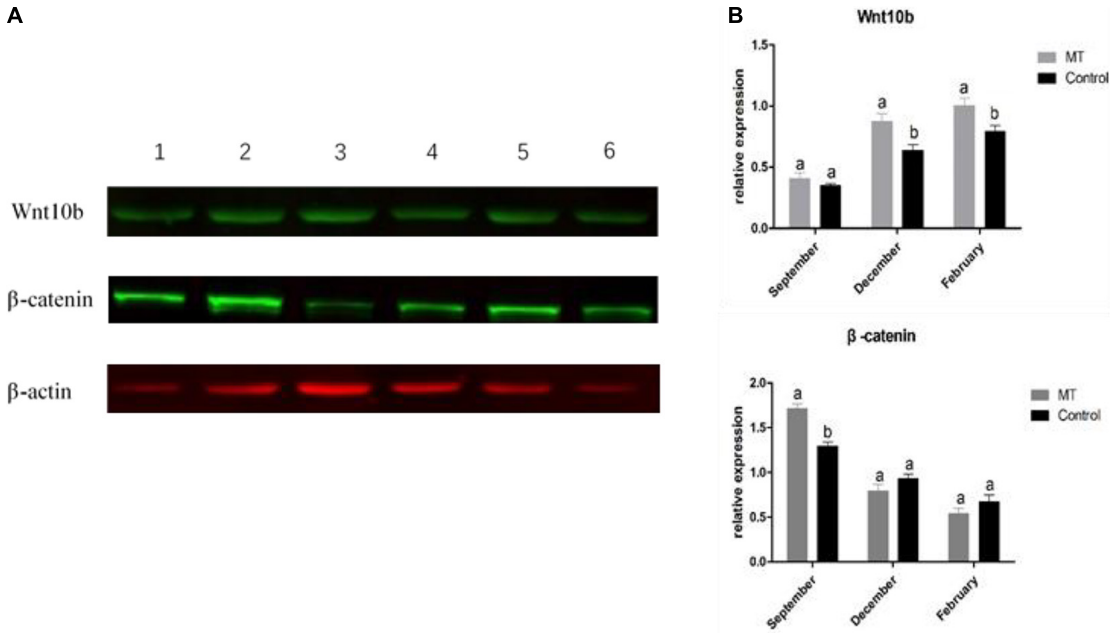

FIGURE 8 | (A) Western blot and quantitative analysis of *Wnt10b* and β-*catenin* genes. The one, two, and three bands were *Wnt10B,*β-*catenin*, and β-*actin* of the test group in February, October, and December, respectively; the four, five, and six bands were *Wnt10B,*β-*catenin*, and β-*actin* of the control group at February, October, and December, respectively. **(B)** The same letter represents no significant difference, while different letters represent significant difference.

already started to go deep into the skin. Therefore, it is speculated that the stimulation of exogenous MT may change the growth cycle of Inner Mongolia cashmere goat hair follicles in the early flourishing period, but it has no obvious effect on the stage from the growth period to the beginning of the next cashmere growth cycle. This finding is consistent with previous studies on the effect of MT on cashmere performance of Inner Mongolia alba cashmere goats (Yang et al., 2020). However, we want to know why the effect of MT implantation on hair follicle growth of cashmere goats is weakened after the growth period, which provides a new direction and idea for future research on MT.

Identification of Differentially Expressed Genes Related to Cashmere Growth Based on Transcriptome Sequencing

Through transcriptome sequencing, we can determine the effect of MT implantation on the gene expression level in skin and hair follicle growth in cashmere goats at different stages. The growth cycle and formation of hair follicles are regulated by molecules and some complex signaling pathways. Some of the signaling pathways function by inhibiting or promoting factors related to hair follicle development, which are eventually transmitted to hair follicle development-related tissues to achieve whole-cycle changes in hair follicles. Therefore, finding regulatory signaling molecules at different developmental stages is the key to studying the growth and development of whole hair follicles. In this study, statistical analysis of differential gene expression showed that the most differentially expressed genes were identified in October, while the least differentially expressed genes were identified in December, indicating that gene expression was up-regulated in the initial stage of secondary hair follicle growth. In general, the activity of secondary hair follicles was the highest in October, which was also confirmed by the identification of the most up-regulated genes in October. With the progression of hair follicle growth and development, the number of up-regulated genes continued to increase, while the number of down-regulated genes began to decrease. It is worth noting that in February, hair follicle activity was lower, but a high number of up-regulated genes among the identified differentially expressed genes were found. We suspect that MT implantation may reactivate secondary hair follicles in the resting period (Wuliji et al., 2006), which is also consistent with previous research results. Finally, through GO functional classification and KEGG signaling pathway analysis, the differentially expressed genes of the experimental group and the control group in February, October, and December were enriched in biological processes, cellular components, and molecular functions. Two different genes related to hair follicular development in the *Wnt*, *MAPK*, and *Notch* signaling pathways, *Wnt10b* and β-*catenin*, were selected for further verification and analysis.

Effect of MT Implantation on the Expression of *Wnt10b* and β-*catenin* Signaling Molecules

Reverse transcription-qPCR was used to verify the gene expression to ensure the accuracy of the study on phenotypic

traits. It has been reported that there are many signaling pathways regulating the periodic growth and development of hair follicles. The *Wnt* signaling pathway is one of the central pathways (Ouji et al., 2006; Wu Z.Y. et al., 2020). *Wnt10b* and β-*catenin* are important genes related to hair follicle development in the *Wnt* signaling pathway in Inner Mongolia cashmere goats. Studies have shown that *Wnt10b* is expressed in hair matrix and inner root sheath cells and promotes the growth of hair matrix cells and hair stem lengthening. Cheng et al. (2016) showed that the expression level of Wnt10b was higher in anagen and lower in catagen and telogen. In this study, to investigate the relationship between MT and *Wnt10b* and β-*catenin* and the mechanism of the influence of MT on cashmere growth, the two genes were quantitatively analyzed by RT-qPCR. The results showed that the expression level of *Wnt10b* was significantly increased after MT implantation in catagen and telogen. In January, the hair follicle transitioned from catagen to telogen, the hair follicles shrank back under the skin, and hair follicle cells underwent apoptosis, while *Wnt10b* promoted hair matrix cell proliferation and hair stem elongation. It plays an important role in the differentiation of follicular epidermal cells (Ouji et al., 2007). Therefore, it was speculated that MT implantation increases the expression level of *Wnt10b* from catagen to telogen, which leads to the reactivation of hair follicles and the growth of cashmere 2 months earlier. *Wnt*/β-*catenin* signaling plays an important role in the growth and development of hair follicles and the proliferation and differentiation of stem cells (Chen et al., 2020). β-*catenin* has lower expression in catagen and telogen but higher expression at the end of anagen (Schmidt-Ullrich and Paus, 2005). However, the results of this study showed that MT implantation increased the expression level of β-*catenin* in late anagen and telogen. To further investigate the underlying mechanism, western blot analysis was used to detect the effect of MT implantation on the protein expression levels of *Wnt10b* and β-*catenin* in hair follicles of cashmere goats.

Previous studies have demonstrated that changes in *Wnt10b* protein expression play an important role in the growth and development of hair follicles (Li et al., 2013). The current opinion is that activation of the *Wnt10b*/β-*catenin* signaling pathway can promote hair follicle status from telogen to anagen and play a key role in the initiation of periodic hair growth. In this study, the western blot results showed that the expression level of *Wnt10b* protein was higher in the experimental group than in the control group in telogen, and the expression level of β-*catenin* protein was higher in the experimental group than in the control group in anagen. PCR results also showed that MT implantation increased the expression level of *Wnt10b* protein in telogen. Therefore, we carefully conclude that hair stromal cells were the first to pick up the signal and proliferate rapidly after MT implantation. At the same time, hair matrix cells release *Wnt10b* into the extracellular matrix and activate the *Wnt10b*/β-*catenin* pathway, which consequently alters the expression level of β-*catenin*. Thus, the β-*catenin* gene can promote the growth of hair follicle stem cells from telogen to anagen (Jones and Jomary, 2002), and the cashmere falls off and is accompanied by secondary cashmere growth.

SUMMARY

The present results demonstrates that MT has beneficial effects on secondary hair follicles throughout the life cycle, and by upregulating the expression of genes related to hair follicle development in cashmere goats, MT regulates the periodic growth of cashmere and induces cashmere to enter the growing period in advance.

Wnt/β-*catenin* signaling plays an important role in the proliferation and differentiation of stem cells by coacting on the growth and development of skin hair follicles. Western blot and PCR results showed that MT preparations increased *Wnt10b* protein expression in the regression period and the resting phase, and prompt examination of β-*catenin* protein in the hair follicle growth period was higher than that in the control group. Therefore, we cautiously conclude that after implantation of MT, hair stromal cells secrete *Wnt10b* into the extracellular matrix to activate the *Wnt10b*/β-*catenin* pathway, thereby changing the expression level of β-*catenin*.

DATA AVAILABILITY STATEMENT

The datasets presented in this study can be found in online repositories. The names of the repository/repositories and accession number(s) can be found below: NCBI (Accession: PRJNA724921, SAMN18865013–SAMN18865021).

ETHICS STATEMENT

The animal study was reviewed and approved by the Ethics Committee of the Inner Mongolia Agricultural University. Written informed consent was obtained from the owners for the participation of their animals in this study.

AUTHOR CONTRIBUTIONS

YW, JiaL, and ZW: conceptualization. WG and ZeL: data curation. FZ, YJZ, and RS: formal analysis. RW, ZhL, and HX: investigation. YHZ: project administration. JinL: resources. JunL and QM: writing – original draft. All authors have read and agreed to the published version of the manuscript.

FUNDING

This research was funded by National Natural Science Foundation of China (31860628, 31860626, and 32060742).

Key Technology Project of the Inner Mongolia Autonomous Region (2020GG0031), Special Fund Project for Landmark Achievements of School of Animal Science of Inner Mongolia Agricultural University ((BZCG202006 and BZCG202106), and Major Science and Technology Projects of Inner Mongolia Autonomous Region (2020ZD0004).

REFERENCES

Basheer, E. A. M., and Abdulbari, H. A. (2018). Visible Light TiO2 Photocatalyst Composite Based on Carbon Microfiber Derived from Human Hair. *ChemistrySelect* 41, 11687–11695. doi: 10.1002/slct.201801161

Cetera, M., Leybova, L., Woo, F. W., Deans, M., and Devenport, D. (2017). Planar cell polarity-dependent and independent functions in the emergence of tissue-scale hair follicle patterns. *Dev. Biol.* 428, 188–203. doi: 10.1016/j.ydbio.2017.06.003

Chen, X., Sun, K., Zhao, S., Geng, T., Fan, X., Sun, S., et al. (2020). Irisin promotes osteogenic differentiation of bone marrow mesenchymal stem cells by activating autophagy via the Wnt//beta-catenin signal pathway. *Cytokine* 136:155292. doi: 10.1016/j.cyto.2020.155292

Duan, C. H., Xu, J. H., and Sun, C. M. (2015). Effects of melatonin implantation on cashmere yield, fibre characteristics, duration of cashmere growth as well as growth and reproductive performance of Inner Mongolian cashmere goats. *J. Anim. Sci. Biotechnol.* 6, 463–468. doi: 10.1186/s40104-015-0023-2

Duan, C. H., Xu, J. H., and Sun, C. M. (2016). Melatonion and cashmere growth in Inner Mongolian cashmere goats. *Can. J. Animal Sci.* 2, 108–113. doi: 10.1139/cjas-2015-0018

Duan, C. H., Xu, J. H., Zhang, Y., Zhang, W., Sun, Y., and Jia, Z. (2017). Effects of melatonin implantation on cashmere growth, hormone concentrations and cashmere yield in cashmere-perennial-type Liaoning cashmere goats. *Anim. Prod. Sci.* 57, 60–64. doi: 10.1071/AN15183

Ge, W., and Wang, S. H. (2018). Melatonin promotes Cashmere goat (Capra hircus) secondary hair follicle growth: a view from integrated analysis of long non-coding and coding RNAs. *Cell Cycle* 17, 1255–1267. doi: 10.1080/15384101.2018.1471318

Han, S. T., Cui, Y., and Helbing, D. L. (2020). Inactivation of Horseradish Peroxidase by Acid for Sequential Chemiluminescent Western Blot. *Biotechnol. J.* 15:e1900397. doi: 10.1002/biot.201900397

Ji, Y. L., Wang, H., and Meng, C. (2012). Melatonin alleviates cadmium-induced cellular stress and germ cell apoptosis in testes. *J. Pineal Res.* 52, 71–79. doi: 10.1111/j.1600-079X.2011.00921.x

Jones, S. E., and Jomary, C. (2002). Secreted Frizzled-related proteins: searching for relationships and patterns. *Bioessays* 24, 811–820. doi: 10.1002/bies.10136

Lanoix, D., Beghdadi, H., and Lafond, J. (2008). Human placental trophoblasts synthesize melatonin and express its receptors. *J. Pineal Res.* 45, 50–60. doi: 10.1111/j.1600-079X.2008.00555.x

Lepage, O., Larson, E. T., and Mayer, I. (2005). Tryptophan affects both gastrointestinal melatonin production and interrenal activity in stressed and nonstressed rainbow trout. *J. Pineal Res.* 38, 264–271.

Li, Y. H., Zhang, K., and Yang, K. (2013). Adenovirus-mediated *wnt10b* overexpression induces hair follicle regeneration. *J. Inves. Dermat.* 1, 42–48. doi: 10.1038/jid.2012.235

Lin, C. M., Yuan, Y. P., and Chen, X. C. (2015). Expression of Wnt/ beta-Catenin signaling,stem-cell markers and proliferating cell markers in rat whisker hair follicles. *J. Mol. Histol.* 46, 233–240. doi: 10.1007/s10735-015-9616-5

Liu, B., Gao, F., Guo, J., Wu, D., Hao, B., Li, Y., et al. (2016). A Microarray-Based Analysis Reveals that a Short Photoperiod Promotes Hair Growth in the Arbas Cashmere Goat. *PLoS One* 11:e0147124. doi: 10.1371/journal.pone.0147124

Mcdonald, B. J., Hoey, W. A., and Hopkins, P. S. (1987). Cyclical fleece growth in cashmere goats. *Aus. J. Agric. Res.* 38, 597–609. doi: 10.1071/AR9870597

Messenger, A. G., and Botchkareva, N. V. (2017). Unraveling the secret life of the hair follicle: from fungi to innovative hair loss therapies. *Exp. Dermatol.* 26:471. doi: 10.1111/exd.13384

Millar, S. E. (2002). Molecular mechanisms regulating hair follicle development. *Invest. Dermatol.* 118, 216–225.

Norton, B. W., and Klören, W. R. L. (1995). Measurement of the components of the cashmere growth cycle in Australian cashmere goats. *Small Ruminan Res.* 17, 263–268. doi: 10.1016/0921-4488(95)00660-d

Ouji, Y., Yoshikawa, M., and Moriya, K. (2007). Effects of Wnt-10b on hair shaft growth in hair follicle cultures. *Biochem. Biophys. Res. Commun.* 359, 516–522. doi: 10.1016/j.bbrc.2007.05.135

Ouji, Y., Yoshikawa, M., and Shiroi, A. (2006). Wnt-10b promotes differentiation of skin epithelial cells in vitro. *Biochem. Biophy. Res. Commun.* 342, 28–35. doi: 10.1016/j.bbrc.2006.01.104

Reiter, R. J., Rosales-Corral, S., and Tan, D. X. (2017). Melatonin as a mitochondria-targeted antioxidant: one of evolution's best ideas. *Cell. Mol. Life Sci.* 74, 3863–3881. doi: 10.1007/s00018-017-2609-7

Salehian, Z., Naderi, N., and Souri, M. (2015). Seasonal variation of fiber follicle activity and wool growth in fattailed Sanjabi sheep in West Iran. *Trop. Anim. Health Prod.* 47, 567–573. doi: 10.1007/s11250-015-0764-0

Schmidt-Ullrich, R., and Paus, R. (2005). Molecular principles of hair follicle induction and morphogenesis. *Bioessays* 27, 247–261. doi: 10.1002/bies.20184

Su, R., Fan, Y., Qiao, X., Li, X., Zhang, L., Li, C., et al. (2018). Transcriptomic analysis reveals critical genes for the hairfollicle of Inner Mongolia cashmere goat from catagen to telogen. *PLoS One* 13:e0204404. doi: 10.1371/journal.pone.0204404

Tamura, H., Kawamoto, M., and Sato, S. (2017). Long-term melatonin treatment delays ovarian aging. *J. Pineal Res.* 62:e12381. doi: 10.1111/jpi.12381

Tan, D., Manchester, L. C., and Reiter, R. J. (1999). Identification of highly elevated levels of melatonin in bone marrow: its origin and significance. *Biochim. Biophys. Acta* 1472, 206–214. doi: 10.1016/S0304-4165(99)00125-7

Trapnell, C., Williams, B. A., Pertea, G., Mortazavi, A., Kwan, G., van Baren, M. J., et al. (2010). Transcript assembly and quantification by RNA-Seq reveals unannotated transcripts and isoform switching during cell differentiation. *Nat. Biotechnol.* 28, 511–551. doi: 10.1038/nbt.1621

Watabe, R., Yamaguchi, T., Kabashima-Kubo, R., Yoshioka, M., and Nishio, D. (2014). Leptin controls hair follicle cycling. *Exp. Dermatol.* 23, 228–229. doi: 10.1111/exd.12335

Watkins, P., and Buxton, A. (1992). *Luxury, Fibres: Rare Materials for Higher Added Value. Special Report*. London: Economist Intelligence Unit.

Wu, P., and Zhang, Y. M., Xing, Y., Xu, W., Guo, H., Deng, F., et al. (2020). The balance of Bmp6 and Wnt10b regulates the telogen-anagen transition of hair follicles. *Cell Commun Signal.* 18: 4. doi: 10.1186/s12964-020-0508-2

Wu, Z. Y., Zhu, Y. L. Liu, H., Liu, G.,and Li, F. (2020). Wnt10b promotes hair follicles growth and dermal papilla cells proliferation via Wnt/beta-Catenin signaling pathway in Rex rabbits. *Biosci. Rep.* 40:BSR20191248. doi: 10.1042/BSR20191248

Wuliji, T., Litherland, A., and Goetsch, A. L. (2006). Evaluation of melatonin and bromocryptine administration in Spanish goats. *Small Rumin. Res.* 66, 11–21. doi: 10.1016/j.smallrumres.2005.04.024

Yang, C. H. (2020). Effect of melatonin administration to lactating cashmere goats on milk production of dams and on hair follicle development in their offspring. *Animal* 14:6. doi: 10.1017/S1751731119002726

Yang, C. H., Duan, C. H., Wu, Z. Y., Li, Y., Luan, Y. Y., Fu, X. J.,et al. (2020). Effects of melatonin administration to cashmere goats on cashmere production and hair follicle characteristics in two consecutive cashmere growth cycles. *Domest. Anim. Endocrinol.* 74:106534. doi: 10.1016/j.domaniend.2020.106534

Yang, X. Z. (2020). Effects of dietary melatonin on hematological immunity, antioxidant defense and antibacterial ability in the Chinese mitten crab, Eriocheir sinensis. *Aquaculture* 529:735578. doi: 10.1016/j.aquaculture.2020.735578

Zawilska, J. B., Jarmak, A., Woldan-Tambor, A., and Nowak, J. Z. (1995). Light-induced suppression of nocturnal serotonin N-acetyltransferase activity in chick pineal gland and retina: a wavelength comparison. *J. Pineal Res.* 19, 87–92. doi: 10.1111/j.1600-079X.1995.tb00175.x

Zhang, Y. J. (2020). Comparative study on seasonal hair follicle cycling by analysis of the transcriptomes from cashmere and milk goats. *Genomics* 112, 332–345. doi: 10.1016/j.ygeno.2019.02.013

Zhang, Y. J., Wu, K. J., Wang, L. L., Wang, Z., Han, W., Chen, D., et al. (2020). Comparative study on seasonal hair follicle cycling by analysis of the transcriptomes from cashmere and milk goats. *Genomics* 112, 332–345.

Zhu, B., Xu, T., Yuan, J., Guo, X., and Liu, D. (2013). Transcriptome sequencing reveals differences between primary and secondary hair follicle-derived dermal papilla cells of the cashmere goat (Capra hircus). *PLoS One* 8:e76282. doi: 10.1371/journal.pone.0076282

Conflict of Interest: The authors declare that the research was conducted in the absence of any commercial or financial relationships that could be construed as a potential conflict of interest.

frontiers in Genetics

ORIGINAL RESEARCH
published: 29 July 2021
doi: 10.3389/fgene.2021.662143

Whole-Transcriptome Analysis of Preadipocyte and Adipocyte and Construction of Regulatory Networks to Investigate Lipid Metabolism in Sheep

Cheng Xiao[1†], Tian Wei[1†], Li Xiang Liu[1,2], Jian Qiang Liu[1], Chun Xin Wang[1], Zhi Yu Yuan[1], Hui Hai Ma[1], Hai Guo Jin[1], Li Chun Zhang[1] and Yang Cao[1]**

[1] Jilin Academy of Agricultural Sciences, Gongzhuling, China, [2] College of Animal Science and Technology, Jilin Agricultural University, Changchun, China

OPEN ACCESS

Edited by:
Rui Su,
Inner Mongolia Agricultural University, China

Reviewed by:
Bao Yuan,
Jilin University, China
Chuzhao Lei,
Northwest A&F University, China
Mohammad Reza Bakhtiarizadeh,
University of Tehran, Iran
Rajwali Khan,
University of Agriculture, Peshawar, Pakistan

***Correspondence:**
Li Chun Zhang
280774981@qq.com
Yang Cao
caoyang003@163.com

[†] These authors have contributed equally to this work

Specialty section:
This article was submitted to Livestock Genomics, a section of the journal Frontiers in Genetics

Received: 31 January 2021
Accepted: 09 June 2021
Published: 29 July 2021

Citation:
Xiao C, Wei T, Liu LX, Liu JQ, Wang CX, Yuan ZY, Ma HH, Jin HG, Zhang LC and Cao Y (2021) Whole-Transcriptome Analysis of Preadipocyte and Adipocyte and Construction of Regulatory Networks to Investigate Lipid Metabolism in Sheep. Front. Genet. 12:662143. doi: 10.3389/fgene.2021.662143

Many local sheep breeds in China have poor meat quality. Increasing intramuscular fat (IMF) content can significantly improve the quality of mutton. However, the molecular mechanisms of intramuscular adipocyte formation and differentiation remain unclear. This study compared differences between preadipocytes and mature adipocytes by whole-transcriptome sequencing and constructed systematically regulatory networks according to the relationship predicted among the differentially expressed RNAs (DERs). Sequencing results showed that in this process, there were 1,196, 754, 100, and 17 differentially expressed messenger RNAs (mRNAs), long non-coding RNAs (lncRNAs), microRNAs (miRNAs), and circular RNAs (circRNAs), respectively. Gene Ontology analysis showed that most DERs enriched in Cell Part, Cellular Process, Biological Regulation, and Binding terms. Kyoto Encyclopedia of Genes and Genomes (KEGG) analysis found that the DERs primarily focused on Focal adhesion, phosphoinositide 3-kinase (PI3K)-Akt, mitogen-activated protein kinase (MAPK), peroxisome proliferator-activated receptor (PPAR) signaling pathways. Forty (40) DERs were randomly selected from the core regulatory network to verify the accuracy of the sequence data. The results of qPCR showed that the DER expression trend was consistent with sequence data. Four novel promising candidate miRNAs (miR-336, miR-422, miR-578, and miR-722) played crucial roles in adipocyte differentiation, and they also participated in multiple and important regulatory networks. We verified the expression pattern of the miRNAs and related pathways' members at five time points in the adipocyte differentiation process (0, 2, 4, 6, 8, 10 days) by qPCR, including miR-336/ACSL4/LncRNA-MSTRG71379/circRNA0002331, miR-422/FOXO4/LncRNA-MSTRG54995/circRNA0000520, miR-578/IGF1/LncRNA-MSTRG102235/circRNA0002971, and miR-722/PDK4/LncRNA-MSTRG107440/circRNA0002909. In this study, our data provided plenty of valuable candidate DERs and regulatory networks for researching the molecular mechanisms of sheep adipocyte differentiation and will assist studies in improving the IMF.

Keywords: whole-transcriptome analysis, adipocyte differentiation, preadipocyte, mature adipocyte, differentially expressed RNAs, regulatory networks, sheep

INTRODUCTION

Small Tail Han sheep, a Chinese endemic breed, possesses high fecundity and strong resistance (Miao et al., 2016). Farmers and breeding enterprises widely raise Small Tail Han sheep to provide for the local consumers in Northeast China. Unfortunately, Small Tail Han sheep can no longer adapt to the current market because it has a slow growth rate and low meat quality (Kashan et al., 2005). Therefore, it is urgent to improve the quality of mutton. Intramuscular fat (IMF) content is closely related to meat quality traits and affects the taste and tenderness of mutton, changes the nutritional composition, and directly affects consumers' purchasing decisions (Zhao et al., 2015). Therefore, increasing the content of IMF is the key to improving meat quality. Many factors affect the accumulation of IMF content including nutrition (Scollan et al., 2017), environment (Lambe et al., 2021), animal breed (Martins et al., 2020), age (Rahemi et al., 2015), gender (Gálvez et al., 2018), and genetic factors (Park et al., 2018). Although excessive caloric intake without a rise in energy expenditure increases IMF (Tang and Lane, 2012), different individuals possess the diverse ability to increase IMF in the same diet condition. The accumulation of IMF is the result of *de novo* lipogenesis and adipocyte differentiation, so when increasing IMF, we need to explore the mechanism of adipocyte differentiation.

Intramuscular adipose contains a high percentage of mature adipocytes, some preadipocytes, and a few other cells (Géloën et al., 1989). Adipocyte differentiation is a process that the preadipocyte differentiates into the mature adipocyte. The regulatory mechanisms of adipocyte differentiation are complex, and many genes (Ntambi and Young-Cheul, 2000), transcription factors (Liu et al., 2020), proteins (Gregoire et al., 1998), and hormones are involved (Obregon, 2008). Genetic factors can affect the accumulation of IMF by regulating *de novo* lipogenesis and adipocyte differentiation (Koutnikova and Auwerx, 2001). Recently, non-coding RNAs that contain long non-coding RNA (lncRNA), circular RNA (circRNA), and microRNA (miRNA) may play a core role in lipid metabolism and adipocyte differentiation (Zeng et al., 2018). LncRNA has more tissue specificity, binds to target genes by cis or trans methods (Tafer and Hofacker, 2008), and develops into pre-miRNA (Friedlander et al., 2012). LncRNA participates in various physiological functions, such as dose compensation effect, epigenetic regulation, cell cycle, and differentiation regulation (Xiao et al., 2015; Xiong et al., 2018). Some studies have reported that lncRNA plays a core role in adipocyte differentiation (Lopez-Pajares, 2016). circRNA, covalently closed by 3-terminal and 5-terminal RNAs, is more stable and conserved than other RNAs (Jeck and Sharpless, 2014). A part of circRNAs can transcribe as the protein; other positions are in intron sequences of the cell nucleus (Li Z. et al., 2015). circRNA may become potential biological markers involved in adipocyte differentiation (Yu et al., 2021). miRNA is a crucial regulatory molecule and can bind to the untranslated region (UTR) of messenger RNAs (mRNAs) to regulate their expression (Ali et al., 2020). miRNA participates in many biological functions, such as cellular growth and differentiation (Lu and Rothenberg, 2018). Many reports have identified that miRNA acts as a vital factor affecting adipocyte differentiation (Shi et al., 2016). Compete endogenous RNA (ceRNA) is a common physiological mechanism that lncRNA and circRNA competitively combine with miRNA (Thomson and Dinger, 2016). circRNA acts as a sponge to absorb miRNA competing with other RNAs (Memczak et al., 2013). Some studies have proven that ceRNA widely exists in adipocyte differentiation and forms the crucial regulatory networks (Xu et al., 2015; Chen et al., 2018). Although many studies related to adipocyte differentiation were published, the detailed molecular mechanism remains unclear, especially non-coding RNA and ceRNA in sheep.

To explore the molecular mechanisms and identify the candidate RNAs in sheep adipocyte differentiation, we compared the changes between preadipocytes and mature adipocytes by whole-transcriptome analysis. Our data provided many novel candidate RNAs, ceRNA networks, and, at the same time, research directions and theoretical basis for related research. This work is meaningful for excavating the molecular mechanism of sheep adipocyte differentiation and increasing IMF.

MATERIALS AND METHODS

Preadipocyte Isolation, Culture, and Differentiation

The Small-Tailed Han sheep was raised as experimental animals in the Jilin Academy of Agricultural Sciences. A 2-month-old healthy male sheep's groin adipose tissue was isolated to extract the preadipocytes. The tissue was washed with ice-cold phosphate-buffered saline (PBS; Sigma-Aldrich, St. Louis, MO, United States) containing 1% penicillin/streptomycin (Sigma) and cut into small pieces, then the tissue blocks were digested for 1 h using collagenase Type II (Sigma) and 0.25% trypsin (Sigma) to collect preadipocytes. The cells were cultured with a complete culture medium containing 10% fetal bovine serum (Gemini Bio-Products, Woodland, CA, United States), 1% penicillin/streptomycin (Sigma), and DMEM-F12 medium (Sigma) in a 37°C and 5% CO_2 incubator (Thermo Fisher Scientific, Waltham, MA, United States) and replaced with new culture medium every 48 h. When the cells are overgrown in the culture dish, they are induced to differentiate into mature adipocytes by the exogenous inducer. The cells were treated with inducer I solution containing 10 mg/ml insulin (Sigma), 1.0 mM dexamethasone (Sigma), 0.5 mM IBMX (Sigma), and complete culture medium for 48 h, inducer II solution containing 10 mg/ml insulin (Sigma) and complete culture medium for 48 h, and then fresh complete culture medium to continue cell culture. The whole process of cell differentiation underwent about 12 days.

Oil Red O Staining

Oil red O staining solution can identify adipocytes because the lipid droplets within the cell can be stained red, but other cells cannot. Oil red O staining occurs on the 12th day when the cells are growing, which is the eighth day when the cells start to differentiate. The adipocytes were washed with PBS buffer three times and fixed with 4% paraformaldehyde solution (Sangon

Biotech Co., Ltd., Shanghai, China) in a 37°C and 5% CO_2 incubator for 30 min. The cells were washed with PBS buffer three times, then cells were treated with Oil red O (Sigma) for 30 min in the incubator. After this, the cells were washed with PBS buffer three times, the staining was observed with a microscope, and pictures were taken.

RNA Extraction and Qualification

The fourth-generation preadipocytes possess fast and stable growth and can be used as experimental cells based on previous experimental experience. Some preadipocytes are regarded as group P, and the remaining cells differentiate into adipocytes as group M. Each group has three repetitions (technical repetition); they are P1, P2, P3 and M1, M2, M3. The cells' total RNA was extracted using TRIzol reagent (Thermo Fisher Scientific, Waltham, MA, United States) according to the instructions, then RNA degradation and contamination were monitored using 1% agarose gels. NanoPhotometer spectrophotometer (IMPLEN, CA, United States) assesses the purity of RNA. Qubit RNA Assay Kit in a Qubit 2.0 Fluorometer (Life Technologies, CA, United States) measured the concentration of RNA. Nano 6000 Assay Kit in a Bioanalyzer 2100 system (Agilent Technologies, CA, United States) evaluated the integrity of RNA (Ma et al., 2019).

Library Preparation

Here, 3 μg total RNA of each sample was used to construct the lncRNA library. The total RNA was digested by DNase I, and ribosomal RNA (rRNA) was removed using Ribo-Zero™ Gold Kit (Illumina, San Diego, United States); at this time, the lncRNA library contains mRNA. Since mRNA contains a specific Poly-A tail, oligo(dT) magnetic beads can specifically bind to the Poly-A tail to separate mRNA. Fragmentation Buffer was added to the reaction system to fragment RNA into short fragments (about 200–500 nt), and then the fragments were used as templates to synthesize the first strand of cDNA with six-base random hexamer primers, and then buffer, dNTPs, RNase H, and DNA Polymerase I were used to synthesize the second strand of cDNA. QiaQuick PCR kit purified cDNA and EB buffer resolved end reparation and single nucleotide A (adenine) addition and adaptor. The target fragment is recovered by agarose gel electrophoresis, the uracil-N-glycosylase (UNG) enzyme degraded the second strand of cDNA, and the suitable fragments were selected as templates for PCR amplification. Finally, agarose gel electrophoresis recovers the target fragments to construct the library. To construct a circRNA library, it is necessary to add an RNase enzyme to remove linear RNA after rRNA is removed, so that circRNA can be obtained. After the RNA of the sample is qualified, the Small RNA Sample Pre Kit constructs the miRNA library; small RNA sequence length is small and has a special structure at the 3′ and 5′ ends (the 5′ end has a complete phosphate group, and the 3′ end has a hydroxyl group). The small RNA is directly connected to both ends with an adaptor, and then reverse transcription is used to synthesize cDNA. Then, after PCR amplification, polyacrylamide gel electrophoresis (PAGE) was performed to separate the target DNA fragments; the cDNA library is recovered by cutting the gel. The constructed library was sequenced using an Illumina system (Agilent Technologies Inc.) by Annoroad Gene Technology Co., Ltd. (Beijing, China).

Raw Data Processing

The original results of Illumina high-throughput sequencing are image data files, which are converted into Raw Reads after Base Calling by bcl2fastq2 software, and the results are stored in the FASTQ (referred to as fq) file format. In the FASTQ format file, each base corresponds to a base quality character, and the ASCII code value corresponding to each base quality character minus 33 (Sanger quality value system) is the sequencing quality score of the base (Phred Quality Score). Different Phred Quality Scores represent different base sequencing error rates. For example, Phred Quality Score values of 20 and 30 indicate base sequencing error rates of 1 and 0.1%, respectively. Raw data contain sequencing adapter sequences and low-quality sequences. To ensure the quality of the information analysis data, we filter raw data sequences and use Cutadapt and fastx_toolkit to remove the adaptor, low-quality reads, reads with an N content greater than 5%, and reads that match ribosomal RNA.

Comparison Analysis and Mapped Reads Assembly

To better identify lncRNAs and mRNAs, clean RNA sequencing (RNA-Seq) reads were mapped to the genome using Hisat2. To identify circRNAs, clean RNA-Seq reads were mapped to the genome using the BWA-MEM algorithm. BWA-MEM can quickly and efficiently compare reads with the genome. For the accuracy of subsequent miRNA analysis, clean miRNA-Seq reads were mapped to the genome using Bowtie software (setting allows one mismatch). The reference genome and gene annotation files were downloaded from the NCBI database. Version: Ovis_aries.NCBI.GCF_002742125.1.v1.0. GCF_002742125.1_Oar_rambouillet_v1.0_genomic. gff.gz. StringTie can quickly assemble transcripts using RNA-Seq alignment results. Reads were divided into different categories, and built splice graph to determine the transcript. Each transcript build flow network for path of heaviest coverage to compute maximum flow to evaluate abundance, and combine the complex data set assemble into a transcript.

Long Non-coding RNA Identification

We mainly screen for three types: long intergenic non-coding RNA (lincRNA), intronic lncRNA, and antisense lncRNA. The basic screening conditions are as follows: (1) The length of the transcript is greater than or equal to 200 bp, and the number of exons is greater than or equal to 2; (2) Calculating the read coverage of each transcript, and transcripts with less than five reads in all samples were removed; (3) gffcompare[1] compares the annotation files of the species to screen out the known mRNA and other non-coding RNA (rRNA, tRNA, snoRNA, snRNA, etc.); (4) Identifying potential lincRNA, intronic lncRNA, and antisense lncRNA according to the class_code information ("u,"

[1] http://ccb.jhu.edu/software/stringtie/gff.shtml

"i," "x") in the comparison result. Through the initial screening of lncRNA in the previous step, a variety of coding potential analysis software is used to screen, mainly Coding-Non-Coding Index (CNCI), Coding Potential Calculator (CPC), Coding Potential Assessment Tool (CPAT for animals only), and PFAM protein domain analysis. Several analysis methods all distinguish the non-coding transcript as the final novel lncRNA data set.

Circular RNA Identification

The current research mainly is on exonic circular RNA (ecircRNA) and the cyclization mechanism: (1) lariat-driven circularization (2) intron pairing-driven circularization. The difference between the two models is whether the first step of cyclization is to form a lariat-driven structure or the introns on both sides of the exon are complementarily paired first. No matter which form it is, it is formed by trans-splicing the splice donor (SD) of the downstream exon of the circRNA and the splice acceptor (SA) of the upstream exon. The main idea of recognizing circRNA: looking for the GT-AG signal next to the junction site. CIRI (Gao et al., 2015) is an efficient and fast circRNA identification tool. BWA-MEM algorithm is used to split and compare the sequences, and then the resulting SAM file is scanned to find paired chiastic clipping (PCC) and paired-end mapping (PEM) sites, as well as GT-AG splicing signals. The sequence with junction site was realigned with a dynamic programming algorithm to ensure the reliability of identifying circRNA.

miRNA Identification

According to the mapped reads, it is compared with the specified species sequence in the miRBase database to identify known miRNAs. Clean Reads that are not annotated as known miRNAs are compared with the non-coding RNA sequence in Rfam (13.0) to realize the annotation of rRNA, tRNA, snRNA, snoRNA, and other non-coding RNAs. For Clean Reads that are not annotated as known miRNA, non-coding RNA, and Repeat, the small RNA derived from mRNA is annotated by matching with the location information of gene exons and introns (100% position overlap). There are still some features of miRNAs, but no sequences have been discovered so far, so novel miRNA predictive analysis is needed. The software miRDeep2 is used to predict novel miRNAs, obtain the matched Clean Reads information of each novel miRNA, and obtain the structure and expression information of each novel miRNA.

Analysis of Differentially Expressed RNAs

The expression levels of the protein-coding genes and lncRNAs were estimated by FPKM (Fragments Per Kilobase of transcript per Million mapped reads), which is a very effective tool for quantitatively estimating gene expression and can eliminate the influence of the difference in gene length and sequencing amount on the calculated gene expression, and the results can be directly used to compare the expressed difference between different samples. Due to the particularity of circRNA, it is difficult to accurately obtain the information of circRNA Reads on all alignments (linear RNA interference), so the usual expression estimation method is to use the number of Junction reads to estimate the expression of circRNA. We selected SRPBM (Spliced Reads per Billion Mapping) (Li Y. et al., 2015) normalization method to quantify the expression of circRNA. TPM (Transcripts Per Million) is used to estimate the expression level of miRNA, which is calculated based on the reads (incompletely mature or degraded) that are aligned to the miRNA precursor and slide in a certain area of the mature body. We selected DEseq2 to analyze the differential expression of RNAs, comparing the treatment group and the reference group. $|\log2\text{Ratio}| \geq 1$ and $p < 0.05$ were set as the threshold in the differential expression analysis.

Target RNA Prediction

LncRNA binds to target genes in Cis or Trans mode. Cis binding method prediction: the protein-coding genes adjacent to lncRNA (upstream and downstream 50 kb) will be screened out as target genes. Trans combination method prediction: when the number of samples is greater than or equal to 6, the target gene is screened according to the correlation coefficient between the expression of lncRNA and mRNA (correlation coefficient ≥ 0.9). The forecasting software is implemented using Annoroad's in-house scripts. There are multiple binding sites of miRNA on the circRNA sequence. When miRNA is adsorbed, it cannot regulate its corresponding target gene, thus acting as a sponge of miRNA molecules, and then we selected miRanda (3.3a) (Enright et al., 2003) for target prediction. MiRanda (Enright et al., 2003) and TargetScan (Agarwal et al., 2015), two target prediction software, were selected to predict miRNA target genes, and the intersection of the two target prediction results is taken as miRNA target genes.

Gene Ontology and Kyoto Encyclopedia of Genes and Genomes Pathway Analysis

GOseq R package (ver. 2.12) conducted Gene Ontology (GO) analysis according to the following rules: differentially expressed genes (DEGs), differentially expressed circular RNA (DEcircRNA)-deriving genes, target genes of differentially expressed long non-coding RNAs (DElncRNAs), and differentially expressed miRNAs (DEmiRNAs). GO analysis was used to annotate the genes with terms under biological process, cellular component, and molecular function categories. KOBAS software (2.0) conducted Kyoto Encyclopedia of Genes and Genomes (KEGG) pathways analysis according to the same rules. GO and KEGG terms featuring $p < 0.05$ were considered significantly enriched.

Regulatory Network Construction

According to the prediction results of target RNAs, we systematically constructed various regulatory networks of the differentially expressed RNAs (DERs) related to sheep adipocyte differentiation. The two-element network was based on the following relationships: target mRNA of lncRNA, target mRNA of miRNA, lncRNA can become miRNA, circRNA adsorbs miRNA.

Then, we constructed ceRNA networks, including the three-element network and four-element network based on various RNAs that can competitively bind the same miRNA response elements (MREs). Cytoscape 3.6.1 visualized the networks.

Quantitative Real-Time PCR Validation

We randomly selected 40 DERs from the regulatory networks to identify the accuracy of sequencing results using qPCR and also explored the expression trend of the RNAs at five time points during the preadipocyte to mature adipocyte period (2, 4, 6, 8, 10 days). The glyceraldehyde-3-phosphate dehydrogenase gene (*Gapdh*) and U6 were internal controls. The total RNA transcribed into the cDNA using a reverse transcription kit (TaKaRa, Japan) as qPCR template, and the glyceraldehyde-3-phosphate dehydrogenase gene (Gapdh) and U6 were internal controls for qPCR. The primer sequences were synthesized by Genewiz Company as **Supplementary Tables 1–4**. qPCR was performed on LightCycler Roche 480 (Roche) with SuperMix Real PreMix Plus (SYBR green) (Roche). The delta-delta CT method calculated the relative expression level of RNAs.

Statistical Analysis

The sequencing data of samples were compared according to the following three groups: M1 vs. P1, M2 vs. P2, and M3 vs. P3. The commonly owned data among the three groups were the final results of the adipocyte differentiation process. R software calculated parameters for the high-throughput sequencing-related data and differential expression analyses. All data representation using means ± SD and a p-value threshold of 0.05 was to infer statistically significant expression changes.

RESULTS

Adipocyte Culture and Differentiation

Adipocytes' differentiation process mainly undergoes two stages: proliferation and differentiation. As shown in **Figure 1**, the non-adherent preadipocytes are spherical with a diameter of 10–30 μm. The cells begin to adhere to the wall and become irregular fusiform after 6 h. When the cells are overgrown in the culture dish, the exogenous inducer promotes the differentiation of the cells into mature adipocytes. Under the microscope, it can be seen that there are lipid droplets inside the cells, and the lipid droplets can be stained by Oil Red O, which indicates that the cells are successfully differentiated.

Overview of RNA Sequencing

As shown in **Table 1**, the quality of the sequencing data is high, the proportion of high-quality clean reads exceeds 95%, and the average percentage of Q30 is above 93%. The clean reads mapping rates of lncRNA and mRNA were more than 93%. We obtained 18,968 RNA transcripts, of which 1,713 known and 5,640 novel lncRNAs were in the P1 group, 1,705 known and 5,640 novel lncRNAs were in the P2 group, 1,680 known and 5,637 novel lncRNAs were in the P3 group, 1,569 known and 5,548 novel lncRNAs were in the M1 group, 1,611 known and 5,537 novel lncRNAs were in the M2 group, and 1,666 known and 5,602 novel lncRNAs were in the M3 group. The mapping rates of circRNA surpass 99% (**Table 1**). We identified 3,480 circRNAs, of which the CLASSIC circRNAs account for more than 80%. The mapping rates of miRNA exceed 97% (**Table 2**). We identified 150 known and 326 novel miRNAs in the P1 group, 150 known and 378 novel miRNAs in the P2 group, 150 known and 375 novel miRNAs in the P3 group, 151 known and 372 novel miRNAs in the M1 group, 149 known and 361 novel miRNAs in the M2 group, and 150 known and 342 novel miRNAs in the M3 group.

Analysis of Differentially Expressed RNAs

Using $|\log2\text{Ratio}| \geq 1$ and $p < 0.05$ as the criteria for screening DERs, the volcano chart shows the number of DERs in each group (**Supplementary Figure 1**). R language draws a cluster map to reflect the expression changes of DERs under different conditions (**Supplementary Figure 2**). DERs of each group are different, and we use the three groups of shared DERs as the final data. **Figure 2** showed that we identified 1,196 DEGs, of which 711 genes were upregulated, and 485 were downregulated. There were 754 DElncRNAs in the process, of which 529 lncRNAs were upregulated, and 225 lncRNAs were downregulated. There were 17 DEcircRNAs in the process, of which 9 circRNAs were upregulated, and 8 circRNAs were downregulated. In addition, 100 DEmiRNAs dysregulated, 46 miRNAs were upregulated, and 54 miRNAs were downregulated between the P and M groups. The DERs' detailed information is in **Supplementary Tables 5–8**.

Gene Ontology and Kyoto Encyclopedia of Genes and Genomes Pathway Analysis

GO analysis showed that the DERs were mainly involved in the cell part of the cellular component classification. Many DERs belonged to cellular processes and biological regulation on the physiological process classification. The molecular function assessment showed that the DERs associated with binding (**Supplementary Figure 3**). KEGG pathway analysis found that DEGs mainly enriched in the Focal adhesion, Axon guidance, and phosphoinositide 3-kinase (PI3K)-Akt signaling pathway. Peroxisome proliferator-activated receptor (PPAR), adipocytokine, and mitogen-activated protein kinase (MAPK) signaling pathways were also significantly enriched, but there was no significant enrichment in Fatty acid biosynthesis, Insulin signaling pathway, fat digestion and absorption, and fatty acid metabolism. The top three lncRNAs were MAPK signaling pathway, endocytosis, and pathways in cancer. Insulin and adipocytokine signaling pathway and fatty acid metabolism enriched significantly, but there was no significant enrichment in fat digestion and absorption, fatty acid biosynthesis, and PPAR signaling pathways. Most circRNAs focused on focal adhesion, FoxO signaling pathway, longevity regulating pathway-worm, axon guidance, and PI3K–Akt signaling pathways. A large number of miRNAs were involved in focal adhesion and PPAR signaling pathways (**Supplementary Figure 4**).

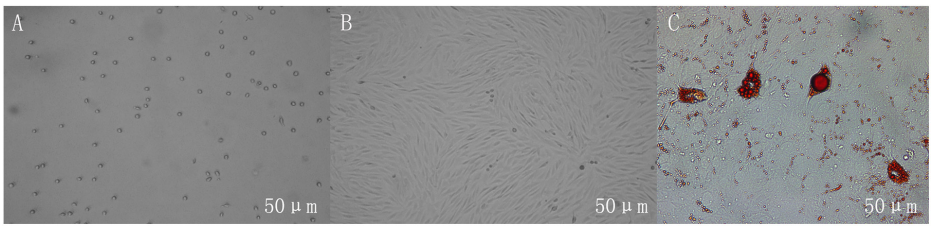

FIGURE 1 | Growth morphology of adipocytes in different periods. **(A)** Non-adherent cells are spherical. **(B)** The adherent cells are irregularly shaped, and the cells are photographed on the fourth day of culture. **(C)** The lipid droplets in differentiated adipocytes can be stained red by Oil Red O, and the cells are photographed on the 12th day of culture. Scales bar: 50 μm.

TABLE 1 | Alignment and quantification statistics in each sample RNA-Seq library.

Sample	P1	P2	P3	M1	M2	M3
Raw reads	70,089,738	70,608,836	89,908,418	83,662,284	84,682,784	83,821,350
Clean reads	67,227,174	67,721,360	86,430,498	80,025,662	81,211,530	80,248,416
Clean Reads rate (%)	95.92	95.91	96.13	95.65	95.9	95.74
Clean Q30 rate (%)	93.39	93.42	94.14	94.37	93.99	94.36
LncRNA and mRNA mapping rate (%)	95.89	96	96.15	93.32	95.86	96.16
circRNA mapping rate (%)	99.99	1	1	99.97	1	1

circRNA, circular RNA; lncRNA, long non-coding RNA; mRNA, messenger RNA; RNA-Seq, RNA sequencing.

TABLE 2 | Alignment and quantification statistics in each sample miRNA library.

Sample	P1	P2	P3	M1	M2	M3
Total reads	22,413,923	18,892,622	18,752,504	24,882,694	25,413,485	20,585,959
Perfect match reads	18,543,399	15,886,883	15,820,075	21,054,917	21,678,813	17,451,683
Match rate (%)	97.45	97.72	97.86	97.76	97.99	97.8
Not match rate (%)	2.55	2.28	2.14	2.24	2.01	2.2

Construction of Regulatory Networks

Two-Element Network

A lncRNA combines with multiple target genes, at the same time, a gene can also be targeted by multiple lncRNAs in the lncRNA–mRNA networks. There were 729 DElncRNAs and 1,844 DE target genes in the three groups. There were 46 DElncRNAs and 24 target miRNAs in the lncRNA–miRNA networks. The lncRNA–mRNA and lncRNA–miRNA regulatory networks were too complex and huge, so the networks were shown clearly in a chart on the manuscript. Detailed information is shown in **Supplementary Tables 9, 10**. **Figures 3A,B** showed circRNA–miRNA and miRNA–mRNA regulatory networks. Detailed information is shown in **Supplementary Tables 11, 12**.

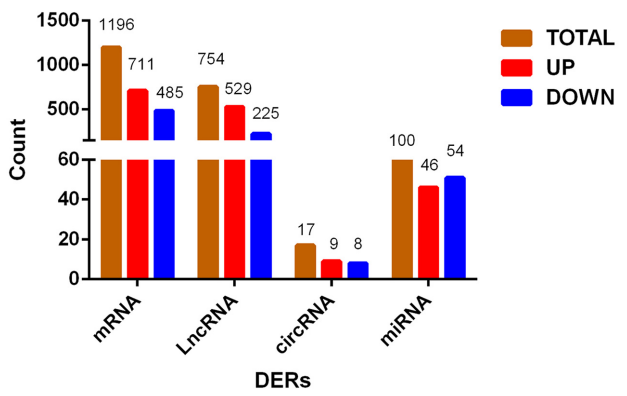

FIGURE 2 | Histogram of differentially expressed RNA shared by three groups. From preadipocytes to mature adipocytes, brown column is the number of total differentially expressed RNAs, red column is RNAs with increased expression, and blue column is RNAs with decreased expression.

Three-Element Network

As shown in **Figure 3C**, 13 novel miRNAs play a central role in the mRNA–miRNA–lncRNA networks. Detailed information is shown in **Supplementary Table 13**. In miRNA–mRNA–circRNA networks, we did not find shared networks in the three groups, but there are shared networks in M1 vs. P1 and M2 vs. P2, and there are other shared networks in M2 vs. P2 and M3 vs. P3. There are six novel miRNAs (miR-336, miR-422, miR-578, miR-722, miR-748, and miR-831) that may play a core role in the regulatory networks (**Figures 3D,E**). Detailed information is shown in **Supplementary Table 14**.

Four-Element Network

In miRNA–mRNA–circRNA–lncRNA networks, we did not find shared networks in the three groups, but there are shared networks in M1 vs. P1 and M2 vs. P2, and there are other shared networks in M2 vs. P2 and M3 vs. P3 (**Figures 3F,G**). Interestingly, six novel miRNAs

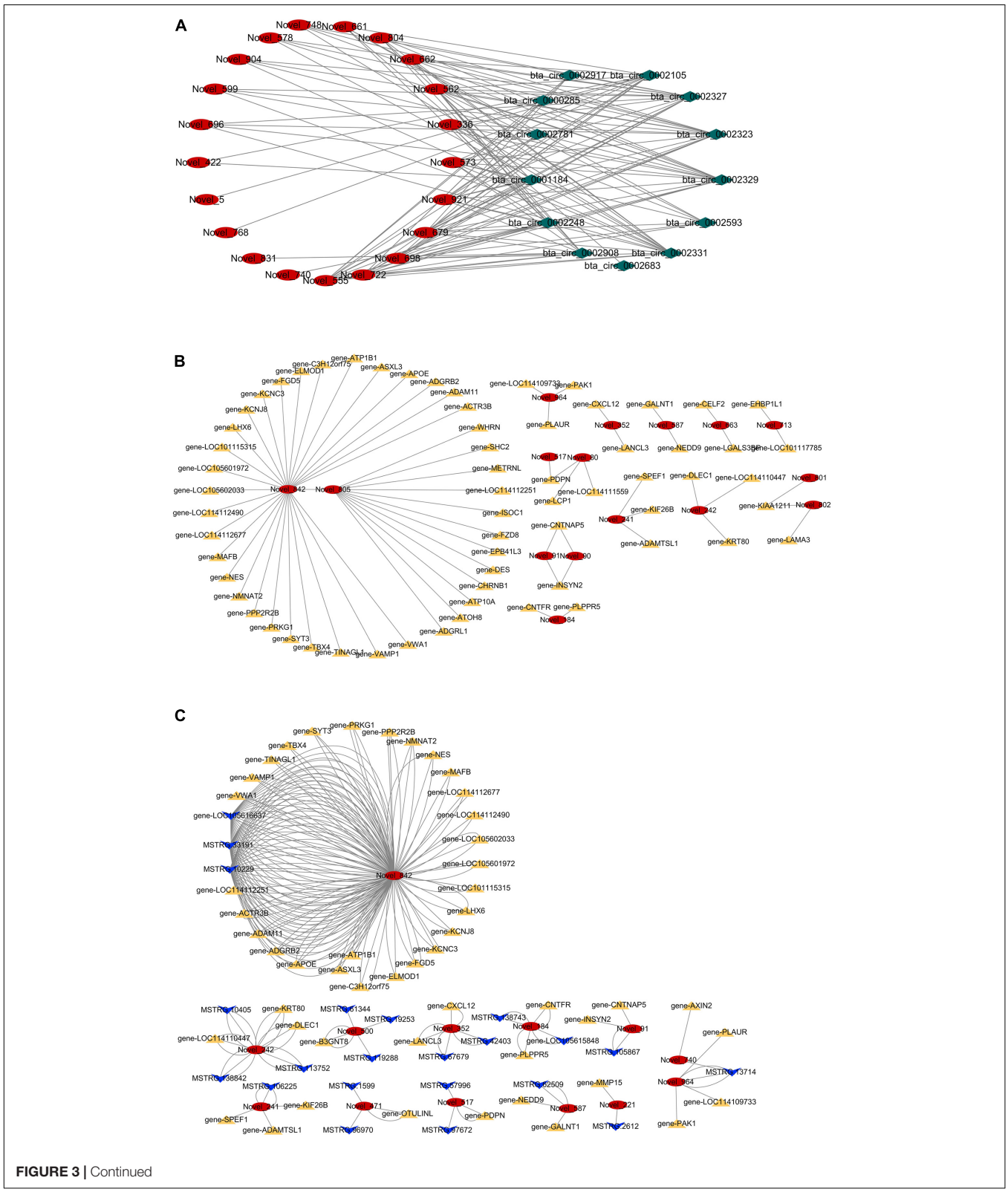

FIGURE 3 | Continued

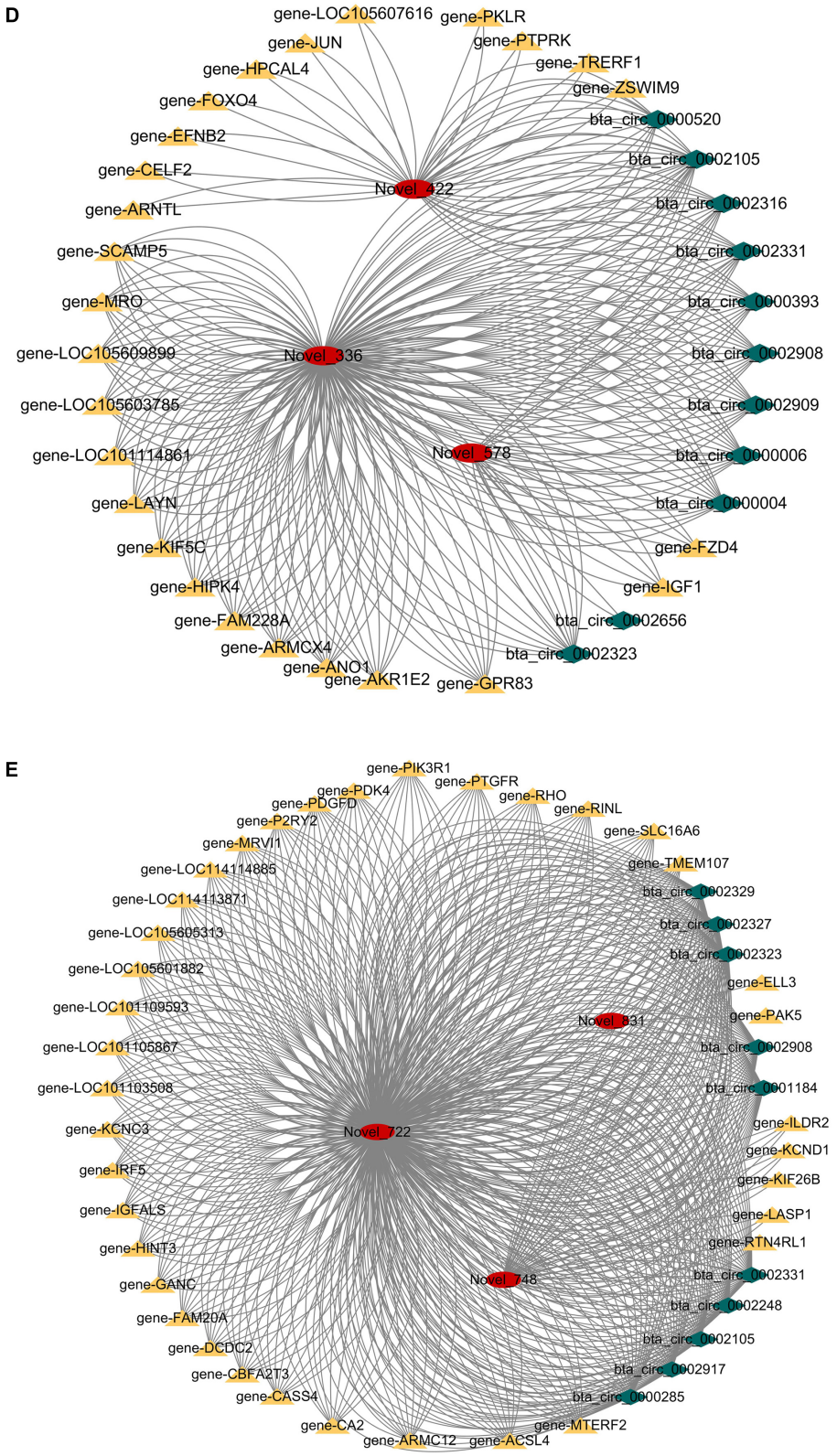

FIGURE 3 | Continued

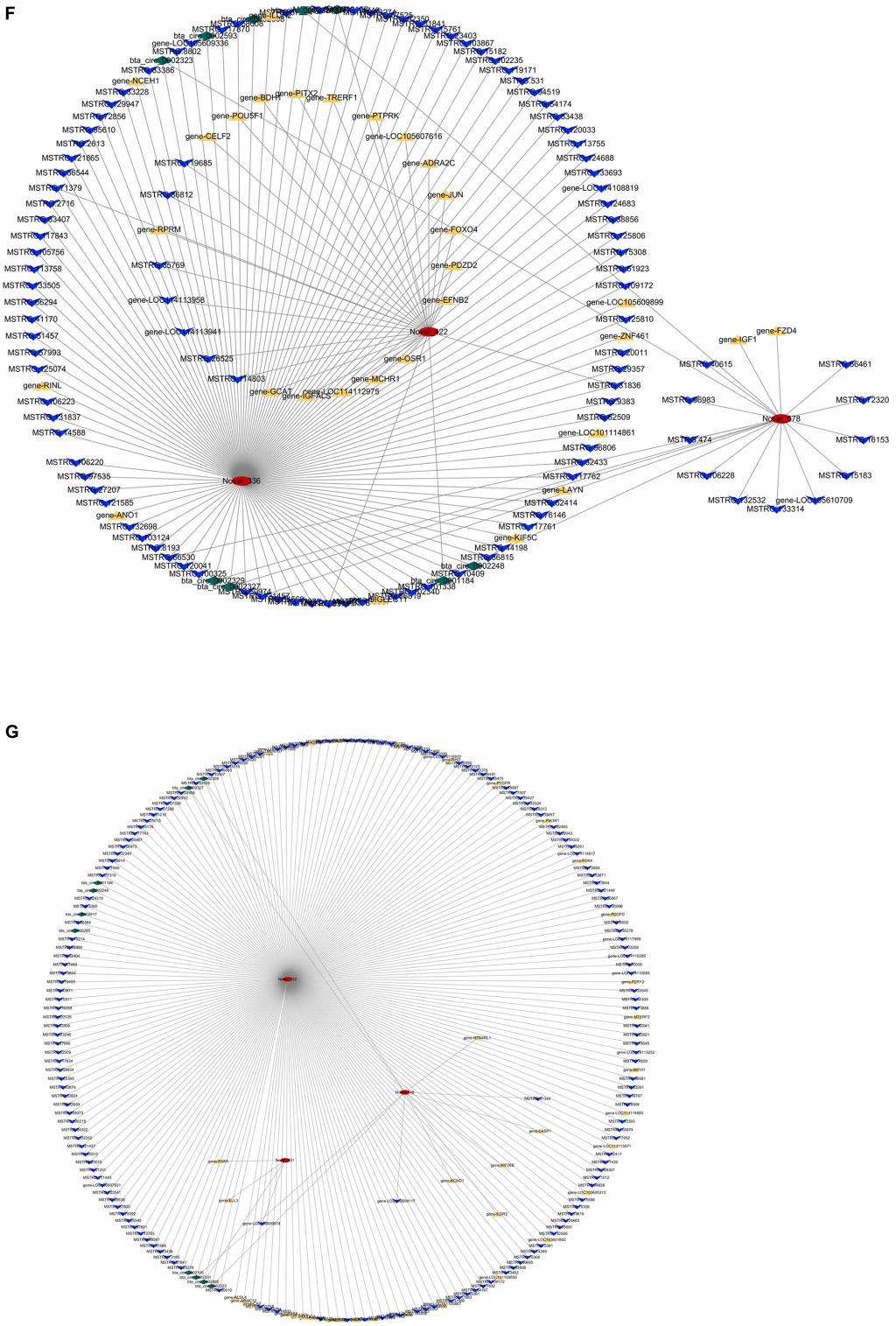

FIGURE 3 | Regulatory networks from preadipocytes to mature adipocytes. **(A)** Circular RNA (circRNA)–microRNA (miRNA) network regulation diagram; the red graphic is miRNA, and the green graphic is circRNA. **(B)** miRNA–messenger RNA (mRNA) network regulation diagram; the yellow graphic is mRNA. **(C)** Long non-coding RNA (lncRNA)–miRNA–mRNA network regulation diagram; the blue graphic is mRNA. **(D)** circRNA–miRNA–mRNA network regulation diagram between M1 vs. P1 and M2 vs. P2 groups. **(E)** circRNA–miRNA–mRNA network regulation diagram between M2 vs. P2 and M3 vs. P3 groups. **(F)** LncRNA–circRNA–miRNA–mRNA network regulation diagram between M1 vs. P1 and M2 vs. P2 groups. **(G)** LncRNA–circRNA–miRNA–mRNA network regulation diagram between M2 vs. P2 and M3 vs. P3 groups.

(miR-336, miR-422, miR-578, miR-722, miR-748, and miR-831) can simultaneously form three-element and four-element networks. Detailed information is shown in **Supplementary Table 15**.

Screening Out Candidate RNAs and Core Networks

Because the number of DERs and networks was large and complex, we screened out the highest expression DERs and core networks. The highest expression of DEGs was screened out based on $|\log FC| > 5$. The highest expression of lncRNAs and circRNAs was chosen based on $|\log FC| > 2$ because the $|\log FC|$ value of DElncRNAs and microRNAs is low (**Table 3**). The $|\log FC|$ value of DEmiRNAs is high, so the highest expression of miRNAs was selected based on $|\log FC| > 10$. miRNAs' detailed information is shown in **Table 4**. The raw data of sequencing have been in the public database (Sequence Read Archive): SUB7601005 and SUB7600133[2,3].

[2]https://submit.ncbi.nlm.nih.gov/subs/sra/SUB7601005/overview
[3]https://submit.ncbi.nlm.nih.gov/subs/sra/SUB7600133/overview

The core networks were screened out based on three- and four-element networks, and they all contained four crucial novel miRNAs (miR-336, miR-422, miR-578, and miR-722). The miRNAs can form various networks because they had many targets, such as the following: miR-336 has 402 target RNAs (58 genes, 328 lncRNAs, 16 circRNAs); miR-422 has 24 target RNAs (11 genes, 11 lncRNAs, 2 circRNAs); miR-578 has 335 targets (46 genes, 273 lncRNAs, 16 circRNAs); miR-722 has 201 target RNAs (24 genes, 163 lncRNAs, 14 circRNAs). We considered the miRNAs as the candidate miRNAs. Detailed information is shown in **Table 5**.

Validation of the Accuracy of RNA Sequencing Data by qPCR

To validate the accuracy of RNA-Seq data, we selected 40 DERs from the highest expression DERs and the core regulatory networks, including four well-known genes that affect the adipocyte differentiation, including Lipoprotein lipase (LPL) (Ailhaud et al., 1985), Fatty acid-binding protein 4 (FABP4) (Moseti et al., 2016), Insulin-like growth factor 1 (IGF1)

TABLE 3 | The highest expression of DERs in M group vs. P group of RNA-Seq.

Description	Log2(M/P group)	Regulation	*p*-value	Position	Biotype
SPINK5	−5.214585327	Down	4.36E−175	chrNC_040256.1:61843953−61931728:+	Protein coding
SLITRK6	−5.742358445	Down	5.89E−62	chrNC_040261.1:66253981−66260610:−	Protein coding
LOC101106199	−6.537740726	Down	2.82E−22	chrNC_040266.1:52094769−52096364:+	Protein coding
SLC9A3	−6.122703226	Down	2.68E−17	chrNC_040267.1:78089680−78123950:+	Protein coding
LOC106990846	−2.073319757	Down	1.01E−89	chrNC_040252.1:67232773−67237128:+	lncRNA
LOC114116841	−2.315348304	Down	0.00094041	chrNC_040262.1:20528946−20533678:+	lncRNA
LOC105602850	−2.367815724	Down	0.003113683	chrNC_040268.1:57249831−57306438:−	lncRNA
LOC114113974	−2.730385804	Down	0.036100724	chrNC_040252.1:4213089−4240720:−	lncRNA
LOC114114545	−2.647923643	Down	0.000519611	chrNC_040255.1:103110999−103142205:+	lncRNA
LOC105604950	−3.845863021	Down	0.000341618	chrNC_040276.1:17541786−17605265:−	lncRNA
LOC105607182	−2.367815724	Down	2.90E−05	chrNC_040253.1:38409442−38410287:−	lncRNA
LOC114110446	−5.145423303	Down	2.20E−05	chrNC_040274.1:5639080−5641719:+	lncRNA
MSTRG.80212	−5.052313898	Down	6.67E−09	chrNC_040262.1:35134262−35138700:+	lncRNA
MSTRG.105803	−4.845863021	Down	0.000147779	chrNC_040268.1:48523635−48527825:+	lncRNA
MSTRG.121783	−5.730385804	Down	1.69E−07	chrNC_040273.1:14918722−14956227:+	lncRNA
bta_circ_0000680	−4.229703279	Down	0.004356129	chrNC_040253.1:777960920.77797217:−	circRNA

circRNA, circular RNA; DER, differentially expressed RNA; lncRNA, long non-coding RNA; RNA-Seq, RNA sequencing.

TABLE 4 | The highest expression of DEmiRNAs in M group vs. P group of RNA-Seq.

Description	Log2(M/P group)	Regulation	*p*-value	Sequence	Biotype
Novel_220	−15.12252412	down	0	ACCACAGGGTAGAACCACGGAC	miRNA
Novel_455	−14.97920218	down	0	CTCAGTCAGCCTTGTGGATGTA	miRNA
Novel_90	−14.53355481	down	0	AAAAGCTGGGTTGAGAGGGCGA	miRNA
Novel_172	−13.97693693	down	0	AACTGTTTGCAGAGGAAACTGAG	miRNA
Novel_169	−13.23737812	down	0	AACTGGCCCACAAAGTCCCGCT	miRNA
Novel_362	−13.0942399	down	0	CAAGTCACTAGTGGTTCCGTTTAGT	miRNA
Novel_890	−11.86052381	down	6.70E−207	TTATCAGAATCTCCAGGGGTACT	miRNA

DEmiRNA, differentially expressed microRNA; miRNA, microRNA; RNA-Seq, RNA sequencing.

TABLE 5 | Core miRNAs of important networks in M group vs. P group of RNA-Seq.

Description	Log2(M/P group)	Regulation	*p*-value	Sequence	Biotype
Novel_366	−6.315266783	Down	4.05E−10	CACAGCTCCAGGGGATGCCGTTC	miRNA
Novel_422	−6.76272576	Down	4.66E−13	CCTCCCCTTCCTCCCTCCCTCCC	miRNA
Novel_578	−4.971312382	Down	9.65E−05	GGGTTTCCCTGGTGGCTCAGA	miRNA
Novel_722	−9.988908241	Down	2.23E−72	TCGCTCAGTCGTGTCCGACTCT	miRNA
Novel_748	−5.525383867	Down	4.38E−06	TCTGGAGGGGCAGAAGGAGAAGC	miRNA
Novel_831	1.057978306	Up	7.77E−95	TGGCAGTGTCTTAGCTGGTTGTTG	miRNA
Novel_842	−5.110346368	Down	7.73E−05	TGGGCGGAGGTGGGGCGGGGGGCCC	miRNA

miRNA, microRNA; RNA-Seq, RNA sequencing.

(Chun et al., 2019), Carnitine palmitoyltransferase 1A (CPT1A) (Calderon et al., 2016), and novel crucial miRNAs (miR-336, miR-422, miR-578, miR-722). The qPCR results were highly consistent with the RNA-Seq data (**Figure 4**). It suggested that RNA-Seq data were credible and accurate. DERs' detailed information is shown in **Tables 6**, **7**.

Validation Expression Trend of Differentially Expressed RNAs in the Process of Adipocyte Differentiation

Although we saw the expression alteration of the DERs between the P and M groups, it still cannot indicate that the RNAs were indeed involved in every period of adipocyte differentiation. We detected the expression trend of the DERs in the adipocyte differentiation period (2–10 days) by qPCR. The results showed that the RNAs had significant changes in the whole process of adipocyte differentiation (**Figure 5**). The RNAs also contained some pathways, such as miR-336/ACSL4/LncRNA-MSTRG71379/circRNA0002331, miR-422/FOXO4/LncRNA-MSTRG54995/circRNA0000520, miR-578/IGF1/LncRNA-MSTRG102235/circRNA0002971, and miR-722/PDK4/LncRNA-MSTRG107440/circRNA0002909. The DERs and networks were indeed involved in the process of sheep adipocyte differentiation. The core regulatory networks of four miRNAs are worthy of attention and in-depth studying.

DISCUSSION

Marbling is a vital standard to measure the quality of meat (Pethick et al., 2004). IMF content can significantly affect a marbling state. Increasing the accumulation of fat in intramuscular can promote the formation of meat marbling and improve meat properties such as taste, flavor, color, etc. (Dodson et al., 2010). The genetic factor leading to the speed of individual accumulating IMF content was different in the same breed and feeding conditions. The reasons may be which genetic factor determines the number of mammalian initial fat cells and the speed rate of adipocyte differentiation (Hocquette et al., 2010). Therefore, it is crucial to explore the potential molecular mechanisms of adipocyte differentiation. At present, a few studies provided candidate RNAs related to meat traits and were used for actual production (Hong et al., 2012; Yuan et al., 2013; Pertea et al., 2016). However, other non-coding RNAs and ceRNA remain less reported in sheep. In this study, we used high-throughput sequencing to compare RNA changes from preadipocytes to mature adipocytes. We obtained plenty of candidate genes and core regulatory networks affecting adipocyte differentiation by qPCR validation. These findings will enable us to understand the molecular mechanisms involved in adipocyte differentiation and expand new researching directions or biomarkers for improving the IMF and quality of mutton.

We found plenty of novel RNA transcripts in the study, especially non-coding RNAs. The number of novel miRNAs and lncRNAs dramatically surpassed that of the known ones. These results deserve attention. The main reasons may be that the reports on non-coding RNAs in sheep adipocyte differentiation were less and leading to lots of novel miRNAs and lncRNAs were not found. At the same time, there is lately no complete genome reference. In this study, a large number of genes involved in adipocyte differentiation were identified, especially well-known genes. The expression trend of the genes was consistent with what others reported (Prosdocimo et al., 2014; Olivecrona, 2016; Li et al., 2017; Kineman et al., 2018; Rodríguez-Calvo et al., 2019), such as LPL, FABP4, Forkhead box-O1 (FoxO1) (Chen et al., 2019), IGF1, and KLF family members. Some studies found that the selective knockdown of Matrix metalloproteinase 2 (MMP2) in mouse adipose cell lines led to a significant reduction (Bauters et al., 2015). Our sequencing data indicated that the MMP2 gene was also significantly increased in sheep adipocyte differentiation. Some reports suggested that Sirtuin 3 (SIRT3) promotes age-related adipogenesis and osteoclast production related to bone loss (Ho et al., 2017). The changing trend of the SIRT3 gene in these studies was consistent with our data. Reported miRNAs related to sheep lipid metabolism were less, especially only a few DEmiRNAs were found in the present study. miR-143 could be associated with obesity and could promote adipocyte differentiation in mice fed with a high-fat diet. We also found that miR-143 was significantly expressed during adipocyte differentiation (Bae et al., 2017). Some studies suggested that miR-181a promoted preadipocyte differentiation in porcine by directly targeting transforming growth factor-beta receptor 1 (TGFBR1) (Zhang et al., 2019). In this study, we also identified miR-181a and TGFBR1, and the expression trends were consistent with previous reports and findings. miR-27a can

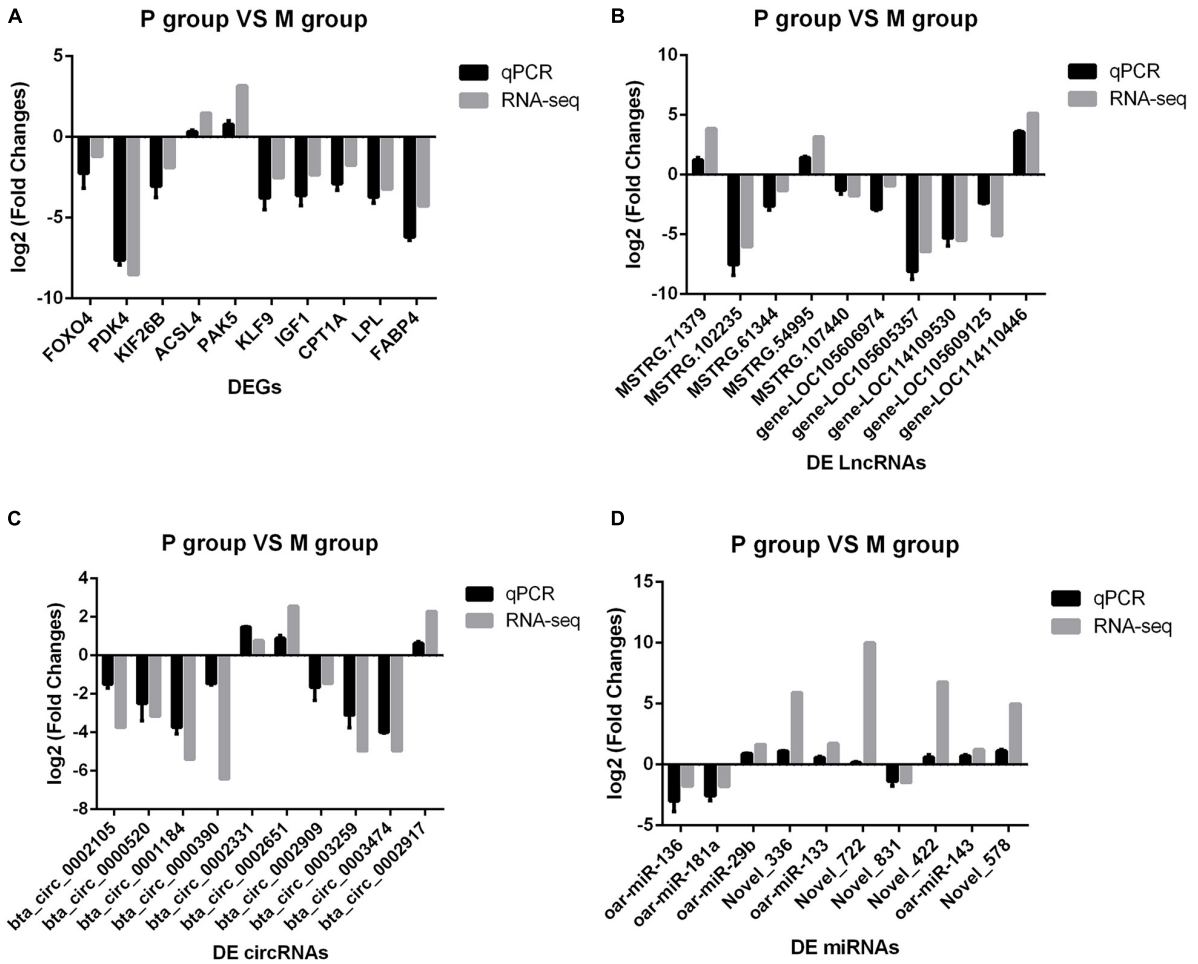

FIGURE 4 | Comparison of sequencing results and qPCR results. The abscissa is differentially expressed RNAs (DERs), the ordinate is Log2(Fold Change), the gray column is the sequencing result, and the black column is the qPCR result. **(A)** Validation of messenger RNA (mRNA) results by qPCR. **(B)** Validation of long non-coding RNA (lncRNA) results by qPCR. **(C)** Validation of circular RNA (circRNA) results by qPCR. **(D)** Validation of microRNA (miRNA) results by qPCR.

promote the proliferation of sheep preadipocytes and inhibit cell differentiation by regulating the expression of RXRα (Deng et al., 2020). Our experiment also identified the expression changes of miR-27a, but the trend was not statistically significant. One potential explanation for this is that our study missed the probability of the period of higher expression of miR-27a. To the best of our knowledge, only a limited number of reports have previously studied the expression profiles of lncRNAs and circRNAs concerning sheep lipid metabolism by searching the NCBI website. Although in the present study we found most lncRNAs and circRNAs affecting adipocyte differentiation, the DERs do not have too much literature for reference. The underlying function of DERs can provide a new research direction. In this study, some known genes affecting adipocyte differentiation had significant changes, such as PPARγ, CCAAT/enhancer-binding proteins (C/EBPα), and sterol regulatory element-binding protein 1 (SREBP1) (Sarjeant and Stephens, 2012). The main reasons may be what genes are only significantly expressed in the early stage of adipocyte differentiation. These trial samples were in preadipocyte and mature adipocyte stages, and the interval time is too long. Therefore, the experiment did not identify these well-known genes' significant expression.

GO enrichment analysis showed that the results of four varieties of RNAs were similar; GO terms all enriched in cell part, cellular process, biological regulation, and binding. Non-coding RNAs made GO enrichment analysis based on targets or related to genes, so the final results were similar. KEGG pathway analysis results for the four varieties of RNAs showed that DERs mostly enriched in focal adhesion, PPAR signaling pathway, cancer, adipocytokine signaling pathway, MAPK signaling pathway, FoxO signal pathway, PI3K/Akt signaling pathways, and so on. A potential explanation for these findings could be that the non-coding RNAs may present different functions and spatiotemporal specific activities. However, we only studied the RNA expression in two periods of cell differentiation. Interestingly, we found many significantly dysregulated genes involved in cancer that participated in adipocyte differentiation.

TABLE 6 | Validation DERs by qPCR.

Description	Log2(M/P group)	Regulation	*p*-value	Position	Biotype
FOXO4	1.206825243	Up	2.38E−29	chrNC_040278.1:66559700−66566788:+	Protein coding
PDK4	8.51278818	Up	0	chrNC_040255.1:14709622−14723348:−	Protein coding
KIF26B	1.958753835	Up	1.40E−264	chrNC_040263.1:34375794−34974888:−	Protein coding
ACSL4	−1.484972615	Down	9.18E−274	chrNC_040278.1:134005859−134080888:+	Protein coding
PAK5	−3.164830284	Down	0.009030858	chrNC_040264.1:2315164−2741382:−	Protein coding
KLF9	2.520358431	Up	0	chrNC_040253.1:71284364−71311713:+	Protein coding
IGF1	2.340239857	Up	0	chrNC_040254.1:183945231−184028095:−	Protein coding
CPT1A	1.738046955	Up	4.08E−262	chrNC_040272.1:47903982−47963597:−	Protein coding
LPL	3.23308832	Up	3.81E−37	chrNC_040253.1:48325425−48351715:−	Protein coding
FABP4	4.280841452	Up	1.62E−10	chrNC_040260.1:62825793−62830309:−	Protein coding
bta_circ_0002105	3.747576644	Up	0.007144757	chrNC_040263.1:236713980.23815809:+	circRNA
bta_circ_0000520	3.162614143	Up	0.040244255	chrNC_040253.1:1914752360.191552199:−	circRNA
bta_circ_0001184	5.825877078	Up	3.30E−08	chrNC_040256.1:159915940.16093665:+	circRNA
bta_circ_0000390	6.410839578	Up	1.71E−11	chrNC_040253.1:1203039920.120348810:+	circRNA
bta_circ_0002331	−0.774234923	Down	5.16E−33	chrNC_040264.1:664698010.66593120:+	circRNA
bta_circ_0002651	−2.559851881	Down	4.34E−05	chrNC_040268.1:55330811O.55331699:+	circRNA
bta_circ_0002909	1.452120761	Up	0.015200022	chrNC_040271.1:30480927O.30573486:+	circRNA
bta_circ_0003259	4.969969066	Up	1.04E−05	chrNC_040276.1:140470320.14062601:+	circRNA
bta_circ_0003474	4.969969066	Up	1.04E−05	chrNC_040278.1:941054400.94114703:−	circRNA
bta_circ_0002917	−2.287418777	Down	5.26E−09	chrNC_040271.1:40105230.4029153:+	circRNA
MSTRG.71379	−3.853768219	Down	3.22E−41	chrNC_040260.1:50049753−50057325:+	lincRNA
MSTRG.102235	6.024501699	Up	1.16E−09	chrNC_040267.1:32049818−32061433:−	lincRNA
MSTRG.61344	1.328310243	Up	7.85E−47	chrNC_040258.1:44623533−44652963:−	Antisense
MSTRG.54995	−3.177513741	Down	0	chrNC_040257.1:26304321−26424276:+	Intronic
MSTRG.107440	1.761467293	Up	0.016201024	chrNC_040268.1:78672493−78673817:+	lincRNA
LOC105606974	0.942039538	up	0.000111223	chrNC_040253.1:258708631−258721999:−	lncRNA
LOC105605357	6.443291333	up	3.23E−87	chrNC_040278.1:12643932−12646966:−	lncRNA
LOC114109530	5.498432887	up	3.97E−07	chrNC_040271.1:52087348−52095154:+	lncRNA
LOC105609125	5.102504211	up	1.12E−05	chrNC_040257.1:63372022−63385936:−	lncRNA
LOC114110446	−5.145423303	down	2.20E−05	chrNC_040274.1:5639080−5641719:+	lncRNA

circRNA, circular RNA; DER, differentially expressed RNA; lincRNA, long intergenic non-coding RNA; lncRNA, long non-coding RNA.

TABLE 7 | Validation DEmiRNAs by qPCR.

Description	Log2(M/P group)	Regulation	*p*-value	Sequence	Biotype
oar-miR-136	1.782238672	Up	5.34E−29	ATCCATTTGTTTTGATGATGGA	miRNA
oar-miR-181a	1.787057294	Up	0	AACATTCAACGCTGTCGGTGAGT	miRNA
oar-miR-29b	−1.635919823	Down	0	TAGCACCATTTGAAATCAGTGT	miRNA
oar-miR-133	−1.727689283	Down	4.20E−67	TTGGTCCCCTTCAACCAGCTGT	miRNA
oar-miR-143	−1.226226546	Down	0	TGAGATGAAGCACTGTAGCTC	miRNA

DEmiRNA, differentially expressed microRNA; miRNA, microRNA.

We systematically constructed regulatory networks affecting adipocyte differentiation. The regulatory networks were complex; therefore, constructed various networks were necessary. In this study, IGF1 can participate in all regulatory networks, and it suggested that IGF1 played a vital role in adipocyte differentiation. We also noticed that miR-336, miR-422,

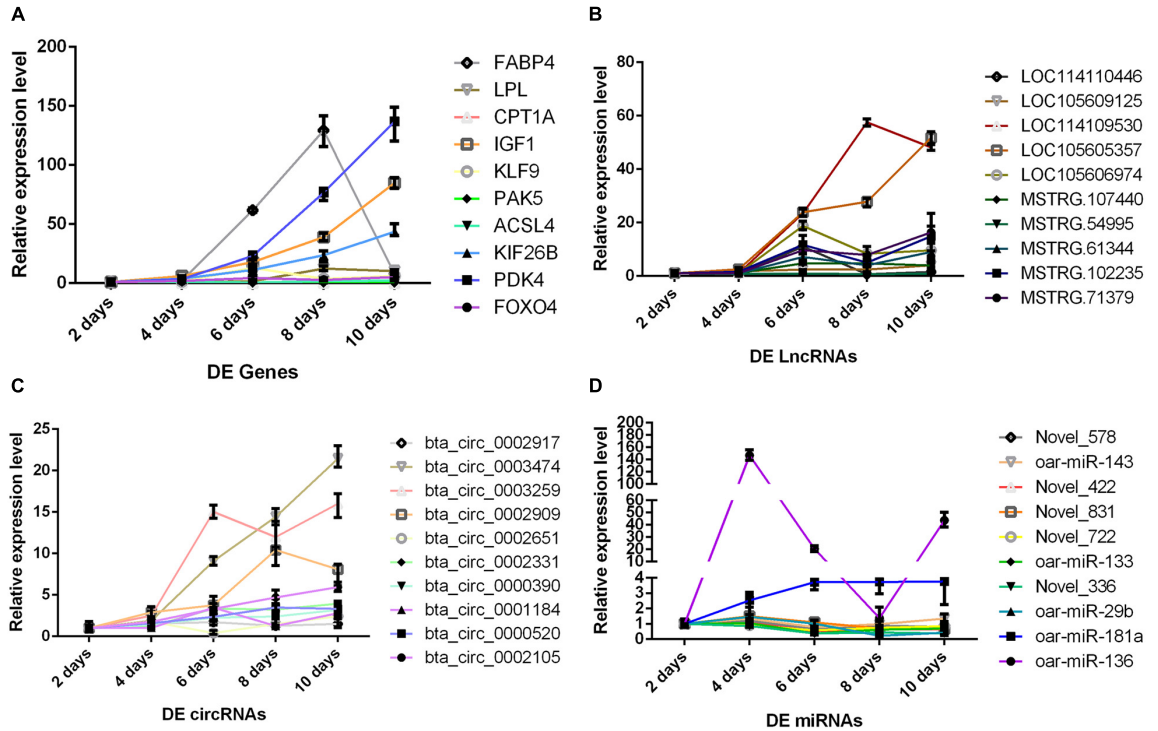

FIGURE 5 | The change trend of differentially expressed RNA during adipocyte differentiation. The abscissa is the different days of cell culture, the ordinate is relative expression level, different colored lines represent different RNAs. **(A)** Messenger RNA (mRNA) results by qPCR. **(B)** Long non-coding RNA (lncRNA) results by qPCR. **(C)** Circular RNA (circRNA) results by qPCR. **(D)** MicroRNA (miRNA) results by qPCR.

miR-578, and miR-722 played core roles in all ceRNA regulatory networks. In this study, although the expression differences of the four new miRNAs (miR-336, miR-422, miR-578, and miR-722) did not seem to be significant in the qPCR results, we can see that the expressions of other network factors related to these four miRNAs are all significant, and these four genes also have significant changes at different stages of the adipocyte differentiation process. Interestingly, we found that all core miRNAs of the circRNA–miRNA–mRNA network participated in the four-element network. However, none of the core miRNAs of the lncRNA–miRNA–mRNA participated in the four-element network, and the reasons were unclear. We chose 40 DERs to detect the expression pattern in the process adipocyte differentiation, from which form many regulatory networks: miR-336/ACSL4/LncRNA-MSTRG71379/circRNA0002331, miR-422/FOXO4/LncRNA-MSTRG54995/circRNA0000520, miR-578/IGF1/LncRNA-MSTRG102235/circRNA0002971, miR-722/PDK4/LncRNA-MSTRG107440/circRNA0002909, and so on. The four networks and their core miRNAs were worthy of the next study. There were some problems encountered during the experiment. For example, the interval time from the P group to the M group was too long. Sequencing results may miss some highly expressed genes or non-coding RNAs in this period. We plan to add a new group of experiments between P and M groups to deal with the problems. In this study, trial data provided the DERs and pathways as practical value and reference for exploring the molecular mechanisms of adipocyte differentiation. This study not only adapts to livestock but also has valuable reference significance for human fat metabolism.

CONCLUSION

We did whole-transcriptome sequencing in the sheep preadipocyte and the mature adipocyte group. We constructed for the first time comprehensive and systematic regulatory networks affecting sheep adipocyte differentiation. Sequencing data contained plenty of well-known and novel genes and non-coding RNAs; some of the DERs may be candidate RNAs, and they played a vital role in sheep adipocyte differentiation. The study identified that the four miRNAs (miR-336, miR-422, miR-578, and miR-722) were valuable for researching the molecular mechanisms of adipocyte differentiation. The four miRNAs involved in the networks also play crucial roles in the process and may be new biomarkers for improving IMF content and meat quality in sheep.

DATA AVAILABILITY STATEMENT

The datasets presented in this study can be found in online repositories. The names of the repository/repositories and accession number(s) are Sequence Read Archive—PRJNA639304, https://www.ncbi.nlm.nih.gov/search/all/?term=PRJNA639304.

ETHICS STATEMENT

The animal study was reviewed and approved by AWEC 2019A05, 16 May 2019. Written informed consent was obtained from the owners for the participation of their animals in this study.

AUTHOR CONTRIBUTIONS

LZ and YC: conceptualization. YC: methodology and writing—review and editing. TW: software. CX: validation, formal analysis, writing—original draft preparation, and visualization. JL: investigation. HM: resources. LL: data curation. CW and ZY: supervision. HJ: project administration. HJ and HM: funding acquisition. All authors have read and agreed to the published version of the manuscript.

FUNDING

This study was supported by the Scientific and Technological Developing Scheme of Jilin Province (20190301006NY), the Jilin Scientific and Technological Development Program (20190301005NY), and the China Agriculture Research System of MOF and MARA (CARS-38 and CARS-39-17).

ACKNOWLEDGMENTS

We thank all the researchers who contributed to this work.

SUPPLEMENTARY MATERIAL

The Supplementary Material for this article can be found online at: https://www.frontiersin.org/articles/10.3389/fgene.2021.662143/full#supplementary-material

Supplementary Figure 1 | Volcano map of different groups of differential RNAs. **(A–C)** Expression profiles of mRNAs and LncRNAs (M1 vs. P1, M2 vs. P2, M3 vs. P3). **(D–F)** Expression profiles of circRNAs (M1 vs. P1, M2 vs. P2, M3 vs. P3). Green points represent down-regulated RNAs; red points represent up-regulated RNAs; gray points represent not significantly expressed RNAs in the volcano plots. **(G–I)** Expression profiles of miRNAs (M1 vs. P1, M2 vs. P2, M3 vs. P3). Blue points represent down-regulated RNAs; yellow points represent up-regulated RNAs; gray points represent not significantly expressed RNAs in the volcano plots. X-axis: Fold change log2 ratio of RNAs. Y-axis: false discovery rate values (-log10 transformed).

Supplementary Figure 2 | Cluster map of different groups of differential RNAs. **(A)** Cluster analysis of mRNAs. **(B)** Cluster analysis of LncRNAs. **(C)** Cluster analysis of circRNAs. **(D)** Cluster analysis of miRNAs. The yellow and blue regions represent increased and decreased RNAs.

Supplementary Figure 3 | Gene ontology (GO) analysis of different groups of differential RNAs. **(A)** GO annotations of DE mRNAs. **(B)** GO annotations of DE LncRNAs. **(C)** GO annotations of DE circRNAs. **(D)** GO annotations of DE miRNAs.

Supplementary Figure 4 | KEGG pathway analysis of different groups of differential RNAs. **(A)** KEGG pathway of DE mRNAs. **(B)** KEGG pathway of DE LncRNAs. **(C)** KEGG pathway of DE circRNAs. **(D)** KEGG pathway of DE miRNAs.

Supplementary Table 1 | Primer sequences of mRNAs.

Supplementary Table 2 | Primer sequences of LncRNAs.

Supplementary Table 3 | Primer sequences of circRNAs.

Supplementary Table 4 | Primer sequences of miRNAs.

Supplementary Table 5 | List of 1,196 DEmRNAs.

Supplementary Table 6 | List of 754 DELncRNAs.

Supplementary Table 7 | List of 17 DEcircRNAs.

Supplementary Table 8 | List of 100 DEmiRNAs.

Supplementary Table 9 | Data of LncRNA binds to miRNA.

Supplementary Table 10 | Data of LncRNA binds to mRNA.

Supplementary Table 11 | Data of circRNA absorbs miRNA.

Supplementary Table 12 | Data of miRNA bind to mRNA.

Supplementary Table 13 | LncRNA-mRNA-miRNA correlation data.

Supplementary Table 14 | circRNA-mRNA-miRNA correlation data.

Supplementary Table 15 | circRNA-LncRNA-mRNA-miRNA correlation data.

REFERENCES

Agarwal, V., Bell, G. W., Nam, J. W., and Bartel, D. P. (2015). Predicting effective microRNA target sites in mammalian mRNAs. *Elife* 4:e05005. doi: 10.7554/eLife.05005

Ailhaud, G., Amri, E., Czerucka, D., Forest, C., Gaillard, D., Grimaldi, P., et al. (1985). Lipoprotein lipase and adipocyte differentiation. *Reprod. Nutr. Dev.* 25, 153–158.

Ali, S. Z., Langden, S. S., Munkhzul, C., Lee, M., and Song, S. J. (2020). Regulatory mechanism of MicroRNA expression in cancer. *Int. J. Mol. Sci.* 21:1723. doi: 10.3390/ijms21051723

Bae, I., Park, P. J., Lee, J. H., Cho, E. G., Lee, T. R., and Kim, S. H. (2017). PPARγ-mediated G-protein coupled receptor 120 signaling pathway promotes transcriptional activation of miR-143 in adipocytes. *Gene* 626, 64–69. doi: 10.1016/j.gene.2017.05.016

Bauters, D., Scroyen, I., Van, H. M., and Lijnen, H. R. (2015). Gelatinase A (MMP-2) promotes murine adipogenesis. *Biochim. Biophys. Acta* 1850, 1449–1456. doi: 10.1016/j.bbagen.2015.04.003

Calderon, D. M., Sebastián, D., Fucho, R., Weber, M., Mir, J. F., García-Casarrubios, E., et al. (2016). Carnitine palmitoyltransferase 1 increases lipolysis, UCP1 protein expression and mitochondrial activity in brown adipocytes. *PLoS One* 11:e0159399. doi: 10.1371/journal.pone.0159399

Chen, C., Cui, Q., Zhang, X., Luo, X., Liu, Y., Zuo, J., et al. (2018). Long non-coding RNAs regulation in adipogenesis and lipid metabolism: emerging insights in obesity. *Cell Signal.* 51, 47–58. doi: 10.1016/j.cellsig.2018.07.012

Chen, J., Lu, Yi, Tian, M., and Huang, Q. (2019). Molecular mechanisms of FOXO1 in adipocyte differentiation.[J]. *J. Mol. Endocrinol.* 62, R239–R253. doi: 10.1530/JME-18-0178

Chun, S. Y., Lim, J., Lee, E. H., Han, M. H., Ha, Y. S., Lee, N. J., et al. (2019). Preparation and characterization of human adipose tissue-derived extracellular matrix, growth factors, and stem cells: a concise review. *Tissue Eng. Regen. Med.* 16, 385–393. doi: 10.1007/s13770-019-00199-7

Deng, K., Ren, C., Fan, Y., Liu, Z., Zhang, G., Zhang, Y., et al. (2020). miR-27a is an important adipogenesis regulator associated with differential lipid accumulation between intramuscular and subcutaneous adipose tissues of sheep. *Domest. Anim. Endocrinol.* 71:106393. doi: 10.1016/j.domaniend.2019.106393

Dodson, M. V., Jiang, Z., Chen, J., Hausman, G. J., Guan, L. L., Novakofski, J., et al. (2010). Allied industry approaches to alter intramuscular fat content and composition in beef animals. *J. Food Sci.* 75, R1–R8. doi: 10.1111/j.1750-3841.2009.01396.x

Enright, A. J., John, B., Gaul, U., Tuschl, T., Sander, C., and Marks, D. S. (2003). MicroRNA targets in Drosophila. *Genome Biol.* 5:R1. doi: 10.1186/Gb-2003-5-1-r1

Friedlander, M. R., Mackowiak, S. D., Li, N., Chen, W., and Rajewsky, N. (2012). miRDeep2 accurately identifies known and hundreds of novel microRNA genes in seven animal clades. *Nucleic Acids Res.* 40, 37–52. doi: 10.1093/var/gkr688

Gálvez, F., Domínguez, R., Pateiro, M., Carballo, J., Tomasevic, I., and Lorenzo, J. M. (2018). Effect of gender on breast and thigh turkey meat quality. *Br. Poult. Sci.* 59, 408–415. doi: 10.1080/00071668.2018.1465177

Gao, Y., Wang, J., and Zhao, F. (2015). CIRI: an efficient and unbiased algorithm for de novo circular RNA identification. *Genome Biol.* 16:4.

Géloën, A., Roy, P. E., and Bukowiecki, L. J. (1989). Regression of white adipose tissue in diabetic rats. *Am. J. Physiol.* 257, E547–E553. doi: 10.1152/append.1989.257.4.E547

Gregoire, F. M., Smas, C. M., and Sul, H. S. (1998). Understanding adipocyte differentiation. *Physiol. Rev.* 78, 783–809. doi: 10.1152/physrev.1998.78.3.783

Ho, L., Wang, L. P., Roth, T. M., Pan, Y., Verdin, E. M., Hsiao, E. C., et al. (2017). Sirtuin-3 promotes adipogenesis, osteoclastogenesis, and bone loss in aging male mice. *Endocrinology* 158, 2741–2753. doi: 10.1210/en.2016-1739

Hocquette, J. F., Gondret, F., Baéza, E., Médale, F., Jurie, C., Pethick, D. W., et al. (2010). Intramuscular fat content in meat-producing animals: development, genetic and nutritional control, and identification of putative markers. *Animal* 4, 303–319. doi: 10.1017/S1751731109991091

Hong, J. S., Noh, S. H., Lee, J. S., Kim, J. M., Hong, K. C., and Lee, Y. S. (2012). Effects of polymorphisms in the porcine microRNA miR-1 locus on muscle fiber type composition and miR-1 expression[J]. *Gene* 506, 211–216. doi: 10.1016/j.gene.2012.06.050

Jeck, W. R., and Sharpless, N. E. (2014). Detecting and characterizing circular RNAs. *Nat. Biotechnol.* 32, 453–461. doi: 10.1038/nbt.2890

Kashan, N., Azar, G., Afzalzadeh, A., Afzalzadeh, A., and Salehi, A. (2005). Growth performance and carcass quality of fattening lambs from fat-tailed and tailed sheep breeds. *Small Rumin Res* 60, 267–271. doi: 10.1016/j.smallrumres.2005.01.001

Kineman, R. D., Del, R. M., and Sarmento, C. A. (2018). 40 YEARS of IGF1: understanding the tissue-specific roles of IGF1/IGF1R in regulating metabolism using the Cre/loxP system.[J]. *J. Mol. Endocrinol.* 61, T187–T198. doi: 10.1530/JME-18-0076

Koutnikova, H., and Auwerx, J. (2001). Regulation of adipocyte differentiation. *Ann. Med.* 33, 556–561. doi: 10.3109/07853890108995966

Lambe, N. R., Clelland, N., Draper, J., Smith, E. M., Yates, J., and Bunger, L. (2021). Prediction of intramuscular fat in lamb by visible and near-infrared spectroscopy in an abattoir environmen. *Meat Sci.* 171:108286. doi: 10.1016/j.meatsci.2020.108286

Li, Y., Ma, Z., Jiang, S., Hu, W., Li, T., Di, S., et al. (2017). A global perspective on FOXO1 in lipid metabolism and lipid-related diseases. *Prog. Lipid Res.* 66, 42–49. doi: 10.1016/j.plipres

Li, Y., Zheng, Q., Bao, C., Li, S., Guo, W., Zhao, J., et al. (2015). Circular RNA is enriched and stable in exosomes: a promising biomarker for cancer diagnosis. *Cell Res.* 25, 981–984. doi: 10.1038/cr.2015.82

Li, Z., Huang, C., Bao, C., Chen, L., Lin, M., Wang, X., et al. (2015). Exon-intron circular RNAs regulate transcription in the nucleus. *Nat. Struct. Mol. Biol.* 22, 256–264. doi: 10.1038/nsmb.2959

Liu, S., Huang, J., Wang, X., and Ma, Y. (2020). Transcription factors regulate adipocyte differentiation in beef cattle. *Anim. Genet.* 51, 351–357. doi: 10.1111/age.12931

Lu, T. X., and Rothenberg, M. E. (2018). MicroRNA. *J. Allergy Clin. Immunol.* 141, 1202–1207. doi: 10.1016/j.jaci.2017.08.034

Lopez-Pajares, V. (2016). Long non-coding RNA regulation of gene expression during differentiation. *Pflugers Arch.* 468, 971–981. doi: 10.1007/s00424-016-1809-6

Ma, N., Pan, J., Ye, X., Yu, B., Zhang, W., and Wan, J. (2019). Whole-transcriptome analysis of APP/PS1 mouse brain and identification of circRNA-miRNA-mRNA networks to investigate AD pathogenesis. *Mol. Ther. Nucleic Acids* 18, 1049–1062. doi: 10.1016/j.omtn.2019.10.030

Martins, J. M., Fialho, R., Albuquerque, A., Neves, J., Freitas, A., Tirapicos Nunes, J., et al. (2020). Portuguese local pig breeds: genotype effects on meat and fat quality traits. *Animals* 10:905. doi: 10.3390/ani10050905

Memczak, S., Jens, M., Elefsinioti, A., Torti, F., Krueger, J., Rybak, A., et al. (2013). Circular RNAs are a large class of animal RNAs with regulatory potency. *Nature* 495, 333–338. doi: 10.1038/nature11928

Miao, X., Luo, Q., Zhao, H., and Qin, X. (2016). Ovarian proteomic study reveals the possible molecular mechanism for hyperprolificacy of Small Tail Han sheep. *Sci. Rep.* 6:27606. doi: 10.1038/srep27606

Moseti, D., Regassa, A., and Kim, W. K. (2016). Molecular regulation of adipogenesis and potential anti-adipogenic bioactive molecules. *Int. J. Mol. Sci.* 17:124. doi: 10.3390/ijms17010124

Ntambi, J. M., and Young-Cheul, K. (2000). Adipocyte differentiation and gene expression. *J. Nutr.* 130, 3122S–3126S. doi: 10.1093/jn/130.12.3122S

Obregon, M. J. (2008). Thyroid hormone and adipocyte differentiation. *Thyroid* 18, 185–195. doi: 10.1089/thy.2007.0254

Olivecrona, G. (2016). Role of lipoprotein lipase in lipid metabolism. *Curr. Opin. Lipidol.* 27, 233–241. doi: 10.1097/MOL.0000000000000297

Park, S. J., Beak, S. H., Jung, D. J. S., Kim, S. Y., Jeong, I. H., Piao, M. Y., et al. (2018). Genetic, management, and nutritional factors affecting intramuscular fat deposition in beef cattle–A review. *Asian Austr. J. Anim. Sci.* 31, 1043–1061. doi: 10.5713/ajas.18.0310

Pertea, M., Kim, D., Pertea, G. M., Leek, J. T., and Salzberg, S. L. (2016). Transcript-level expression analysis of RNA-seq experiments with HISAT, StringTie and Ballgown. *Nat. Protoc.* 11, 1650–1667. doi: 10.1038/nprot.2016.095

Pethick, D. W., Harper, G. S., and Oddy, V. H. (2004). Growth, development and nutritional mainpulation of marbling in cattle. *Aust. J. Exp. Agr.* 44, 705–715. doi: 10.1071/ea02165

Prosdocimo, D. A., Anand, P., Liao, X., Zhu, H., Shelkay, S., Artero-Calderon, P., et al. (2014). Kruppel-like factor 15 is a critical regulator of cardiac lipid metabolism. *J. Biol. Chem.* 289, 5914–5924. doi: 10.1074/jbc.M113.531384

Rahemi, H., Nigam, N., and Wakeling, J. M. (2015). The effect of intramuscular fat on skeletal muscle mechanics: implications for the elderly and obese. *J. R. Soc. Interface* 12:20150365. doi: 10.1098/rsif.2015.0365

Rodríguez-Calvo, R., Girona, J., Rodríguez, M., Samino, S., Barroso, E., de Gonzalo-Calvo, D., et al. (2019). Fatty acid binding protein 4 (FABP4) as a potential biomarker reflecting myocardial lipid storage in type 2 diabetes. *Metabolism* 96, 12–21. doi: 10.1016/j.metabol.2019.04.007

Sarjeant, K., and Stephens, J. M. (2012). Adipogenesis. *Cold Spring Harb. Perspect. Biol.* 4:a008417. doi: 10.1101/cshperspect.a008417

Scollan, N. D., Price, E. M., Morgan, S. A., Huws, S. A., and Shingfield, K. J. (2017). Can we improve the nutritional quality of meat? *Proc. Nutr. Soc.* 76, 603–618. doi: 10.1017/S0029665117001112

Shi, C., Huang, F., Gu, X., Zhang, M., Wen, J., Wang, X., et al. (2016). Adipogenic miRNA and meta-signature miRNAs involved in human adipocyte differentiation and obesity. *Oncotarget* 7, 40830–40845. doi: 10.18632/oncotarget.8518

Tafer, H., and Hofacker, I. L. (2008). RNAplex: a fast tool for RNA-RNA interaction search. *Bioinformatics* 24, 2657–2663. doi: 10.1093/bioinformatics/btn193

Tang, Q. Q., and Lane, M. D. (2012). Adipogenesis: from stem cell to adipocyte. *Annu. Rev. Biochem.* 81, 715–736. doi: 10.1146/annurev-biochem-052110-115718

Thomson, D. W., and Dinger, M. E. (2016). Endogenous microRNA sponges: evidence and controversy. *Nat. Rev. Genet.* 17, 272–283. doi: 10.1038/nrg.2016.20

Xiao, T., Liu, L., Li, H., Sun, Y., Luo, H., Li, T., et al. (2015). Long noncoding rna adinr regulates adipogenesis by transcriptionally activating C/EBP alpha. *Stem Cell Rep.* 5, 856–865. doi: 10.1016/j.stemcr.2015.09.007

Xiong, Y., Yue, F., Jia, Z., Gao, Y., Jin, W., Hu, K., et al. (2018). A novel brown adipocyte-enriched long non-coding RNA that is required for brown adipocyte differentiation and sufficient to drive thermogenic gene program in white adipocytes. *Biochim. Biophys. Acta Mol. Cell Biol. Lipids.* 1863, 409–419. doi: 10.1016/j.bbalip.2018.01.008

Xu, S., Chen, P., and Sun, L. (2015). Regulatory networks of non-coding RNAs in brown/beige adipogenesis. *Biosci. Rep.* 35:e00262. doi: 10.1042/BSR20150155

Yu, G., Yang, Z., Peng, T., and Lv, Y. (2021). Circular RNAs: rising stars in lipid metabolism and lipid disorders. *J. Cell Physiol.* 236, 4797–4806. doi: 10.1002/jcp.30200

Yuan, Z., Li, J., Li, J., Gao, X., Gao, H., and Xu, S. (2013). Effects of DGAT1 gene on meat and carcass fatness quality in Chinese commercial cattle. *Mol. Biol. Rep.* 40, 1947–1954. doi: 10.1007/s11033-012-2251-2

Zhang, Z., Gao, Y., Xu, M. Q., Wang, C. J., Fu, X. H., Liu, J. B., et al. (2019). miR-181a regulate porcine preadipocyte differentiation by targeting TGFBR1. *Gene* 681, 45–51. doi: 10.1016/j.gene.2018.09.046

Zhao, X. H., Yang, Z. Q., Bao, L. B., Wang, C. Y., Zhou, S., Gong, J. M., et al. (2015). Daidzein enhances intramuscular fat deposition and improves meat quality in finishing steers. *Exp. Biol. Med.* 240, 1152–1157. doi: 10.1177/1535370214564755

Zeng, Y., Ren, K., Zhu, X., Zheng, Z., and Yi, G. (2018). Long noncoding RNAs: advances in lipid metabolism. *Adv. Clin. Chem.* 87, 1–36. doi: 10.1016/bs.acc.2018.07.001

Conflict of Interest: The authors declare that the research was conducted in the absence of any commercial or financial relationships that could be construed as a potential conflict of interest.

Publisher's Note: All claims expressed in this article are solely those of the authors and do not necessarily represent those of their affiliated organizations, or those of the publisher, the editors and the reviewers. Any product that may be evaluated in this article, or claim that may be made by its manufacturer, is not guaranteed or endorsed by the publisher.

frontiers in Veterinary Science

ORIGINAL RESEARCH
published: 03 August 2021
doi: 10.3389/fvets.2021.644474

Identification of Photoperiod-Induced LncRNAs and mRNAs in Pituitary Pars Tuberalis of Sheep

Qing Xia[1†], *Mingxing Chu*[1†], *Xiaoyun He*[1], *Qiuyue Liu*[2], *Xiaosheng Zhang*[3], *Jinlong Zhang*[3], *Xiaofei Guo*[3] *and Ran Di*[1*]

[1] Key Laboratory of Animal Genetics and Breeding and Reproduction of the Ministry of Agriculture and Rural Affairs, Institute of Animal Science, Chinese Academy of Agricultural Sciences, Beijing, China, [2] Institute of Genetics and Developmental Biology, Chinese Academy of Sciences, Beijing, China, [3] Tianjin Institute of Animal Sciences, Tianjin, China

OPEN ACCESS

Edited by:
Rui Su,
Inner Mongolia Agricultural University, China

Reviewed by:
Gan Shangquan,
Xinjiang Academy of Agricultural and Reclamation Sciences, China
Wei Sun,
Yangzhou University, China
Zhuanjian Li,
Henan Agricultural University, China
Hugues Dardente,
Institut National de recherche pour l'agriculture, l'alimentation et l'environnement (INRAE), France

***Correspondence:**
Ran Di
dirangirl@163.com

[†]These authors share first authorship

Specialty section:
This article was submitted to Livestock Genomics, a section of the journal Frontiers in Veterinary Science

Received: 21 December 2020
Accepted: 24 June 2021
Published: 03 August 2021

Citation:
Xia Q, Chu M, He X, Liu Q, Zhang X, Zhang J, Guo X and Di R (2021) Identification of Photoperiod-Induced LncRNAs and mRNAs in Pituitary Pars Tuberalis of Sheep. Front. Vet. Sci. 8:644474. doi: 10.3389/fvets.2021.644474

The pituitary pars tuberalis (PT) is the regulating center of seasonal reproduction, which can sense the melatonin signal and eventually cause downstream changes of GnRH secretion through TSHβ. Recently, lncRNAs have been identified in animal reproductive-related tissues, and they play important roles in reproductive regulation. Therefore, in this study, we expect to identify photoperiod-induced lncRNAs and genes in pituitary PT of sheep by comparison of expression profiles between short photoperiod (SP) and long photoperiod (LP). Through RNA-Seq, a total of 55,472 lncRNAs were identified in pituitary PT of Sunite ewes. The number of differentially expressed (DE) genes and lncRNAs between SP and LP increased gradually with the extension of LP (from LP7 to LP42). The notable LP-induced candidate genes included *EYA3*, *TSHB*, *SIX1*, *DCT*, *VMO1*, *AREG*, *SUV39H2*, and *EZH2*, and SP-induced genes involved *ENSOARG00000012585, CHGA*, *FOS*, *SOCS3*, and *TH*. In enriched pathways for DE genes and lncRNA target genes between SP and LP, the reproduction- and circadian-related pathways were highlighted. In addition, the interactome analysis of lncRNAs and their targets implied that *MSTRG.209166* and its *trans*-target *TSHB*, *MSTRG.288068* and its *cis*-target *SIX1*, and *ENSOARG00000026131* and its *cis*-target *TH* might participate in regulation of seasonal reproduction. Together, these results will help to determine important photoperiod-induced lncRNAs and genes and give us some new insights into the epigenetic regulation of seasonal reproduction in sheep.

Keywords: lncRNAs, mRNAs, photoperiod, sheep, pituitary pars tuberalis

INTRODUCTION

The reproductive activity of some animal species inhabiting the temperate zone is limited in specific seasons in order to maximize the survival possibility of their offspring. According to the different seasons of breeding, these animals are categorized as long photoperiod (LP) breeders and short photoperiod (SP) breeders (1, 2). Among them, sheep belongs to the SP breeder (3); that is, they are mostly bred in autumn and winter. For example, Sunite sheep in China exhibit obvious seasonal reproductive behavior throughout the year, i.e., estrus from August to March of the next year and anestrus from April to July (2, 4).

Seasonal reproduction is an important factor limiting the production effciency of the sheep industry; therefore, research on the molecular basis of seasonal reproduction of sheep is indispensable for possible artificial regulation of this trait in the future. However, the molecular mechanism and regulatory network of seasonal reproduction are not very clear until now.

Pituitary pars tuberalis (PT) plays an important role of transmission center in the seasonal reproduction of animals. The pineal gland first converts external photoperiod signals into biological signals (nocturnal melatonin secretion), which causes photoperiod-induced signals (*EYA3*, *TSHB*, etc.) alternation in PT. Thus, the thyrotrophin secreted by the anterior pituitary will increase in long days, which acts on TSH receptor-expressing cells in the adjacent mediobasal hypothalamus, leading to type III thyroid hormone deiodinase (DIO3) switch to type II thyroid hormone deiodinase (DIO2). DIO2 regulates the thyroid hormone in the hypothalamus, controlling the activity of the hypothalamus–pituitary–gonad axis to exhibit the summer phenotypes by direct (GnRH neuron) or indirect (*KISS1*/*RFRP* system) ways (5, 6). Besides, the photoperiod-induced gene expression in PT is mainly affected by photoperiod, independently of the TH status (6). However, molecular changes related to seasonal reproduction in medio-basal hypothalamus are regulated not only by photoperiod but also by TH. Therefore, PT is the best ideal tissue for seasonal reproduction analyses. So far, several important genes involved in the regulation of seasonal reproduction have been discovered in PT. For example, LP-induced genes (e.g., *EYA3* and *TSHβ*) and an SP-induced gene (*CHGA*) were revealed in PT of sheep (3, 7, 8). Their expression levels had a remarkable change in different photoperiods. In recent years, long non-coding RNAs (lncRNAs) are considered as key regulators of gene expression because they play crucial roles in transcriptional and post-transcriptional regulation. In sheep, many lncRNAs have been identified in reproduction-related tissues, such as ovary, uterus, and germ cells (9–12). Moreover, lncRNAs play important roles in many aspects of sheep reproductive regulation, such as fecundity (12, 13), gonadal development (14), and sex hormone response (15). However, the functions of lncRNAs in animal PT on seasonal reproduction are unknown. Therefore, one purpose of this research is to seek the new photoperiod-induced genes and lncRNAs in PT of sheep by transcriptome sequencing. Another objective is to explore the potential relationship between genes and lncRNAs by target prediction and joint analysis of their co-expression in PT of sheep. These results will give us some new insights into the epigenetic regulation of seasonal reproduction in sheep.

METHODS

Ethical Statement

All the animals were authorized by the Science Research Department (in charge of animal welfare issue) of the Institute of Animal Sciences, Chinese Academy of Agricultural Sciences (IAS-CAAS; Beijing, China). In addition, ethical approval of animal survival was given by the animal ethics committee of IAS-CAAS (No. IAS2018-3, April 10, 2018).

Animal and Tissue Acquirement

Experiments were conducted on 12 adult Sunite ewes (2–3 years old; weight 30–40 kg), which were selected from a farm in Urat Middle Banner (40° 75′ north latitude), Bayan Nur City, Inner Mongolia Autonomous Region, China, and maintained in a farm in the Tianjin Institute of Animal Sciences, Tianjin (39° 13′ north latitude), China. All ewes were raised under the same conditions, with free access to water and feed. Construction of ovariectomized (OVX) and estradiol-implanted sheep model and light control experiment were previously described in detail (2, 12). Ewes were ovariectomized and estradiol-implanted (E_2, Sigma Chemical Co., St. Louis, MO, USA) to maintain plasma estradiol levels of 3–5 pg/ml (6, 16) in October, 2016, according to the model developed by Karsch et al. (1984) (17). This OVX + E_2 model normalizes the level of circulating E_2 (12), which uncovers the well-documented central seasonal shift in the negative feedback action of E_2 on gonadotropin secretion (18). After the surgery, the ewes recovered for 30 days before artificial light control. Then, in November 2016, all ewes were brought indoors and submitted to a light program simulating the outdoor photoperiodic condition by time-control switch. Firstly, all ewes were kept in artificial SP with lights on during 10:30–18:30 (SP, 8:16 h light/dark) for 21 days and switched to LP with lights on during 06:30–22:30 (LP, 16:8 h light/dark) for 42 days, with free access to water and food. Ewes were euthanized [intravenous pentobarbital (100 mg/kg)] at ZT4 [4 h after lights on] of SP21, LP7, LP21, and LP42 (8, 19–21). Consistent with the specific location described by Wood et al. (7) and Lomet et al. (6), the PT tissue (**Figure 1**) of each ewe was immediately collected and stored at −80°C for total RNA extraction.

RNA Extraction, Library Construction, and Sequencing

Pituitary PT tissues were used for RNA extraction with TRIzol Reagent (Invitrogen, Carlsbad, CA, USA) according to the manufacturer's instruction. Examination involving the integrality and quality of the isolated RNA was performed via electrophoresis and the RNA Nano 6000 Assay Kit of the Bioanalyzer 2100 system (Agilent Technologies, Santa Clara, CA, USA).

The rRNA was depleted from 3 μg of total RNA using Ribo-Zero TM Gold Kits (Epicentre, Madison, WI, USA). Sequencing libraries of the 12 samples (SP21, $n = 3$; LP7, $n = 3$; LP21, $n = 3$; LP42, $n = 3$) were generated using NEB Next Ultra Directional RNA LibraryPrep Kit for Illumina (NEB, Ipswich, MA, USA) according to the manufacturer's instructions, and index codes were used to label the sequences of each sample. After cluster generation, the library preparations were sequenced on an Illumina Hiseq platform (Illumina, San Diego, CA, USA). Raw data of the performed RNA-seq have been recorded in the SRA public database (Accession number of BioProject: PRJNA680667).

Reference Genome Mapping and Transcriptome Assembly

Raw data in fastq format were processed through in-house perl scripts. In this step, clean reads were obtained by removing

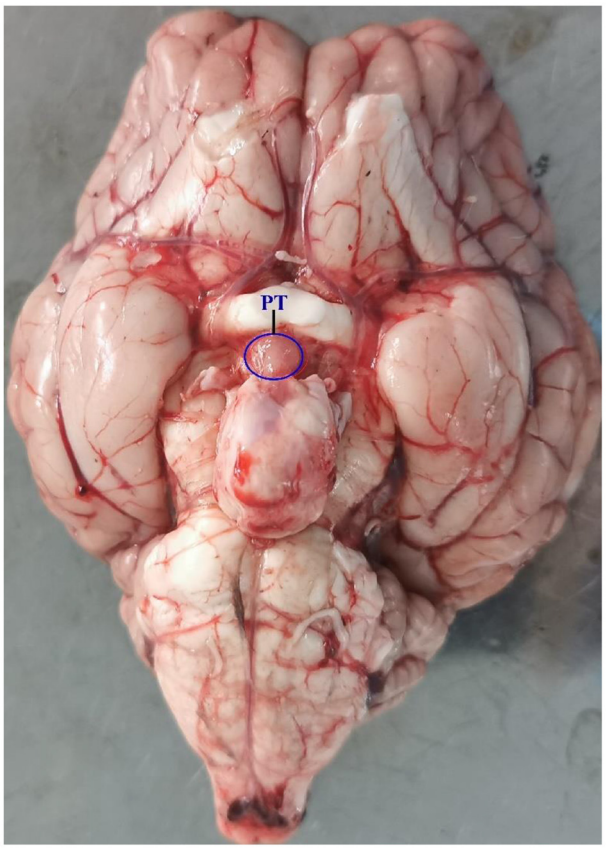

FIGURE 1 | The location of PT tissue in Sunite sheep.

reads with adapter contamination, reads that contained poly-N, and low-quality reads from raw data. Simultaneously, the Q20, Q30, and GC contents of the clean data were calculated. All downstream analysis was based on high-quality clean data. HiSAT2 (22) was used to align clean reads of each sample to the sheep reference genome *Oar_v3.1*. StringTie (23) was used for transcriptome assembly and reconstruction. Thus, known lncRNA and mRNA transcripts were identified, and the position of transcripts was obtained.

LncRNA Identification and Differentially Expression Analysis

Novel lncRNAs with more than two exons and lengths of more than 200 nt were predicted by CNCI (24), CPC (25), PFAM (26), and CPAT (27) software after transcriptome assembly. The fragments per kilobase per million mapped reads [FPKM (28)] values were calculated to represent the expression of genes and lncRNAs. To determine the effect of photoperiod on genes and lncRNAs expression in PT of sheep, the expression of genes and lncRNAs at every time point of LP (LP7, LP 21, or LP 42) was compared with the SP21 group using DESeq, i.e., SP 21 vs. LP 7, SP 21 vs. LP 21, and SP 21 vs. LP 42. In addition, $p < 0.05$ and |Fold change| >1 was considered standard of differential expression between the SP and LP.

GO and KEGG Pathway Enrichment Analysis of Differentially Expressed Genes and lncRNAs

Gene Ontology (GO) enrichment analysis of differentially expressed genes or lncRNA target genes was implemented by the GOseq R package, in which gene length bias was corrected (29). GO classifies functions into three groups: cellular components, molecular functions, and biological processes. The KEGG biological pathways database (http://www.genome.jp) is a central public database for understanding high-level functions and regulatory network research. Enrichment analysis was performed on each pathway in KEGG using a hypergeometric test. According to significant threshold (p-value: 0.05), the genes were screened and enriched for the pathways. Next, the significance of the pathway enrichment analysis was corrected by FDR, and the corrected p-value (q-value) was obtained.

Construction of Integral lncRNA–mRNA Interaction Networks

The primary role of lncRNAs, which are a type of non-coding RNA, is to regulate their target genes by cis-regulating nearby protein-coding genes and trans-regulating distal protein-coding genes. Here, protein coding genes with a distance of <100 Kb were assumed to be the cis-target genes, and Pearson correlation coefficients with the lncRNAs of >0.95 were assumed to represent the trans-target genes (30).

To further reveal the potential roles of lncRNAs that are involved in modulating the reproductive process, integral interaction networks containing lncRNAs and their corresponding target genes were built using Cytoscape software (31) in each comparison (SP 21 vs. LP 7, SP 21 vs. LP 21, and SP 21 vs. LP 42), which include cis- and trans-forms of regulation.

RNA-seq Data Validation

EYA3, *TSHB*, *CHGA*, *MSTRG.209166*, *MSTRG.22781*, and *MSTRG.42035* were selected to validate the accuracy of RNA sequencing *via* the reverse-transcription quantitative polymerase chain reaction (RT-qPCR). *GAPDH* was used as an internal reference to normalize target gene expression. All primers used in the RT-qPCR are shown in **Supplementary Table 1**. cDNA was used to perform RT-qPCR after reverse transcription from total RNA to cDNA. The RT-qPCR reaction conditions were as follows: 95°C for 15 min, followed by 40 cycles of 95°C for 10 s and 60°C for 30 s. The data obtained from RT-qPCR reaction were then calculated using the $2^{-\Delta\Delta Ct}$ method (32, 33) and processed by SPSS 19.0 with a one-way analysis of variance. The results are presented as means ± standard deviation. Furthermore, $p < 0.05$ was regarded as statistically significant.

RESULTS

Summary of Transcriptome Sequencing Data

To identify differentially expressed lncRNAs and genes between SP and LP, RNA libraries of different photoperiods were constructed. After removing low-quality sequences, a total of

TABLE 1 | Summary of raw reads after quality control and mapping to the reference genome.

Photoperiod	Sample	Raw reads	Clean reads	Clean reads rate (%)	Q30 (%)	Mapped reads	Mapping rate (%)
SP21	SP2101	125,660,438	122,442,196	97.44	96.91	115,418,878	94.26
	SP2102	125,942,826	122,243,686	97.06	95.9	114,892,152	93.99
	SP2103	132,973,810	129,237,768	97.19	95.94	121,797,173	94.24
LP7	LP701	113,017,724	109,422,884	96.82	94.45	102,336,864	93.52
	LP702	120,666,156	116,544,984	96.58	94.44	108,968,477	93.50
	LP703	120,732,238	117,373,382	97.22	96.09	110,710,654	94.32
LP21	LP2101	109,242,794	106,213,878	97.23	93.56	98,166,189	92.42
	LP2102	123,453,896	119,838,276	97.07	96.16	113,659,315	94.84
	LP2103	122,212,386	116,562,600	95.38	92.52	108,893,984	93.42
LP42	LP4201	112,488,634	109,485,312	97.33	93.83	101,355,097	92.57
	LP4202	108,789,602	105,051,072	96.56	94.51	98,080,693	93.36
	LP4203	123,811,728	120,508,540	97.33	95.94	113,375,002	94.08

SP, short photoperiod; LP, long photoperiod; Q30, the rate of bases whose quality is >30 Phred value in clean reads.

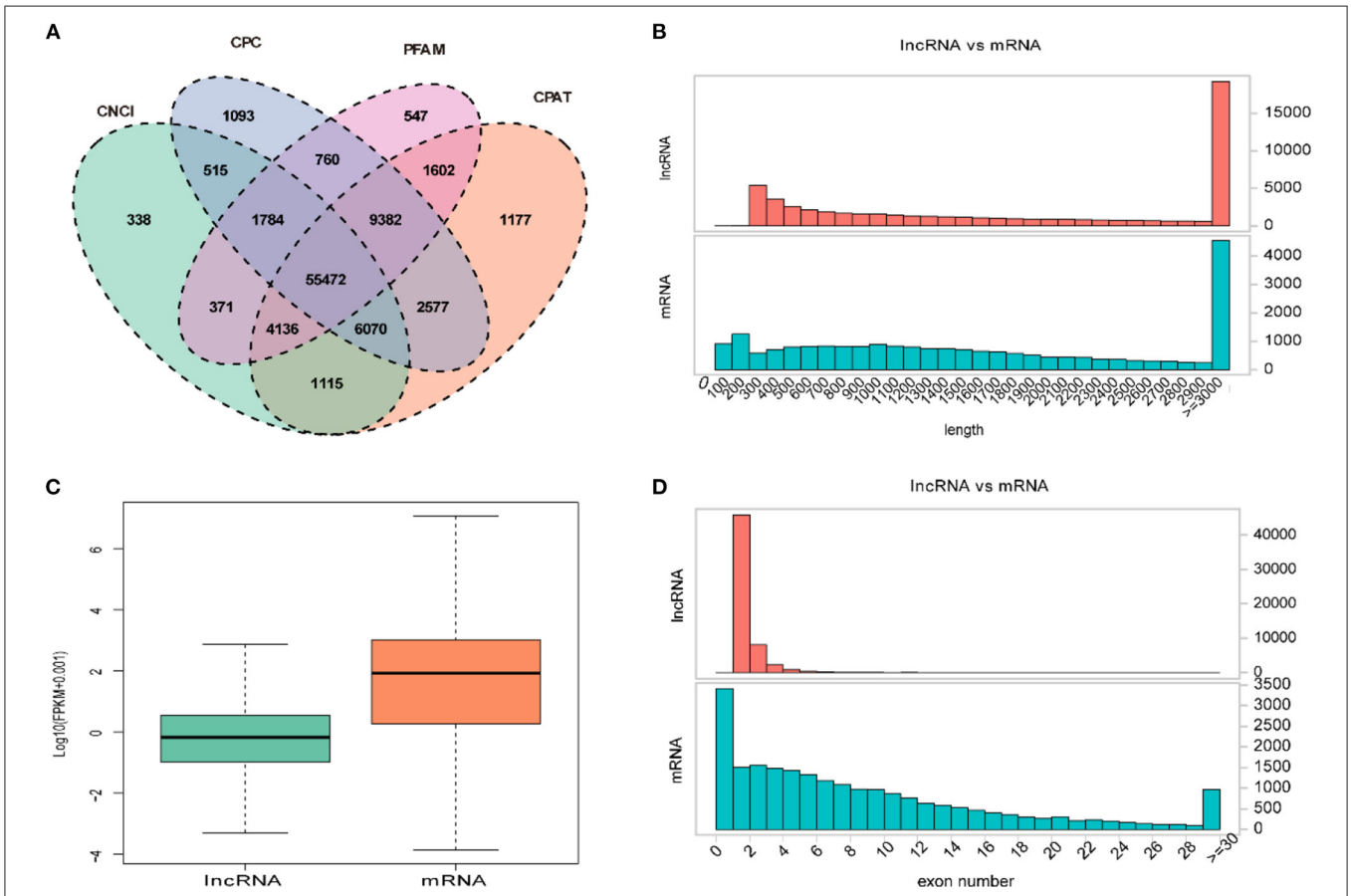

FIGURE 2 | Expression characteristics of lncRNAs and genes in the PT of ewes. **(A)** Venn diagram for screening lncRNAs by four software (CNCI, CPC, CAPT, and PFAM). The sum of the numbers in each large oval represents the total number of non-coding transcripts from each software, and the overlapping parts of the oval represent the non-coding transcripts common to the software. **(B)** The length distribution of lncRNAs and mRNAs. **(C)** The expression level of lncRNAs and mRNAs. **(D)** The exon number distribution of lncRNAs and mRNAs.

1,394,924,578 clean reads with >92.52% of Q30 were obtained after sequencing all 12 libraries. Approximately 92–95% of the reads were successfully aligned to the *Ovis aries* reference genome (*Oar_v3.1*) (**Table 1**).

Overall, a total of 55,472 lncRNAs were identified in PT of 12 ewes using four programs (CNCI, CPC, PFAM, and CAPT) (**Figure 2A**). The length distribution of lncRNAs was consistent with that of protein-coding gene (**Figure 2B**). Of them, the

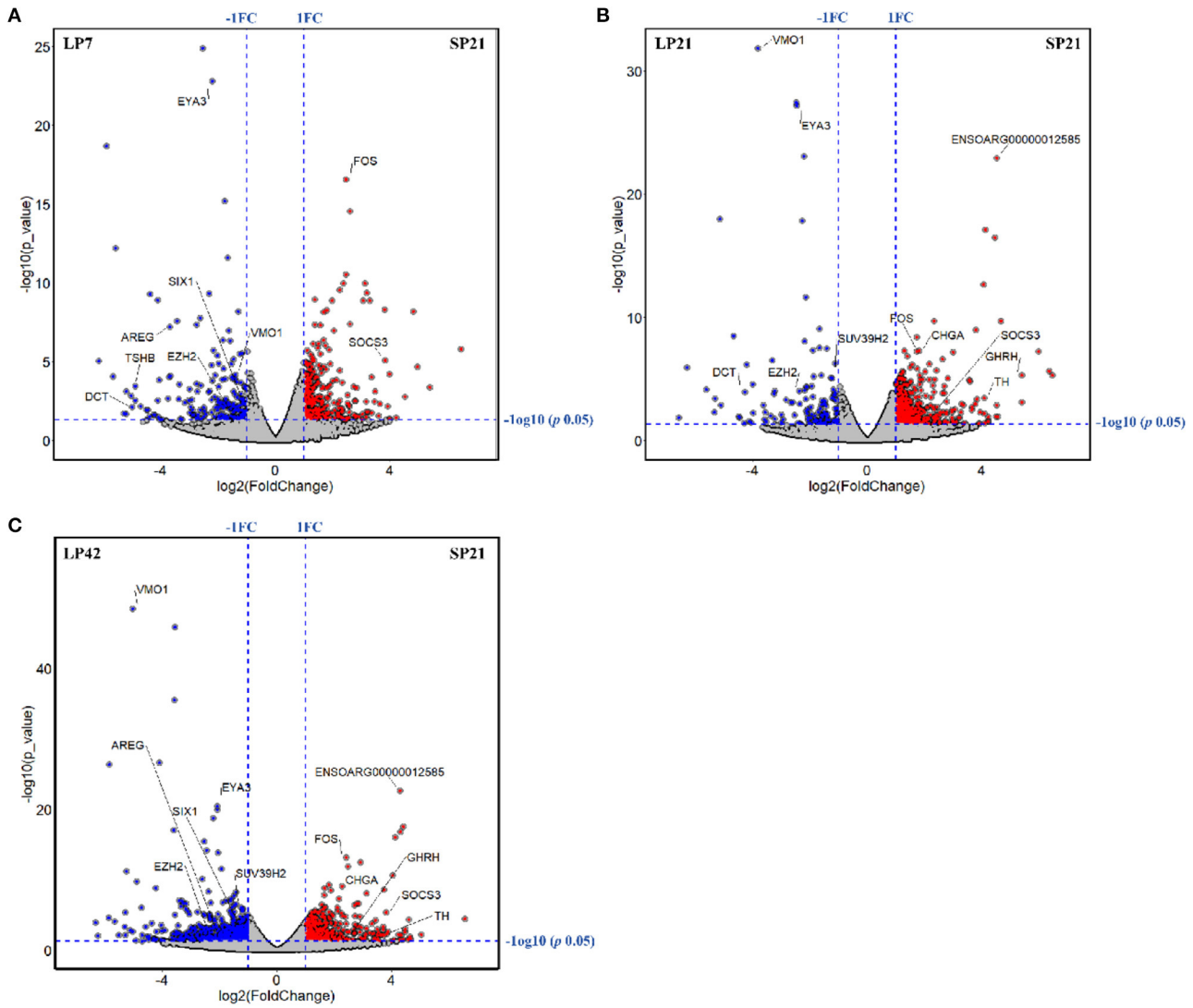

FIGURE 3 | The volcano plots of differentially expressed genes between long photoperiod (LP) and short photoperiod (SP) in PT of Sunite sheep. **(A)** The results of LP7 vs. SP21; **(B)** the results of LP21 vs. SP21; **(C)** the results of LP42 vs. SP21.

transcripts of lncRNAs and mRNAs with lengths of more than 3,000 bp accounted for the majority, and its number in lncRNAs was significantly greater than that in mRNAs (**Figure 2B**). However, transcript levels of lncRNAs were lower than those of mRNAs in the PT of Sunite ewes (**Figure 2C**). Most of the lncRNAs have only two or three exons, whereas mRNAs contain a wide range of exons from 2 to 30 (**Figure 2D**).

Photoperiod-Induced Factor Analysis Through Differentially Expressed Genes and lncRNAs

The number of differentially expressed (DE) genes between SP and LP increased gradually with the extension of LP (from LP7 to LP42). Specifically, there were 499 DE mRNAs in SP21 vs. LP7, in which *FOS*, *SOCS3*, *EYA3*, *TSHB*, *SIX1*, *DCT*, *VMO1*, *AREG*, and *EZH2* were related to reproduction (**Figure 3A**). In SP21 vs. LP21, 625 DE mRNAs were detected, including *CHGA*, *FOS*, *SOCS3*, *GHRH*, *TH*, *EYA3*, *TSHB*, *DCT*, *VMO1*, *SUV39H2*, and *EZH2* that were associated with reproduction (**Figure 3B**). In addition, 874 DE mRNAs were screened between the SP21 and LP42 group. Of them, the genes related to reproduction included *CHGA*, *FOS*, *SOCS3*, *GHRH*, *TH*, *EYA3*, *TSHB*, *SIX1*, *VMO1*, *AREG*, and *EZH2* (**Figure 3C**). The top 10 DE mRNAs in each contrast group are shown in **Table 2**. Among these genes, there are specific differentially expressed genes (*FOS*, *TMEM200A*, *MLIP*, *PMP2*, *PRX*, and *SPTBN5* and seven novel genes) that are different from previous reports (6, 7). Besides, for the top genes, it is worth paying attention to those genes that appear in the above contrast groups simultaneously,

TABLE 2 | The top 10 differentially expressed mRNAs in three comparisons between LP and SP.

Comparisons	Gene	*p*-value	Log2foldchange	Up/Down	Gene name
LP7 vs. SP21	ENSOARG00000014847	1.29E−25	−2.531934183	Up	*ENSOARG00000014847*
	ENSOARG00000003071	1.55E−23	−2.209131416	Up	*EYA3*
	ENSOARG00000002985	2.10E−19	−5.881442781	Up	*ENSOARG0000000298*
	ENSOARG00000001783	2.83E−17	2.460057284	Down	*FOS*
	ENSOARG00000017954	6.56E−16	−1.77693187	Up	*ACSL4*
	ENSOARG00000012585	2.89E−15	2.610496836	Down	*ENSOARG00000012585*
	ENSOARG00000015485	6.34E−13	−5.568818193	Up	*DQA*
	ENSOARG00000020015	2.54E−12	−1.658620427	Up	*TMEM200A*
	ENSOARG00000000857	3.00E−11	2.448160683	Down	*ENSOARG00000000857*
	ENSOARG00000003776	1.04E−10	3.130953431	Down	*ENSOARG00000003776*
LP21 vs. SP21	ENSOARG00000007112	1.47E−32	−3.819122926	Up	*VMO1*
	ENSOARG00000005662	9.30E−29	−9.037863894	Up	*ENSOARG00000005662*
	ENSOARG00000017954	3.92E−28	−2.474582452	Up	*ACSL4*
	ENSOARG00000003071	6.86E−28	−2.454903078	Up	*EYA3*
	ENSOARG00000008195	8.26E−24	−2.196263967	Up	*CYP4V2*
	ENSOARG00000012585	1.20E−23	4.510495819	Down	*ENSOARG00000012585*
	ENSOARG00000018081	1.59E−23	−8.570717405	Up	*BPIFC*
	ENSOARG00000008250	1.05E−18	−5.150050353	Up	*KLKB1*
	ENSOARG00000014847	1.50E−18	−2.278049468	Up	*ENSOARG00000014847*
	ENSOARG00000009143	7.84E−18	4.11635763	Down	*ENSOARG00000009143*
LP42 vs. SP21	ENSOARG00000009116	2.03E−56	−7.230483397	Up	*PMP2*
	ENSOARG00000007112	2.98E−49	−5.030524117	Up	*VMO1*
	ENSOARG00000017954	1.45E−46	−3.565896967	Up	*ACSL4*
	ENSOARG00000006792	2.83E−43	−7.98187898	Up	*MLIP*
	ENSOARG00000006630	3.02E−36	−3.574968045	Up	*PRX*
	ENSOARG00000020448	2.35E−27	−4.099272015	Up	*SPTBN5*
	ENSOARG00000008250	4.24E−27	−5.842338208	Up	*KLKB1*
	ENSOARG00000018081	1.34E−23	−8.659205306	Up	*BPIFC*
	ENSOARG00000012585	2.18E−23	4.291991999	Down	*ENSOARG00000012585*
	ENSOARG00000003071	3.48E−21	−2.091523071	Up	*EYA3*

and they are the most likely photoperiodic-induced factors in the regulation of seasonal reproduction. To sum up, the notable LP-induced genes included *EYA3*, *TSHB*, *VMO1, DCT*, and *EZH2*. SP-induced genes involved *ENSOARG00000012585*, *CHGA*, *FOS*, *SOCS3*, and *TH*. For lncRNAs, the number of DE lncRNAs was also increasing with the extension of the LP. Specifically, 1,887, 2,038, and 2,614 DE lncRNAs were detected in the SP21 vs. LP7 group (**Supplementary Table 5**), SP21 vs. LP21 group (**Supplementary Table 6**), and SP21 vs. LP42 group (**Supplementary Table 7**), respectively. These DE lncRNAs may be involved in the regulation of the expression of important genes for seasonal reproductive trait. Besides, our results had some common overlap DE mRNAs with the reports of Wood et al. (2015) and Lomet et al. (2017) (6, 7). The detailed information is shown in **Supplementary Table 8**.

GO Annotation and KEGG Enrichment Analysis of DE Genes and lncRNAs

GO and KEGG analyses were conducted for the differentially expressed mRNAs and target genes of differentially expressed lncRNAs. The top 10 enriched GO terms for lncRNAs and mRNAs of SP21 vs. LP7 (blue), SP21 vs. LP21 (orange), and SP21 vs. LP42 (green) are shown in **Figures 4A,B** (data in **Supplementary Tables 9–11** for lncRNAs and **Supplementary Tables 12–14** for mRNAs). The following GO terms are noteworthy, including neuron terms (such as neuron part, axon, synapse part, and response to stimulus), receptor terms (such as cell surface receptor signaling pathway and receptor complex), regulation of apoptosis process, regulation of cell death, regulation of cell proliferation, and metabolic process (such as regulation of metabolic process and positive regulation of phosphorus metabolic process). In order to further focus on the function of differentially expressed genes between SP and LP, we constructed a simplified network of related statistically significant GO terms (**Figure 4C**) for differentially expressed genes overlapping between SP and three of LP points using the Cytoscape add-on ClueGO (34, 35). The results emphasized enrichment for cell proliferation and differentiation, cell response and pathway, cell death and regulation, and the cytokine process, which might play an important role in the

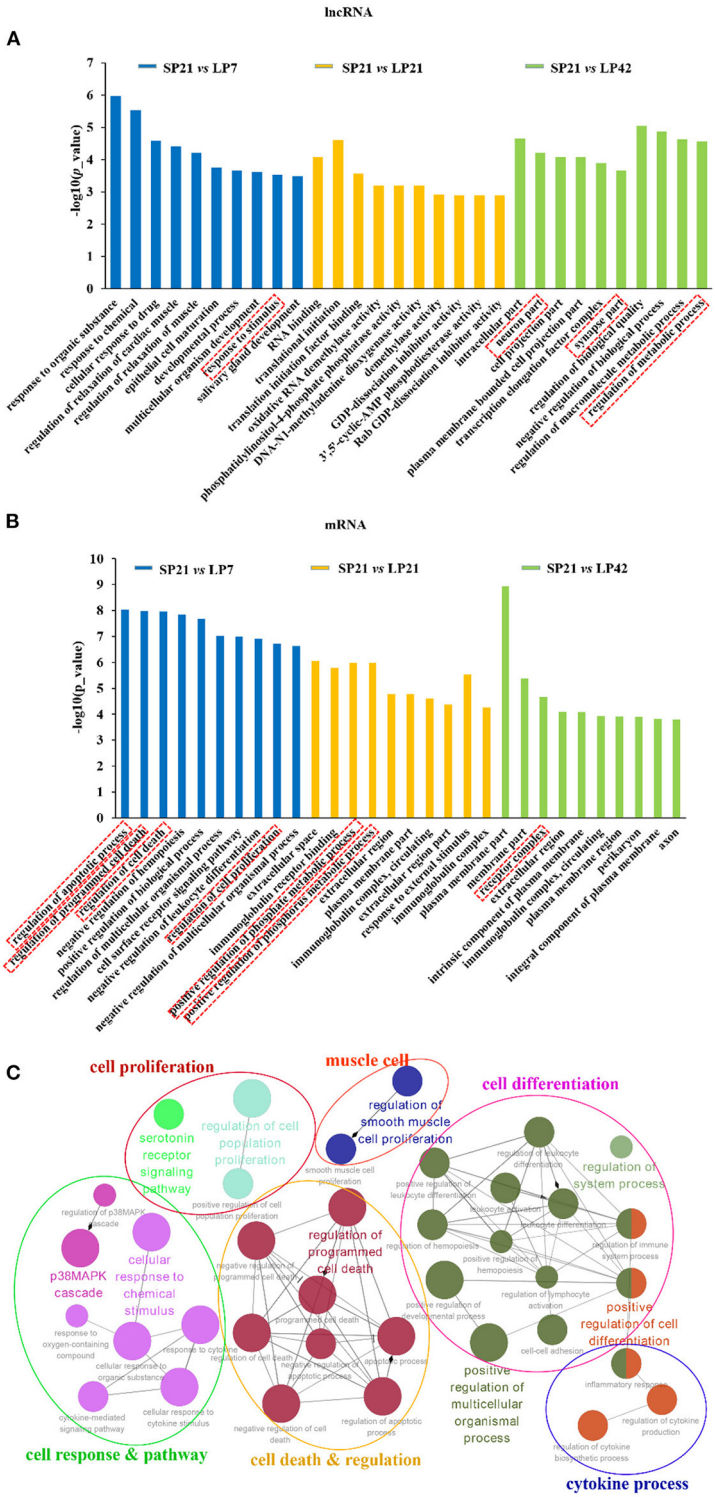

FIGURE 4 | Top enriched Gene Ontology (GO) terms of differentially expressed lncRNAs and genes between short photoperiod and long photoperiod in PT of Sunite sheep. **(A)** The top GO terms of target genes of differentially expressed LncRNAs; **(B)** the top GO terms of differentially expressed mRNAs. The GO terms in blue are from SP21 vs. LP7; those in orange are from SP21 vs. LP21, and those in green are from SP21 vs. LP42. **(C)** A simplified network of related statistically significant GO terms ($p < 0.01$) using the Cytoscape add-on ClueGO (34, 35). The network of overlap DE genes among SP21 vs. LP7, LP21, and LP42 are shown. The filled colored circles (nodes) represent each statistically significant parent GO term. The lines (edges) between the nodes show that there are overlapping genes within each term. The colored ovals group these parent GO terms into more generic functional descriptions. The red boxes represent the seasonal reproduction-related terms.

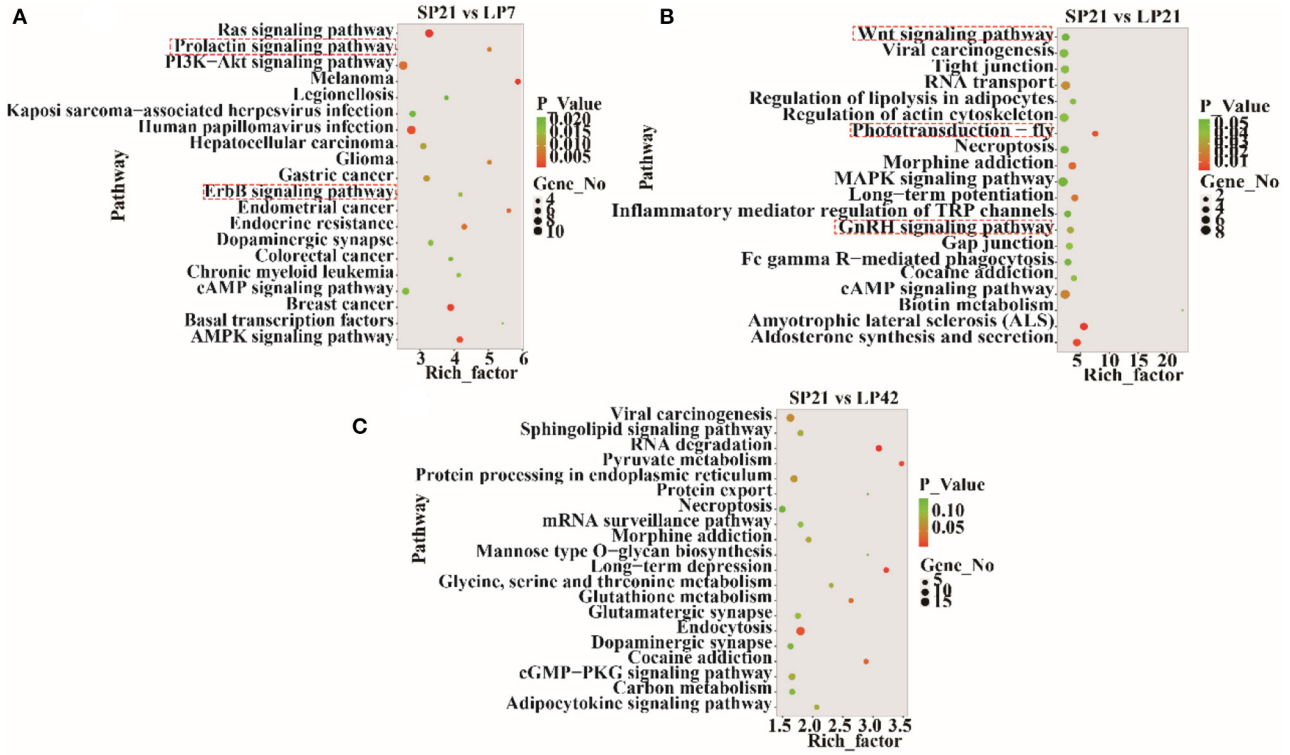

FIGURE 5 | KEGG pathway analysis for target genes of differentially expressed lncRNAs between short photoperiod and long photoperiod in PT of Sunite sheep. **(A)** Top 20 enrichment pathways in SP21 vs. LP7. **(B)** Top 20 enrichment pathways in SP21 vs. LP21. **(C)** Top 20 enrichment pathways in SP21 vs. LP42. Rich_factor is defined as the amount of differentially expressed genes enriched in the pathway/amount of all genes in the background gene set. The red boxes represent the seasonal reproduction-related terms.

regulation of seasonal breeding in sheep at the level of the PT/MBH (36, 37).

The top 20 enriched KEGG pathways for target genes of differentially expressed lncRNAs and pathways for differentially expressed mRNAs are shown in **Figures 5**, **6**, respectively. The most interesting pathways included reproduction-related pathways (Prolactin signaling pathway, ErbB signaling pathway, Wnt signaling pathway, MAPK signaling pathway, and GnRH signaling pathway in **Figure 5**; ErbB signaling pathway and MAPK signaling pathway in **Figure 6**), circadian related pathways (phototransduction-fly in **Figure 5**; circadian entrainment in **Figure 6**), and neuroactive ligand–receptor interaction, TNF signaling pathway, tyrosine metabolism, and neuroactive ligand–receptor interaction pathway (detailed data in **Supplementary Tables 15–17** for lncRNAs and **Supplementary Tables 18–20** for mRNAs). Here, we also combined the overlap DE genes from three comparisons and assigned KEGG terms to create a simplified network of related statistically significant KEGG terms (34, 35) (**Figure 7**). **Figure 7** also showed that many differentially expressed genes between SP and LP are enriched in pathways related to reproduction, such as signaling (prolactin signaling pathway, cAMP signaling pathway, and JAK-STAT signaling pathway), neuron, neurotransmitters, and cell process.

LncRNA–mRNA Network Construction

The differentially expressed lncRNAs and their target genes were selected to construct the lncRNA–mRNA network with co-expression information. In the network of SP21 vs. LP7, 23 differentially expressed lncRNAs and 21 target genes were included, among which the *trans* relationship between *MSTRG.209166* and *TSHB* was hinted (**Figure 8A**, **Supplementary Table 21**). In SP21 vs. LP21, 29 differentially expressed lncRNAs and 26 target genes were selected to construct network. Notably, *MSTRG.209166* was also found to *trans*-regulate *TSHB* and *MSTRG.235014 cis*-regulated *DDC*, because the two genes were important for seasonal reproduction (**Figure 8B**, **Supplementary Table 22**). In SP21 vs. LP42, 102 differentially expressed lncRNAs and 91 target genes formed a more sophisticated network. For several key genes of seasonal reproduction, several target combinations between lncRNAs and them were highlighted. For example, they implied that *MSTRG.209166 trans*-regulated *TSHB*, *MSTRG.288068 cis*-regulated *SIX1*, *MSTRG.272793 cis*-regulated *KIT*, and *ENSOARG00000026131 cis*-regulated *TH* (**Figure 8C**, **Supplementary Table 23**).

Gene Expression Validation

A total of six genes, namely, three mRNAs (*EYA3*, *TSHB*, and *CHGA*) related to seasonal reproduction and three random

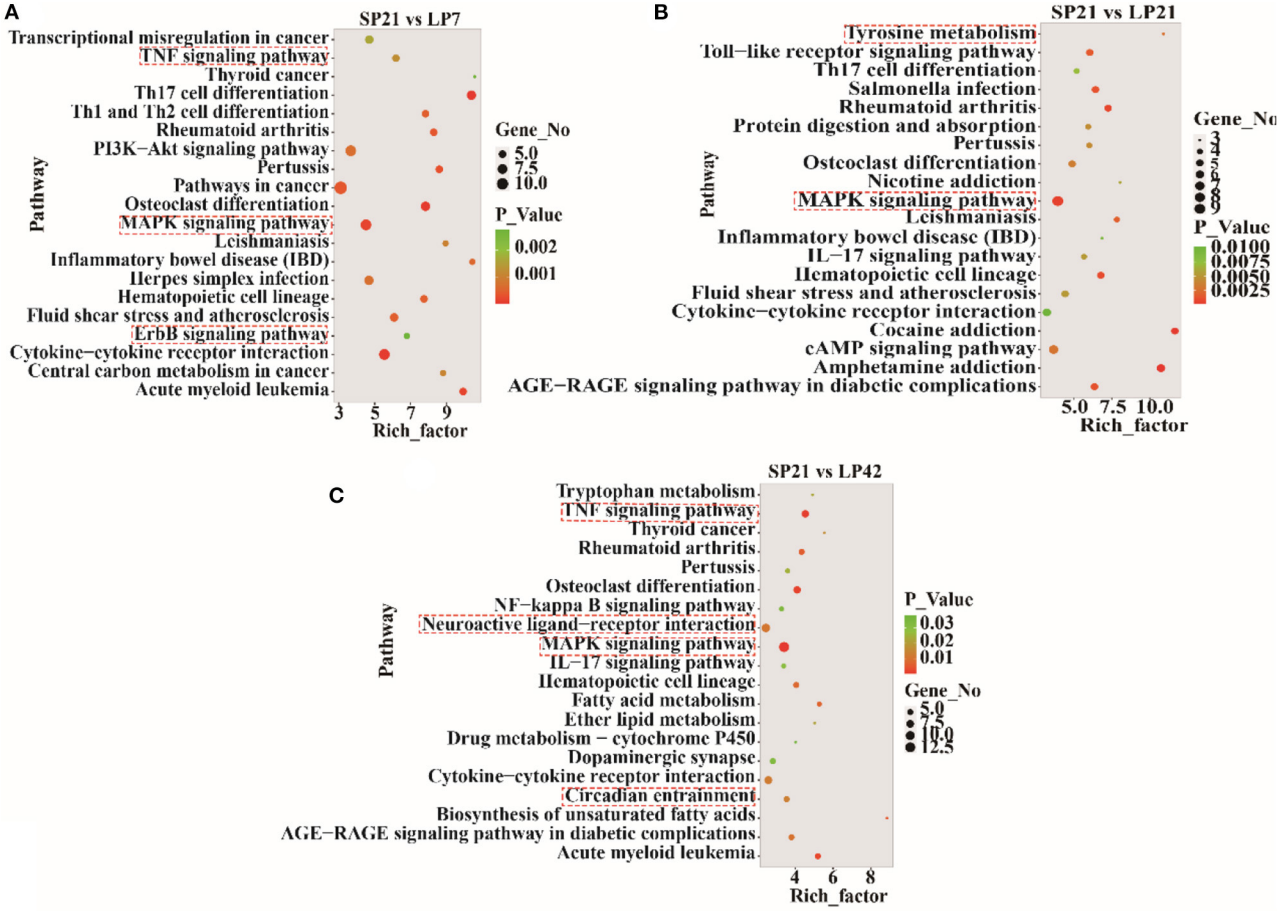

FIGURE 6 | KEGG pathway analysis of differentially expressed mRNAs between short photoperiod and long photoperiod in PT of Sunite sheep. **(A)** Top 20 enrichment pathways in SP21 vs. LP7. **(B)** Top 20 enrichment pathways in SP21 vs. LP21. **(C)** Top 20 enrichment pathways in SP21 vs. LP42. Rich_factor is defined as the amount of differentially expressed genes enriched in the pathway/amount of all genes in the background gene set. The red boxes represent the seasonal reproduction-related terms.

lncRNAs (*MSTRG.290436*, *MSTRG.22781*, and *MSTRG.17707*), were selected for RT-qPCR verification. The results indicated that there is a similar expression pattern between RNA-Seq and RT-qPCR data (**Figure 9**).

DISCUSSION

Seasonal reproduction is a result of adaptation of animal reproductive activities to environmental changes, which is essential for breeding success and survival of future generations. However, the detailed molecular mechanism of animal seasonal reproduction has not been fully revealed. So far, several key genes for seasonal reproduction have been found in animals, including *EYA3* gene in Japanese quail (38) and sheep (8), the vasoactive intestinal peptide (*VIP*) gene in Yangzhou goose (39), *TSHB* in sheep (8), *TSHB* and pituitary adenylate cyclase activating polypeptide (*PACAP*) in mice (19, 40), and *CHGA* and Tachykinin 1 (*TAC1*) in sheep (3, 7), which are mainly expressed in the pituitary PT. The pituitary PT is an important regulatory center for seasonal reproductive traits. Therefore, it was used as the target tissue in this study and the first objective of this study is to screen new candidate photoperiod-induced genes in PT of sheep.

Combined with the results of gene differential expression, GO, and KEGG pathway enrichment analyses, some important candidate genes were screened out. They included *CHGA*, *FOS*, *SOCS3*, *EYA3*, *TSHB*, *SIX1*, *GHRH*, *DCT*, *TH*, *VMO1*, *AREG*, *SUV39H2*, and *EZH2*, which were mainly involved in the following pathways: reproduction-related pathways, TNF signaling pathway, circadian entrainment, and tyrosine metabolism. Specifically, LP-induced genes included *EYA3*, *VMO1*, *TSHB*, *SIX1*, *GHRH*, *DCT*, *TH*, *VMO1*, *AREG*, *SUV39H2*, and *EZH2* and SP-induced genes involved *ENSOARG00000012585*, *CHGA*, *FOS*, *SOCS3*, and *TH*. Wood et al. (7) reported *CHGA* as a SP-activator, which had a significantly high expression at SP compared with LP in PT of rams. Our results in PT of ewes also further confirm that *CHGA* is a SP-induced gene. For *FOS*, *SOCS3*, and *ENSOARG00000012585*,

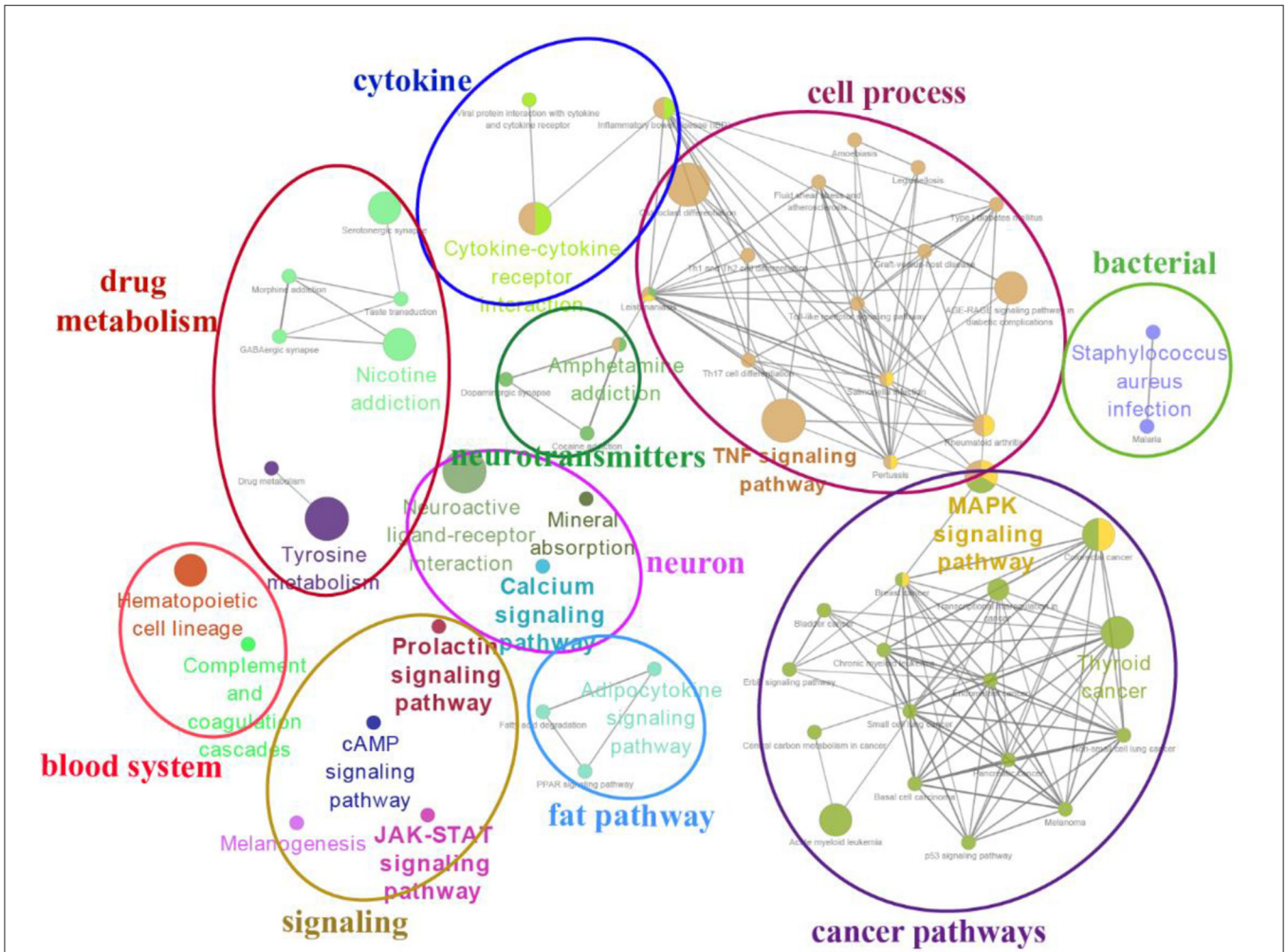

FIGURE 7 | A simplified network of related statistically KEGG pathways using the Cytoscape add-on ClueGO (34, 35). The network of overlap DE genes among SP21 vs. LP7, LP21, and LP42 are shown. The filled colored circles (nodes) represent each statistically parent KEGG pathway. The lines (edges) between the nodes show that there are overlapping genes within each pathway. The colored ovals group these parent KEGG pathways into more generic functional descriptions.

they may be considered as new candidate SP-induced genes in PT, whose function in PT need further analysis. The suprachiasmatic nuclei of the hypothalamus (SCN) are the master circadian clock in mammals. The role of *FOS* and *SOCS3* in SCN has been reported in long-day breeding animals (redheaded bunting, rat, and hamster), which are enriched in the TNF signaling pathway and circadian entrainment. Their expression patterns under SP and LP are opposite to those of short-day breeding animals (41–43). For example, *FOS* is predominantly expressed in the SCN of redheaded buntings under LP conditions (42). Moreover, our results showed that *FOS* was highly expressed in pituitary PT of sheep under SP. Photoperiod also modulated *SOCS3* gene expression and maintained its expression in a high level in the SCN of hamsters during LP compared with SP (44). Then, *SOCS3* conveys seasonal changes into leptin sensitivity in the Siberian hamster (44).

So far, several LP-induced genes have been revealed. *EYA3* and *TSHB*, as LP-induced genes, displayed a marked increase from SP to LP in PT of sheep (3, 7, 45). Similarly, in this study, *EYA3* and *TSHB* were LP-induced and went up at LP compared with SP in PT of ewes, further certifying the findings of previous studies (8, 15, 46). In both sheep and mouse, *EYA3* and its partner *SIX1* synergistically act as upstream inducers of the *TSHB* transcription to induce the expression of *TSHB* (8, 19). Furthermore, *TSHB* acts locally on *TSHR*-expressing cells in the adjacent basal hypothalamus, leading to altered expression of *DIO2* (5, 6, 47). Then, *DIO2* can regulate the secretion of TH in the basal hypothalamus and further modulate the transition of reproductive status through the spatial structure of GnRH neurons (7). When the GnRH neurons were wrapped by ependymal cells, little GnRH were released into pituitary, which caused the decrease of LH and FSH secretion, and eventually sheep entered the state of anestrus (7).

Tyrosine metabolism can mediate the biological effects of many hormones and cytokines on reproduction, immunity, and cell growth (48, 49). In this study, the DE *DCT* was enriched

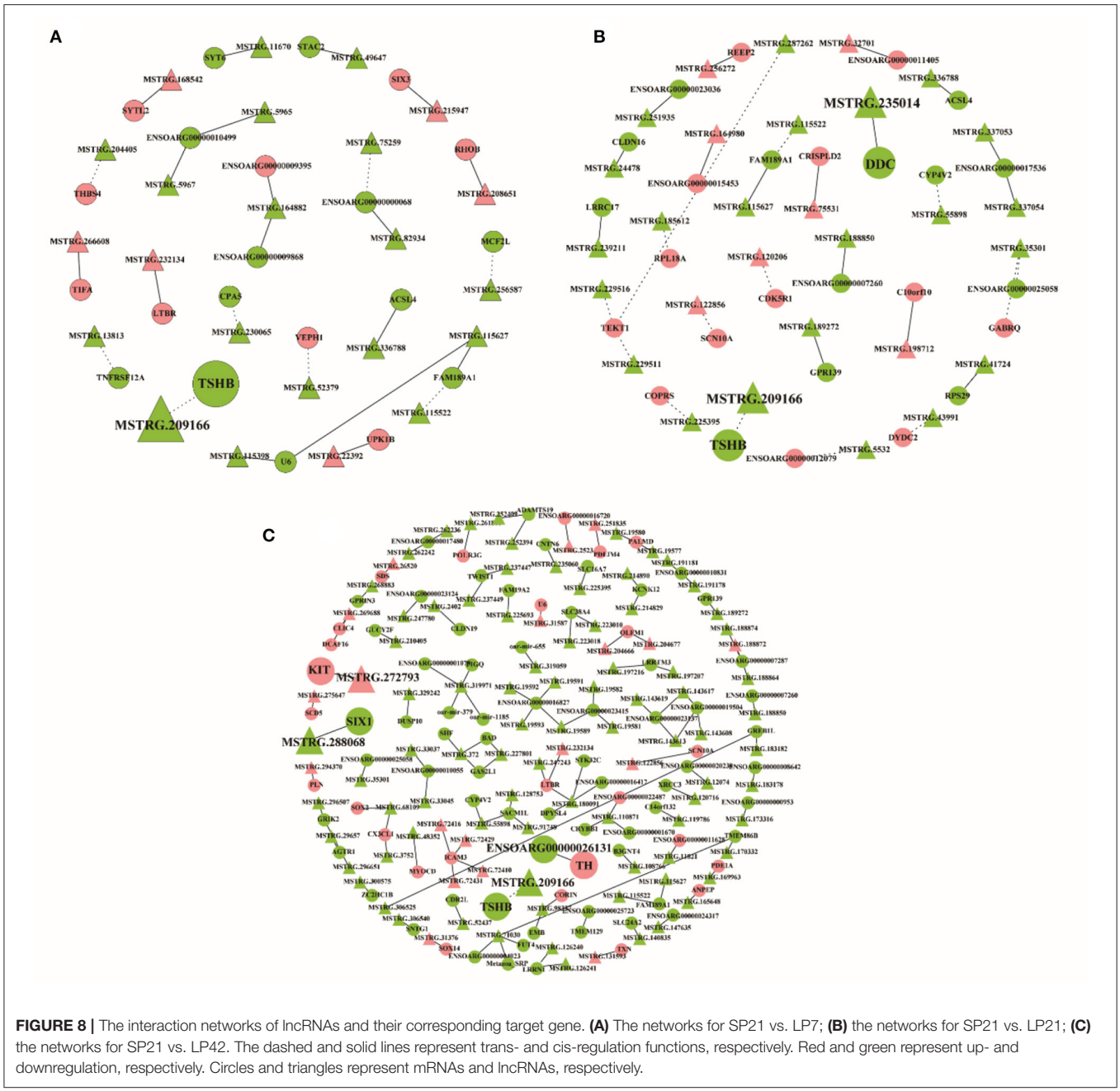

FIGURE 8 | The interaction networks of lncRNAs and their corresponding target gene. **(A)** The networks for SP21 vs. LP7; **(B)** the networks for SP21 vs. LP21; **(C)** the networks for SP21 vs. LP42. The dashed and solid lines represent trans- and cis-regulation functions, respectively. Red and green represent up- and downregulation, respectively. Circles and triangles represent mRNAs and lncRNAs, respectively.

in the tyrosine metabolism pathway. *DCT* was found as a novel long-day marker, whose expression levels in tanycytes lining the infra-lateral walls and floor of the ovine third ventricle showed marked increase with the extension of the photoperiod (6, 45). Similarly, in this study, *DCT* was significantly upregulated during LP compared with SP in PT of sheep. These results suggested that *DCT* expression was crucial for initiation of anestrus in sheep. Previous research has shown that *TH* can modulate *DCT* expression (46). *DCT* is a part of, or is driven by, the circannual clock in sheep. Therefore, these characteristics—LP induction and circannual changes in expression—place *DCT* in a list of key genes involved in seasonal timing, which had included *TSHB*, *EYA3*, *DIO2*, and *DIO3* (45, 46).

In this study, the expression level of *VMO1*, *AREG*, *SUV39H2*, and *EZH2* was also significantly higher during LP than those at SP in PT of sheep. As secreted factors, *VMO1* and *AREG* were found to be acutely induced by LP in MBH of Ile-de-France ewes (6). In polyovular species, the LH-driven signaling can promote oocyte maturation and cumulus expansion by *AREG*. In addition, murine data indicated that LH binding to LHCGR in mural granulosa cells will up-regulate *AREG* (50). However, the function of *AREG* gene in PT is still unknown,

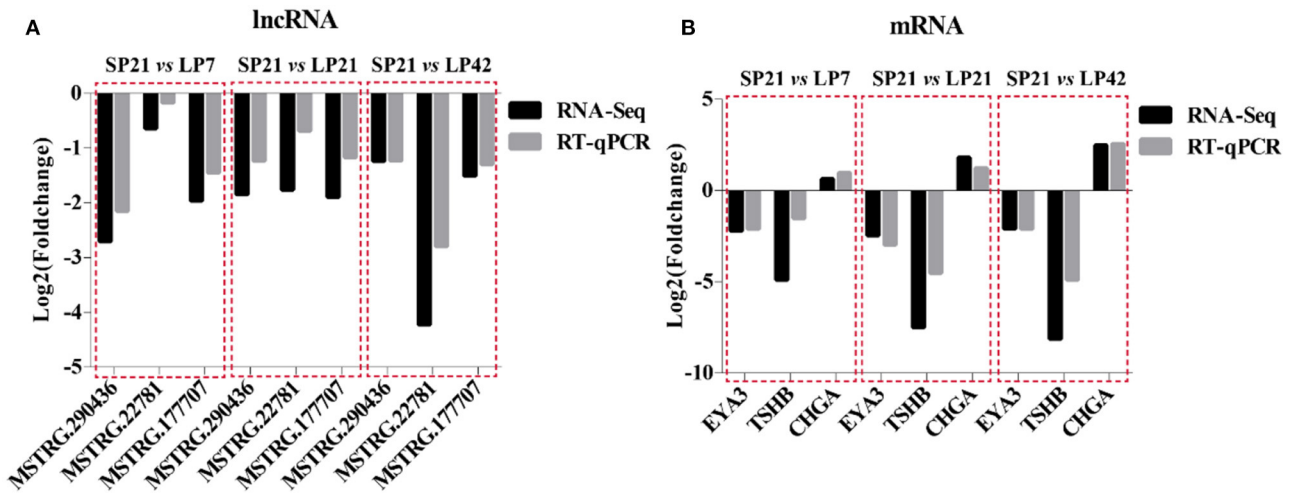

FIGURE 9 | Validation of RNA-Sequencing (RNA-seq) data using RT-qPCR. **(A)** RNA-Seq and RT-qPCR results of three selected differentially expressed lncRNAs in PT of Sunite sheep at different photoperiods. **(B)** RNA-Seq and RT-qPCR results of three selected differentially expressed mRNAs in PT of Sunite sheep at different photoperiods.

and it may be considered as a candidate LP-induced gene to analyze. For two histone methyltransferases genes, *SUV39H2* and *EZH2*, the results about seasonal changes of their expression in the PT are consistent with the hypothesis that epigenetic changes in PT cells are involved in circannual timing (6). Besides, the acute LP responsiveness of most of these markers (*TSHB*, *VMO1*, *EZH2*, and *EYA3*) is also in accordance with the findings from Dardente et al. (45) and Lomet et al. (6) in Ile-de-France ewes.

In recent years, studies have indicated that lncRNAs play important roles in many aspects of sheep reproductive regulation, such as fecundity (12, 13), gonadal development (14), and sex hormone response (15). As epigenetic regulators, lncRNAs can regulate the expression of reproduction-related genes. Thus, the other objective of this study is to predict lncRNAs that target key genes for seasonal reproduction in PT of sheep. Firstly, our result showed that the sequence length and exon number of mRNAs and lncRNAs in sheep pituitary have different patterns with those in hypothalamus of sheep (3,448 nt and 2.5 exons) (13). This implies that lncRNAs have tissue-specific characteristics. Then, through lncRNA–mRNA network construction, several notable target combinations between lncRNAs and key genes for seasonal reproduction were predicted. They specifically included the *trans* relationship between *MSTRG.209166* and *TSHB* and *cis* relationships between *MSTRG.235014* and *DDC*, *MSTRG.272793* and *KIT*, and *ENSOARG00000026131* and *TH*. Importantly, the *trans* relationship between *MSTRG.209166* and *TSHB* was shared among all of the comparison groups (SP vs. LP), which suggested that *MSTRG.209166* might play an important role in seasonal reproduction by regulating the expression of *TSHB*. TSHB is an important hub in the pathway of seasonal reproduction, so this study provides a new molecular object (*MSTRG.209166*) for the follow-up epigenetic regulation study of seasonal reproduction in sheep. In addition, the several candidate lncRNAs mentioned above (e.g., *MSTRG.235014*, *MSTRG.272793*, and *ENSOARG00000026131*) are also worthy of in-depth analysis.

CONCLUSION

In summary, our study provided a genome-wide view of lncRNA and mRNA expression profiling in pituitary PT of sheep during LPs and SPs. Several new candidate photoperiod-induced genes and lncRNAs targeting key genes of seasonal reproduction were predicted in PT of sheep. These results will provide new clues for understanding the molecular regulation of seasonal reproduction in sheep.

DATA AVAILABILITY STATEMENT

The datasets presented in this study can be found in online repositories. The names of the repository/repositories and accession number(s) can be found below: NCBI BioProject; PRJNA680667.

ETHICS STATEMENT

The animal study was reviewed and approved by The Science Research Department (in charge of animal welfare issue) of the Institute of Animal Sciences, Chinese Academy of Agricultural Sciences (IAS-CAAS; Beijing, China) (No. IAS2018-3,10 April 2018). Written informed consent was obtained from the owners for the participation of their animals in this study.

AUTHOR CONTRIBUTIONS

QX and MC: design of experiment and analysis for PT of sheep. QL and XH: construction of the OVX+E2 sheep model and light control experiment. RD: Experimental guidance and writing. XZ, JZ, and XG: light control experiment and collection of samples.

FUNDING

This research was funded by the following bodies: the National Natural Science Foundation of China (31861143012, 31472078, and 31772580), the Earmarked Fund for China Agriculture Research System (CARS-38), the Agricultural Science and Technology Innovation Program of China (ASTIP-IAS13), the China High-level Talents Special Support Plan Scientific and Technological Innovation Leading Talents Program (W02020274), the Tianjin Agricultural Science and Technology Achievements Transformation and Popularization Program (201704020), and the Youth Innovative Research and Experimental Project of Tianjin Academy of Agricultural Sciences (2020013). The APC was funded by the National Natural Science Foundation of China (31861143012). The funding bodies had no role in the design of the study and collection, analysis, and interpretation of data and in writing the manuscript.

SUPPLEMENTARY MATERIAL

The Supplementary Material for this article can be found online at: https://www.frontiersin.org/articles/10.3389/fvets.2021.644474/full#supplementary-material

REFERENCES

1. Ebling FJP, Foster DL. Photoperiod requirements for puberty differ from those for the onset of the adult breeding season in female sheep. *J Reprod Fertil.* (1988) 84:283–93. doi: 10.1530/jrf.0.0840283
2. La Y, He X, Zhang L, Di R, Chu M. Comprehensive analysis of differentially expressed profiles of mRNA, lncRNA, and circRNA in the uterus of seasonal reproduction sheep. *Genes.* (2020) 11:301. doi: 10.3390/genes11030301
3. Dupré SM, Miedzinska K, Duval CV, Yu L, Goodman RL, Lincoln GA, et al. Identification of Eya3 and TAC1 as long-day signals in the sheep pituitary. *Curr Biol.* (2010) 20:829–35. doi: 10.1016/j.cub.2010.02.066
4. Li X Y, He X Y, Liu Q Y, Wang X Y, Guo X F, Xia Q, et al. Expression pattern analysis of TAC1 and PRLR genes in different reproductive states of sheep. *Acta Vet Zootech Sin.* (2018) 49:253–62.
5. Hanon EA, Lincoln GA, Fustin J-M, Dardente H, Masson-Pévet M, Morgan PJ, et al. Ancestral TSH mechanism signals summer in a photoperiodic mammal. *Curr Biol.* (2008) 18:1147–52. doi: 10.1016/j.cub.2008.06.076
6. Lomet D, Juliette C, Chesneau D, Dubois E, Hazlerigg D, Dardente H. The impact of thyroid hormone in seasonal breeding has a restricted transcriptional signature. *Cell Mol Life Sci.* (2018) 75:905–19. doi: 10.1007/s00018-017-2667-x
7. Wood SH, Christian HC, Miedzinska K, Saer BRC, Johnson M, Paton B, et al. Binary switching of calendar cells in the pituitary defines the phase of the circannual cycle in mammals. *Curr Biol.* (2015) 25:2651–62. doi: 10.1016/j.cub.2015.09.014
8. Dardente H, Wyse CA, Birnie MJ, Dupré SM, Loudon ASI, Lincoln GA, et al. A molecular switch for photoperiod responsiveness in mammals. *Curr biol.* (2010) 20:2193–8. doi: 10.1016/j.cub.2010.10.048
9. Miao X, Luo Q, Zhao H, Qin X. Ovarian transcriptomic study reveals the differential regulation of miRNAs and lncRNAs related to fecundity in different sheep. *Sci Rep.* (2016) 6:35299. doi: 10.1038/srep35299
10. Miao X, Luo Q, Zhao H, Qin X. Co-expression analysis and identification of fecundity-related long non-coding RNAs in sheep ovaries. *Sci Rep.* (2016) 6:39398. doi: 10.1038/srep39398
11. Feng X, Li F, Wang F, Zhang G, Pang J, Ren C, et al. Genome-wide differential expression profiling of mRNAs and lncRNAs associated with prolificacy in Hu sheep. *Biosci Rep.* (2018) 38:BSR20171350. doi: 10.1042/BSR20171350
12. He X, Tao L, Zhong Y, Di R, Xia Q, Wang X, et al. Photoperiod induced the pituitary differential regulation of lncRNAs and mRNAs related to reproduction in sheep. *PeerJ.* (2021) 9:e10953. doi: 10.7717/peerj.10953
13. Zhang ZB, Tang JS, Di R, Liu QY, Wang XY. Comparative transcriptomics reveal key sheep (Ovis aries) hypothalamus LncRNAs that affect reproduction. *Animals.* (2019) 9:152. doi: 10.3390/ani9040152
14. Mulvey BB, Olcese U, Cabrera JR, Horabin JI, An interactive network of long non-coding RNAs facilitates the Drosophila sex determination decision. *Biochim Biophys Acta.* (2014) 1839:773–84. doi: 10.1016/j.bbagrm.2014.06.007
15. Li W, Notani D, Ma Q, Tanasa B, Nunez E, Chen AY, et al. Functional roles of enhancer RNAs for oestrogen-dependent transcriptional activation. *Nature.* (2013) 498:516–20. doi: 10.1038/nature12210
16. Smith JT, Clay CM, Caraty A, Clarke IJ. KiSS-1 messenger ribonucleic acid expression in the hypothalamus of the ewe is regulated by sex steroids and season. *Endocrinology.* (2007) 148:1150–7. doi: 10.1210/en.2006-1435
17. Karsch FJ, Bittman EL, Foster DL, Goodman TL, Legan SJ, Robinson JE. Neuroendocrine basis of seasonal reproduction. *Recent Prog Horm Res.* (1984) 40:185–232. doi: 10.1016/B978-0-12-571140-1.50010-4
18. Legan SJ, Karsch FJ, Foster DL. The endocrin control of seasonal reproductive function in the ewe: a marked change in response to the negative feedback action of estradiol on luteinizing hormone secretion. *Endocrinology.* (1977) 101:818–24. doi: 10.1210/endo-101-3-818
19. Masumoto KH, Ukai-Tadenuma M, Kasukawa T, Nagano M, Uno KD, Tsujino K, et al. Acute induction of Eya3 by late-night light stimulation triggers TSHβ expression in photoperiodism. *Curr Biol.* (2010) 20:2199–06. doi: 10.1016/j.cub.2010.11.038
20. Wood S, Loudon A. Clocks for all seasons: unwinding the roles and mechanisms of circadian and interval timers in the hypothalamus and pituitary. *J Endocrinol.* (2014) 222:R39–59. doi: 10.1530/JOE-14-0141
21. Tsujino K, Narumi R, Masumoto KH, Susaki EA, Shinohara Y, Abe T, et al. Establishment of TSH β real-time monitoring system in mammalian photoperiodism. *Genes Cells.* (2013) 18:575–88. doi: 10.1111/gtc.12063
22. Pertea M, Kim D, Pertea GM, Leek JT, Salzberg SL. Transcript-level expression analysis of RNA-seq experiments with HISAT, StringTie and Ballgown. *Nat Protoc.* (2016) 11:1650–67. doi: 10.1038/nprot.2016.095
23. Pertea M, Pertea GM, Antonescu CM, Chang TC, Mendell JT, Salzberg SL. StringTie enables improved reconstruction of a transcriptome from RNA-seq reads. *Nat Biotechnol.* (2015) 33:290–5. doi: 10.1038/nbt.3122
24. Sun L, Luo HT, Bu DC, Zhao GG, Yu K. Utilizing sequence intrinsic composition to classify protein-coding and long non-coding transcripts. *Nucleic Acids Res.* (2013) 41:e166. doi: 10.1093/nar/gkt646
25. Kong L, Zhang Y, Ye Z Q, Liu X Q, Zhao S Q, Wei L, et al. CPC: assess the protein-coding potential of transcripts using sequence features and support vector machine. *Nucleic Acids Res.* (2007) 35:W345–9. doi: 10.1093/nar/gkm391
26. El-Gebali S, Mistry J, Bateman A, Eddy S R, Luciani A, Potter S C, et al. The Pfam protein families database in 2019. *Nucleic Acids Res.* (2019) 47:D427–32. doi: 10.1093/nar/gky995

27. Wang L, Jung PH, Surendra D, Wang S, Jean-Pierre K, Li W. CPAT: Coding-Potential Assessment Tool using an alignment-free logistic regression model. *Nucleic Acids Res.* (2013) 41:e74. doi: 10.1093/nar/gkt006
28. Trapnell C, Williams BA, Pertea G, Mortazavi A, Pachter L. Transcript assembly and quantification by RNA-Seq reveals unannotated transcripts and isoform switching during cell differentiation. *Nat Biotechnol.* (2010) 28:511–5. doi: 10.1038/nbt.1621
29. Young M D, Wakefield M J, Smyth G K, Oshlack A. Gene ontology analysis for rna-seq: accounting for selection bias. *Genome Biol.* (2010) 11:R14. doi: 10.1186/gb-2010-11-2-r14
30. Fatica A, Bozzoni I. Long non-coding RNAs: new players in cell differentiation and development. *Nat Rev Genet.* (2014) 15:7–21. doi: 10.1038/nrg3606
31. Shannon P, Markiel A, Ozier O, Baliga N S, Wang J T, Ramage D, et al. Cytoscape: a software environment for integrated models of biomolecular interaction networks. *Genome Res.* (2003) 13:2498–504. doi: 10.1101/gr.1239303
32. Livak KJ, Schmittgen TD. Analysis of relative gene expression data using real-time quantitative PCR and the 2(-delta delta C(T)) method. *Methods.* (2001) 25:402–8. doi: 10.1006/meth.2001.1262
33. Livak KJ. Analyzing real-time PCR data by the comparative c(t) method. *Nat Protoc.* (2008) 3:1101–8. doi: 10.1038/nprot.2008.73
34. Bindea G, Mlecnik B, Hackl H, Charoentong P, Tosolini M, Kirilovsky A, et al. ClueGO: a Cytoscape plug-in to decipher functionally grouped gene ontology and pathway annotation networks. *Bioinformatics.* (2009) 25:1091–3. doi: 10.1093/bioinformatics/btp101
35. Bindea G, Galon J, Mlecnik B. CluePedia Cytoscape plugin: pathway insights using integrated experimental and in silico data. *Bioinformatics.* (2013) 29:661–3. doi: 10.1093/bioinformatics/btt019
36. Lincoln GA, Andersson H, Hazlerigg D. Clock genes and the long-term regulation of prolactin secretion: evidence for a photoperiod/circannual timer in the pars tuberalis. *J Neuroendocrinol.* (2003) 15:390–7. doi: 10.1046/j.1365-2826.2003.00990.x
37. Dardente H, Migaud M. Thyroid hormone and hypothalamic stem cells in seasonal functions. *Vitam Horm.* (2021) 116:91–131. doi: 10.1016/bs.vh.2021.02.005
38. Nakao N, Ono H, Yamamura T, Anraku T, Takagi T, Higashi K, et al. Thyrotrophin in the pars tuberalis triggers photoperiodic response. *Nature.* (2008) 452:317–22. doi: 10.1038/nature06738
39. Zhu HX, Chen Z, Shao XB, Yu JN, Wei CK, Dai ZC, et al. Reproductiveaxis gene regulation during photostimulation and photorefractoriness in Yangzhou goose ganders. *Front Zool.* (2017) 14:11. doi: 10.1186/s12983-017-0200-6
40. Hannibal J, Georg B, Fahrenkrug J. PAC1- and VPAC2 receptors in light regulated behavior and physiology: studies in single and double mutant mice. *PLos ONE.* (2017) 12:e0188166. doi: 10.1371/journal.pone.0188166
41. Veen DRvd, Pol-Meijer MMTvd, Jansen K, Smeets M, Zee EAVD, Gerkema MP. Circadian rhythms of c-FOS expression in the suprachiasmatic nuclei of the common vole (Microtus arvalis). *Chronobiol In.* (2008) 25:481–99. doi: 10.1080/07420520802254403
42. Majumdar G, Yadav G, Rani S, Kumar V. A photoperiodic molecular response in migratory redheaded bunting exposed to a single long day. *Gen Comp Endocrinol.* (2014) 204:104–13. doi: 10.1016/j.ygcen.2014.04.013
43. Jennings KJ, Chasles M, Cho H, Mikkelsen J, Bentley G, Keller M, et al. The preoptic area and the RFamide-related peptide neuronal system gate seasonal changes in chemosensory processing. *Integr Comp Biol.* (2017) 57:1055–65. doi: 10.1093/icb/icx099
44. Alexander T, Claire E, Moar KM, Logie TJ, Adam CL, Mercer JG, et al. Photoperiodic regulation of leptin sensitivity in the Siberian hamster, Phodopus sungorus, is reflected in arcuate nucleus SOCS-3 (suppressor of cytokine signaling) gene expression. *Endocrinology.* (2004) 145:1185–93. doi: 10.1210/en.2003-1382
45. Dardente H, Lomet D, Chesneau D, Pellicer-Rubio MT, Hazlerigg D. Discontinuity in the molecular neuroendocrine response to increasing daylengths in Ile-de-France ewes: is transient Dio2 induction a key feature of circannual timing? *J Neuroendocrinol.* (2019) 31:e12775. doi: 10.1111/jne.12775
46. Dardente H, Lomet D. Photoperiod and thyroid hormone regulate expression of L-Dopachrome tautomerase (Dct), a melanocyte stem-cell marker, in tanycytes of the ovine hypothalamus. *J Neuroendocrinol.* (2018) 30:e12640. doi: 10.1111/jne.12640
47. Trivedi AK, Sur S, Sharma A, Taufique ST, Kumar V. Temperature alters the hypothalamic transcription of photoperiod responsive genes in induction of seasonal response in migratory redheaded buntings. *Mol Cell Endocrino.* (2019) 493:110454. doi: 10.1016/j.mce.2019.110454
48. Rui H, Xu J, Mehta S, Fang H, Williams J, Dong F, et al. Activation of the Jak2-Stat5 signaling pathway in Nb2 lymphoma cells by an anti-apoptotic agent, aurintricarboxylic acid. *J Biol Chem.* (1998) 273:28–32. doi: 10.1074/jbc.273.1.28
49. Zhao Y, Kan FWK. Human OVGP1 enhances tyrosine phosphorylation of proteins in the fibrous sheath involving AKAP3 and increases sperm-zona binding. *J Assist Reprod Genet.* (2019) 36:1363–77. doi: 10.1007/s10815-019-01502-0
50. Park JY. EGF-like growth factors as mediators of LH action in the ovulatory follicle. *Science.* (2004) 303:682–4. doi: 10.1126/science.1092463

Conflict of Interest: The authors declare that the research was conducted in the absence of any commercial or financial relationships that could be construed as a potential conflict of interest.

Publisher's Note: All claims expressed in this article are solely those of the authors and do not necessarily represent those of their affiliated organizations, or those of the publisher, the editors and the reviewers. Any product that may be evaluated in this article, or claim that may be made by its manufacturer, is not guaranteed or endorsed by the publisher.

frontiers in Genetics

DATA REPORT
published: 17 August 2021
doi: 10.3389/fgene.2021.714852

iSheep: an Integrated Resource for Sheep Genome, Variant and Phenotype

Zhong-Huang Wang[1,2†], Qiang-Hui Zhu[2,3†], Xin Li[2,3†], Jun-Wei Zhu[1], Dong-Mei Tian[1], Si-Si Zhang[1], Hai-Long Kang[1,2], Cui-Ping Li[1], Li-Li Dong[1], Wen-Ming Zhao[1,2] and Meng-Hua Li[4*]*

[1] National Genomics Data Center, Beijing Institute of Genomics, Chinese Academy of Sciences (China National Center for Bioinformation), Beijing, China, [2] College of Life Sciences, University of Chinese Academy of Sciences (UCAS), Beijing, China, [3] CAS Key Laboratory of Animal Ecology and Conservation Biology, Institute of Zoology, Chinese Academy of Sciences, Beijing, China, [4] College of Animal Science and Technology, China Agricultural University, Beijing, China

Keywords: iSheep, databases, variant, phenotype, annotation

OPEN ACCESS

Edited by:
Rui Su,
Inner Mongolia Agricultural University, China

Reviewed by:
Feng Wang,
Nanjing Agricultural University, China
Yu Jiang,
Northwest A and F University, China

****Correspondence:***
Wen-Ming Zhao
zhaowm@big.ac.cn
Meng-Hua Li
menghua.li@cau.edu.cn

† These authors have contributed equally to this work

Specialty section:
This article was submitted to Livestock Genomics, a section of the journal Frontiers in Genetics

Received: *26 May 2021*
Accepted: *23 July 2021*
Published: *17 August 2021*

Citation:
Wang Z-H, Zhu Q-H, Li X, Zhu J-W, Tian D-M, Zhang S-S, Kang H-L, Li C-P, Dong L-L, Zhao W-M and Li M-H (2021) iSheep: an Integrated Resource for Sheep Genome, Variant and Phenotype. Front. Genet. 12:714852. doi: 10.3389/fgene.2021.714852

INTRODUCTION

Sheep (*Ovis aries*), one of the main and oldest livestock in the world, are particularly beneficial to human society by supplying wool, meat, milk, and skins. They have been domesticated *ca.* 8,000–12,000 years B.P. (Zeder, 2008). Being one of the earliest domesticated animals and one of the closest animals to human, sheep are also useful in revealing the history of early human settlements and expansions by analyzing their patterns of genetic variants (Zhao et al., 2017; Hu et al., 2019a; Deng et al., 2020).

The completion of a sheep reference genome (Jiang et al., 2014) and rapid advancement in high-throughput sequencing technologies have greatly accelerated the understanding of domestication, evolution and genetic mechanisms underlying various phenotypic traits in sheep (Lv et al., 2014; Yang et al., 2016; Alberto et al., 2018; Naval-Sanchez et al., 2018; Li et al., 2020). With the amount of increasing genomic data, establishing a systematic database in sheep for data archiving, analyzing and visualization becomes particularly essential, since so far only few databases are available for sheep compared with a variety of integrated resources established in mice (Laulederkind et al., 2013), dogs (Tang et al., 2019) and cattle (Elsik et al., 2016).

To date, one of the most widely accessible genetic databases for sheep is the International Sheep Genomics Consortium (ISGC, https://www.sheephapmap.org/). The ISGC database contains sheep genome assemblies and variants of 935 sheep representing 69 breeds from 21 countries. The ISGC database consists of around 50 million filtered variants called using GATK and Samtools programs based on the reference genome assembly Oar_v3.1. Also, it comprises the results at European Variation Archive (EVA) and the genotypes of several SNP chip arrays (Illumina 15K, 50K and HD 600K SNP chips). For the EVA database, users can't obtain complete VCF files in its variant browser. Meanwhile, the EVA data set has gathered a large amount of genetic data, but the information on raw sequencing, annotation, breed and phenotype still remains underdeveloped. Another public database, dbSNP (https://www.ncbi.nlm.nih.gov/snp/), was established in 1999 by the National Center for Biotechnology Information (NCBI, https://www.ncbi.nlm.nih.gov/), which has collected variation information of *Homo sapiens*, *Mus musculus* and other species (Sherry et al., 2001). However, dbSNP has discontinued to update non-human variations since 2017 (https://ncbiinsights.ncbi.nlm.nih.gov/2017/05/09/phasing-out-support-for-non-human-genome-organism-data-in-dbsnp-and-dbvar/#more-1122), which brings inconvenience for research communities to use non-human variations. As a complementary resource to the dbSNP, the Genome Variation Map (GVM, https://ngdc.cncb.ac.cn/gvm/) is dedicated to collecting, integrating, and visualizing different types of genome variations for a series

of species from all over the world (Song et al., 2018; Li et al., 2021). Up to 2021, the latest version of GVM has included 355 next generation sequencing (NGS) deposits of wild and domestic sheep (Li et al., 2021), which is a large data set, but lacks functional genetic variants and related information.

Here, we present iSheep (https://ngdc.cncb.ac.cn/isheep/), a specialized, integrated, and open-access resource for sheep. It consists of whole genome raw sequencing data, genomic variants, functional annotations, breed information and phenotypic traits (including morphological, production and disease-resistance traits). It also provides a world-wide public and free data service. Furthermore, iSheep incorporates online data analysis tools for data mining, genome navigation and annotation, which will not only be useful for the sheep research communities but also benefit a large number of sheep breeders.

MATERIALS AND METHODS

The pipeline for database construction is shown in **Figure 1**, and details are described in Data collection, Data processing, and Database implementation.

Data Collection

Whole-genome sequencing (WGS) data with a depth of 4∼40× coverage were collected from two sources: 126 samples from the GVM database, and 229 samples from Yang et al. (2016) and Hu et al. (2019a). All the raw WGS data were deposited in the Genome Sequence Archive (GSA, https://ngdc.cncb.ac.cn/gsa/), which is a core data resource of the National Genomics Data Center (NGDC, https://ngdc.cncb.ac.cn/) and archives raw sequence data.

The Ovine SNP BeadChip data including Ovine Illumina 50K BeadChip of 1,512 samples and Ovine Infinium HD 600K SNP BeadChip of 911 samples are from seven published papers (Aken et al., 2016; Ren et al., 2016; Peng et al., 2017; Xu et al., 2017, 2018; Chen et al., 2018; Gao et al., 2018) (**Supplementary Table 1**). All the Illumina 50K BeadChip and HD 600K BeadChip data were merged and submitted separately to the GVM.

The breed information was derived from 19 public websites and a book (**Supplementary Table 2**). The information on GWAS was acquired from 52 published papers using genome-wide association studies (GWAS) method in PubMed (**Supplementary Table 3**).

Data Processing

Whole genome sequence (WGS) reads were mapped to the sheep reference genome Oar v4.0 (https://www.ncbi.nlm.nih.gov/assembly/GCF_000298735.2) by Burrows-Wheeler Aligner (BWA) v.0.7.10-r789 (Li and Durbin, 2009). Mapping results were then converted into BAM format and sorted by SortSam in Picard package v.2.1.1 ("Picard Toolkit." 2019. Broad Institute, GitHub Repository. http://broadinstitute.github.io/picard/; Broad Institute). MarkDuplicates in Picard was used to remove duplicated reads. INDEL realignment and correction of base quality were performed through GATK v.3.7 (McKenna et al., 2010). HaplotypeCaller and GenotypeGVCFs in GATK were then used for variants calling and joint genotyping. After filtering, the non-redundant variants were identified and assigned with 'oas' number corresponding to 'rs' number in European Variation Archive (EVA) (https://www.ebi.ac.uk/eva/). SNP Chip data of Illumina 50K BeadChip and HD BeadChip were updated to Oar v.4.0, transformed into VCF format using plink v.1.9 (Purcell et al., 2007), and then mapped to the WGS variant sites identified above.

We integrated the variants obtained above according to the position on the chromosomes, performed annotations of variants using VEP v.84 (McLaren et al., 2016), and obtained corresponding information on genes, transcriptomes, and proteins. We also calculated minor allele frequency (MAF) for each variant using vcftools v.0.1.13 (Danecek et al., 2011). Besides, NCBI Genome Remapping Service (https://www.ncbi.nlm.nih.gov/genome/tools/remap) was also used to find corresponding variant position in Oar Rambouillet v.1.0 from Oar v.4.0.

Breed information was collected from the public repositories, including Wikipedia, Domestic Animal Diversity Information System (DAD-IS 3), Breeds of Livestock, Sheep101, Roy's Farm, and Animal Genetic Resources in China: Sheep and Goats (**Supplementary Table 2**). To provide a unified description of phenotype, we defined a few rules to standardize the breed information, for example, using the most popular name to nominate the breed name. GWAS information was curated from published papers associated with GWAS in sheep manually. Among 152 related publications, 922 Associations relative to 110 traits were extracted from 52 papers published from the years of 2011 to 2019 (**Supplementary Table 3**). Finally, we used the online tool LiftOver (http://genome.ucsc.edu/cgi-bin/hgLiftOver) to correct the coordinates of each curated genotype.

Database Implementation

iSheep is implemented by frameworks of springboot version 1.5.9 (https://spring.io/projects/spring-boot/) and mybatis version 1.3.1 (https://mybatis.org/), and data were stored and retrieved through MySQL 8.0 (http://www.mysql.org; a free and popular relational database management system). Web user interfaces were developed by JSP (JavaServer Pages; a technology facilitating rapid development of dynamic web pages based on the Java programming language), HTML (HyperText Markup Language), CSS (Cascading Style Sheets), AJAX (Asynchronous JavaScript and XML; a set of web development techniques to create asynchronous applications without interfering with the display and behavior of the existing page), JQuery (a cross-platform and feature-rich JavaScript library; http://jquery.com, version 3.3.1) and Bootstrap (https://getbootstrap.com, version 4.1.3). Genomic visualization was achieved by Dalliance (Down et al., 2011).

RESULTS

Data Contents and Statistics

iSheep integrates phenotypic and genotypic data modules containing Breeds, Samples, Genome-wide association study (GWAS), Variants and Genes. The modules (i.e., Breeds, Samples, GWAS and Genes) can be related by the module Variants

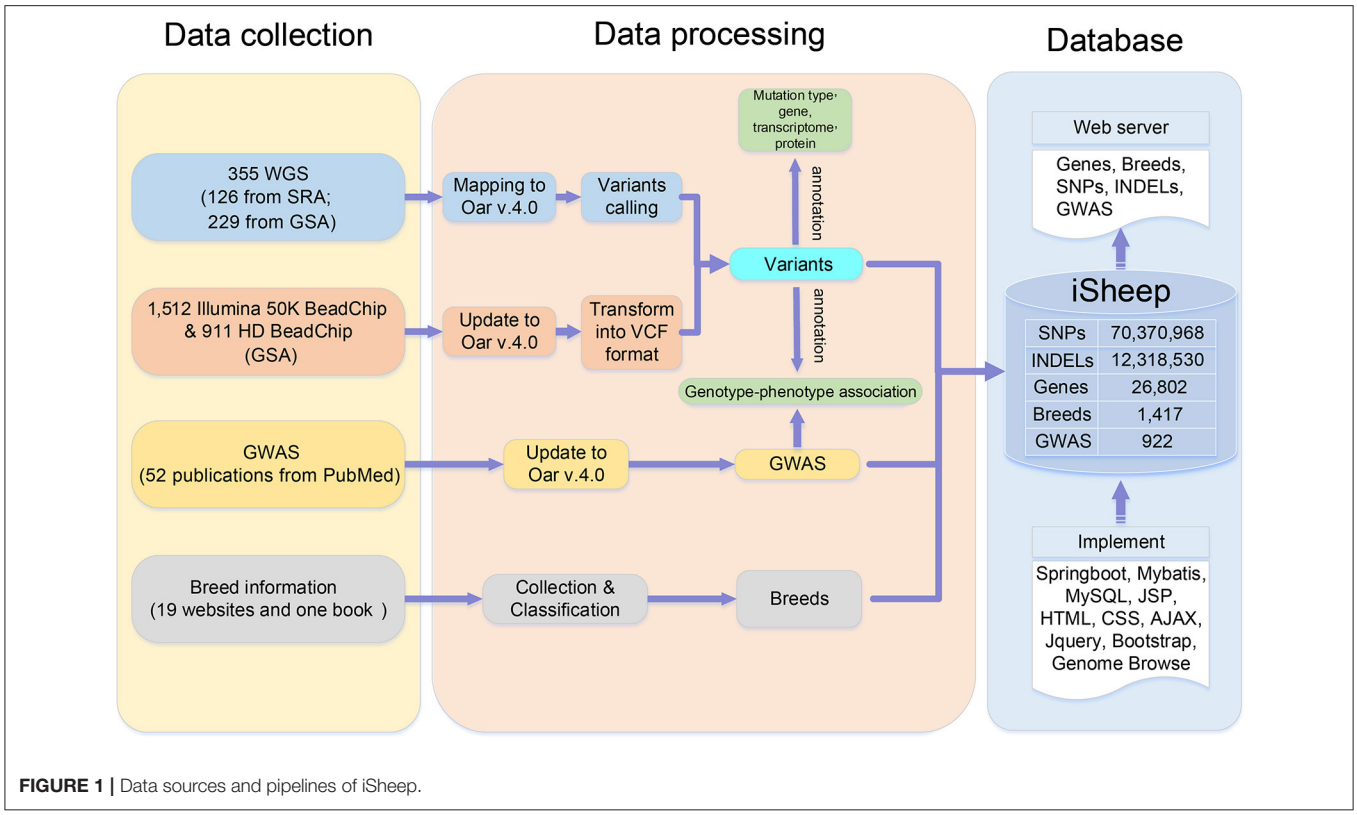

FIGURE 1 | Data sources and pipelines of iSheep.

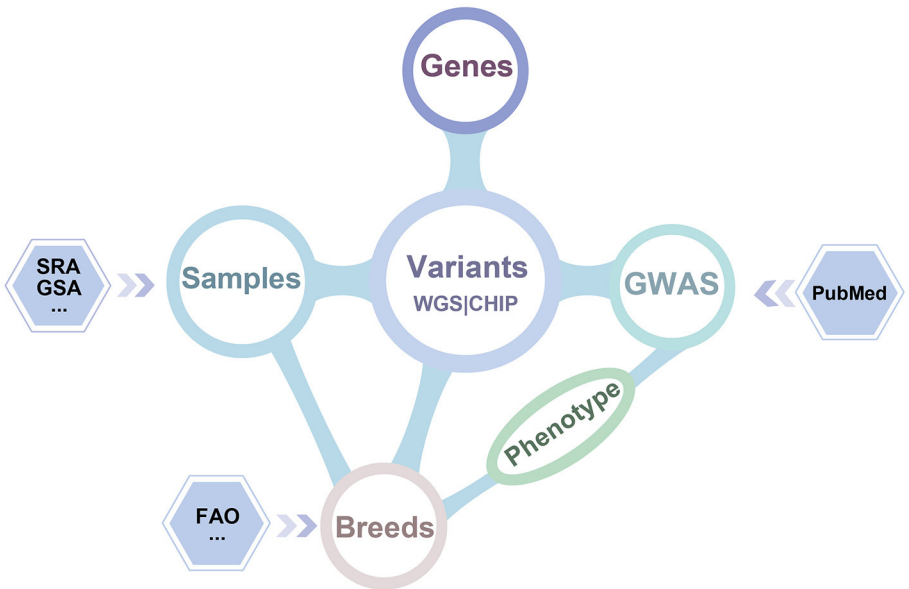

FIGURE 2 | Dataset relationship of iSheep. The iSheep integrates multiple types of data set with inter-connections between each other: (*i*) The Variants called from 355 samples' whole genome sequence data and 2,423 samples' chip data which have been deposited in Genome Sequence Archive (GSA) and Sequence Read Archive (SRA); (*ii*) Genes with variation annotation; (*iii*) GWAS dataset containing manually curated publications of genome-wide variant-trait associations in specific breeds; (*iv*) The sample information and corresponding breed information.

(**Figure 2**). In details, we collected whole-genome sequencing (WGS) data of 355 sheep, SNP BeadChip data of 2,423 sheep, 26,802 genes annotated in the sheep genome, 1,417 breeds, and 922 variant-trait associations from 52 publications. Moreover,

TABLE 1 | Data statistics of iSheep.

Data content	Data statistics
Variants	82,689,498
SNPs	70,370,968
INDELs	12,318,530
Genes	26,802
lincRNA	3,481
Protein coding	19,953
Pseudogene	2,949
misc RNA	255
tRNA	55
miRNA	106
Samples	
Whole-genome sequencing (WGS)	355
Ovine Illumina 50K SNP BeadChip	1,512
Ovine Infinium HD SNP BeadChip (600K)	911
Phenotypes	
Breeds	1,417
Associations	922
Ontology	110
Disease-resistance trait	23
Meat and carcass trait	33
Milk trait	7
Production and reproduction	33
Wool trait	14
Publications	52

different data sets have been translated into usable information through standard data processing (**Figure 1**). Also, we provide a unified data service for the sheep research communities.

In total, the information on variants contains 70,370,968 SNPs and 12,318,530 INDELs (**Table 1**), and it was annotated to 24 consequence types. The results showed that the variants located in noncoding regions (e.g., intergenic regions, introns, upstream/downstream regions of genes and 3′/5′ prime UTRs) occupy the largest proportion (∼ 99.09%) of the genomes, whereas the variants located in coding regions such as synonymous and missense only account for no more than 1% (**Supplementary Table 4**). The gene information mainly includes gene name, location, symbol, gene type and functional descriptions (**Figure 3A**). The breed information includes breed name, distribution, usage, and phenotypic characteristics (**Figure 3B**). The phenotype information consists of five categories such as production and reproduction, meat and carcass, milk, disease-resistance, and wool traits (**Figure 3C**).

Retrieving and Browsing Data

iSheep provides an online documentation to help users familiarize with the database and a convenient way to retrieve and download data through a uniform user interface. The advanced search engines are designed in different modules to improve the usability and accessibility.

(*i*) In the Breeds module, basic information about 1,417 breeds is listed by integrating the content of 20 resources (**Supplementary Table 2**). Users are able to search breeds of interests through the key words such as breed name and/or country name, and then filter the breed by usage or body size. Detailed information including images and morphological, production, reproduction and other phenotypic characteristics has been curated and integrated in system, and is linked with breed name for further displayed.

(*ii*) In the GWAS module, 922 variant-trait associations and 111 traits are manually curated from 52 publications (**Supplementary Table 3**). To unify the representation of biological traits, the trait entities are divided into a suite of ontologies by using the standard of sheep QTLdb (Hu et al., 2019b). When a trait term is selected, basic descriptive information on association, trait and publication will be automatically mapped and displayed on the right panel (**Figure 3C**), where users could view the detailed information for different species. Additionally, for each publication, its bibliographic details are collectively summarized in the Publications module. Therefore, the mapping between GWAS traits and ontology terms would be useful to identify new potential genetic variants by providing all related associations across different species.

(*iii*) In the Variants module, variants called from 355 whole genome sequences and SNP BeadChip of 2,423 individuals, and annotated genes are showed. To support information search and exploration, powerful retrieve functions are designed for users to filter variants by name, position, consequence types and/or minor allele frequency, while users can also choose the sequencing technologies to locate the concerned data sets. Typically, the elaborate information of each variant marked with annotation label, for example functional change or not, makes the selection of the specific variation much easier. Through clicking variant, the detailed and structured information (e.g., genes, SNPs and INDELs) with a visualized bar is shown, and also, the concerned genotypes of this variant in 355 sheep WGS samples are showed (**Figure 3D**). Specially, if the variant maps to a SNP site in 600 K and/or 50 K BeadChip, the SNP genotypes in the chip(s) will be linked out, with the total number of the samples pooled in chips up to 2,423 individuals from 47 sheep breeds.

In other modules, such as the Samples and Genes, there are searching engines for further data query, providing the external links to the data sources to find more detail information.

Morphological and Phenotypic Traits Survey Using iSheep

The integration and correlation of multiple data types in sheep make iSheep a knowledge base, which brings a convenient way for users. Based on the Variants module, users can obtain all corresponding information in other different modules (i.e., Genes, Breeds, Samples and GWAS) of iSheep. For example, through the Associations in GWAS module, users can filter out the traits "white to black" or "white spotted", and then choose one variant (e.g., "oas24670730") in the result page (**Figure 3C**). The detailed information of this variation will be listed and the extensional information of Beadchip data will be linked out (**Figure 3D**). In this example, the breed "Duolang" will be extracted because of its the highest mutation frequency among all breeds (**Figure 3E**). Besides that, the image and quantifiable

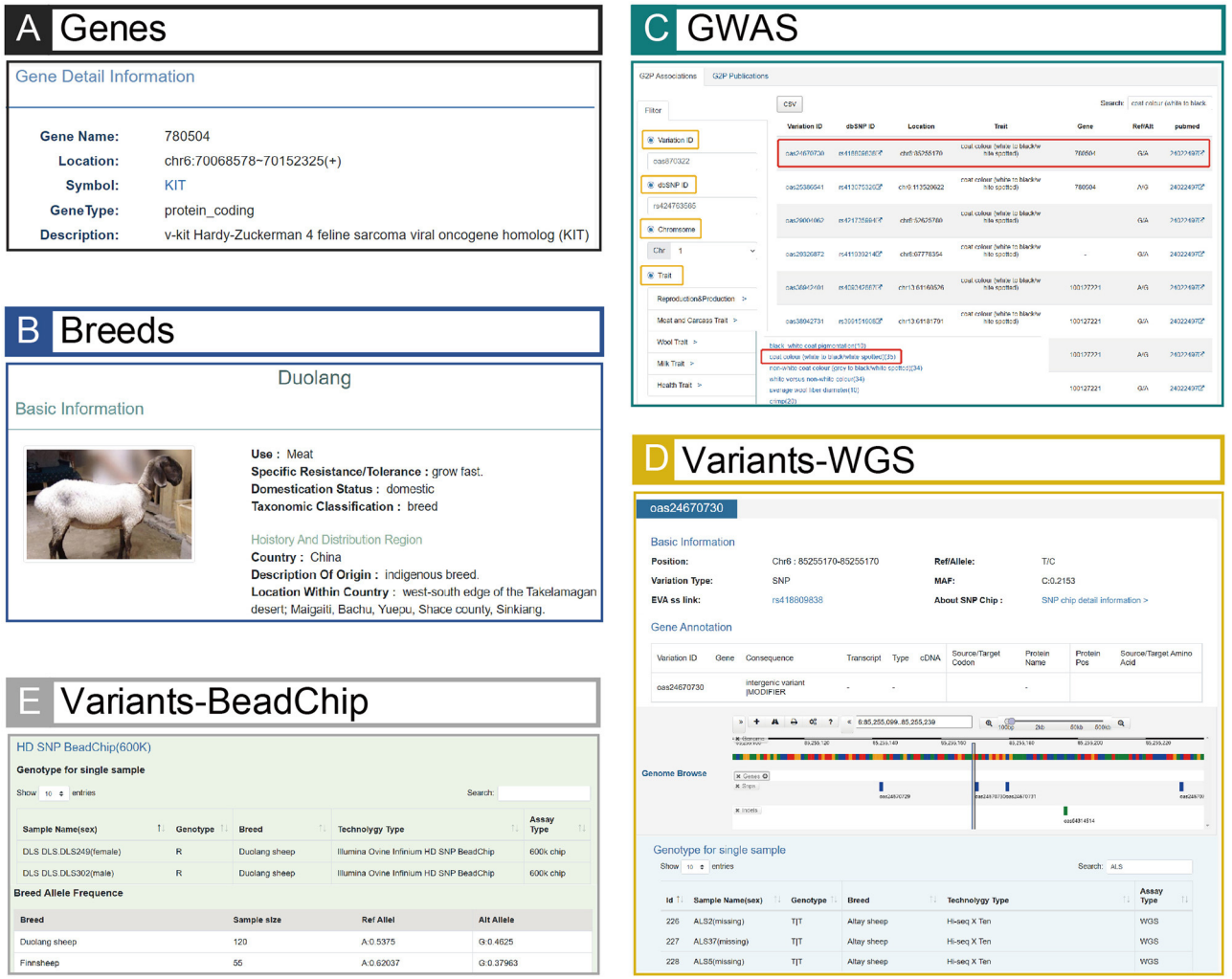

FIGURE 3 | Screenshots of GWAS, Variants, Breeds and Genes modules. **(A)** An example searching result of GWAS. The result page is linked to Genes **(E)** and Variants **(B)**, and the page can jump to corresponding pages when relevant buttons (e.g., variant ID: oas24670730, or gene name: 780504) are clicked. **(B)** An example result of Variants (variant ID: oas24670730). The result page shows detailed information of this example and links to extensional information of BeadChip data **(C)**. **(C)** An example result in BeadChip of Variants (variant ID: oas24670730). The result page is linked to **(B)** when the users click "SNP chip detail information >", and Duolang sheep with the highest mutation frequency in this example is shown in the table. **(D)** Phenotypic data of Duolang sheep. **(E)** Page of the gene (gene name: 780504) related to the variant (variant ID: oas24670730) in **(A)**.

phenotype data of this sheep breed (**Figure 3B**) and the related genes (**Figure 3A**) of this variant will be connected.

Online Tools of iSheep

iSheep provides two online tools for users to analyze data. The first one is Comparison, which can be used to compare SNPs between two or more individuals. The results show the information of different samples' genotypes on variant sites and make it more convenient for users to focus on their interested SNPs. The second is Genome browse, which helps users to better visualize the locus of variants in the genome. Users can easily visualize the interested region with genes, transcripts, SNPs, INDELs and other elements. Further, users can export their results in the SVG format.

DISCUSSION

By integrating omics data of sheep, variants, and phenotype, we have developed a new sheep database, iSheep, which provides an easy access for users to download raw re-sequencing/variant data, perform their personalized analyses online, and visualize and export results. Compared with some available sheep databases, such as ISGC and dbSNP which are not updated in time, iSheep excels in the following aspects: (*i*) Fast updated with multiple data types and resources (i.e., WGS data, variant data, gene data, breed data and GWAS data). Besides the domestic sheep data, iSheep provides raw re-sequencing and variant data for various wild sheep including argali (*O. ammon*), Asian

mouflon (*O. orientalis*), bighorn (*O. canadensis*) and thinhorn (*O. dalli*), which makes it more convenient to investigate demographic history and domestication of sheep; (*ii*) Multiple options for keyword searching; (*iii*) Comprehensive annotations for variants and phenotypes, comprising 922 variant-trait associations for 110 phenotypic traits; and (*iv*) A user-friendly website with functional online tools including Comparison and Genome Browse.

The overall goal of iSheep is to provide a comprehensive resource for sheep studies. In the future, we will continue to improve gene annotations and exploit additional applications after integrating new data types such as transcriptomics and proteomics, and continue to collect more phenotypic data to increase breed traceability. The development of online tools for omics data analysis will also be our focus. In addition, we are striving to develop an online tool for performing imputation of missing genotypes for the same SNP position based on existing genotypes in our database.

DATA AVAILABILITY STATEMENT

The original contributions presented in the study are included in the article/**Supplementary Material**, further inquiries can be directed to the corresponding author/s.

AUTHOR CONTRIBUTIONS

M-HL and W-MZ conducted and designed this study. Z-HW, Q-HZ, J-WZ, D-MT, H-LK, C-PL, and S-SZ collected data and implemented the database. XL, Z-HW, and Q-HZ wrote the first draft of the manuscript. M-HL and W-MZ reviewed and edited the final manuscript. All authors reviewed and approved the paper for publication.

FUNDING

This study was funded by grants from the National Key Research and Development Program-Key Projects of International Innovation Cooperation between Governments (2017YFE0117900), the National Natural Science Foundation of China (Nos. 31825024, 31661143014, and 31972527), the Second Tibetan Plateau Scientific Expedition and Research Program (STEP) (No. 2019QZKK0501), the External Cooperation Program of Chinese Academy of Sciences (152111KYSB20190027), the Taishan Scholars Program of Shandong Province (No. ts201511085) and Strategic Priority Research Program of the Chinese Academy of Sciences (XDB38050300).

ACKNOWLEDGMENTS

We are grateful to the late Zhi-Fa Wang and a number of other persons for providing samples for generating the molecular data. Meanwhile, we also thank China National Center for Bioinformation (CNCB) members for maintaining servers and computing resources.

SUPPLEMENTARY MATERIAL

The Supplementary Material for this article can be found online at: https://www.frontiersin.org/articles/10.3389/fgene.2021.714852/full#supplementary-material

REFERENCES

Aken, B. L., Ayling, S., Barrell, D., Clarke, L., Curwen, V., Fairley, S., et al. (2016). The Ensembl gene annotation system. *Database* 2016:baw093. doi: 10.1093/database/baw093

Alberto, F. J., Boyer, F., Orozco-terWengel, P., Streeter, I., Servin, B., de Villemereuil, P., et al. (2018). Convergent genomic signatures of domestication in sheep and goats. *Nat. Commun.* 9, 1–9. doi: 10.1038/s41467-018-03206-y

Chen, Z.-H., Zhang, M., Lv, F.-H., Ren, X., Li, W.-R., Liu, M.-J., et al. (2018). Contrasting patterns of genomic diversity reveal accelerated genetic drift but reduced directional selection on X-chromosome in wild and domestic sheep species. *Genome Biol. Evol.* 10, 1282–1297. doi: 10.1093/gbe/evy085

Danecek, P., Auton, A., Abecasis, G., Albers, C. A., Banks, E., DePristo, M. A., et al. (2011). The variant call format and VCFtools. *Bioinformatics* 27, 2156–2158. doi: 10.1093/bioinformatics/btr330

Deng, J., Xie, X.-L., Wang, D.-F., Zhao, C., Lv, F.-H., Li, X., et al. (2020). Paternal origins and migratory episodes of domestic sheep. *Curr. Biol.* 30, 4085–4095.e4086. doi: 10.1016/j.cub.2020.07.077

Down, T. A., Piipari, M., and Hubbard, T. J. P. (2011). Dalliance: interactive genome viewing on the web. *Bioinformatics* 27, 889–890. doi: 10.1093/bioinformatics/btr020

Elsik, C. G., Unni, D. R., Diesh, C. M., Tayal, A., Emery, M. L., Nguyen, H. N., et al. (2016). Bovine genome database: new tools for gleaning function from the Bos taurus genome. *Nucleic. Acids. Res.* 44, D834–D839. doi: 10.1093/nar/gkv1077

Gao, L., Xu, S.-S., Yang, J.-Q., Shen, M., and Li, M.-H. (2018). Genome-wide association study reveals novel genes for the ear size in sheep (Ovis aries). *Anim. Genet.* 49, 345–348. doi: 10.1111/age.12670

Hu, X.-J., Yang, J., Xie, X.-L., Lv, F.-H., Cao, Y.-H., Li, W.-R., et al. (2019a). The genome landscape of tibetan sheep reveals adaptive introgression from argali and the history of early human settlements on the Qinghai–Tibetan Plateau. *Mol. Biol. Evol.* 36, 283–303. doi: 10.1093/molbev/msy208

Hu, Z.-L., Park, C. A., and Reecy, J. M. (2019b). Building a livestock genetic and genomic information knowledgebase through integrative developments of animal QTLdb and CorrDB. *Nucleic. Acids. Res.* 47, D701–D710. doi: 10.1093/nar/gky1084

Jiang, Y., Xie, M., Chen, W., Talbot, R., Maddox, J. F., Faraut, T., et al. (2014). The sheep genome illuminates biology of the rumen and lipid metabolism. *Science* 344, 1168–1173. doi: 10.1126/science.1252806

Lauledерkind, S. J. F., Hayman, G. T., Wang, S.-J., Smith, J. R., Lowry, T. F., Nigam, R., et al. (2013). The rat genome database 2013—data, tools and users. *Brief. Bioinformatics* 14, 520–526. doi: 10.1093/bib/bbt007

Li, C., Tian, D., Tang, B., Liu, X., Teng, X., Zhao, W., et al. (2021). Genome Variation Map: a worldwide collection of genome variations across multiple species. *Nucleic. Acids. Res.* 49, D1186–D1191. doi: 10.1093/nar/gkaa1005

Li, H., and Durbin, R. (2009). Fast and accurate short read alignment with Burrows–Wheeler transform. *Bioinformatics* 25, 1754–1760. doi: 10.1093/bioinformatics/btp324

Li, X., Yang, J., Shen, M., Xie, X.-L., Liu, G.-J., Xu, Y.-X., et al. (2020). Whole-genome resequencing of wild and domestic sheep identifies genes associated with morphological and agronomic traits. *Nat. Commun.* 11:2815. doi: 10.1038/s41467-020-16485-1

Lv, F.-H., Agha, S., Kantanen, J., Colli, L., Stucki, S., Kijas, J. W., et al. (2014). Adaptations to climate-mediated selective pressures in sheep. *Mol. Biol. Evol.* 31, 3324–3343. doi: 10.1093/molbev/msu264

McKenna, A., Hanna, M., Banks, E., Sivachenko, A., Cibulskis, K., Kernytsky, A., et al. (2010). The genome analysis toolkit: a MapReduce framework for analyzing next-generation DNA sequencing data. *Genome Res.* 20, 1297–1303. doi: 10.1101/gr.107524.110

McLaren, W., Gil, L., Hunt, S. E., Riat, H. S., Ritchie, G. R. S., Thormann, A., et al. (2016). The ensembl variant effect predictor. *Genome Biol.* 17, 1–14. doi: 10.1186/s13059-016-0974-4

Naval-Sanchez, M., Nguyen, Q., McWilliam, S., Porto-Neto, L. R., Tellam, R., Vuocolo, T., et al. (2018). Sheep genome functional annotation reveals proximal regulatory elements contributed to the evolution of modern breeds. *Nat. Commun.* 9, 1–13. doi: 10.1038/s41467-017-02809-1

Peng, W.-F., Xu, S.-S., Ren, X., Lv, F.-H., Xie, X.-L., Zhao, Y.-X., et al. (2017). A genome-wide association study reveals candidate genes for the supernumerary nipple phenotype in sheep (Ovis aries). *Anim. Genet.* 48, 570–579. doi: 10.1111/age.12575

Purcell, S., Neale, B., Todd-Brown, K., Thomas, L., Ferreira, M. A. R., Bender, D., et al. (2007). PLINK: a tool set for whole-genome association and population-based linkage analyses. *Am. J. Hum. Genet.* 81, 559–575. doi: 10.1086/519795

Ren, X., Yang, G.-L., Peng, W.-F., Zhao, Y.-X., Zhang, M., Chen, Z.-H., et al. (2016). A genome-wide association study identifies a genomic region for the polycerate phenotype in sheep (*Ovis aries*). *Sci. Rep.* 6, 1–8. doi: 10.1038/srep21111

Sherry, S. T., Ward, M. H., Kholodov, M., Baker, J., Phan, L., Smigielski, E. M., et al. (2001). dbSNP: The NCBI Database of Genetic Variation. *Nucleic. Acids. Res.* 29, 308–311. doi: 10.1093/nar/29.1.308

Song, S., Tian, D., Li, C., Tang, B., Dong, L., Xiao, J., et al. (2018). Genome Variation Map: a data repository of genome variations in BIG Data Center. *Nucleic. Acids. Res.* 46, D944–D949. doi: 10.1093/nar/gkx986

Tang, B., Zhou, Q., Dong, L., Li, W., Zhang, X., Lan, L., et al. (2019). iDog: an integrated resource for domestic dogs and wild canids. *Nucleic. Acids. Res.* 47, D793–D800. doi: 10.1093/nar/gky1041

Xu, S.-S., Gao, L., Xie, X.-L., Ren, Y.-L., Shen, Z.-Q., Wang, F., et al. (2018). Genome-Wide Association Analyses Highlight the Potential for Different Genetic Mechanisms for Litter Size Among Sheep Breeds. *Front. Genet.* 9:118. doi: 10.3389/fgene.2018.00118

Xu, S.-S., Ren, X., Yang, G.-L., Xie, X.-L., Zhao, Y.-X., Zhang, M., et al. (2017). Genome-wide association analysis identifies the genetic basis of fat deposition in the tails of sheep (Ovis aries). *Anim. Genet.* 48, 560–569. doi: 10.1111/age.12572

Yang, J., Li, W.-R., Lv, F.-H., He, S.-G., Tian, S.-L., Peng, W.-F., et al. (2016). Whole-genome sequencing of native sheep provides insights into rapid adaptations to extreme environments. *Mol. Biol. Evol.* 33, 2576–2592. doi: 10.1093/molbev/msw129

Zeder, M. A. (2008). Domestication and early agriculture in the Mediterranean Basin: origins, diffusion, and impact. *Proc. Natl. Acad. Sci. U.S.A.* 105, 11597–11604. doi: 10.1073/pnas.0801317105

Zhao, Y.-X., Yang, J., Lv, F.-H., Hu, X.-J., Xie, X.-L., Zhang, M., et al. (2017). Genomic reconstruction of the history of native sheep reveals the peopling patterns of nomads and the expansion of early pastoralism in East Asia. *Mol. Biol. Evol.* 34, 2380–2395. doi: 10.1093/molbev/msx181

Conflict of Interest: The authors declare that the research was conducted in the absence of any commercial or financial relationships that could be construed as a potential conflict of interest.

The reviewer FW declared a past co-authorship with several of the authors XL, M-HL to the handling Editor.

frontiers in Genetics

ORIGINAL RESEARCH
published: 18 August 2021
doi: 10.3389/fgene.2021.715526

Role of Sulfur Metabolism Gene and High-Sulfur Gene Expression in Wool Growth Regulation in the Cashmere Goat

Yuan Chai[1], Yanyong Sun[1,2], Bin Liu[3], Lili Guo[1], Zaixia Liu[1], Le Zhou[1], Lingli Dai[1], Chunyan Jia[1], Wenguang Zhang[1,4] and Chun Li[5]**

[1] College of Animal Science, Inner Mongolia Agricultural University, Hohhot, China, [2] College of Animal Science and Veterinary Medicine, Tianjin Agricultural University, Tianjin, China, [3] Nei Mongol BioNew Technology Co., Ltd., Hohhot, China, [4] Kunming Institute of Zoology, Chinese Academy of Sciences, Kunming, China, [5] College of Animal Science and Technology, Inner Mongolia University for Nationalities, Tongliao, China

Sulfur, an essential mineral element for animals, mainly exists in the form of organic sulfur-containing amino acids (SAAs), such as cystine, methionine, and cysteine, within the body. The content, form, and structure of sulfur play an important role in determining the wool fiber quality. In addition, keratin-associated proteins, one of the most crucial wool fiber components, are rich in SAAs. However, sulfur metabolism from the blood to the skin and hair follicles remains unclear. In this study, we analyzed high-sulfur protein gene and sulfur metabolism genes in the cashmere goat and explored the effects of melatonin on their expression. In total, 53 high-sulfur protein genes and 321 sulfur metabolism genes were identified. We found that high-sulfur protein genes were distributed in the 3–4 and 144M regions of chromosome 1 and the 40–41M region of chromosome 19 in goats. Moreover, all year round, allele-specific expression (ASE) is higher in the 40–41M region of chromosome 19 than in the other regions. Total of 47 high-sulfur protein genes showed interaction with transcription factors and cofactors with ASE. These transcription factors and cofactors were inhibited after melatonin implantation. The network analysis revealed that melatonin may activate the sulfur metabolism process via the regulation of the genes related to cell energy metabolism and cell cycle in the skin, which provided sufficient SAAs for wool and cashmere growth. In conclusion, our findings provide a new insight into wool growth regulation by sulfur metabolism genes and high-sulfur protein genes in cashmere goats.

Keywords: high sulfur protein gene, sulfur metabolic gene, allele specific expression, melatonin, hair growth

OPEN ACCESS

Edited by:
Shaobin Li,
Gansu Agricultural University, China

Reviewed by:
Jianning He,
Qingdao Agricultural University, China
Shuting Xiong,
Hunan Agricultural University, China
Ruiwen Fan,
Shanxi Agricultural University, China

****Correspondence:***
Wenguang Zhang
atcgnmbi@aliyun.com
Chun Li
lichun1985@126.com

Specialty section:
This article was submitted to Livestock Genomics, a section of the journal Frontiers in Genetics

Received: *27 May 2021*
Accepted: *29 July 2021*
Published: *18 August 2021*

Citation:
Chai Y, Sun Y, Liu B, Guo L, Liu Z, Zhou L, Dai L, Jia C, Zhang W and Li C (2021) Role of Sulfur Metabolism Gene and High-Sulfur Gene Expression in Wool Growth Regulation in the Cashmere Goat. Front. Genet. 12:715526. doi: 10.3389/fgene.2021.715526

INTRODUCTION

The sulfur content directly affects the properties of wool fibers, including cashmere wool fibers. Notably, sulfur-containing amino acids (SAAs), differentially expressed genes (DEGs), methionine, and cysteine play an important metabolic and functional role in animals. In a study, SAA supplementation was found to significantly increase wool production and sulfur concentration

Abbreviations: ASE, allele specific expression; SAA, sulfur amino acids; PFs, primary follicles; SFs, secondary follicles; HQ, high quality; LQ, low quality; DEGs, differentially expressed genes; SNP, single nucleotide polymorphisms; WGCNA, weight gene co-expression network analysis; CDS, the coding sequences; LEfSe, linear discriminant analysis Effect Size.

in wool (Sherlock et al., 2001). Moreover, wool fiber cystine content was directly proportional to the dietary SAA levels and thus to the wool quality. Moreover, daily supplementation with 2 g of cysteine or 2.46 g of methionine improved wool production per unit area of skin by 35–130% and wool sulfur content by 24–35% (Reis and Schinekel, 1961; Reis and Schinckel, 1963). Nutritional supply of SAAs significantly alters the mitotic rate of hair follicle bulb cells: higher SAA supplementation leads to increased proliferation and differentiation of follicle bulb cells and further keratinization (Hynd, 1989). Cellular uptake of cysteine is mediated by various transporters, often with tissue-specific distribution. Downes et al. (1962) studied cysteine uptake in human hair follicles and outer root sheath cells *ex vivo* and found that fibroblasts demonstrated cysteine uptake and that the cysteine transporter ASC was present in hair follicles and outer root sheath cells. Cysteine is also the main component of keratinized proteins in feathers, and in birds, the demand for cysteine is fulfilled via the transsulfuration pathway. Inhibition of the transsulfuration pathway can affect hair follicle development, skin thickness, and growth in broilers; moreover, this inhibition is associated with the upregulation of hepatic cystathionine synthase and cystathionine lyase mRNAs (Silva et al., 2018). Silva et al. (2019) randomized chicks into control and cysteine-deficient groups for 49 days and measured their skin layer thickness and hair follicle length and thickness on days 10, 24, 34, and 49 after treatment, respectively. Chicken epidermis in the cysteine-deficient group had thinner and shorter hair follicles with increased cystathionine synthase and cystathionine lyase mRNA expression—indicating a disruption in the transsulfuration pathway (Silva et al., 2019).

Sulfur metabolism is interwoven through various life processes, where it contributes to their vitality. Ongoing studies on the role of sulfur in goat wool fiber growth are mainly focused on sulfur's nutritional effect, its suitable dietary level, and the nitrogen–sulfur ratio, but without much attention to the underlying molecular mechanisms. Wang et al. (2006) found that related hormones changed in cashmere goats after melatonin implantation and that it regulated nitrogen distribution in the body and the villus, thus promoting cashmere wool growth. Sulfur metabolism is closely related to nitrogen metabolism (Wang and Jia, 1999).

To date, the knowledge on the expression pattern of sulfur metabolism genes in cashmere goats remains limited. In this study, we hypothesize that sulfur metabolism genes interact with melatonin to regulate villus growth. Here, high-sulfur protein family genes, sulfur metabolism genes, and melatonin in cashmere goats are used as entry points to study the important genes involved in the regulation of villus growth, eventually elucidating the underlying signal transduction networks.

MATERIALS AND METHODS

Experimental Animals and Sample Collection

Six 16-month-old female cashmere goats from Hanshan, Inner Mongolia were included in this study. They were divided into two groups (n = 3 in each group): melatonin implantation (treatment group) and melatonin non-implantation (control group). In total, we collected 72 blood and 72 skin samples over 12 months (12 each from each goat).

During the experiment, 2 mg/kg body weight melatonin was implanted subcutaneously behind the ears of the treatment group goats, whereas no melatonin was implanted in the control group. One month after implantation, scapula skin samples (size, 1 cm^2) and venous blood samples were collected and quickly frozen and stored at -80°C in liquid nitrogen. The melatonin concentration in plasma were tested (**Supplementary Figure 1**).

Moreover, primary follicles (PFs) and secondary follicles (SFs) were collected in each month from four female cashmere goats from Inner Mongolia. PF samples were collected from 12 months of the year and SF samples were collected from August to February of the following year. These PFs and SFs were plucked from the side of the torso of the goats at the beginning of each month. First, the cashmere and wool were separated by careful observation, and then the cashmere and wool were quickly pulled out from the torso of the goats. Use chloroform sterilized scissors to cut the hair follicles 1 cm away from the root of the cashmere and wool. The PF and SFs were immediately frozen without any chemical solutions in liquid nitrogen for storage and transported until RNA isolation. In total, 12 PFs and 8 SFs samples were collected.

RNA-seq Library Construction and Sequencing Using Blood and Skin Samples

Total RNA was extracted from all blood and skin samples using TRIzol reagent (TaKaRa), according to the manufacturer's instructions. The blood and skin samples at –80°C were thawed (skin material was ground in liquid nitrogen). 1 ml TRIzol reagent was added and thoroughly mixed. The supernatants were obtained after the samples were centrifuged at 12,000 *g*, for 10 min at 4°C. The top layer was collected after chloroform was added. A 1:1 V of isopropanol was added to each tube before being centrifuged at 12,000 *g* for 10 min at 4°C. The supernatants were discarded and the remaining pellets were washed with 1 ml of 75% ethanol and centrifuge at 7500 *g* for 5 min. All of the residual ethanol was then removed and the pellets were allowed to air dry for 4 min. The RNA samples were then redissolved in 30 μl of DEPC (Diethyl Pyrocarboanate) treated H2O and stored at –80°C. After the RNA samples were quantitated, mRNAs was enriched with oligo (DT) magnetic beads. Then, the fragment buffer was added to break the mRNA into shorter fragments. We used the mRNA as the template, single-stranded cDNA was synthesized using a randomized hexamer, followed by the synthesis of double-stranded cDNA by adding buffer, dNTPs, DNA polymerase I, and RNase H. The double-stranded cDNA was then purified using AMPure XP beads, and then the second strand of cDNA containing U was degraded using USER enzyme. Purified double-stranded cDNA was then repaired at the end, followed by the addition of a tail and connection to the sequencing connector. Next, AMPure XP beads were used to select the fragment size. Finally, the final library was

obtained via PCR amplification and purification. After RNA-seq library construction, Qubit 2.0 was used for preliminary quantification, followed by library insert size detection using Agilent 2100. After the inserts met the expectations, Q-PCR was used to accurately quantify the effective concentration of the library and ensure the quality of the library. In total, 72 libraries from skin samples and 72 libraries from blood samples have been constructed.

Single-Molecule Long-Read Sequencing and Optimization of Hair Follicle Gene Structure in Cashmere Goat

Total RNA used for constructing an Iso-Seq library: mRNA was reverse-transcribed and then amplified using SMARTer PCR cDNA Synthesis Kit and PrimeSTAR GXL DNA Polymerase. The subsequent library construction was performed using the SMRTbell Template Prep Kit 1.0, and its library sequencing was performed on a PacBio RS II. The full-length transcriptome was analyzed using SMRTLink; it mainly included three stages: CCS acquisition, classification, and clustering. We used the Quiver algorithm in combination with the non-full-length sequences to polishing the consensus isoforms obtained through clustering and screen high-quality (HQ) and low-quality (LQ) sequences for subsequent analysis. Based on the full-length transcripts after polishing (HQ + LQ), the sequences were aligned to the reference genome (Capra hircus ARS1) by using the alignment software program Gmap (Wu and Watanabe, 2005). Only the sequences with identity > 0.9 and coverage > 0.85 in the alignment results were selected. The sequences with differences in the last exon at the 5′ end were merged using ToFU for collapse (with the options: –dun-merge-5-shorter). The GFF annotation file of the collapsed transcript was compared with that of the reference genome using gffcompare. The start and end positions of known genes were also optimized.

DEG Analysis

High-quality clean data obtained by filtering data according to strict standards can be used for further research and publication. When the N content in any sequencing read is >10% of the base number of the read, the paired reads should be removed. Moreover, when the LQ base number ($Q \leq 5$) base present in any sequencing read is >50% of the base number of the read, the paired reads should be removed. We used HISAT to match the read segments to the reference genome, which was obtained from the goat reference genome and its corresponding genome annotation file in the NCBI database (*ARS1*) (Dong et al., 2013). DEGs were detected using limma in the R package (Ritchie et al., 2015) with default parameters to screen out DEGs according to FPKM. The genes with $|\log_2 fc| > 1$ and $P < 0.05$ were identified as DEGs.

Weight Gene Coexpression Network and ASE Analyses

In the control group, 86 sulfur metabolism genes were differentially expressed in the blood and skin, whereas 4839 genes were coexpressed. A coexpression network was thus constructed using the weight gene coexpression network analysis (WGCNA) (Langfelder and Horvath, 2008) in R package for 4839 genes with 86 sulfur metabolism functional DEGs used as traits. The parameter β was given a default value from 1 to 30, as determined by the function SFT $powerestimate, with the minimum number of modules chosen to be 30.

BAM files were single-nucleotide polymorphisms (SNPs) called with samtools to generate BCF files, which were converted to VCF files using bcftools, containing genotype data for individuals. Heterozygous SNPs in an individual were filtered with the criteria that the individual's genotype was heterozygous, the coverage was >30 in both REF and ALT reads for both individual and SNP sites in a month, and finally, high confidence expressed SNPs were obtained.

Next, for ASE, we defined a haplotype concordant with the reference genome as ref allele and its homologous chromosome as ALT allele. The probability of occurrence of each allele was calculated via binomial distribution. A corresponding *P*-value of ≤0.05 was considered to indicate significance.

RESULTS

Genome-Wide Identification, Characterization, and Expression Profile of High-Sulfur Genes in Cashmere Goats

To run a complete search for identifying high-sulfur genes in the goat genome, two methods were used: We first searched the high-sulfur for protein sequences based on the published high-sulfur protein sequences in human (Khan et al., 2014) and sheep (Gong et al., 2016) and the Hidden Markov Model. For the sequence not found using the first method, we used the second method, where the published human and sheep high-sulfur protein sequences were employed as a query to perform blast against the goat reference proteome with identity score ranked first, alignment length equal to sequence length, and mismatches of <5. In total, 53 genes were assigned as high-sulfur protein genes in cashmere goats (**Supplementary Table 1**). All the high-sulfur protein genes are distributed in the 3M–4M and 144M regions of goat chromosome 1 and the 40M–41M region of goat chromosome 19 (**Figure 1**).

Single-molecule long-read sequencing of hair type in cashmere goat transcriptome data was used to complement and correct the 35 high-sulfur protein gene sequences in the cashmere goat. Consequently, 35 high-sulfur protein genes with relatively complete and accurate sequences were finally obtained (**Supplementary Table 2**). To classify the high-sulfur protein gene family in the cashmere goat, we built a phylogenetic tree using all the 53 high-sulfur protein sequences in cashmere goats, humans, and sheep using the NJ method. This tree illustrated that high-sulfur proteins in the cashmere goat can be divided into 12 subfamilies (**Figure 2**). We designated these subfamilies according to the human and sheep high-sulfur protein classification. No members were present in the *KRTAP*5, *KRTAP*23, and *KRTAP*12 subfamily. In contrast, 7, 4, 4, 14, 6, 12,

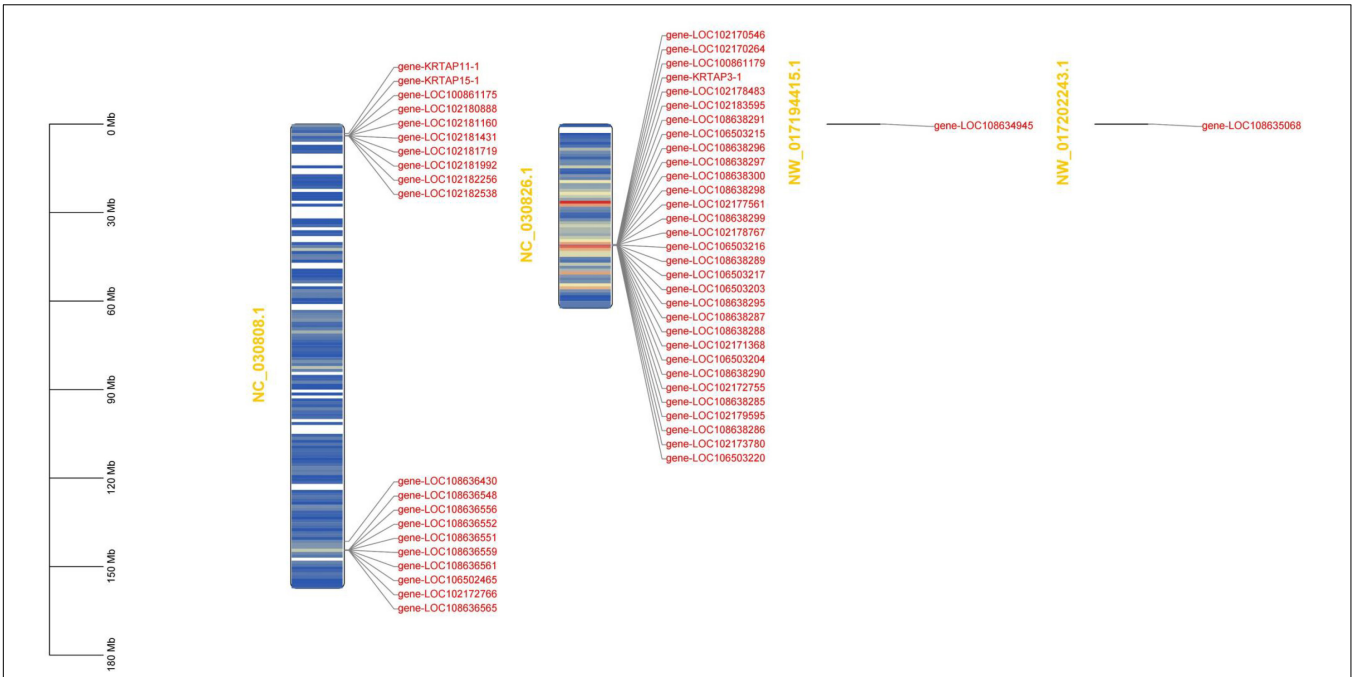

FIGURE 1 | Chromosomal mapping of 53 high-sulfur protein genes.

2, 5, 1, 1, 1, and 2, high-sulfur proteins were found to belong to the *KRTAP*1, *KRTAP*2, *KRTAP*3, *KRTAP*4, *KRTAP*9, *KRTAP*10, *KRTAP*11, *KRTAP*13, *KRTAP*15, *KRTAP*16, *KRTAP*17, and *KRTAP*24 subfamilies, respectively.

The conserved motifs in the high-sulfur proteins were further investigated using the online tool MEME (Bailey et al., 2009), and a total of 20 conserved motifs were detected (**Supplementary Table 3**). The height of each stacked letter in **Figure 3** represents the probability that the amino acid appears at the site, with a high frequency of cysteine (**Figure 3**). The structures of the motifs demonstrated that the motifs are conserved within each subfamily—indicating that the gene function within the families was quite conserved. Of them, the motifs 8, 4, and 7 were conserved in *KRTAP*10. Moreover, motifs 4, 13, 1, and 8 were conserved in *KATAP*9, *KATAP*1, *KRTAP*3, and *KRTAP*13, respectively (**Figure 4**).

We found that 53 high-sulfur protein genes were expressed in skin variably over 1 year. In contrast, only three genes—namely *KRTAP11-1*, *LOC102170546*, and *LOC108638285*—were expressed in blood, but at a low level (**Figure 5B**). The expression of high-sulfur protein genes in the skin demonstrated a decreasing trend from February to May, followed by an increasing trend from June to September (**Figure 5A**).

Weight gene coexpression network analysis was used to identify the coding sequences (CDS) with coordinated amino acid expression patterns. Here, we divided the 9355 CDS (Cys $\geq$ 3) of the goat reference proteome into six modules. The number of CDS in each module was 1724, 6437, 621, 428, 69, and 76, and a total of 5160 genes were annotated. Of these, 52 high-sulfur protein genes were annotated in the yellow-green module, and the protein amino acid expression pattern was found to be different from that of other genes. Moreover, cysteine abundance was noted to be highest, followed by that of serine (**Figure 6**).

Profiling High-Sulfur Protein Gene ASE in Cashmere Goats

Gene expression profiling using RNA-seq and genotyping were performed on data. We identified 172771 SNPs. We further counted the number of ASE per 1M region of chromosome 19. Moreover, TBtools (Chen et al., 2020) was used to display it in the form of a heat map. The results indicated a higher number of ASE in the 40–41M region of chromosome 19 compared with other regions (**Figure 7A**). The number of high-sulfur protein genes with ASE ranged from 35 to 43 for all months of the year in the control group (**Supplementary Table 4**) and from 37 to 45 for all months of the year in the treatment group (**Supplementary Table 5**). In total, 308 regions with different numbers of ASE between the control and treatment groups were detected; here, the region of difference number ASE was defined as the ratio of the two groups (min/max) $\leq$ 0.3. The locations at which ASE occurred differed between the 12 months (**Figure 7B**). The total number of ASE sites was higher in the control group than in the treatment group, indicating that melatonin inhibited ASE. Moreover, annotation revealed that these regions contained 856 genes, of which 16 genes play important roles in the Hippo signaling pathway (P = 0.008; **Supplementary Figure 2**). Furthermore, 37 transcription factors and 60 transcription cofactors were scattered throughout these regions.

After melatonin implantation, the expression of 26 transcription cofactors and 22 transcription factors changed, all of which showed higher expression levels in the control group

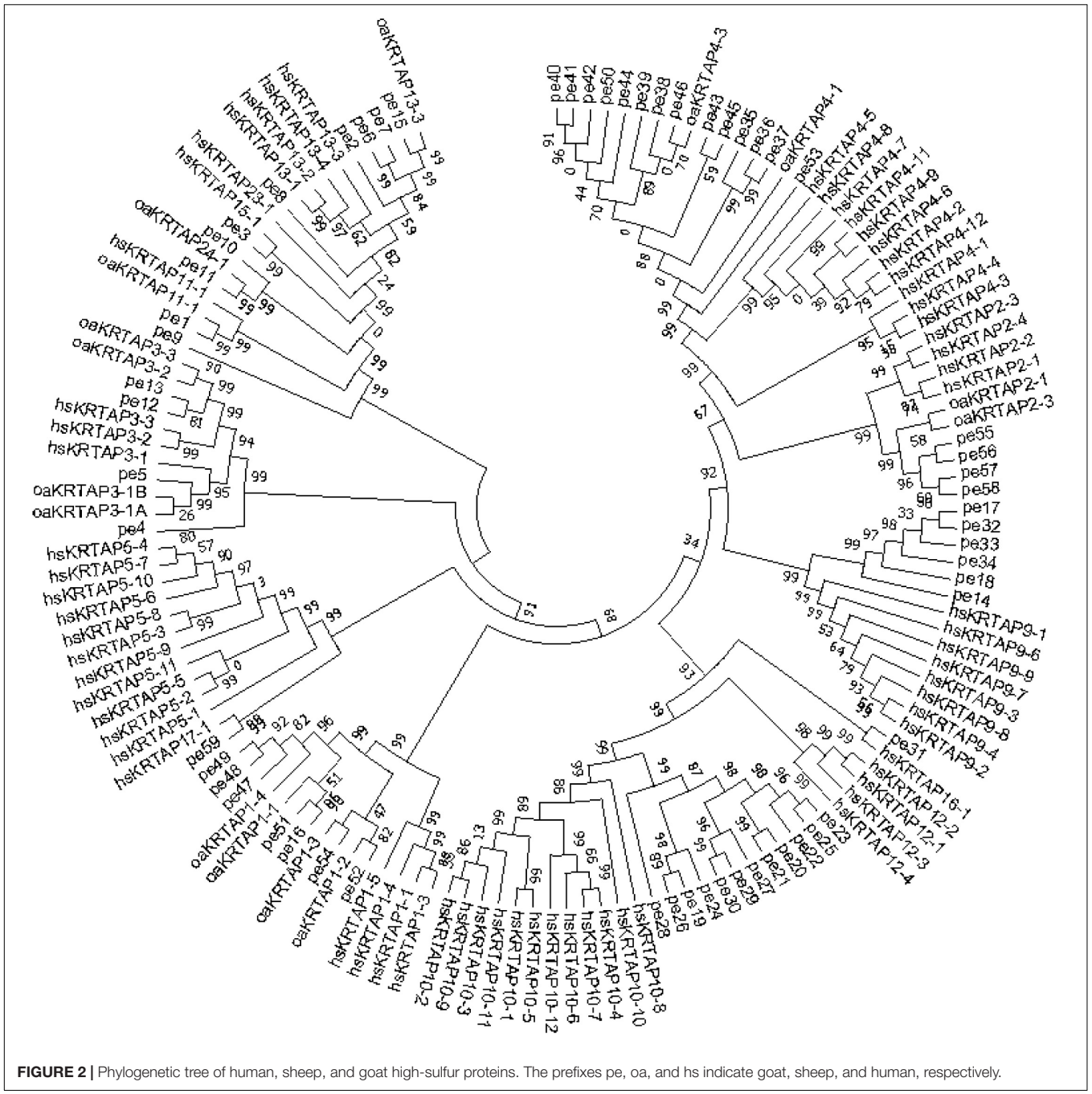

FIGURE 2 | Phylogenetic tree of human, sheep, and goat high-sulfur proteins. The prefixes pe, oa, and hs indicate goat, sheep, and human, respectively.

from August to December. Moreover, the expression pattern changed in the treatment group, with elevated expression levels in May and April (**Supplementary Figure 3**).

In total, 47 high-sulfur protein genes were used to construct a coexpression network using Pearson's correlation with a cutoff ($|adj| \geq 0.98$, $P \leq 0.01$; **Figure 8**). We found that the regulation between 18 high-sulfur protein genes and 17 transcription factors as well as 18 transcription factor cofactor genes was relatively more complex. Moreover, 29 high-sulfur protein genes and *ELF5* (the key gene of the regulatory network) were noted to constitute a regulatory network. Pearson's correlation analysis revealed positive regulatory relationships between the high-sulfur proteins and all the transcription factors and cofactors.

Identification of Sulfur Metabolism Gene Expression Patterns in Cashmere Goat Blood and Skin

We, next, ran a complete search for sulfur metabolism genes in the cashmere goat genome using all the annotated pathway of the sulfur metabolism from GO database[1]. In total, 29

[1]http://geneontology.org/

FIGURE 3 | Amino acid frequency of 20 conserved motifs. Each letter represents an amino acid; the larger the letter in a motif, the higher is amino acid frequency.

species were found to cover 116 sulfur metabolism pathways with a total of 1789 sulfur metabolism genes, including 321 sulfur metabolism genes in the cashmere goat. In total, 10, 1, and 310 sulfur metabolism genes were specifically expressed in the skin, in the blood, and in both the skin and blood, respectively.

In total, 20 GO terms incorporating the cofactor metabolic process, sulfur compound biosynthetic and metabolic process, acyl-CoA metabolic process, mucopolysaccharide metabolic process, and sulfur compound catabolic process were enriched significantly (**Supplementary Figure 4**). For sulfur metabolism genes, the expression patterns may play important roles in the growth of different wools. Therefore, we analyzed sulfur metabolism gene expression all year round. The results showed that changes in the blood and skin mainly occurred between June and July. In the skin, a total of 320 genes expression showed a significantly elevated trend from January to June, with a slow decrease in expression after July. In the blood, the expression of 311 sulfur metabolism genes showed an overall decreasing trend between January and June, with the lowest expression in June and a gradual increase after July (**Figure 9**).

We then investigated the transcriptional differences that characterize preferentially or specifically expressed genes in each development stage of skin and blood. Over the year, the skin had 43, 40, 37, 46, 43, 46, 45, 41, 39, 43, 36, and 39 genes with upregulated expression and had 16, 12, 8, 8, 9, 12, 11, 14, 13, 12, 16, and 14 genes with downregulated expression compared with that in blood (**Supplementary Table 6**). Over the study months, the number of tissue-specific genes varied between 3 and 9, with a total of 15 genes showing tissue-specific expression. These results suggested the potential function of sulfur metabolism genes have important roles in cashmere goat skin.

Global Transcriptome Analysis for Tissue-Specific Functional Pathway

The transcriptome analysis of the blood and skin tissues at different development stages of the control and treatment groups was performed to provide crucial system-level insights into molecular mechanisms underlying wool and cashmere development and melatonin. The transcriptome data from skin and blood samples were 99.09% (**Supplementary Table 7**) and 98.55% (**Supplementary Table 8**) valid, respectively. In total, 23,108 and 23,050 genes were identified in the skin of the control and treatment groups, respectively. Moreover, 21,378 and 21,304 genes were identified in the blood of the control and treatment groups, respectively. Furthermore, 56–57% and 59–60% of genes exhibited medium expression level (FPKM = 5–100) in skin and blood of the different groups, respectively.

We then analyzed the changes in gene expression associated with treatment and control for different tissues (blood vs. skin). There were 6,327 DEGs in the control group ($|\log_2 fc| > 1$, $P < 0.05$), with 3,715 genes upregulated in the skin and 2,612 genes upregulated in the blood. The number of upregulated DEGs in the treatment group was 3634 in the skin and 2607 in the blood.

Gene set enrichment analysis (GSEA) was then used to find enriched GO gene-sets upregulated in the blood and skin of the treatment and control groups. The results were generated after scoring DEGs using the Signal2Noise statistic. Only gene-sets that passed conservative significance thresholds (FDR < 25%)

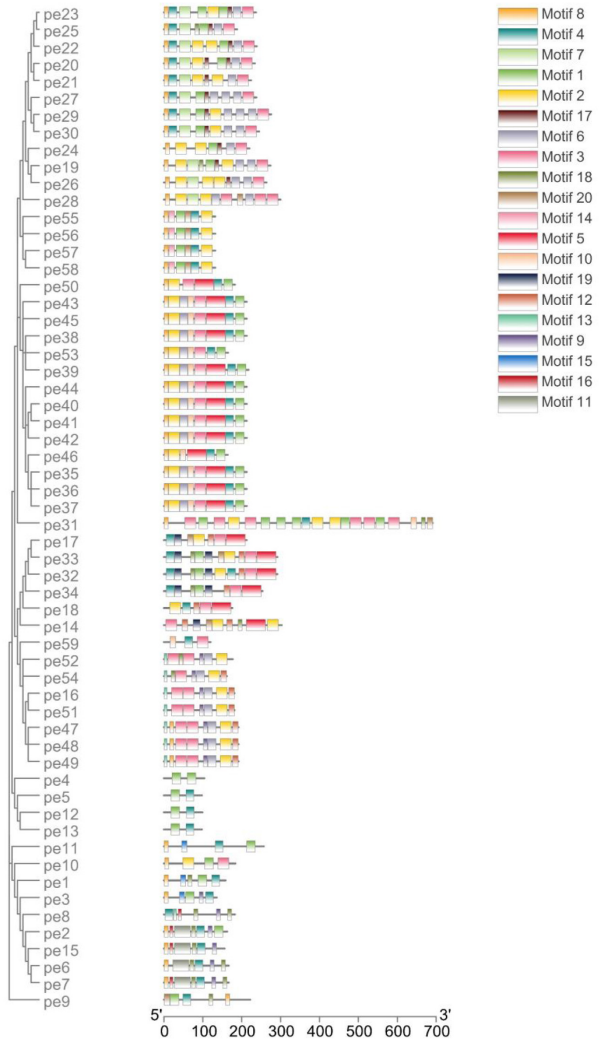

FIGURE 4 | Distribution of conserved motifs of high-sulfur protein genes.

were selected for display in the Enrichment Map; consequently, 780 and 504 gene-sets were enriched in the skin and blood of the control group, respectively, and 824 and 504 gene-sets were enriched in the skin and blood of the treatment group, respectively. Of all the pathways enriched by the DEGs in control (blood vs. skin) and treatment (blood vs. skin) groups, 522 functional pathways of cell development regulation were strongly correlated with each other; moreover, these pathways were correlated with the WNT canonical pathway, BMP signaling pathway, cell motility, kinase activity, and muscle tissue development activity (**Supplementary Figure 5A**). This two-enrichment visualization demonstrated the same (all red or all blue) or different enrichment across the two data sets. Here, we noted that the agreement between the control and treatment groups was noted at very high-most nodes, which are all one color, thus indicating that these gene-sets have tissue-specific upregulation (**Figure 10**). In the treatment group, 11 gene-sets were significantly enriched in the blood but not in the skin, and gene-sets with stronger upregulation only in the skin were present in nine functional pathways (**Supplementary Figure 5B**). In total, 10 gene-sets were enriched in the control group and only constituted a minor portion of the blood map. Moreover, gene-sets with stronger enrichment only in the skin were present in 12 functional pathways (**Supplementary Figure 5C**). In total, 15 functional pathways in the control group were upregulated in the blood, but an opposite result was noted in the treatment group, and up regulated in the skin (**Supplementary Figure 5D**). Actin filament organization, GTPase binding, rho GTPase binding, ruffle membrane, and small GTPase-mediated signal transduction gene-set were strongly induced in the blood after melatonin treatment. Thus, these five functional pathways could be more dependent on melatonin in the blood (**Supplementary Figure 5D**).

Effect of Melatonin on Sulfur Metabolism Gene and Tissue-Specific Gene Expression Changes

To understand the tissue-specific expression patterns of all genes, we clustered all their expression patterns (4389 genes) by using WGCNA. We identified three main gene modules, where the turquoise modules represent the tissue-specific expression patterns (**Figure 11**), including 3629 genes. This module demonstrated a more pronounced and patterned regulation by tissues but were less patterned by development stages.

Gene set enrichment analysis (Subramanian et al., 2005) and Enrichment Map (Daniele et al., 2010) were used to analyze upregulated pathway including the turquoise module genes in the blood and skin. The results showed that many of the key pathways in the turquoise module were also tissue-specific (**Figure 12**). In the skin, 168 upregulated pathways were enriched, including sulfur compound metabolic, cellular amino acid catabolic, organic acid biosynthetic, and WNT signaling pathways. There were 687 upregulated pathways in the blood, including adaptive immune response, innate immune response, immune system development, and regulation of leukocyte migration. The network simultaneously showed the pathways upregulated in the blood and skin; here, blue and red nodes denoted the upregulated pathways in the blood and skin, respectively. Most nodes of the node were of one color, whereas the remaining pathways were both blue and red, demonstrating that a subset of gene-sets both regulated metabolic processes in the blood and skin.

The enriched pathways in blood appeared in most functional groups (blue nodes), indicating that the response of blood to the expression of genes with tissue-specific expression patterns was relatively strong. The immune-related pathways were significantly upregulated in the blood, whereas the oxidation-related pathways were significantly upregulated in the skin.

In general, there were fewer pathways upregulated in the skin than in the blood (168 vs. 687). Many of the gene-sets upregulated only in the skin were associated with amino acid metabolism, sulfur compound biosynthesis, and transport kinase function. The tissue-specific modules were positively or negatively correlated with 86 sulfur metabolism genes, with

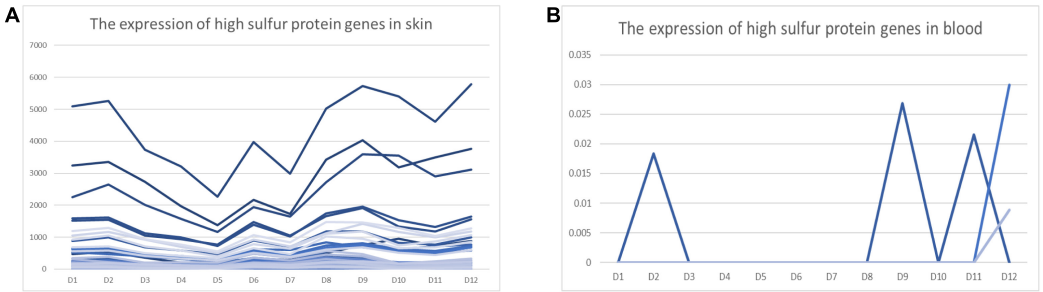

FIGURE 5 | FPKM of high-sulfur protein genes over the 12 study months. Abscissa represents month, and ordinate represents FPKM. D represents the control group.

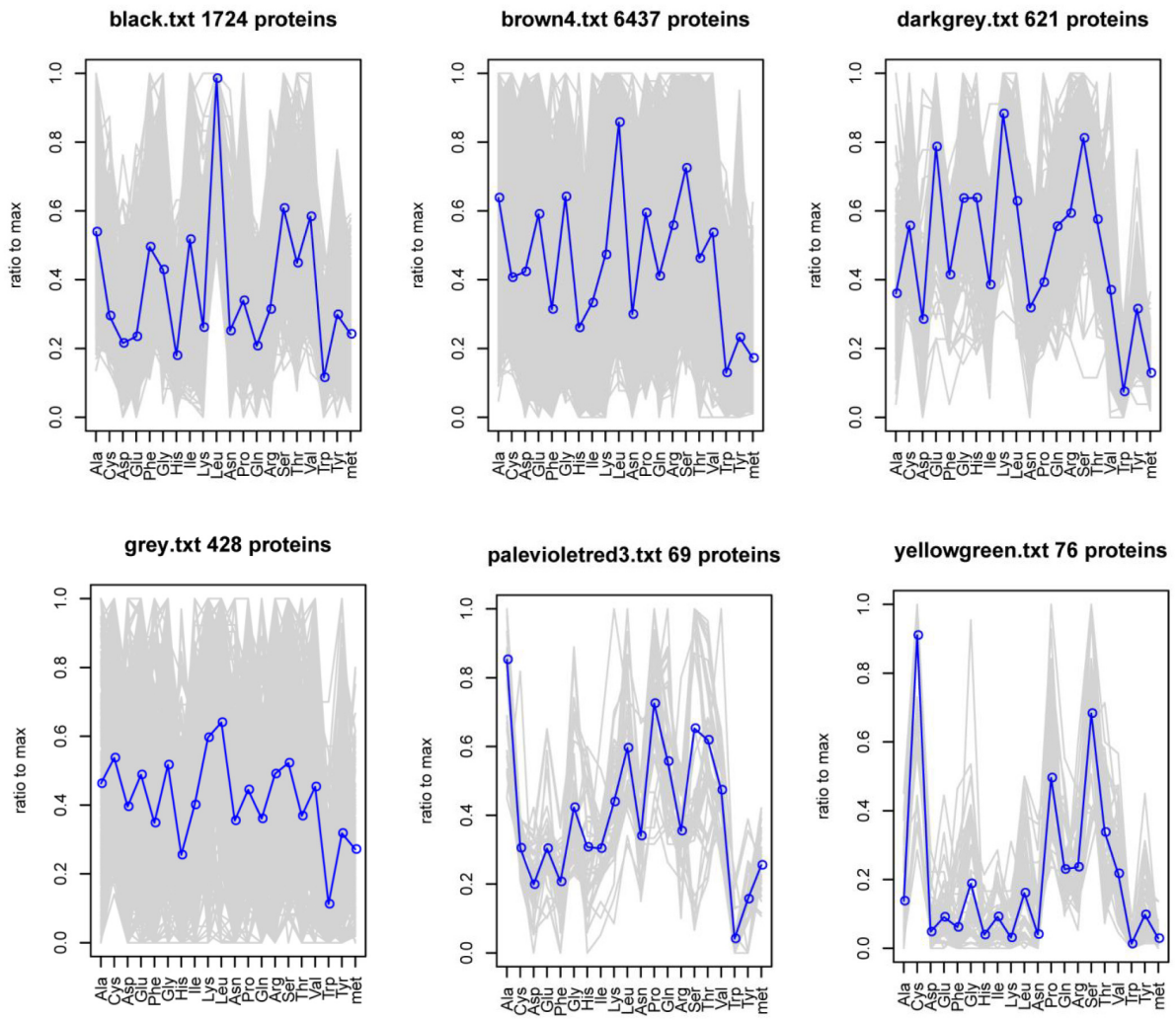

FIGURE 6 | Abundance of 20 amino acids in each CDS in the module.

a correlation coefficient of >9.8; moreover, the correlation coefficient of individual module was 0.99 ($P < 1e^{-20}$), indicating that the module obtained via WGCNA was high reliable (**Supplementary Figure 6**).

According to the WGCNA results, we constructed coexpression modules, and part of the genes in the tissue-specific module involved in pathway specificity were upregulated in the skin, such as those related to amino acid metabolism, sulfur

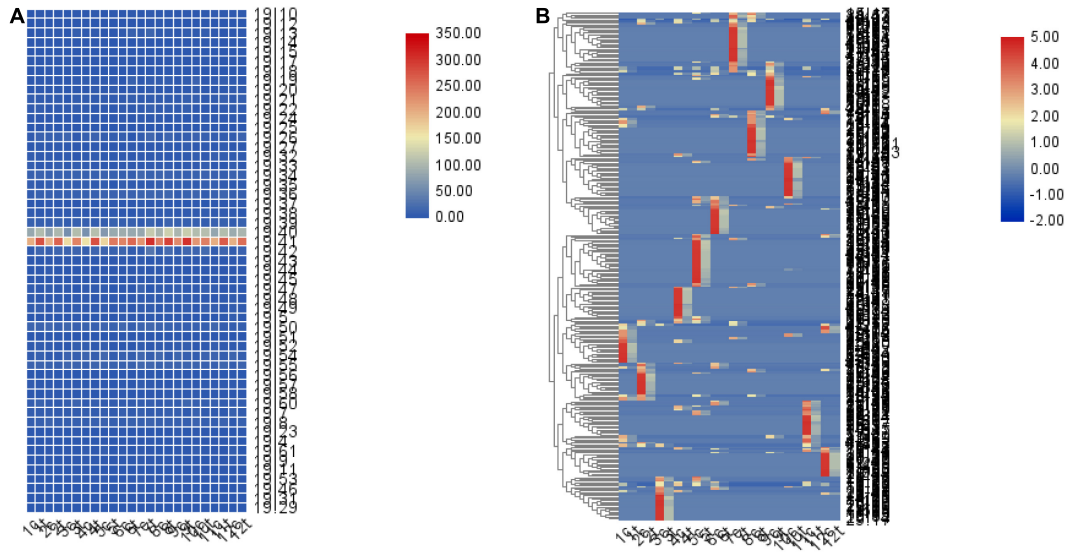

FIGURE 7 | Heat map of the number of ASE loci in the 1M region. **(A)** Quantitative heat map of ASE loci in every 1M region of chromosome 19. **(B)** A total of 308 regions exhibiting differences in the proportion of ASE sites between the control and treatment groups (minimum/maximum $\leq$ 0.3), and the locations at which ASE numbers differed between months. The number represents the month, c represents the control group, t represents the treatment group.

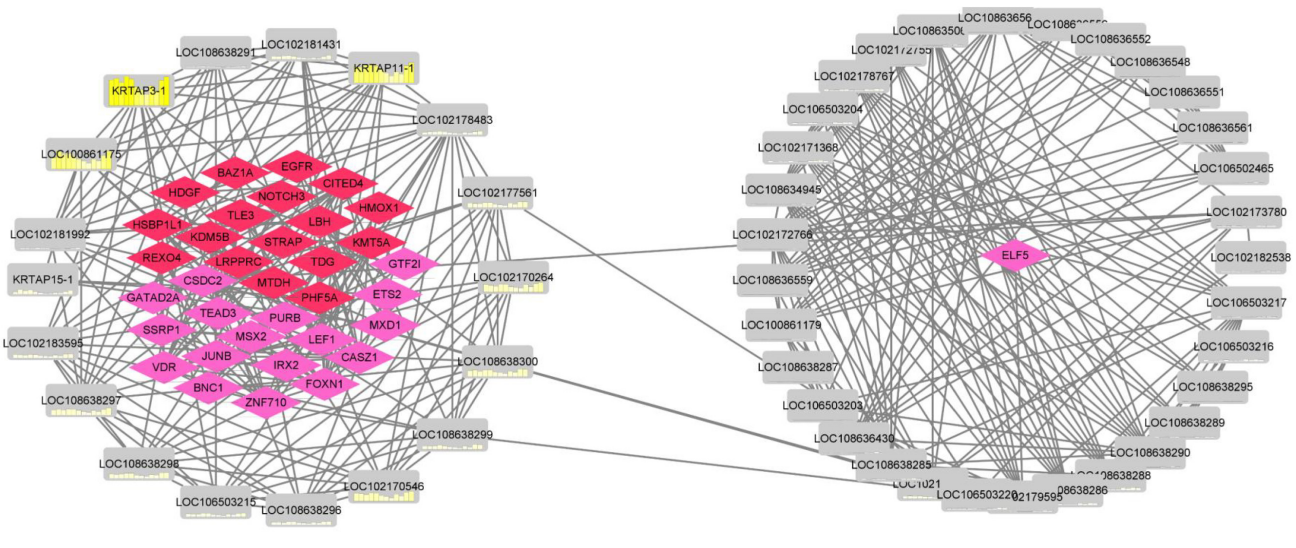

FIGURE 8 | Coexpression regulatory network of high-sulfur protein gene, transcription factor, and transcription cofactor. The red node represents transcription factor, the pink node represents transcription factor cofactor, and the gray node represents high sulfur protein gene. The yellow node shows the expression over 12 months.

compound biosynthesis, and transport kinase function. Because various biological metabolic processes are not caused by a single factor, the development of gene interaction networks not only provides an effective way to probe complex metabolic processes but also improves the comprehensiveness of our research. Based on this, we constructed an interactive regulatory network between the tissue-specific genes and sulfur metabolism genes.

For network construction, genes were screened from the turquoise module and linear discriminant analysis effect size (LEfSe) (Segata et al., 2011) was used to elucidate tissue-specific genes for network construction. LEfSe, which judged the factors most likely to explain the different categories, was used to search for biomarkers. Filtering was performed on the basis of the GS of genes and phenotypic traits in the WGCNA results, and genes with a GS of top3 were selected as positively correlated. In total, 258 relation pairs were obtained with GS $\geq$ 0.85 and $P \leq 1e^{15}$ involving 122 turquoise genes. LEfSe results illustrated 23 genes with tissue-specific expression in the treatment group, but no genes with tissue-specific expression were noted in the control group (**Supplementary Figure 7**). Based on the 23 genes with tissue-specific expression and the sulfur metabolism gene regulatory network, *VAT*1, *PGRMC*1, and *SLC31A*1 were

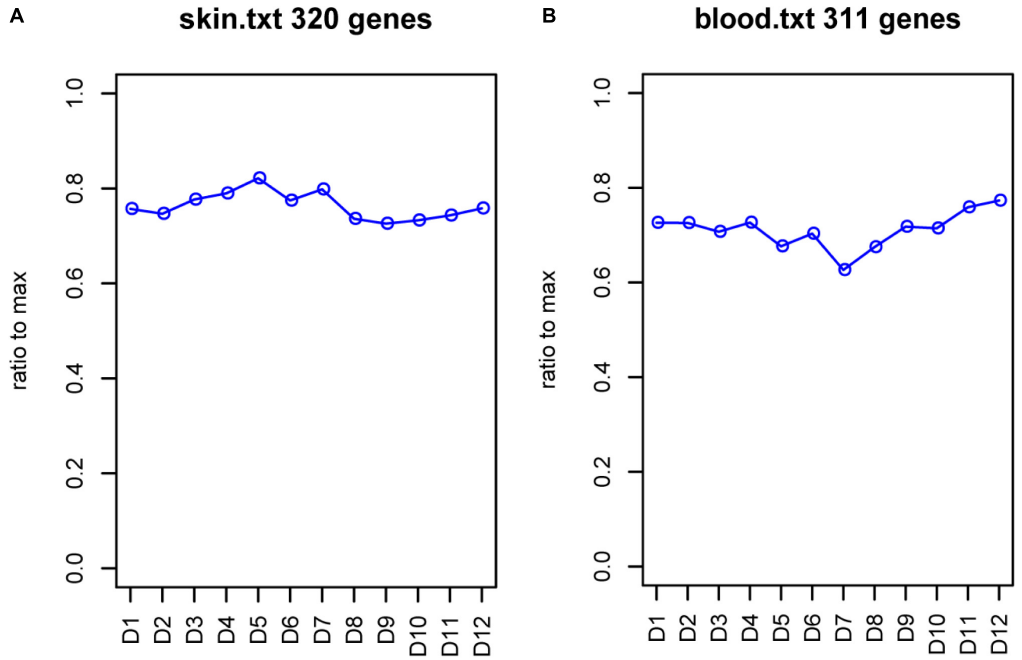

FIGURE 9 | FPKM of sulfur metabolism genes. **(A)** FPKM of sulfur metabolism genes in skin. **(B)** FPKM of sulfur metabolism genes in blood. Abscissa represents month, and ordinate represents ratio to max. D represents the control group.

found to be hub genes (**Figure 13**)—all of which were highly and less expressed in the skin and blood of the treatment group, respectively.

Although we constructed coexpression modules between the tissue-specific genes and sulfur metabolism genes, the specific biological function of these genes was unknown. By using Database for Annotation, Visualization and Integrated Discovery (DAVID, version 6.7) (Huang et al., 2009), we performed functional enrichment analysis for all genes in the regulatory network. The results indicated that genes in the regulatory network were enriched to a result closely related to the tissue biological functions. For instance, the tissue-specific gene *VAT*1—highly expressed specifically in skin tissue after the implantation of melatonin—is mainly involved in the oxidation–reduction process, and regulates 11 genes involved in fatty acid metabolism (*THEM*5, *ENPP*2, *DSEL*, *ACSL*1, *FAR*2, *ELOVL*4, *ELOVL*3, *ACOT*6, *ACSBG*1, *NDNF*, and *PDK*4). There are four genes involved in cysteine and SAA metabolism (*CTH*, *CDO*1, *AHCY*, and *MAT1A*). Among these, *CTH* interacts with *PSMD*12, *CDO*1 with *ST6GALNAC2* and *SLC25A4*, *AHCY* with *YWHAE* and *TUBA1C*, and *MAT1A* with *RAD23B*. After melatonin implantation, *PSMD*12, *ST6GALNAC2*, *SLC25A4*, *TUBA1C,* and *RAD23B* were upregulated in the skin. The function of these genes was most related to cell energy metabolism and cell cycle.

DISCUSSION

Sulfur is an essential mineral for organisms it not only functions as a structural component but also performs specific functions in cellular metabolism (Mcnab et al., 1990). In sheep, the high-sulfur protein genes family comprises six members; of these, *KRTAP*4 and *KRTAP*5 are the ultra–high-sulfur protein genes, containing eight members in total: *KRTAP*4-1, *KRTAP*4-2, *KRTAP*4-3, *KRTAP*5-1, *KRTAP*5-2, *KRTAP*5-3, *KRTAP*5-4, and *KRTAP*5-5 (Gong et al., 2016). The high and ultra–high-sulfur protein genes are located on human chromosomes 17q21.2, 21q22.1, 21q22.3, 11p15.5, and 11q13.4 (Rogers et al., 2006).

Studies have shown that in sheep, sulfur and SAAs play a specific role in metabolism; the sulfur levels in erythrocytes and plasma proteins (mainly those containing cystine and methionine) are higher in sheep than in cattle, horses, and dogs (Mапкова and Wang, 1954). Cystine metabolized from glutathione in blood is a constituent of wool proteins (Mапкова and Wang, 1954). Then, the sulfur metabolism during the enrichment of sulfur from the blood to the skin is extremely important. Here, we performed deep transcriptome sequencing on samples obtained from cashmere goat blood and skin; moreover, the expression patterns of high-sulfur protein genes were systematically analyzed to provide further insights into the molecular mechanism underlying sulfur's role in cashmere goats' wool growth regulation.

Significant ($P \leq 0.01$) interactions were noted between 47 high-sulfur protein genes and transcription factors and cofactors with ASE. However, the ASE of these transcription factors and cofactors was inhibited by melatonin. Thirteen genes in the interaction network were functionally associated with the functional of hair growth.

*Elf*5 (Driskell et al., 2013) and *EGR*1 (Phan et al., 2020) directly regulate *KRT*18 expression, and *Elf*5 may play a role in mediating fibroblast growth factor regulatory processes. *LEF*1 in fibroblasts can promote skin repair and hair follicle regeneration, and it

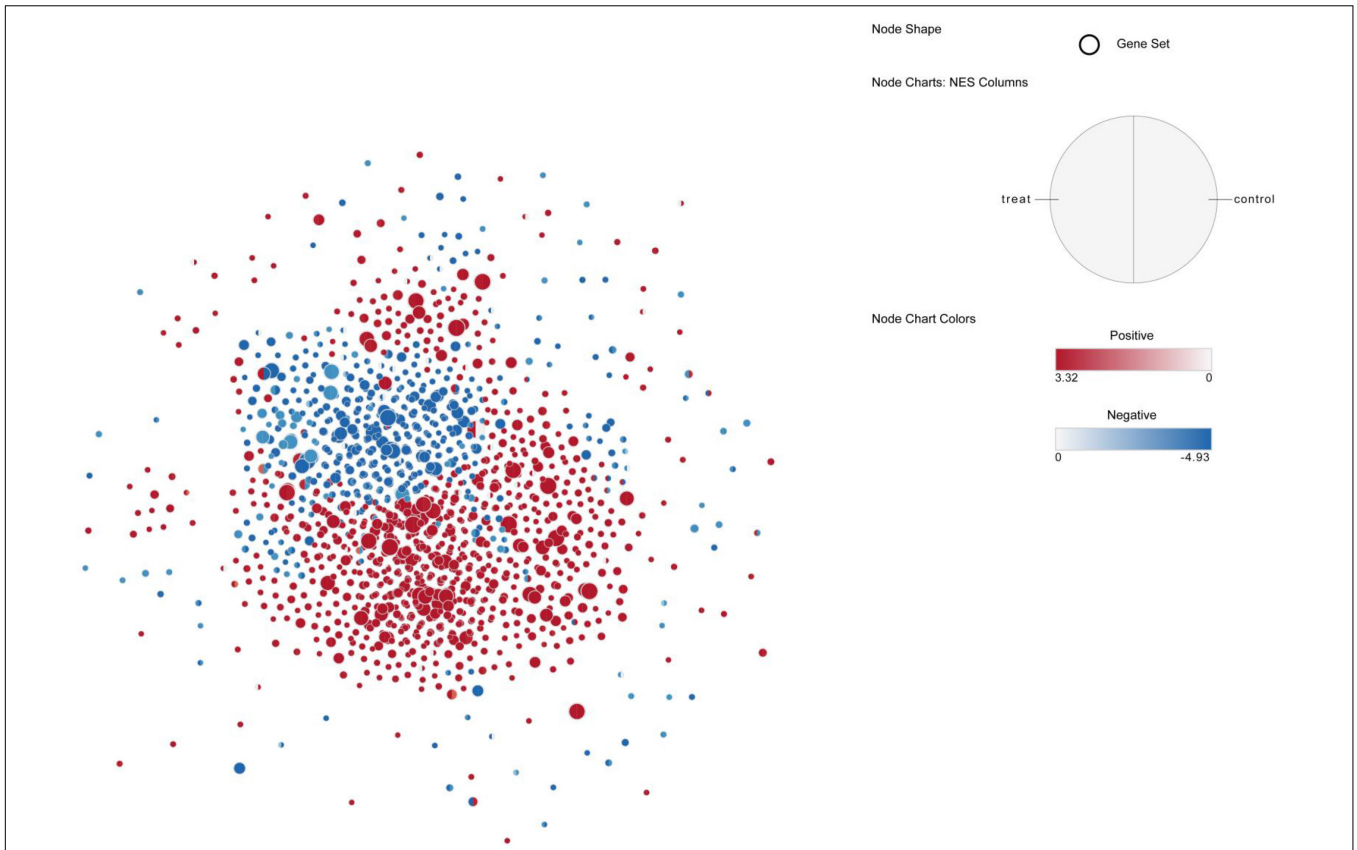

FIGURE 10 | Up-regulated pathway network of blood and skin in control and treat, the red node indicates that the pathway is up-regulated in the skin, and the blue node indicates that the pathway is up-regulated in the blood, the left half of the node represents treat and the right side represents control.

is a key effector in the WNT signaling pathway involved in hair follicle morphogenesis. WNT target gene transcription is repressed by *TLE*3, and β-catenin directly competes with TLE proteins for TCF/LEF binding to complete gene regulation at WNT pathway activation.

β-Catenin inhibition by *VDR* promotes keratinocyte proliferation and hair follicle differentiation (Hu et al., 2014). *JUB* via WNT/β-catenin signaling can induce epithelial–mesenchymal transition in liver cancer cells (Wang et al., 2018). Loss of functional FOXN1 also has profound effects on epidermal keratinization and epidermal adhesion (Mecklenburg et al., 2010). Mutant *GTF2I* can induce thymic epithelial cell transformation and metabolic alterations (Kim et al., 2020). TGF-β regulates many cellular processes, including cell proliferation and differentiation. Moreover, STRAP is a TGF-β inhibitor of signaling and an important regulator of cell proliferation. TGF-β receptors I and II interact and negatively regulate TGF-β-induced gene expression (Kim et al., 2007). Furthermore, MSX2 is involved in keratin formation (Ma et al., 2003). Downregulation of KHSRP expression in the skin can inhibit mir-198 expression and enhance FSTL1 expression, which stimulates keratinocyte migration (Briata et al., 2016). *KDM5B* is important in cell differentiation, stem cell self-renewal, and other developmental processes (Han et al., 2016). *TEAD*3 can promote human epidermal growth (Li et al., 2020).

In general, mice lacking EGFR fail to develop hair (Tripurani et al., 2018). Thus, it is speculated that the interaction of transcription factors and cofactors with high-sulfur protein genes is upregulated to promote villus growth after melatonin implantation, further enriching current knowledge on high-sulfur protein gene family functions.

In addition to providing sulfur required for maintaining redox reaction, the metabolism of these SAAs produces proteins with a role in maintaining the spatial structure of hair, where intermediary metabolites mediate intercellular and intracellular signaling, thus promoting epigenetic regulation of gene expression and collectively contributing to hair growth (Ward and Denicola, 2019).

With regard to the underlying mechanism of sulfur, we first identified 321 sulfur metabolism genes in the cashmere goat and observed the expression of these genes in skin and blood tissues. Sulfur metabolism gene expression changes in the blood and skin mainly occurred between June and July, and the number of sulfur metabolism genes in the skin was significantly higher than that in the blood. These results suggested a potential function of sulfur metabolism genes which may have important roles to the skin of the cashmere goats. The skin has been highlighted as valuable candidate tissues for research transport system for cysteine (Thomas et al., 2007). Evidence from the coexpression network analysis revealed the sulfur metabolism genes associated

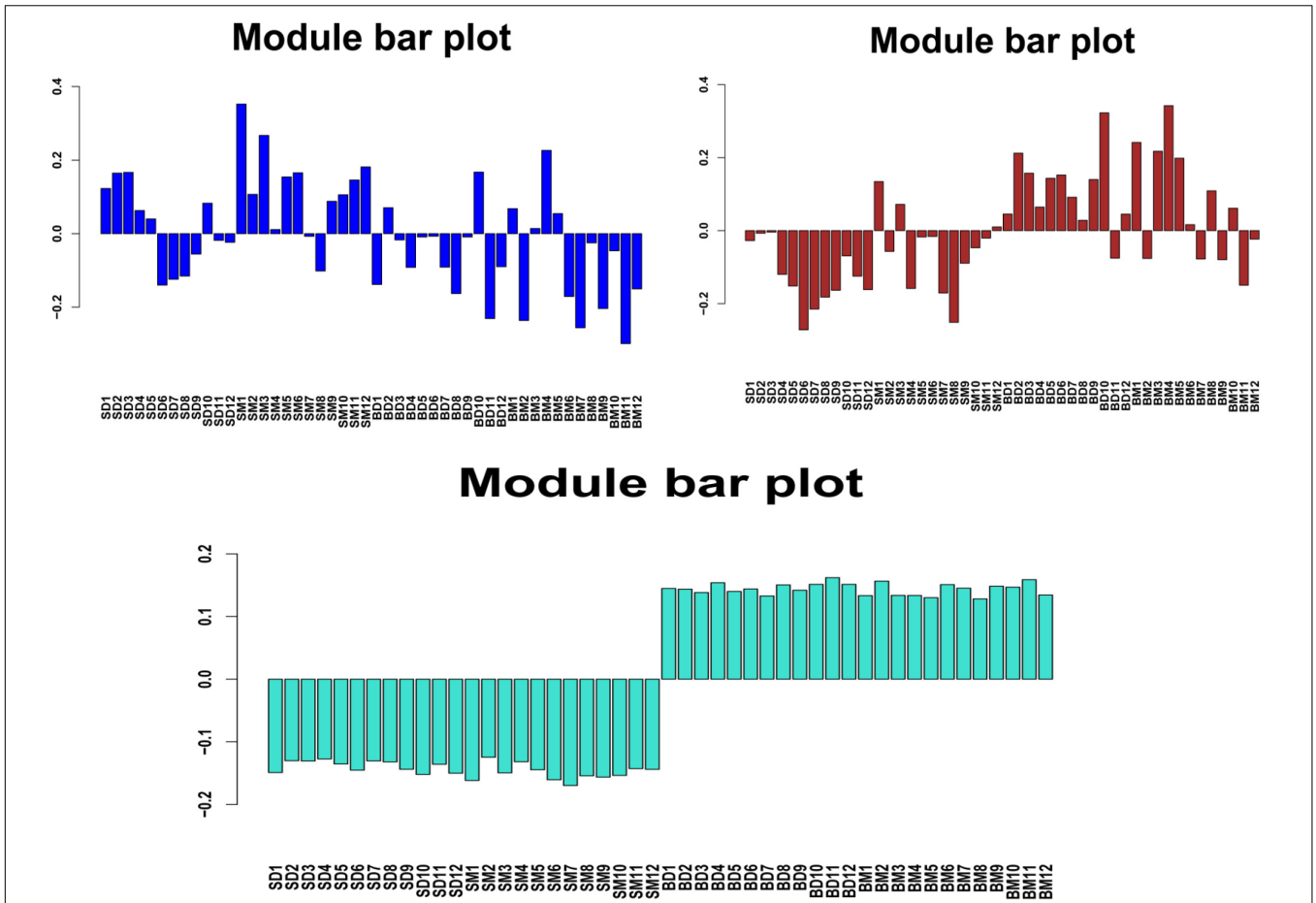

FIGURE 11 | Block eigenvalue bar chart. SD and SM represents the skin samples in the control and treatment groups, respectively, and BD and BM represents the blood samples in the control and treatment groups, respectively.

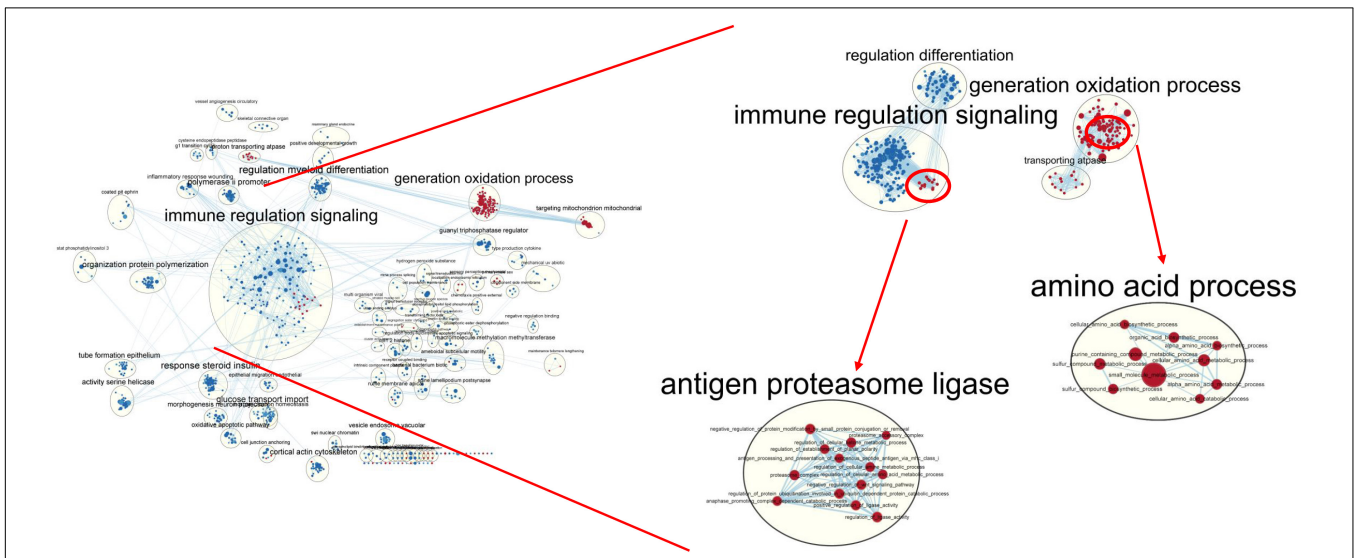

FIGURE 12 | Global network of enrichment results of turquoise module genes. The red and blue nodes indicate that the pathway is upregulated in the skin and blood, respectively.

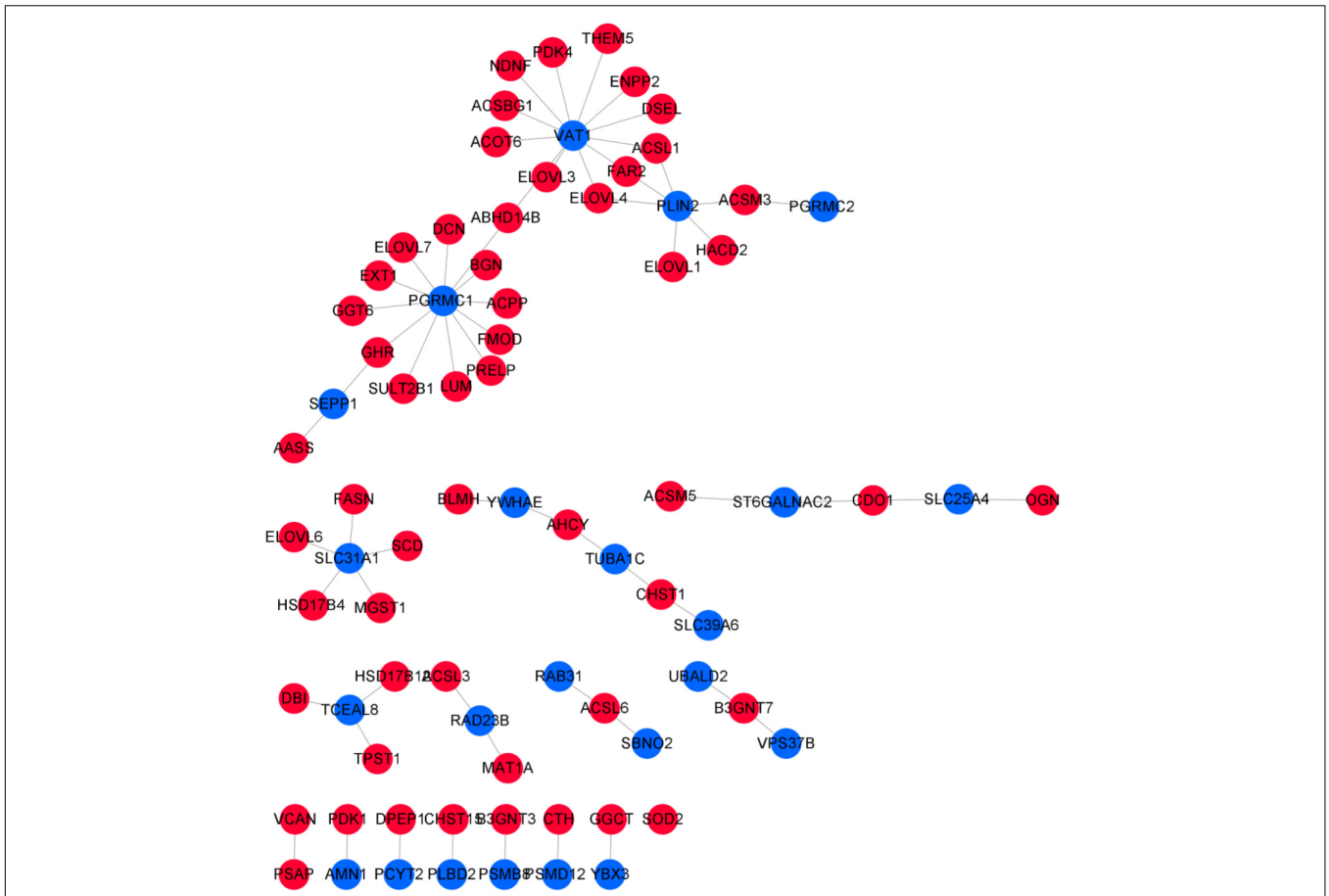

FIGURE 13 | Correlation network of sulfur metabolism genes and tissue-specific expressed genes. The blue nodes represent tissue-specific genes, and the red nodes represent sulfur metabolism genes.

with 23 tissue-specific genes, which were only upregulated in the skin or blood after melatonin implantation. For instance, *CTH*, *CDO*1, *AHCY*, and *MAT1A* were found to be involved in cysteine and SAA metabolism. *CTH* interacts with *PSMD*12, *CDO*1 with *ST6GALNAC2* and *SLC25A4*, *AHCY* with *YWHAE* and *TUBA1C*, and *MAT1A* with *RAD23B*.

Moreover, *PSMD*12 plays a key role in regulating the cell cycle, DNA damage repair, and apoptosis (Saez and Vilchez, 2014; Küry et al., 2017; Contreras et al., 2018; Okumura et al., 2018). *PSMD*12 knockdown can inhibit cell growth and migration (Du et al., 2020). *ST6GALNAC2* has functions in the PI3K/AKT pathway (Ren et al., 2014), which is involved in many cellular processes, including proliferation, differentiation, apoptosis, cell cycle progression, and cell motility (Bellacosa et al., 2005; Engelman et al., 2006). *SLC25A4* has been implicated to have many transport functions for various molecules on the mitochondrial membrane, including ATP/ADP and amino acids, which are molecules constituting cellular energy sources (Albahde et al., 2020).

TUBA1C overexpression is mainly associated with cell cycle regulation. Yin et al. (2019) found that *YWHAE* and *TUBA1C* are functionally related in keratinocytes. We also found that *YWHAE* interacts with *TUBA1C* and both genes were specifically upregulated in the skin after melatonin treatment. Notably, *PSMD*12, *ST6GALNAC2*, *SLC25A4*, *YWHAE*, *TUBA1C*, and *RAD23B* were all upregulated specifically in the skin after melatonin implantation, and the functions of these genes were mostly related to cellular energy metabolism and cell cycle. The energy required for cashmere wool growth comes from a series of oxidation–reduction reactions during cellular metabolism, which are facilitated by different molecules with constituent sulfur atoms (Thomas et al., 2007). The tissue-specific gene *VAT*1 was highly and specifically expressed in the skin tissue after melatonin implantation. This gene is mainly involved in redox processes and regulates 11 genes involved in fatty acid metabolism: *THEM*5, *ENPP*2, *DSEL*, *ACSL1*, *FAR*2, *ELOVL*4, *ELOVL*3, *ACOT*6, *ACSBG1*, *NDNF*, and *PDK*4. These results highlight the potential role of melatonin in skin in upregulated expression of genes involved in cellular energy metabolism as well as those involved in cell cycle and activation of sulfur metabolic processes provides sufficient SAAs for cashmere wool development.

Intracellular targets where melatonin exerts biological actions are receptors, and they are divided into membrane receptors [melatonin type 1 (MT1) and type 2 (MT2) receptors] and nuclear receptors (RORα, RORβ, and RORγ) (Liu et al., 2016).

MT1 and MT2 receptors have been detected in mammalian skin (Söderquist et al., 2015). Human skin primarily transcribes *MT1*, whereas *MT*2 is expressed along with *MT1* in specific conditions. In contrast, mouse skin shows exclusive expression of *MT*2. In human skin, *MT*1 has been detected in the differentiated layer of the epidermis, the outer and inner root sheaths of HF, sweat glands, and blood vessels, whereas *MT2* has been detected in the inner root sheath, sweat glands, and blood vessels (Slominski et al., 2018). In contrast, cashmere goat skin tissues showed no expression of membrane receptors. Expression of only *ROR*α, a nuclear receptor, was detected in the skin of cashmere goat (Wang, 2016).

Based on the overall panoramic regulatory network, we concluded that melatonin affects the pathways involved in the DEG between blood and skin, and the pathways demonstrated spatially specific upregulation trends; for example, after melatonin implantation, the ErbB signaling pathway was found to be upregulated only in the blood from control cashmere goats, whereas only the Notch signaling pathway was noted to be upregulated only in the treated cashmere goat skin.

CONCLUSION

In total, 53 high-sulfur protein genes and 321 sulfur metabolism genes were identified and further analyzed for their expression in the skin and blood tissue. These high-sulfur protein genes are distributed in the 3–4M and 144M regions of chromosome 1 and the 40–41M region of chromosome 19 in goats. We found that ASE in the 40–41M region of chromosome 19 was significantly higher than that in the other regions over the entire study year. In total, 47 high-sulfur protein genes were found to interact with ASE transcription factors and cofactors. The ASE transcription factors and cofactors were inhibited after melatonin implantation. We also constructed a regulatory network of tissue-specific genes and sulfur metabolism genes and found that melatonin possibly activates the sulfur metabolism process by regulating the genes related to cell energy metabolism and cell cycle in the skin. This can provide sufficient SAAs for cashmere wool growth. Our findings offer a new insight into wool growth regulation by sulfur metabolism genes and high-sulfur protein genes in cashmere goats.

DATA AVAILABILITY STATEMENT

The datasets analyzed for this study can be found in the Genome Sequence Archive in BIG Data Center, Beijing Institute of Genomics (BIG), Chinese Academy of Sciences, under accession numbers CRA004599 and CRA004598 that are publicly accessible at https://ngdc.cncb.ac.cn/gsa.

ETHICS STATEMENT

The animal study was reviewed and approved by the Special Committee on Scientific Research and Academic Ethics of Inner Mongolia Agricultural University [Approval No. (2020)056].

AUTHOR CONTRIBUTIONS

YC: writing–original draft preparation and writing–reviewing and editing. WZ: supervision and project administration, and writing–reviewing and editing. YS, BL, LG, ZL, LZ, LD, and CJ: experimental sample and data analysis. CL: funding acquisition. YS: contributed as co-author. All authors contributed to the article and approved the submitted version.

FUNDING

The reported work was supported by the National Natural Science Foundation of China (nos. 31672385, 31402052), Inner Mongolia Natural Science Foundation (no. 2019MS03078), from the Special Open Project on the Construction of Mongolian Pharmacy Doctoral Station for National Service with Special Needs (no. MDMYBJ2019004), and the Doctoral Scientific Research Foundation of Inner Mongolia University for Nationalities (no. BS308). The funding played a role in the design of the study and the collection, analysis, and interpretation of data.

ACKNOWLEDGMENTS

We thank study participants for their contribution.

SUPPLEMENTARY MATERIAL

The Supplementary Material for this article can be found online at: https://www.frontiersin.org/articles/10.3389/fgene.2021.715526/full#supplementary-material

Supplementary Figure 1 | The average content of melatonin of cashmere goat in different months.Blue line is the treat group and red line is the control.

Supplementary Figure 2 | KEGG pathway analysis of 856 genes.

Supplementary Figure 3 | Expression pattern of 26 transcription cofactors and 22 transcription factors. D is the control group, M is the implantation group, and the number is the month.

Supplementary Figure 4 | KEGG pathway of sulfur metabolism genes.

Supplementary Figure 5 | (A) Global network of gene enrichment in the blood and skin samples of the control and treatment groups. **(B)** Pathways upregulated specifically in the treatment group skin and blood. **(C)** Pathways upregulated specifically in the control group skin and blood. **(D)** Upregulated specifically in the treatment and control group skin and blood. The red and blue node indicates that the pathway is up-regulated in the skin and blood, respectively, and the left and right halves of the node represent the treatment and control groups, respectively.

Supplementary Figure 6 | Correlations between module eigengenes and sulfur metabolism genes. The numbers within the heat map represent correlations, and *P*-values (in parentheses; red, positively correlated, and blue, negatively correlated) for the module-trait associations.

Supplementary Figure 7 | LEfSe highlights 23 tissue-specific consistently DEGs between the treatment group blood and skin.

REFERENCES

Albahde, M. A. H., Zhang, P., Zhang, Q., Li, G. Q., and Wang, W. L. (2020). Upregulated Expression of TUBA1C Predicts Poor Prognosis and Promotes Oncogenesis in Pancreatic Ductal Adenocarcinoma via Regulating the Cell Cycle. *Front. Oncol.* 10:49. doi: 10.3389/fonc.2020.00049

Bailey, T. L., Mikael, B., Buske, F. A., Frith, M., Grant, C. E., Clementi, L., et al. (2009). MEME Suite: tools for motif discovery and searching. *Nucleic Acids Res.* 37, W202–W208. doi: 10.1093/nar/gkp335

Bellacosa, A., Kumar, C. C., Cristofano, A. D., and Testa, J. R. (2005). Activation of AKT kinases in cancer: implications for therapeutic targeting. *Adv. Cancer Res.* 94, 29–86. doi: 10.1016/S0065-230X(05)94002-5

Briata, P., Bordo, D., Puppo, M., Gorlero, F., Rossi, M., Perrone-Bizzozero, N., et al. (2016). Diverse roles of the nucleic acid-binding protein KHSRP in cell differentiation and disease. *Wiley Interdiscip. Rev. RNA* 7, 227–240. doi: 10.1002/wrna.1327

Chen, C. J., Chen, H., Zhang, Y., Thomas, H. R., Frank, M. H., and He, R. X. (2020). TBtools: an integrative toolkit developed for interactive analyses of big biological data. *Mol. Plant* 13, 1194–1202. doi: 10.1016/j.molp.2020.06.009

Contreras, L., Calderon, R. I., Varela-Ramirez, A., Zhang, H. Y., Quan, Y., Das, U., et al. (2018). Induction of apoptosis via proteasome inhibition in leukemia/lymphoma cells by two potent piperidones. *Cell. Oncol.* 41, 623–636. doi: 10.1007/s13402-018-0397-1

Daniele, M., Isserlin, R., Stueker, O., Emili, A., and Bader, G. D. (2010). Enrichment map: a network-based method for gene-set enrichment visualization and interpretation. *Plos One* 5:e13984. doi: 10.1371/journal.pone.0013984

Dong, Y., Xie, M., Jiang, Y., Xiao, N. Q., Du, X. Y., Zhang, W. G., et al. (2013). Sequencing and automated whole-genome optical mapping of the genome of a domestic goat (*Capra hircus*). *Nat. Biotechnol.* 31, 135–141. doi: 10.1038/nbt.2478

Downes, A. M., Lyne, A. G., and Clarke, W. H. (1962). Radioautographic studies of the incorporation of 35s cystine into wool. *Aust. J. Biol. Sci.* 15, 713–719. doi: 10.1071/bi9620713

Driskell, R. R., Lichtenberger, B. M., Hoste, E., Kretzschmar, K., Simons, B. D., Charalambous, M., et al. (2013). Distinct fibroblast lineages determine dermal architecture in skin development and repair. *Nature.* 504, 277–281. doi: 10.1038/nature12783

Du, X. N., Shen, X., Dai, L., Bi, F., Zhang, H., and Lu, C. F. (2020). PSMD12 promotes breast cancer growth via inhibiting the expression of pro-apoptotic genes. *Biochem. Biophys. Res. Commun.* 526, 368–374. doi: 10.1016/j.bbrc.2020.03.095

Engelman, J. A., Luo, J., and Cantley, L. C. (2006). The evolution of phosphatidylinositol 3-kinases as regulators of growth and metabolism. *Nat. Rev. Genet.* 7, 606–619. doi: 10.1038/nrg1879

Gong, H., Zhou, H. T., Forrest, R. H. J., Li, S. B., Wang, J. Q., Dyer, J. M., et al. (2016). Wool keratin-associated protein genes in sheep—a review. *Genes* 7:24. doi: 10.3390/genes7060024

Han, M., Xu, W., Cheng, P., Jin, H. C., and Wang, X. (2016). Histone demethylase lysine demethylase 5B in development and cancer. *Oncotarget* 8, 8980–8991. doi: 10.18632/oncotarget.13858

Hu, L., Bikle, D. D., and Oda, Y. (2014). Reciprocal role of vitamin D receptor on β-catenin regulated keratinocyte proliferation and differentiation. *J. Steroid Biochem. Mol. Biol.* 144, 237–241. doi: 10.1016/j.jsbmb.2013.11.002

Huang, D. W., Sherman, B. T., and Lempicki, R. A. (2009). Systematic and integrative analysis of large gene lists using DAVID bioinformatics resources. *Nat. Protoc.* 4, 44–57. doi: 10.1038/nprot.2008.211

Hynd, P. I. (1989). "Factors influencing cellular events in the wool follicle," in *The Biology of Wool and Hair*, eds G. E. Rogers, P. J. Reis, K. A. Ward, and R. C. Marshall (London: Chapman and Hall), 169–184.

Khan, I., Maldonado, E., Vasconcelos, V., O'Brien, S. J., Johnson, W. E., Antunes, A., et al. (2014). Mammalian keratin associated proteins (KRTAPs) subgenomes: disentangling hair diversity and adaptation to terrestrial and aquatic environments. *BMC Genomics* 15:779. doi: 10.1186/1471-2164-15-779

Kim, C. J., Choi, B. J., Song, J. H., Park, Y. K., Cho, Y. G., Nam, S. W., et al. (2007). Overexpression of serine-threonine receptor kinase-associated protein in colorectal cancers. *Pathol. Int.* 57, 178–182. doi: 10.1111/j.1440-1827.2007.02078.x

Kim, K. I, Rao, G. H., Zhao, X. L., Fan, R. Z., Avantaggiati, M. L., Wang, Y., et al. (2020). Mutant GTF2I induces cell transformation and metabolic alterations in thymic epithelial cells. *Cell Death Differ.* 27, 2263–2279. doi: 10.1038/s41418-020-0502-7

Küry, S., Besnard, T., Ebstein, F., Khan, T. N., Gambin, T., Douglas, J., et al. (2017). De novo disruption of the proteasome regulatory subunit PSMD12 causes a syndromic neurodevelopmental disorder. *Am. J. Hum. Genet.* 100, 352–363. doi: 10.1016/j.ajhg.2017.01.003

Langfelder, P., and Horvath, S. (2008). WGCNA: an R package for weighted correlation network analysis. *Bmc Bioinformatics* 9:559. doi: 10.1186/1471-2105-9-559

Li, J. T., Tiwari, M., Xu, X., Chen, Y. F., Tamayo, P., and Sen, G. L. (2020). TEAD1 and TEAD3 play redundant roles in the regulation of human epidermal proliferation. *J. Invest. Dermatol.* 140, 2081–2084. doi: 10.1016/j.jid.2020.01.029

Liu, J., Clough, S. J., Hutchinson, A. J., Adamah-Biassi, E. B., Popovska-Gorevski, M., and Dubocovich, M. L. (2016). MT1 and MT2 Melatonin Receptors: A Therapeutic Perspective. *Annu. Rev. Pharmacol. Toxicol.* 56, 361–383. doi: 10.1146/annurev-pharmtox-010814-124742

Ma, L., Liu, J., Wu, T., Plikus, M., Jiang, T. X., Bi, Q., et al. (2003). 'Cyclic alopecia' in Msx2 mutants: defects in hair cycling and hair shaft differentiation. *Development.* 130, 379–389. doi: 10.1242/dev.00201

Маткова, КВ, and Wang, H. M. (1954). Sulfur metabolism and wool growth in sheep. *Chin. J. Vet. Med.* 107–111.

Mcnab, A. R., Andrus, P., Wagner, T. E., Buhl, A. E., Waldon, D. J., Kawabe, T. T., et al. (1990). Hair-specific expression of chloramphenicol acetyltransferase in transgenic mice under the control of an ultra-high-sulfur keratin promoter. *Proc. Natl. Acad. Sci. U. S. A.* 87, 6848–6852. doi: 10.1073/pnas.87.17.6848

Mecklenburg, L., Tychsen, B., and Paus, R. (2010). Learning from nudity: lessons from the nude phenotype. *Exp. Dermatol.* 14, 797–810. doi: 10.1111/j.1600-0625.2005.00362.x

Okumura, T., Ikeda, K., Ujihira, T., Okamoto, K., Horie-Inoue, K., Takeda, S., et al. (2018). Proteasome 26S subunit PSMD1 regulates breast cancer cell growth through p53 protein degradation. *J. Biochem.* 163, 19–29. doi: 10.1093/jb/mvx053

Phan, Q. M., Fine, G. M., Salz, L., Herrera, G. G., Wildman, B. B., Driskell, I. M., et al. (2020). Lef1 expression in fibroblasts maintains developmental potential in adult skin to regenerate wounds. *eLife* 9:e60066. doi: 10.7554/eLife.60066

Reis, P. J., and Schinckel, P. G. (1963). Some aspects of sulfur containing amino acids on the growth and composition of wool. *Aust. J. Biol. Sci.* 16:218. doi: 10.1071/bi9640532

Reis, P. J., and Schinekel, P. G. (1961). Nitrogen utilization and wool production by sheep. *Aust. J. Agric. Res.* 12, 335–352. doi: 10.1071/ar9610335

Ren, D., Jia, L., Li, Y., Gong, Y. X., Liu, C., Zhang, X., et al. (2014). ST6GalNAcII mediates the invasive properties of breast carcinoma through PI3K/Akt/NF-κB signaling pathway. *IUBMB Life* 66, 300–308. doi: 10.1002/iub.1268

Ritchie, M. E., Belinda, P., Wu, D., Hu, Y. F., Law, C. W., Shi, W., et al. (2015). limma powers differential expression analyses for RNA-sequencing and microarray studies. *Nucleic Acids Res.* 43:e47. doi: 10.1093/nar/gkv007

Rogers, M. A., Langbein, L., Praetzel-Wunder, S., Winter, H., and Schweizer, J. (2006). Human hair keratin-associated proteins(KAPs). *Int. Rev. Cytol.* 251, 209–263. doi: 10.1016/S0074-7696(06)51006-X

Saez, I., and Vilchez, D. (2014). The mechanistic links between proteasome activity, aging and age-related diseases. *Curr. Genomics* 15, 38–51. doi: 10.2174/138920291501140306113344

Segata, N., Izard, J., Waldron, L., Gevers, D., Miropolsky, L., Garrett, W. S., et al. (2011). Metagenomic biomarker discovery and explanation. *Genome Biol.* 12:R60. doi: 10.1186/gb-2011-12-6-r60

Sherlock, R. G., Harris, P. M., Lee, J., Wickham, G. A., Woods, J. L., and McCutcheon, S. N. (2001). Intake and long-term cysteine supplementation change wool characteristics of Romney sheep. *Aust. J. Agric. Res.* 52, 29–36. doi: 10.1071/ar00031

Silva, J. H. V. D., González-Cerón, F., Howerth, E. W., Rekaya, R., and Aggrey, S. E. (2018). Inhibition of the Transsulfuration Pathway Affects Growth and Feather Follicle Development in Meat-Type Chickens. *Anim. Biotechnol.* 30, 175–179. doi: 10.1080/10495398.2018.1461634

Silva, J. H. V. D., González-Cerón, F., Howerth, E. W., Rekaya, R., and Aggrey, S. E. (2019). Alteration of dietary cysteine affects activities of genes of the transsulfuration and glutathione pathways, and development of skin tissues

and feather follicles in chickens. *Anim. Biotechnol.* 31, 203–208. doi: 10.1080/10495398.2019.1577253

Slominski, A. T., Hardeland, R., Zmijewski, M. A., Slominski, R. M., Reiter, R. J., and Paus, R. (2018). Melatonin: a cutaneous perspective on its production, metabolism, and functions. *J. Invest. Dermatol.* 138, 490–499. doi: 10.1016/j.jid.2017.10.025

Söderquist, F., Hellström, P. M., and Cunningham, J. L. (2015). Human gastroenteropancreatic expression of melatonin and its receptors MT1 and MT2J. *PLoS One* 10:e0120195. doi: 10.1371/journal.pone.0120195

Subramanian, A., Tamayo, P., Mootha, V. K., Mukherjee, S., Ebert, B. L., Gillette, M. A., et al. (2005). Gene set enrichment analysis: a knowledge-based approach for interpreting genome-wide expression profiles. *Proc. Natl. Acad. Sci. U. S. A.* 102, 15545–15550. doi: 10.1073/pnas.0506580102

Thomas, N., Tivey, D. R., Penno, N. M., Nattrass, G., and Hynd, P. I. (2007). Characterization of transport systems for cysteine, lysine, alanine, and leucine in wool follicles of sheep. *J. Anim. Sci.* 85, 2205–2213. doi: 10.2527/jas.2006-541

Tripurani, S. K., Yan, W., Fan, Y. X., Rahimi, M., Wong, L., Lee, M. H., et al. (2018). Suppression of Wnt/β-catenin signaling by EGF receptor is required for hair follicle development. *Mol. Biol. Cell* 29, 2784–2799. doi: 10.1091/mbc.E18-08-0488

Wang, H. (2016). Changes of Hair Growth And Related Hormones in Blood and the Expression of Genes in Skin of Liaoning Cashmere Goats. Shenyang Agricultural University: 9–10.

Wang, H., Wang, J., Shi, X. L., and Ding, Y. T. (2018). JUB induces epithelial-mesenchymal transition via the Wnt/β-catenin signaling pathway in hepatocellular carcinoma cells. *Int. J. Clin. Exp. Pathol.* 11, 1374–1382.

Wang, L. F., Lu, D. X., Sun, H. Z., Zhao, X. Y., and Shan, D. (2006). Effects of photoperiod and melatonin on nitrogen partitioning and cashmere growth in inner mongolia white cashmere goats. *Sci. Agric. Sin.* 39, 1004–1010.

Wang, N., and Jia, Z. H. (1999). Comprehensive evaluation of the optimal nitrogen to sulfur ratio in diet of inner Mongolian white cashmere goats. *Acta Zoonutrimenta Sin.* 11, 228–235.

Ward, N. P., and Denicola, G. M. (2019). Sulfur metabolism and its contribution to malignancy. *Int. Rev. Cell Mol. Biol.* 347, 39–103. doi: 10.1016/bs.ircmb.2019.05.001

Wu, T. D., and Watanabe, C. K. (2005). GMAP: a genomic mapping and alignment program for mRNA and EST sequences. *Bioinformatics* 21, 1859–1875. doi: 10.1093/bioinformatics/bti310

Yin, S. J., Lee, J. R., Kwak, H., Lee, B., Han, J. W., Hahn, M., et al. (2019). Functional study of 14-3-3 protein epsilon (YWHAE) in keratinocytes: microarray integrating bioinformatics approaches. *J. Biomol. Struct. Dyn.* 38, 1–17. doi: 10.1080/07391102.2019.1637282

Conflict of Interest: BL was employed by the company Nei Mongol BioNew Technology Co. Ltd.

The remaining authors declare that the research was conducted in the absence of any commercial or financial relationships that could be construed as a potential conflict of interest.

Publisher's Note: All claims expressed in this article are solely those of the authors and do not necessarily represent those of their affiliated organizations, or those of the publisher, the editors and the reviewers. Any product that may be evaluated in this article, or claim that may be made by its manufacturer, is not guaranteed or endorsed by the publisher.

frontiers in Genetics

ORIGINAL RESEARCH
published: 29 September 2021
doi: 10.3389/fgene.2021.732097

Five SNPs Within the *FGF5* Gene Significantly Affect Both Wool Traits and Growth Performance in Fine-Wool Sheep (*Ovis aries*)

Haiyu Zhao†, Ruixue Hu†, Fadi Li† and Xiangpeng Yue†*

State Key Laboratory of Grassland Agro-Ecosystems, Key Laboratory of Grassland Livestock Industry Innovation, Ministry of Agriculture and Rural Affairs, Engineering Research Center of Grassland Industry, Ministry of Education, College of Pastoral Agriculture Science and Technology, School of Life Sciences, Lanzhou University, Lanzhou, China

OPEN ACCESS

Edited by:
Xin Wang,
Northwest A&F University, China

Reviewed by:
Sangang He,
Xinjiang Academy of Animal Science, China
ChunLei Zhang,
Jiangsu Normal University, China

***Correspondence:**
Xiangpeng Yue
lexp@lzu.edu.cn

†ORCID:
Haiyu Zhao
orcid.org/0000-0001-7431-5089
Ruixue Hu
orcid.org/0000-0001-6749-4787
Fadi Li
orcid.org/0000-0002-0143-4199
Xiangpeng Yue
orcid.org/0000-0002-0633-359X

Specialty section:
This article was submitted to Livestock Genomics, a section of the journal Frontiers in Genetics

Received: *28 June 2021*
Accepted: *31 August 2021*
Published: *29 September 2021*

Citation:
Zhao H, Hu R, Li F and Yue X (2021) Five SNPs Within the FGF5 Gene Significantly Affect Both Wool Traits and Growth Performance in Fine-Wool Sheep (Ovis aries). Front. Genet. 12:732097. doi: 10.3389/fgene.2021.732097

Fibroblast growth factor 5 (*FGF5*) gene, a member of fibroblast growth factor superfamily, plays significant roles in the regulation of the hair growth cycle during the development of mammalian hair follicles as well as the skeletal muscle development. In this study, DNA sequencing was used to scan the putative SNPs within the full-length of *FGF5* gene, and SNPscan high-throughput technique was applied in the individual genotyping of 604 crossbred sheep. 10 SNPs were identified within *FGF5* gene while five of them located in intron 1 could be genotyped, namely SNP1 (g. 105914953 G > A), SNP2 (g. 105922232 T > C), SNP3 (g. 105922244 A > G), SNP4 (g. 105922334 A > T) and SNP5 (g. 105922340 G > T). All these SNPs were in accord with the Hardy-Weinberg equilibrium ($P > 0.05$), and displayed the moderate polymorphism with PIC values ranging from 0.302 to 0.374. Thereafter, the correlation analysis between each SNP locus and economic traits including wool length, greasy wool weight and growth performance of sheep was systematically implemented. In our results, SNP1, SNP3, SNP4 and SNP5 were significantly associated with wool length, greasy wool weight and growth traits of SG sheep ($P < 0.05$); SNP1, SNP2, SNP3, and SNP4 were significantly correlated with wool length and growth traits of SSG sheep ($P < 0.05$). Meanwhile, our study revealed a strong linkage disequilibrium (LD) relationship among these SNPs ($r^2 > 0.33$), except for SNP3 and SNP4 sites ($r^2 = 0.30$). Combination genotype analysis showed that combination genotypes were significantly associated with mean fiber diameter of SG ($P < 0.05$), and body weight trait of SSG ($P < 0.01$). The above findings suggested that these SNP loci might affect economic traits synergistically and could be regarded as potential molecular markers for improving both wool production and growth performance of fine-wool sheep, which lay a molecular foundation for the breeding of fine dual-purpose sheep thereby accelerating the pace of sheep breeding.

Keywords: sheep, *FGF5* gene, single nucleotide polymorphism, wool quality traits, growth performance, body weight, association

INTRODUCTION

Sheep, as an important source of wool, mutton and milk production, is economically influential in the textile and meat industry. Thus, during the last decades, to increase the wool and mutton production, extensive efforts have been made to improve the production potential of sheep products by various research/breeding institutions (Rochus et al., 2020; Erdenee et al., 2021). For instance, Merino sheep crossing with local alpine fine-wool sheep can breed an excellent dual-purpose sheep, with good fine wool length and growth performance. In China, South African mutton merino and Gansu alpine fine wool cross developed a new variety, SG crossbred sheep (South African mutton merino ♂× Gansu alpine fine wool ♀, SG); subsequently, South African mutton merino and SG sheep cross bred another variety, SSG crossbred sheep (South African mutton merino ♂× SG ♀, SSG). SG and SSG sheep varieties have demonstrated good adaptabilities to local climate, improves growth rate and undegraded wool quality. However, both their wool production and growth traits still need to be further improved. Compared with traditional cross-breeding techniques, molecular marker-assisted selection (MAS) breeding has the advantages of low cost, obvious effect and short breeding cycle. Therefore, taking full advantages of the MAS method, the exploration of crucial candidate genes and genetic markers related with wool production as well as growth performance is essential for the improvement of SG and SSG sheep varieties.

Single nucleotide polymorphism (SNP) is defined as a single base-pair substitution in the genomic DNA sequence that occurs with high frequency in the population (Vignal et al., 2002). It is regarded as the most preferable DNA marker in genetic and molecular breeding since its tracking availability, ease of interpretation and suitability for various genotyping techniques (Kruglyak, 1997). Many studies conferred that SNP markers could be used for the breeding of livestock, of which the fundamental goal is to use these mutations as useful markers for the prediction of superior animals concerning the desired production traits (Xiang et al., 2018; Bi et al., 2021; Gautason et al., 2021). Nowadays, the candidate gene association study (CGAS) (Moon, 2019) has been widely used to identify genetic variants of candidate genes and their potential association with certain genotype traits (Pryce et al., 2011; Locke et al., 2015). The success of CGAS largely depends on the choice of candidate genes to be studied, of which the biological function should be relevant to the studied traits (Wilkening et al., 2009; Gebreselassie et al., 2020). For the current sheep breeding, the detailed genetic mutation analyses of crucial genes related to wool production and growth traits are far from enough.

Wool traits and growth performance of sheep are complex physiological and biochemical properties influenced by genetics, the environment and nutrition etc. Many signaling pathways and related factors are involved in the regulation of these economic traits. Among them, fibroblast growth factors (FGFs) are a family of factors that play important roles in promoting and regulating the growth of fibroblasts. Fibroblast growth factor 5 (FGF5) has been verified as a famous dominant inhibitor of hair elongation in many studies. For example, FGF5-null mouse exhibited a long hair phenotype (Nesterova et al., 2010; Zhang et al., 2020); loss-of-function mutations within *FGF5* associated with long-hair phenotypes have been described in many mammalian species, including humans (Higgins et al., 2014), cats (Drögemüller et al., 2007), dogs (Cadieu et al., 2009), rabbits (Xu et al., 2020) and donkeys (Legrand et al., 2014). In addition, the mouse *FGF5* gene was reported to be able to inhibit skeletal muscle development in the limb (Clase et al., 2000). All these findings triggered great interest in the roles of *FGF5* gene in breeding improved wool production and growth of animals. However, although *FGF5* gene has been identified to be polymorphic in many species, there is not any causal mutations that have been identified to be associated with wool traits or the growth performance in sheep.

Therefore, in this study, taking full advantage of our well-established hybrid sheep strain, we investigated the genetic variations of *FGF5* gene in SG and SSG sheep groups. The identified SNPs are significantly correlated with both the wool traits and growth performance of sheep, thereby could be used as candidate molecular markers for the breeding of fine dual types sheep thus accelerating the pace of sheep breeding.

MATERIALS AND METHODS

All experiment protocols were reviewed and approved by the Ethics Committee of College of Pastoral Agriculture Science and Technology, Lanzhou University (Ethic approval No: 2010-1 and 2010-2). All efforts were taken to minimize animal suffering.

Sample Collection and Genomic DNA Extraction

In this study, A total of 401 South African mutton merino (♂) × Gansu alpine fine wool (♀) crossbred sheep (SG sheep) and 203 South African mutton merino (♂) × SG (♀) crossbred sheep (SSG sheep) were selected randomly from sheep-breeding farms in Wuwei City, Gansu Province, China. The sheep were yearlings or adults (2∼2.5 years old), and they were all reared in very similar conditions with appropriate environment and suitable feeding. Blood samples of all individuals were collected. Detailed records of the mean fiber diameter (MFD), greasy wool weight (GWW), wool length in five body parts (shoulder, side, thigh, notum, and abdomen) as well as five indicators of growth performance including body weight, body height, body length, chest girth, and shin circumference were available for all selected individuals (as shown in **Table 1** and **Supplementary Table 1**).

Genomic DNA was extracted from blood samples using the method previously published (Zhao et al., 2013). Their qualities were then assayed using Nanodrop 2000 Spectrophotometer based on the $1.8 < OD260/280 < 2.0$ standard. All qualified genomic DNA samples were diluted to the working concentration of 50 ng/μL and stored at −20°C for further experiments.

Primer Design and DNA Pool Construction

According to the sheep *FGF5* gene sequence (GenBank accession No. NC_019463.2) in the NCBI database, seven pairs of primers

(as shown in **Supplementary Table 2**) were designed for the amplification of the full-length of *FGF5* gene by using Primer Premier 6.0 software. DNA pooling sequencing was used to screen putative SNPs in each amplified fragment. In order to determine the presence of SNPs within the sheep *FGF5* gene, a total of 30 DNA pools were constructed, and each pool was composed of genomic DNA samples derived from 20 sheep individuals.

SNP Screening and SNPscan Genotyping

To screen genetic variations cost-effectively, putative SNP identification in sheep *FGF5* gene was achieved by sequencing PCR products of the pooled DNA samples. Briefly, the PCR products were validated by 1.0% agarose gel electrophoresis, then purified and sequenced directly using Sanger sequencing by AoKeDingSheng Biotechnology Company (Beijing, China). To screen the candidate SNPs, sequence alignments were carried out by using DNAstar (DNAstar, United States) and chromas (Technelysium Pty Ltd., Australia) softwares. SNPs were identified by the presence of double peaks at each single locus in the chromatograms. Subsequently, quality control analysis was performed on the candidate SNPs, and the qualified SNPs were genotyped in all 604 sheep samples by using the commercial SNPscan^{TM} high-throughput method (Tianhao Biotech, Shanghai, China).

The PCR amplification was performed in the 25.0 μL reaction condition containing 1.0 μL genomic DNA (50 ng/μL), 0.4 μL of each forward/reverse primer (10 pmol/μL), 12.5 μL of 2 × Taq PCR Super Mix (TranGen Biotech, China) and 10.7 μL of ddH_2O. The PCR amplification protocol contained a pre-denaturation at 95°C for 5 min and denaturation at 94°C for 30 s, followed by annealing for 30 s at the optimal temperature, 35 cycles of elongation at 72°C for 30 s, and a final extension at 72°C for 5 min with subsequent cooling to 4°C.

Statistical Analysis

Genotypic and allelic frequencies were estimated based on the obtained genotyping results by using Microsoft Excel software. Genetic parameters including the polymorphism information content (PIC), effective allele number (Ne), homozygosity (Ho) and expected heterozygosity (He) were calculated using the Nei's method (Nei and Roychoudhury, 1974). The allele frequencies of each SNP were calculated for departure from Hardy-Weinberg equilibrium (HWE) by using the χ^2-test.

According to the characteristics of the source of sheep sample and the effects of gender, age and variety, a statistical analysis model was established as $Y_{ijklm} = \mu + G_i + s_j + p_k + e_{ijklm}$, in which Y_{ijklm} refers to the measured value of the phenotypic trait, μ represents the population mean, G_i is the genotype effect, s_j is the gender effect, p_k is the field effect, and e_{ijklm} is the random residual. The effect of birth type had no significant impact on the phenotypic value of wool traits and growth performance, therefore it had been leaving out in our linear model (Bromley et al., 2000). SPSS 22.0 software (IBM) was used to analyze the association between the individual genotypes and the phenotype of the wool traits and growth performance, as well as the combination genotype analysis. The least-squares method was set to fit the linear model (LSE) for comparison. The general linear model (GLM) of ANOVA was used to analyze the relationships between the genotypes and economic traits. According to the correlation coefficients (D'/r^2), the pattern of pairwise Linkage disequilibrium (LD) between SNP loci was estimated and visualized as previously described (Zou et al., 2021). The case of $D' = 1$ or $r^2 = 1$ is known as complete LD. Values of $D' < 1$; $r^2 > 0.33$ indicate strong LD.

RESULTS

Identification of Five SNPs Within Sheep *FGF5* Gene

According to our DNA sequencing and sequence alignments results based on 604 sheep samples, 10 putative SNPs were identified within *FGF5* gene while only five of them could be genotyped, namely SNP1 (g. 105914953 G > A), SNP2 (g. 105922232 T > C), SNP3 (g. 105922244 A > G), SNP4 (g. 105922334 A > T) and SNP5 (g. 105922340 G > T). They are all intron mutations located in the first intron of sheep *FGF5* gene. The sequence chromatograms of heterozygous genotypes were illustrated in **Figure 1**.

Genotypic and Allelic Frequencies and Population Indexes

Genotypic frequencies, allelic frequencies, as well as the genetic parameters including heterozygosity (He), homozygosity (Ho), effective allele numbers (Ne) and the polymorphism information content (PIC) of five SNP loci within *FGF5* gene in the SG and SSG crossbred sheep group were evaluated (as shown in **Table 2** and **Supplementary Table 3**). The genotypic frequencies of homozygous wild alleles in SNP1, SNP2, SNP3 and SNP5 were all higher than that of mutation alleles, except the SNP4 locus. Based on the χ^2-test, these five identified SNPs of *FGF5* gene were all in accordance with the Hardy-Weinberg equilibrium ($P > 0.05$). Besides, five SNPs within the *FGF5* gene all displayed moderate polymorphism, with PIC values ranging from 0.302 to 0.374.

TABLE 1 | The information of sheep and the economic traits measured.

Population	Age	Sex	Sample size	Measured economic traits
SG	Adult	Female	401	Wool length, mean fiber diameter, the greasy wool weight and growth performance
SSG	Yearling	Male	203	Wool length, mean fiber diameter, and growth performance

SG, South African mutton merino (♂) and Gansu alpine fine wool (♀) crossbred sheep; SSG, South African mutton merino (♂) and SG (♀) crossbred sheep.

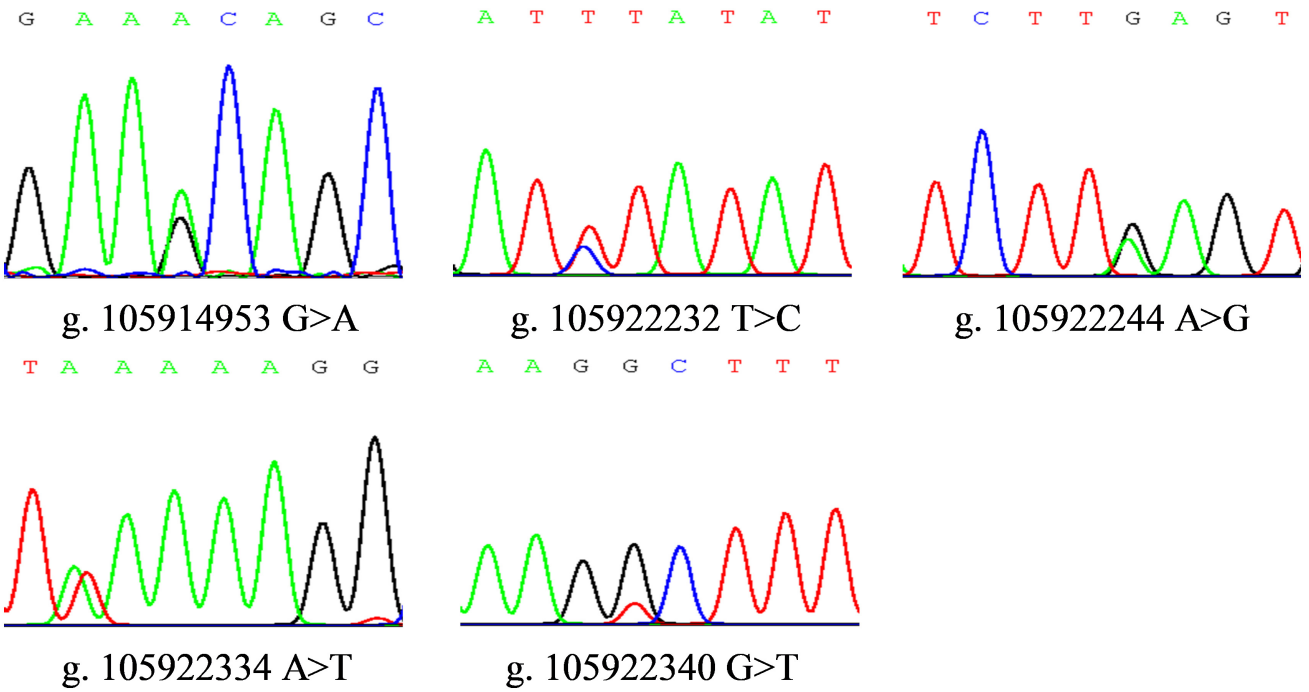

FIGURE 1 | Sequence chromatograms of five SNP loci within sheep *FGF5* gene.

Association Analysis of SNPs With Wool Production Traits

The wool traits of the female SG sheep group were recorded from five body parts, namely shoulder, side, thigh, notum, and abdomen. Moreover, the other parameters like mean fiber diameter and greasy wool weight of SG sheep were also recorded in this study. Based on the above information, we explored the correlations between these SNPs of *FGF5* gene and the economic traits. Association analysis showed that the SNP1 (g.105914953 G > A) was significantly correlated with abdomen wool length, and AA carriers showed the best wool length ($P < 0.05$); SNP4 (g.105922334 A > T) was significantly associated with the greasy wool weight, and AA carriers had the best greasy wool weight compared with other carriers ($P < 0.01$); SNP5 (g.105922340 G > T) was also correlated with natural wool length in the abdomen, and GG genotype exhibited significantly improved wool length in comparison with the GT genotype ($P < 0.05$) (**Table 3** and **Supplementary Table 4**).

In addition, the wool length and fiber diameter data of the male SSG sheep group were also available from five body parts, namely shoulder, side, thigh, notum, and abdomen. Our correlation analysis showed that both SNP1 and SNP3 (g.105914953 G > A; g.105922244 A > G) were significantly correlated with thigh wool length ($P < 0.05$); SNP2 (g.105922232 T > C) was significantly associated with the mean fiber diameter ($P < 0.05$); SNP4 (g.105922334 A > T) was correlated with natural wool length in the notum, and AT genotype demonstrated improved wool length compared with other genotypes ($P < 0.05$) (**Table 4**).

Association Analysis of *FGF5* SNPs With Growth Performance

Association analysis demonstrated that the identified SNPs within *FGF5* gene were also significantly correlated with growth traits of female SG sheep, including SNP3 (g.105922244 A > G), SNP4 (g.105922334 A > T) and SNP5 (g.105922340 G > T). SNP3, SNP4, SNP5 had a significant influence on the body height ($P < 0.05$), and AA, AA, and TT carriers had significantly improved body height than that of other carriers, respectively (**Table 5**). For the male SSG sheep, association analysis demonstrated that SNP1 (g.105914953 G > A), SNP2 (g.105922232 T > C) sites had significant effects on body weight ($P < 0.05$), and GG, CC carriers had improved weight trait than that of other carriers (**Table 6**).

Linkage Disequilibrium Analysis of SNP Loci Within Sheep *FGF5* Gene

In this study, since all these five SNPs were significantly associated with various sheep economic traits, are there any correlation relationships among these SNP loci? To further understand this question, linkage disequilibrium (LD) analysis between SNP1, SNP2, SNP3, SNP4 and SNP5 were analyzed (**Figure 2** and **Supplementary Table 5**). SNP1 had a strong LD relationship with SNP2, SNP3, SNP4 and SNP5 ($r^2 > 0.33$); SNP2 had a strong LD relationship with SNP1, SNP3, SNP4 and SNP5 ($r^2 > 0.33$); SNP3 locus had a strong LD relationship with SNP1, SNP2, SNP5 loci ($r^2 > 0.33$); SNP4 site had a strong LD relationship with SNP1, SNP2 and SNP5 sites ($r^2 > 0.33$); and SNP5 was strongly

TABLE 2 | The genetic diversity of sheep *FGF5* gene.

SNP Loci	Genotypic frequencies			Allele frequencies		Genetic parameter				
	D	H	R	Reference	Mutation	Ho	He	Ne	PIC	HWE (*P*-value)
SNP1	0.570 (342)	0.370 (222)	0.060 (36)	0.755	0.245	0.630	0.370	1.587	0.302	0.997
SNP2	0.341 (204)	0.489 (293)	0.170 (102)	0.585	0.415	0.514	0.486	1.944	0.368	0.854
SNP3	0.547 (328)	0.382 (229)	0.072 (43)	0.738	0.263	0.613	0.387	1.632	0.312	0.727
SNP4	0.220 (130)	0.510 (302)	0.270 (160)	0.475	0.525	0.501	0.499	1.995	0.374	0.577
SNP5	0.484 (275)	0.396 (255)	0.120 (68)	0.682	0.318	0.566	0.434	1.766	0.340	0.448

Genotype frequency: D, homozygous wild type genotype; H, heterozygous mutant genotype; R, homozygous mutant genotype; Ho, homozygosity; He, heterozygosity; Ne, effective allele numbers; PIC, polymorphism information content; HWE, Hardy–Weinberg equilibrium.

TABLE 3 | The correlation analysis of SNPs with wool production related indicators in SG sheep.

Loci	Genotypes	Natural wool length (cm)					MFD (μm)	GWW (kg)
		Shoulder	Side	Thigh	Notum	Abdomen		
SNP1	AA	6.17 ± 0.08	6.69 ± 0.10	6.33 ± 0.08	6.37 ± 0.08	**4.67 ± 0.10^{a}**	21.63 ± 0.15	3.59 ± 0.05
	GA	6.15 ± 0.09	6.43 ± 0.15	6.21 ± 0.10	6.37 ± 0.12	**4.31 ± 0.11^{b}**	21.80 ± 0.20	3.59 ± 0.07
	GG	6.23 ± 0.20	6.25 ± 0.18	6.00 ± 0.12	6.28 ± 0.14	**4.59 ± 0.29^{ab}**	21.98 ± 0.49	3.63 ± 0.18
SNP2	CC	6.07 ± 0.08	6.56 ± 0.10	6.23 ± 0.09	6.30 ± 0.08	4.51 ± 0.10	21.59 ± 0.18	3.55 ± 0.06
	CT	6.20 ± 0.09	6.65 ± 0.13	6.30 ± 0.09	6.41 ± 0.11	4.55 ± 0.12	21.81 ± 0.19	3.57 ± 0.06
	TT	6.34 ± 0.18	6.22 ± 0.15	6.20 ± 0.14	6.34 ± 0.16	4.55 ± 0.20	21.76 ± 0.29	3.78 ± 0.11
SNP3	GG	6.13 ± 0.08	6.68 ± 0.10	6.29 ± 0.08	6.36 ± 0.08	4.61 ± 0.09	21.57 ± 0.15	3.63 ± 0.05
	AG	6.22 ± 0.10	6.45 ± 0.14	6.30 ± 0.10	6.38 ± 0.12	4.45 ± 0.13	21.89 ± 0.21	3.54 ± 0.07
	AA	6.21 ± 0.18	6.25 ± 0.15	5.94 ± 0.11	6.24 ± 0.11	4.49 ± 0.29	22.02 ± 0.42	3.64 ± 0.16
SNP4	AA	6.30 ± 0.17	6.35 ± 0.17	6.16 ± 0.14	6.47 ± 0.18	4.60 ± 0.17	21.58 ± 0.28	**3.86 ± 0.10^{a}**
	AT	6.18 ± 0.08	6.60 ± 0.12	6.34 ± 0.09	6.39 ± 0.09	4.45 ± 0.10	21.88 ± 0.17	**3.55 ± 0.06^{B}**
	TT	6.06 ± 0.09	6.58 ± 0.11	6.18 ± 0.10	6.24 ± 0.09	4.63 ± 0.14	21.52 ± 0.21	**3.50 ± 0.06^{B}**
SNP5	GG	6.19 ± 0.09	6.71 ± 0.11	6.28 ± 0.09	6.39 ± 0.09	**4.74 ± 0.12^{a}**	21.54 ± 0.16	3.62 ± 0.06
	GT	6.11 ± 0.09	6.42 ± 0.13	6.31 ± 0.10	6.35 ± 0.11	**4.33 ± 0.11^{b}**	22.03 ± 0.19	3.53 ± 0.07
	TT	6.30 ± 0.16	6.44 ± 0.16	6.07 ± 0.10	6.31 ± 0.12	**4.53 ± 0.19^{ab}**	21.57 ± 0.35	3.73 ± 0.12

Letters with different genotypes in same trait (a, b/A, B) means significantly at $P < 0.05/P < 0.01$, respectively.
The bold values indicate significant differences.
MFD, mean fiber diameter; GWW, greasy wool weight.

linked with SNP1, SNP2, SNP3, and SNP4 sites ($r^2 > 0.33$). These close links among five loci suggested that there might be a certain synergistic effect on regulating the above economic traits of sheep.

Combination Genotype Analysis Between Five SNP Loci and Sheep Economic Traits

According to the genotype distribution of five SNP sites in SG and SSG sheep population. In the order of SNP1-SNP2-SNP3-SNP4-SNP5, there were 19 combination genotypes. The detailed information of these 19 combination genotypes were shown in **Supplementary Table 6**. Other combination genotypes which were not present or had only one or two occurrences, were not analyzed. For the SG sheep, the combination genotypes were significantly associated with Mean Fiber Diameter ($P < 0.05$) (**Figure 3** and **Supplementary Table 7**), whereas for the SSG sheep, combination genotypes were significantly corrected with Body Weight trait ($P < 0.01$) (**Figure 4** and **Supplementary Table 8**). Results with no significant correlation between combination genotypes and other phenotypic traits are not shown in this section.

DISCUSSION

Wool production traits and the growth performance of sheep greatly affect the development of the whole sheep breeding industry. In recent years, to meet the growing needs of the Chinese sheep market, the sheep industry has gradually switched its focus from wool to wool-mutton production. Therefore, it

TABLE 4 | The correlation analysis of SNPs with wool production related indicators in SSG sheep.

Loci	Genotypes	Natural wool length (cm)					MFD (μm)
		Shoulder	Side	Thigh	Notum	Abdomen	
SNP1	AA	7.72 ± 0.13	7.95 ± 0.15	**7.58 ± 0.10^{b}**	7.99 ± 0.13	5.44 ± 0.11	20.94 ± 0.28
	GA	7.72 ± 0.13	7.93 ± 0.17	**7.48 ± 0.12^{b}**	7.87 ± 0.17	5.37 ± 0.13	20.89 ± 0.38
	GG	8.31 ± 0.47	8.64 ± 0.90	**8.53 ± 0.62^{a}**	8.83 ± 0.83	5.26 ± 0.55	24.80 ± 0.70
SNP2	CC	7.56 ± 0.18	7.95 ± 0.21	7.54 ± 0.14	7.81 ± 0.18	5.31 ± 0.15	**21.54 ± 0.42^{ab}**
	CT	7.79 ± 0.13	8.02 ± 0.15	7.55 ± 0.11	8.04 ± 0.14	5.48 ± 0.11	**20.55 ± 0.29^{b}**
	TT	7.91 ± 0.22	7.88 ± 0.28	7.79 ± 0.22	8.05 ± 0.26	5.38 ± 0.22	**21.88 ± 0.57^{a}**
SNP3	GG	7.74 ± 0.14	7.93 ± 0.14	**7.60 ± 0.10^{ab}**	8.02 ± 0.12	5.47 ± 0.11	21.13 ± 0.28
	AG	7.69 ± 0.13	7.99 ± 0.18	**7.48 ± 0.13^{b}**	7.82 ± 0.17	5.36 ± 0.14	20.82 ± 0.40
	AA	8.34 ± 0.44	8.25 ± 0.71	**8.31 ± 0.54^{a}**	8.71 ± 0.69	5.03 ± 0.35	20.43 ± 1.67
SNP4	AA	7.93 ± 0.17	7.95 ± 0.20	7.71 ± 0.17	**8.01 ± 0.20^{ab}**	5.41 ± 0.17	21.06 ± 0.49
	AT	7.83 ± 0.14	8.12 ± 0.17	7.63 ± 0.11	**8.20 ± 0.15^{a}**	5.54 ± 0.12	20.90 ± 0.29
	TT	7.49 ± 0.21	7.84 ± 0.24	7.49 ± 0.15	**7.67 ± 0.19^{b}**	5.27 ± 0.17	21.19 ± 0.54
SNP5	GG	7.76 ± 0.15	7.92 ± 0.16	7.66 ± 0.11	8.09 ± 0.14	5.44 ± 0.11	21.25 ± 0.28
	GT	7.70 ± 0.13	8.01 ± 0.17	7.48 ± 0.13	7.84 ± 0.16	5.45 ± 0.13	20.72 ± 0.39
	TT	8.02 ± 0.31	8.03 ± 0.41	7.81 ± 0.27	8.15 ± 0.34	5.01 ± 0.28	20.63 ± 0.82

Letters with different genotypes in same trait (a, b) means significantly at $P < 0.05$.
The bold values indicate significant differences.
MFD, mean fiber diameter.

TABLE 5 | Correlation analysis of SNPs within the *FGF5* gene with body size in SG sheep.

Loci	Genotypes	Body weight (kg)	Chest girth (cm)	Body height (cm)	Body length (cm)	Shin circumference (cm)
SNP1	AA	38.54 ± 0.42	80.86 ± 0.44	64.33 ± 0.33	67.77 ± 0.45	7.37 ± 0.06
	GA	38.25 ± 0.58	81.59 ± 0.58	64.55 ± 0.36	68.34 ± 0.56	7.37 ± 0.08
	GG	40.51 ± 1.15	82.26 ± 1.14	65.79 ± 0.87	68.63 ± 1.41	7.55 ± 0.16
SNP2	CC	38.44 ± 0.48	80.90 ± 0.51	63.99 ± 0.41	67.37 ± 0.54	7.40 ± 0.08
	CT	38.53 ± 0.50	81.35 ± 0.51	64.68 ± 0.31	68.48 ± 0.50	7.34 ± 0.07
	TT	39.54 ± 0.89	81.97 ± 0.85	65.45 ± 0.72	68.32 ± 0.97	7.52 ± 0.13
SNP3	GG	38.48 ± 0.43	80.85 ± 0.44	**64.16 ± 0.34^{b}**	67.68 ± 0.47	7.40 ± 0.07
	AG	38.68 ± 0.57	81.38 ± 0.58	**64.64 ± 0.35^{ab}**	68.47 ± 0.55	7.30 ± 0.08
	AA	39.28 ± 1.15	83.14 ± 1.06	**66.10 ± 0.84^{a}**	68.33 ± 1.28	7.62 ± 0.16
SNP4	AA	39.59 ± 0.73	81.86 ± 0.83	**65.97 ± 0.65^{a}**	69.56 ± 0.92	7.39 ± 0.12
	AT	38.30 ± 0.48	81.23 ± 0.48	**64.20 ± 0.30^{b}**	67.81 ± 0.46	7.37 ± 0.07
	TT	38.66 ± 0.55	81.03 ± 0.59	**64.32 ± 0.46^{b}**	67.61 ± 0.62	7.40 ± 0.08
SNP5	GG	38.59 ± 0.47	81.05 ± 0.49	**64.38 ± 0.37^{ab}**	67.84 ± 0.52	7.41 ± 0.07
	GT	38.29 ± 0.53	81.24 ± 0.54	**64.26 ± 0.32^{b}**	67.78 ± 0.50	7.33 ± 0.08
	TT	39.83 ± 0.81	82.06 ± 0.87	**65.81 ± 0.74^{a}**	69.58 ± 1.04	7.48 ± 0.12

Letters with different genotypes in one growth trait (a, b) means significantly at $P < 0.05$.
The bold values indicate significant differences.

is particularly important to take into account the breeding of improved wool production as well as the growth performance in sheep. Single nucleotide polymorphisms (SNPs) are regarded as the most preferable DNA marker in genetic and molecular breeding since its tracking availability, ease for interpretation, and suitability for genotyping techniques (Kruglyak, 1997; Wang et al., 2019), therefore it has been widely used in the modern genetic breeding of livestock.

In this study, ten SNP mutations within *FGF5* gene were identified in the hybrid SG and SSG sheep while only five of them were focused for genotyping and subsequent association analysis. This is because: (1) technically, only these five SNPs could be genotyped by the probe-based SNPscan method; (2) these five intronic SNPs are adjacent therefore are more likely to exhibit linkage and combined genotype effects; (3) according to previous studies, intronic SNPs as molecular markers also play important roles in the animal genetics and breeding. These intronic SNPs were all consistent with the Hardy-Weinberg equilibrium ($P > 0.05$), and all displayed moderate polymorphism, with a high adaptability under the circumstances of environmental changes. In addition, their associations with wool production and growth traits of sheep were investigated, and our results revealed that these five SNPs within *FGF5* gene were all significantly correlated with sheep economic traits.

TABLE 6 | Correlation analysis of SNPs within the *FGF5* gene with body size in SSG sheep.

Loci	Genotypes	Body weight (kg)	Chest girth (cm)	Body height (cm)	Body length (cm)	Shin circumference (cm)
SNP1	AA	**47.87 ± 0.74^{b}**	92.94 ± 0.67	71.85 ± 0.38	74.60 ± 0.44	9.99 ± 0.09
	GA	**46.87 ± 0.81^{b}**	92.77 ± 0.86	71.91 ± 0.39	74.29 ± 0.45	10.08 ± 0.12
	GG	**53.93 ± 3.76^{a}**	94.13 ± 3.52	73.75 ± 1.28	76.25 ± 1.70	10.15 ± 0.42
SNP2	CC	**49.78 ± 1.09^{a}**	94.51 ± 0.97	72.31 ± 0.53	75.37 ± 0.63	10.19 ± 0.13
	CT	**46.57 ± 0.70^{b}**	92.21 ± 0.70	71.72 ± 0.35	74.22 ± 0.43	9.96 ± 0.09
	TT	**47.47 ± 1.37^{ab}**	92.44 ± 1.36	72.03 ± 0.67	74.24 ± 0.64	9.99 ± 0.19
SNP3	GG	47.96 ± 0.78	92.94 ± 0.67	72.00 ± 0.37	74.67 ± 0.44	10.01 ± 0.09
	AG	47.31 ± 0.80	93.10 ± 0.88	71.75 ± 0.41	74.33 ± 0.48	10.08 ± 0.12
	AA	47.95 ± 2.84	91.11 ± 2.92	73.00 ± 0.85	74.89 ± 0.99	9.89 ± 0.35
SNP4	AA	47.59 ± 1.09	93.04 ± 0.79	72.15 ± 0.46	74.29 ± 0.55	9.98 ± 0.14
	AT	47.38 ± 0.81	93.04 ± 0.79	72.01 ± 0.39	74.52 ± 0.47	10.05 ± 0.10
	TT	48.28 ± 1.20	93.36 ± 1.14	71.89 ± 0.62	75.00 ± 0.70	10.07 ± 0.14
SNP5	GG	47.85 ± 0.83	92.89 ± 0.76	71.98 ± 0.44	74.85 ± 0.51	10.00 ± 0.09
	GT	47.27 ± 0.82	92.75 ± 0.81	71.98 ± 0.37	74.47 ± 0.42	10.11 ± 0.12
	TT	49.58 ± 1.68	94.12 ± 1.80	71.82 ± 0.67	73.59 ± 0.87	9.85 ± 0.17

Letters with different genotypes in one growth trait (a, b) means significantly at $P < 0.05$.
The bold values indicate significant differences.

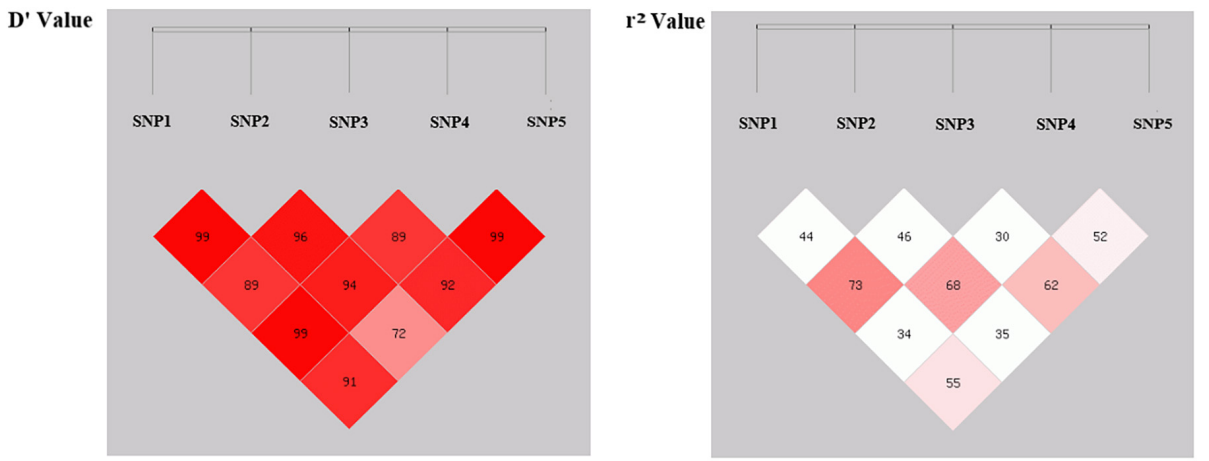

FIGURE 2 | Linkage disequilibrium (LD) analysis of five SNP loci within sheep *FGF5* gene.

For the wool traits of sheep, SNP1, SNP4 and SNP5 were significantly associated with the wool length and greasy wool weight of SG sheep ($P < 0.05$), and SNP1, SNP2, SNP3 and SNP4 were closely correlated with wool length of SSG sheep ($P < 0.05$). These results suggested that all these five SNP mutations might play important roles in the wool production of sheep, and the observed differences of these SNP loci in SG and SSG sheep might be caused by the breed specificity. According to previous studies, the fibroblast growth factor 5, as a member of the fibroblast growth factor superfamily (FGFs), plays an important role in the regulation of the hair growth cycle during the development of mammalian hair follicles (Schneider et al., 2009; Hu et al., 2021). *FGF5* gene could inhibit murine normal hair growth, and its loss of function mutation caused abnormal hair growth by extending the hair growth cycle (Sundberg et al., 1997; Kim et al., 2020). Similar studies also have been conducted in many other species, for example, Hattori et al. (1996) found that hair growth in rat was associated with *FGF5* gene mutation. In humans, previous studies have identified *FGF5* as a crucial gene regulating hair growth and hair loss (Kim et al., 2020). In goats and sheep, CRISPR Cas9 technology has been used to produce functional deletion mutations in *FGF5* gene, and the hair length of mutant individuals was significantly longer than that of the wild type (Hu et al., 2017; Li et al., 2017; Su et al., 2020). All these results have indicated that the presence of *FGF5* gene may affect the hair growth of animals, and the growth of hair could be promoted by altering the expression of *FGF5* gene. In this study, five SNPs within *FGF5* gene identified in Chinese crossbred sheep might significantly influence wool length, which strongly suggests that these genetic variations could be regarded as effective molecular markers for wool sheep breeding.

For the growth performance, SNP3, SNP4 and SNP5 were found to be significantly associate with the body height of SG sheep ($P < 0.05$), and SNP1, SNP2 were significantly correlated

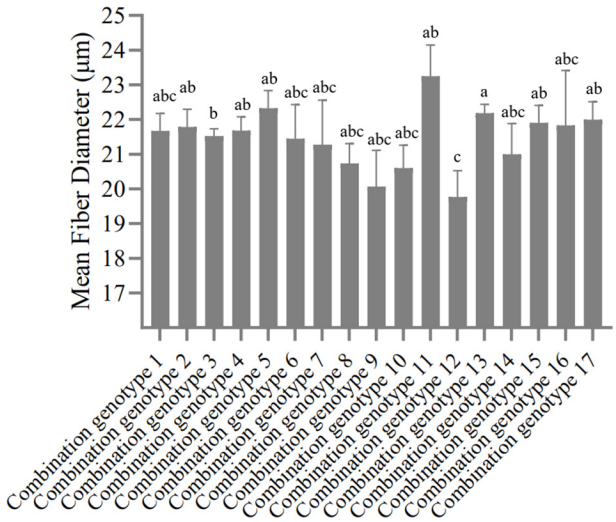

FIGURE 3 | Association analysis between 17 combination genotypes of five SNP loci and Mean Fiber Diameter in SG sheep. Different letters (a, b, c) show significant difference ($P < 0.05$).

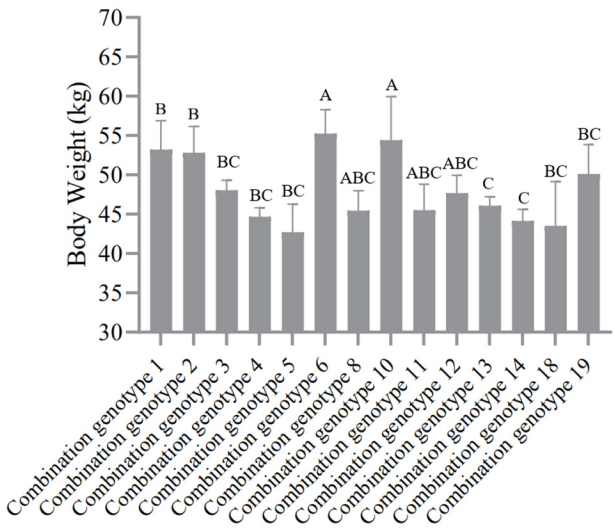

FIGURE 4 | Association analysis between 14 combination genotypes of five SNP loci and Body Weight in SSG sheep. Different letters (A, B, C) show significant difference ($P < 0.01$).

with the bodyweight of SSG sheep ($P < 0.05$). These results suggested that these SNPs might influence the growth and development of sheep. Zhang et al. (2015) have cloned the coding sequence of *FGF5*, and qPCR analyses have shown that *FGF5* was widely expressed in various tissues including the skin, muscle, spleen, liver, heart and brain of sheep. In addition, *FGF5* gene has been documented to be able to inhibit mouse skeletal muscle development in the limb (Clase et al., 2000). The ectopic expression of *FGF5* significantly stimulated the tenascin expression, the proliferation and expansion of connective tissue fibroblasts throughout the developing limb, as well as promoted the formation of connective tissue. The above studies strongly support our findings that *FGF5* gene could act as a candidate gene of sheep growth and development. However, further studies are still needed to explore the functional mechanisms of how these SNPs within sheep *FGF5* gene affect the body height and weight of hybrid sheep in our study. Intriguingly, our results pointed out that, in SG sheep, individuals with heterozygous genotypes performed inferiority phenotypes both in the wool length and body weight, leading to a hint that a positive correlation might exist in wool development and body weight. In the Merino sheep, increased live weight was found to result in a moderate correlated increase in wool development (Mortimer et al., 2017). Moreover, weight traits have also been identified to have a moderate positive direct genetic correlation with fleece length in Columbia, Polypay, Rambouillet, and Targhee sheep (Bromley et al., 2000). However, the same effect of heterozygous was not applied to SSG sheep, due to the breed specificity, as well as the limitation of sample size.

Previous studies have well-documented that different gene mutations can be linked with each other thereby affecting the economic traits of animals, such as litter size and growth performance of goats (Wang et al., 2019, 2020). Since all these five SNP loci are significantly associated with the economic traits of sheep, is there a certain synergistic effect among them? Based on this assumption, this study further analyzed the linkage disequilibrium (LD) relationship among these loci and the results revealed that there might be a strong linkage disequilibrium relationship among the five SNPs ($r^2 > 0.33$), and the r^2 value between SNP3 and SNP4 was close to the threshold of strong linkage disequilibrium state ($r^2 = 0.30$), suggesting that all these five SNPs might play a synergistic role in the selection and breeding of sheep with both fine wool traits and improved growth performance. In addition, we performed the combination genotype analysis between different combination genotypes and economic traits of SG and SSG sheep. Interestingly, our results showed that combination genotypes were significantly associated with Mean Fiber Diameter of SG ($P < 0.05$), and Body Weight of SSG ($P < 0.01$), which illustrated that the combined selection of these five SNPs might be meaningful and beneficial to the improvement of economic traits of sheep. Given that there hasn't been any report on the associations between genetic variations of *FGF5* gene and wool and growth traits in sheep, our study here suggested that functional mutations of *FGF5* might play important roles in both sheep growth and wool production, and these five SNP loci within *FGF5* gene could be used as candidate molecular markers, which is of great significance for the improvement of crossbred sheep breeding.

Limitations of the study: In the present research, we focused on the correlation analysis between *FGF5* SNPs or combination genotypes with various sheep economic traits. We speculate that these linked SNPs may affect the expression of *FGF5* gene thereby modulating wool traits and growth performance of sheep. However, these findings are based mostly on association. Thus, future research on the genotype dependent gene and protein expression levels, especially in hair follicle, muscle and skeleton will provide important insight into the underlying mechanisms.

CONCLUSION

In this study, five SNPs loci within the sheep *FGF5* gene were identified in two hybrid sheep strains. Among them, SNP1, SNP3, SNP4 and SNP5 were significantly associated with wool length, greasy wool weight and growth performance of SG sheep, and SNP1, SNP2, SNP3, and SNP4 were significantly correlated with wool length and growth traits of SSG sheep. Meanwhile, there were strong linkage disequilibrium relationships among these SNPs. In addition, combination genotypes were significantly associated with mean fiber diameter of SG, and body weight trait of SSG. These above findings suggested that these newly discovered linked SNPs might be utilized as potential molecular markers in the breeding of dual types of sheep with improved wool traits and growth performance.

DATA AVAILABILITY STATEMENT

The original contributions presented in the study are included in the article/**Supplementary Material**, further inquiries can be directed to the corresponding author/s.

ETHICS STATEMENT

The animal study was reviewed and approved by the Ethics Committee of College of Pastoral Agriculture Science and Technology, Lanzhou University (Ethic approval No: 2010-1 and 2010-2).

AUTHOR CONTRIBUTIONS

RH performed the experiments. RH and HZ analyzed the data. HZ prepared the manuscript. FL and XY designed the experiments and discussed the results. HZ and XY revised the manuscript. All authors contributed and approved the current submission.

FUNDING

This research was funded by Gansu Province Major Science and Technology Projects (20ZD7NA004), the Fundamental Research Funds for the Central Universities (lzujbky-2019-74), the "Double First-Class" Research Start-up Funds of Lanzhou University (561119203) and the China Agriculture Research System of MOF and MARA (CARS-38).

ACKNOWLEDGMENTS

We would like to thank all the technicians in breeding farms for their kind support during the sample collection.

SUPPLEMENTARY MATERIAL

The Supplementary Material for this article can be found online at: https://www.frontiersin.org/articles/10.3389/fgene.2021.732097/full#supplementary-material

REFERENCES

Bi, Y., Zhang, S., Li, J., He, L., Kang, Y., Chen, H., et al. (2021). The mRNA expression profile of the goat prion protein testis-specific (PRNT) gene and its associations with litter size. *Theriogenology* 165, 69–75. doi: 10.1016/j.theriogenology.2021.02.013

Bromley, C. M., Snowder, G. D., and Van Vleck, L. D. (2000). Genetic parameters among weight, prolificacy, and wool traits of Columbia, Polypay, Rambouillet, and Targhee sheep. *J. Anim. Sci.* 78, 846–858. doi: 10.2527/2000.784846x

Cadieu, E., Neff, M. W., Quignon, P., Walsh, K., Chase, K., Parker, H. G., et al. (2009). Coat variation in the domestic dog is governed by variants in three genes. *Science* 326, 150–153. doi: 10.1126/science.1177808

Clase, K. L., Mitchell, P. J., Ward, P. J., Dorman, C. M., Johnson, S. E., and Hannon, K. (2000). FGF5 stimulates expansion of connective tissue fibroblasts and inhibits skeletal muscle development in the limb. *Dev. Dyn.* 219, 368–380.

Drögemüller, C., Rüfenacht, S., Wichert, B., and Leeb, T. (2007). Mutations within the FGF5 gene are associated with hair length in cats. *Anim. Genet.* 38, 218–221. doi: 10.1111/j.1365-2052.2007.01590.x

Erdenee, S., Akhatayeva, Z., Pan, C., Cai, Y., Xu, H., Chen, H., et al. (2021). An insertion/deletion within the CREB1 gene identified using the RNA-sequencing is associated with sheep body morphometric traits. *Gene* 775:145444. doi: 10.1016/j.gene.2021.145444

Gautason, E., Schönherz, A. A., Sahana, G., and Guldbrandtsen, B. (2021). Genomic inbreeding and selection signatures in the local dairy breed Icelandic Cattle. *Anim. Genet.* 52, 251–262. doi: 10.1111/age.13058

Gebreselassie, G., Berihulay, H., Jiang, L., and Ma, Y. (2020). Review on genomic regions and candidate genes associated with economically important production and reproduction traits in sheep (Ovies aries). *Animals* 10:33. doi: 10.3390/ani10010033

Hattori, Y., Yamasaki, M., and Itoh, N. (1996). The rat FGF-5 mRNA variant generated by alternative splicing encodes a novel truncated form of FGF-5 1. *Biochim. Biophys. Acta* 1306, 31–33. doi: 10.1016/0167-4781(19)60001-1

Higgins, C. A., Petukhova, L., Harel, S., Ho, Y. Y., Drill, E., Shapiro, L., et al. (2014). FGF5 is a crucial regulator of hair length in humans. *Proc. Natl. Acad. Sci. U. S. A.* 111, 10648–10653. doi: 10.1073/pnas.1402862111

Hu, R., Fan, Z. Y., Wang, B. Y., Deng, S. L., Zhang, X. S., Zhang, J. L., et al. (2017). RAPID COMMUNICATION: generation of FGF5 knockout sheep via the CRISPR/Cas9 system12. *J. Anim. Sci.* 95, 2019–2024. doi: 10.2527/jas.2017.1503

Hu, X., Hao, F., Li, X., Xun, Z., Gao, Y., Ren, B., et al. (2021). Generation of vegf knock-in cashmere goat via the crispr/cas9 system. *Int. J. Biol. Sci.* 17, 1026–1040. doi: 10.7150/ijbs.55559

Kim, Y. J., Jung, N., Kim, N., Ha, J. C., Park, J. H., Han, K., et al. (2020). Effect of cysteine-free human fibroblast growth factor-5s mutant (FGF5sC93S) on hair growth. *Dermatol. Ther.* 33:e14530. doi: 10.1111/dth.14530

Kruglyak, L. (1997). The use of a genetic map of biallelic markers in linkage studies. *Nat. Genet.* 17, 21–24. doi: 10.1038/ng0997-21

Legrand, R., Tiret, L., and Abitbol, M. (2014). Two recessive mutations in fgf5 are associated with the long-hair phenotype in donkeys. *Genet. Sel. Evol.* 46:65. doi: 10.1186/s12711-014-0065-5

Li, W. R., Liu, C. X., Zhang, X. M., Chen, L., Peng, X. R., He, S. G., et al. (2017). CRISPR/Cas9-mediated loss of FGF5 function increases wool staple length in sheep. *FEBS J.* 284, 2764–2773. doi: 10.1111/febs.14144

Locke, A. E., Kahali, B., Berndt, S. I., Justice, A. E., Pers, T. H., Day, F. R., et al. (2015). Genetic studies of body mass index yield new insights for obesity biology. *Nature* 518, 197–206. doi: 10.1038/nature14177

Moon, K. H. (2019). Screening of Genetic Factor in the Interaction Between Periodontitis and Metabolic Traits Using Candidate Gene Association Study (CGAS). *Biochem. Genet.* 57, 466–474. doi: 10.1007/s10528-018-9899-9

Mortimer, S. I., Hatcher, S., Fogarty, N. M., van der Werf, J. H. J., Brown, D. J., Swan, A. A., et al. (2017). Genetic parameters for wool traits, live weight, and ultrasound carcass traits in Merino sheep. *J. Anim. Sci.* 95, 1879–1891. doi: 10.2527/jas.2016.1234

Nei, M., and Roychoudhury, A. K. (1974). Sampling variances of heterozygosity and genetic distance. *Genetics* 76, 379–390. doi: 10.1093/genetics/76.2.379

Nesterova, A., Nizamutdinov, I., Golovatenko-Abramov, P., and Konyukhov, B. (2010). Fluctuations of BMP signaling pathway during hair cycles in skin of mice with mutant genes we, wal and Fgf5go. *J. Dermatol. Sci.* 60, 201–203. doi: 10.1016/j.jdermsci.2010.10.002

Pryce, J. E., Hayes, B. J., Bolormaa, S., and Goddard, M. E. (2011). Polymorphic regions affecting human height also control stature in cattle. *Genetics* 187, 981–984. doi: 10.1534/genetics.110.123943

Rochus, C. M., Jonas, E., and Johansson, A. M. (2020). Population structure of five native sheep breeds of Sweden estimated with high density SNP genotypes. *BMC Genet.* 21:27. doi: 10.1186/s12863-020-0827-8

Schneider, M. R., Schmidt-Ullrich, R., and Paus, R. (2009). The Hair Follicle as a Dynamic Miniorgan. *Curr. Biol.* 19, R132–R142. doi: 10.1016/j.cub.2008.12.005

Su, R., Gong, G., Zhang, L., Yan, X., Wang, F., Zhang, L., et al. (2020). Screening the key genes of hair follicle growth cycle in Inner Mongolian Cashmere goat based on RNA sequencing. *Arch. Anim. Breed.* 63, 155–164. doi: 10.5194/aab-63-155-2020

Sundberg, J. P., Rourk, M. H., Boggess, D., Hogan, M. E., Sundberg, B. A., and Bertolino, A. P. (1997). Angora Mouse Mutation: altered Hair Cycle, Follicular Dystrophy, Phenotypic Maintenance of Skin Grafts, and Changes in Keratin Expression. *Vet. Pathol.* 34, 171–179. doi: 10.1177/030098589703400301

Vignal, A., Milan, D., SanCristobal, M., and Eggen, A. (2002). A review on SNP and other types of molecular markers and their use in animal genetics. *Genet. Sel. Evol.* 34, 275–305. doi: 10.1186/1297-9686-34-3-275

Wang, X., Yang, Q., Zhang, S., Zhang, X., Pan, C., Chen, H., et al. (2019). Genetic effects of single nucleotide polymorphisms in the goat gdf9 gene on prolificacy: true or false positive? *Animals* 9:886. doi: 10.3390/ani9110886

Wang, Z., Zhang, X., Jiang, E., Yan, H., Zhu, H., Chen, H., et al. (2020). InDels within caprine IGF2BP1 intron 2 and the 3'-untranslated regions are associated with goat growth traits. *Anim. Genet.* 51, 117–121. doi: 10.1111/age.12871

Wilkening, S., Chen, B., Bermejo, J. L., and Canzian, F. (2009). Is there still a need for candidate gene approaches in the era of genome-wide association studies? *Genomics* 93, 415–419. doi: 10.1016/j.ygeno.2008.12.011

Xiang, G., Ren, J., Hai, T., Fu, R., Yu, D., Wang, J., et al. (2018). Editing porcine IGF2 regulatory element improved meat production in Chinese Bama pigs. *Cell. Mol. Life Sci.* 75, 4619–4628. doi: 10.1007/s00018-018-2917-6

Xu, Y., Liu, H., Pan, H., Wang, X., Zhang, Y., Yao, B., et al. (2020). CRISPR/Cas9−mediated disruption of fibroblast growth factor 5 in rabbits results in a systemic long hair phenotype by prolonging anagen. *Genes* 11:297. doi: 10.3390/genes11030297

Zhang, L., He, S., Liu, M., Liu, G., Yuan, Z., Liu, C., et al. (2015). Molecular cloning, characterization, and expression of sheep FGF5 gene. *Gene* 555, 95–100. doi: 10.1016/j.gene.2014.10.036

Zhang, R., Li, Y., Jia, K., Xu, X., Li, Y., Zhao, Y., et al. (2020). Crosstalk between androgen and Wnt/β-catenin leads to changes of wool density in FGF5-knockout sheep. *Cell Death Dis.* 11:407. doi: 10.1038/s41419-020-2622-x

Zhao, H., Wu, X., Cai, H., Pan, C., Lei, C., Chen, H., et al. (2013). Genetic variants and effects on milk traits of the caprine paired-like homeodomain transcription factor 2 (PITX2) gene in dairy goats. *Gene* 532, 203–210. doi: 10.1016/j.gene.2013.09.062

Zou, C., Massonnet, M., Minio, A., Patel, S., Llaca, V., Karn, A., et al. (2021). Multiple independent recombinations led to hermaphroditism in grapevine. *Proc. Natl. Acad. Sci. U. S. A.* 118:e2023548118. doi: 10.1073/pnas.2023548118

Conflict of Interest: The authors declare that the research was conducted in the absence of any commercial or financial relationships that could be construed as a potential conflict of interest.

Publisher's Note: All claims expressed in this article are solely those of the authors and do not necessarily represent those of their affiliated organizations, or those of the publisher, the editors and the reviewers. Any product that may be evaluated in this article, or claim that may be made by its manufacturer, is not guaranteed or endorsed by the publisher.

frontiers in Genetics

ORIGINAL RESEARCH
published: 30 September 2021
doi: 10.3389/fgene.2021.735827

Differential Methylation and Transcriptome Integration Analysis Identified Differential Methylation Annotation Genes and Functional Research Related to Hair Follicle Development in Sheep

Yuezhen Tian[1], Xuemei Yang[2], Jianwen Du[2], Weidan Zeng[2], Weiwei Wu[1], Jiang Di[1], Xixia Huang[2] and Kechuan Tian[1]**

[1]The Key Laboratory for Genetics Breeding and Reproduction of Xinjiang Cashmere and Wool Sheep, Institute of Animal Science, Xinjiang Academy of Animal Sciences, Urumqi, China, [2]College of Animal Science, Xinjiang Agricultural University, Urumqi, China

OPEN ACCESS

Edited by:
Xin Wang,
Northwest A and F University, China

Reviewed by:
Wenlin Bai,
Shenyang Agricultural University, China
Wei Sun,
Yangzhou University, China

***Correspondence:**
Xixia Huang
au-huangxixia@163.com
Kechuan Tian
woolcashmere@163.com

Specialty section:
This article was submitted to Livestock Genomics, a section of the journal Frontiers in Genetics

Received: 03 July 2021
Accepted: 30 August 2021
Published: 30 September 2021

Citation:
Tian Y, Yang X, Du J, Zeng W, Wu W, Di J, Huang X and Tian K (2021) Differential Methylation and Transcriptome Integration Analysis Identified Differential Methylation Annotation Genes and Functional Research Related to Hair Follicle Development in Sheep. Front. Genet. 12:735827. doi: 10.3389/fgene.2021.735827

Hair follicle growth and development are a complex and long-term physiological process, which is regulated by a variety of physical factors and signal pathways. Increasing the understanding of the epigenetic regulation and function of candidate genes related to hair follicle development will help to better understand the molecular regulatory mechanisms of hair follicle development. In this study, the methylated DNA immunoprecipitation sequencing (MeDIP-seq) was used to obtain the genome-wide methylation map of the hair follicular development of Super Merino sheep in six stages (fetal skin tissue at 65 d, 85 d, 105 d, 135 d, 7 d, and 30 d after birth). Combined with the results of previous RNA-sequencing, 65 genes were screened out that were both differential methylation and differential expression, including EDN1, LAMC2, NR1D1, RORB, MyOZ3, and WNT2 gene. Differential methylation genes were enriched in Wnt, TNF, TGF-beta, and other signaling pathways related to hair follicle development. The bisulfite sequencing PCR results and MeDIP-seq were basically consistent, indicating that the sequencing results were accurate. As a key gene in the Wnt signaling pathway, both differential methylation and expression gene identified by MeDIP-seq and RNA-seq, further exploration of the function of WNT2 gene revealed that the DNA methylation of exon 5 (CpG11 site) promoted the expression of WNT2 gene. The overexpression vector of lentivirus pLEX-MCS-WNT2 was constructed, and WNT2 gene effectively promoted the proliferation of sheep skin fibroblasts. The results showed that WNT2 gene could promote the growth and development of skin and hair follicles. The results of this study will provide a theoretical basis for further research on sheep hair follicle development and gene regulation mechanisms.

Keywords: sheep, hair follicle development, DNA methylation, MeDIP-seq, fibroblast, WNT2

INTRODUCTION

With the development of textile industry, people's demand for high-quality wool is increasing, and China has been relying on imported wool to meet the demand of domestic production for a long time. In order to break the foreign monopoly on the ultra-fine wool sheep market, improve the grade and level of the fine wool sheep industry in China, and protect the diversity of sheep breeds, it is of great significance to select and improve the fine wool sheep breeds in China to meet the market demand. Super Merino sheep is a new breed of ultra-fine wool independently bred in China. This breed has been jointly bred by several units in Xinjiang, Inner Mongolia, Jilin and other provinces since 2000. With ultra-fine Australian Merino sheep as the male parent, and Chinese Merino sheep Xinji fine wool sheep and Aohan fine wool sheep as the female parent, the method of progressive hybridization has been adopted. After 14 years of selection and breeding, the new breed of ultra-fine wool for worsted with wool fineness of 17.0 ~ 19.0 μm was approved and named in 2014. However, the regulation mechanism of wool growth and hair follicle development is still unclear. Therefore, it is necessary to further breed Super Merino sheep as an excellent local ultra-fine wool breed in China and to explore the mechanism related to the development of its hair follicles.

Hair is the product of hair follicle growth and development, and hair follicle is the skin of the derivatives, its structure and properties have important effects on yield and quality of hair (Cao et al., 2017; Zhao et al., 2020a), so increasing related studies on hair follicle is necessary. Hair follicle growth and development are a complex and long-term physiological process regulated by the variety of physical factors and signaling pathways, and gene expression is one of the decisive factors influencing the growth of sheep hair (Sulayman et al., 2019; Zhang et al., 2019a). DNA methylation is an important epigenetic mechanism that plays a role in several biological processes, such as gene expression and genomic imprinting (Freitag and Selker, 2005; Devos et al., 2021), and also plays a role by regulating the expression of genes related to hair follicle development (Zou et al., 2016; Wang et al., 2020; Li et al., 2021). At present, researchers have obtained the transcriptome regulation network of hair follicle development in some varieties of sheep through multi-omics (Sulayman et al., 2019; Li et al., 2020), but few epigenetic markers related to it have been found. Therefore, further studies are needed to integrate the results of multi-omics studies, in order to better analyze the regulation mechanism of hair follicle development.

Methylated DNA immunoprecipitation sequencing (MeDIP-seq) is a high-throughput sequencing technology based on the principle of antibody enrichment, which specifically binds 5mC bound antibodies to DNA methylation fragments on the genome, and then enriches and rebinds specifically (Zhou et al., 2018; Ben Maamar et al., 2021). This method has high specificity and is convenient and suitable for DNA methylation analysis. Compared with the whole-genome bisulfate sequencing method, the cost is lower and the genome-wide methylation status can be estimated unbiased. Therefore, this method was used in this study to analyze the genome-wide methylation level (Willems et al., 2016; Kim et al., 2018).

In order to explore the potential regulatory relationships among epigenetic regulation, gene expression, and gene function, this study will continue to explore regulation mechanism of genes that are both differential methylation and differential expression in different hair follicle stages (Sulayman et al., 2019), including differential methylation regions (DMRs) and differential methylation genes (DMGs; Chen et al., 2018a; Zhang et al., 2019b). As the encoding gene of methyltransferase, DNMT1, DNMT3a, and DNMT3b are involved in the regulation of target gene methylation (Yu et al., 2021). Therefore, the expression levels of DNMTs genes in different hair follicle development stages will be explored in this study. Then, WNT2 is a differential methylation and differential expression gene in different stages of hair follicle development, and WNT2 is also a key gene in the Wnt signaling pathway related to hair follicle development (Fu and Hsu, 2013; Chen et al., 2018a; Zhou et al., 2020). Therefore, we chose WNT2 gene to further explore its regulation and functional mechanism of methylation in hair follicle development. Firstly, we will explore the DNA methylation, mRNA, and protein expression level of exon 5 of WNT2 gene, and analyze the relationship between DNA methylation and expression level of this gene. Secondly, lentivirus PLEX-MCS-WNT2 expression vector will be constructed, and the function of WNT2 gene will be preliminarily verified. And then, the lentivirus pLEX-MCS-WNT2 expression vector will be co-transfected into sheep skin fibroblasts. Finally, the proliferation of sheep skin fibroblasts can be identified by CCK-8 method to further determine the effect of WNT2 gene on the development of hair follicles. The results of this study will provide a theoretical basis for the subsequent research on the development of hair follicles and the mechanism of gene regulation in sheep hair. It is of great significance to explain the regulatory network of hair follicle development from the perspective of molecular and epigenetic mechanisms.

MATERIALS AND METHODS

Samples Collection and Cell Culture

All Super Merino sheep used in this study were raised in the Xinjiang Science and Innovation Breeding Center (Latitude 43°01′08″–44°06′11″N, Longitude 86°37′56″–88°58′22″E), Xinjiang Uygur Autonomous Region, China. All selected sheep were pluriparous sheep about 2 to 3 years old. The ewes were in estrus at the same time and were mated with the semen of the same ram and were managed under the same environmental and nutritional conditions. In this study, fetal skin tissue at 65 d, 85 d, 105 d, and 135 d at embryonic period and 7 d and 30 d after birth (labeled as G1, G2, G3, G4, G5, and G6, respectively) were collected, and three lambs were collected at each stage (Sulayman et al., 2019).

After collection and treatment, the samples were quickly placed into a cryopreservation tube and stored in a liquid nitrogen. In addition, five ewes with an average fiber diameter of 16.9 μm (extremely fine group) and five ewes with an average fiber diameter of 19.53 μm (extremely thick group) were selected. Skin tissue samples (2 cm × 2 cm) from the left scapula were collected and cryopreserved in liquid nitrogen for DNA, RNA, and protein extraction for further WNT2 gene function verification. Experiments were performed according to the Regulations for the Administration of Affairs Concerning Experimental Animals and approved by the Xinjiang Agricultural University.

The sheep skin fibroblasts used in this experiment were donated by the Biotechnology Institute of Xinjiang Academy of Animal Science. The cells were seeded in a petri dish containing 20% fetal bovine serum and 1% antibiotics in 5% CO_2 at 37°C.

Genomic DNA, RNA, and Protein Extraction

The AllPrep DNA/RNA Mini Kit (80204, Qiagen) was used to extract genomic DNA from skin tissue of Super Merino sheep at six stages of hair follicle development: 65 d, primary hair follicles formation; 85 d, secondary hair follicle bud formation; 105 d, differentiation of secondary hair follicles; 135 d, secondary hair follicles mature; and 7 d and 30 d, after birth (Ablat et al., 2017). The extracted genomic DNA was subjected to NanoDrop One spectrophotometer and Qubit 2.0 (Q33216, Invitrogen) electrophoresis for qualified quality inspection and further experiment.

Tissues RNA was extracted by the AllPrep DNA/RNA Mini Kit (80204, Qiagen), and RNA concentration was determined using NanoDrop 2000 nucleic acid detector. After agarose gel electrophoresis, cDNA was synthesized using reverse transcription kit (PrimeScript RT reagent Kit with gDNA Eraser) and stored for further experiment in the −20°C refrigerator.

Tissue samples of 50–100 mg were triturated in liquid nitrogen, and protein samples were extracted from the skin tissues of the 10 sheep individuals (five extremely fine group and five extremely thick group sheep) according to the instructions of highly efficient RIPA tissue/cell rapid lysate. The extracted protein samples were detected according to the instructions of the Pierce TM BCA Protein Assay Kit, and the qualified protein samples were stored at −20°C.

MeDIP-seq Analysis

DNA libraries were constructed as: G1, G2, G3, G4, G5, and G6. MeDIP-seq was performed as previously described by previous method (Miao et al., 2020). Purified DNA was analyzed on NanoDrop One spectrophotometer (Thermo Fisher Scientific, Waltham, MA, United States) and quantified using a Qubit (Thermo Fisher Scientific, Waltham, MA, United States). DNA was recovered with AMPure XP beads (Beckman Coulter, Inc., Indianapolis, IN, United States) and utilized for MeDIP using a Magnetic Methylated DNA Immunoprecipitation Kit (Diagenode Inc., Denville, NJ, United States) according to the manufacturer's protocol. DNA size was verified using an Agilent DNA-1000 Kit on an Agilent 2100 Bioanalyzer (Agilent Technologies, Santa Clara, CA, United States). After MeDIP, the remaining DNA was PCR-amplified with sequencing primers and the DNA libraries were quantified using a Qubit fluorometer (Thermo Fisher Scientific, Waltham, MA, United States) according to the Qubit user guide, and subsequently used for sequencing (Illumina Hiseq2500, Illumina). The raw data were aligned to the *Ovis aries* genome (version 0.12.8) using default parameters (Li et al., 2021). The number of reads was assessed using the chi-squared test and false discovery rate; results with $p < 0.05$ were considered significant. MACS (version 1.4.2) software was applied to search the peak enrichment area, and the enrichment area of the sample peak was obtained.

According to the previous RNA-seq results of our research group (Sulayman et al., 2019), the tissues of the animals used were the same as that of the MeDIP-seq. According to the results of the two analysis, genes/regions that were both differentially methylated and differentially expressed were screened to provide a basis for subsequent analysis.

GO and KEGG Pathway Analysis

DMGs were subjected to GO functional analysis and KEGG pathway analysis by DAVID. The GO enrichment analysis provided all significantly enriched GO terms for comparison with the DMGs to determine the genomic background and filters of the DMGs that corresponded to biological functions. Pathway analysis for the DMGs was performed using the KEGG tool, which is a digital representation of the biological system (Kanehisa et al., 2006). GO enrichment analysis for the DMGs was performed using the GOseq R package (Young et al., 2010). GO enrichment can classify DMG according to biological processes, cell components, molecular functions, etc. KEGG pathway can also be significantly enriched by the GO enrichment principle, and corrected values of $p < 0.05$ were considered significantly enriched by the DMGs.

Bisulfite Sequencing PCR

The differential methylation and differentially expressed genes related to the regulation of hair follicle development in 105 d and 135 d of embryonic period were selected for bisulfite sequencing PCR (BSP) analysis. Genomic DNA was processed according to the instructions of the EZ DNA Methylation-GOIDTM Kit. We downloaded the sequences of *Ovis aries* EDN1, LAMC2, NR1D1, RORB, MYOZ3, and WNT2 gene from NCBI database and designed the primer pairs of BSP by MethPrimer online software. The modified DNA was amplified by PCR, as previously reported (Fan et al., 2020). PCR amplification product was purified by the PCR product purification kit (Tiangen). After agarose gel electrophoresis and concentration determination, the purified product was linked to PMD19-T vector (Takara). Three positive clones from each sample were selected and sent to Shanghai Sangong for sequencing.

Expression Analysis of DNMTs, EDN1, and WNT2 Genes in Sheep

Fetal skin tissue at 65 d, 85 d, 105 d, 135 d, and 7 d and 30 d after birth (labeled as G1, G2, G3, G4, G5, and G6, respectively) were used, and three samples were collected at each stage. According to the sequences of sheep DNMT1, DNMT3a, DNMT3b, and EDN1 provided by the NCBI, the reference gene was GAPDH, and Primer Premier 5.0 software was used to design the quantitative primers. The cDNA template was used for qRT-PCR amplification. The total system was 25 μl, including 1 μl cDNA, and each sample had three replicates. The amplification reaction was carried out in Bio-Rad CFX96 fluorescent quantitative PCR instrument.

The gene expressions of WNT2 of the skin, heart, liver, spleen, lung, kidney, and muscle tissue of left shoulder of the lambs at 135 d (hair follicle maturation period) were identified. According to the sequences of sheep WNT2, the reference gene was GAPDH (Kang et al., 2020). The amplification procedures and systems were same as above.

Construction of Lentivirus pLEX-MCS-WNT2 Expression Vector

The restriction endonuclease *XhoI* and *NotI* were used to digest the WNT2 fragment and the vector by double enzyme digestion. Restrictive endonuclease NotI and XhoI restriction sites and protective bases were introduced. Forward primers: aacgagatatcgggtcccGCGGCCGCATGAACGCCT, reverse primers: tgtgttctcgtcgtgcccCTCGAGTCATGTCGGAGCCG. The digested product was recovered according to the agarose gel DNA recovery kit. The recovered product was linked to the pLEX-MCS vector, and the ligated product was added to the DH5α capable cells. The correct bacterial colonies were selected for expanded culture. Meanwhile, the recombinant plasmid was extracted using the instructions of Tiangen endotoxin-free plasmid DNA small extraction kit.

Transfection of Recombinant Plasmid and Cell Proliferation Assay

Sheep skin fibroblasts were evenly inoculated into 24-well plates with 1×10^5 cells per well and cultured in a CO_2 incubator. When the confluence degree of sheep skin fibroblasts reached 70–80%, the co-infection test of the recombinant plasmid was carried out (Saadeldin et al., 2020). Each sample was repeated with six Wells. The transfection test groups were blank group (no treatment), control group (only lentivirus), and experimental group (lentivirus and WNT2).

After transfection for 48 h, sheep skin fibroblasts were digested with trypsin and added to the basic medium to stop digestion. 1 ml DMEM was added to each well and inoculated to 96-well plate at 100 μl/well and given 10 μl CCK-8 solution. After treatment for 0, 24 h, 48 h, and 72 h, the absorbance at 450 nm was measured with a microplate analyzer. The OD value represented the relative growth level of sheep fibroblasts, and the cell proliferation curve was plotted.

TABLE 1 | A statistics of data preprocessing results.

Sample No	Raw reads	Quality trimed	Adaptor trimed	Clean reads	Clean ratio(%)
No.1 (G1-1)	53,845,124	495,554	47,925	53,115,802	98.65%
No.2 (G1-2)	54,982,106	503,671	48,811	54,242,600	98.66%
No.3 (G1-3)	57,072,144	514,604	50,548	56,303,779	98.65%
No.4 (G1-1)	63,036,942	564,459	56,251	62,222,198	98.71%
No.5 (G1-2)	57,441,046	518,801	51,159	56,654,443	98.63%
No.6 (G1-3)	51,338,890	465,642	46,059	50,675,433	98.71%
No.7 (G1-1)	52,919,506	473,483	47,374	51,807,185	97.90%
No.8 (G1-2)	60,987,212	561,587	55,349	60,181,362	98.68%
No.9 (G1-3)	54,714,588	485,909	49,407	54,014,211	98.72%
No.10 (G1-1)	66,545,134	592,933	59,103	65,681,906	98.70%
No.11 (G1-2)	58,959,386	540,447	54,116	58,142,509	98.61%
No.12 (G1-3)	63,980,500	576,058	54,460	63,147,351	98.70%
No.13 (G1-1)	69,863,230	637,525	61,321	68,941,380	98.68%
No.14 (G1-2)	59,941,976	516,709	53,274	59,179,417	98.73%
No.15 (G1-3)	78,318,998	711,762	69,293	77,307,653	98.71%
No.16 (G1-1)	58,779,108	530,707	52,018	58,022,063	98.71%
No.17 (G1-2)	41,052,114	365,460	35,157	40,082,620	97.64%
No.18 (G1-3)	53,542,530	486,401	47,371	52,857,557	98.72%

Effective reads ratio = Clean reads/raw reads.

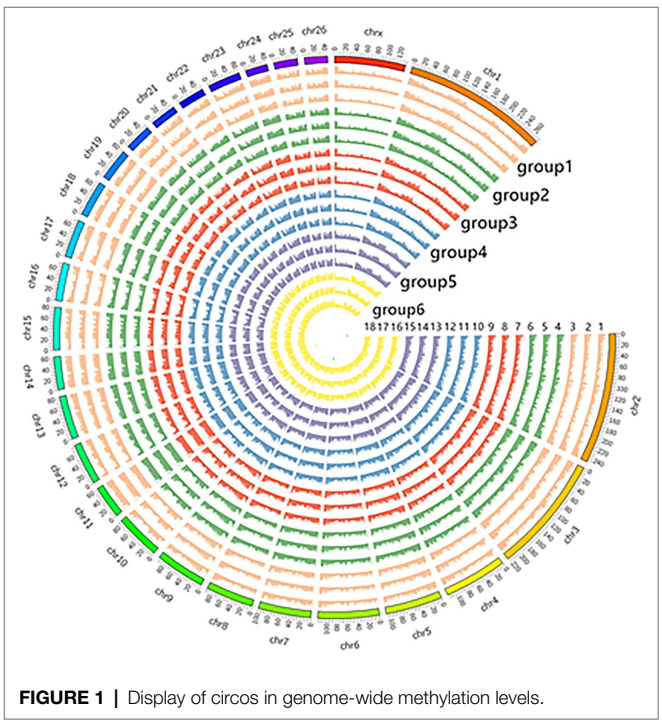

FIGURE 1 | Display of circos in genome-wide methylation levels.

Statistical Analysis

The relative expression level of the target gene was calculated using the method of $2^{-\triangle\triangle Ct}$. The SPSS19.0 software was used for one-way ANOVA and independent sample t test, and Duncan method was used for multiple comparisons. $p < 0.05$ indicated significant difference, and $p < 0.01$ indicated significant difference. The relative expression level of WNT2 protein in the skin tissues of Sub-Merino sheep with different fineness was determined by ImageJ. Data were presented as mean ± SEM.

RESULTS

Global Mapping of DNA Methylation in Skin Tissue of Six Stages

The number of original reads provided by each sample after sequencing was about 6G, and the proportion of base mass greater than 20 (Q20) per direction was more than 94%, which could be used for subsequent analysis (**Table 1**). Illumina NovaSeq was used to analyze the MeDIP-seq of skin tissues of 18 samples from six periods of Super Merino sheep, and the Clean ratio was between 97.64 and 98.73%. The obtained clean reads were compared with the reference genome of *Ovis aries* by Bowtie software, and the only matched reads were used for subsequent analysis. The circos graph of genome-wide DNA methylation level was drawn using circos software, with the length of 100 kb as the window. Both autosomes (1–26) and sex chromosomes (X) are rich in sequence enrichment peaks (**Figure 1**). The number of Peak scanned in individuals range from 75,514 to 129,618, and most of them are distributed in the intergenic region and promoter region (**Figure 2**). The raw sequencing data has been uploaded to the NCBI database (https://www.ncbi.nlm.nih.gov/).

MeDIP-seq and RNA-seq Combination Analysis

Through differential methylation analysis of two adjacent periods, a total of 596 differentially methylated genes were obtained, among which 256 were up-methylated genes and 340 were down-methylated genes. The down-methylated genes were more than up-methylated genes. There were 93 differentially methylated genes in the G1/G2 group, 89 differentially methylated genes in the G2/G3 group, 76 differentially methylated genes in the G3/G4 group, 64 differentially methylated genes in the G4/G5 group, 69 differentially methylated genes in the G5/G6 group, and 205 differentially methylated genes in the G6/G1 group. Two of the DMGs were present in all six comparison groups (**Figure 3**).

DNA methylation will affect gene expression to some extent, so the 596 differentially methylated genes screened in this study were overlapped with the differentially expressed genes previously screened by our group, and a total of 65 both differentially methylated and differentially expressed genes were identified in two adjacent periods (**Table 2**).

Gene Ontology and Pathway Enrichment Analysis

In order to assess whether the genes associated with differential methylation were enriched in certain biological processes or pathways, we conducted gene ontology and pathway analyses using the DMGs. DAVID was used to perform GO and KEGG enrichment analysis on the differentially methylated genes obtained at six stages to screen the biological functions and signaling pathways related to the hair follicle development of Super Merino sheep. The GO functional annotation showed that 1,046 GO entries were enriched, including 76 entries for cellular components, 124 entries for molecular functions, and 846 entries for biological processes. The enrichment of biological processes was mainly due to the regulatory effects of the generation of immune-related products, chemokines, enzyme activities, and apoptosis processes of epithelial and endothelial cells. Go items related to hair follicle development: hair follicle development, hair cycle process, skin epidermis development, and cell differentiation (**Figure 4**).

KEGG enrichment analysis showed that differentially methylated genes were enriched in 220 signaling pathways, and Top 15 was selected according to the enrichment degree. Among them, metabolic pathways contained the most differentially methylated genes, and these genes were enriched in WNT signaling pathway, TNF signaling pathway, MAPK signaling pathway, TGF-beta signaling pathway, ECM-receptor interaction, and other signaling pathways related to hair follicle development (**Figure 4**).

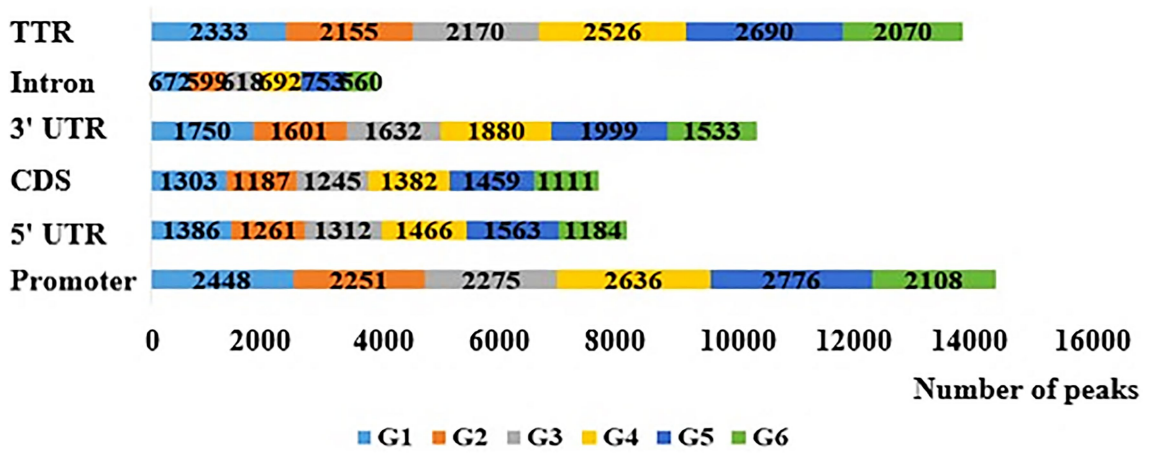

FIGURE 2 | Distribution of peaks in different gene elements in the six stage. Promoter is 2,000 bp upstream of transcription start site and TTR is 5,000 bp downstream of transcription stop site.

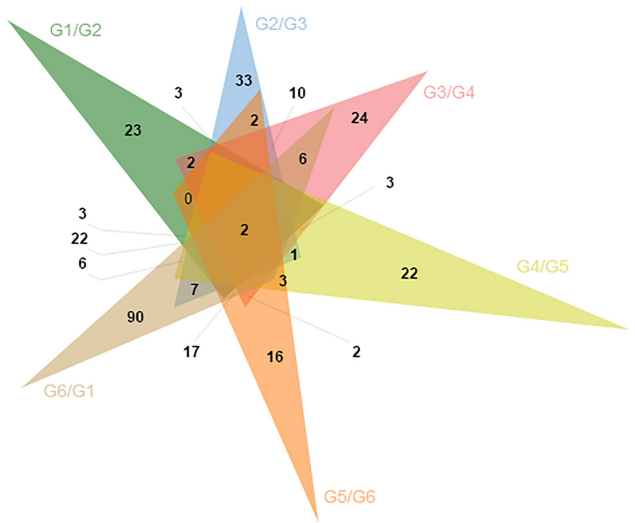

FIGURE 3 | The Venn of differential methylation genes in the six group comparisons.

TABLE 2 | Genes obtained from unite analysis of methylated DNA immunoprecipitation sequencing (MeDIP-Seq) and RNA-Seq.

Stages	Genes	Gene counts
G1/G2	*LAMC2, ARHGAP36, PADI3, NR1D1, EDN1*	5
G2/G3	*GABRB2, FABP3, B2M, PLIN5, CAPN3, K38, SELE, SLC5A1, MAPK13, CDKN1A*	10
G3/G4	*MYOZ3, MX1, RORB, WNT2, SLC5A1, EDN1, SLC14A1*	7
G5/G6	None	0
G6/G1	*SFN, AK1, LPIN1, AQP5, ACP5, DCT, NR1D1, RHOF, PQLC1, G6PD, ARHGAP36, GSN, SFTPC, TUBA4A, ITM2C, AZIN2, PADI3, B4GALT7, IGF1, IFT27, TSPAN5, TOB2, MYOZ3, SCD5, MMP14, B2M, SDR16C5, ATP7B, ACACA, MC1R, TIMP2, CYGB, AVPR1B, TLR5, SELP, LAMC2, IL2RA, REM1, HSD17B2, FURIN, SERPINA1, CRYAB, ARNTL, GHR, EDN1, NFKBIA, GNAI2, SLC25A27, AQP4, FHL1*	50

Differential Methylation Genes Related to Hair Follicle Development in Super Merino Sheep

Bisulfite sequencing PCR primers of EDN1, LAMC2, NR1D1, RORB, MYOZ3, and WNT2 genes were used for PCR amplification using bisulfite modified DNA as template (**Table 3**). The target fragment in the DMR region of EDN1 gene was 279–551 bp, the product size was 273 bp, there were 10 methylation sites, and the GC content ranged from 50 to 56%. The target fragment in the DMR region of LAMC2 gene was 198–497 bp, the product size was 300 bp, there were 16 methylation sites, and the GC content ranged from 60 to 64%. The target fragment in the DMR region of NR1D1 gene was 296–476 bp, the product size was 181 bp, there were 7 methylation sites, and the GC content ranged from 53.85 to 54.17%. The target fragment in the DMR region of RORB gene was 281–492 bp, the product size was 212 bp, there were 4 methylation sites, and the GC content ranged from 46.15 to 57.69%. The target fragment in the DMR region of MYOZ3 gene was 327–523 bp, the product size was 197 bp, there were 8 methylation sites, and the GC content ranged from 55.52–62.95% (**Supplementary Figures S1–S5**).

The methylation patterns of the sequencing genes corresponding to DMR were determined by sequence alignment analysis, and the methylation patterns of the five genes at 105d and 135d in the embryonic period were plotted. The results showed that the methylation rate of EDN1 gene was 54.44% at 105d and 42.22% at 135d in embryo. The methylation rate of LAMC2 gene was 52.78% at 105d and 85.43% at 135d. The methylation rate of NR1D1 gene was 96.83% at 105d and 90.48% at 135d. The methylation rate of RORB gene was 88.89% at 105d and 80.56% at 135d. The methylation rate of MYOZ3 gene was 66.06% at 105d and 56.94% at 135d (**Figure 5**). The methylation levels of EDN1, NR1D1, RORB, and MYOZ3 genes at 105d were higher than that of 135d at embryonic stage, while that of LAMC2 was the opposite.

The DNA methylation of the pre- and post-100 bp of exon 5 of WNT2 gene in the skin tissue of Super Merino sheep was analyzed. The sequence alignment result found a total of 13 CpG sites were consistent with the results predicted by MethPrimer software (**Figure 6**). Three positive monoclones of WNT2 gene from the two groups (extremely fine group and extremely thick group) of Super Merino sheep were selected and sequenced. The DNA methylation patterns of WNT2 gene in the skin tissue of Super Merino sheep in two groups were represented by the black and white origin diagram. The methylation levels of the fine group and the thick group were both higher and the difference was not significant ($p > 0.05$), and methylation ratios were 92.31 and 88.21%, respectively (**Figure 5**).

Expression of DNMTs, EDN1, and WNT2 Genes in Sheep Skin Tissue

Gene sequences of DNMT1, DNMT3a, DNMT3b, EDN1, and WNT2 in sheep were provided according to the NCBI, and GAPDH was used as the internal reference gene. The primer sequences were shown in **Table 4**.

The relative expression level of DNMT1 gene in G1 stage was significantly higher than that in G2 and G3 stages ($p < 0.01$), and significantly higher than that in G4, G5, and G6 stages ($p < 0.05$; **Figure 7A**). The change of DNMT3a gene expression increased first and then decreased, that is, it slowly increased from G1 period, reached the highest in G3 period, and then decreased. The expression level of this gene in G1, G2, and G3 was significantly higher than that in G5 and G6 ($p < 0.01$), and the expression level in G1 and G3 was significantly higher than that in G4 ($p < 0.05$; **Figure 7B**). With the hair follicle development, the expression pattern of DNMT3b in skin tissue showed a sequential pattern, that is, the trend of gradual decline. The expression level of this gene at G1 stage was significantly higher than that at G6 stage ($p < 0.05$), and there

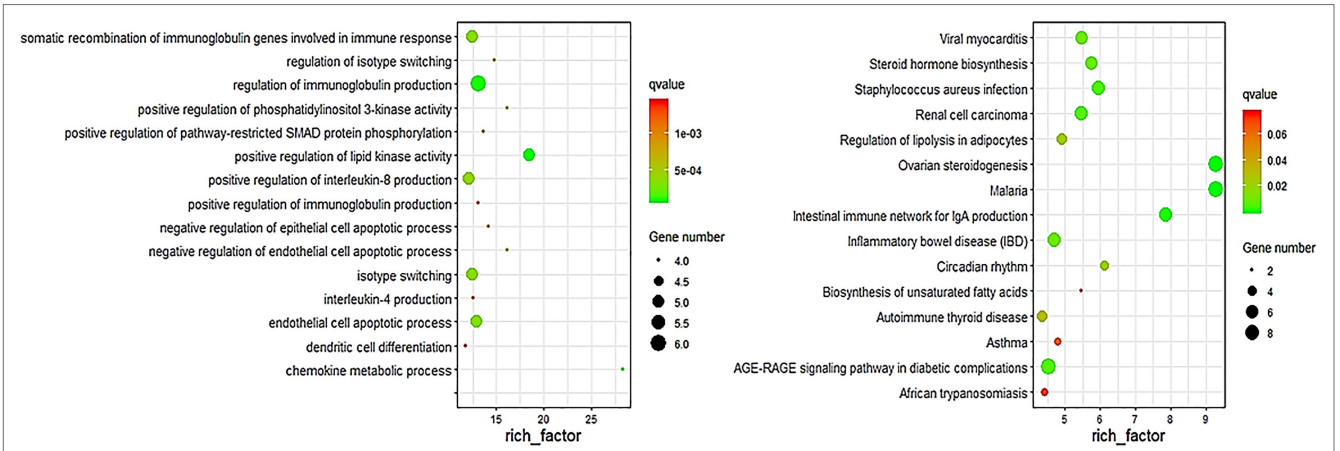

FIGURE 4 | Top 15 biological processes of GO enrichment and pathway enrichment.

TABLE 3 | Primers for amplicon of bisulfite sequencing PCR.

DMR	Gene	Primer sequence	Product Length
Chr20:43020501–43021000	*EDN1*	F: GGGTTTGTTTGAAGTTTTTTATTTA R: CCACTAAATCTCTTTACCTTCTTTTC	273 bp
Chr12:62293501–62294000	*LAMC2*	F: TTAGGTATTTTGGGGAAAGTTGTAG R: ACACACCACCTCCTCTATCTCTAAC	300 bp
Chr11:39923001–39923500	*NR1D1*	F: GAGGATGTGATATTTTAGGTAGTT R: CCATAATATTATCATTAAAAACAAAC	181 bp
Chr2:61615501–61616000	*RORB*	F: TGGATAGTTTTTTGTTGTAAGGATTG R: TCCAATATAAACCCAATCTCCTCTAT	212 bp
Chr5:59476501–59476600	*MYOZ3*	F: TGTTGAGTTATTGAAGGGTATTTTATT R: TTCCAAATCTCTCCCTAAACAAC	197 bp
Chr5:57479471–57480746	*WNT2*	F: GAAGTTATGTGTTGTGGTAGAGGTTA R: CCTTACAAATCCAATAAAATCCTTAC	230 bp

was no significant difference between G2, G3, G4, G5, and G6 stages ($p > 0.05$; **Figure 7C**).

The results of WNT2 gene expression in different tissues at 135d in embryonic period showed that the Δct value of skin was the smallest, so skin was used as the control group to calculate the expression amount. WNT2 gene was expressed in all tissues, but the expression levels were different. The expression level of WNT2 gene in skin tissue was significantly higher than that in the other six tissues ($p < 0.01$), and the expression level of WNT2 gene in heart, liver, spleen, lung, kidney, and muscle was not significantly different ($p > 0.05$; **Figure 8**).

Study on Relationship Between Methylation Expression and mRNA Expression in Super Merino Sheep

Western Blot was used to detect the expression of WNT2 protein in the skin tissues of Super Merino sheep with different fineness, and it was found that WNT2 protein was expressed in each individual in the very fine group and the very thick group. According to gray value calculation (**Figure 9**), the expression level of WNT2 protein in the very fine group was 1.74 times higher than that in the very thick group ($p < 0.05$), and the expression pattern of WNT2 protein in the two groups was consistent with the mRNA expression pattern and the change trend of DNA methylation level of WNT2 gene, both of which were higher in the very fine group than in the very thick group.

Each CpG site of WNT2 gene had different methylation levels in the skin tissues of Super Merino sheep with different fineness, among which CpG11 site had the largest difference in methylation levels between the two groups (**Figure 10**). Correlation analysis was conducted on each CpG site and its expression level in the extremely fine group and the extremely thick group. As shown in **Table 2**, there was a significant positive correlation between the methylation level of CpG11 site and its mRNA expression level ($p < 0.05$, $r^2 = 0.693$; **Table 5**).

Effect of WNT2 Gene on Proliferation of Sheep Skin Fibroblasts

The lentiviral vector pLEX-MCS was linked to the target fragment of WNT2 gene. The results of agarose gel electrophoresis were consistent with the results of the target fragment. Then, the recombinant plasmid pLEX-MCS-WNT2 was successfully constructed (**Supplementary Figure S6**). Sequencing was

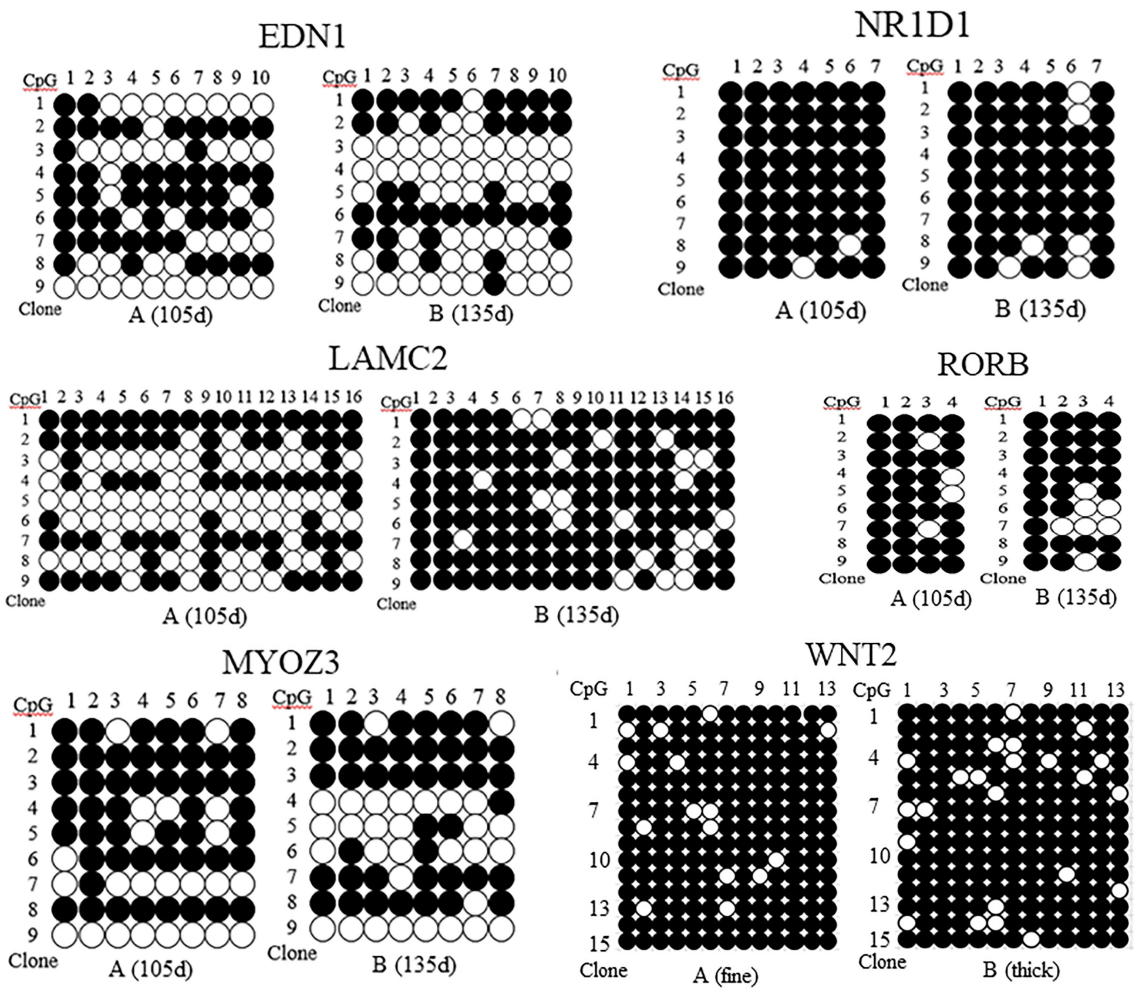

FIGURE 5 | Methylation patterns of EDN1, NR1D1, LAMC2, RORB, MYOZ3, and WNT2 gene in skin tissues of Super Merino sheep with different stages and fineness. ●, indicates methylation; ○, indicates no methylation. (A) (fine), the extremely fine group; (B) (thick), the extremely thick group.

performed on the recombinant plasmid pLEX-MCS-WNT2 successfully identified by double enzyme digestion test (*XhoI*/*NotI*), and it was found that the recombinant plasmid pLEX-MCS-WNT2 successfully obtained the original sequence in the CDS region of WNT2 gene (**Supplementary Figure S7**).

The proliferation of sheep skin fibroblasts transfected with lentivirus pLEX-MCS-WNT2 expression vector was detected by CCK-8 method. OD value represented the proliferation efficiency of sheep skin fibroblasts. With the increase of detection time, the proliferation level of sheep skin fibroblasts increased in blank group, control group, and experimental group, but the proliferation level in blank group was lower than that in the other two groups (**Figure 11**). At 24 h and 48 h. The proliferation level in experimental group was significantly higher than that in control group ($p < 0.01$); the proliferation levels at 72 h were significantly higher than those in the control group ($p < 0.05$). The proliferation level of the control group at 24 h was significantly higher than that of the blank group ($p < 0.01$); the proliferation level at 48 h was significantly higher than that in blank group ($p < 0.05$); and the proliferation level at 72 h was significantly higher than that in blank group ($p < 0.01$). The results showed that WNT2 gene could promote the proliferation of sheep skin fibroblasts.

DISCUSSION

The quality of wool is determined by the structure and characteristics of hair follicles, so it is of great significance to improve wool quality to improve the regulation mechanism of hair follicle structure and development. Increasing functional molecules have been identified and characterized for each stage in hair follicle development of mice (Nakamura et al., 2013; Saxena et al., 2019; Zhao et al., 2020b). However, there are few reports regarding the machinery underlying fine sheep hair follicle morphogenesis due to technical difficulties and high costs. Although there are conservative signals in hair follicle development among mice, different physiology and

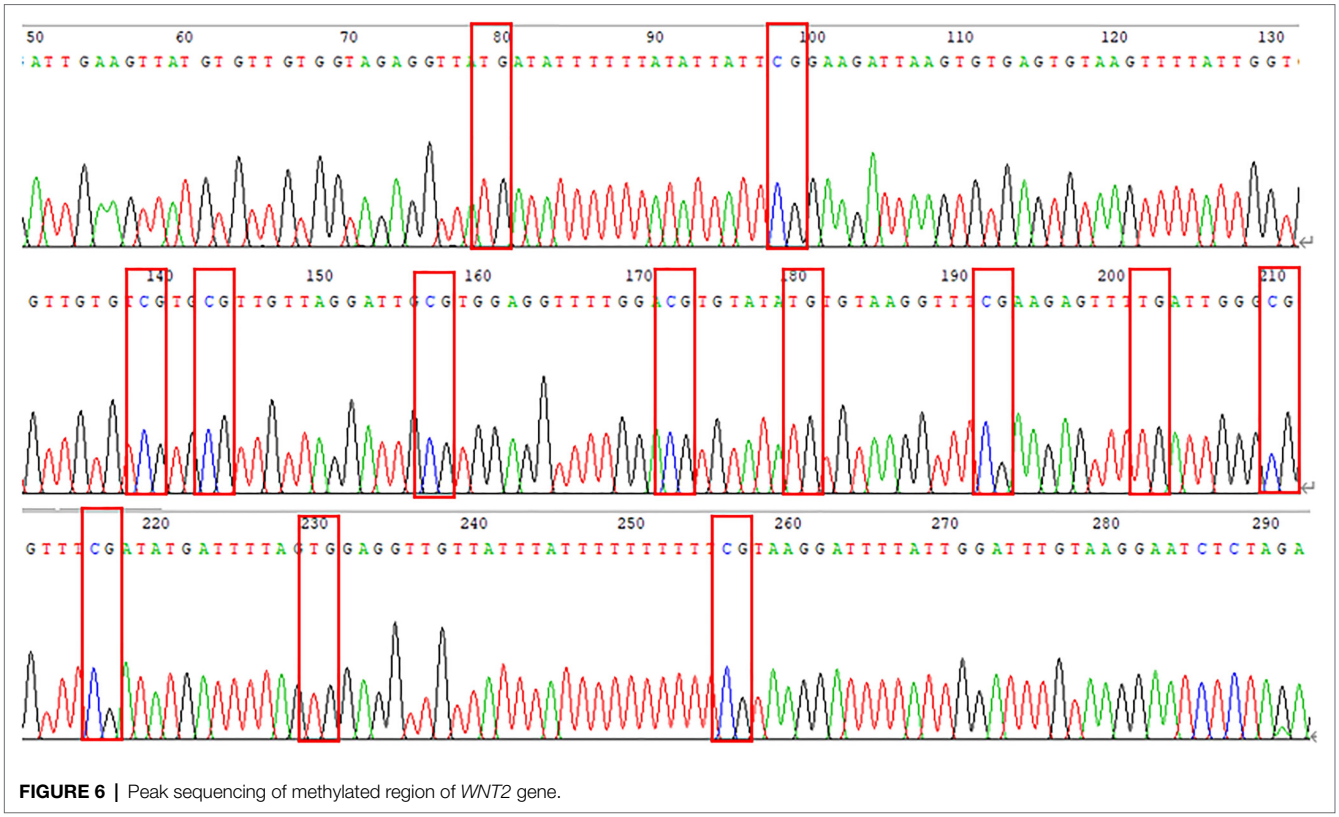

FIGURE 6 | Peak sequencing of methylated region of *WNT2* gene.

TABLE 4 | PCR primers of qRT-PCR.

Gene	Primer sequence	Product Length/bp	Tm (°C)	GenBank No
DNMT1	F:CAGACGTGTGAGCCGAGTGAAC R:CGAGATGCCTGCTTGGTGGAAG	117	61	NC_040256
DNMT3a	F:CGTCTCGGCTCCAGATGTTCTTC R:CGATGTAGCGGTCCACCTGAATG	180	60	NC_040254
DNMT3b	F:TACCTCACCATCGACCTCACAGAC R:TGCTCTCCTGCTGGCTGTCC	94	60	NC_040264
EDN1	F:GAAAGCCTGGGACAACCGAAAGAG R:TTGATGCTGTTGCTGATGGTCTCC	123	60	NC_040271
WNT2	F:GAAGTTATGTGTTGTGGTAGAGGTTA R:CCTTACAAATCCAATAAAATCCTTAC	109	59	NC_040255
GAPDH	F:GAGATCAAGAAGGTGGTGAAGCAG R:GTAGAAGAGTGAGTGTCGCTGTTG	113	60	NC_040254

regulation mechanisms exist between mice and sheep. Meanwhile, there are few studies on epigenetic markers and functional mechanisms related to hair follicle development in sheep. Taken together, further exploration and integration of the results of multi-omics studies are needed in order to better understand the regulation mechanism of hair follicle development.

The well-known genome-wide association study (GWAS) approach has been used to explain the variation in desired phenotypes among animals; however, in humans, the DNA sequence variation identified by GWAS is estimated to account for less than 30% of the phenotypic variation (Langevin and Kelsey, 2013). Therefore, in the current era of omics, epigenome-wide association studies (EWAS) may help to fill the gap between large-scale genomic information and related applications (Michels et al., 2013; Lee et al., 2014). Studies have shown that DNA methylation can lead to phenotypic changes in feeding and environmental conditions, resulting in productivity changes and animal disease risk (Boddicker et al., 2016; Tao et al., 2019; Tanwar et al., 2020). For example, a comparison of DNA methylation distribution between fast and slow growing broilers found that a total of 13,294 methylation genes were detected, of which 132 differentially methylated genes were related to growth and metabolism (Hu et al., 2013). Therefore, it is of great significance to explore the DNA methylation pattern of hair follicle development and the mechanism of candidate genes for improving wool quality breeding.

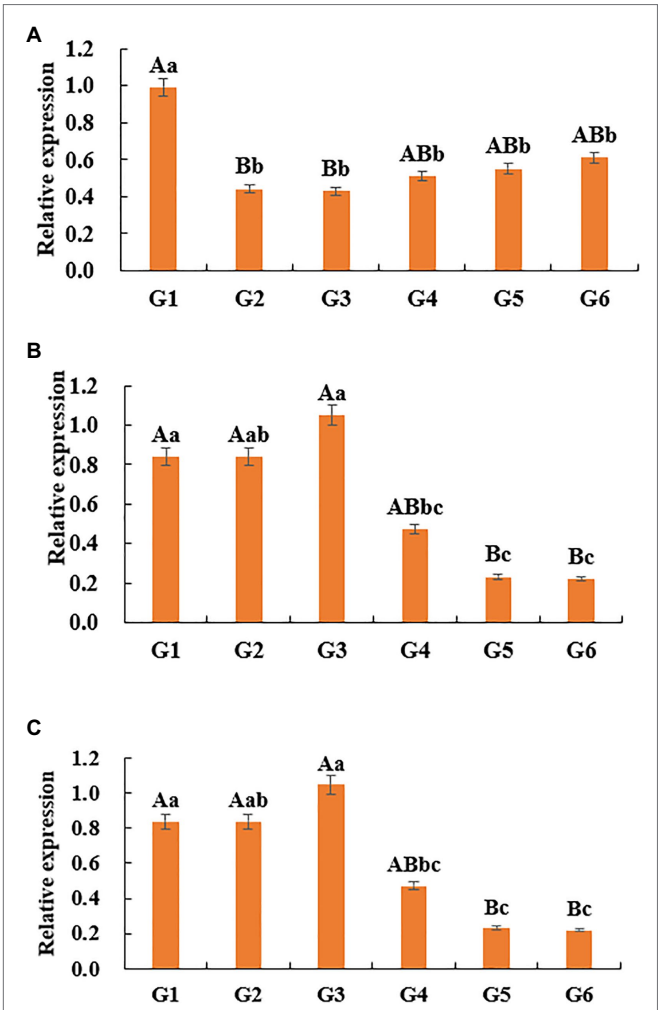

FIGURE 7 | Relative expression of *DNMTs* genes in skin tissues of Super Merino sheep. **(A)** The relative expression of *DNMT1* gene. **(B)** The relative expression of *DNMT3a* gene. **(C)** The relative expression of *DNMT3b* gene. Different lowercase letters indicate significant difference ($p < 0.05$), and different uppercase letters indicate extremely significant difference ($p < 0.01$), the same letter expressed surprise was not significant ($p > 0.05$).

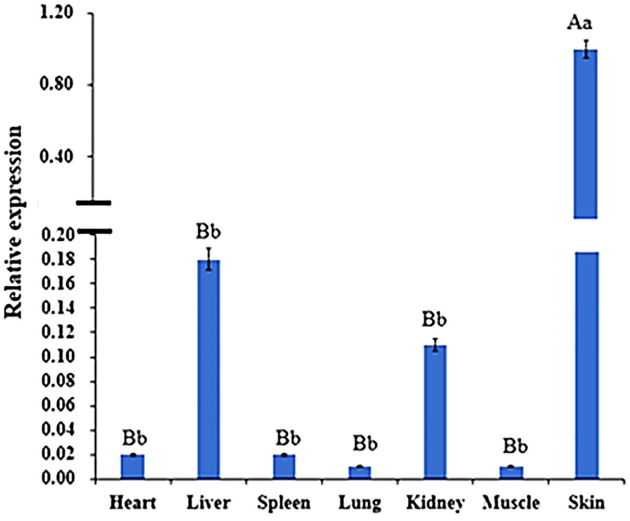

FIGURE 8 | Expression of *WNT2* gene in different tissues at 135 d of embryonic stage. Different lowercase letters indicate significant difference ($p < 0.05$), and different uppercase letters indicate extremely significant difference ($p < 0.01$), the same letter expressed surprise was not significant ($p > 0.05$).

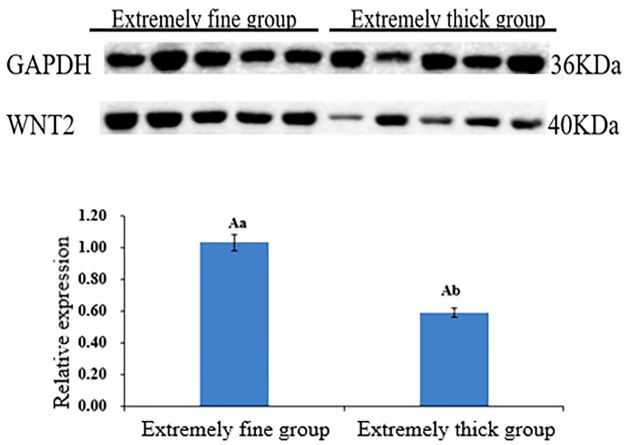

FIGURE 9 | Relative expression levels of WNT2 protein in skin tissue of Super Merino sheep with different fineness. Different capital letters indicate significant differences ($p < 0.01$), and same capital letters indicate no significant differences ($p > 0.01$); different lowercase letters indicate significant differences ($p < 0.05$).

In this study, the MeDIP-seq technique was used to map the genome-wide methylation of skin tissue of Super Merino sheep during six stages of hair follicle development (Ablat et al., 2017). Results found 596 differentially methylated genes. Combined with the results of transcriptome sequencing, we found 65 genes that were both differentially methylated and differentially expressed at different stages of hair follicle development, including EDN1, LAMC2, NR1D1, RORB, MyOZ3, and WNT2 gene (**Table 2**). GO enrichment analysis showed that these differentially expressed genes were mainly distributed in biological processes, molecular functions, and cell composition. KEGG pathway enrichment analysis showed that most of the differentially methylated genes were distributed in metabolism, cancer, and some signaling pathways. Among them, Wnt/β-catenin, as a classical signaling pathway, was first found to be related to hair follicle development (Leirós et al., 2012). This indicated that the MeDIP sequencing results of this study are reliable. Meanwhile, comparison of dibisulfite sequencing results and MeDIP-seq results showed that the methylation levels of these differentially methylated regions were also basically consistent with the results of MeDIP-seq sequencing (**Figure 5**). It was proved that the MeDIP-seq data obtained in this study were reliable and could be used for the analysis of skin tissue of Super Merino sheep at different follicle development stages.

Considering the critical role of the Wnt signaling pathway in the development of hair follicles, as well as the result of MeDIP-seq,

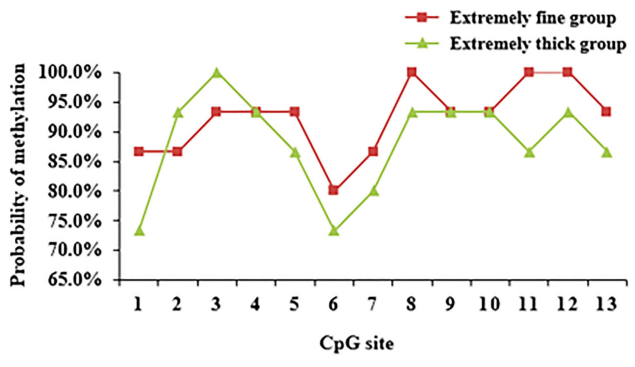

FIGURE 10 | DNA methylation level of CpG loci of *WNT2* gene in skin tissue of Super Merino Sheep with different fineness.

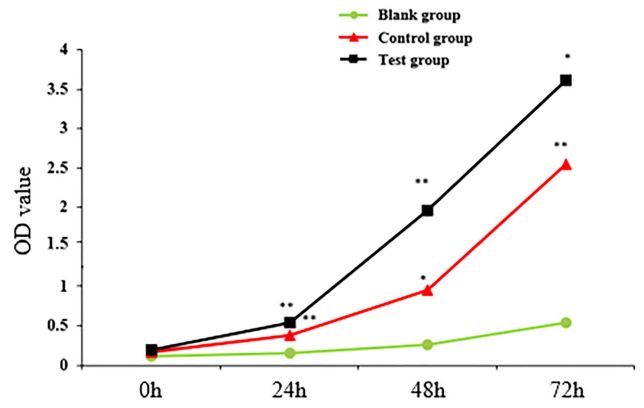

FIGURE 11 | Detection of sheep skin fibroblast proliferation efficiency. * indicates significant difference ($p < 0.05$), and ** indicates extremely significant difference ($p<0.01$). Unmarked means the difference is not significant ($p > 0.05$).

we want to further explore the methylation pattern and functional mechanism of WNT2 gene in the process of hair follicle development. Result showed WNT2 gene was widely expressed in the heart, liver, spleen, lung, kidney, muscle, and skin tissue of Super Merino sheep at 135 d of embryonic period, and the expression level in the skin tissue was significantly higher than that in other tissues ($p < 0.05$). It suggesting that WNT2 gene has an important effect on the growth and development of skin and hair follicle (**Figure 8**). The expression of mRNA and protein of WNT2 gene in the extremely fine group was significantly higher than that in the extremely thick group ($p < 0.05$), which showed that WNT2 gene is a key factor regulating the early development of sheep hair follicles. In addition, the CpG11 methylation level of WNT2 gene was positively correlated with the mRNA expression ($p < 0.05$), which indicated that the DNA methylation level of WNT2 gene promoted the expression of WNT2 gene, and then positively regulated the wool fiber diameter. This might be because the primer designed in this study selected the exon 5 of WNT2 gene, and it was the last exon of WNT2 gene. The influence of DNA methylation level in last exon region on the transcription level was greater than that in the promoter region, and the methylation of this region was positively correlated with gene expression (Yang et al., 2014; Singer et al., 2015). This is consistent with previous reports (Fraga et al., 2003; Zhang et al., 2006). These results showed the CpG11 site could be used as a candidate epigenetic marker (**Table 5**).

This study has verified that WNT2 gene was related to hair follicle development, and the DNA methylation level of WNT2 gene has a certain effect on wool fiber diameter. In order to further study, the regulation of WNT2 gene on hair follicle development, the lentivirus pLEX-MCS-WNT2 expression vector, was successfully constructed and transfected into sheep skin fibroblasts. It was found that WNT2 gene could promote the proliferation of sheep skin fibroblasts. It was further suggested that WNT2 gene could promote the growth and development of skin and hair follicles. According to previous study, Chen et al. (2018b) found that miR-125a can directly recognize and bind to the 3'UTR region of WNT2, and the regulation of WNT2 expression by miRNA may depend on transcriptional degradation. miR-125a also regulates hair follicle development by affecting the expression of WNT2-concordant genes in the Wnt signaling pathway, such as CTNNB1, LEF-1, PPARd, and TGFB1, so the relationship between miR-125a and WNT2 gene in the process of hair follicle development can be further explored. Studies also found androgens deregulate dermal papilla cells secreted factors involved in normal hair follicle stem cell differentiation *via* the inhibition of the canonical Wnt signaling pathway (Leirós et al., 2012). It was found that WNT2 is a Wntl protein involved in the classical Wnt/β-catenin pathway, and other WNT5a proteins involved in non-classical pathways. Studies have shown that classical pathways have a greater impact on induced hair follicle formation (Lin et al., 2015). Taken together, these results indicated that WNT2 gene may participate in hair follicle development through a variety of signaling ways, and its specific research is still worthy of further exploration.

CONCLUSION

In this study, the MeDIP-seq technology was used to obtain the genome-wide methylation map in six stages of hair follicular development of Super Merino sheep. Combined with the results of previous transcriptome sequencing, 65 genes were screened out that were both differentially methylated and differentially expressed, including EDN1, LAMC2, NR1D1, RORB, MyOZ3, and WNT2 gene. Differential methylated genes were enriched in Wnt, TNF, TGF-Beta, and other signaling pathways related to hair follicle development. Further exploration of the function of WNT2 gene revealed that the DNA methylation level of its exon 5 promoted the expression of this gene. The overexpression vector of lentivirus pLEX-MCS-WNT2 was constructed, and WNT2 gene effectively promoted the proliferation of sheep skin fibroblasts. These results revealed the epigenetic regulation mechanism of hair follicle development and the regulation mechanism of WNT2 gene. It could promote the growth and development of skin and hair follicles and provide theoretical basis for sheep wool breeding.

TABLE 5 | Correlation between mRNA expression of *WNT2* gene and CpG site.

Relation	CpG1	CpG2	CpG3	CpG4	CpG5	CpG6	CpG7
expression	−0.228	−0.474	−0.265	0.036	0.098	0.128	0.450
	CpG8	CpG9	CpG10	CpG11	CpG12	CpG13	
	0.102	0.036	0.170	0.693*	0.313	0.353	

**means significant correlation ($p < 0.05$), unmarked means no correlation ($p > 0.05$).*

DATA AVAILABILITY STATEMENT

The datasets presented in this study can be found in online repositories. The names of the repository/repositories and accession number(s) can be found at NCBI (accession: PRJNA750351 and PRJNA750354).

ETHICS STATEMENT

The animal study was reviewed and approved by the Faculty Animal Policy and Welfare Committee of Xinjiang Academy of Animal Sciences under contract.

AUTHOR CONTRIBUTIONS

XH and KT designed the experiment, contributed to the revision of the manuscript, and assisted in revising the final version of the manuscript. YT, XY, and JD performed all the experiments. WZ, WW, and JD collected the sheep samples. YT prepared all the figures and tables and drafted the manuscript. All authors have read and approved the final manuscript.

FUNDING

This research was funded by the Natural Science Foundation of Xinjiang Province (nos. 2019D01B07 and 2020D03016), the Special Fund for the National Natural Science Foundation of China (no. 31760655), the China Postdoctoral Science Foundation (no. 2017M623287), and the China Agriculture Research System of MOF and MARA (CARS-39). YT was supported by the Tianshan Elite Project in Xinjiang Province.

SUPPLEMENTARY MATERIAL

The Supplementary Material for this article can be found online at: https://www.frontiersin.org/articles/10.3389/fgene.2021.735827/full#supplementary-material

REFERENCES

Ablat, S., Tian, Y., Xu, Q., He, J., Zhao, B., Xu, X., et al. (2017). Study on Fetal Skin Hair Follicle Structure and Morphological Development of Subo Merino Sheep. *Sci. Agric. Sin.* 50, 3226–3235. doi: 10.3864/j.issn.0578-1752.2017.16.017

Ben Maamar, M., Sadler-Riggleman, I., Beck, D., and Skinner, M. K. (2021). Genome-wide mapping of DNA methylation 5mC by methylated DNA immunoprecipitation (MeDIP)-sequencing. *Methods Mol. Biol.* 2198, 301–310. doi: 10.1007/978-1-0716-0876-0_23

Boddicker, R. L., Koltes, J. E., Fritz-Waters, E. R., Koesterke, L., Weeks, N., Yin, T., et al. (2016). Genome-wide methylation profile following prenatal and postnatal dietary omega-3 fatty acid supplementation in pigs. *Anim. Genet.* 47, 658–671. doi: 10.1111/age.12468

Cao, Y., Jin, H. G., Ma, H. H., and Zhao, Z. H. (2017). Comparative analysis on genome-wide DNA methylation in longissimus dorsi muscle between small tailed Han and Dorper×small tailed Han crossbred sheep. *Asian Australas. J. Anim. Sci.* 30, 1529–1539. doi: 10.5713/ajas.17.0154

Chen, X., Shen, L. H., Gui, L. X., Yang, F., Li, J., Cao, S. Z., et al. (2018a). Genome-wide DNA methylation profile of prepubertal porcine testis. *Reprod. Fertil. Dev.* 30, 349–358. doi: 10.1071/RD17067

Chen, Y., Zhao, B., Liu, M., Wang, J., Qiu, X., Zhu, C., et al. (2018b). MicroRNAs profiling identifies miR-125a and its target gene Wnt2 in skins of different haired rabbits. *Front. Genet.* 9:628. doi: 10.3389/fgene.2018.00628

Devos, J., Behrouzi, A., Paradis, F., Straathof, C., Li, C., Colazo, M., et al. (2021). Genetic potential for residual feed intake and diet fed during early- to mid-gestation influences post-natal DNA methylation of imprinted genes in muscle and liver tissues in beef cattle. *J. Anim. Sci.* 99:skab140. doi: 10.1093/jas/skab140

Fan, Y., Liang, Y., Deng, K., Zhang, Z., Zhang, G., Zhang, Y., et al. (2020). Analysis of DNA methylation profiles during sheep skeletal muscle development using whole-genome bisulfite sequencing. *BMC Genomics* 21:327. doi: 10.1186/s12864-020-6751-5

Fraga, M. F., Ballestar, E., Montoya, G., Taysavang, P., Wade, P. A., and Esteller, M. (2003). The affinity of different MBD proteins for a specific methylated locus depends on their intrinsic binding properties. *Nucleic Acids Res.* 31, 1765–1774. doi: 10.1093/nar/gkg249

Freitag, M., and Selker, E. U. (2005). Controlling DNA methylation: many roads to one modification. *Curr. Opin. Genet. Dev.* 15, 191–199. doi: 10.1016/j.gde.2005.02.003

Fu, J., and Hsu, W. (2013). Epidermal Wnt controls hair follicle induction by orchestrating dynamic signaling crosstalk between the epidermis and dermis. *J. Invest. Dermatol.* 133, 890–898. doi: 10.1038/jid.2012.407

Hu, Y., Xu, H., Li, Z., Zheng, X., Jia, X., Nie, Q., et al. (2013). Comparison of the genome-wide DNA methylation profiles between fast-growing and slow-growing broilers. *PLoS One* 8:e56411. doi: 10.1371/journal.pone.0083821

Kanehisa, M., Goto, S., Hattori, M., Aoki-Kinoshita, K. F., Itoh, M., Kawashima, S., et al. (2006). From genomics to chemical genomics: new developments in KEGG. *Nucleic Acids Res.* 34, D354–D357. doi: 10.1093/nar/gkj102

Kang, Z., Zhang, S., Jiang, E., Wang, X., Wang, Z., Chen, H., et al. (2020). circFLT1 and lncCCPG1 sponges miR-93 to regulate the proliferation and differentiation of adipocytes by promoting lncSLC30A9 expression. *Mol. Ther. Nucleic Acids* 22, 484–499. doi: 10.1016/j.omtn.2020.09.011

Kim, W., Park, H., Seo, K. S., and Seo, S. (2018). Characterization and functional inferences of a genome-wide DNA methylation profile in the loin (longissimus dorsi) muscle of swine. *Asian Australas. J. Anim. Sci.* 31, 3–12. doi: 10.5713/ajas.16.0793

Langevin, S. M., and Kelsey, K. T. (2013). The fate is not always written in the genes: epigenomics in epidemiologic studies. *Environ. Mol. Mutagen.* 54, 533–541. doi: 10.1002/em.21762

Lee, J. R., Hong, C. P., Moon, J. W., Jung, Y. D., Kim, D. S., Kim, T. H., et al. (2014). Genome-wide analysis of DNA methylation patterns in horse. *BMC Genomics* 15:598. doi: 10.1186/1471-2164-15-598

Leirós, G. J., Attorresi, A. I., and Balañá, M. E. (2012). Hair follicle stem cell differentiation is inhibited through cross-talk between Wnt/β-catenin and androgen signalling in dermal papilla cells from patients with androgenetic alopecia. *Br. J. Dermatol.* 166, 1035–1042. doi: 10.1111/j.1365-2133.2012.10856.x

Li, S., Chen, W., Zheng, X., Liu, Z., Yang, G., Hu, X., et al. (2020). Comparative investigation of coarse and fine wool sheep skin indicates the early regulators for skin and wool diversity. *Gene* 758:144968. doi: 10.1016/j.gene.2020.144968

Li, X. J., Liu, L. Q., Dong, H., Yang, J. J., Wang, W. W., Zhang, Q., et al. (2021). Comparative genome-wide methylation analysis of longissimus dorsi muscles in Yorkshire and Wannanhua pigs. *Anim. Genet.* 52, 78–89. doi: 10.1111/age.13029

Lin, C. M., Yuan, Y. P., Chen, X. C., Li, H. H., Cai, B. Z., Liu, Y., et al. (2015). Expression of Wnt/β-catenin signaling, stem-cell markers and proliferating cell markers in rat whisker hair follicles. *J. Mol. Histol.* 46, 233–240. doi: 10.1007/s10735-015-9616-5

Miao, X., Luo, Q., Xie, L., Zhao, H., and Qin, X. (2020). Comparative DNA methylome analysis of estrus ewes reveals the complex regulatory pathways of sheep fecundity. *Reprod. Biol. Endocrinol.* 18:77. doi: 10.1186/s12958-020-00633-9

Michels, K. B., Binder, A. M., Dedeurwaerder, S., Epstein, C. B., Greally, J. M., Gut, I., et al. (2013). Recommendations for the design and analysis of epigenome-wide association studies. *Nat. Methods* 10, 949–955. doi: 10.1038/nmeth.2632

Nakamura, M., Schneider, M. R., Schmidt-Ullrich, R., and Paus, R. (2013). Mutant laboratory mice with abnormalities in hair follicle morphogenesis, cycling, and/or structure: an update. *J. Dermatol. Sci.* 69, 6–29. doi: 10.1016/j.jdermsci.2012.10.001

Saadeldin, I. M., Swelum, A. A., Zakri, A. M., Tukur, H. A., and Alowaimer, A. N. (2020). Effects of acute hyperthermia on the Thermotolerance of cow and sheep skin-derived fibroblasts. *Animals* 10:545. doi: 10.3390/ani10040545

Saxena, N., Mok, K. W., and Rendl, M. (2019). An updated classification of hair follicle morphogenesis. *Exp. Dermatol.* 28, 332–344. doi: 10.1111/exd.13913

Singer, M., Kosti, I., Pachter, L., and Mandel-Gutfreund, Y. (2015). A diverse epigenetic landscape at human exons with implication for expression. *Nucleic Acids Res.* 43, 3498–3508. doi: 10.1093/nar/gkv153

Sulayman, A., Tian, K., Huang, X., Tian, Y., Xu, X., Fu, X., et al. (2019). Genome-wide identification and characterization of long non-coding RNAs expressed during sheep fetal and postnatal hair follicle development. *Sci. Rep.* 9:8501. doi: 10.1038/s41598-019-44600-w

Tanwar, V. S., Ghosh, S., Sati, S., Ghose, S., Kaur, L., Kumar, K. A., et al. (2020). Maternal vitamin B12 deficiency in rats alters DNA methylation in metabolically important genes in their offspring. *Mol. Cell. Biochem.* 468, 83–96. doi: 10.1007/s11010-020-03713-x

Tao, S., Zhou, T., Saelao, P., Wang, Y., Zhu, Y., Li, T., et al. (2019). Intrauterine growth restriction alters the genome-wide DNA methylation profiles in small intestine, liver and longissimus Dorsi muscle of Newborn piglets. *Curr. Protein Pept. Sci.* 20, 713–726. doi: 10.2174/1389203720666190124165243

Wang, S., Li, F., Liu, J., Zhang, Y., Zheng, Y., Ge, W., et al. (2020). Integrative analysis of Methylome and transcriptome reveals the regulatory mechanisms of hair follicle morphogenesis in cashmere goat. *Cell* 9:969. doi: 10.3390/cells9040969

Willems, E., Guerrero-Bosagna, C., Decuypere, E., Janssens, S., Buyse, J., Buys, N., et al. (2016). Differential expression of genes and DNA methylation associated with prenatal protein undernutrition by albumen removal in an avian model. *Sci. Rep.* 6:20837. doi: 10.1038/srep20837

Yang, X., Han, H., De Carvalho, D. D., Lay, F. D., Jones, P. A., and Liang, G. (2014). Gene body methylation can alter gene expression and is a therapeutic target in cancer. *Cancer Cell* 26, 577–590. doi: 10.1016/j.ccr.2014.07.028

Young, M. D., Wakefield, M. J., Smyth, G. K., and Oshlack, A. (2010). Gene ontology analysis for RNA-seq: accounting for selection bias. *Genome Biol.* 11:R14. doi: 10.1186/gb-2010-11-2-r14

Yu, M., Qin, C., Li, P., Zhang, Y., Wang, Y., Zhang, J., et al. (2021). Hydrogen gas alleviates sepsis-induced neuroinflammation and cognitive impairment through regulation of DNMT1 and DNMT3a-mediated BDNF promoter IV methylation in mice. *Int. Immunopharmacol.* 95:107583. doi: 10.1016/j.intimp.2021.107583

Zhang, B., Ban, D., Gou, X., Zhang, Y., Yang, L., Chamba, Y., et al. (2019b). Genome-wide DNA methylation profiles in Tibetan and Yorkshire pigs under high-altitude hypoxia. *J. Anim. Sci. Biotechnol.* 10:25. doi: 10.1186/s40104-019-0316-y

Zhang, R., Wu, H., and Lian, Z. (2019a). Bioinformatics analysis of evolutionary characteristics and biochemical structure of FGF5 gene in sheep. *Gene* 702, 123–132. doi: 10.1016/j.gene.2019.03.040

Zhang, X., Yazaki, J., Sundaresan, A., Cokus, S., Chan, S. W., Chen, H., et al. (2006). Genome-wide high-resolution mapping and functional analysis of DNA methylation in arabidopsis. *Cell* 126, 1189–1201. doi: 10.1016/j.cell.2006.08.003

Zhao, R., Li, J., Liu, N., Li, H., Liu, L., Yang, F., et al. (2020a). Transcriptomic analysis reveals the involvement of lncRNA-miRNA-mRNA networks in hair follicle induction in Aohan fine wool sheep skin. *Front. Genet.* 11:590. doi: 10.3389/fgene.2020.00590

Zhao, X., Tian, G. G., Fang, Q., Pei, X., Wang, Z., and Wu, J. (2020b). Comparison of RNA m6A and DNA methylation profiles between mouse female germline stem cells and STO cells. *Mol. Ther. Nucleic Acids* 23, 431–439. doi: 10.1016/j.omtn.2020.11.020

Zhou, T., Chen, Y., Zhao, B., Hu, S., Li, J., Liu, M., et al. (2020). Characterization and functional analysis of SIAH1 during skin and hair follicle development in the angora rabbit (Oryctolagus cuniculus). *Hereditas* 157:10. doi: 10.1186/s41065-020-00126-0

Zhou, X., Yang, S., Yan, F., He, K., and Zhao, A. (2018). Genome-wide DNA methylation profiles of porcine ovaries in estrus and proestrus. *Physiol. Genomics* 50, 714–723. doi: 10.1152/physiolgenomics.00052.2017

Zou, C., Fu, Y., Li, C., Liu, H., Li, G., Li, J., et al. (2016). Genome-wide gene expression and DNA methylation differences in abnormally cloned and normally natural mating piglets. *Anim. Genet.* 47, 436–450. doi: 10.1111/age.12436

Conflict of Interest: The authors declare that the research was conducted in the absence of any commercial or financial relationships that could be construed as a potential conflict of interest.

Publisher's Note: All claims expressed in this article are solely those of the authors and do not necessarily represent those of their affiliated organizations, or those of the publisher, the editors and the reviewers. Any product that may be evaluated in this article, or claim that may be made by its manufacturer, is not guaranteed or endorsed by the publisher.

frontiers in Veterinary Science

ORIGINAL RESEARCH
published: 26 October 2021
doi: 10.3389/fvets.2021.689589

Effects of Slaughter Age on Myosin Heavy Chain Isoforms, Muscle Fibers, Fatty Acids, and Meat Quality in *Longissimus Thoracis* Muscle of Tibetan Sheep

Gaoliang Bao, Xiu Liu, Jiqing Wang, Jiang Hu, Bingang Shi, Shaobin Li and Yuzhu Luo**

Gansu Key Laboratory of Herbivorous Animal Biotechnology, Faculty of Animal Science and Technology, Gansu Agricultural University, Lanzhou, China

OPEN ACCESS

Edited by:
Joanna Szyda, Wroclaw University of Environmental and Life Sciences, Poland

Reviewed by:
Guihong Fu, Hunan Agricultural University, China
Mariangela Caroprese, University of Foggia, Italy

***Correspondence:**
Shaobin Li
lisb@gsau.edu.cn
Yuzhu Luo
luoyz@gsau.edu.cn

Specialty section:
This article was submitted to Livestock Genomics, a section of the journal Frontiers in Veterinary Science

Received: *01 April 2021*
Accepted: *21 September 2021*
Published: *26 October 2021*

Citation:
Bao G, Liu X, Wang J, Hu J, Shi B, Li S and Luo Y (2021) Effects of Slaughter Age on Myosin Heavy Chain Isoforms, Muscle Fibers, Fatty Acids, and Meat Quality in Longissimus Thoracis Muscle of Tibetan Sheep. Front. Vet. Sci. 8:689589. doi: 10.3389/fvets.2021.689589

Tibetan sheep is one of the dominant livestock at Qinghai-Tibet Plateau, which is the main food source of local people. In order to investigate the effect of slaughter age on meat quality, fatty acid profile and expression of myosin heavy chain (MyHC) isoform genes were analyzed in Tibetan sheep. A total of 24 Tibetan sheep including 4 months old (4 m), 1.5 years old (1.5 y), 3.5 years old (3.5 y), and 6 years old (6 y) were randomly selected. The results indicated that the MyHC IIx and MyHC IIb mRNAs increased with age, whereas MyHC IIa mRNA decreased. MyHC I mRNA was highest at 3.5 y. There were differences in the muscle fiber types of Tibetan sheep at different ages. Intramuscular fat (IMF) was highest at 1.5 y, the pH_{45min} and pH_{24h} value of 6 y sheep were lower than the other groups, the shear force increased with age ($p < 0.05$), and drip loss increased with age ($p < 0.01$). Tibetan sheep at 1.5 y had lower saturated fatty acid (SFA) contents and higher monounsaturated fatty acid (MUFA) contents ($p < 0.05$). Different muscle fiber types influence the meat quality and fatty acid composition of Tibetan sheep with increasing age. These results demonstrated the effect of age on meat quality of Tibetan sheep through regulation of expression of the MyHC isoforms which changed the myofiber types, and 1.5 y Tibetan sheep meat was more suitable for a healthy human diet.

Keywords: muscle fiber, meat quality, fatty acid, MyHC isoform, Tibetan sheep

INTRODUCTION

Consumers, especially from developed countries, are more health conscious and pay more attention to nutritional and physicochemical qualities of the meat products they consume (1). Nutritional and physicochemical qualities are affected by various factors including the slaughter age (2), breed, sex, and diet of the animal (3). Animal age is an important influencing factor that can affect both the meat quality and fatty acid profile (4). The intramuscular fat (IMF) content accumulates with increasing age, improving water holding capacity and juiciness (5). Abhijith et al. have found that meat tenderness of boer goats decreased with increasing slaughter age (6). Guo et al. demonstrated

that the shear force of pork increased with slaughter age, while IMF content first decreased and then increased (7). The Tibetan sheep is the most numerous livestock (>50 million) on the Qinghai-Tibet Plateau and is also the main meat source for local people (8). Tibetan sheep is well-known for its highly nutritious, superior meat quality and strong resistance to harsh environments. However, effects of slaughter age on fatty acids and meat quality of Tibetan sheep remains unknown.

The energy level of the muscles of animals at slaughter affects the energy metabolism of the muscle during the post-mortem period, causing differences in meat quality (9). Glycolysis is a very important energy pathway in cells during the post-mortem period, and the glycolysis rate is influenced by muscle fiber type (10). There are mainly four muscle fiber types in adult mammalian skeletal muscle: MyHC I (types I), MyHC IIa (types IIa), MyHC IIb (types IIb), and MyHC IIx (types IIx) (11, 12). Moreover, the structure, function, and metabolism of the four muscle fiber types are different. The myosin heavy chain (MyHC) gene directly regulates the type of muscle fibers through gene expression and has an important impact on meat quality (10). Besides, the proportions of different muscle fibers change with age in humans, and this transformation also occurs in the muscles of animals, such as pigs, chickens, sheep, and mice (13). Different types of muscle fibers contain different contents of myoglobin, mitochondria, glycogen, and fat, affecting their metabolic characteristics, which will lead to differences in muscle quality including in terms of muscle tenderness, color, and IMF (14). Previous studies have underlined the relationship between muscle fiber types and meat quality and fatty acid. Renand et al. found that IMF content is an important factor in determining eating quality including tenderness, juiciness, and flavor, and IMF content is positively correlated with meat tenderness (15). Alasnier et al. demonstrated that the percentage of type I muscle fibers in beef was positively correlated with IMF content (16). Tenderness is an important indicator for evaluating meat quality, which is the key factor affecting consumer purchasing and market acceptance (17). Therkildsen et al. and Ryu et al. demonstrated that the proportion of type I muscle fibers was positively correlated with the juiciness and flavor of meat but negatively correlated with drip loss and brightness of the flesh color (18, 19). Conversely, the more percentage of type IIB muscle fibers, the drier and harder the meat (20). Joo et al. found that muscle fiber type composition is an important factor influencing fatty acid composition in Hanwoo muscle (21). Han et al. found that appropriate fiber level addition in diets could improve meat quality through regulation the expression of myofiber types (20). However, effects of muscle fiber types on fatty acids and meat quality of Tibetan sheep remains unclear.

Therefore, the objective of the present study was to determine the changes of muscle fiber types with increasing age to evaluate the more suitable slaughter age of Tibetan sheep by determining the meat qualities and fatty acid. The associations of muscle fiber types and expression of MyHC isoform genes on meat quality of the *Longissimus thoracis* (LT) in Tibetan sheep at four growth stages (4 m, lamb; 1.5 y, young sheep; 3.5 y, adult sheep and 6 y sheep) were analyzed.

MATERIALS AND METHODS

Ethics Statement

This animal study was reviewed and approved by the Faculty Animal Policy and Welfare Committee of Gansu Agricultural University (Ethic approval file No. GSAU-Eth-AST-2021-001).

Animals and Muscle Sampling

A total of 24 Tibetan sheep ewes representing four stages of growth (4 m, 1.5 y, 3.5 y, and 6 y) with each stage having six individuals were randomly selected from the same flock of Haiyan County, Qinghai Province, China (3,500 m above sea level). All sheep had the same nutrition and were raised under the same environmental conditions with natural light and free access to food and water. All these sheep were exsanguinated humanely according to Islamic customs, peeled, and split down the midline according to standard operating procedures. Each muscle sample of *Longissimus thoracis* at the 12th and 13th rib was collected from the carcass immediately after slaughter; after rinsing with saline and de-RNAase water, RT-qPCR samples were collected in cryotubes and stored in liquid nitrogen immediately. Meanwhile, two pieces of the left LT muscles between the 12th and 13th ribs were sampled, one of them snap-frozen in liquid nitrogen for ATP staining, and another one was fixed in 4% paraformaldehyde (PFA) for HE staining. Carcasses were then chilled at 4°C for 24 h for further meat quality analysis.

Meat Quality Measurements

The pH of the LT muscle between the 12th and 13th ribs was measured at 45 min (pH_{45min}) and 24 h (pH_{24h}) after slaughter using a portable pH meter (Testo 205 portable waterproof pH, Testo Instruments International Trading Ltd., Shanghai, China) by inserting directly into the samples. The electrode was calibrated with pH 4.00 and pH 7.00 buffer before determination. Each sample was measured three times, and the average value was used for statistical analyses. Meat color was measured using a Minolta chromameter (CR-300; Minolta Camera Co., Osaka, Japan) calibrated against a standard white tile (8 mm diameter aperture, D65 illuminant and 10° standard observer angle) at 45 min and 24 h after slaughter at three positions on the surface of the cross-section of LT after exposing the sample to air for 30 min at 4°C. Results were expressed as lightness (L*), redness (a*), and yellowness (b*) (22). For cooking loss analysis, 300-g samples were steamed in a water bath to a core temperature of 70°C. The cooking loss was calculated as the percentage of weight change before and after cooking (23). The shear force was measured at the 12th to 13th ribs according to the method of Honikel (24). Forty-eight hours after slaughter, the samples were cooked within a plastic bag set in a water bath at 75°C until the internal temperature of the sample reached 70°C; it was then cooled down to room temperature. Five slices of meat each with a diameter of 1.27 cm were cut from each sample with a cylindrical core drill, the slices being cut perpendicular to the fiber direction with a shearing device (C-LM3B; Runhu Instrument Co., Ltd., Guangzhou, China). Following the method of Latorre et al. (25), approximately 25 g of muscle from the 12th and 13th ribs were used to analyze drip loss. The muscle samples were trimmed to

2 × 3 × 5 cm along the length of the fiber and suspended in an inflatable plastic bag, then stored at 4°C for 24 h. The drip loss was calculated as the proportion of lost weight compared to the initial weight. The content of IMF in the LT at the 12th to 13th ribs was measured by the Soxhlet extraction method using a solvent (petroleum ether) and expressed as weight as a percentage of wet muscle tissue (26), with three replicates for each sample.

Fatty Acid Profile

Fatty acids in the LT of Tibetan sheep were determined according to the method by Juárez et al. (27) with several modifications. The meat samples were ground in liquid nitrogen; 1.0 g of the ground sample was Heated by a water bath with 0.7 ml of 10 mol·L^{-1} KOH solution and 5.3 ml anhydrous methanol (chromatographically pure), at 55°C for 1.5 h. The test tube and contents were then cooled to room temperature, mixed with 0.58 ml 12 mol·L^{-1} H_2SO_4 solution, and the free fatty acid was methylated and placed in a water bath at 55°C for 1.5 h. It was then cooled to room temperature, 3 ml n-hexane was added, then transferred to a centrifuge tube and centrifuged at 3,000 rpm for 5 min. The supernatant was filtered into short thread vials (Beijing Labgic Technology Co., Ltd., Beijing, China) using a 0.22 μm nylon syringe, and stored at −20°C for fatty acid methyl esters (FAMEs) analysis. FAMEs were separated and quantified on a Shimadzu GC2010 Plus with a Flame Ionization Detector (FID), a split injector, and an AOC-20i auto-injector. A Restek FAMEWAX capillary column (0.25 mm × 30 m × 0.25 μm) was used. The initial oven temperature was 140°C for 5 min, then increased to 200°C at a rate of 2°C per minute, and then to 230°C at a rate of 6°C per minute, then temperature was maintained for 20 min. FAME peaks were identified and quantified by the comparison of their retention times with those produced from a mixture of 37 FAME standards (Supelco 47,885-U; Sigma-Aldrich, St. Louis, MO, USA), and then serially diluted to five concentrations ranging from 10 to 0.625 g L^{-1}. Fatty acid analysis was conducted in triplicate for each sample.

HE Staining

HE staining analysis was conducted as described by Zhang et al. (28). 1 × 2 × 0.5 cm sample was soaked to 4% paraformaldehyde solution for 24 h. After formalin fixation and dehydration, samples were encased in paraffin wax and sliced into 4-μm-thick histological sections. Tissue sections were stained with hematoxylin–eosin, and images were collected using an upright microscope (IX71; Olympus Microsystems Ltd., Tokyo, Japan). Then, at least 100 muscle fibers were randomly selected for measurement of their diameter using Image-Pro Plus 6.0 (Media Cybernetics Inc., Rockville, MD, USA) image analysis software.

Myosine ATPase Staining

The contractile fibers type (Type I, IIA, IIx, and IIB) of LT muscles were identified using the myosin ATPase staining technique as previously described by Sen et al. (29) with some modifications. Acid pre-incubation ATP enzyme histochemical staining was undertaken. After the sections were dried, acid buffer (0.2 mol/L sodium acetate 49 ml, 0.2 mol/L glacial acetic acid 45 ml, pH 4.63) was added for 10 min. The sections were then removed and incubated with acid ATPase solution. This involved adding 5 ml of ATPase working solution, then 0.6 g adenosine disodium triphosphate and 15 ml of distilled water to dilute, resulting in a pH value of 9.4–9.5. These sections were then washed two to three times for 2 min each time. Acid ATPase incubation solution was added and the sections were incubated at 37°C for 2 h. The working solution was then removed, the sections were then placed in 1% calcium chloride solution for 6 min, the solution was then removed, and the sections were placed in 2% cobalt chloride solution and then washed three times with distilled water, for 5 min each time. Ammonium sulfide solution was added to the sections to develop their color, for about 1 min. They were then washed with tap water three times and transparently mounted using ethanol dehydrated xylene.

The succinate dehydrogenase staining technique described by Nachlas et al. (30) was used to identify the metabolic types (oxidized and glycolytic) of the LT muscle fibers. The muscle fibers were observed using a microscope (×100, Olympus BX61; Olympus Corporation, Tokyo, Japan) and connected to an image capture system (Clemex image analysis software; Vision Lite, Montreal, Canada). Image-Pro Plus 6.0 (Media Cybernetics Inc.) analysis software was used for data analysis of type I, type IIA, and type IIB fibers. Type I fibers are usually dark brown, type IIA + IIX fibers have the lightest coloration, and the color of type IIB fibers are between type I and IIA + IIX types.

Quantitative Real-Time PCR Analysis

Total RNA was extracted from LT muscle samples of Tibetan sheep using Trizol Reagent (Shanghai Yuanye Biotechnology Co., Ltd., Shanghai, China). The experimental operation was carried out according to the product instructions. The purity and concentration of the extracted RNA were measured by an ultraviolet spectrophotometer, and then it was stored at −80°C. The Prime Script™ RT reagent Kit with gDNA Eraser was used for cDNA reverse transcription. The reverse-transcribed cDNA was stored at −20°C for the next analysis.

The NCBI database and Primer Premier 5 software (Premier Biosoft, Palo Alto, CA, USA) were used to design primers to amplify the MyHC isoform genes and a housekeeping gene for qPCR. The primer sequences and PCR conditions are listed in **Table 1**. cDNA was used as a template and the SYBR Green Pro Taq HS qPCR Kit (Accurate Biology, Hunan, China) was used for RT-qPCR. The thermal cycling parameters were as follows: an initial denaturation step at 95°C for 10 min followed by 40 cycles of denaturation at 95°C for 15 s and annealing and extension at 60°C for 1 min. The expression of different MyHC mRNAs were determined as $2^{-\Delta\Delta Ct}$, where ΔCt was the difference in Ct between the MyHC and glyceraldehyde 3-phosphate dehydrogenase (GAPDH). The relative amounts of MyHCI, IIa, IIx, and IIb were expressed as the percentage of total MyHC transcripts.

Statistical Analysis

All statistical analyses of the difference were performed using one-way analysis of variance (ANOVA) by IBM SPSS 22.0 (SPSS

TABLE 1 | Primer sequences and annealing temperatures used for RT-qPCR.

GenBank accession No.	Gene	Primer sequence (5′-3′)	Annealing temperature (°C)
XM_004010325.3	MyHC I	F: GCAAGAAGAGGAGTGAGGCA	60
		R: GGCAGCAATGACCGCAAA	
XM_027974884.1	MyHC IIa	F: CTGAGGAGGCTGAGGAACA	60
		R: TCAGGACACGATCACTCTTCA	
XM_027974882.1	MyHC IIx	F: AACAACTTCCAGAAACCCAAAC	60
		R: GTACAGCCCGACCACCGT	
XM_027974883.1	MyHC IIb	F: TGAGGCAACAAAGAATCTTA GAAAC	60
		R: AAGTGGAGCTGAGTGTCCTTC	
NM_001190390	GAPDH	F: GTCGGAGTGAACGGATTTGG	60
		R: ACGATGTCCACTTTGCCAGT	

Inc., Chicago, IL, USA). Significance among the groups was investigated by Duncan's multiple range tests. Data are shown as the means ± standard error (S.E). Pearson correlation analysis was used to analyze the relationship between meat quality traits and muscle fiber characteristics. GraphPad Prism v6.04 Software (GraphPad Software Inc., San Diego, CA, USA) was used to analyze the dynamics and plot the graphs. Each experiment was replicated at least thrice.

RESULTS

Muscle Development at Different Growth Stages of Tibetan Sheep

HE staining was undertaken to analyze the muscle development of Tibetan sheep at different growth stages (**Figure 1**), including muscle fiber diameter, area, and density. The muscle fiber density of 4 m was significantly larger than other groups ($p < 0.05$), and there was no significant difference among 1.5, 3.5, and 6 y ($p > 0.05$; **Figure 1B**). Muscle fiber area in the 4 m and 1.5 y Tibetan sheep was significantly lower than other two groups, and muscle fiber diameter increased significantly with increasing age ($p < 0.05$; **Figure 1D**).

Meat Quality of Tibetan Sheep at Different Growth Stages

The meat quality of 4 m, 1.5 y, 3.5 y, and 6 y Tibetan sheep are shown in **Table 2**. L_{45min}, L_{24h}, and b_{45min} values of 4 m Tibetan sheep were significantly higher than 1.5, 3.5, and 6 y animals ($p < 0.01$), and the a_{45min} value of 3.5 y Tibetan sheep was lowest ($p < 0.01$). Except for b_{24h} of 4 m, a_{24h} and b_{24h} of 6 y were significantly higher than the other groups ($p < 0.05$). The pH_{45min} of 4 m and 3.5 y Tibetan sheep meat was higher than that of 1.5 and 6 y sheep ($p < 0.01$). After being stored at 4°C for 24 h, pH declined in all groups. The IMF content of 1.5 and 3.5 y was higher than that of 4 m and 6 y animals ($p < 0.01$). The shear force of the muscles of 4 m was the lowest, and it gradually increased with increasing age ($p < 0.01$). The drip loss increased with increasing slaughter age ($p < 0.01$), while the cooking loss of 6 y was the lowest among the four groups ($p < 0.01$).

Fatty Acid Profile at Different Growth Stages of Tibetan Sheep

The effect of slaughter age on the fatty acid composition of the LT muscle of Tibetan sheep is shown in **Table 3**. There are 26 fatty acids detected in the LT muscle of Tibetan sheep. The SFA content of 4 m and 1.5 y sheep was lower than the other two groups, and there was no significant difference between 4 m and 1.5 y sheep, while SFA contents increased in 3.5 y Tibetan sheep ($p = 0.032$). The highest content of MUFA, C14:1, C17:1, and C18:2n6t was in 1.5 y Tibetan sheep ($p < 0.05$).

Tibetan Sheep Muscle Fiber Types

The LT muscle fibers of Tibetan sheep were classified into three types (I, IIa + IIx, and IIb) based on the acid stability of myosin ATPase and the glycolytic rate (**Figure 2A**). There was no significant difference in the proportion of MyHC I muscle fiber content in the four groups ($p > 0.05$). The maximum proportion of MyHC IIa + IIx in 3.5 y Tibetan sheep was 70.89%, which was higher than that in 1.5 and 6 y Tibetan sheep ($p < 0.05$). The proportion of MyHC IIb was 19.06% at 1.5 y and was higher than that in 4 m and 3.5 y of Tibetan sheep ($p < 0.05$; **Figure 2B**). There was no significant difference in the diameter of MyHC I, MyHC IIa + IIx, and MyHC IIb fibers between the four growth stages ($p > 0.05$). However, the diameter of each type of muscle fiber was different ($p < 0.05$), with MyHC IIb having the largest diameter (**Figure 2C**). There was no significant difference in the muscle fiber density of MyHC I, MyHC IIa + IIx, and MyHC IIb ($p > 0.05$); however, MyHC IIa + IIx had the highest density ($p < 0.01$; **Figure 2D**). There was no significant difference in fiber area composition of MyHC I, MyHC IIa + IIx, and MyHC IIb ($p > 0.05$). MyHC IIb fiber area composition was larger than that of MyHC I and MyHC IIa + IIx ($p < 0.01$; **Figure 2E**).

Expression of MyHC Genes at Different Growth Stages

The MyHC I, MyHC IIa, MyHC IIx, and MyHC IIb mRNA expressions were analyzed by RT-qPCR. As shown in **Figure 3**, the MyHC I mRNA was the lowest at 4 m ($p < 0.05$) and then increased with age, reaching the highest level at 3.5 years. The MyHC IIa mRNA decreased with increasing age while the MyHC IIx and MyHC IIb mRNA were the least in 4 m Tibetan sheep and gradually increased with age ($p < 0.05$). The MyHC IIb mRNA was lower than MyHC I, MyHC IIa, and MyHC IIx in the LT muscle of Tibetan sheep ($p < 0.05$).

Correlation Analysis

Positive correlations were found between L_{45min} and MyHC IIa + IIx type muscle fiber density (0.333, $p < 0.01$) and MyHC IIa expression (0.602, $p < 0.01$; **Table 4**). Negative correlations were found between the L_{45min} value and MyHC I expression (−0.669, $p < 0.01$), MyHC IIx expression (−0.561, $p < 0.01$), and MyHC IIb expression (−0.378, $p < 0.01$). A positive correlation was found between the shear force and MyHC IIb diameter (0.265, $p < 0.05$), and negative correlations between shear force

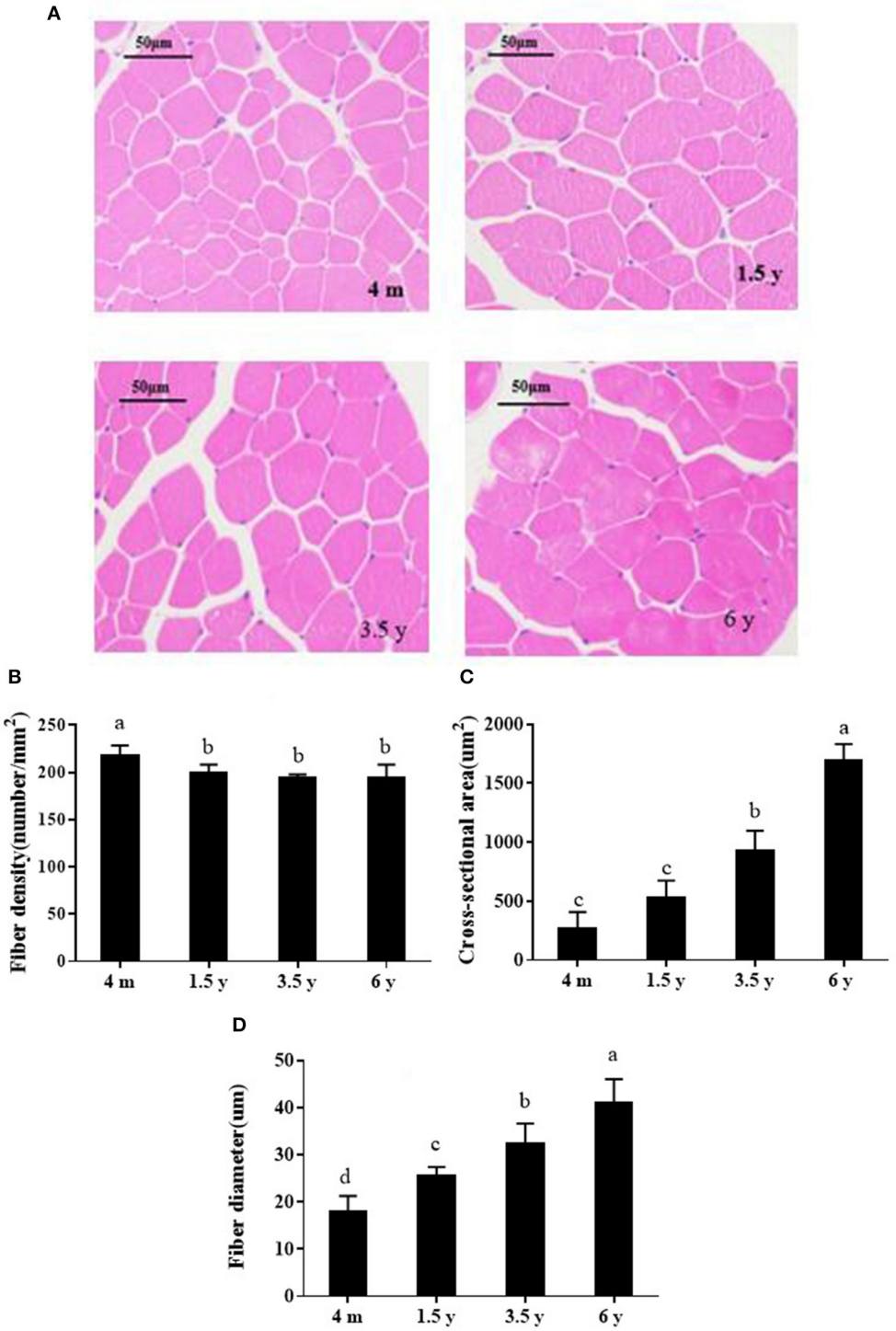

FIGURE 1 | (A) HE-stained photos of the muscle fibers of Tibetan sheep at different growth stages (×200). **(B–D)** Show muscle fiber density, area and diameter, respectively. Data are shown as the means ± S.E. Different letters (a–d) indicate significant differences between different growth stages ($p < 0.05$). 4 m, 4 months old; 1.5 y, 1.5 years old; 3.5 y, 3.5 years old; 6 y, 6 years old.

and MyHC IIa + IIx type muscle fiber density (−0.261, $p < 0.05$), MyHC IIb density (−0.352, $p < 0.01$), MyHC I expression (−0.321, $p < 0.01$), and MyHC IIa expression (−0.735, $p < 0.01$), with positive correlations between shear force and MyHC IIx expression (0.862, $p < 0.01$), MyHC IIb expression (0.797, $p < 0.01$), and fiber diameter (0.707, $p < 0.01$). A positive correlation

TABLE 2 | Effect of different muscle fiber types on meat quality for Tibetan sheep slaughtered at different ages.

Item	4 m	1.5 y	3.5 y	6 y	*p*-Values
L_{45min}	33.78 ± 1.42^{a}	26.54 ± 1.46^{b}	26.45 ± 1.59^{b}	26.97 ± 2.44^{b}	<0.001
a_{45min}	20.25 ± 0.99^{a}	19.39 ± 1.64^{a}	17.85 ± 1.85^{b}	19.27 ± 1.54^{a}	<0.001
b_{45min}	8.81 ± 1.13^{a}	6.98 ± 0.66^{b}	7.56 ± 2.25^{b}	6.90 ± 0.99^{b}	<0.001
L_{24h}	36.16 ± 2.15^{a}	30.24 ± 2.66^{b}	27.55 ± 3.05^{c}	29.96 ± 4.32^{b}	<0.001
a_{24h}	20.21 ± 1.43^{b}	20.02 ± 1.43^{b}	19.07 ± 1.57^{b}	22.59 ± 2.86^{a}	<0.001
b_{24h}	9.64 ± 1.41^{ab}	9.06 ± 0.89^{b}	8.42 ± 2.63^{b}	10.88 ± 2.27^{a}	0.002
pH_{45min}	6.77 ± 0.10^{a}	6.63 ± 0.08^{b}	6.74 ± 0.10^{a}	6.50 ± 0.13^{c}	<0.001
pH_{24h}	5.44 ± 0.06^{a}	5.48 ± 0.25^{a}	5.35 ± 0.06^{b}	5.25 ± 0.06^{c}	<0.001
IMF (%)	1.60 ± 0.32^{b}	2.46 ± 0.49^{a}	2.36 ± 0.39^{a}	1.63 ± 0.26^{b}	<0.001
Shear force (*N*)	26.87 ± 3.17^{d}	42.86 ± 3.64^{c}	50.77 ± 4.18^{b}	59.96 ± 3.85^{a}	<0.001
Drip loss (%)	2.30 ± 0.14^{c}	2.57 ± 0.34^{b}	3.00 ± 0.43^{a}	3.25 ± 0.33^{a}	<0.001
Cooking loss (%)	39.18 ± 1.05^{a}	37.53 ± 0.88^{b}	38.18 ± 1.53^{b}	36.50 ± 1.10^{c}	<0.001

$^{a-d}$Within a row, values with different superscript letters significantly differ ($p < 0.05$). Values are shown as the mean values ± S.E.
IMF, intramuscular fat content.
p-Values refer to comparisons of meat quality between four different slaughter age.

TABLE 3 | Effect of slaughter age on the fatty acid profile of LT muscle of Tibetan sheep (g/100 g).

Fatty acid	4 m	1.5 y	3.5 y	6 y	*p*-Values
C10:0	0.63 ± 0.098	0.58 ± 0.066	0.50 ± 0.086	0.59 ± 0.014	0.912
C12:0	0.58 ± 0.123^{b}	0.57 ± 0.062^{b}	0.64 ± 0.035^{ab}	0.86 ± 0.125^{a}	0.101
C14:0	4.12 ± 0.191^{a}	2.05 ± 0.019^{b}	2.15 ± 0.056^{b}	3.49 ± 0.407^{a}	0.002
C14:1	0.66 ± 0.250^{b}	1.37 ± 0.276^{a}	0.58 ± 0.031^{b}	0.67 ± 0.041^{b}	0.038
C15:0	0.65 ± 0.011	0.55 ± 0.373	0.26 ± 0.069	0.52 ± 0.012	0.339
C16:0	23.61 ± 1.021^{a}	18.81 ± 0.011^{c}	20.62 ± 0.951*b*^{c}	21.00 ± 0.353^{b}	0.012
C16:1	1.30 ± 0.005^{b}	1.19 ± 0.027^{bc}	1.08 ± 0.081^{c}	1.50 ± 0.070^{a}	0.006
C17:0	0.84 ± 0.018^{c}	1.10 ± 0.235^{bc}	1.19 ± 0.012^{b}	1.82 ± 0.018^{a}	0.005
C17:1	0.37 ± 0.015^{c}	0.67 ± 0.005^{a}	0.49 ± 0.016^{b}	0.54 ± 0.030^{b}	<0.001
C18:0	15.88 ± 0.105^{c}	21.68 ± 0.107^{b}	23.85 ± 0.569^{a}	21.06 ± 0.281^{b}	<0.001
C18:1n9t	3.47 ± 0.158^{bc}	3.54 ± 0.412^{b}	4.74 ± 0.105^{a}	2.58 ± 0.479^{c}	0.013
C18:1n9c	34.12 ± 1.409	34.94 ± 0.132	32.25 ± 1.392	34.20 ± 0.694	0.059
C18:2n6t	0.35 ± 0.004^{b}	0.54 ± 0.008^{a}	0.25 ± 0.008^{b}	0.32 ± 0.078^{b}	0.007
C18:2n6c	4.76 ± 0.879	4.85 ± 0.428	4.53 ± 0.445	3.39 ± 0.024	0.249
C20:0	0.20 ± 0.075	0.32 ± 0.057	0.24 ± 0.051	0.30 ± 0.071	0.333
C18:3n6	0.10 ± 0.067	0.14 ± 0.013	0.14 ± 0.030	0.10 ± 0.011	0.531
C20:1	2.73 ± 0.053^{a}	1.60 ± 0.223^{bc}	1.37 ± 0.147^{c}	2.29 ± 0.511^{ab}	0.028
C18:3n3	0.92 ± 0.155	0.72 ± 0.177	0.80 ± 0.134	0.76 ± 0.108	0.589
C21:0	0.26 ± 0.146	0.31 ± 0.362	0.45 ± 0.128	0.45 ± 0.118	0.759
C20:2	0.18 ± 0.092	0.14 ± 0.061	0.14 ± 0.029	0.14 ± 0.022	0.827
C22:0	0.53 ± 0.025^{a}	0.41 ± 0.060^{ab}	0.34 ± 0.041^{b}	0.52 ± 0.063^{a}	0.048
C20:3n6	0.10 ± 0.003	0.14 ± 0.015	0.15 ± 0.018	0.12 ± 0.006	0.062
C22:1n9	0.09 ± 0.102	0.52 ± 0.494	0.38 ± 0.049	0.37 ± 0.006	0.461
C20:4n6	2.34 ± 0.142^{a}	1.64 ± 0.313^{b}	1.57 ± 0.350^{b}	1.15 ± 0.088^{b}	0.038
C20:5n3	0.67 ± 0.078	0.79 ± 0.086	0.56 ± 0.194	0.55 ± 0.013	0.259
C22:6n3	0.55 ± 0.020	0.84 ± 0.185	0.73 ± 0.165	0.71 ± 0.064	0.281
SFA	47.29 ± 1.626^{b}	46.37 ± 1.040^{b}	50.23 ± 0.260^{a}	50.61 ± 0.604^{a}	0.032
MUFA	42.75 ± 1.478^{b}	43.82 ± 0.805^{a}	40.90 ± 1.061^{c}	42.15 ± 0.303^{b}	0.045
PUFA	9.97 ± 3.111	9.81 ± 0.235	8.88 ± 1.321	7.24 ± 0.301	0.180
n-3	2.13 ± 0.214	2.35 ± 0.447	2.09 ± 0.494	2.02 ± 0.186	0.813
n-6	7.65 ± 2.803	7.32 ± 0.151	6.64 ± 0.798	5.09 ± 0.136	0.128

$^{a-c}$Within a row, values with different superscript letters differ ($p < 0.05$). Data are shown as the mean values ± S.E.
SFA, MUFA, PUFA, and n represent saturated fatty acid, mono unsaturated fatty acid, poly unsaturated fatty acid, and omega, respectively.
p-Values represent statistical comparisons of fatty acid profiles between the four slaughter ages.

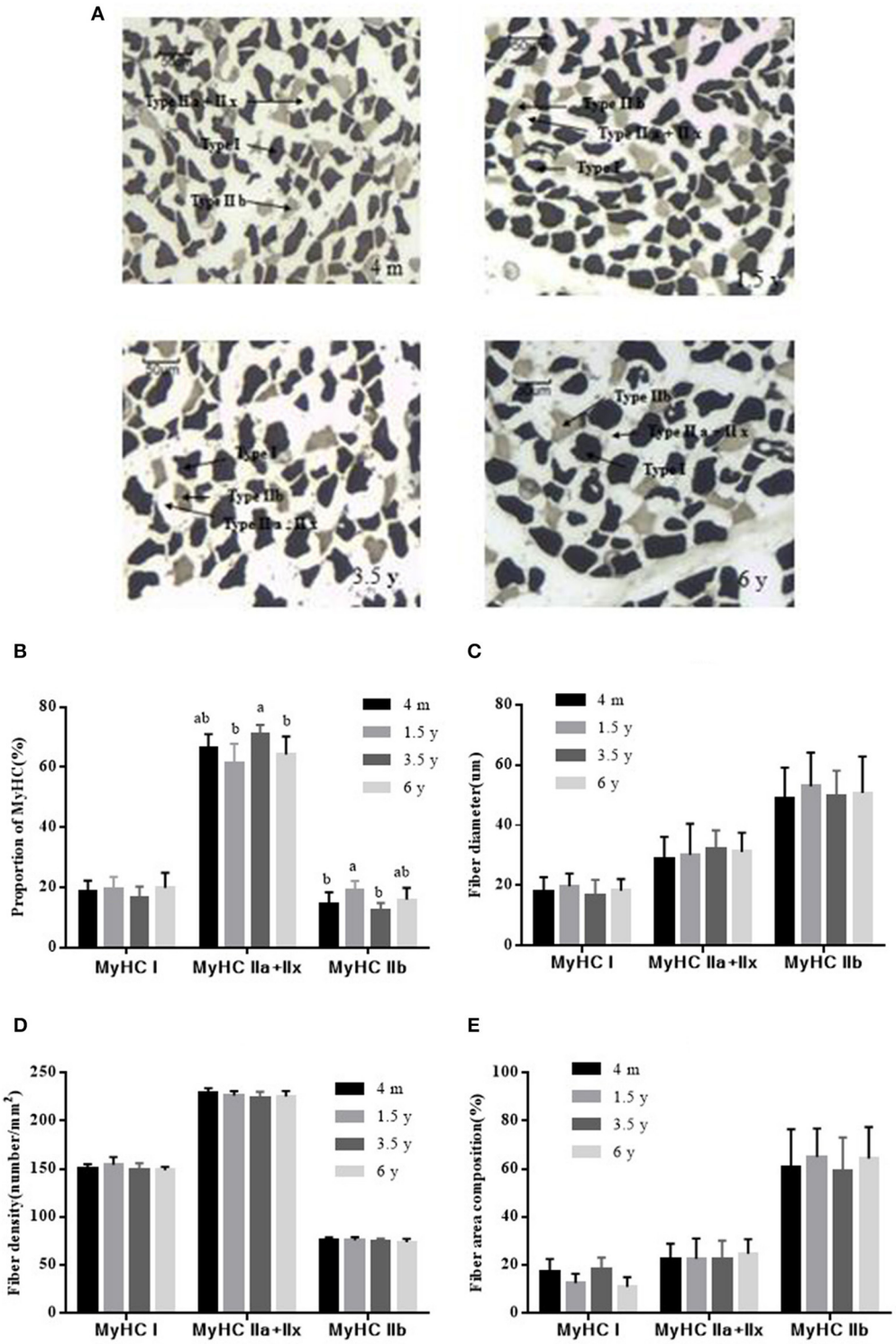

FIGURE 2 | ATPase staining to determine the type of Tibetan sheep muscle fiber (×100). **(A)** Type I fiber was stained dark, the type IIa + IIx fiber was unstained, the type IIb fiber was stained gray. **(B)** Proportions of MyHC I, MyHC IIa + IIx, and MyHC IIb in the LT muscle of Tibetan sheep at different growth stages. **(C)** The diameter of MyHC I, MyHC IIa + IIx, and MyHC IIb at different growth stages. **(D)** Fiber density analysis of MyHC I, MyHC IIa + IIx, and MyHC IIb at different growth stages. **(E)** Fiber area composition of MyHC I, MyHC IIa + IIx, and MyHC IIb at different growth stages. Data are shown as the means ± S.E. Different letters (a,b) indicate significant between different growth stages ($p < 0.05$).

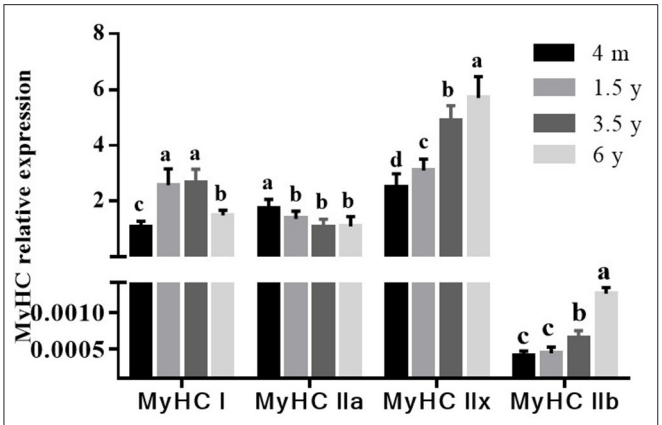

FIGURE 3 | Effect of slaughter age on muscle fiber type-related gene expressions in Tibetan sheep. The mRNA levels were measured by real-time quantitative PCR. The MyHC I, MyHC IIa, MyHC IIx, and MyHC IIb mRNA levels were normalized to the amount of GAPDH mRNA. Data are shown as the means ± S.E. Different letters (a–d) indicate significant differences between different slaughter age ($p < 0.05$).

was found between the IMF and MyHC I expression (0.692, $p < 0.01$), and a negative correlation was found between IMF and MyHC IIb expression (−0.327, $p < 0.01$).

DISCUSSION

Sheep meat is an important source of animal protein across the world and is popular for its leanness, lack of fat, tenderness, juiciness, and nutrition (31). Tibetan sheep lives on the Qinghai-Tibet Plateau in China, is famous for its individual flavor, palatability, and nutrition. Meat color is one of the most important physical indicator of meat quality. In this study, the meat color of L_{45min} in Tibetan sheep was the highest in the 4 m group and significantly higher than that of other age groups. This could be because 4 m meat has more moisture and a greater myoglobin content with more type I muscle fiber (32). However, some studies have found that the *L*-value of the meat gradually increased with animal age (33). The a value and b value of the 4 m group were higher compared to the other groups, similar to the results of Warner et al. (34) but contrary to the results of Gardner et al. (5). In general, muscle fiber types at birth are composed of oxidative fibers (35). Under a high-altitude environment with lower temperature and thinner oxygen level, there were more type I muscle fibers and myoglobin content in young animals, which would result in a higher a value (36). In this study, the b value of the 4 m Tibetan sheep was highest, contrary to the results of Mashele et al. (37). After being stored at 4°C for 24 h, the color value of Tibetan sheep meat was increased.

The glycogen content gradually decreased post-mortem, glycogen degraded into lactic acid by glycolysis until the activity of glycolytic enzymes was inhibited, which resulted in pH value continued decline. In this study, the pH_{45min} of Tibetan sheep meat post-mortem was close to neutral, and the 4 m group was the highest, and there were more slow-twitch fibers in 4 m Tibetan sheep meat. Bertol et al. found that pork pH_{45min} was related to the total amount of muscle fibers present, and that pig meat with more fibers had a smaller fiber size, higher pH_{45min}, and lower drip loss (38). The pH_{24h} value showed decline from 1.5 to 6 y; pH_{24h} value was lowest in 6 y Tibetan sheep. It is generally believed that the rate and extent of pH decline is mainly related to glycolysis post-mortem, with glycogen degraded into lactic acid and H^+. Previous studies also found that there was a difference of the rate of glycolysis post-mortem between different muscle fibers types, which influence the meat quality by changing the speed and degree of pH decline (39). The more glycolytic fibers, the more the rate of glycolysis, which resulted in the accumulation of lactic acid, and the pH declined rapidly, finally influencing the meat quality (40). Therefore, the percentage of type IIB fibers in sheep meat was negatively correlated with pH value (18). Muscles harboring higher percentages of fast-twitch fiber tend to have a more rapid pH decline than muscles with a higher percentage of slow-twitch fiber (41).

IMF content is an important factor that influences meat quality, which is affected by genetic and environmental factors such as genotype, gender, feeding system, and age. IMF content is positively correlated with tenderness (15). A previous study using Sudan Black B and Oil Red O for histochemical staining showed that all type I fibers contained neutral lipids while IIA and IIB fibers contained only 26 and 1%, respectively (42). Therefore, the percentage of type I fibers was positively correlated with the IMF content of cattle meat (43). Type I muscle fibers are to the benefit of juiciness and flavor, while type IIB fiber content is often associated with harder meat. There is a consistent correlation between type I muscle fiber and meat tenderness (15). In this study, the IMF content in the 1.5 and 3.5 y Tibetan sheep meat was highest. There were more mitochondria and myoglobin of type I muscle fibers on the electron transfer chain. Kim et al. and Liu et al. found that the more glycolytic muscle fiber types and the less oxidized muscle fiber types in muscle leads to a rapid pH decline post-mortem, which made white meat (44, 45). The meat quality depends largely on the muscle fiber types. The different slaughter ages of animal influence meat quality by regulating the composition of muscle fibers, and each muscle fiber type content changed with increasing age (46). The shear force is one of the most important physical indicators of meat tenderness. In this study, the shear force showed continued increase with age. Abhijith et al. reported that the shear force of Boer goat meat increased significantly with age (6). Drip loss and cooking loss were associated with tenderness and juiciness. In this study, there was a lower drip loss of 4 m, which was associated with more type I muscle fiber. And similar to results of Turan et al. who found young animal had higher meat quality in terms of tenderness and water holding capacity (47).

Fatty acids are important nutrients for the human body and have important physiological functions. In this study, there were 26 fatty acids detected in the LT muscle of Tibetan sheep, including 10 SFAs, seven MUFAs, and nine PUFAs. MUFA is of great significance for reducing cardiovascular diseases with its function of reducing total cholesterol, enhancing the activity of antioxidant enzymes, reducing blood pressure and blood sugar levels, preventing deterioration in memory,

TABLE 4 | Pearson correlations (two-tailed test, $N = 72$) between various indicators.

	A	B	C	D	E	F	G	H	I	J	K	L	M	N	O	P	Q	R	S	T	U	V	W
A	1	0.414**	0.531**	0.768**	−0.012	0.125	−0.724**	0.309**	0.204	−0.420**	−0.157	0.499**	0.009	−0.093	−0.250*	0.006	0.333**	0.199	−0.669**	0.602**	−0.561**	−0.378**	−0.616**
B		1	0.311**	0.465**	0.465**	0.340**	−0.302**	−0.042	0.178	−0.146	−0.217	0.224	0.097	0.086	−0.058	−0.013	0.244*	0.168	−0.427**	0.413**	−0.307**	−0.087	−0.221
C			1	0.389**	0.110	0.552**	−0.379**	0.348**	0.059	−0.119	−0.052	0.369**	−0.077	0.240*	−0.053	0.257*	0.176	0.057	−0.283*	0.326**	−0.295*	−0.262*	−0.393**
D				1	0.203	0.345**	−0.586**	0.167	0.119	−0.372**	−0.242*	0.365**	0.051	0.000	−0.028	−0.057	0.279*	0.171	−0.565**	0.453**	−0.531**	−0.295*	−0.566**
E					1	0.728**	0.268*	−0.344**	−0.130	−0.209	0.233*	−0.338**	0.005	0.172	0.130	−0.007	0.105	0.013	−0.333**	0.009	0.261*	0.464**	0.087
F						1	0.140	−0.208	−0.120	−0.247*	0.162	−0.181	−0.015	0.282*	0.165	0.159	0.035	−0.032	−0.313**	−0.005	0.153	0.312**	−0.092
G							1	−0.513**	−0.483**	0.120	0.582**	−0.592**	−0.033	0.049	0.265*	−0.056	−0.261*	−0.352**	−0.321**	−0.735**	0.862**	0.797**	0.707**
H								1	0.185	0.096	−0.232*	0.479**	−0.209	0.079	−0.057	0.045	−0.022	0.152	0.031	0.334**	−0.468**	−0.627**	−0.319**
I									1	0.272*	−0.525**	0.285*	0.244*	−0.080	−0.218	0.137	0.301*	0.369**	0.084	0.399**	−0.493**	−0.535**	−0.362**
J										1	−0.336**	−0.083	0.098	0.128	−0.127	0.139	−0.180	0.066	0.692**	−0.152	−0.063	−0.327**	0.053
K											1	−0.231	−0.251*	0.106	0.118	−0.356**	−0.120	−0.296*	−0.174	−0.455**	0.785**	0.738**	0.535**
L												1	−0.195	−0.081	−0.150	−0.025	0.154	0.221	−0.108	0.445**	−0.517**	−0.579**	−0.449**
M													1	−0.182	0.000	−0.107	0.013	0.082	0.044	−0.012	−0.132	−0.026	−0.055
N														1	0.061	0.039	0.020	0.085	0.036	−0.007	0.036	0.038	−0.014
O															1	−0.110	−0.081	−0.511**	0.009	−0.151	0.191	0.269*	0.160
P																1	0.146	−0.069	0.098	0.131	−0.236*	−0.190	−0.111
Q																	1	0.086	−0.266*	0.232*	−0.309**	−0.161	−0.245*
R																		1	0.037	0.164	−0.349**	−0.344**	−0.328**
S																			1	−0.430**	0.158	−0.190	0.231
T																				1	−0.696**	−0.520**	−0.579**
U																					1	0.841**	0.707**
V																						1	0.654**
W																							1

*A, B, C, D, E, F, G, H, I, J, K, L, M, N, O, P, Q, R, S, T, U, V, and W, respectively, represent L_{45min}, a_{45min}, b_{45min}, L_{24h}, a_{24h}, b_{24h}, shear force, pH_{45min}, pH_{24h}, IMF, drip loss, cooking loss, fiber diameter of MyHC I, fiber diameter of MyHC IIa + IIx, fiber diameter of MyHC IIb, fiber density of MyHC I, fiber density of MyHC IIa + IIx, fiber density of MyHC IIb, mRNA expression of MyHC I, mRNA expression of MyHC IIa, mRNA expression of MyHC IIx, and mRNA expression of MyHC IIb, fiber diameter. *Correlation is significant at $P < 0.05$, **Correlation is significant at $P < 0.01$.*

and promoting growth and development (48). In this study, the highest MUFA contents were detected in the 1.5 y Tibetan sheep, which then reduced with increasing age. Zhang et al. found that lamb meat had the least MUFA content, complementing the results of our study (1). PUFA plays an important role in stabilizing cell membrane function, regulating gene expression, maintaining cytokine and lipoprotein balance, resisting cardiovascular diseases, and promoting growth and development (49) with a variety of functions within biological systems (1). In this study, PUFA contents showed continued decline with increasing age, which was consistent with the results of Zhang et al. (1). C18:2n6c is an essential fatty acid and the precursor fatty acid for the synthesis of conjugated linoleic acid (CLA). In this study, content of C18:2n6c was highest in the 1.5 y Tibetan sheep. C20:5n3 and C22:6n3 are important PUFA with the function of reducing platelet aggregation and blood lipids, preventing coronary heart disease, improving memory, and preventing brain senescence (50). C20:5n3 and C22:6n3 contents in the 1.5 y group were higher compared to other groups.

In this study, expression differences of these myosin heavy chains were found in the LT muscle of Tibetan sheep at different ages. Correlations were found between muscle fiber type and meat quality, and muscle fiber types largely influence the meat quality of Tibetan sheep. This result was supported by previous studies. Hwang et al. have found that there was a positive correlation between shear force and Type IIb muscle fiber and Type IIb area in Korean native black goat (51). Overall, the complex metabolic characteristics of muscle may play a more important role in determining the meat quality of Tibetan sheep.

CONCLUSION

In conclusion, the results of the present study indicated that the meat tenderness and water holding capacity of Tibetan sheep decreased with increasing age, IMF of 1.5 y Tibetan sheep was the highest. Age influenced the ultimate pH and meat color; higher MUFA and some PUFA content were observed in 1.5 y of Tibetan sheep. The above results demonstrated that 1.5 y was a more suitable slaughter age of Tibetan sheep for a healthy human diet. Age influenced the meat quality, which was possibly associated with the transformation of oxidative muscle fiber to glycolytic muscle fiber.

DATA AVAILABILITY STATEMENT

The original contributions presented in the study are included in the article/**Supplementary Material**, further inquiries can be directed to the corresponding author/s.

ETHICS STATEMENT

The animal study was reviewed and approved by the Faculty Animal Policy and Welfare Committee of Gansu Agricultural University.

AUTHOR CONTRIBUTIONS

GB: data curation and writing—original draft. XL and JH: formal analysis, methodology, and software. JW and BS: investigation, validation, methodology, and software. SL: funding acquisition and writing—review and editing. YL: project administration, supervision, and writing—review and editing. All authors contributed to the article and approved the submitted version.

FUNDING

This research was funded by the Basic Research Creative Groups of Gansu Province (17JR5RA137), the Fuxi Young Talents Fund of Gansu Agricultural University (Gaufx-03Y04), the Projects of Gansu Agricultural University (GSAU-ZL-2015-033), and Key R&D Projects in Gansu Province (18YF1WA082).

ACKNOWLEDGMENTS

We thank colleagues in the laboratory and our collaborators for their useful suggestions. We thank Dr. Wenhao Li of Qinghai University who provided the help during the field work.

SUPPLEMENTARY MATERIAL

The Supplementary Material for this article can be found online at: https://www.frontiersin.org/articles/10.3389/fvets.2021.689589/full#supplementary-material

REFERENCES

1. Zhang R, Yoo MJ, Gathercole J, Reis MG, Farouk MM. Effect of animal age on the nutritional and physicochemical qualities of ovine bresaola. *Food Chem.* (2018) 254:317–25. doi: 10.1016/j.foodchem.2018.02.031
2. Veiseth E, Shackelford S, Wheeler T, Koohmaraie M. Factors regulating lamb longissimus tenderness are affected by age at slaughter. *Meat Sci.* (2004) 68:635–40. doi: 10.1016/j.meatsci.2004.05.015
3. Priolo A, Micol D, Agabriel J. Effects of grass feeding systems on ruminant meat colour and flavour. A review. *Anim Res.* (2001) 50:185–200. doi: 10.1051/animres:2001125
4. Nogalski Z, Pogorzelska-Przybyłek P, Sobczuk-Szul M, Nogalska A, Modzelewska-Kapituła M, Purwin C. Carcass characteristics and meat quality of bulls and steers slaughtered at two different ages. *Ital J Anim Sci.* (2017) 17:1–10. doi: 10.1080/1828051X.2017.1383861
5. Gardner GE, Hopkins DL, Greenwood PL, Cake MA, Boyce MD, Pethick DW. Sheep genotype, age and muscle type affect the expression of metabolic enzyme markers. *Austr J Exp Agric.* (2007) 47:1180–9. doi: 10.1071/EA07093
6. Abhijith A, Warner RD, Ha M, Dunshea FR, Leury BJ, Zhang M, et al. Effect of slaughter age and post-mortem days on meat quality of *longissimus* and *semimembranosus* muscles of Boer goats. *Meat Sci.* (2021) 175:108466. doi: 10.1016/j.meatsci.2021.108466
7. Guo ZY, Chen XL, Chen DW, Li M, Yin J, Yu B, et al. Effects of slaughter age on carcass traits and meat quality of crossbred (Duroc×Landrace×Yorkshire) finishing pigs. *Anim Biotechnol.* (2021) 2021:1–7. doi: 10.1080/10495398.2021.1916512

8. Wang X, Xu T, Zhang X, Geng Y, Kang S, Xu S. Effects of dietary protein levels on growth performance, carcass traits, serum metabolites, and meat composition of Tibetan sheep during the cold season on the Qinghai-Tibetan Plateau. *Animals.* (2020) 10:801. doi: 10.3390/ani10050801
9. Zhao JP, Zhao GP, Jiang RR, Zheng MQ, Chen JL, Liu RR, et al. Effects of diet-induced differences in growth rate on metabolic, histological, and meat-quality properties of 2 muscles in male chickens of 2 distinct broiler breeds. *Poult Sci.* (2012) 91:237–47. doi: 10.3382/ps.2011-01667
10. Kang YK, Choi YM, Lee SH, Choe JH, Kim BC. Effects of myosin heavy chain isoforms on meat quality, fatty acid composition, and sensory evaluation in Berkshire pigs. *Meat Sci.* (2011) 89:384–9. doi: 10.1016/j.meatsci.2011.04.019
11. Brooke MH, Kaiser KK. Muscle fiber types: how many and what kind? *Arch Neurol.* (1970) 23:369–79. doi: 10.1001/archneur.1970.00480280083010
12. Lefaucheur L, Hoffman RK, Gerrard DE, Okamura CS, Rubinstein N, Kelly A. Evidence for three adult fast myosin heavy chain isoforms in type II skeletal muscle fibers in pigs. *J Anim Sci.* (1998) 76:1584–93. doi: 10.1016/S0168-1591(97)00123-8
13. Yoshioka M, Boivin A, Bolduc C, St-Amand J. Gender difference of androgen actions on skeletal muscle transcriptome. *J Mol Endocrinol.* (2007) 39:119–33. doi: 10.1677/JME-07-0027
14. Kim GD, Ryu YC, Jo C, Lee JG, Yang HS, Jeong JY, et al. The characteristics of myosin heavy chain-based fiber types in porcine longissimus dorsi muscle. *Meat Sci.* (2014) 96:712–8. doi: 10.1016/j.meatsci.2013.09.028
15. Renand G, Picard B, Touraille C. Relationships between muscle characteristics and meat quality traits of young Charolais bulls. *Meat Sci.* (2001) 59:49–60. doi: 10.1016/S0309-1740(01)00051-1
16. Alasnier C, Rémignon H, Gandemer G. Lipid characteristics associated with oxidative and glycolytic fibres in rabbit muscles. *Meat Sci.* (1996) 43:213–24. doi: 10.1016/S0309-1740(96)00015-0
17. Anderson MJ, Lonergan SM, Fedler CA, Prusa KJ, Binning JM, Huff-Lonergan E. Profile of biochemical traits influencing tenderness of muscles from the beef round. *Meat Sci.* (2012) 91:247–54. doi: 10.1016/j.meatsci.2012.01.022
18. Therkildsen M, Melchior LL, Bang HG, Vestergaard M. Effect of growth rate on tenderness development and final tenderness of meat from Friesian calves. *Anim Sci.* (2002) 74:253–64. doi: 10.1017/S1357729800052425
19. Ryu YC, Kim BC. Comparison of histochemical characteristics in various pork groups categorized by postmortem metabolic rate and pork quality. *J Anim Sci.* (2006) 84:894. doi: 10.1111/j.1439-0396.2005.00584.x
20. Han P, Li P, Zhou W, Fan L, Wang B, Liu H, et al. Effects of various levels of dietary fiber on carcass traits, meat quality and myosin heavy chain I, IIa, IIx and IIb expression in muscles in Erhualian and Large White pigs. *Meat Sci.* (2020) 169:108160. doi: 10.1016/j.meatsci.2020.108160
21. Joo ST, Hwang YH, Frank D. Characteristics of Hanwoo cattle and health implications of consuming highly marbled Hanwoo beef. *Meat Sci.* (2017) 132:45–51. doi: 10.1016/j.meatsci.2017.04.262
22. Zhao J, Li K, Su R, Liu W, Ren Y, Zhang C, et al. Effect of dietary Tartary buckwheat extract supplementation on growth performance, meat quality and antioxidant activity in ewe lambs. *Meat Sci.* (2017) 134:79–85. doi: 10.1016/j.meatsci.2017.07.016
23. Qin X, Zhang T, Cao Y, Deng B, Zhao J. Effects of dietary sea buckthorn pomace supplementation on skeletal muscle mass and meat quality in lambs. *Meat Sci.* (2020) 166:108141. doi: 10.1016/j.meatsci.2020.108141
24. Honikel KO. Reference methods for the assessment of physical characteristics of meat. *Meat Sci.* (1998) 49:447–57. doi: 10.1016/s0309-1740(98)00034-5
25. Latorre MA, Medel P, Fuentetaja A, Lázaro R, Mateos GG. Effect of gender, terminal sire line and age at slaughter on performance, carcass characteristics and meat quality of heavy pigs. *Ani Sci.* (2003) 77:33–45. doi: 10.1046/j.1365-2052.2003.01032.x
26. Folch J, Lees M, Stanley GHS. A simple method for the isolation and purification of total lipides from animal tissues. *J Biol Chem.* (1957) 226:495–509. doi: 10.1016/S0021-9258(18)64849-5
27. Juárez M, Polvillo O, Contò M, Ficco A, Ballico S, Failla S. Comparison of four extraction/methylation analytical methods to measure fatty acid composition by gas chromatography in meat. *J Chromatogr A.* (2008) 1190:327–32. doi: 10.1016/j.chroma.2008.03.004
28. Zhang J, Ma G, Guo Z, Yu Q, Han L, Han M, et al. Study on the apoptosis mediated by apoptosis-inducing-factor and influencing factors of bovine muscle during postmortem aging. *Food Chem.* (2018) 266:359–67. doi: 10.1016/j.foodchem.2018.06.032
29. Sen U, Sirin E, Ensoy U, Aksoy Y, Ulutas Z, Kuran M. The effect of maternal nutrition level during mid-gestation on postnatal muscle fibre composition and meat quality in lambs. *Anim Product Sci.* (2016) 56:834. doi: 10.1071/AN14663
30. Nachlas MM, Tsou KC, De Souza E, Cheng CS, Seligman AM. Cyochemical demonstration of succinic dehydrogenase by the use of a new p-nitrophenyl substituted ditetrazole. *J Histochem Cytochem.* (1957) 5:420–36. doi: 10.1177/5.4.420
31. Mcafee AJ, Mcsorley EM, Cuskelly GJ, Moss BW, Wallace JM, Bonham MP, et al. Red meat consumption: an overview of the risks and benefits. *Meat Sci.* (2010) 84:1–13. doi: 10.1016/j.meatsci.2009.08.029
32. Wittenberg JB. Myoglobin function reassessed. *J Exp Biol.* (2003) 206:2011–20. doi: 10.1242/jeb.00243
33. Hopkins DL, Stanley DF, Martin LC, Toohey ES, Gilmour AR. Genotype and age effects on sheep meat production. 3 meat quality. *Austr J Exp Agric.* (2007) 47:1155–64. doi: 10.1071/EA06299
34. Warner RD, Pethick DW, Greenwood PL, Ponnampalam EN, Banks RG, Hopkins DL. Unravelling the complex interactions between genetics, animal age and nutrition as they impact on tissue deposition, muscle characteristics and quality of Australian sheep meat. *Aust J Exp Agric.* (2007) 47:1229–38. doi: 10.1071/EA07229
35. Takemasa T, Sugimoto K, Miyazaki M, Machida M, Ikeda SI, Hitomi Y, et al. Simple method for the identification of oxidative fibers in skeletal muscle. *Eur J Appl Physiol.* (2004) 91:357–9. doi: 10.1007/s00421-003-1035-8
36. Joo ST, Kauffman RG, Kim BC, Kim CJ. The relationship between color and water-holding capacity in post-rigor porcine Longissimus muscle. *J Muscle Foods.* (2010) 6:211–26. doi: 10.1111/j.1745-4573.1995.tb00568.x
37. Mashele GA, Parker ME, Schreurs NM. Effect of slaughter age between 5 to 14 months of age on the quality of sheep meat. *Paper Presented at: New Zealand Society of Animal Production.* Vol. 77. New Zealand: Society of Animal Production. (2017). p. 177–80.
38. Bertol TM, Campos RMLD, Ludke JV, Terra NN, Figueiredo EAPD, Coldebella A, et al. Effects of genotype and dietary oil supplementation on performance, carcass traits, pork quality and fatty acid composition of backfat and intramuscular fat. *Meat Sci.* (2013) 93:507–16. doi: 10.1016/j.meatsci.2012.11.012
39. Wang HJ, Pu JN, Chen DW, Tian G, Mao XB. Effects of dietary amylose and amylopectin ratio on growth performance, meat quality, postmortem glycolysis and muscle fibre type transformation of finishing pigs. *Arch Anim Nutr.* (2019) 73:194–207. doi: 10.1080/1745039X.2019.1583518
40. Ryu YC, Kim BC. The relationship between muscle fiber characteristics, postmortem metabolic rate, and meat quality of pig longissimus dorsi muscle. *Meat Sci.* (2005) 71:351–7. doi: 10.1016/j.meatsci.2005.04.015
41. Choi YM, Ryu YC, Kim BC. Influence of myosin heavy and light chain isoforms on early postmortem glycolytic rate and pork quality. *Meat Sci.* (2007) 76:281–8. doi: 10.1016/j.meatsci.2006.11.009
42. Karlsson AH, Klont RE, Fernandez X. Skeletal muscle fibres as factors for pork quality. *Livestock Product Sci.* (1999) 60:255–69. doi: 10.1016/S0301-6226(99)00098-6
43. Joo ST, Kim GD, Hwang YH, Ryu YC. Control of fresh meat quality through manipulation of muscle fiber characteristics. *Meat Sci.* (2013) 95:828–36. doi: 10.1016/j.meatsci.2013.04.044
44. Kim JM, Lim KS, Ko KB, Ryu YC. Estimation of pork quality in live pigs using biopsied muscle fibre number composition. *Meat Sci.* (2017) 137:130–3. doi: 10.1016/j.meatsci.2017.11.020
45. Liu F, Xu Q, Dai R, Ni Y. effects of natural antioxidants on colour stability, lipid oxidation and metmyoglobin reducing activity in raw beef patties. *Acta Sci Polonorum Technol Aliment.* (2015) 14:37–44. doi: 10.17306/J.AFS.2015.1.4
46. Pette D, Staron RS. Myosin isoforms, muscle fiber types, and transitions. *Microsc Res Tech.* (2015) 50:500–9. doi: 10.1002/1097-0029(20000915)50:6<500::AID-JEMT7>3.0.CO;2-7

47. Turan A, Yalcintan H, Orman A, Ekiz B. Effects of gender and slaughter age on meat quality of Anatolian water buffaloes. *Trop Anim Health Product*. (2021) 53:415. doi: 10.1007/s11250-021-02835-8
48. Legako JF, Dinh TTN, Miller MF, Brooks JC. Effects of USDA beef quality grade and cooking on fatty acid composition of neutral and polar lipid fractions. *Meat Sci*. (2014) 100:246–55. doi: 10.1016/j.meatsci.2014.10.013
49. Henry GE, Momin RA, Nair MG, Dewitt DL. Antioxidant and cyclooxygenase activities of fatty acids found in food. *Agric Food Chem*. (2002) 50:2231–4. doi: 10.1021/jf0114381
50. Smet SD, Raes K, Demeyer D. Meat fatty acid composition as affected by fatness and genetic factors: a review. *Anim Res*. (2004) 53:81–98. doi: 10.1051/animres:2004003
51. Hwang YH, Bakhsh A, Lee J-G, Joo S-T. Differences in muscle fiber characteristics and meat quality by muscle type and age of korean native black goat. *Food Sci Anim Resour*. (2019) 39:988–99. doi: 10.5851/kosfa.2019.e92

Conflict of Interest: The authors declare that the research was conducted in the absence of any commercial or financial relationships that could be construed as a potential conflict of interest.

Publisher's Note: All claims expressed in this article are solely those of the authors and do not necessarily represent those of their affiliated organizations, or those of the publisher, the editors and the reviewers. Any product that may be evaluated in this article, or claim that may be made by its manufacturer, is not guaranteed or endorsed by the publisher.

frontiers in Genetics

ORIGINAL RESEARCH
published: 15 November 2021
doi: 10.3389/fgene.2021.710449

Isobaric Tags for Relative and Absolute Quantification-Based Proteomics Reveals Candidate Proteins of Fat Deposition in Chinese Indigenous Sheep With Morphologically Different Tails

*Caiye Zhu, Heping Cheng, Na Li, Tiaoguo Liu and Youji Ma**

College of Animal Science and Technology, Gansu Agricultural University, Lanzhou, China

Background: Chinese indigenous sheep can be classified into two types according to their tail morphology: fat-rumped and thin-tailed sheep, of which the typical breeds are Altay sheep and Tibetan sheep, respectively.

Methods: To identify the differentially expressed proteins (DEPs) underlying the phenotypic differences between tail types, we used isobaric tags for relative and absolute quantification (iTRAQ) combined with multi-dimensional liquid chromatography tandem-mass spectrometry (LC-MS/MS) technology to detect candidate proteins. We then subjected these to a database search and identified the DEPs. Finally, bioinformatics technology was used to carry out Gene Ontology (GO) functional and Kyoto Encyclopedia of Genes and Genomes (KEGG) pathway analyses.

Results: A total of 3,248 proteins were identified, of which 44 were up-regulated and 40 were down-regulated DEPs. Analyzing their GO function terms and KEGG pathways revealed that the functions of these DEPs are mainly binding, catalytic activity, structural molecule activity, molecular function regulator, and transporter activity. Among the genes encoding the DEPs, *APOA2*, *GALK1*, *ADIPOQ*, and *NDUFS4* are associated with fat formation and metabolism.

Conclusion: The *APOA2*, *GALK1*, *ADIPOQ*, and *NDUFS4* genes may be involved in the deposition of fat in the tail of sheep. This study provides a scientific basis for the breeding of thin-tailed sheep.

Keywords: iTRAQ, fat deposit, type of tail, sheep, bioinformatics analysis

OPEN ACCESS

Edited by:
Xin Wang,
Northwest A&F University, China

Reviewed by:
Ran Di,
Institute of Animal Sciences (CAAS), China
Suxu Tan,
Michigan State University, United States

****Correspondence:***
Youji Ma
yjma@gsau.edu.cn

Specialty section:
This article was submitted to Livestock Genomics, a section of the journal Frontiers in Genetics

Received: *16 May 2021*
Accepted: *31 August 2021*
Published: *15 November 2021*

Citation:
Zhu C, Cheng H, Li N, Liu T and Ma Y (2021) Isobaric Tags for Relative and Absolute Quantification-Based Proteomics Reveals Candidate Proteins of Fat Deposition in Chinese Indigenous Sheep With Morphologically Different Tails. Front. Genet. 12:710449. doi: 10.3389/fgene.2021.710449

INTRODUCTION

To enable their adaptation to various environments, long-term natural selection has produced sheep breeds differing starkly in their individual phenotypes. The difference in tail type is one of the main changes in the evolutionary process of sheep. Studies have shown that fat-tailed sheep emerged 5,000 years ago, having gradually formed after the long-tailed Asian thin-tailed sheep were

first domesticated (Moradi et al., 2012). However, fat-tailed sheep now account for about 25% of the total number of sheep in the world and are widely distributed; in China, 80% of sheep breeds are fat-tailed sheep (Wei et al., 2015). The unique way of depositing fat in the tail or buttocks of sheep is considered a key change following the domestication process (Ryder, 1991). It is generally believed the fat stored in the tail can produce enough energy in extremely harsh geographical and climatic environments, thus playing a crucial role in the survival of sheep (Farahani et al., 2010). Almost all fat-tailed sheep have better adaptability and better resistance to stress than other local breeds of sheep (Moradi et al., 2012). Fat-tailed sheep have most of the fat deposited in their tail, which invariably lessens fat deposition in other parts of the carcass, thereby affecting meat quality, because more feed is required to deposit fat than to produce meat (Negussie, 2003). It is estimated that the forage consumed to produce 1 kg of fat can yield 2 kg of lean meat (Gan et al., 2013). The fat deposited in the tail not only changes the quality of the lamb but also hinders the breeding of sheep, diminishing the economic benefits of raising them.

Isobaric tags for relative and absolute quantification (iTRAQ) are a proteome quantification technology with high throughput and high sensitivity. This technology uses a variety of isotope reagents to label the N-terminus of protein polypeptides or lysine side chain groups and simultaneously analyzes the protein expression between two and eight samples *via* high-resolution mass spectrometry; it is a high-throughput screening technique commonly used in quantitative proteomics in recent years (Lu et al., 2017; Wang et al., 2017; Yang et al., 2017). For example, Zhang et al. (2019) used iTRAQ technology to identify 30 differential proteins in chicken liver tissue under different concentrations of ammonia and Forde et al. (2014), Yang et al. (2017) used iTRAQ and liquid chromatography tandem-mass spectrometry (LC-MS/MS) technology to process protein extracts from the uterine fluid of pregnant cows at different time periods (10, 13, 16, and 19 days of pregnancy), finding significant changes in protein content of the uterine fluid across these four experimental periods. He et al. (2018) performed an iTRAQ-based quantitative proteomic analysis of horn tissues from both scurs and normal two-horned and four-horned individuals; their results indicated that the PI3K-Akt signaling pathway was the most significant, possibly affecting the formation of the extracellular matrix in horn that ultimately leads to the development of deformed horn tissue. Xu et al. (2019) used iTRAQ to identify critical proteins affecting milk fat in dairy cattle. Using the iTRAQ approach, Li et al. (2017) examined 27 fiber samples representing nine fiber types from sheep and goats and found differentially abundant proteins that are important to the structural components of hair, as well as some genes related to hair growth and fatty acid synthesis.

MATERIALS AND METHODS

Sample Collections

Three Altay sheep were randomly selected from Altay in Xinjiang Province and three Tibetan sheep from Tianzhu in Gansu Province (**Figure 1**). The tail length, width, and circumference of Altay sheep are 22 ± 2.7, 36 ± 1.8, and 98 ± 4.3 cm, respectively. The tail length, width, and circumference of Tibetan sheep are 15 ± 3.2, 4 ± 1.1, and 7 ± 0.3 cm, respectively. Approximately 0.5 g of tail fat tissue was removed from each sheep. After rinsing each tissue sample with normal saline, it was stored on dry ice and brought to the laboratory, where all samples were stored at −80°C until used.

Protein Extraction and Peptide Digestion

Protein extraction was done using the SDT (4% SDS, 100 mM Tris/HCL pH 7.6, and 0.1 M DTT) cleavage method (WisNiewski et al., 2009), with the BCA method used for protein quantification. Next, an appropriate amount of protein was taken from each sample for its attempted digestion by the filter-aided sample preparation (FASP) method, after which the C_{18} cartridge was used to desalt the enzymatic peptides. After the peptides were lyophilized, 40 μl of dissolution was added to reconstitute them, and the peptide $D_{280\ nm}$ value finally measured.

Isobaric Tags for Relative and Absolute Quantification Labeling

From each sample, 100 μg peptide was taken and the instructions of the AB SCIEX iTRAQ labeling kit followed accordingly, then the labeled peptides mixed.

Strong Cation Exchange Chromatographic Classification

Each group of labeled peptides was mixed, with the AKTA Purifier 100 (AKTA avant25 Cytiva) used for classification. Buffer A consisted of 10 cM KH_2PO_4 and 25% ACN, at pH 3.0, and buffer B of 10 cM KH_2PO_4, 500 mM KCL, and 25% ACN, at pH 3.0. The chromatographic column was equilibrated with liquid A, a given sample loaded onto the chromatographic column by the injector, using a flow rate set to 1 ml/min. The liquid phase gradient went was follows: 0% B liquid for 25 min; linear gradient of B liquid from 0 to 10%, for 25–32 min; linear gradient of liquid B from 10 to 20%, for 32–42 min; linear gradient of liquid B from 20 to 45%, for 42–47 min, linear gradient of liquid B from 45 to 100%, for 47–52 min; and lastly, for 52–60 min, liquid B was maintained at 100%. After 60 min, the B liquid was reset to 0%. Absorbance at 214 nm was monitored during the elution process, and eluted components were collected every 1 min, freeze-dried, and desalted by using the C18 cartridge.

Liquid Chromatography Tandem-Mass Spectrometry

Each graded sample was separated by the high-performance liquid chromatography (HPLC) liquid phase system Easy nLC by using a nanoliter flow rate. Buffer A consisted of 0.1% formic acid in water, and B was 0.1% formic acid-acetonitrile (acetonitrile: 84%). The chromatographic column was equilibrated with 95% liquid A. The sample was loaded onto the loading column by the autosampler, separated by the analytical column, and the flow rate was set to 300 nl/min. After the sample was separated by chromatography, mass spectrometry was performed by a

FIGURE 1 | (A) Altay sheep with their fat-rumped tail and **(B)** Tibetan sheep with the thin-tailed type.

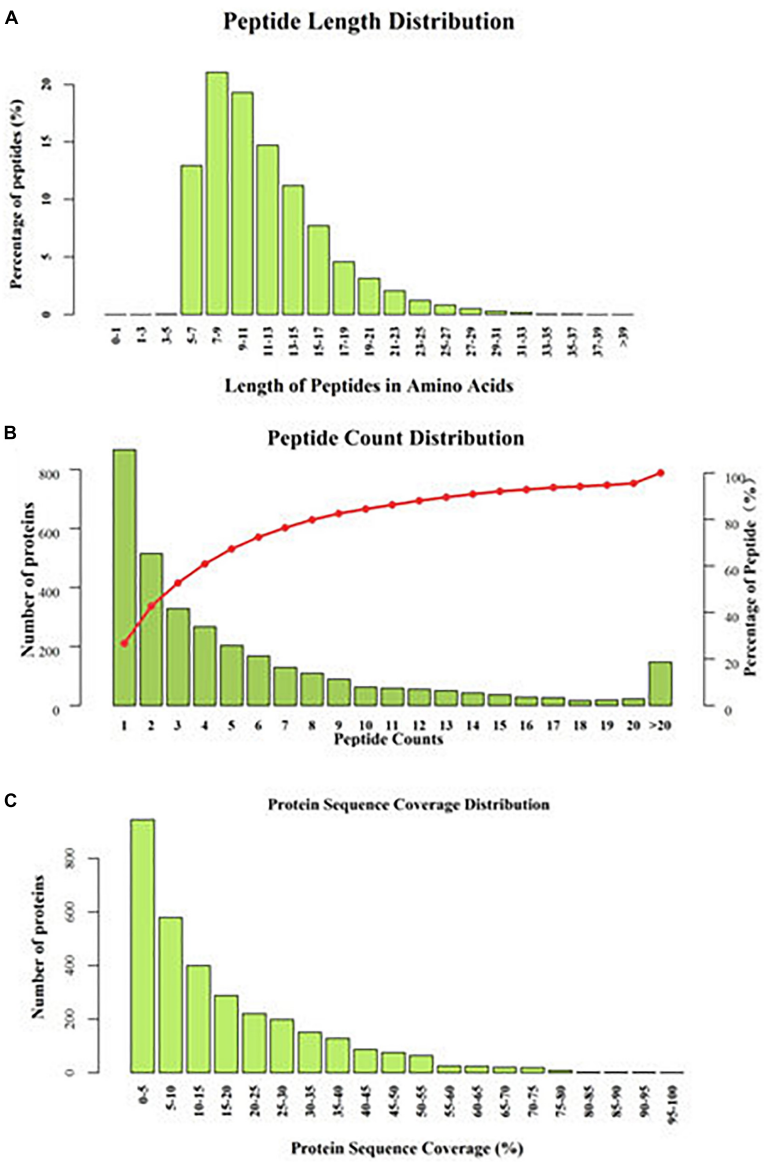

FIGURE 2 | Information for the peptides and proteins identified by iTRAQ **(A–C)**.

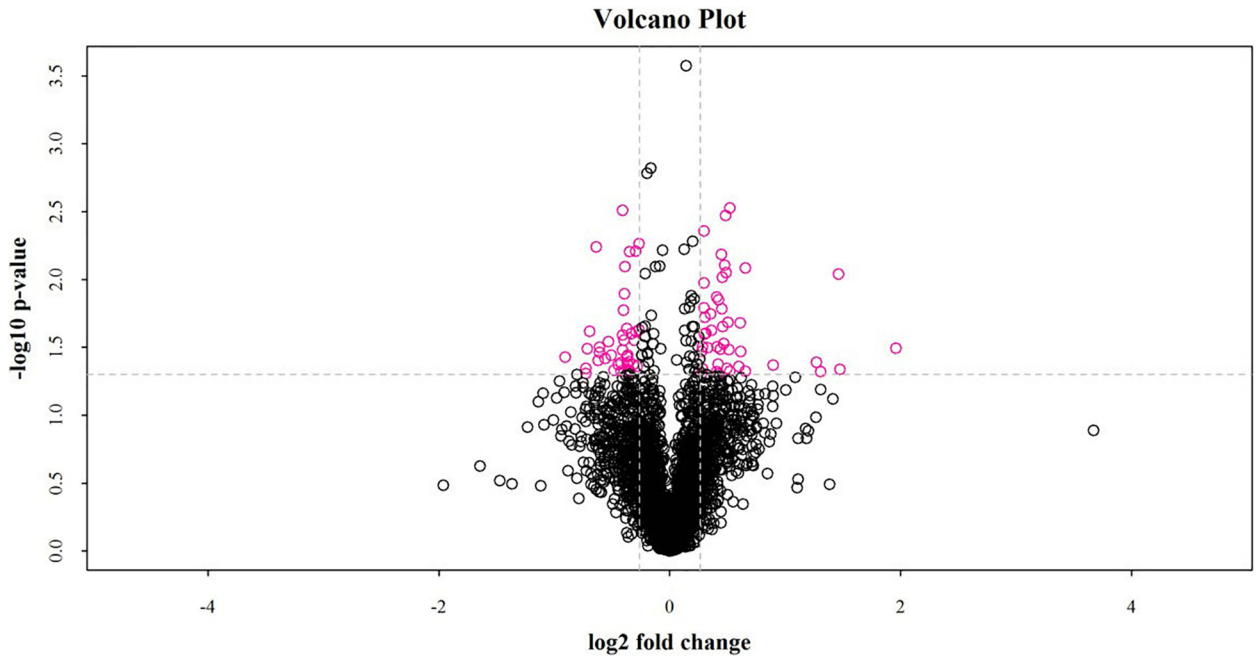

FIGURE 3 | Volcano plot of differentially expressed proteins between fat-rumped and thin-tailed sheep. The red dots in the picture are proteins found to be significantly different, and the black dots are proteins with no such difference.

Q-Exactive mass spectrometer. The detection method applied was "formal ion," the scanning range of precursor ion was 300–1,800 m/z, the resolution of primary mass spectrometry was 70,000 at 200 m/z, the AGC target was $1e^6$, the maximum IT was 50 ms, and the dynamic exclusion time is 60 s. The mass-to-charge ratios of peptides and peptide fragments were collected accordingly as follows: 20 fragment spectra were collected after each full scan; the MS2-activation type was HCD; the isolation window was 2 m/z; the secondary mass spectrometry resolution was 17,500, at 200 m/z; normalized collision energy was 30 eV; and the underfill ratio was 0.1%.

Protein Identification and Quantitative Analysis

The ensuing raw data from the mass spectrometry analysis were contained in a RAW file. Both Mascot v2.2 (Carmona et al., 2015) and Proteome Discover v1.4 software (Kim et al., 2014) were used for database checking and quantitative analysis. Each protein contained at least one specific peptide during its identification. The screening criteria for differential proteins were a $P < 0.01$ with an fold-change (FC) ≥ 2 or ≤ 0.85 (Götz et al., 2008).

Bioinformatics Analysis

We used the Blast2GO to perform a Gene Ontology (GO) annotation of the target protein collection. This process includes sequence alignment, GO mapping, GO annotation, and InterProScan annotation augmentation. The KAAS [Kyoto Encyclopedia of Genes and Genomes (KEGG) Automatic Annotation Server] software was used to annotate the KEGG pathways of the target protein collection against the KEGG database.[1] Fisher's exact test was used to compare the distribution of each GO classification or KEGG pathway in the target protein collection versus the overall protein collection. GO functional terms and enriched KEGG pathways with $P < 0.05$ were considered significant.

Protein Cluster Analysis

First, the quantitative information of the target protein collection was normalized [normalized to (−1, 1) interval]. Next, we used the "Complexheatmap" package for the R software platform (v3.4) to simultaneously categorize the two dimensions of sample and protein expression (distance algorithm: Euclidean and connection method: average linkage), from which a hierarchical clustering heat map was generated.

Protein Interaction Network Analysis

Based on the information available in the IntAct[2] or STRING[3] database, the target protein or an indirect interaction relationship was searched for. Cytoscape software (v3.2.1) was used to generate an interaction network and analyze it.

Western Blot Verification

For this assay, 50–100 mg tail fat tissue was placed in an Eppendorf tube and shredded. Then, 1 ml of the tissue cell lysate was put on ice for 3 h and then centrifuged at 12,000 rpm, at 4°C for 10 min, whose supernatant fluid was collected for

[1]http://www.genome.jp

[2]http://www.ebi.ac.uk./intact/main.xhtml

[3]http://string-db.org/

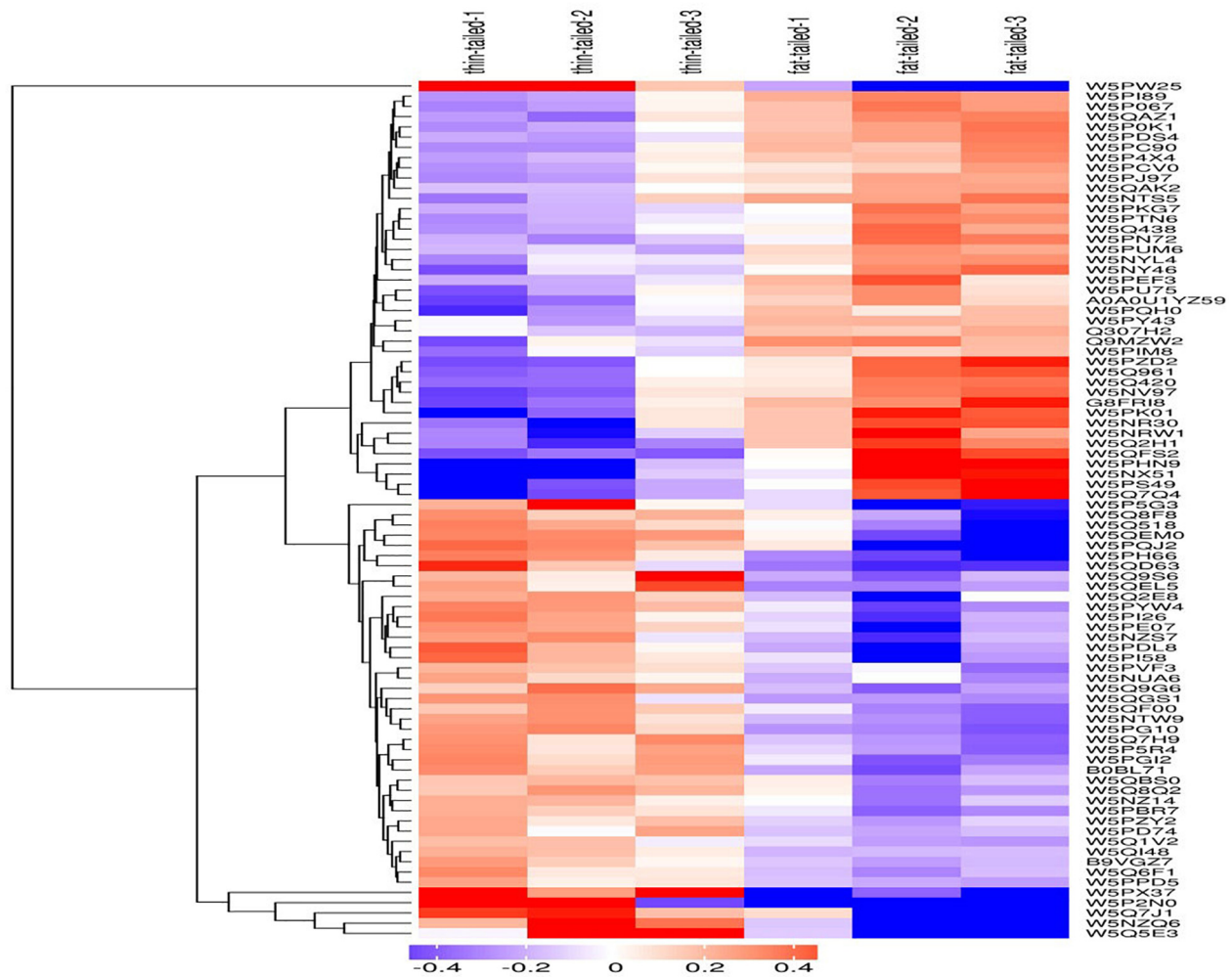

FIGURE 4 | Results from the cluster analysis of differentially expressed proteins in the thin-tailed versus fat-tailed sheep. The logarithm of protein expression in different samples is displayed in different colors on the heat map. Red represents significantly up-regulated proteins, blue represents significantly down-regulated proteins, and gray represents those proteins lacking quantitative information.

use in another new EP tube. A total protein sample of about 10 μl was taken, to which 10 μl of loading buffer was added, and then boiled 3–5 min to denature the protein. Next, SDS-PAGE gel electrophoresis was conducted, and protein transferred to a PVDF membrane. Finally, according to the antigen–antibody reaction, a western blot analysis of the target protein was carried out.

RESULTS

Protein Profile by the Isobaric Tags for Relative and Absolute Quantification Analysis

By comparing the information obtained by iTRAQ proteomics technology and the database results, 3,248 proteins were identified from 20,120 peptides by searching against the Uniprot_Ovis_aries_27827_20180612 database. According to their segment length distribution, these peptides mainly consisted of 7–21 amino acids (**Figure 2A**), a reasonable length, indicating the data set is of high quality. Most protein peptides had counts of 1–13 (**Figure 2B**). Protein sequence coverage is shown in **Figure 2C**.

TABLE 1 | Fat-related genes found in tail tissue of sheep.

Protein name	Gene name	*P*-value	Functional description
NADH:ubiquinone oxidoreductase subunit S4	*NDUFS4*	0.022	Intramuscular fat deposition
Galactokinase 1	*GALK1*	0.024	Related to fatty liver
Apolipoprotein A2	*APOA2*	0.042	Fat deposition
Adiponectin	*ADIPOQ*	0.033	Regulates fat metabolism

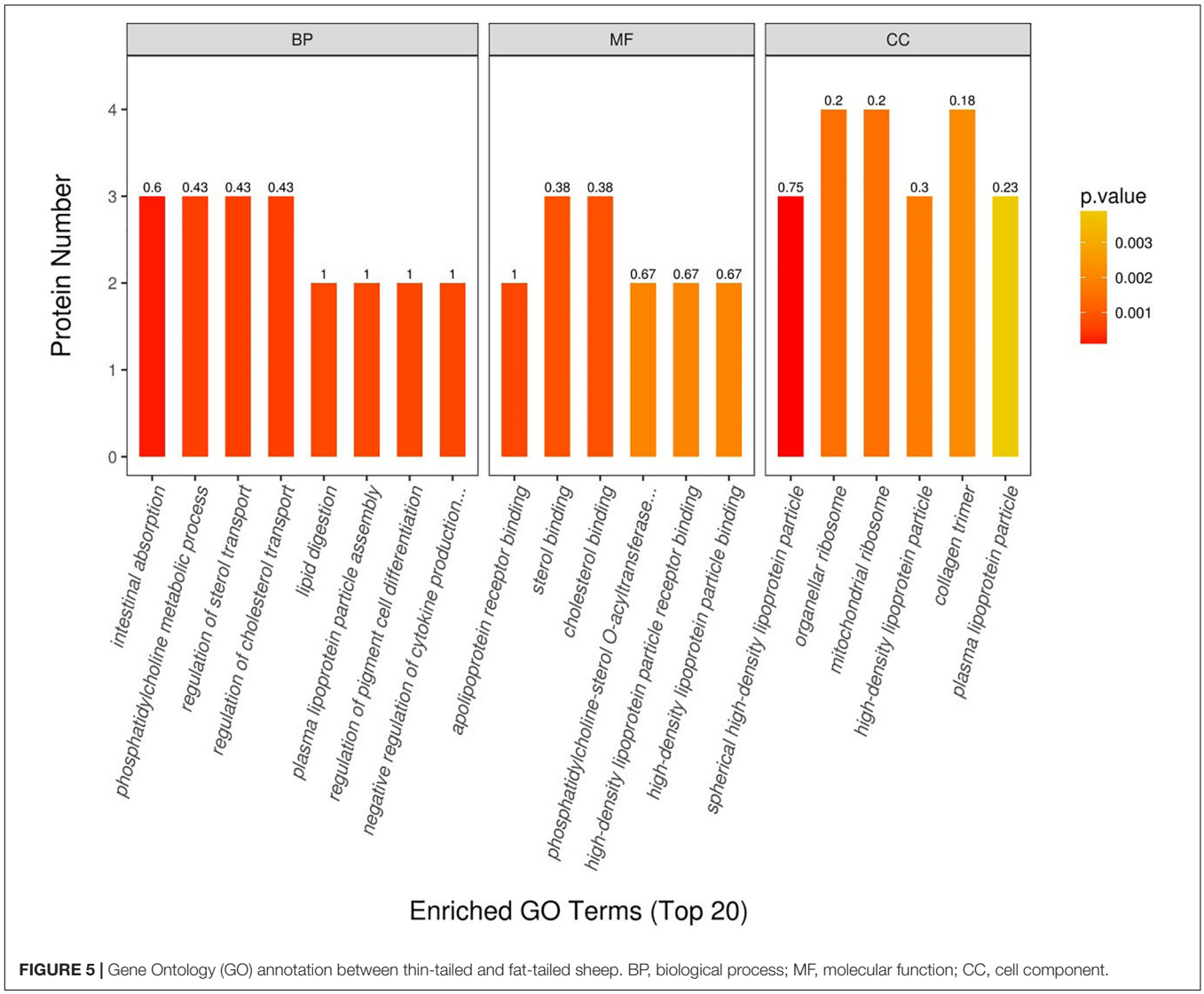

FIGURE 5 | Gene Ontology (GO) annotation between thin-tailed and fat-tailed sheep. BP, biological process; MF, molecular function; CC, cell component.

Screening of Differentially Expressed Proteins

Between the fat-rumped and thin-tailed sheep, 44 up-regulated and 40 down-regulated proteins were identified, giving a total of 84 differentially expressed proteins (DEPs). A volcano graph (**Figure 3**) was drawn using two factors: the protein expression difference fold-change and the *P*-value from the *t*-test.

Cluster Analysis of Differentially Expressed Proteins

In this study, the hierarchical clustering algorithm was used to perform cluster analysis on the DEPs of the comparison group. These results were displayed in the form of a heat map. As **Figure 4** shows, using criteria of a fold-change greater than 1.2 times and $P < 0.05$ for the *t*-test, the DEPs obtained by the screening can effectively separate the comparison components. Accordingly, this supports the screening rationale for DEPs we employed.

Among the corresponding differentially expressed genes (DEGs) for the proteins, we found some genes related to fat synthesis and metabolism (**Table 1**).

Bioinformatics

Gene Ontology Enrichment Analysis

We used Blast2GO[4] software (Götz et al., 2008) to perform the GO functional annotation on all proteins identified in this study and then implemented a GO enrichment analysis of DEPs (tested by Fisher's exact test method), as shown in **Figure 5**. These results uncovered important biological processes, such as intestinal absorption, regulation of sterol transport, regulation of cholesterol transporter, phosphatidylcholine metabolic process, and plasma lipoprotein particle assembly. In terms of molecular functions, those of apolipoprotein receptor binding, sterol binding, cholesterol binding, high-density lipoprotein particle binding, and high-density lipoprotein particle receptor binding

[4]https://www.blast2go.com/

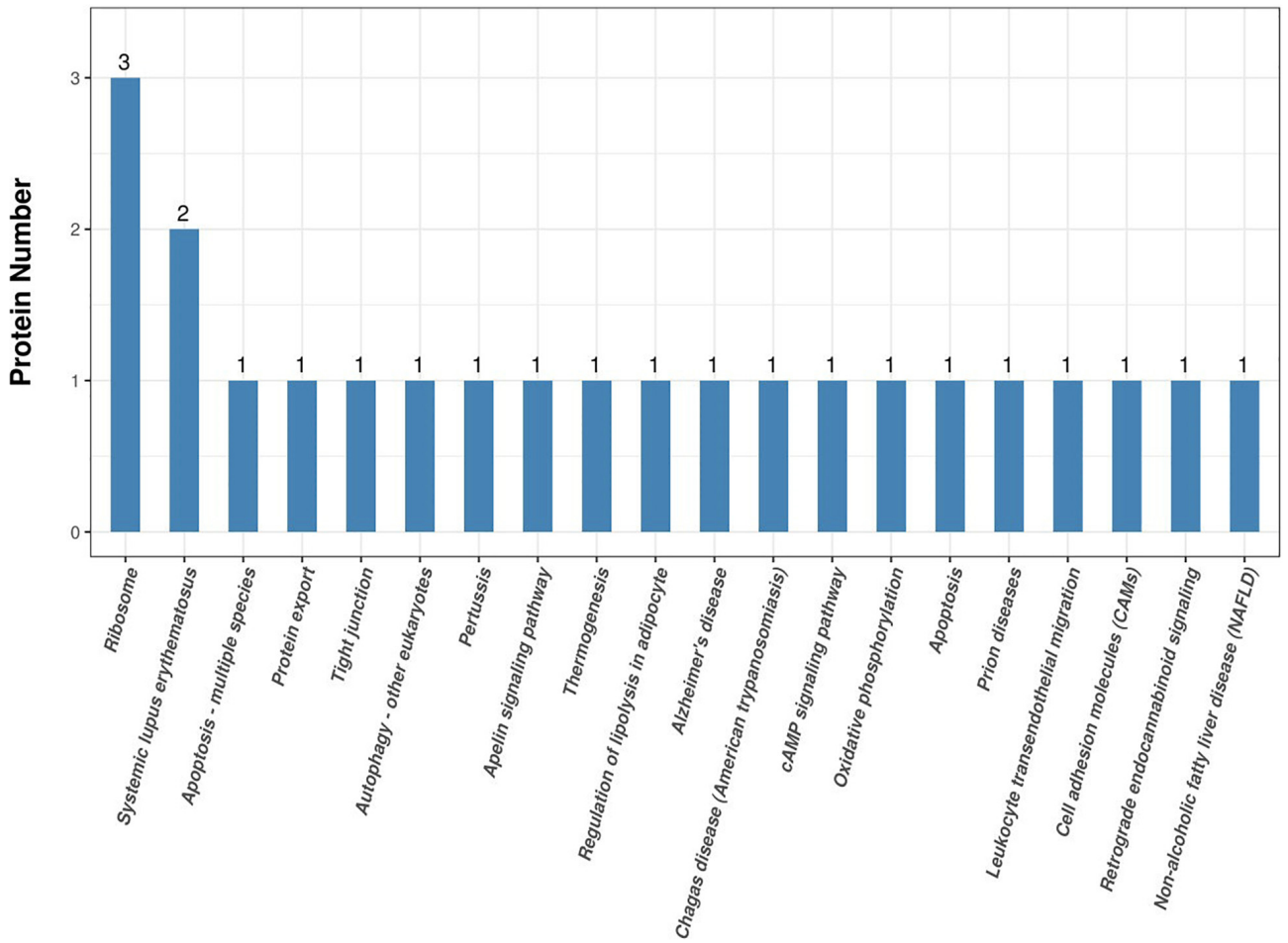

FIGURE 6 | Kyoto Encyclopedia of Genes and Genomes (KEGG) pathway results.

were found dominant in sheep tail tissue. Localized proteins, such as spherical high-density lipoprotein particle, organellar ribosome, mitochondrial ribosome, high-density lipoprotein particle, and collagen trimer, were also all changed significantly between the thin-tailed and fat-tailed comparison group.

Kyoto Encyclopedia of Genes and Genomes Pathway Enrichment Analysis

Annotating the KEGG pathway of proteins that were significantly differentially expressed helped us to better understand the metabolic or signaling pathways that these proteins may be involved in. Specifically, it revealed the series of changes in proteins that occur from the cell surface to the nucleus. These results are shown in **Figure 6**. The most significant enrichment occurred in the ribosome. They are involved in regulation of transcription, DNA template, cytoplasmic translation, rRNA processing, protein serine/threonine kinase activity, viral nucleocapsid, cytosolic large ribosomal subunit, positive regulation of transcription from RNA polymerase II promoter, herpes simplex infection, viral carcinogenesis, and Ras signaling pathway.

Differential Protein Interaction Network Analysis

Cytoscape software was used to analyze the network interaction functioning of the DEPs; the results are given in **Figure 7**. Each functional module is composed of multiple functional nodes. In the network interaction diagram, each functional node is a differential protein, and the functional nodes mapped to important functional modules are core differential proteins.

Western Blot Validation

We extracted the adipose tissue protein in the tail of the fat-tailed sheep group and the thin-tailed group and detected the DEGs by western blot after an SDS-PAGE (**Figure 8**). The proteins were subsequently transferred onto PVDF (GE Healthcare, United Kingdom) and then blocked in 5% non-fat milk (Millipore, United States). The antibodies for WB were aggrecan mouse monoclonal antibody and rabbit polyclonal antibody (Abcam, Cambridge, United Kingdom); goat anti-rabbit IgG and goat anti-mouse IgG were labeled with horseradish peroxidase (HRP) as secondary antibodies.

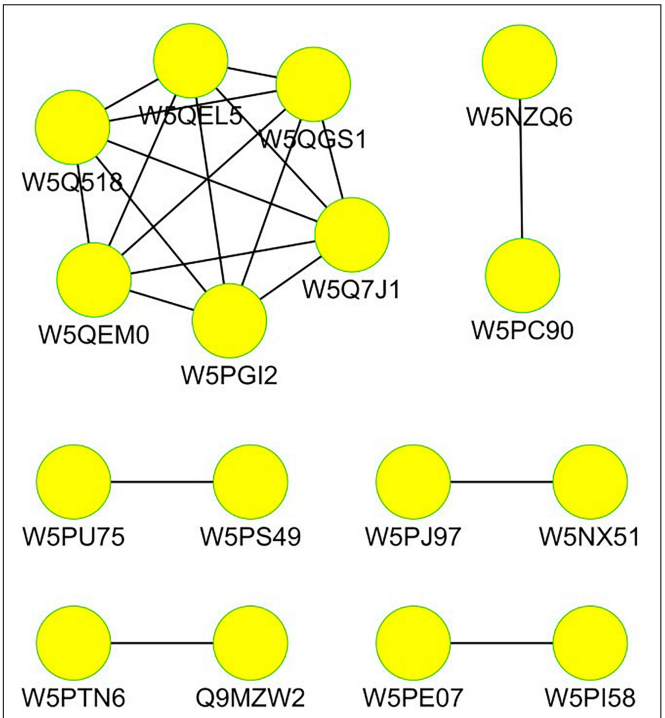

FIGURE 7 | Interacting network of the differentially expressed proteins in the tails of sheep.

These results showed that the *NDUFS4*, *GALK1*, *APOA2*, and *ADIPOQ* genes are differentially expressed in tissues between fat-rumped and thin-tailed sheep.

DISCUSSION

In this study, Altay and Tibetan sheep were used as experimental groups. Altay sheep have fat-rumped tails whereas the Tibetan sheep have thin tails, and the two breeds are distributed in different regions of China. Altay sheep are mainly distributed in Fuhai and Fuyun counties in the Altay region of Xinjiang Uygur Autonomous Region. The production area is dominated by typical continental climate, with an annual average temperature of 4.0°C, an extreme minimum temperature of −42.7°C, an annual snow cover of 200–250 days, and a snow thickness of 15–20 cm. The fat deposited on the buttocks forms a rounded fat hip, which is wide, straight, and rich. There is a shallow groove in the middle of the lower edge of the fat hip, which is divided into two symmetrical halves. Tibetan sheep are native to the Qinghai–Tibet Plateau and are mainly distributed in the Tibet Autonomous Region and Qinghai. The central production area is located at 26°50′–36°53′ north latitude and 78°25′–99°06′ east longitude. It is located in the southwestern part of the Qinghai–Tibet Plateau with an average elevation of over 4,000 m. The climate is characterized by long sunshine, strong radiation, low temperature, large temperature difference, clear and wet long night rain, dry winter and spring, high wind pressure, low air pressure, and low oxygen content. The two breeds have different genetic backgrounds; the Altay sheep belong to the Kazakh sheep line and the Tibetan sheep belong to the Tibetan sheep line, making genes associated with the different tail phenotypes easier to detect. Here we successfully used iTRAQ technology to analyze the differential proteins in tail fat tissue samples of these breeds differing in tail types. These proteins are not comprehensive using the method. The enrichment analysis only uses these detectable proteins. Therefore, the enrichment analysis is not accurate.

The protein interaction network is constituted by the interaction of proteins to participate in all aspects of life processes such as biological signal transmission, gene expression regulation, energy and material metabolism, and cell cycle regulation. A systematic analysis of the interactions of a large number of proteins in biological systems is of great significance for understanding the working principles of proteins in biological systems, understanding the reaction mechanism of energy material metabolism, and understanding the functional connections between proteins. In mammals, fatty acid metabolism is intricate, and some key proteins play a vital role (Ivessa et al., 2013). In the analysis of differential protein pathways, it is significantly enriched in pathways such as metabolism and fat synthesis pathways, and these differential proteins regulate different biological pathways and ultimately lead to the difference in fat deposition in the tails of fat-tailed sheep and lean-tailed sheep. Apolipoprotein A2 (*APOA2*) plays an important role in fat metabolism. In recent years, the *APOA2* gene has been used often as a candidate gene for fat deposition, and its genetic polymorphism distribution among different poultry was studied to find genetic markers related to production traits to inform and guide breeding production.

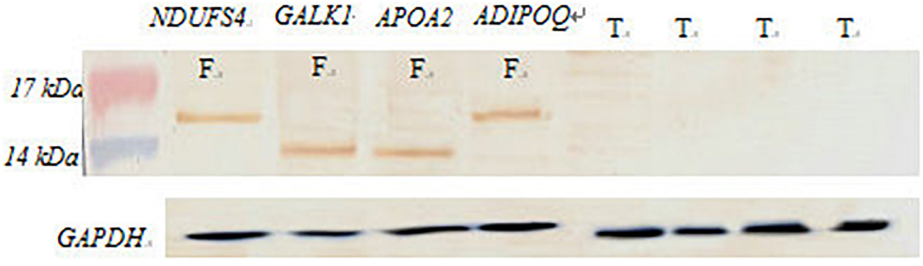

FIGURE 8 | Western blot verification. F, fat-rumped sheep; T, thin-tailed sheep.

A research by Song et al. (2013). demonstrated that the *APOA2* gene is a also a key gene for fat deposition in pigs. This gene was also identified in our study, so it could also be involved in fat deposition that occurs in the tail of sheep. The *NDUFS4* gene encodes the respiratory chain NADH dehydrogenase in the mitochondrial membrane, and previous studies have shown that the mitochondria play a key role in adipocyte differentiation. Mckay et al. (2003) found that chemical inhibition of the mitochondrial respiratory chain leads to reduced fat deposition in nematodes and 3T3-L1 cell lines. A work by Zhang et al. (2019) proved that the transcript abundance of *NDUFS4* mRNA expression in the longest back (posterior) muscle was significantly higher in the high-intramuscular fat (IMF) than low-IMF Laiwu pig, and its expression in the IMF-rich Laiwu pig also significantly exceeded that of the IMF-poor large white pig, prompting the authors to speculate that *NDUFS4* affects the deposition of IMF (Song et al., 2013). Adiponectin (*ADIPOQ*) is the first adipose tissue found in mice, by Scherer et al. (1995) who named it as a fat cell complement-related protein. *ADIPOQ* plays an important role in regulating fat metabolism, mainly by binding to receptors and acting on target tissues to exert biological effects. Animal breeds, in having different growth periods and tissue parts, as well as physiological conditions, are expected to influence how *ADIPOQ* regulates lipid metabolism, which in turn affects fat deposition in animals.

CONCLUSION

The iTRAQ technology was used to compare the fat proteins in the tail of Altay sheep and Tibetan sheep, and the DEPs obtained were analyzed. It is speculated that certain genes, namely, *APOA2*, *GALK1*, *ADIPOQ*, and *NDUFS4*, could be involved in the regulation of fat deposition in the tail of sheep.

DATA AVAILABILITY STATEMENT

The mass spectrometry proteomics data have been deposited to the ProteomeXchange Consortium via the PRIDE (Carmona et al., 2015) partner repository and data are available via ProteomeXchange with identifier PXD029488.

ETHICS STATEMENT

The animal study was reviewed and approved by the Gansu Agricultural University (Lanzhou, China), approval no. GSAU-AEW-2017-0003.

AUTHOR CONTRIBUTIONS

CZ conceived and designed the experiments, performed the experiments, and wrote the manuscript. YM, NL, TL, and HC analyzed the data and contributed reagents, materials, and analysis tools. All authors contributed to the article and approved the submitted version.

FUNDING

This work was supported by the National Natural Science Foundation of China (Grant No. 32060748), the Scientific Research Start-up Funds for Openly Recruited Doctors (Grant No. 2017RCZX-16), the Fuxi Young Talents Fund of Gansu Agricultural University (Grant No. GAUfx-04Y012), and Gansu Youth Science and Technology Fund Project (20JR5RA017).

REFERENCES

Carmona, R., Zafra, A., Seoane, P., Castro, A. J., Guerrero-Fernandez, D., Castillo-Castillo, T., et al. (2015). ReprOlive: a database with linked data for the olive tree (*Olea europaea* L.) reproductive transcriptome. *Front. Plant Sci.* 6:625. doi: 10.3389/fpls.2015.00625

Farahani, A. H. K., Shahrbabak, H. M., Shahrbabak, M. M., and Yeganeh, H. M. (2010). Relationship of fat-tail and body measurements with some economic important traits in fat-tail Makoei breed of Iranian sheep. *Afr. J. Biotechnol.* 9, 5989–5992.

Forde, N., McGettigan, P. A., Mehta, J. P., O'Hara, L., Mamo, S., Bazer, F. W., et al. (2014). Proteomic analysis of uterine fluid during the pre-implantation period of pregnancy in cattle. *Reproduction* 147, 575–587. doi: https://doi.org/10.1530/REP-13-0010

Gan, S.-Q., Zhang, W., Song, T.-Z., Shen, M., Liang, Y.-W., Yang, J.-Q., et al. (2013). Polymoriphism detection and analysis of novel snp on x chromosome between fat-tailed and thin-tailed sheep breeds. *Southwest China J. Agric. Sci.* 26, 2066–2070.

Götz, S., García-Gómez, J. M., Terol, J., Williams, T. D., Nagaraj, S. H., Nueda, M. J., et al. (2008). High-throughput functional annotation and data mining with the Blast2GO suite. *Nucleic Acids Res.* 36, 3420–3435. doi: 10.1093/nar/gkn176

He, X.-H., Chen, X.-F., Pu, Y.-B., Guan, W.-J., Song, S., Zhao, Q.-J., et al. (2018). iTRAQ-based quantitative proteomic analysis reveals key pathways responsible for scurs in sheep(Ovis aries). *农业科学学报:英文版* 17, 1843–1851. doi: 10.1016/S2095-3119(17)61894-X

Ivessa, N. E., Rehberg, E., Kienzle, B., Seif, F., Hermann, R., Hermann, M., et al. (2013). Molecular cloning, expression, and hormonal regulation of the chicken microsomal triglyceride transfer protein. *Gene* 523, 1–9. doi: 10.1016/j.gene.2013.03.102

Kim, M. S., Pinto, S. M., Getnet, D., Nirujogi, R. S., Manda, S. S., Chaerkady, R., et al. (2014). A draft map of the human proteome. *Nature* 509, 575–581. doi: 10.1038/nature13302

Li, Y., Zhou, G., Zhang, R., Guo, J., Li, C., Martin, G., et al. (2017). Comparative proteomic analyses using iTRAQ-labeling provides insights into fiber diversity in sheep and goats. *J. Proteomics* 172, 82–88. doi: 10.1016/j.jprot.2017.10.008

Lu, X., Luan, S., Dai, P., Meng, X., Cao, B., Luo, K., et al. (2017). iTRAQ-based comparative proteome analysis for molecular mechanism of defense against acute ammonia toxicity in Pacific White shrimp *Litopenaeus vannamei*. *Fish Shellfish Immunol.* 74, 52–61. doi: 10.1016/j.fsi.2017.12.030

Mckay, R. M., Mckay, J. P., Avery, L., and Graff, J. M. (2003). C. elegans: a model for exploring the genetics of fat storage. *Dev. Cell* 4, 131–142. doi: 10.1016/S1534-5807(02)00411-2

Moradi, M. H., Nejati-Javaremi, A., Moradi-Shahrbabak, M., Dodds, K. G., and McEwan, J. C. (2012). Genomic scan of selective sweeps in thin and fat tail sheep breeds for identifying of candidate regions associated with fat deposition. *BMC Genetics* 13:10. doi: 10.1186/1471-2156-13-10

Negussie, E. (2003). Patterns of growth and partitioning of fat depots in tropical fat-tailed Menz and Horro sheep breeds. *Meat Sci.* 64, 491–498. doi: 10.1016/S0309-1740(02)00227-9

Ryder, M. L. (1991). Rare sheep under communism. *United Kingdom* 18, 337–339.
Scherer, P. E., Williams, S., Fogliano, M., Baldini, G., and Lodish, H. F. (1995). A novel serum protein similar to C1q, produced exclusively in adipocytes. *J. Biol. Chem.* 270, 26746–26749. doi: 10.1074/jbc.270.45.26746
Song, Z. Y., Shi, X., Hao, Y., Qian, G., Lili, Z., and Gongshe, Y. (2013). Analysis of expression patterns of key genes during the pig (*Sus scrofa*) mature adipocyte dedifferentiation based on a novel ceiling culture model. *J. Agric. Biotechnol.* 21, 379–387. doi: 10.1016/j.cbd.2019.100602
Wang, Z., Shang, P., Li, Q., Wang, L., Chamba, Y., Zhang, B., et al. (2017). iTRAQ-based proteomic analysis reveals key proteins affecting muscle growth and lipid deposition in pigs. *Sci. Rep.* 7:46717. doi: 10.1038/srep46717
Wei, C., Wang, H., Liu, G., Wu, M., Cao, J., Liu, Z., et al. (2015). Genome-wide analysis reveals population structure and selection in Chinese indigenous sheep breeds. *BMC Genomics* 16:194. doi: 10.1186/s12864-015-1384-9
WisNiewski, J. R., Zougman, A., Nagaraj, N., and Mann, M. (2009). Universal sample preparation method for proteome analysis. *Nat. Methods* 6, 359–362. doi: 10.1038/nmeth.1322
Xu, L., Shi, L., Liu, L., Liang, R., Li, Q., Li, J., et al. (2019). Analysis of liver proteome and identification of critical proteins affecting milk fat, protein and lactose metabolism in dariy cattle with iTRAQ. *Proteomics* 19:e1800387. doi: 10.1002/pmic.201800387
Yang, M., Song, D., Cao, X., Wu, R., Liu, B., Ye, W., et al. (2017). Comparative proteomic analysis of milk-derived exosomes in human and bovine colostrum and mature milk samples by iTRAQ-coupled LC-MS/MS. *Food Res. Int.* 92, 17–25. doi: 10.1016/j.foodres.2016.11.041
Zhang, Y., Gou, W., Zhang, Y., Zhang, H., and Wu, C. (2019). Insights into hypoxic adaptation in Tibetan chicken embryos from comparative proteomics. *Comp. Biochem. Physiol. Part D Genomics Proteomics* 31:100602. doi: 10.1016/j.cbd.2019.100602

Conflict of Interest: The authors declare that the research was conducted in the absence of any commercial or financial relationships that could be construed as a potential conflict of interest.

Publisher's Note: All claims expressed in this article are solely those of the authors and do not necessarily represent those of their affiliated organizations, or those of the publisher, the editors and the reviewers. Any product that may be evaluated in this article, or claim that may be made by its manufacturer, is not guaranteed or endorsed by the publisher.

frontiers in Veterinary Science

ORIGINAL RESEARCH
published: 18 November 2021
doi: 10.3389/fvets.2021.732440

chi-miR-324-3p Regulates Goat Granulosa Cell Proliferation by Targeting *DENND1A*

Yufang Liu[1,2], *Yulin Chen*[1,2], *Zuyang Zhou*[1,2], *Xiaoyun He*[1], *Lin Tao*[1], *Yanting Jiang*[3], *Rong Lan*[3], *Qionghua Hong*[3]* *and Mingxing Chu*[1]*

[1] Key Laboratory of Animal Genetics, Breeding and Reproduction of Ministry of Agriculture and Rural Affairs, Institute of Animal Science, Chinese Academy of Agricultural Sciences, Beijing, China, [2] College of Life Sciences and Food Engineering, Hebei University of Engineering, Handan, China, [3] Yunnan Animal Science and Veterinary Institute, Kunming, China

Granulosa cell (GC) proliferation provides essential conditions for ovulation in animals. A previous study showed that *DENND1A* plays a significant role in polycystic ovary syndrome. However, the modulation of *DENND1A* in GCs remains unclear. Our previous integrated analysis of miRNA–mRNA revealed that the 3'-untranslated region of *DENND1A* could be a target of chi-miR-324-3p. In this study, we used quantitative reverse transcription polymerase chain reaction (RT-qPCR) to investigate *DENND1A* expression in ovarian tissues of high- and low-yielding goats. Furthermore, dual-fluorescent reporter vector experiments, Cell Counting Kit-8 (CCK-8) assay, and RT-qPCR were used to elucidate the regulatory pathway of chi-miR-324-3p-*DENND1A* in GCs. The results revealed an opposite tendency between the expressions of chi-miR-324-3p and *DENND1A* in the ovaries of high- and low-yielding goats. The CCK-8 assay indicated that chi-miR-324-3p overexpression significantly suppressed GC proliferation, whereas chi-miR-324-3p inhibition promoted GC proliferation. In addition, the expressions of GC proliferation markers *LHR*, *Cylin D2,* and *CDK4* showed the same tendency. The dual-fluorescent reporter assay revealed that chi-miR-324-3p directly targeted *DENND1A*, and the RT-qPCR results revealed that *DENND1A* expression was inhibited by chi-miR-324-3p. In summary, chi-miR-324-3p inhibited the proliferation of GCs by targeting *DENND1A*.

Keywords: chi-miR-324-3p, *DENND1A*, granulosa cells, proliferation, goat

OPEN ACCESS

Edited by:
Rui Su,
Inner Mongolia Agricultural University, China

Reviewed by:
Lifan Zhang,
Nanjing Agricultural University, China
Xianyong Lan,
Northwest A&F University, China
Yinghui Ling,
Anhui Agricultural University, China

***Correspondence:**
Qionghua Hong
yxh7168@126.com
Mingxing Chu
mxchu@263.net

Specialty section:
This article was submitted to Livestock Genomics, a section of the journal Frontiers in Veterinary Science

Received: *29 June 2021*
Accepted: *14 October 2021*
Published: *18 November 2021*

Citation:
Liu Y, Chen Y, Zhou Z, He X, Tao L, Jiang Y, Lan R, Hong Q and Chu M (2021) chi-miR-324-3p Regulates Goat Granulosa Cell Proliferation by Targeting DENND1A. Front. Vet. Sci. 8:732440. doi: 10.3389/fvets.2021.732440

INTRODUCTION

Ovaries, which have two functions, the cyclical production of fertilizable ova and steroid hormones, are important organs for economic animals (1). Follicles are the fundamental unit of mammalian ovaries, and the complex regulation of follicular dynamics dictates the degree of prolificacy in different species (2). The process of physical contact between granulosa cells (GCs) and oocytes can aid in oocyte growth, maturation, and, ultimately, ovulation. The proliferation of GCs is elementary for follicle and oocyte development, ovulation, and luteinization (3). Many factors can promote the proliferation of GCs, including genes, transcription factors, non-coding RNAs, and hormones. *BMPR-IB*, a gene that is well-known for its mutation in prolific sheep, was knocked out using the CRISPR-Cas technology in goat GCs, which resulted in the higher expressions of *R-Smads*, *LHR*, and *FSHR* in the *BMPR-IB* knocked out GCs compared with those in the GCs in which *BMPR-IB*

was not knocked out (4). Other genes were also found to play an important role in GC development, such as *GDF9*, *BMP15,* and *YAP1* (5–7).

Studies have shown that miRNA as a regulator influences the development of GCs. miR-224 is a promising marker of polycystic ovary syndrome (PCOS), and the overexpression of miR-224 reduces cell expansion and expression of oocyte development-associated genes (8). miR-101-3p mimics and negative control were transfected into goat GCs, and RNA-seq was used to construct the cDNA libraries. Studies have suggested that miR-101-3p targeted to *STC1* regulates the expression of *STAR*, *CYP19A1*, *CYP11A1*, and 3β-HSD steroid hormone synthesis-associated gene, thereby promoting the secretion of E_2 and P_4 (3). Additionally, miR-383 and miR-320 regulate steroid hormone secretion in GCs, whereas miR-21-5p, miR-503, miR-424, and miR-503 are involved in ovulation, follicular-luteal transformation, and luteinization (9–11). miR-324-3p is involved in various cancer development processes, which promote tumor growth by targeting *DACT1* and activating the Wnt/β-catenin pathway in hepatocellular carcinoma (12). Recently, a new study demonstrated that lncRNA H1FX-AS1 targeted *DACT1* and inhibited cervical cancer by sponging miR-324-3p (13). Fang et al. revealed that lncRNA SNHG22 facilitated malignant phenotypes in triple-negative breast cancer by sponging miR-324-3p and upregulating *SUDS3* (14). However, the function of miR-324-3p in regulating GC proliferation remains unknown.

DENND1A, which encodes for a clathrin-binding protein that is a member of the connecdenn family and a guanine nucleotide-exchange factor, is located at 9q22.32 (15). A previous study revealed a *DENND1A* variant, DENND1A.V2, which was upregulated in the theca cells of women with PCOS, and reduced *CYP17A1* expression and androgen secretion (16). Several studies have found that polymorphisms of *DENND1A* were related to an increased risk of PCOS (17, 18). Therefore, the previous studies showed that *DENND1A* plays a crucial role in PCOS. However, the function of *DENND1A* in GCs is still unknown. In our previous study, integrated analysis of miRNA–mRNA results revealed that *DENND1A* is a target gene of chi-miR-324-3p. Hence, we deduced that chi-miR-324-3p inhibits GC proliferation in PCOS by suppressing *DENND1A* expression.

In this study, we aimed to identify the roles of chi-miR-324-3p in the proliferation of goat GCs and the relationship of chi-miR-324-3p with *DENND1A*. The findings demonstrated that chi-miR-324-3p could regulate GC proliferation by targeting *DENND1A*. Overall, this study provides new evidence supporting the potential application of chi-miR-324-3p to prolific goats.

MATERIALS AND METHODS

Ethics Statement

This study and all the experimental procedures were approved by the Science Research Department (in charge of animal welfare issue) of the Institute of Animal Sciences and Chinese Academy of Agricultural Sciences (IAS-CAAS) (Beijing, China). Ethical approval was also provided by the animal ethics committee of IAS-CAAS (No. IAS2019-63).

Animal Tissue Collection

Female native domestic goats, known as Yunshang black goats, were used in this study. According to their yield records (at least two-born litter size), 277 female goats (152 high yielding goat and 125 low yielding goat) with no significant differences in weight and height were grouped into either the high-yielding group (average litter size 3.00 ± 0.38) or low-yielding group (average litter size 1.32 ± 0.19) ($p < 0.05$). All goats were bred under the same conditions, with free access to water and feed in a goat farm located in Yunnan Province. In the follicular phase, three high-yielding (high litter size group, HF) and three low-yielding goats (low litter size group, LF) were selected from the batch of goats according to their litter size. The ovarian tissues were collected from goats, frozen immediately in liquid nitrogen, and subsequently stored at −80°C until RNA extraction.

Cell Culture and Transfection

Following previously described methods, primary goat GCs were isolated from the follicles of ovarian tissues in the follicular phase (19). The diameter of the GCs in the follicular phase was over 3.5 mm. The isolated cells were seeded in 6-mm plates and maintained in a complete medium [DMEM/F12 (1:1), 10% FBS, and 1% penicillin/streptomycin] as described by Yang et al. (20). When the cell confluence was >90%, the cells were transferred to 10-mm plates for the next experiment.

RNA Extraction

According to the manufacturer's protocol, total RNA was isolated from ground ovarian tissue powder and goat primary GCs using TRIzol reagent (Invitrogen, Carlsbad, CA, USA). The purity and concentration of the RNA samples were evaluated using a NanoDrop 2000 spectrophotometer (Thermo Scientific, Wilmington, DE, USA). Standard denaturing agarose gel electrophoresis was used to determine the presence of contamination and degradation.

Vector Construction

The 3′ untranslated region (UTR) of *DENND1A* containing the predicted target site, including wild type (WT) and mutant type (MUT), were cloned into pmiR-RB-Report vector [named pmiR-RB-DENND1A-WT and pmiR-RB-DENND1A-MUT; isolated using *Xho*I and *Not*I (Takara, Dalian, China)], respectively. The insert sequence was synthesized by RiboBio company, including the wild/mutant sequences, miRNA mimic, mimic-NC, inhibitor, and inhibitor NC (RiboBio, Guangzhou, China).

Dual-Luciferase Reporter Analysis

HEK293T, a human cell line of renal epithelial cells, was used to validate the miRNA target. Cells were seeded into 24-well plates. Cotransfection with 200 ng of target mRNA-3'-UTR-WT or target mRNA-3'-UTR-MUT and 10 μl of miRNA mimic or mimic-NC was performed using Lipofectamine 2000 (Invitrogen, USA). Subsequently, luciferase activity was measured using the Dual-Luciferase Reporter Assay System (Promega, WI, USA) at 48 h post-Transfection. The assays were performed in triplicate.

Real-Time Polymerase Chain Reaction Assay

According to the manufacturer's instructions, reverse transcription was performed using a PrimeScript™ RT reagent kit (TaKaRa, Dalian, China), for mRNA and miRcute Plus miRNA First-Strand cDNA kit (TIANGEN, Beijing, China) for miRNA. RT-qPCR was performed using SYBR Green qPCR Mix (TaKaRa, Dalian, China) for mRNAs and miRcute Plus miRNA qPCR kit (TIANGEN, Beijing, China) for miRNAs using RocheLight Cycler®480 II system (Roche Applied Science, Mannheim, Germany). The qPCR for mRNAs was performed as follows: initial denaturation at 95°C for 5 min, followed by 40 cycles of denaturation at 95°C for 5 s, and finally annealing at 60°C for 30 s. In contrast, the qPCR for miRNAs was performed as follows: initial denaturation at 95°C for 15 min, followed by 40 cycles of denaturation at 94°C for 20 s, and finally annealing at 60°C for 34 s. The data were analyzed using the $2^{-\Delta\Delta Ct}$ method. *LHR*, *Cylin D2*, and *CDK4* were selected as GC proliferation markers (21). Goat *RPL19* gene and U6 gene were used as a reference gene for normalizing target gene data. The sequences of RT-qPCR primers are listed in **Table 1**.

Ethynyldeoxyuridine Incorporation Assay

GC proliferation was quantified using an ethynyldeoxyuridine (EdU) kit according to the manufacturer's protocol (Beyotime). Cells were seeded into 96-well plates as described above. One hundred microliters of 50 μM EdU was aliquoted to each well and cells were incubated an additional 3 h. Cells were then washed with PBS and fixed with 4% paraformaldehyde for 30 min. To neutralize excess aldehyde groups, 50 μl of 2 mg/ml of glycine was aliquoted per well and incubated with cells for 15 min. Subsequently, 100 μl of 0.5% Triton X-100 in PBS was aliquoted per well and incubated with cells for 15 min. After rinsing, 100 μl of Apollo reagent was added, and the cells were incubated in the dark for 30 min at room temperature. Cells were washed with PBS and then nuclei were stained with Hoechst 33,342 reaction solution for 30 min in the dark. EdU-stained cells were visualized and quantified using a fluorescence microscope. Three fields were randomly selected for quantification and statistical analysis.

TABLE 1 | Primer sequences used for quantitative-polymerase chain reaction in this study.

Gene name	GenBank accession number	Primer sequence 5′-3′	Product size (bp)
DENND1A	XM_018055747.1	F: AACGCTCTGAAAATCGAGCC	228
		R: CAGCTTATCACTCCCGGCAT	
LHR	NM_001314279.1	F: CGGCTGGCTTTTTCACTGTT	226
		R: GGGAGGCAAATGCTGACCTT	
Cylin D2	XM_005680985.3	F: ATGTGGATTGCCTCAAAGCC	152
		R: CAGGTCGATATCCCGAACATC	
CDK4	XM_005680266.3	F: GAGCATCCCAATGTTGTCAGG	172
		R: ACTGGCGCATCAGATCCTTT	
RPL19	XM_005693740.3	F: ATCGCCAATGCCAACTC	154
		R: CCTTTCGCTTACCTATACC	
chi-miR-324-3p		F: CCCCAGGTGCTGCT	
U6		F: CAAGGATGACACGCAAATTCG	

Cell Counting Kit-8 Assay of GCs

GCs were inoculated into 96-well plates with approximately 100 μl of cell suspension per well in three replicates. Cells were then incubated for 2–4 h at 37°C in an incubator, and used for subsequent experiments after cell apposition/adequate confluency was reached more than 90%. Cell proliferation assay was conducted using the Cell Counting Kit-8 (CCK-8) method (Beyotime, Beijing, China). Goat GCs were cultured in 96-well plates and measured by adding 10 μl of CCK-8 solution per well as per protocol. After the addition of CCK-8 solution, absorbance at 450 nm was measured at 0, 6, 12, 24, 48, and 72 h.

Statistical Analysis

Statistical analyses of RT-qPCR results and graphs were conducted using GraphPad Prism (v.5.0) (San, Diego, CA, USA). Statistical significance of the data was tested using paired *t*-tests. The results were presented as means ± SEM of three replicates, and the statistical significance was represented by p-values < 0.05 ($^{*}p < 0.05$) and p-values < 0.01 ($^{**}p < 0.01$).

RESULTS

Expressions of chi-MiR-324-3p and DENND1A in Ovarian Tissues

It has been predicted in a previous study that as a *DENND1A* regulator, chi-miR-324-3p is expressed in goat ovarian tissues in the follicular phase. To illustrate the correlation of the predicted miRNA–mRNA pair, the expression patterns of chi-miR-324-3p and its putative target *DENND1A* were investigated in HF (high-yielding group) and LF (low-yielding group). As shown in **Figure 1**, opposite expression patterns of chi-miR-324-3p and *DENND1A* were observed in the high-yielding group (**Figure 1**). This indicated a negative correlation between the expressions of chi-miR-324-3p and *DENND1A*.

Overexpression of chi-MiR-324-3p Suppressed GC Proliferation

To investigate the regulatory function of chi-miR-324-3p on GC proliferation, an overexpression experiment was performed by transfecting a chi-miR-324-3p mimic into goat GCs (**Figure 2A**). The EdU, CCK-8 assay and analysis of the expressions of GC proliferation factors were used for validating the functions of chi-miR-324-3p in GCs. The results revealed that the GCs proliferation was significantly lower in the mimic group than that in the mimic-NC group (**Figures 2B,C**) ($p < 0.05$). The expressions of *LHR, Cylin D2,* and *CDK4* were also significantly lower in the mimic group than in the mimic-NC group (**Figure 2D**) ($p < 0.05$). These results demonstrated that the overexpression of chi-miR-324-3p inhibited the proliferation of goat GCs.

Inhibition of chi-MiR-324-3p Promoted the Proliferation of GCs

To further explore the role of chi-miR-324-3p in goat GCs, chi-miR-324-3p inhibitor was transfected into goat GCs (**Figure 3A**).

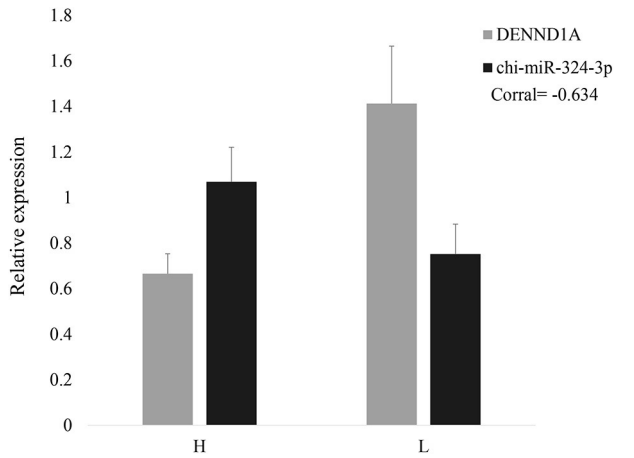

FIGURE 1 | Relative expressions of *DENND1A* and chi-miR-324-3p in goat ovarian tissues in high- and low-yielding groups. H represents the high-yielding group; L represents the low-yielding group.

The EdU and CCK-8 assay revealed that the GC proliferation in the inhibitor group was significantly higher than that of the inhibitor-NC group (**Figures 3B,C**) ($p < 0.05$). The mRNA expression of GC proliferation markers was significantly upregulated after inhibitor transfection (**Figure 3D**) ($p < 0.05$). These results demonstrated that the inhibition of chi-miR-324-3p could promote the proliferation of goat GCs.

DENND1A Is a chi-MiR-324-3p Target

In a previous study, it was revealed that *DENND1A* is a potential target of chi-miR-324-3p. To verify whether *DENND1A* is the direct target gene of chi-miR-324-3p, two plasmids containing either the WT or MUT 3'-UTR of *DENND1A* were constructed (**Figure 4A**). Subsequently, cotransfection of chi-miR-324-3p mimic or mimic-NC into 293T cells was performed. Notably, chi-miR-324-3p markedly decreased the activity of WT *DENND1A* compared with the negative control, but no significant changes were noted for the MUT (**Figure 4B**). These findings indicated that chi-miR-324-3p can directly target the 3'-UTR of *DENND1A*.

Expression of DENND1A Is Regulated by chi-MiR-324-3p

To examine the validity of the putative target, chi-miR-324-3p mimic or mimic-NC was transfected into goat GCs. RT-qPCR data revealed that the transcriptional levels of *DENND1A* were

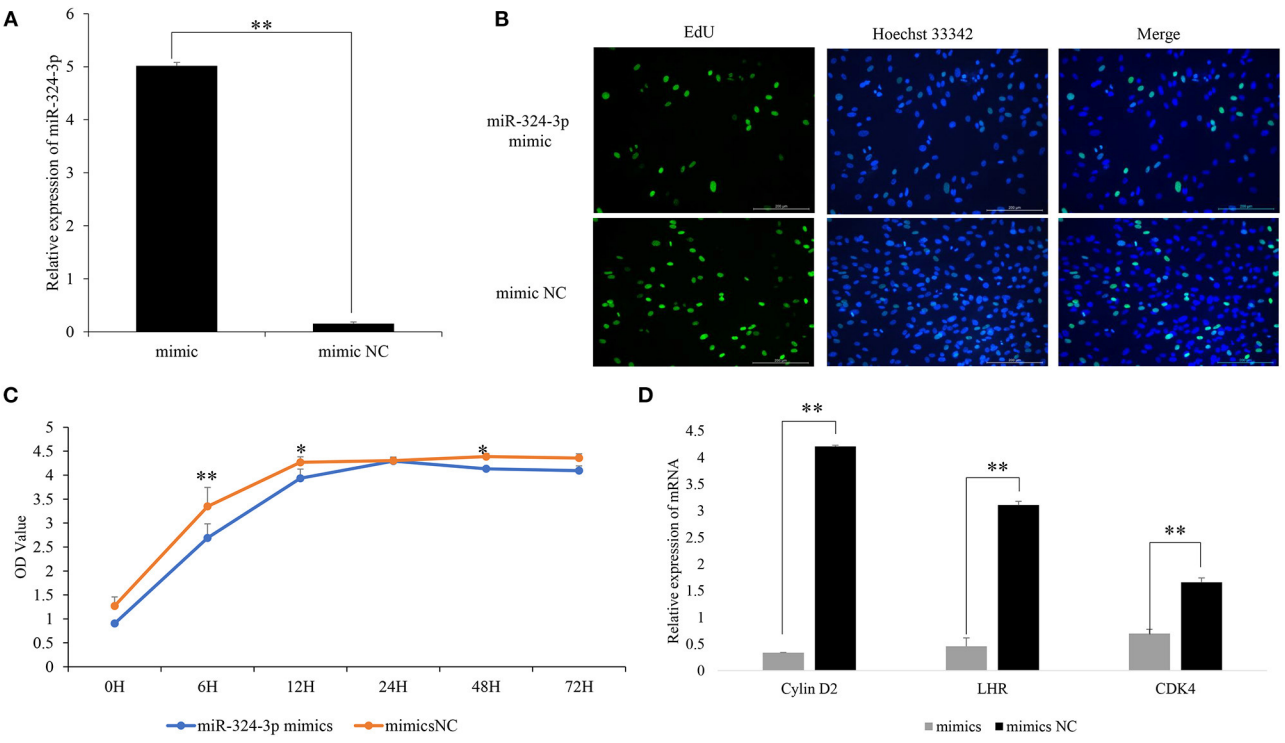

FIGURE 2 | Overexpression of chi-miR-324-3p in goat GCs. **(A)** Relative expression of miR-324-3p. **(B)** The result of EdU assay. **(C)** CCK-8 assay of goat GCs with miR-324-3p mimic and mimic NC transfection at 0–72 h. **(D)** Relative expressions of *LHR*, *CDK4*, and *Cylin D2* in transfected chi-miR-324-3p mimic and mimic NC at 48 h. $*p < 0.05$; $**p < 0.01$. CCK-8, Cell Counting Kit-8; GC, granulosa cell.

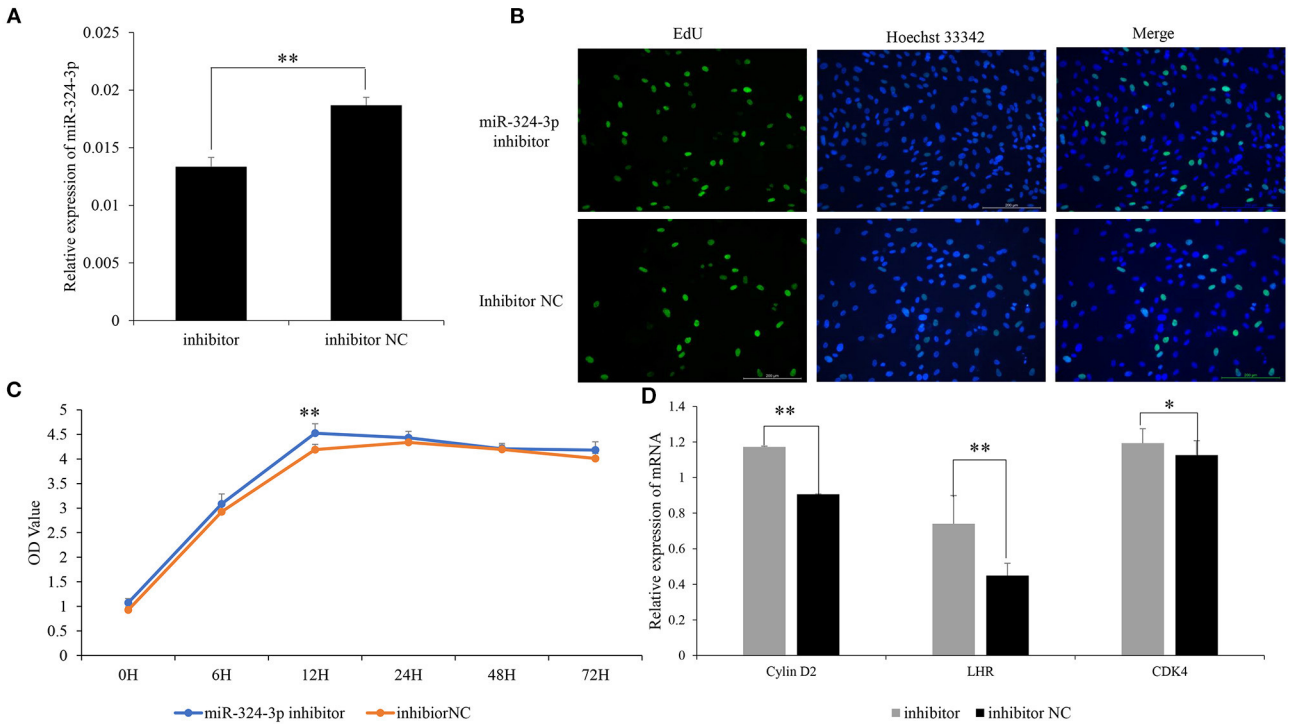

FIGURE 3 | Inhibited chi-miR-324-3p expression in goat GCs. **(A)** Relative expression of miR-324-3p. **(B)** The result of EdU assay. **(C)** CCK-8 assay of goat GCs with miR-324-3p mimic and mimic NC transfection at 0–72 h. **(D)** Relative expressions of *LHR*, *CDK4*, and *Cylin D2* in transfected chi-miR-324-3p mimic and mimic NC at 48 h. $^{*}p < 0.05$; $^{**}p < 0.01$. CCK-8, Cell Counting Kit-8; GC, granulosa cell.

different between the mimic and mimic-NC groups (**Figure 5**). Thus, we concluded that chi-miR-324-3p directly targets the 3'-UTR of *DENND1A* to suppress its mRNA translation in goat GCs.

DISCUSSION

The key candidate gene associated with prolific traits in goats remains unknown. In our study of RNA-seq, chi-miR-324-3p and *DENND1A* showed differential expression levels in high- and low-yielding goats and chi-miR-324-3p was predicted to target *DENND1A* (data unpublished). In this study, we found and validated the function of chi-miR-324-3p in goat GCs. Our results indicated that chi-miR-324-3p regulated GC proliferation by targeting *DENND1A*.

The DENN domain is a common, evolutionarily ancient, and conserved protein module; there are eight families and *DENND1A* is a member of these. *DENND1A* was detected by proteomic analysis of clathrin-coated vesicles (22). Its variant is associated with hyperandrogenism and irregular menses and is a risk variant for PCOS as documented by the NIH criteria (23). *DENND1A* is expressed in the theca cells and testes; therefore, it may be associated with hyperandrogenism by increasing androgen levels (24). In this study, the high expression of *DENND1A* was associated with prolific traits in goats; chi-miR-324-3p directly acted on the 3'-UTR of *DENND1A* in the 293T cell line. Meanwhile, our overexpression and inhibition experiments on chi-miR-324-3p further verified that the expressions of *DENND1A* and chi-miR-324-3p showed opposite trends in goat GCs. Some studies have suggested that *DENND1A* regulates Rab GTPases, which are important for calcium regulated exocytosis in pituitary cells and for basal and GnRH-induced gonadotropin release (25, 26). Moreover, *DENND1A* has been reported to participate in endocytosis and receptor trafficking in the cellular membrane. Furthermore, high methylation existed in the *DENND1A* intron in aging oocytes (16, 27). Regardless, the effects of *DENND1A* on goat GC proliferation remain experimentally unclarified. Here, we provide new insights for understanding that *DENND1A* might be a key gene involved in goat GC proliferation that is regulated by chi-miR-324-3p. Taken together, these experimental results support the conclusion that *DENND1A* is involved in GC proliferation.

A previous study reported that miR-324-3p can promote the dysregulation of the expression of genes involved in cell death and apoptosis, cAMP and Ca^{2+} signaling, cell stress, and metabolism (28). Notably, miR-324-3p inhibition was highly and significantly correlated with cell proliferation and apoptosis. miR-324-3p, which is highly upregulated in maternal blood in the second trimester, is associated with fetal growth (29). miR-324-3p has also been reported to increase the incidence of ectopic pregnancy according to the analysis of tissues obtained from voluntarily terminated pregnancy, which has a repressive interaction with 3'-UTR of *KISS1* (30). In addition,

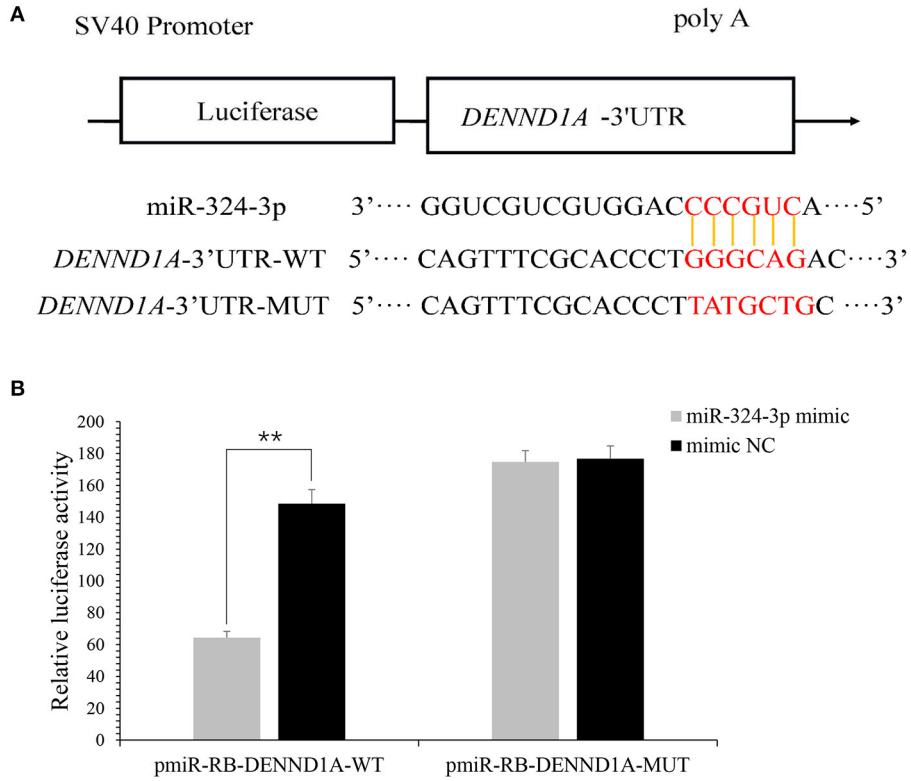

FIGURE 4 | *DENND1A* is directly targeted by chi-miR-324-3p. **(A)** Predicted binding sites of chi-miR-324-3p in the 3'-UTR of *DENND1A*. The red section is the seed region of chi-miR-324-3p. **(B)** Relative luciferase activities of 293T cells cotransfected with the *DENND1A* 3'-UTR wild-type and mutant dual-luciferase reporter and chi-miR-324-3p mimic and mimic NC at 48 h. UTR, untranslated region. $^{**}P < 0.01$.

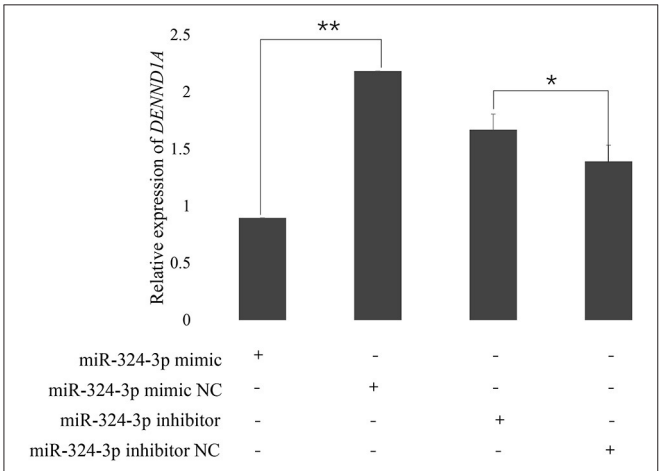

FIGURE 5 | Expression of *DENND1A* in goat GCs transfected with chi-miR-324-3p mimic or mimic NC, and inhibitor or inhibitor-NC at 48 h. *RPL19* was used as the reference gene. Results are representative of the mean (±standard deviation) of three independent analyses. $^{*}p < 0.05$; $^{**}p < 0.01$.

miR-324-3p overexpression in ectopic pregnancy is responsible for decreased KISS1/kisspeptin expression (31). Our previous studies have demonstrated that chi-miR-324-3p can regulate the development of ovaries in prolific goats by targeting *DENND1A* (data unpublished). Moreover, there is evidence that miR-324-3p plays crucial roles in ovary development and cell proliferation. Furthermore, miR-324-3p is related to SKOV3 cell viability, invasion, and migration *via* overexpression in ovarian cancer (32). Furthermore, a study demonstrated that miR-324-3p expression in PCOS rats is remarkably downregulated and confirmed that the overexpression of miR-324-3p represses proliferation and induces the apoptosis of GCs by targeting *WNT2B* (33). Using the CCK-8 assay, our results indicated that chi-miR-324-3p could inhibit goat GC proliferation, as demonstrated by the low expression of GC proliferation markers. We used goat ovaries in the follicular phase and the primary GCs as the animal material. Thus, we propose a new mechanism for the roles of chi-miR-324-3p in goat GCs.

In summary, our study reveals that chi-miR-324-3p regulates goat GC proliferation by directly targeting *DENND1A*. These data expand our mechanistic understanding of GC proliferation and ovary development in which miRNAs play an important role.

DATA AVAILABILITY STATEMENT

The original contributions presented in the study are included in the article/supplementary material, further inquiries can be directed to the corresponding authors.

ETHICS STATEMENT

The animal study was reviewed and approved by the Science Research Department (in charge of animal welfare issue) of the Institute of Animal Sciences and Chinese Academy of Agricultural Sciences (IAS-CAAS) (Beijing, China) for all the experimental procedures mentioned. Ethical approval was provided by the animal ethics committee of IASCAAS (No. IAS2019-63).

AUTHOR CONTRIBUTIONS

Conceptualization: YFL and MXC; Methodology: YFL, ZYZ, LT and MXC; Validation: YFL, YLC and ZYZ; Formal Analysis: YFL and MXC; Investigation: YFL, ZYZ, LT, YLC, XYH, YTJ, RL, QHH and MXC; Resources: YFL, ZYZ, LT and MXC; Data Curation: YFL, ZYZ, LT, and MXC; Writing-Original Draft Preparation: YFL and MXC; Supervision: MXC; Project Administration: YFL, QHH and MXC; Funding Acquisition: QHH and MXC. All authors have read and agreed to the published version of the manuscript.

FUNDING

This research was funded by the Agricultural Science and Technology Innovation Program of China (CAAS-ZDRW202106 and ASTIP-IAS13), the China Agriculture Research System of MOF and MARA (CARS-38), the Major Science and Technology Special Plan of Yunnan Province (202102AE090039), and the Basic Research Foundation Key Project of Yunnan Province (202001AS070002).

REFERENCES

1. Hafez ESE, Hafez B. Folliculogenesis, egg maturation, and ovulation. In: Hafez B, Hafez E, editors. *Reproduction in Farm Animals.* Philadelphia, PA: Lippincott Williams and Wilkins (2000). p. 68–81. doi: 10.1002/9781119265306.ch5
2. Sharma GT, Majumdar AC. Control of follicular steroidogenesis in early- and late-luteal phase goat ovaries. *Small Ruminant Res.* (1999) 34:111–7. doi: 10.1016/S0921-4488(99)00006-1
3. An XP, Ma HD, Liu YH, Li F, Song YX, Li G, et al. Effects of miR-101-3p on goat granulosa cells in vitro and ovarian development in vivo via STC1. *J Anim Sci Biotechnol.* (2020) 11:102. doi: 10.1186/s40104-020-00506-6
4. Kumar S, Punetha M, Jose B, Bharati J, Khanna S, Sonwane A, et al. Modulation of granulosa cell function via CRISPR-Cas fuelled editing of BMPR-IB gene in goats (Capra hircus). *Sci Rep.* (2020) 10. doi: 10.1038/s41598-020-77596-9
5. Md Hasanur A, Jibak L, Takashi M. GDF9 and BMP15 induce development of antrum-like structures by bovine granulosa cells without oocytes. *J Reprod Dev.* (2018) 64:423–31. doi: 10.1262/jrd.2018-078
6. Zhu GQ, Fang C, Li J, Mo CH, Wang YJ, Li J. Transcriptomic diversification of granulosa cells during follicular development in chicken. *Sci Rep.* (2019) 9:5462. doi: 10.1038/s41598-019-41132-1
7. Lv XM, He CB, Huang C, Wang HB, Hua GH, Wang ZF, et al. Timely expression, and activation of YAP1 in granulosa cells is essential for ovarian follicle development. *FASEB J.* (2019) 33:10049–64. doi: 10.1096/fj.201900179RR
8. Li X, Wang H, Sheng Y, Wang Z. MicroRNA-224 delays oocyte maturation through targeting Ptx3 in cumulus cells. *Mech Dev.* (2017) 143:20–5. doi: 10.1016/j.mod.2016.12.004
9. Yin MM, Wang XR, Yao GD, Lü MR, Liang M, Sun YP, et al. Transactivation of microRNA-320 by microRNA-383 regulates granulosa cell functions by targeting E2F1 and SF-1 proteins. *J Biol Chem.* (2014) 289:18239–57. doi: 10.1074/jbc.M113.546044
10. Samuel G, Dessie SW, Ijaz A, Sudeep S, Md Munir H, Michael H, et al. MicroRNA expression profile in bovine granulosa cells of preovulatory dominant and subordinate follicles during the late follicular phase of the estrous cycle. *PLoS ONE.* (2015) 10:e0125912. doi: 10.1371/journal.pone.0125912
11. Hari Om P, Dawit T, Michael H, Samuel G, Eva H, Christiane N, et al. MicroRNA-424/503 cluster members regulate bovine granulosa cell proliferation and cell cycle progression by targeting SMAD7 gene through activin signaling pathway. *J Ovarian Res.* (2018) 11:34. doi: 10.1186/s13048-018-0410-3
12. Tuo H, Wang YF, Wang L, Yao BW, Li Q, Wang C, et al. MiR-324-3p promotes tumor growth through targeting DACT1 and activation of Wnt/β-catenin pathway in hepatocellular carcinoma. *Oncotarget.* (2017) 8:65687–98. doi: 10.18632/oncotarget.20058
13. Shi XH, Huo JZ, Gao XP, Cai H, Zhu WP. A newly identified lncRNA H1FX-AS1 targets DACT1 to inhibit cervical cancer via sponging miR-324-3p. *Cancer Cell Int.* (2020) 20:358. doi: 10.1186/s12935-020-01385-7
14. Fang X, Zhang J, Li CY, Liu JJ, Shi ZD, Zhou P. Long non-coding RNA SNHG22 facilitates the malignant phenotypes in triple-negative breast cancer via sponging miR-324-3p and upregulating SUDS3. *Cancer Cell Int.* (2020) 20:252. doi: 10.1186/s12935-020-01321-9
15. Kulkarni R, Teves ME, Han AX, McAllister JM, Strauss JFIII. Colocalization of polycystic ovary syndrome candidate gene products in theca cells suggests novel signaling pathways. *J Endocr Soc.* (2019) 3:2204–23. doi: 10.1210/js.2019-00169
16. McAllister JM, Modi B, Miller BA, Biegler J, Bruggeman R, Legro RS, et al. Overexpression of a DENND1A isoform produces a polycystic ovary syndrome theca phenotype. *Proc Natl Acad Sci USA.* (2014) 111:E1519–27. doi: 10.1073/pnas.1400574111
17. Gammoh E, Arekat MR, Saldhana FL, Madan S, Ebrahim BH, Almawi WY. DENND1A gene variants in Bahraini Arab women with polycystic ovary syndrome. *Gene.* (2015) 560:30–3. doi: 10.1016/j.gene.2015.01.034
18. Bao S, Cai JH, Yang SY, Ren Y, Feng T, Jin T, et al. Association of DENND1A gene polymorphisms with polycystic ovary syndrome: a meta-analysis. *J Clin Res Pediatr Endocrinol.* (2016) 8:135–43. doi: 10.4274/jcrpe.2259
19. Sharma AK, Sharma RK. Effect of prostaglandins E2 and F2α on granulosa cell apoptosis in goat ovarian follicles. *Iran J Vet Res.* (2020) 21:97–102.
20. Yang DQ, Wang L, Lin PF, Jiang TT, Wang N, Zhao F, et al. An immortalized steroidogenic goat granulosa cell line as a model system to study the effect of the endoplasmic reticulum (ER)-stress response on steroidogenesis. *J Reprod Dev.* (2017) 63:27–36. doi: 10.1262/jrd.2016-111
21. Sullivan MW, Stewart-Akers A, Krasnow JS, Berga SL, Zeleznik AJ. Ovarian responses in women to recombinant follicle-stimulating hormone and luteinizing hormone (LH): a role for LH in the final stage of follicular maturation. *J Clin Endocrinol Metab.* (1999) 84:228–32. doi: 10.1210/jc.84.1.228
22. Girard M, Allaire PD, McPherson PS, Blondeau F. Non-stoichiometric relationship between clathrin heavy and light chains revealed by quantitative comparative proteomics of clathrin-coated vesicles from brain and liver. *Mol Cell Proteomics.* (2005) 4:1145–54. doi: 10.1074/mcp.M500043-MCP200
23. Welt CK, Styrkarsdottir U, Ehrmann DA, Gudmar T, Gudmundur A, Gudmundsson JA, et al. Variants in DENND1A are associated with polycystic ovary syndrome in women of European ancestry. *J Clin Endocrinol Metab.* (2012) 7:1342–7. doi: 10.1210/jc.2011-3478
24. Strauss JF, McAllister JM, Urbanek M. Persistence pays off for PCOS gene prospectors. *J Clin Endocrinol Metab.* (2012) 97:2286–8. doi: 10.1210/jc.2012-2109
25. Tasaka K, Masumoto N, Mizuki J, Ikebuchi Y, Ohmichi M, Kurachi H, et al. Rab3B is essential for GnRH-induced gonadotrophin release from anterior pituitary cells. *J Endocrinol.* (1998) 157:267–74. doi: 10.1677/joe.0.1570267

26. Marat AL, Dokainish H, McPherson PS. DENN domain proteins: regulators of Rab GTPases. *J Biol Chem.* (2011) 286:13791–800. doi: 10.1074/jbc.R110.217067
27. Pawel K, Amin H, Joseph AZ, Caesar ZL, Ken R, Matthew LS, et al. Epigenetic clock and methylation study of oocytes from a bovine model of reproductive aging. *Aging Cell.* (2021) 20:e13349. doi: 10.1111/acel.13349
28. Ignacio D, Eva CS, Raquel DT, Javier ÁM, de Rojas-de Petro ES, Domínguez-Rodríguez A, et al. miR-125a, miR-139 and miR-324 contribute to Urocortin protection against myocardial ischemia-reperfusion injury. *Sci Rep.* (2017) 7:8898. doi: 10.1038/s41598-017-09198-x
29. Rodosthenous RS, Burris HH, Sanders AP, Just AC, Dereix AE, Svensson K, et al. Second trimester extracellular microRNAs in maternal blood and fetal growth: an exploratory study. *Epigenetics.* (2017) 12:804–10. doi: 10.1080/15592294.2017.1358345
30. Romero-Ruiz A, Avendano MS, Dominguez F, Lozoya T, Molina-Abril H, Sangiao-Alvarellos S. Deregulation of miR-324/KISS1/kisspeptin in early ectopic pregnancy: mechanistic findings with clinical and diagnostic implications. *Am J Obstet Gynecol.* (2019) 220:e1–e17. doi: 10.1016/j.ajog.2019.01.228
31. Ghafouri-Fard S, Shoorei H, Taheri M. The role of microRNAs in ectopic pregnancy: a concise review. *Noncoding RNA Res.* (2020) 5:67–70. doi: 10.1016/j.ncrna.2020.04.002
32. Liu QY, Jiang XX, Tian HN, Guo HL, Guo H, Guo Y. Long non-coding RNA OIP5-AS1 plays an oncogenic role in ovarian cancer through targeting miR-324-3p/NFIB axis. *Eur Rev Med Pharmacol Sci.* (2020) 24:7266–75. doi: 10.26355/eurrev_202007_21881
33. Jiang YC, Ma JX. The role of MiR-324-3p in polycystic ovary syndrome (PCOS) via targeting WNT2B. *Eur Rev Med Pharmacol Sci.* (2018) 22:3286–93. doi: 10.26355/eurrev_201806_15147

Conflict of Interest: The authors declare that the research was conducted in the absence of any commercial or financial relationships that could be construed as a potential conflict of interest.

Publisher's Note: All claims expressed in this article are solely those of the authors and do not necessarily represent those of their affiliated organizations, or those of the publisher, the editors and the reviewers. Any product that may be evaluated in this article, or claim that may be made by its manufacturer, is not guaranteed or endorsed by the publisher.

frontiers in Veterinary Science

ORIGINAL RESEARCH
published: 22 November 2021
doi: 10.3389/fvets.2021.709737

Effects of *FecB* Mutation on Estrus, Ovulation, and Endocrine Characteristics in Small Tail Han Sheep

Xiangyu Wang[1†], *Xiaofei Guo*[2†], *Xiaoyun He*[1], *Qiuyue Liu*[3], *Ran Di*[1], *Wenping Hu*[1], *Xiaohan Cao*[1], *Xiaosheng Zhang*[2], *Jinlong Zhang*[2] *and Mingxing Chu*[1*]

[1] *Key Laboratory of Animal Genetics, Breeding and Reproduction of Ministry of Agriculture and Rural Affairs, Institute of Animal Science, Chinese Academy of Agricultural Sciences, Beijing, China,* [2] *Institute of Animal Husbandry and Veterinary Medicine, Tianjin Academy of Agricultural Sciences, Tianjin, China,* [3] *Institute of Genetics and Developmental Biology, The Innovation Academy for Seed Design, Chinese Academy of Sciences, Beijing, China*

The Booroola fecundity gene (*FecB*) has a mutation that was found to increase the ovulation rate and litter size in Booroola Merino sheep. This mutation is also associated with the fecundity of small-tail han (STH) sheep, an important maternal breed used to produce hybrid offspring for mutton production in China. Previous research showed that the *FecB* gene affects reproduction in STH sheep, based on litter size records. However, the effects of this gene on estrus, ovulation, and endocrine characteristics in these sheep remain unclear. Here, we analyzed the traits mentioned earlier and compared them among the three *FecB* genotypes of STH ewes using estrus synchronization. Overall, 53 pluriparous ewes were selected from among 890 STH ewes and subjected to *FecB* genotyping for experiments to characterize estrous and ovulation rates. *FecB* heterozygous (+B) ewes presented an earlier onset of estrus (42.9 ± 2.2 h) and a shorter estrous cycle (17.2 ± 0.2 days) ($P \leq 0.05$). The ovulation rates increased with the increasing copy number of the B allele ($P \leq 0.01$). Ovulation time showed no significant differences among the three *FecB* genotypes. The serum concentrations of follicle-stimulating hormone (FSH), luteinizing hormone, estrogen (E_2), and progesterone (P_4) were measured in 19 of the ewes. Serum concentrations of E_2 and FSH dramatically varied around the time of behavioral estrus. In *FecB* mutant homozygous (BB) ewes, E_2 concentration had two peaks, which were higher ($P \leq 0.05$) than those of ++ genotypes. FSH concentration of BB ewes was higher ($P \leq 0.05$) than that of the ++ ewes just after estrus. The expression of the estrogen receptor 1 (*ESR1*) gene in the +B genotype was higher than in the other genotypes. Based on the data for the reproductive performance of STH ewes with the three *FecB* genotypes, our study suggests that the development of follicles in ewes with the B allele is dependent on the response to FSH regulated by E_2 in the early stage. +B ewes, exhibiting moderate ovulation and litter size and a shorter estrous cycle, can be highly recommended in sheep crossbreeding systems for commercial mutton production. Moreover, this study provides useful information to conserve better and use the genetic resources of STH sheep in China.

Keywords: sheep, *FecB* gene, estrus, ovulation, reproduction hormones, hormone receptors

OPEN ACCESS

Edited by:
Xin Wang,
Northwest A&F University, China

Reviewed by:
Zhongwei Wang,
Institute of Hydrobiology, Chinese Academy of Sciences (CAS), China
Gan Shangquan,
Xinjiang Academy of Agricultural and Reclamation Sciences (XAARS), China

***Correspondence:**
Mingxing Chu
chumingxing@caas.cn

[†] *These authors have contributed equally to this work*

Specialty section:
This article was submitted to Livestock Genomics, a section of the journal Frontiers in Veterinary Science

Received: *14 May 2021*
Accepted: *08 October 2021*
Published: *22 November 2021*

Citation:
Wang X, Guo X, He X, Liu Q, Di R, Hu W, Cao X, Zhang X, Zhang J and Chu M (2021) Effects of FecB Mutation on Estrus, Ovulation, and Endocrine Characteristics in Small Tail Han Sheep. Front. Vet. Sci. 8:709737. doi: 10.3389/fvets.2021.709737

INTRODUCTION

The *FecB* gene, also called *BMPR1B* (bone morphogenetic protein receptor type 1B), was initially identified in prolific Booroola Merino sheep. These sheep have a mutation (A746G) in the coding region of the *FecB* gene, leading to the substitution of glutamine for arginine in the protein (1–5). The *FecB* gene was shown to have an additive effect on ovulation rate and an effect on litter size that varies from additive to dominant depending on the genotype (6). Moreover, the *FecB* gene might be associated with a higher concentration of follicle-stimulating hormone (FSH) in peripheral blood during the estrous cycle (7–9). It has been reported that progesterone concentrations in Booroola ewes were 25% higher than in control Merino ewes during days 9–11 of the estrous cycle, although the difference did not reach significance (7, 10). *In vitro*, in the absence or presence of FSH, granulosa cells from BB ewes were found to be less responsive to the activity of *GDF5* and *BMP4*, resulting in higher progesterone secretion (3). In addition, it was suggested that granulosa cells carrying this *FecB* mutation might result in reduced proliferation but earlier responsiveness to LH in small follicles (11, 12). The estrous cycle is an external phenotype that is influenced by reproductive hormones (13). Small-tail han (STH) sheep are well known as a high-fecundity breed. The *FecB* mutation in this breed originates from Central Asian sheep, unlike the mutation in Booroola sheep (14). The average litter size of STH primiparous ewes is 2.00, and that of pluriparous ewes is 2.61. Many reports about frequency distributions of the *FecB* gene described that segregations of this gene are found in STH sheep. The +B and BB genotypes are the dominant genotypes in this breed, and the frequency of the B allele is greater than 0.5 (15). The *FecB* gene was shown to significantly affect litter size in STH sheep and other Chinese sheep breeds (16). Because of their excellent reproductive performance, STH sheep are widely used as the female parent in crossbreeding to improve the production efficiency of commercial mutton sheep. In the modern sheep industry, laparoscopic artificial insemination (AI) is being used to maximize reproductive potential. To achieve successful laparoscopic AI, the sheep breed and the signs of behavioral estrus are key factors to be taken into account (17). Based on research on Booroola Merino sheep, it was assumed that the *FecB* gene affects reproductive performance (4, 18). Unlike Booroola Merino sheep, STH sheep are a breed exhibiting year-round estrus. However, there has been little research on the effects of the *FecB* gene on the phenotypes of estrous time, estrous onset, estrous duration, estrous cycle, and subsequent ovulation time in this sheep breed. Therefore, there is a need to evaluate these factors.

Here, estrus and ovulation time traits were measured in three groups of estrus-synchronized STH ewes with different *FecB* genotypes. Combining estrus and ovulation data, we further analyzed the differences in hormonal patterns of the three genotypes in estrous cycles. By analyzing the expression profiles of hormone receptors in granulosa cells of preovulatory follicles in the different genotypes, we also analyzed how hormones coordinate with their receptors to generate signaling cascades that regulate follicle selection and maturation. This research should provide additional insight into the effect of the *FecB* gene on estrus and ovulation events and benefit future sheep reproductive production in China.

MATERIALS AND METHODS

Animals and Genotyping of *FecB* Gene by TaqMan Assay

Jugular vein blood and litter size data of 890 healthy non-pregnant ewes aged approximately 3 years were collected randomly from a herd in southwest Shandong Province, China. These ewes were genotyped for the *FecB* gene by the TaqMan method. Primer sequences of *FecB*-TaqMan and its probe sequences are listed in **Table 1**. The 6-μl reaction system contained 1 μl of DNA, 3 μl of 2× TaqMan Universal Master Mix II (Thermo Fisher Scientific Inc., Waltham, MA, USA), 0.3 μl of each *FecB*-TaqMan primer, 0.15 μl of two probe primers, and 1.9 μl of H_2O. Polymerase chain reaction (PCR) amplification was performed on a Roche LightCycler 480 II System (Roche, Basel, Switzerland) under the following PCR conditions: incubation at 95°C for 10 min, followed by 40 cycles of 95°C for 30 s and 60°C for 1 min. The allelic discrimination data were analyzed using endpoint genotyping with the hydrolysis probe protocol.

Pluriparous ewes ($n = 53$) with similar body conditions were selected and divided into three groups based on the *FecB* genotype (23 wild-type ++ ewes, 16 heterozygote +B ewes, and 14 homozygous mutant BB ewes) for subsequent experiments.

Experimental Treatment and Design

During the spring, estrus synchronization in these three groups was performed using a controlled internal drug release device (CIDR) (EAZI-BREED® CIDR® Sheep and Goat Device, Pfizer Animal Health, Auckland, New Zealand) with 300 mg of progesterone in all ewes for 12 days without any use of exogenous hormones for superovulation. Only 250,000-IU vitamin A and 25,000-IU vitamin D were injected to protect the vaginal epithelium when the CIDR was inserted. Estrus synchronization was performed on ewes twice with an interval of 14 days. In the first synchronization of estrus in 53 sheep of the three genotypes, estrus response, estrus onset, estrus duration, ovulation time, ovulation rate, and hormonal patterns in these estrous cycles were recorded. In the second experiment, cumulus cells were collected from 12 ewes. All ewes were maintained in a barn with food and water *ad libitum*.

Estrus Determination

After removal of the CIDR, eight rams with proven high serving capacity were selected as teasers wearing an apron around their hypogastrium to detect estrus in the ewes. The 53 experimental ewes (23 ++, 16 +B, 14 BB) and rams were raised separately. CIDRs were removed at 6:00 a.m. Teasing was initially performed every 6 h (at 6:00, 12:00, 18:00, and 24:00) for 96 h (19–22). Teasing was subsequently performed

TABLE 1 | TaqMan primer and probe sequences for genotyping and Quantitative PCR primer information.

Gene	GenBank ID	Usage	Primer sequence (5′–3′)	
BMPR1B	NC_019463.2	Genotyping	Forward primer	CCAGCTGGTTCCGAGAGACA
			Reverse primer	CTTATACTCACCCAAGATGTTTTCATG
			Probe-A	AAATATATCAGACGGTGTTG-MGB
			Probe-G	AAATATATCGGACGGTGTTG-MGB
FSHR	NM_001009289.1	Quantitative PCR	Forward primer	CAAAGATCCTCCTGGTCCTGTTC
			Reverse primer	GTTCCTGGTGAAGATGGCGTAG
LHCGR	NM_001278566.2		Forward primer	GCTGAGAGTGAACTGAGTGACTG
			Reverse primer	CTGGTTCGGGAGCACATTGG
INHA	NM_001308579.1		Forward primer	GACTGGACAGACAGGAGACC
			Reverse primer	AGGACAACGCAGCAGGAG
ESR1	XM_027972563.1		Forward primer	TGCCATGTTTCAAACCCATCTTC
			Reverse primer	TCTATGACCAATGACCTCTCTGTG
CYP19A1	NM_001123000.1		Forward primer	TCGTCCTGGTCACCCTTCTG
			Reverse primer	CGGTCTCTGGTCTCGTCTGG
CYP17A1	NM_001009483.1		Forward primer	CTTACCATTGACAAAGGCACAGAC
			Reverse primer	GCTTAATGATGGCGAGATGAGTTG
RPL19	XM_004012836.2		Forward primer	F:AATGCCAATGCCAACTC
			Reverse primer	R:CCCTTTCGCTACCTATACC

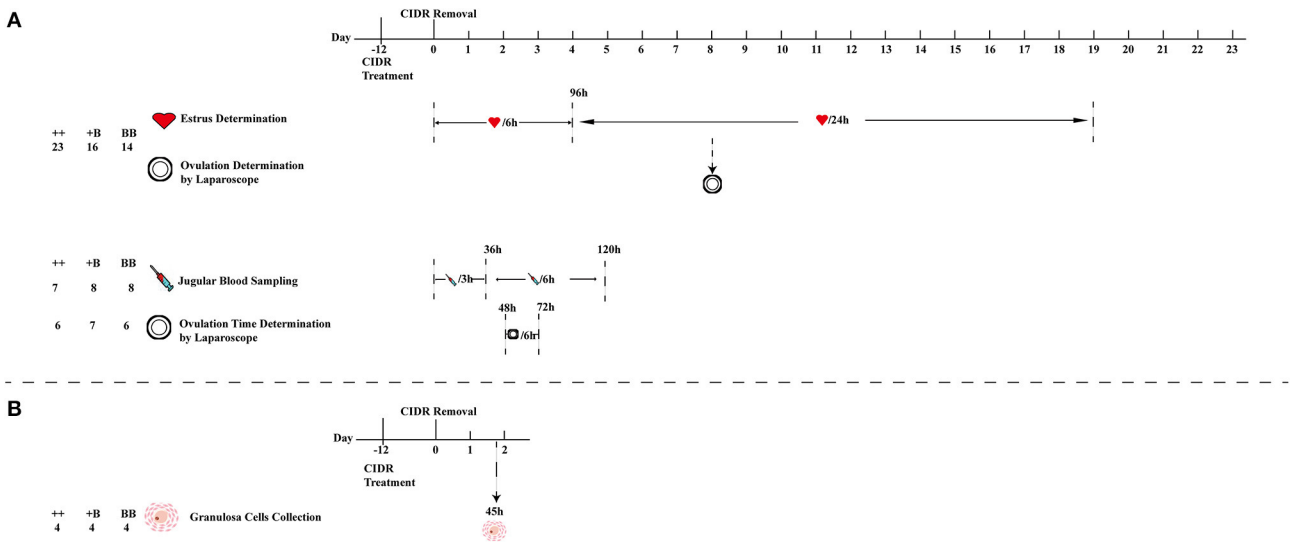

FIGURE 1 | Schematic workflow of estrus and ovulation determination, blood sampling, and granulosa cell collection. **(A)** First estrus synchronization of 53 ewes (23 ++, 16 +B, and 14 BB) for estrus and ovulation rate determination, 23 (7 ++, 8 +B and 8 BB) ewes from 53 ewes were selected for blood sampling, and 19 (6 ++, 7 +B and 6 BB) ewes from 53 ewes for ovulation time and rate determination. **(B)** Second estrus synchronization of 12 ewes for cumulus cell collection from follicles (>3 mm) at 45 h after CIDR removal.

only once a day at 6:00 a.m. until the initiation of the next estrus. Following established definition and procedures, traits of estrus response, estrus onset, and estrus duration of ewes of the three groups in the first estrous cycle were recorded and calculated (22). The first estrus was defined from the ewes' first accepted mount, and the estrous cycle was defined as the interval from the last refused mount to the next one. Details of the experimental process of estrus determination are presented in **Figure 1**.

Ovulation Determination

We randomly selected 6 ++ ewes, 7 +B ewes, and 6 BB ewes from among the 53 ewes of the three experimental groups to determine the ovulation time and rate by a modified version of the method reported by Romano et al. (22, 23). Laparoscopy was performed to determine ovulation at 48, 54, 60, 66, and 72 h after CIDR removal. The intervals from CIDR removal and estrus onset to first ovulation were respectively defined as the times elapsed from CIDR removal and estrus

onset to the time halfway between the first appearance of preovulatory follicles and their disappearance. The intervals from CIDR removal and estrus onset to the last ovulation were respectively defined as the times elapsed from CIDR removal and estrus onset to the time halfway between the last appearance of preovulatory follicles and their disappearance. The ovulation rate (the number of corpora lutea on both ovaries) was also recorded for all 53 sheep in the three groups using laparoscopy on day 8 after CIDR removal (**Figure 1**).

Blood Sampling and Hormonal Assays

Blood samples for testing hormone levels were collected from 7 ++, 8 +B, and 8 BB ewes from among the 53 ewes at the same time to determine the time of ovulation in the same batch. After removal of the CIDR at 06:00 a.m., 10 ml of jugular vein blood was collected in BD SST tubes (BD, San Diego, CA, USA) every 3 h for a 36-h period (24). From 36 to 120 h, blood was collected every 6 h. Jugular vein blood was kept at room temperature for 30 min, followed by centrifugation at 1,500×*g* for 10 min (25). The concentration of follicle-stimulating hormone (FSH) was determined using a commercial FSH [^{125}I]-labeled radioimmunoassay (RIA) kit (B03-FSH; Beijing North Institute of Biological Technology, BNIBT, Beijing, P. R. China). The sensitivity of the kit was <1.0 mIU/ml. The coefficient of variation (CV) in each batch was <10%, and the CV across the batch was <15%. Luteinizing hormone (LH) was quantified using a commercial LH [^{125}I]-labeled RIA kit (B04-LH; BNIBT). The kit sensitivity was 1.0 mIU/ml, and intra- and inter-batch CVs were <10 and <15%, respectively. The estradiol (E_2) concentration was tested using an E_2 RIA kit (B05-E2; BNIBT), the sensitivity of which was <2 pg/ml. The CVs for each batch and between the batches were <10 and 15%, respectively. Progesterone (P_4) was quantified using RIA kits (B08-P; BNIBT) with a sensitivity of <0.1 ng/ml, intra-batch CV of <10%, and inter-batch CV of <15%. To ensure the accuracy of hormone detection, triplicate assays were performed for each sample. The details are presented in **Figure 1**.

Granulosa Cell Collection and Real-Time Quantitative Polymerase Chain Reaction

Ewes (4 ++, 4 +B, and 4 BB) were used for estrus synchronization. At 45 h after CIDR removal, cumulus–oocyte complexes were aspirated from follicles > 3 mm in diameter with a syringe containing Dulbecco's phosphate-buffered saline (Thermo Fisher Scientific Inc.). Then, the cumulus–oocyte complexes were washed with Dulbecco's phosphate-buffered saline and digested with hyaluronidase. After 5 min of centrifugation at 2,000 rpm, the granulosa cells were gathered and lysed in 1 ml of Trizol (Thermo Fisher Scientific Inc.). The lysate was immediately frozen in liquid nitrogen and stored at −80°C for further RNA extraction.

Total RNA from cumulus cells was isolated following the Trizol protocol. One microgram of RNA was reverse-transcribed with PrimeScript RT Reagent Kit (TaKaRa, Shiga, Japan). Real-time quantitative PCR was performed on the LightCycler 480 Real-Time PCR system (Roche, Switzerland) with the SYBR Premix Ex Taq kit (TaKaRa), as described (26). Primer sequences for quantitative PCR are listed in **Table 1**. Ribosomal protein L19 (RPL19) was used as an internal reference gene, and the $2^{-\Delta\Delta Ct}$ method was used to determine the relative expression levels in messenger RNA analysis (27).

Data Analysis

Statistical analysis was performed using the generalized linear model Statistical Analysis System release 8.12 (SAS Institute Inc., NC, USA). All data are presented as the mean ± standard error of the mean, and $P \leq 0.05$ was considered significant. $P \leq 0.01$ was considered extremely significant. The statistical analyses of genotype frequency, allele frequency, and polymorphism information content were performed with reference to the formulas reported by Guo et al. (28). Traits in estrus determination, ovulation time, hormone concentrations in serum, and gene expression were continuous data. The normality of these continuous data was analyzed using the Shapiro–Wilk normality test. One-way analysis of variance was used to analyze the effect of *FecB* mutations on these normally distributed data. The data of the first estrus and estrus cycle were not normally distributed, so the Kruskal–Wallis nonparametric test was applied. Repeated-measures analysis of variance was adopted to analyze how hormonal (FSH, LH, E_2, and P_4) concentrations changed in different *FecB* genotypes over time. The estrus response was a binary variable, so Pearson's Chi-squared test was adopted to analyze the estrus response. Litter size and ovulation, traits measured as counts, are usually modeled by the Poisson distribution, so we analyzed the genotypic effects on litter size and ovulation rate through a generalized Poisson regression with log–link function using the generalized linear model GENMOD procedure of SAS. For litter size data, we set $Y_j = 0, 1, \ldots, \infty$ to be the litter size of individual sheep. The expectation (E) and the variance of litter size were calculated as $E\left(Y_j\right) = var\left(Y_j\right) = \mu_j$, where $\mu_j = \exp(\alpha_0 + X_j\beta + Z_j\gamma)$, α_0 is the intercept, β is a 3 × 1 vector for parity, and γ is a 3 × 1 vector for genotype. The ovulation data from 53 and 19 sheep were analyzed separately, letting $Y_j = 0, 1, \ldots, \infty$ be the ovulation rate of an individual. The expectation and the variance of ovulation rate were equivalent, $E\left(Y_j\right) = var\left(Y_j\right) = \mu_j$, where $\mu_j = \exp(\alpha_0 + X_j\beta)$, α_0 is the intercept, and β is a 3 × 1 vector for genotyping.

RESULTS

Characteristics of the *FecB* Gene in Small-Tail Han Ewes and Its Association With Litter Size

Using a TaqMan probe-based method, the allele and genotype frequencies of the *FecB* gene in experimental STH ewes were determined, as presented in **Table 2**. The frequencies of ++, +B, and BB genotypes were 0.16, 0.46, and 0.38, respectively; accordingly, the frequencies of the + and B alleles were 0.4

TABLE 2 | Genetic characteristics of *FecB* gene in STH ewes.

Polymorphic site	Genotype	Number of samples	Genotype frequency	Allele	Allele frequency	χ^2(P)	Polymorphism information content
FecB	++	142	0.16	+	0.40	0.61 (0.44)	0.47
	+B	413	0.46	B	0.60		
	BB	335	0.38				

TABLE 3 | Litter size of STH ewes in different parities and *FecB* genotypes.

Genotype	Litter size (Mean ± SEM)			
	First	Second	Third	Overall mean
++	1.77 ± 0.08 (115)^{A}	1.73 ± 0.09 (73)^{A}	2.05 ± 0.22 (20) ^{A}	1.78 ± 0.06 (208)^{A}
+B	2.04 ± 0.04 (330)^{B}	2.25 ± 0.06 (224)^{b}	2.76 ± 0.11 (85) ^{B}	2.21 ± 0.03 (639)^{B}
BB	2.32 ± 0 0.05 (251)^{C}	2.51 ± 0.07 (162)^{c}	3.00 ± 0.17 (54) ^{B}	2.46 ± 0.04 (467)^{C}
	P (Genotype) < 0.01**			
	P (Parity) < 0.01**			

Numbers of litter size analyzed for each genotype are indicated in brackets. Values with same capital letter for same column have no significant difference (P > 0.05). Values with different lowercases or capital for same line differ significantly (P ≤ 0.05). Double asterisk (**) indicates extreme significance (P ≤ 0.01).

and 0.6, respectively. Chi-squared fitness testing showed that *FecB* gene mutations were under Hardy–Weinberg equilibrium in the randomly selected ewes ($P > 0.05$). The polymorphism information content of the *FecB* gene exceeded 0.3, reflecting moderate polymorphism, implying that the selection potential of the sites was considerable. For the polymorphic sites of *FecB*, the results of variance analysis as shown in **Table 3** indicated that the litter size increased with increasing copy numbers of the B allele. Genotype and parity were shown to have significant effects on litter size. In each parity group, the mean litter size of the ++ genotype ewes was significantly smaller than in the other two genotypes. With increasing parity, the differences in litter size between BB and +B genotypes decreased. There was no significant difference in litter size between the BB ewes and +B ewes in terms of parity above two.

Estrus Performance After Estrus Synchronization

A total of 53 STH ewes of similar ages (2.9 ± 0.1 years) and weights (72.5 ± 1.9 kg) were selected for an estrus determination experiment based on the estrus synchronization technique. After CIDR removal, apart from the estrus duration (32.6 ± 1.4 h), all other estrous cycle indexes were significantly affected by *FecB* (**Table 4**). The first estrus for +B STH ewes was 23.6 ± 1.9 h from CIDR removal, which was earlier than in the ++ and BB genotypes at 32.6 ± 2.4 and 30.4 ± 1.6 h, respectively ($P < 0.05$). The cumulative estrus response is shown in **Figure 2**; all ewes presented estrus. The STH ewes with the +B genotype had an earlier response to estrus synchronization treatment, whereas the response of BB STH ewes had a narrower distribution.

The onset of estrus in +B STH ewes was 42.9 ± 2.2 h from CIDR removal, which was also earlier than in ++ and BB genotypes with 51.5 ± 2.0 and 50.0 ± 1.7 h ($P < 0.05$). Compared with 17.9 ± 0.1 and 17.9 ± 0.2 days in the STH ewes with ++ and BB genotypes, a shorter estrous cycle of 17.2 ± 0.2 days was observed in the ewes with the +B genotype. The findings suggested that STH ewes with *FecB* heterozygosity (+B) may exhibit an earlier first estrus, earlier estrus onset, and a shorter estrous cycle.

TABLE 4 | Estrus and ovulation comparison in STH ewes of three *FecB* genotypes.

Genotype	++	+B	BB	Total
Number of samples	23	16	14	53
Age (y)	2.8 ± 0.1	2.8 ± 0.2	3.0 ± 1.1	2.8 ± 0.1
Weight (kg)	73.8 ± 2.7	73.0 ± 4.6	70.1 ± 3.1	72.5 ± 1.9
Estrus response	23	16	14	53
First estrus (h)	32.6 ± 2.4^{a}	23.6 ± 1.9^{b}	30.4 ± 1.6^{a}	29.3 ± 1.3
Estrus onset (h)	51.5 ± 2.0^{a}	42.9 ± 2.2^{b}	50.0 ± 1.7^{a}	48.5 ± 1.3
Last estrus (h)	65.0 ± 2.4^{a}	56.3 ± 2.9^{b}	63.4 ± 2.9^{ab}	61.9 ± 1.6
Estrus duration (h)	32.4 ± 2.3	32.6 ± 2.3	33.0 ± 3.1	32.6 ± 1.4
Estrus cycle (d)	17.9 ± 0.1^{a}	17.2 ± 0.2^{b}	17.9 ± 0.2^{a}	17.7 ± 0.1
Ovulation Rate	1.09 ± 0.02^{A}	2.38 ± 0.13^{b}	3.07 ± 0.35^{c}	2.02 ± 0.17

Values with same lowercase for same line have no significant difference (P > 0.05). Values with different lowercases or capital for same line differ significantly (P ≤ 0.05) or extreme significantly (P ≤ 0.01).

Ovulation Times and Rates in Small-Tail Han Ewes

Ovulation times and rates in STH ewes among the three genotype groups were observed laparoscopically. The mean interval from CIDR removal to first ovulation in STH ewes was 58.1 ± 2.7 h (**Table 5**). We noted that the interval from CIDR removal to

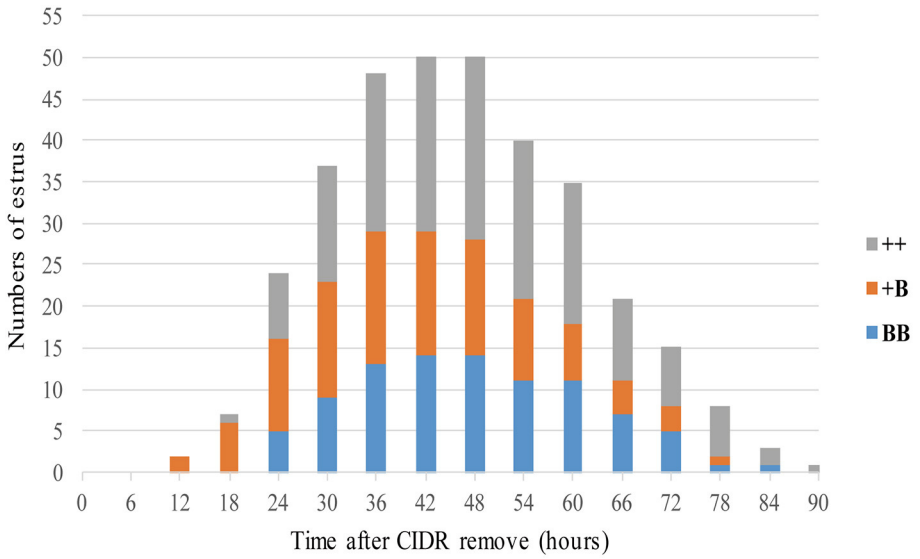

FIGURE 2 | Numbers of ewes in estrus among three *FecB* genotype groups after CIDR removal.

TABLE 5 | Ovulation traits of STH ewes in three *FecB* genotypes.

Items	Genotype		
	++	+B	BB
Number of samples	6	7	6
Interval from CIDR removal to first ovulation(h)	63.0 ± 5.8	52.2 ± 4.4	58.0 ± 3.3
Interval from estrus onset to first ovulation(h)	9.5 ± 2.9	10.2 ± 0.7	9.3 ± 2.0
Interval from CIDR removal to last ovulation(h)	63.3 ± 5.8	55.8 ± 4.4	62.0 ± 3.6
Interval from estrus onset to last ovulation(h)	9.8 ± 3.1	13.8 ± 3.4	13.3 ± 2.3
Ovulation Rate	1.17 ± 0.41^{a}	2.43 ± 0.98^{B}	2.00 ± 0.63^{b}

Values with same lowercase for same line have no significant difference ($P > 0.05$). Values with different lowercases or capital for same line differ significantly ($P \leq 0.05$) or extreme significantly ($P \leq 0.01$).

first ovulation for +B STH ewes appeared to be shorter (52.2 ± 4.4 h), albeit not significantly ($P = 0.30$). The mean intervals from first estrus and estrus onset to first ovulation in STH ewes were 26.3 ± 2.0 and 9.7 ± 1.2 h, respectively. The three *FecB* genotype groups did not differ significantly in any of the variables related to ovulation time. For the ewes with *FecB* mutation, the ovaries did not expel eggs simultaneously. Endoscopy performed every 6 h to estimate the time of ovulation indicated that all ovulations occurred in a period no longer than 6 h. The ovulation rate was measured successfully in the 53 STH ewes (**Table 4**). The ovulation rate of BB ewes (3.07 ± 0.35) was significantly higher than that of +B ewes (2.38 ± 0.13; $P \leq 0.01$). Meanwhile, the ovulation rate of +B ewes was also highly significantly higher than that of ++ ewes (1.09 ± 0.02; $P \leq 0.01$). The *FecB* mutation significantly influenced the ovulation rate of STH ewes.

Serum Concentrations of P_4, Follicle-Stimulating Hormone, Luteinizing Hormone, and E_2 During a Synchronized Estrous Cycle in Small-Tail Han Ewes

The serum concentrations of FSH, LH, E_2, and P_4 were measured during an intact synchronized estrous cycle in 7 ++, 8 +B, and 8 BB ewes for 5 days after CIDR removal. Data presented in **Figure 3** show the mean endocrine profiles of these ewes. Upon CIDR withdrawal, the P_4 concentration rapidly dropped to a low level. E_2 and FSH concentrations started to increase and peaked at approximately 27 h, which was aligned with the first estrus time. At 60 h after CIDR removal, the peaks of E_2 and P_4 dropped before the LH peak. FSH concentration peaked at 72 h after the LH peak. These four hormone concentrations peaked over 60–72 h.

The time of the first estrus of +B STH ewes was earlier than those of the other two genotypes. To investigate the changes of endocrine characteristics in serum before and after estrus, mean FSH, LH, E_2, and P_4 concentrations were calculated in relation to their levels of each individual's time of the first estrus (hour 0; see **Figure 4**). In the three genotypes, P_4 dropped at around hour 0, whereas P_4 concentrations in BB ewes were higher than those in +B and ++ ewes. E_2 increased from hour 0 to 3 in all three genotypes. In BB ewes, E_2 exhibited two peaks (−6 and 3 h), at which the E_2 concentrations were higher ($P \leq 0.05$) than in the ++ genotypes. In ++ and +B ewes, the FSH concentrations dropped before hour 0. The FSH concentrations of ++ and BB ewes increased after hour 0 and peaked at hour 3. BB ewes had significantly higher ($P \leq 0.05$) FSH concentrations than ++ ewes. LH concentrations increased at −3 h and decreased at 3 h, particularly in BB ewes. LH concentrations at 3 h were lower ($P \leq 0.05$) than in the ++ ewes, whereas those in +B ewes were intermediate.

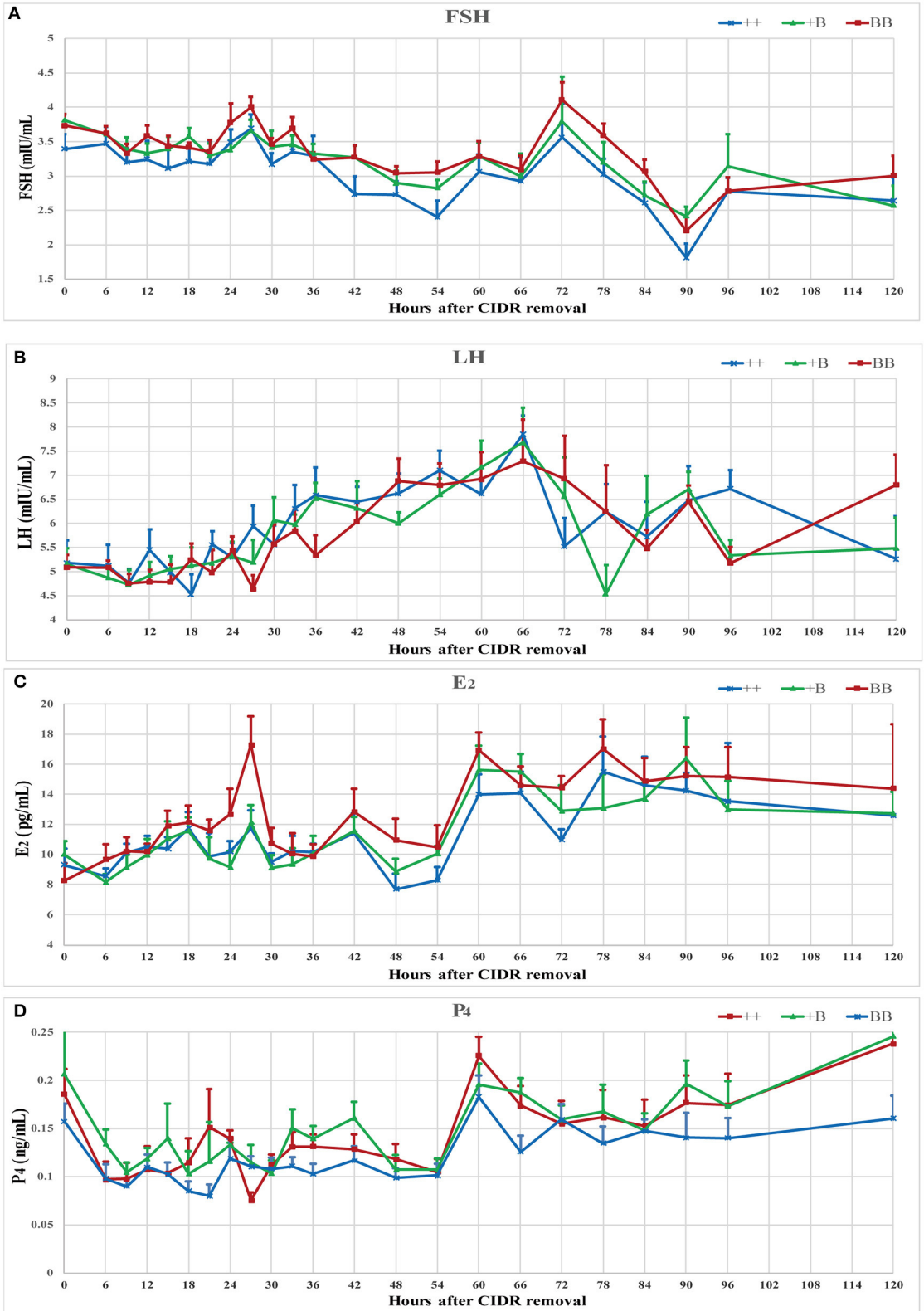

FIGURE 3 | Endocrine profiles of reproductive hormone (FSH, LH, E_2, and P_4) in ewes of three *FecB* genotypes during a synchronized estrous cycle. **(A)** Mean ± SEM of serum FSH (mU/ml), **(B)** Mean ± SEM of serum LH (mU/ml), **(C)** Mean ± SEM of serum E_2 (pg/ml), and **(D)** Mean ± SEM of serum P_4 (pg/ml).

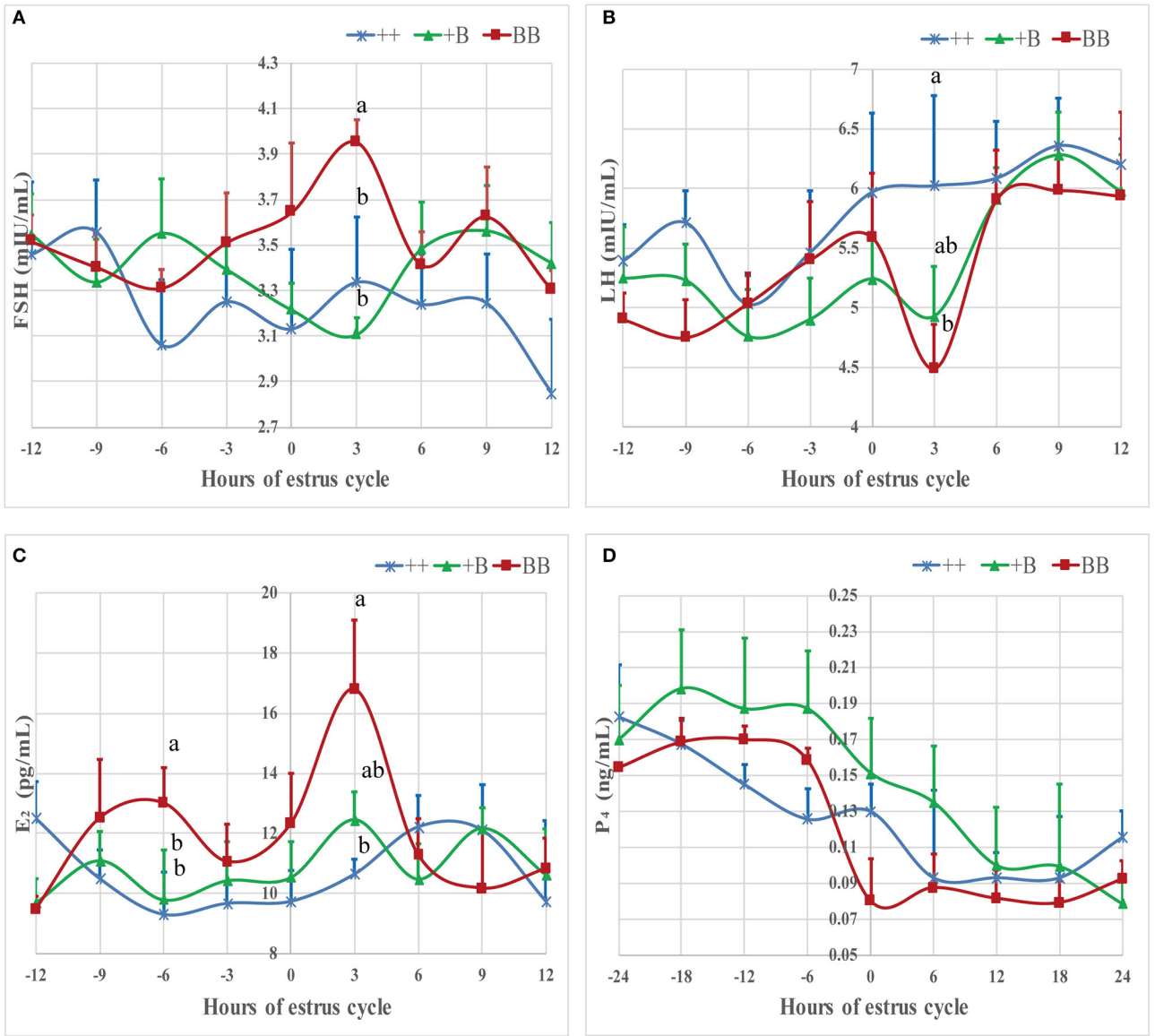

FIGURE 4 | Mean ± SEM of serum FSH, LH, E_2, and P_4 concentration before and after initiation of first estrus (hour 0 is initiation of first estrus) in different FecB genotype ewes. Values with same capital letter for same column have no significant difference ($P > 0.05$). Values with different lowercases or capital for same line differ significantly ($P \leq 0.05$). **(A)** Mean ± SEM of serum FSH (mU/ml), **(B)** Mean ± SEM of serum LH (mU/ml), **(C)** Mean ± SEM of serum E_2 (pg/ml), and **(D)** Mean ± SEM of serum P_4 (pg/ml).

Gene Expression in Granulosa Cells

Taking together the results of the temporal trends in reproductive hormone levels and estrus and ovulation times, granulosa cells were derived from preovulatory dominant follicles approximately 45 h after CIDR removal. Total RNA was extracted and subjected to quantitative real-time PCR to analyze the expression of steroidogenic genes, cytochrome P450, family 17, subfamily A, polypeptide 1 (*CYP17A1*) and cytochrome P450, family 19, subfamily A, polypeptide 1 (*CYP19A1*); gonadotropin receptors, follicle-stimulating hormone receptor (*FSHR*) and luteinizing hormone/choriogonadotropin receptor (*LHCGR*); estrogen receptor 1 (*ESR1*); and the inhibin subunit alpha (*INHA*) (**Figure 5**). Expressions of the genes for the FSH and LH receptors were detected during the preovulatory stage, whereas no significant differences in the expression of these two genes were observed across the three genotypes. The expression of *ESR1* in the +B genotype was higher ($p \leq 0.05$) than in the wild-type (++) genotype. *ESR1* expression in the BB genotype was higher than that in the wild type, but this did not reach significance. There was a trend for an increase of *INHA* expression with increasing *FecB* mutant copy number ($P = 0.08$). The expression of *CYP17A1* and *CYP19A1*, markers of preovulatory follicles, also appeared at 45 h after CIDR removal when we collected the sample.

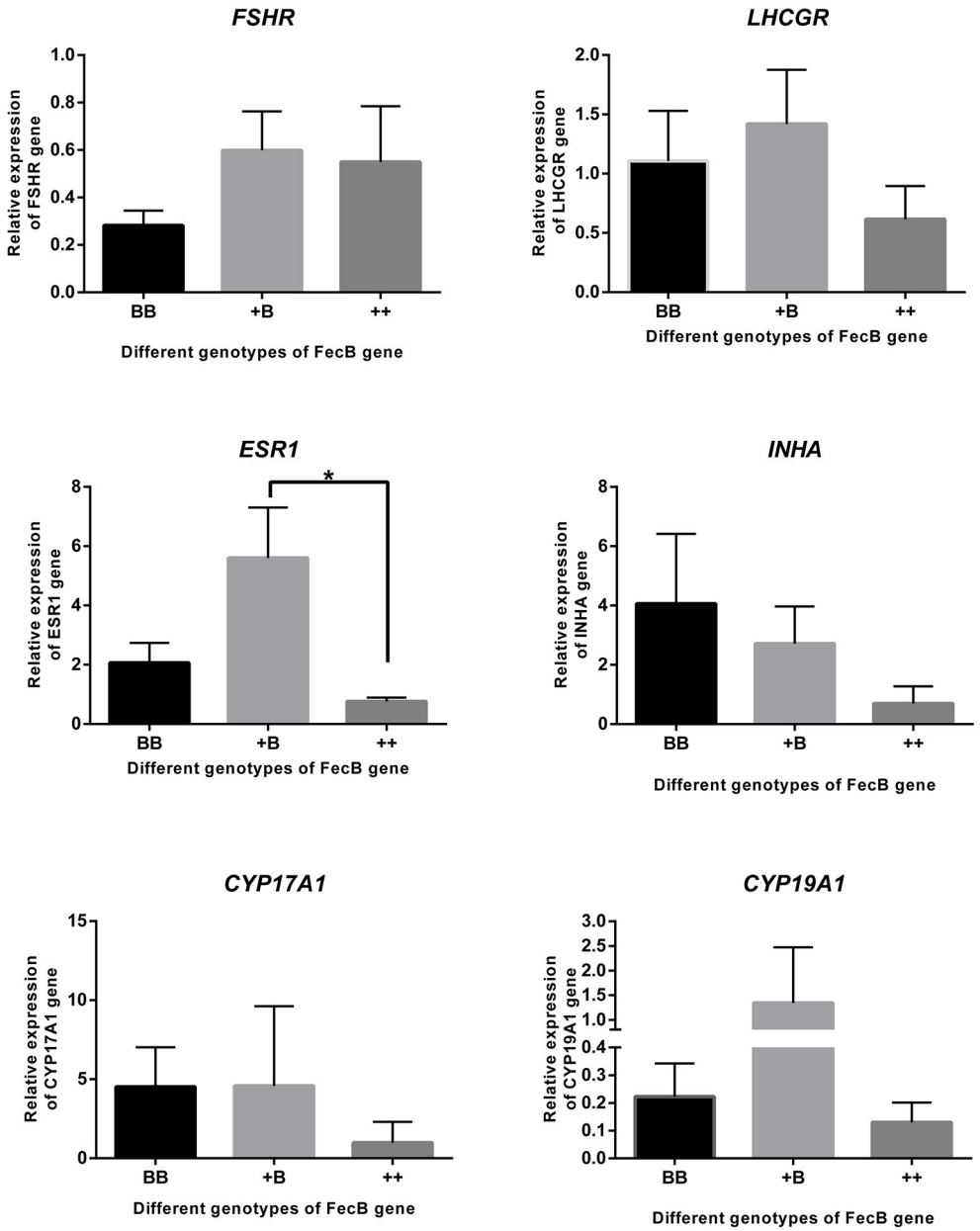

FIGURE 5 | Gene expression in granulosa cells. *FSHR*, *LHCGR*, *ESR1*, *INHA CYP17A1,* and *CYP19A1* genes were quantified using RNA from cumulus cells of follicles (>3 mm) by real-time PCR analysis. Data are mean ± SEM of relative expression level calculated by $2^{-\Delta\Delta Ct}$ method using *RPL19* gene as reference. An asterisk indicates a significant difference ($P \leq 0.05$) between means from wild-type (++) and heterozygous sheep of *FecB* mutation (+B).

DISCUSSION

STH sheep are derived from ancient northern Mongolian sheep, which are widely raised throughout northern China. The effect of *FecB* mutation in STH matches that identified in Booroola Merino sheep: it can significantly increase the litter size of STH sheep (16, 29, 30). Genetic analysis of the *FecB* gene in this study showed that the three *FecB* genotypes are still not fixed in this STH sheep population collected from a population set aside for conservation. The *FecB* gene showed moderate polymorphisms, meaning that no significant selection response has occurred in the last decade (15, 31). This is good news regarding the protection of genetic diversity and of benefit for efforts to exploit the genetic resources of STH sheep in China.

The *BMPR1B* gene is a member of the transforming growth factor-β superfamily, which is critical for skeletal development, organ formation, and embryo development. Many studies have shown that *FecB* mutations influence ovulation rate, litter size, reproductive endocrinology, adrenal gland size, body mass, follicular development, fetal growth, milk production, and

sperm concentration, among others (32–36). With regard to reproductive endocrinology, such mutations can control external estrous characteristics and affect oocyte development. However, little research has been reported on the correlation between *FecB* mutation and estrous characteristics in STH sheep. Here, the estrous indexes of *FecB* heterozygous (+B) STH sheep differed from those in the other genotype groups, presenting an earlier first estrus, earlier estrus onset, and a shorter estrous cycle. However, no differences were observed in ovulation time among the three *FecB* STH genotypes. An investigation of ++ and +B ewes from a three-quarters Romney Marsh × one-quarter Booroola Merino flock after spontaneous estrus induced with progesterone treatment during the reproductive season also found that the *FecB* gene cannot change the duration of ovulation (37). The duration from the first estrus to ovulation was longer in +B STH sheep than in the ++ and BB groups. These results indicate that the *FecB* mutation accelerated the onset of estrus in heterozygote +B STH sheep but had no effect on the onset of ovulation. The +B genotype constituted almost half (0.46) of the total in the STH sheep group; the fecund +B genotype sheep are usually used as maternal parents in crossbreeding programs in commercial mutton production (15). *FecB* gene mutation can result in a change in the estrous phenotype, which is usually the main indicator for determining whether to perform AI (38). When using estrus synchronization with AI in mutton production, we should establish marker-assisted mating and breeding programs. Considering the production cost, prohibition on the use of castrated rams for estrus detection, and the full use of high-breeding-value rams, timed insemination is the optimal mating strategy (39). Combining previous research results and the data of ovulation time from CIDR measured in the three STH *FecB* genotype groups, it was recommended that fixed-time AI be performed between 48 and 60 h after CIDR removal (40, 41).

These results are consistent with previous findings showing that *FecB* mutations appear to have no effect on endocrine profiles (42). In our research, ewes with an *FecB* mutation showed premature estrus. We calculated the individual endocrine data after the time of the first estrus. Before estrus, the ewes with the BB genotype exhibited a peak in E_2 level, which was the highest among the three genotypes. After estrus, E_2 exhibited a second peak. During the growing follicle stage, E_2 downregulates the synthesis and secretion of LH and FSH *via* negative feedback to the hypothalamus and pituitary (43). Our results showed that FSH was not markedly inhibited in the BB genotype; on the contrary, FSH showed significant elevation with a peak at 3 h after estrus. This is in accordance with research on the peripheral FSH concentrations in an F_2 population from a cross between Booroola Merino and Scottish Blackface sheep during the breeding season (44). As the follicles mature, E_2 levels peak, and then positive feedback begins, triggering the release of preovulatory LH and an FSH surge (45). The interval from estrus onset to first ovulation suggested that the ewes started estrus approximately 10 h after estrus was detected. LH secretion in ewes peaked at 9 h after estrus. The concentration of FSH was lower than the peak at 3 h after estrus. Increasing FSH of BB ewes accelerated follicle development, meaning that the follicles reached maturity while still having a small diameter. Before ovulation, the FSH concentration decreased during follicle selection, and LH increased to enable the follicles to survive and proceed to ovulation (46). During antral follicle development, the expression of estrogen receptors and *CYP19A1* and E_2 concentrations significantly increase in granulosa cells (47). The expression pattern of estrogen receptors was similar to that of *CYP19A1* among the three genotypes; in our results, only the expression of *ESR1* was affected by *FecB* mutation. *CYP17A1* and *CYP19A1* play important roles in the steroidogenic pathway. *CYP17A1* expression was higher in the large follicles. LH *via* *LHCGR* induced the messenger RNA expression of *CYP17A1* in ovaries (48, 49). In the large follicles that we collected, we detected the expression of *CYP17A1* and *LHCGR*. The expression in the ewes with the *FecB* mutation was slightly higher than in the wild type. We also detected the expression of *FSHR* in mature follicles, in agreement with previous findings (50). These two receptors, *FSHR* and *LHCGR*, have been reported to adjust the FSH and LH signaling cascades in granulosa cells and to regulate follicular development and ovulation (51).

Here, STH ewes of ++, +B, and BB genotypes showed significant increases in ovulation rate, and *FecB* mutation carriers had significantly larger litters than the wild-type sheep. These findings are in accordance with previous research reported by Davis et al. (52, 53). Combining the data on litter size, we conclude that the effect of the *FecB* gene on litter size is based on the regulation of the ovulation rate. However, litter size is influenced not only by ovulation rate but also by fertilization, embryonic survival, implantation, placentation, and parity (54). Moreover, *FecB* homozygotes were reported to have a smaller litter size than the heterozygotes in Australian Booroola Merino sheep (55). Therefore, an excessive ovulation rate should be avoided in ewes to prevent lower reproductive efficiency, and sheep with *FecB* heterozygosity exhibiting a higher ovulation rate and larger litter size are recommended for commercial hybrid sheep production in China.

CONCLUSION

With the exception of ovulation rate, our results show that the estrus performance of *FecB* heterozygote ewes differed from that of *FecB* homozygote and wild-type ewes, as revealed using estrus synchronization. The development of follicles in ewes with the B allele depended on the response to FSH in the early stage of estrus. *FecB* heterozygote ewes, exhibiting moderate ovulation and litter size and a shorter estrous cycle, can be highly recommended in sheep crossbreeding systems for commercial mutton production. Moreover, the findings obtained in this study should be useful for improving conservation and to better exploit the genetic resources of STH sheep.

DATA AVAILABILITY STATEMENT

The original contributions presented in the study are included in the article/**Supplementary Materials**, further inquiries can be directed to the corresponding author/s.

ETHICS STATEMENT

All experimental procedures conducted in this study were performed in accordance with the guidelines set by the Ethics Committee of the Institute of Animal Science, Chinese Academy of Agricultural Sciences, and approved by the committee (no. IASCAAS-AE-03, 12 December 2016).

AUTHOR CONTRIBUTIONS

XW, XG, and MC designed this study. XW and XG performed the experimental, processed and analyzed the data, drafted the manuscript, and prepared all the figures and tables. XH and XC collected some serum samples. XW, XG, XZ, and JZ detected the ovulation time and rate. QL, RD, WH, and MC contributed to revisions of the manuscript. All authors read and approved the final manuscript.

FUNDING

This work was supported by the National Natural Science Foundation of China (Nos. 31772580, 31501926, and 31902150), Agricultural Science and Technology Innovation Program of China (CAAS-ZDRW202106 and ASTIP-IAS13), Central Public-Interest Scientific Institution Basal Research Fund (No. 2018ywf-yb-2), Earmarked Fund for China Agriculture Research System (CARS-38), Tianjin Agricultural Science and Technology Achievements Transformation and Popularization Program (Grant No. 201704020), Natural Science Foundation of Tianjin (No. 20JCQNJC00630), and the Natural Science Foundation of Jilin Province (20210101376JC).

ACKNOWLEDGMENTS

We thank the staff of the Tianjin Institute of Animal Sciences for sheep care and management. We also thank Chengjun Huang and Kuanfeng Zhu for helping with the collection of serum samples and Mingyu Shang for help with data collection. We are grateful to Dr. Shizhong Xu (Department of Botany and Plant Sciences, University of California, Riverside) and Dr. Fuping Zhao (Institute of Animal Science, Chinese Academy of Agricultural Sciences) for statistical modeling guidance. We thank Liwen Bianji (Edanz) (http://www.liwenbianji.cn/) for editing the English text of a draft of this manuscript.

SUPPLEMENTARY MATERIAL

The Supplementary Material for this article can be found online at: https://www.frontiersin.org/articles/10.3389/fvets.2021.709737/full#supplementary-material

REFERENCES

1. Liu Q, Pan Z, Wang X, Wenping HU, Ran DI, Yao Y, et al. Progress on major genes for high fecundity in ewes. *Front Agr Sci Eng.* (2014) 1:282–90. doi: 10.15302/J-FASE-2014042
2. Davis GH, Montgomery GW, Allison AJ, Kelly RW, Bray AR. Segregation of a major gene influencing fecundity in progeny of Booroola sheep. *N Z L J Agr Res.* (1982) 67:525–9. doi: 10.1080/00288233.1982.10425216
3. Mulsant P, Lecerf F, Fabre S, Schibler L, Monget P, Lanneluc I, et al. Mutation in bone morphogenetic protein receptor-IB is associated with increased ovulation rate in Booroola Mérino ewes. *Proc Natl Acad Sci U S A.* (2001) 98:5104–9. doi: 10.1073/pnas.091577598
4. Wilson T, Wu XY, Juengel JL, Ross IK, Lumsden JM, Lord EA, et al. Highly prolific Booroola sheep have a mutation in the intracellular kinase domain of bone morphogenetic protein IB receptor (ALK-6) that is expressed in both oocytes and granulosa cells. *Biol Reprod.* (2001) 64:1225–35. doi: 10.1095/biolreprod64.4.1225
5. Souza CJ, Macdougall C, Macdougall C, Campbell BK, Mcneilly AS, Baird DT. The Booroola (FecB) phenotype is associated with a mutation in the bone morphogenetic receptor type 1 B (BMPR1B) gene. *J Endocrinol.* (2001) 169:1–6. doi: 10.1677/joe.0.169r001
6. Fogarty NM. A review of the effects of the Booroola gene (FecB) on sheep production. *Small Rumin Res.* (2009) 85:75–84. doi: 10.1016/j.smallrumres.2009.08.003
7. Xia Y, O'Shea T, Murison R, Mcfarlane JR. Concentrations of progesterone, follistatin, and follicle-stimulating hormone in peripheral plasma across the estrous cycle and pregnancy in merino ewes that are homozygous or noncarriers of the Booroola gene. *Biol Reprod.* (2003) 69:1079–84. doi: 10.1095/biolreprod.102.005512
8. McNatty KP, Fisher M, Collins F, Hudson NL, Heath DA, Ball K, et al. Differences in the plasma concentrations of FSH and LH in ovariectomized Booroola FF and ++ ewes. *J Reprod Fertil.* (1989) 85:705–13. doi: 10.1530/jrf.0.0850705
9. Fleming JS, Tisdall DJ, Greenwood PJ, Hudson NL, Heath DA, Mcnatty KP. Expression of the genes for alpha inhibin, beta A inhibin and follistatin in the ovaries of Booroola ewes which were homozygotes or non-carriers of the fecundity gene FecB. *J Mol Endocrinol.* (1992) 8:265–73. doi: 10.1677/jme.0.0080265
10. Bindon BM. Reproductive biology of the Booroola Merino sheep. *Aust J Biol Sci.* (1984) 37:163–89. doi: 10.1071/BI9840163
11. Mcnatty KP, Heath DA, Hudson NL, Lun S, Juengel JL, Moore LG. Gonadotrophin-responsiveness of granulosa cells from bone morphogenetic protein 15 heterozygous mutant sheep. *Reproduction.* (2009) 138:545–51. doi: 10.1530/REP-09-0154
12. Juengel JL, Davis GH, McNatty KP. Using sheep lines with mutations in single genes to better understand ovarian function. *Reproduction.* (2013) 146:R111–23. doi: 10.1530/REP-12-0509
13. K.A. Raheem. A review of reproductive events in sheep. *J Sustain Agric Environ.* (2014) 15:258–75.
14. Notter DR. Genetic aspects of reproduction in sheep. *Reprod Domest Anim.* (2008) 43:122–8. doi: 10.1111/j.1439-0531.2008.01151.x
15. Hua GH, Yang LG. A review of research progress of *FecB* gene in Chinese breeds of sheep. *Anim Reprod Sci.* (2009) 116:1–9. doi: 10.1016/j.anireprosci.2009.01.001
16. Chu M, Jia L, Zhang Y, Jin M, Chen H, Fang L, et al. Polymorphisms of coding region of BMPR - IB gene and their relationship with litter size in sheep. *Mol Biol Rep.* (2011) 38:4071–6. doi: 10.1007/s11033-010-0526-z
17. Gourley DD, Riese RL. Laparoscopic artificial insemination in sheep. *Vet Clin North Am Food Anim Pract.* (1990) 6:615–33. doi: 10.1016/S0749-0720(15)30836-7
18. Souza CJ, Campbell BK, McNeilly AS, Baird DT. Bone morphogenetic proteins and folliculogenesis: lessons from the Booroola mutation. *Reprod Suppl.* (2003) 61:361–70.
19. J.E. Romano. Effect of service on estrus duration in dairy goats. *Theriogenology.* (1993) 40:77–84. doi: 10.1016/0093-691X(93)90342-3
20. J.E. Romano. Effects of different stimuli of service on estrus duration in dairy goats. *Theriogenology.* (1994) 42:875–9. doi: 10.1016/0093-691X(94)90455-R
21. Romano JE, Benech A. Effect of service and vaginal-cervical anesthesia on estrus duration in dairy goats. *Theriogenology.* (1996) 45:691–6. doi: 10.1016/0093-691X(95)00415-5
22. Romano JE, Alkar A, Fuentes-Hernández VO, Amstalden M. Continuous presence of male on estrus onset, estrus duration, and

ovulation in estrus-synchronized Boer goats. *Theriogenology.* (2016) 85:1323–7. doi: 10.1016/j.theriogenology.2015.12.018
23. Romano JE, Fernandez Abella D. Effect of service on duration of oestrus and ovulation in dairy goats. *Anim Reprod Sci.* (1997) 47:107–12. doi: 10.1016/S0378-4320(96)01633-8
24. Drouilhet L, Taragnat C, Fontaine J, Duittoz A, Mulsant P, Bodin L, et al. Endocrine characterization of the reproductive axis in highly prolific Lacaune sheep homozygous for the FecLL mutation. *Biol Reprod.* (2010) 82:815–24. doi: 10.1095/biolreprod.109.082065
25. Bernini P, Bertini I, Luchinat C, Nincheri P, Staderini S, Turano P. Standard operating procedures for pre-analytical handling of blood and urine for metabolomic studies and biobanks. *J Biomol NMR.* (2011) 49:231–43. doi: 10.1007/s10858-011-9489-1
26. Guo X, Wang X, Liang B, Di R, Liu Q, Hu W, et al. Molecular cloning of the B4GALNT2 gene and its single nucleotide polymorphisms association with litter size in small tail han sheep. *Animals.* (2018) 8:160. doi: 10.3390/ani8100160
27. Livak KJ, Schmittgen TD. Analysis of relative gene expression data using real-time quantitative PCR and the 2−ΔΔCT method. *Methods.* (2001) 25:402–8. doi: 10.1006/meth.2001.1262
28. Guo XF, Hu WP, Lang XZ, Li QL, Wang XY, Di R, et al. Two single nucleotide polymorphisms sites in α1-AT gene and their association with somatic cell score in Chinese Holstein cows. *J Biol Res.* (2017) 24:8. doi: 10.1186/s40709-017-0065-z
29. Chu MX, Liu ZH, Jiao CL, He YQ, Fang L, Ye SC, et al. Mutations in BMPR-IB and BMP-15 genes are associated with litter size in Small Tailed Han sheep (Ovis aries). *J Anim Sci.* (2007) 85:598–603. doi: 10.2527/jas.2006-324
30. Qi MY, Xu LQ, Zhang JN, Li MO, Lu MH, Yao YC. Effect of the Booroola fecundity (FecB) gene on the reproductive performance of ewes under assisted reproduction. *Theriogenology.* (2020) 142:246–50. doi: 10.1016/j.theriogenology.2019.10.038
31. Wang W, Liu S, Li F, Pan X, Li C, Zhang X, et al. Polymorphisms of the Ovine BMPR-IB, BMP-15 and FSHR and Their Associations with Litter Size in Two Chinese Indigenous Sheep Breeds. *Int J Mol Sci.* (2015) 16:11385–97. doi: 10.3390/ijms160511385
32. Pardeshi VC, Maddox JM, Kadoo NY, Gupta VS. Genetic modulation of the FecB gene expression. *ACIAR Proc Series.* (2009) 133:57–65.
33. Smith P, Hudson NL, Corrigan KA, Shaw L, Smith T, Phillips DJ, et al. Effects of the Booroola gene (FecB(B)) on bodymass, testis development and hormone concentrations during fetal life. *J Reprod Fertil.* (1993) 98:41.
34. Souza CJ, Baird DT. The Booroola (FecB) mutation is associated with smaller adrenal glands in young adult ewes. *Reprod Biomed Online.* (2004) 8:414–8. doi: 10.1016/S1472-6483(10)60925-X
35. Kumar S, Mishra AK, Kolte AP, Arora AL, Singh D, Singh VK. Effects of the Booroola (FecB) genotypes on growth performance, ewe's productivity efficiency and litter size in Garole x Malpura sheep. *Anim Reprod Sci.* (2008) 105:319–31. doi: 10.1016/j.anireprosci.2007.03.012
36. Gootwine E, Zenu A, Bor A, Yossafi S, Rosov A, Pollott GE. Genetic and economic analysis of introgression the B allele of the FecB (Booroola) gene into the Awassi and Assaf dairy breeds. *Livest Prod Sci.* (2001) 71:49–58. doi: 10.1016/S0301-6226(01)00240-8
37. Souza C, Moraes J, Chagas LM. Effect of the Booroola gene on time of ovulation and ovulatory dynamics. *Anim Reprod Sci.* (1994) 37:7–13. doi: 10.1016/0378-4320(94)01324-1
38. Godfrey RW, Collins JR, Hensley EL. Behavioral and endocrine responses of hair sheep ewes exposed to different mating stimuli around estrus. *Theriogenology.* (2001) 55:877–84. doi: 10.1016/S0093-691X(01)00450-2
39. Olivera-Muzante J, Fierro S, López V, Gil J. Comparison of prostaglandin- and progesterone-based protocols for timed artificial insemination in sheep. *Theriogenology.* (2011) 75:1232–8. doi: 10.1016/j.theriogenology.2010.11.036
40. Fierro S, Viñoles C, Olivera-Muzante J. Long term prostaglandin based-protocols improve the reproductive performance after timed artificial insemination in sheep. *Theriogenology.* (2017) 90:109–13. doi: 10.1016/j.theriogenology.2016.11.031
41. Ezzat AA, Ahmed MN, Elabdeen MAAEZ, Sabry AM. Estrus synchronization in ossimi sheep by progestins. *Alex J Vet Sci.* (2016) 51:207–14.
42. Campbell BK, Baird DT, Souza CJ, Webb R. The FecB (Booroola) gene acts at the ovary: in vivo evidence. *Reproduction.* (2003) 126:101–11. doi: 10.1530/reprod/126.1.101
43. Goodman RL, Gibson M, Skinner DC, Lehman MN. Neuroendocrine control of pulsatile GnRH secretion during the ovarian cycle: evidence from the ewe. *Reprod Suppl.* (2002) 59:41–56.
44. Boulton MI, Haley CS, Springbett AJ, Webb R. The effect of the Booroola (FecB) gene on peripheral FSH concentrations and ovulation rates during oestrus, seasonal anoestrus and on FSH concentrations following ovariectomy in Scottish Blackface ewes. *J Reprod Fertil.* (1995) 103:199–207. doi: 10.1530/jrf.0.1030199
45. Juengel JL. How the quest to improve sheep reproduction provided insight into oocyte control of follicular development. *J R Soc N Z.* (2018) 48:143–63. doi: 10.1080/03036758.2017.1421238
46. Baird DT, Campbell BK. Follicle selection in sheep with breed differences in ovulation rate. *Mol Cell Endocrinol.* (1998) 145:89–95. doi: 10.1016/S0303-7207(98)00174-9
47. Duan H, Ge W, Yang S, Lv J, Ding Z, Hu J, et al. Dihydrotestosterone regulates oestrogen secretion, oestrogen receptor expression, and apoptosis in granulosa cells during antral follicle development. *J Steroid Biochem Mol Biol.* (2021) 207:105819. doi: 10.1016/j.jsbmb.2021.105819
48. Kamalludin MH, Garcia-Guerra A, Wiltbank MC, Kirkpatrick BW. Trio, a novel high fecundity allele: I. Transcriptome analysis of granulosa cells from carriers and noncarriers of a major gene for bovine ovulation rate. *Biol Reprod.* (2018) 98:323–34. doi: 10.1093/biolre/iox133
49. Guo YX, Duan CH, Hao QH, Liu YQ, Li T, Zhang YJ. Effect of short-term nutritional supplementation on hormone concentrations in ovarian follicular fluid and steroid regulating gene mRNA abundances in granulosa cells of ewes. *Anim Reprod Sci.* (2019) 211:106208. doi: 10.1016/j.anireprosci.2019.106208
50. Regan SLP, McFarlane JR, O'Shea T, Andronicos N, Arfuso F, Dharmarajan A, et al. Flow cytometric analysis of FSHR, BMRR1B, LHR and apoptosis in granulosa cells and ovulation rate in merino sheep. *Reproduction.* (2015) 150:151–63. doi: 10.1530/REP-14-0581
51. Wayne CM, Fan H-Y, Cheng X, Richards JS. Follicle-stimulating hormone induces multiple signaling cascades: evidence that activation of rous sarcoma oncogene, RAS, and the epidermal growth factor receptor are critical for granulosa cell differentiation. *Molecular Endocrinology.* (2007) 21:1940–57. doi: 10.1210/me.2007-0020
52. Davis GH. Major genes affecting ovulation rate in sheep. *Genet Sel Evol.* (2005) 37:S11–23. doi: 10.1186/1297-9686-37-S1-S11
53. Davis GH. Fecundity genes in sheep. *Anim Reprod Sci.* (2004) 82:247–53. doi: 10.1016/j.anireprosci.2004.04.001
54. Lim W, Bae H, Bazer FW, Song G. Stimulatory effects of fibroblast growth factor 2 on proliferation and migration of uterine luminal epithelial cells during early pregnancy. *Biol Reprod.* (2017) 96:185–98. doi: 10.1095/biolreprod.116.142331
55. Prior J, Ghalsasi PM, Walkden-Brown SW, Chavan KM, Kulkarni SR, Nimbkar C. Smallholder sheep owners' views on the value and management of Deccani crossbred FecB-carrier ewes with a higher twinning percentage: implications for a future introgression extension program. *ACIAR Proc Series.* (2009) 199–211.

Conflict of Interest: The authors declare that the research was conducted in the absence of any commercial or financial relationships that could be construed as a potential conflict of interest.

Publisher's Note: All claims expressed in this article are solely those of the authors and do not necessarily represent those of their affiliated organizations, or those of the publisher, the editors and the reviewers. Any product that may be evaluated in this article, or claim that may be made by its manufacturer, is not guaranteed or endorsed by the publisher.

Advantages of publishing in Frontiers

OPEN ACCESS
Articles are free to read for greatest visibility and readership

FAST PUBLICATION
Around 90 days from submission to decision

HIGH QUALITY PEER-REVIEW
Rigorous, collaborative, and constructive peer-review

TRANSPARENT PEER-REVIEW
Editors and reviewers acknowledged by name on published articles

Frontiers
Avenue du Tribunal-Fédéral 34
1005 Lausanne | Switzerland

Visit us: www.frontiersin.org
Contact us: frontiersin.org/about/contact

REPRODUCIBILITY OF RESEARCH
Support open data and methods to enhance research reproducibility

DIGITAL PUBLISHING
Articles designed for optimal readership across devices

FOLLOW US
@frontiersin

IMPACT METRICS
Advanced article metrics track visibility across digital media

EXTENSIVE PROMOTION
Marketing and promotion of impactful research

LOOP RESEARCH NETWORK
Our network increases your article's readership